Manresa School of Engineering

Doctoral program in Natural Resources and Environment

Doctoral thesis by compendium of publications

Environmental and occupational characterisation of coals and dust from coal mining

Pedro Trechera Ruiz

Barcelona, November 2021

Supervisors:

Dr. Teresa Moreno Pérez

(IDAEA-CSIC)

Dr. Xavier Querol Carceller

(IDAEA-CSIC)

Tutor:

Dr. M. Montserrat Solé Sardans

(EPSEM-EMIT)

ACKNOWLEDGMENTS

Abans de tot, voldria agrair el suport incondicional a totes les persones que directament o indirectament han aportat el seu gra de sorra per poder realitzar aquesta tesi. Sembla mentida, però una tesi doctoral no és una feina fàcil, i menys encara en temps de Covid. Hi ha moments per a tot, esforços, sacrificis, estrès, aprenentatge, alegries, vivències, quatre anys donen per a molt, i un cop l'acabes et sents molt orgullós de la feina feta. Per això voldria agrair a totes les persones que m'han ajudat d'una manera o altra a fer-ho possible. Moltíssimes gràcies!

Primerament agrair tot el suport i dedicació que m'han brindat els meus directors de tesi, Teresa Moreno i Xavier Querol. Moltíssimes gràcies per confiar en mi des d'un bon principi i per donar-me l'oportunitat de realitzar aquesta tesi doctoral, tot i que aquest món del carbó era nou per a mi. He de dir que em sento molt orgullós d'haver tingut dos grans professionals de supervisors i que acabo molt satisfet. Sense dubte, si tirés quatre anys enrere tornaria, a començar amb vosaltres. Gràcies per tot el que m'heu ensenyat, per prestar-me el vostre temps (que no ha sigut poc), consells, correccions, anècdotes, campanyes, viatges, experiències i de moltes altres, però sobretot i el més important en l'àmbit personal, pel vostre tracte, sentit comú i el vostre costat més humà que m'heu mostrat. Gràcies per haver-me aplanat el camí, mil gràcies! Especialment a tu Xavi, gràcies per introduir-me fins al fons en el món del carbó, per les teves infinites idees, propostes i solucions! Acabo la tesi content, perquè no t'he matat a disgustos!!

M'agradaria destacar la gran ajuda que obtingut durant la meva tesi per part de la Natalia Moreno i la Patricia Córdoba. Desinteressadament les dues sempre s'han mostrat obertes a col·laborar, corregir i ensenyar-me tècniques i experiments nous. A més, han estat un gran suport per a mi, sempre disposades a compartir el seu temps, per molta feina que tinguessin. Sobretot a la Patri, a la que hem molestat molt amb tots els problemes que sorgien al laboratori. Moltíssimes gràcies a totes dues!

Agrair a la Universitat Politècnica de Catalunya, a l'Escola Politècnica Superior d'Enginyeria de Manresa i al seu programa de Doctorat en Recursos Naturals i Medi Ambient. Gràcies a la meva tutora, Montserrat Sole Sardans, però sobretot, gràcies a la Llúcia Rexach per la seva ajuda, facilitat i sempre estar quan se l'ha necessitat.

I would like to express my gratitude to all the colleagues of the ROCD project, since it is thanks to them and to the project that this thesis has been possible. Thank you for all the samples, for the experience gained, conferences held, and trips made. Thanks to Robert Lah, Diane Johnson, Tomasz Pindel, Aleksander Wrana, Ali Arif and Richard Ghimsky and all other colleagues. Especially to Ben Williamson for his dedication and interest in helping, a great team leader and an inspiring person. Also, to Wes, for the help and talks!

Many thanks to all my colleagues from the China University of Geosciences that I met during my two weeks there. There, for making our sampling possible, for a very comfortable stay and for the experience of visiting different areas and mines, in China. I am very grateful for being given this opportunity. Also, I personally wanted to thank Xinguo Zhuang, Baoqing Li, Jing Li, Yunfei Shangguan and Chen Yao, who excelled in scientific knowledge and in hospitality too. Thank you for the support given to this thesis and the support and warmth offered during our time in China. Especially to Yunfei, whose friendship was invaluable!

Tanks to Frank Kelly's team from Imperial College London, MRC-PHE Center for Environment and Health for providing me the opportunity to carry out new tests, tests and for the comfortable accommodation provided. Especially to Ana Oliete and Stav Friedman for their guidance and instruction on all the necessary techniques all the necessary analytical techniques.

Thanks to the group of Gaelle Uzu, from the University of Grenoble Alpes, France, and her team Jean Luc Jaffrezo and Takeoua Mhadhbi for the performance of oxidative potential analysis, help in interpretation and support. Also, to Konrad Kandler from Technical University Darmstadt, thank you very much.

Gràcies a tots els companys/es de IDAEA-EGAR que he compartit durant aquests quatre anys. Moltíssimes gràcies per crear un bon ambient de treball i fer-me sentir sempre com a casa, us estic molt agraït. En especial als PhD que han passat pel 1543, Cris, Carla, Tolis, Marina, Alessia, Joaquim, Jordi, Anna i Maria, fent d'ell un despatx especial, amb molt bon rotllo. Sense oblidar-me de la resta de PhD que m'han acompanyat durant aquests anys, Marta, Jesus, Marten, Amaia, Cristina Carnero i Antonio Pacito. Especialment a l'Adolfo, gran company de lab i amb un cor que no li cap al pit. Gràcies també a la Maria Izquierdo, per les seves xerrades, sobretot en aquesta recta final. Agrair als responsables del lab 1541, Diana, Rebeca i Mar, per tot el material que els hi he "robat". Agrair a la Mercè, Silvia i Rafa per sempre "colar-me" les meves digestions. A més, gràcies Rafa per solucionar mil i un problemes que sorgien amb els equips, ets tot un manetes. Agrair també el treball de la Garay i Elena. En definitiva, us desitjo ho millor a tots/es!

També agrair als companys del CCiTUB de la UB, al servei de microanàlisis i ICTS nanbioses del IQAC-CSIC i a l'equip de Environmental Toxicology de IDAEA-CSIC per permetre l'anàlisis de les meves mostres. Sobretot a Jose Portugal, que encara que no hagin obtingut resultats a toxicologia he aprés moltes coses, i a la Susana Vilchez, amb la que hi he passat molt bones estones analitzant la grandària de partícula.

Gràcies a la família, sobretot a la Carme, Teresa, Ignasi, Aleix i Dani per fer-ho tot més fàcil i donar-me tant de suport sempre. Als meus grans àvis també. Als bons amics i amigues que tinc, de la Secu, Uni, Castells, Futbol, Vilallonga, TGN, Bimbes i de molts altres! Gràcies també a algunes professores de la UB, com Núria Serrano, Anna Grandas i sobretot a tu Elisabet Bosch, sense saber-ho em vau despertar la curiositat pel món científic. Also, thanks Renata!

Gracias Sara, aunque seas la pequeña eres un gran reflejo donde mirarse, cariñosa y con una sonrisa de oreja a oreja. Gracias Papa, gracias a ti he aprendido a no rendirme nunca y, sobre todo, a disfrutar de la vida. Gracias Mama, por tu lucha y entrega para que todo salga adelante, pase lo que pase siempre has sabido ver el lado positivo a las cosas, te estaré eternamente agradecido.

Per últim, gràcies Pluto! El gran terratrèmol i pesadilla de la casa, però que en tendresa no el guanya ningú. Gràcies Bimba! Encara que no m'entenguis, sé que em comprens i ets capaç d'animar-me, sense separar-te mai del meu costat. I moltíssimes gràcies a tu Mire, sempre recolzant-me en tot el que faig. Gràcies per aguantar el meu caos i tindre tanta paciència, per entendre'm en tot moment i sobretot, per transformar màgicament els mals moment en riures i diversió. Amb tu tot és més fàcil!

ABSTRACT

Coal has been a valuable resource in our society for several centuries but its benefits as an energy source are partially counterbalanced by the environmental damage caused by pollutant emissions. Although many global agreements and policies have been proposed in an attempt to reduce the use of fossil fuels, such as the Paris Agreement on climate change to reduce greenhouse gas emissions, coal is still currently produced and consumed on a massive scale. Moreover, it has been predicted that this scenario is likely to continue over the next three decades.

Exposure to high coal dust levels is widely recognised as a major occupational hazard for coal miners. Over the course of time, mining law regulations, advances in mining engineering and the increased safety awareness of coal miners have all encouraged improvements in occupational protection. Despite this, however, exposure to coal dust during mining and handling remains the cause of coal mine dust lung diseases (CMDLD) such as coal workers' pneumoconiosis (CWP), silicosis, and progressive massive fibrosis (PMF). This may be at least in part due to improved technological efficiency of the mining machinery used to work coal, resulting in the emission of finer particles and higher concentrations of coal dust, an effect that has been linked to CMDLD increasingly affecting younger coal workers. In spite of these ongoing changes in mining methods and dust emissions, however, there remains a notable paucity of parallel studies on health-relevant issues linked to particulate matter (PM) inhalation in modern coal mines.

The main objective of this PhD thesis is the study of coal mine dust patterns produced by different types of mining operations and different types of coal. In addition, the potential links between oxidative potential (OP) of coal dust and its geochemistry have been investigated in order to identify indicators of potential concern for human health. To these ends, extensive particle size, chemical, mineralogical and OP analyses were carried out on: i) deposited coal mine dust collected in from different areas in underground and open-pit coal mines; ii) a selection of powdered coal samples from in-seam channel profiles covering a wide and contrasting variety of coal geochemistry patterns. In both cases, the respirable fractions (<4 μm) were extracted and analysed to simulate actual suspended respirable coal dust (PM_4). The novelty of these sampling and analytical programmes made it necessary to calibrate and validate new methodologies, and design and implement new protocols, in order to separate the respirable fractions of dust and obtain comprehensive particle size, geochemical and mineralogical characterisations.

The results of this thesis are summarised in five scientific articles in high-impact journals. Article #1 introduces the subject and includes a review of major health-relevant coal dust geochemical patterns. Articles #2 to #4 show results from the sampling of deposited coal dust in a number of underground coal mines (China and Europe) and an open-pit coal mine (China), and describe the separation and characterisation of respirable fractions. The samples were collected from different zones of the coal mines in order to encompass the most relevant mining operations being undertaken. In addition, in Article #5, powdered coal seam samples, covering a wide range of geochemical patterns from China, were used to separate and characterise their respective respirable fractions.

In Articles #3 to #5 the respirable coal dust samples were selected (according to size and geochemistry) in order to evaluate the relationships among OP markers (ascorbic acid, AA; glutathione, GSH; and dithiothreitol, DTT). This toxicological methodology was applied using cross-correlation and multilinear regression analyses on underground mine dust samples (Article #3), open-pit mine samples (Article #4) and powdered coal samples (Article #5). The approach was repeated including both respirable fractions from deposited coal mine dust and from powdered coal samples (Article #5).

In addition, suspended coal dust measurements were reported in Articles #2 to #4 (Europe and China), including online ambient measurement of $PM_{2.5}$, PM_{10}, BC and UFP (PM <2.5 µm, <10 µm, black carbon, and ultrafine particles, respectively) around several mining operations in the open-pit mine (Article #4).

The results of this thesis demonstrate that coal dust particle size is a key parameter controlling coal dust resuspension. The particle size is highly influenced by moisture content and ash yield of coal dust, with a negative and positive correlation, respectively, with the percentage of fine particles in deposited dust.

Based on observed coal dust levels, the results also provide evidence that respirable coal dust levels are markedly higher in the working front areas. From there, dust concentrations decrease markedly, although with the finer fractions being easily transported to other parts of the mine which, in addition, receive dust contributions from other emission sources such as gangue mining and handling, coal transport, salts from acid mine drainage (AMD), machinery wear and weathering of gunited walls. These contributions markedly modify the coal dust size and geochemical composition, in comparison to the dust from the coal working front.

Thus, both concentrations and geochemical patterns of coal dust are noticeably influenced by the mining operations carried out in a given mine area. Working and handling coal produces relatively coarser mine dust, with variable proportions of mineral matter and coaly matrix, whereas working and handling gangue materials produces fine and high-ash dust enriched in clay minerals, quartz and calcite. In contrast, the access galleries are characterised by lower dust levels, but contain higher amounts of Ca-bearing mineral species and higher contents of potentially hazardous dust components (such acidic sulphate species, Fe, As, Sb, among others) from salts derived from infiltrated phreatic waters affected by AMD.

When respirable fractions of the dust samples were analysed, it was observed that most of the elemental ratios of this respirable dust versus the parent deposited dust were less than or similar to 1.0. In contrast, ratios for clay minerals and a number of metals (Se, Mo, Pb, Zn, Sn, As, Cu, Sb, Ni, Co and Cr) were >1.0, indicating their enrichment in the respirable fraction due to their relatively finer mode of occurrence. Such enrichments may indicate the presence of dust from sources other than the working front coal dust emissions, such as AMD and machinery wear. This is also suggested by the fact that a number of these elements have higher concentrations in PM_{10} compared with the respirable deposited dust. Accordingly, even if PM levels are markedly lower away from the working fronts, it remains important to monitor coal dust in other areas of the mine because of potentially increased occupational exposure to a number of metals.

The total OP (OP^{TOT}) results presented here, together with an article published in 2021 on Turkish coal mine dust, are the first ones investigating links of geochemical patterns between mine dust

and OP. In this present study, total OP (OP^{TOT}) values obtained for coal dust are markedly lower than those reported from PM from subway systems, ambient air PM from areas with high domestic biomass burning and roadside sites. It was found that OP^{AA} is mostly linked with inorganic species within the coal mine dust, whereas OP^{GSH} and OP^{DTT} are linked with organic species of coal. The main drivers were found to be Fe, pyrite, sulphate minerals and anatase for OP^{AA}, as well as moisture content, Ca, Mg, Na and Ba, for OP^{GSH} and OP^{DTT}. Furthermore, the correlations of the contents of most of these components in dust or coal with the OP^{AA}, OP^{GSH} and OP^{DTT} increase only in high-rank coal or high coal-rank mine dust (mostly bituminous in this study).

Results for the evaluation of the impact of coal geochemical patterns on the OP (Article #5) demonstrated that the high pyrite coals and high ash yields and contents of anatase, quartz, S, Ti and various trace metals, such as Mn, Mo and U, are linked to increased OP^{AA}. On the other hand, as described for coal dust, the content of the organic coal matrix seems to control the OP^{GSH} and OP^{DTT} of the powdered coal samples. Thus, these results are similar to the ones obtained for the respirable coal dust samples, indicating that the extraction of the respirable fraction of powdered coal seam samples for subsequent geochemical and OP analysis can be used as a broad indicator of the OP of the coal mine dust.

The results on OP markers are in agreement with those from prior studies and modelling results supplying evidence for the associations of the generation of reactive oxidative species (ROS). This is especially the case for the strong correlations between Fe or pyrite with OP^{AA}, which supports the relevance of the Fe and pyrite contents in inhalable particles from coal dust for oxidative stress, including the possibility of links to lung injury and CWP development.

PM_{10} measurements reported in this study demonstrate the importance of the effectiveness of dust control measures implemented in underground and open-pit coal mines in order to reduce airborne dust concentrations. Of special relevance here are the high levels of fine dust recorded in areas of gangue handling without control measures in the open-pit mine. Additionally, online ambient measurements of BC and UFP record moderate exposure levels, with the highest levels being close to those of traffic sites in urban areas. The lower atmospheric dispersion at the bottom of the open-pit mine, in contrast with the top areas, added to the higher machinery activity and truck density, together result in higher levels of these pollutants.

The results of this PhD thesis underline the importance of continued research on dust in coal mining environments in the context of improving working conditions for coal miners, especially given that intensive coal production in countries such as China is likely to continue for decades to come.

RESUM

El carbó ha estat un recurs molt valuós a la nostra societat durant segles, però els seus beneficis com a font d'energia sempre han estat en part contrarestats pel dany ambiental causat per les seves emissions contaminants. Tot i que s'han proposat molts acords i polítiques per reduir l'ús de les energies fòssils, com ara l'Acord de París sobre el canvi climàtic, que promou la reducció de les emissions de gasos hivernacle, el carbó es segueix consumint i produint actualment a gran escala. A més, es pronostica que aquest escenari romandrà intacte durant les properes tres dècades.

L'exposició a nivells elevats de pols de mineria és considerat com un factor de gran risc ocupacional per als miners del carbó. Al llarg del temps, les regulacions mineres, els avenços en l'enginyeria minera i la conscienciació en la seguretat dels treballadors del carbó han fomentat millores en la protecció ocupacional. Tot i això, l'exposició a la pols de carbó durant la seva mineria i manipulació continua sent la principal causa de malalties pulmonars derivades de la pols del carbó (CMDLD), com la pneumoconiosi dels miners del carbó (CWP), la silicosi i la fibrosi massiva progressiva (PMF). Això, en part, és probablement degut a la millora en l'eficiència tecnològica de la maquinària minera usada per treballar el carbó, resultant en l'emissió de partícules més fines i concentracions més altes de pols de carbó (per ser capaç d'explotar majors quantitats), un efecte que ha estat relacionat amb l'increment de CMDLD, afectant fins i tot treballadors més joves. No obstant això, malgrat els canvis en els mètodes miners i les seves emissions de pols, continua existint una notable escassetat d'estudis paral·lels sobre temes rellevants per a la salut, relacionant-los amb la inhalació de partícules a les mines de carbó modernes.

L'objectiu principal d'aquesta tesi doctoral és l'estudi dels patrons de la pols de carbó produïts pels diferents tipus d'operacions mineres i l'estudi dels principals patrons composicionals de diferents tipus de carbó, cobrint un ampli rang geoquímic. A més, la relació entre el potencial oxidatiu (OP) i la geoquímica de la pols de carbó va ser investigada amb la finalitat d'identificar possibles indicadors o traçadors potencials que puguin perjudicar la salut humana. Amb aquesta finalitat, es van dur a terme anàlisis de mida de partícula, químics, mineralògics i d'OP per a: i) la pols de carbó recol·lectat en diferents zones i processos miners per a mines de carbó subterrànies i de cel obert, ii) una selecció de mostres de perfils de capes de carbó moltes, cobrint una àmplia i contrastada varietat de paràmetres geoquímics dels carbons explotats actualment a la Xina. En tots dos casos, les fraccions respirables (<4 μm) van ser separades i analitzades per simular la pols de carbó respirable en suspensió (PM_4). La novetat d'aquests protocols de mostreig i anàlisi van requerir tasques de calibratge i validació d'aquestes noves metodologies, i dissenyar i implementar nous mètodes per separar les fraccions respirables de pols i obtenir caracteritzacions completes de mida de partícula, geoquímiques i mineralògiques.

Els resultats d'aquesta tesi doctoral estan inclosos en cinc articles científics publicats en revistes d'alt impacte. L'Article #1 és introductori i conté una revisió dels patrons geoquímics de la pols de mineria del carbó més rellevants per la salut humana. De l'Article #2 al #4 es mostren resultats per al mostreig de pols de carbó dipositat a nombroses mines de carbó subterrànies (Xina i Europa) i una mina de cel obert (Xina), i descriu la separació i caracterització de fraccions respirables. Les mostres es van recollir a diferents zones de les mines per tal de cobrir les

operacions mineres més significatives. També, les mostres de carbó molt de l'Article #5, comprenent un ampli rang de patrons geoquímics a la Xina, es van utilitzar per separar i caracteritzar detalladament les fraccions de pols respirable.

Als Articles #3 a #5 van ser seleccionades mostres de pols respirable (d'acord amb la seva mida i els patrons geoquímics) per tal d'avaluar les relacions entre els marcadors OP (àcid ascòrbic, AA; glutatió, GSH; i dithiothreitol, DTT) amb els patrons fisicoquímics més rellevants, duent a terme una anàlisi de relació creuada i regressió multilineal per a les mostres de pols de mines subterrànies (Article #3), mostres de pols de la mina de cel obert (Article #4) i mostres de carbó molt (Article #5). Finalment, les anàlisis van ser repetides incloent totes les fraccions respirables de les mostres dipositades de pols de carbó i de les mostres de carbó molt (Article #5).

A més de les mesures de pols de mina respirable extretes de pols sedimentada o de carbó molt, es van reportar mesures directes de pols de mina en suspensió dels Articles #2 a #4 (Europa i la Xina), incloent-hi mesures ambientals de $PM_{2.5}$, PM_{10}, BC i UFP (PM <2.5 µm, <10 µm, carboni negre, i partícules ultrafines, respectivament) al voltant de diverses operacions mineres a la mina de cel obert (Article #4).

Els resultats d'aquesta tesi doctoral demostren que la mida de partícula de la pols és un paràmetre clau per al control de la resuspensió de la pols de mina de carbó. Els resultats també mostren que la mida de partícula és altament influenciable pels continguts d'humitat i cendra de la pols de mina de carbó, que estan negativament i positivament correlacionats, respectivament, amb el percentatge de les partícules fines en el pols sedimentat/dipositat.

Basant-se en l'observació dels nivells de pols de carbó, els resultats evidencien que els nivells de fracció respirable són marcadament superiors a les àrees del front de treball de la capa de carbó. Des d'allà, la pols decreix considerablement, encara que les fraccions fines siguin fàcilment transportades a altres parts de la mina on també reben contribucions d'altres fonts d'emissió, com ara de la mineria i manipulació dels estèrils, del transport del carbó, de sals del drenatge àcid de mines, del desgast de la maquinària i de l'erosió de galeries gunitades. Aquestes contribucions modifiquen notablement la mida de la pols de mina i la seva composició, en comparació amb la pols provinent del front de treball on és explotada directament la capa de carbó.

Els resultats mostren, doncs, que els nivells i patrons geoquímics de la pols de mina de carbó estan notablement influenciats per les operacions mineres dutes a terme a cada zona específica de la mina. La manipulació i el treball del carbó generen una pols relativament gruixuda, amb proporcions variables de contingut mineral i matriu orgànica; mentre que la manipulació i el treball dels estèrils produeixen pols fina i amb alt contingut en cendra, enriquit en minerals com argila, quars i calcita; els accessos a les galeries estan caracteritzats per baixos continguts en pols, però amb una proporció més alta en material respirable, que contenen espècies minerals enriquides a Ca, i també components potencialment perillosos (espècies sulfatades àcides, Fe, As, Sb, entre d'altres) derivats de les sals de les aigües freàtiques infiltrades, que es veuen afectades pel drenatge àcid de mines.

L'anàlisi de les fraccions respirables de les mostres de pols va mostrar que la major part de les ràtios d'aquesta pols respirable versus la pols dipositada original va ser menor o similar a 1.0. En canvi, les ràtios per a minerals de l'argila i alguns metalls (Se, Mo, Pb, Zn, Sn, As, Cu, Sb, Ni, Co i

Cr) van assolir valors >1.0, indicant el seu enriquiment en la fracció respirable a causa del seu mode d'ocurrència més fi. Aquests enriquiments poden indicar la presència de pols provinent d'altres fonts diferents de les emissions de pols de carbó del front de treball, com ara el drenatge àcid de la mina i el desgast de la maquinària. Això també és suggerit pel fet que diversos d'aquests elements també tenen concentracions més elevades en PM_{10}, comparats amb la pols respirable dipositada. Llavors, encara que els nivells de PM són marcadament inferiors lluny del front de treball de la capa de carbó, el seu enriquiment en determinats metalls i sals evidencia la importància de monitoritzar la pols de mineria a les altres àrees de la mina, i no tan sols al front de treball de la capa.

Els resultats d'OP total (OP^{TOT}) presentats aquí, juntament amb els d'un article publicat el 2021 sobre la pols de mina de carbó a mines turques, són els pioners en investigar les connexions dels patrons geoquímics de la pols de mina i OP. En aquesta tesi doctoral, els valors d'OP^{TOT} obtinguts per a la pols de carbó són marcadament inferiors als d'altres estudis de PM publicats provinents dels sistemes de metro urbà, PM de l'aire ambiental d'àrees amb altes emissions de crema de biomassa domèstica i de carrers urbans transitats. Es va trobar que les espècies inorgàniques de la pols de carbó estan més relacionades amb OP^{AA}, mentre que les espècies orgàniques estan més relacionades amb OP^{GSH} i OP^{DTT}. Es va poder evidenciar que les especies i elements que governen l'OP^{AA} són Fe, pirita, minerals sulfatats i anatasa, mentre que per l'OP^{GSH} i OP^{DTT} són els continguts en humitat (reflectint el contingut en matèria orgànica carbonosa), Ca, Mg, Na i Ba. A més, les correlacions de les concentracions de la major part d'aquests components a la pols de mina o al carbó amb OP^{AA}, OP^{GSH} i OP^{DTT} van incrementar quan van ser avaluats només els carbons o pols de carbó d'alt rang (bituminosos en aquest estudi).

Els resultats de l'avaluació de les característiques geoquímiques dels carbons explotats a la Xina que controlen l'OP de la pols potencialment generada durant la seva extracció i manipulació (Article #5) demostren que els continguts en pirita, cendra, anatasa, quars, S, Ti i diversos metalls traça, com Mn, Mo i U, governen l'OP^{AA}. D'altra banda, igual que el deduït per a la pols de mina, és el contingut en la matèria orgànica carbonosa el que governa els nivells d'OP^{GSH} i OP^{DTT} de les mostres de carbó molt. Aquests resultats són similars als obtinguts a la pols de mina de carbó respirable, indicant que l'extracció de la fracció respirable de les mostres de capes de carbó per ales posteriors anàlisis geoquímica i d'OP es poden utilitzar com a indicador de l'OP de la pols de mina de carbó, atenent les limitacions indicades anteriorment, de les possibles fonts de pols addicionals a la del front de treball a la capa.

Els resultats dels indicadors d'OP concorden amb estudis i models previs que proporcionen evidències d'associacions de determinats elements i espècies en la pols de mineria amb la generació d'espècies reactives de l'oxigen (ROS). Especialment pel que fa a les marcades correlacions entre Fe i pirita amb OP^{AA}, que demostren la rellevància dels continguts de Fe i pirita en pols de mina i de carbó inhalables amb l'estrès oxidatiu, incloent-hi la possibilitat de provocar malalties pulmonars i el desenvolupament de CWP.

Els mesuraments de PM_{10} realitzats en aquest estudi demostren la importància d'aplicar mesures efectives per al control de la pols de mineria a les mines de carbó subterrànies i de cel obert per reduir-ne la concentració. Especialment rellevants són els alts nivells de pols fina mesurats en àrees on els estèrils són manipulats, sense mesures de control, a la mina de cel obert. També, els mesuraments in situ i en continu de BC i UFP van mostrar nivells d'exposició

moderats, obtenint-se nivells d'exposició en cel obert comparables als típicament enregistrats en entorns de trànsit urbà intens. Òbviament aquest no era el cas per als nivells de PM, sent aquests molt superiors a la mina. La baixa dispersió atmosfèrica al fons de la mina a cel obert, en comparació amb les àrees més elevades, combinat amb una densa maquinària minera i el dens trànsit de la zona, proporciona elevats nivells de contaminants, especialment UFP i PM.

Els resultats d'aquesta tesi doctoral subratllen la importància de continuar investigant sobre les propietats i nivells de pols a la mineria del carbó en el context de la millora de les condicions laborals dels miners, especialment atès que, probablement, es mantindrà una producció de carbó molt elevada a països com la Xina durant les dècades vinents.

RESUMEN

El carbón ha sido un recurso muy valioso en nuestra sociedad durante siglos; sin embargo, sus beneficios como fuente de energía siempre han sido parcialmente contrarrestados por el daño ambiental causado por sus emisiones contaminantes. Aunque se han propuesto muchos acuerdos y políticas para reducir el uso de las energías fósiles, como el Acuerdo de París sobre el cambio climático que trata de reducir las emisiones de gases invernadero, el carbón se sigue consumiendo y produciendo actualmente a gran escala. Además, se pronostica que este escenario permanezca intacto durante las siguientes tres décadas.

La exposición a elevados niveles de polvo de minería es considerada un factor de riesgo ocupacional muy importante para los mineros del carbón. Durante el paso del tiempo, las regulaciones mineras, los avances en la ingeniería minera y la mayor consciencia de la seguridad de los trabajadores del carbón ha fomentado mejoras en la protección ocupacional. A pesar de ello, la exposición ocupacional al polvo de carbón durante su minería y manipulación sigue siendo la principal causa de enfermedades pulmonares del polvo del carbón (CMDLD), como la neumoconiosis (CWP), la silicosis y la fibrosis masiva progresiva (PMF). Esto, en parte, probablemente se deba a la mejora en la eficiencia tecnológica de la maquinaria minera usada para trabajar el carbón, resultando en la emisión de partículas más finas y concentraciones más altas de polvo de carbón (al explotarse mayores cantidades de carbón), un efecto que ha estado relacionado con el incremento de CMDLD, afectando incluso a trabajadores más jóvenes. Sin embargo, a pesar de los cambios en los métodos mineros y sus emisiones de polvo, sigue existiendo una notable escasez de estudios paralelos sobre temas relevantes para la salud, relacionándolos con la inhalación de partículas en las minas de carbón modernas.

El principal objetivo de esta tesis doctoral es el estudio de los patrones de polvo de carbón producidos por los diferentes tipos de operaciones mineras y el estudio de los principales patrones de distintos tipos de carbón cubriendo un amplio rango geoquímico. Además, se ha investigado la relación entre el potencial oxidativo (OP) y la geoquímica del polvo de carbón con el propósito de identificar posibles indicadores potenciales que puedan perjudicar la salud humana. Con estos fines, se llevaron a cabo análisis de tamaño de partícula, químicos, mineralógicos y de OP para: i) el polvo de carbón recolectado en diferentes zonas y procesos mineros para minas de carbón subterráneas y de cielo abierto, ii) una selección de muestras de perfiles de capas de carbón molidas cubriendo una amplia y contrastada variedad de parámetros geoquímicos de carbones explotados en China. En ambos casos, las fracciones respirables (<4 µm) fueron extraídas y analizadas para simular el polvo de carbón respirable en suspensión (PM_4). La novedad de estos protocolos de muestreo y análisis hizo necesario calibrar y validar las nuevas metodologías, y diseñar e implementar nuevos métodos, con el fin de separar las fracciones respirables de polvo y obtener caracterizaciones completas de tamaño de partícula, geoquímicas y mineralógicas.

Los resultados de esta tesis doctoral se incluyen en cinco artículos científicos publicados en revistas de alto impacto. El Artículo #1 es introductorio y contiene una revisión de los patrones geoquímicos más relevantes en la salud humana. En los Artículos #2 a #4 se muestran resultados para el muestreo de polvo de carbón depositado en numerosas minas de carbón subterráneas (China y Europa) y una mina de cielo abierto (China), asimismo se describe la separación y

caracterización de fracciones respirables. Las muestras fueron recogidas en diferentes zonas de las minas de carbón con el fin de cubrir las operaciones mineras más significativas realizadas en ellas. Además, las muestras de carbón pulverizado del Artículo #5, que comprenden un amplio rango de patrones geoquímicos en China, fueron utilizadas para separar y caracterizar detalladamente sus fracciones respirables.

En los Artículos #3 a #5, se seleccionaron muestras de polvo de mina y carbón molido (de acuerdo con su tamaño y los patrones geoquímicos) para evaluar las relaciones entre los marcadores OP (ácido ascórbico, AA; glutatión, GSH; y ditiotreitol, DTT) con los patrones fisicoquímicos más relevantes, llevando a cabo un análisis de relación cruzada y regresión multilineal para las muestras de polvo de minas subterráneas (Artículo #3), muestras de polvo de la mina de cielo abierto (Artículo #4) y muestras de carbón pulverizado (Artículo #5). Por último, se repitieron los análisis incluyendo todas las muestras de las fracciones respirables de las muestras depositadas de polvo de carbón y de las muestras de carbón pulverizado (Artículo #5).

Además de las medidas de polvo de carbón respirable extraídas de polvo sedimentado o carbón pulverizado, se llevaron a cabo medidas directas de medidas in-situ y en continuo de polvo de mina en suspensión en los Artículos #2 a #4 (Europa y China), incluyendo medidas en aire ambiente de niveles de $PM_{2.5}$, PM_{10}, BC y UFP (PM <2.5 µm, <10 µm, carbono negro, y partículas ultrafinas, respectivamente) en torno a varias operaciones mineras en la mina de cielo abierto (Artículo #4).

Los resultados de esta tesis doctoral demuestran que el tamaño de partícula del polvo de mina es un parámetro clave para el control de su suspensión. Los resultados también muestran que el tamaño de partícula del polvo depende de los contenidos de humedad y ceniza del mismo, que están negativa y positivamente correlacionados, respectivamente, con el porcentaje de las partículas finas en el polvo sedimentado/depositado.

Basándose en la observación de los niveles de polvo de mina de carbón, los resultados evidencian que los niveles de fracción respirable son marcadamente superiores a las áreas del frente de trabajo de la capa de carbón. Desde allí, el polvo decrece considerablemente, aunque las fracciones finas sean fácilmente transportadas a otras partes de la mina, donde también reciben contribuciones de otras fuentes de emisión, como por ejemplo de la minería y manipulación de los estériles, transporte del carbón, sales del drenaje ácido de minas, desgaste de la maquinaria y erosión de galerías gunitadas. Estas contribuciones modifican notablemente el tamaño del polvo de mina y su composición, en comparación con el polvo proveniente del frente de trabajo donde se explota directamente la capa de carbón.

Los resultados muestran, pues, que los niveles y patrones geoquímicos del polvo de mina de carbón están notablemente influenciados por las operaciones mineras llevadas a cabo en cada zona específica de la mina. La manipulación y el trabajo del carbón generan un polvo relativamente grueso, con proporciones variables de contenido mineral y matriz orgánica; mientras que la manipulación y el trabajo de los materiales de los estériles producen polvo fino y con alto contenido en ceniza, enriquecido en minerales como arcilla, cuarzo y calcita; los accesos a las galerías están caracterizados por bajos contenidos en polvo, pero con mayor proporción en material respirable, que contienen especies minerales enriquecidas en Ca, y

también componentes potencialmente peligrosos (especies sulfatadas ácidas, Fe, As, Sb, entre otros) derivados de las sales de las aguas freáticas infiltradas, que se ven afectadas por el drenaje ácido de minas.

El análisis de las fracciones respirables de las muestras de polvo mostró que la mayor parte de las ratios de concentración de las especies y elementos estudiados en ese polvo respirable versus el polvo depositado original fue menor o similar a 1.0. En cambio, ratios para minerales de la arcilla y algunos metales (Se, Mo, Pb, Zn, Sn, As, Cu, Sb, Ni, Co y Cr) alcanzó valores >1.0, indicando su enriquecimiento en su fracción respirable debido a su modo de ocurrencia más fino. Estos enriquecimientos pueden indicar la presencia de polvo proveniente de otras fuentes distintas a las emisiones de polvo de carbón del frente de trabajo, como el drenaje ácido de la mina y emisiones del desgaste de la maquinaria. Ello se ve corroborado por el hecho de que varios de estos elementos también tienen concentraciones más elevadas en PM_{10}, comparados con el polvo respirable depositado. Así pues, aunque los niveles de PM son marcadamente inferiores lejos del frente de trabajo de la capa de carbón, su enriquecimiento en determinados metales y sales evidencian la importancia de monitorizar el polvo de minería en diferentes áreas de la mina, y no tan solo en el frente de trabajo de la capa.

Los resultados de OP total (OP^{TOT}) presentados aquí, junto con los de un artículo publicado en 2021 de polvo de mina de carbón en minas turcas, son pioneros en investigar las conexiones de los patrones geoquímicos del polvo de mina y OP. En esta tesis doctoral, los valores de OPTOT obtenidos para el polvo de carbón son marcadamente inferiores a los de otros estudios de PM publicados provenientes de los sistemas de metro urbano, PM en aire ambiente de áreas con altas emisiones de quema de biomasa doméstica y de calles urbanas transitadas. Se dedujo que las especies inorgánicas del polvo de carbón están más relacionadas con OP^{AA}, mientras que las especies orgánicas lo están con OP^{GSH} y OP^{DTT}. Las especies y/o elementos que controlaron el OP^{AA} fueron Fe, pirita, minerales sulfatados y anatasa, mientras que para los indicadores OP^{GSH} y OP^{DTT} fueron los contenidos en humedad (reflejando el contenido en materia orgánica carbonosa), Ca, Mg, Na y Ba. Además, las correlaciones de las concentraciones de la mayor parte de estos componentes en polvo de mina o carbón pulverizado con OP^{AA}, OP^{GSH} y OP^{DTT} incrementaron cuando fueron evaluados sólo los carbones o polvo de carbón de alto rango (bituminosos en este estudio).

Los resultados de la evaluación de las características geoquímicas de los carbones explotados en China que controlan el OP del polvo potencialmente generado durante su extracción y manipulación (Artículo #5) demuestran que los contenidos en pirita, ceniza, anatasa, cuarzo, S, Ti y varios metales traza, como Mn, Mo y U, gobiernan la OP^{AA}. Por otra parte, al igual que lo deducido para el polvo de mina, es el contenido en la materia orgánica carbonosa el que gobierna los niveles de OP^{GSH} y OP^{DTT} de las muestras de carbón molido. Estos resultados son similares a los obtenidos en el polvo de mina de carbón respirable, indicando que la extracción de la fracción respirable de las muestras de capas de carbón pulverizado para su posterior análisis geoquímico y de OP se pueden utilizar como indicador del OP del polvo de mina de carbón, atendiendo a las limitaciones indicadas anteriormente, de las posibles fuentes de polvo adicionales a la del frente de trabajo en la capa.

Los resultados de los indicadores de OP concuerdan con los de estudios y modelos previos que proporcionan evidencias de asociaciones de determinados elementos y especies en polvo de

minería con la generación de especies reactivas del oxígeno (ROS). Especialmente en lo referente a las marcadas correlaciones entre Fe y pirita con OP^{AA}, que demuestran la relevancia de los contenidos de Fe y pirita en polvo de mina y de carbón inhalables con el estrés oxidativo, incluyendo la posibilidad de provocar enfermedades pulmonares y el desarrollo de CWP.

Las mediciones de PM_{10} realizadas en este estudio demuestran la importancia de aplicar medidas efectivas para el control del polvo de minería en las minas de carbón subterráneas y de cielo abierto para reducir su concentración. Especialmente relevantes son los altos niveles de polvo fino medidos en áreas donde los estériles son manipulados sin medidas de control, en la mina de cielo abierto. También, las mediciones in-situ y online de BC y UFP mostraron niveles de exposición moderados, obteniéndose niveles de exposición en cielo abierto comparables a los típicamente registrados en entornos de tráfico urbano intenso. Obviamente este no era el caso para los niveles de PM, siendo estos muy superiores en la mina. La baja dispersión atmosférica en el fondo de la mina de cielo abierto, en comparación con las áreas más elevadas, combinado con la alta maquinaria usada, y el denso tráfico de la zona, proporciona elevados niveles de contaminantes, en especial UFP y PM.

Los resultados de esta tesis doctoral subrayan la importancia de seguir investigando sobre las propiedades y niveles de polvo en la minería del carbón en el contexto de la mejora de las condiciones laborales de los mineros; en especial debido a que probablemente se mantenga una producción de carbón muy elevada, en países como China, durante las próximas décadas.

ACRONYMS

WF	Working Front
PM	Particulate Matter
PSD	Particle Size Distribution
CWP	Coal Workers' Pneumoconiosis
ROS	Reactive Oxygen Species
D_{50}	Mass Median Diameter Particle Size
TSP	Total Suspended Particles
UFP	Ultrafine Particles
PMF	Progressive Massive Fibrosis
CMDLD	Coal Mine Dust Lung Diseases
NIOSH	National Institute for Occupational Safety and Health
PRC	People's Republic of China
OP	Oxidative Potential
AA	Ascorbic Acid
GSH	Glutathione
DTT	Dithiothreitol
CWF	Coal Working Front
RCS	Respirable Crystalline Silica
IARC	International Agency for Research on Cancer
AMD	Acid Mine Drainage
CP	Channel Profile
DD	Deposited Dust
RDD	Respirable Deposited Dust (< 4 μm)
CP_4	Respirable Channel Profile (< 4 μm)
ROCD	Reducing risks from Occupational exposure to Coal Dust
USCB	Upper Silesia Coal Basin
VCB	Velenje Coal Basin
PV	Premogovnik Velenje

JSW	Jastrzębska Spółka Węglowa SA
PGG	Polska Grupa Górnicza SA
BWC	Bituminous Southwest China
BSC	Bituminous South China
SSC	Subbituminous South China
ANC	Anthracite North China
BNW	Bituminous Northwest China
TH	Tailings Handling
RT	Roads Traffic
BC	Black Carbon
CUG	China University of Geosciences
WR	Weight Residual
XRD	X-Ray Diffraction
ICDD	International Centre for Diffraction Data
RIR	Reference Intensity Ratio
ad	Air Dried
db	Dry Basis
TWA	Time-Weighted Average
OEL	Occupational Exposure Limits

CONTENTS

Chapter 1

INTRODUCTION

1. INTRODUCTION

Literature on the history of coal utilisation does not clarify where it was first used and mined. However, related sources indicate that its origins were in China, in zones with a lack of wood. Coal use dating from 1000-300 BCE was later extended to several regions of China for heating, cooking and smelting steel (Dodson et al., 2014; Gelegdorj et al., 2007). The Greeks also had discovered coal but, regarded it as a *"geological curiosity rather than as a useful mineral"* (Daemen, 2004). Early use of coal documented in Europe notably includes the Romans in Britain, who took great advantage of its calorific qualities, with coal rapidly becoming an integral part of everyday life, including domestic use, the manufacture of metal artefacts and weapons, and even religious ceremonies (Daemen, 2004; Smith, 1997). But it was not until the 18th century, largely thanks to Thomas Newcomen and James Watt in Britain, that coal gained its status as a vital source of fuel worldwide, providing the resources required for the Industrial Revolution, and stimulating great advances in technology and energy production (Daemen, 2004).

1.1. What is coal?

Although coal is one of the most complex fossil materials, and taking into account that each coal is unique (Orem and Finkelman, 2003), a broad standard definition is a chemically heterogeneous combustible carbonaceous sedimentary black rock (Finkelman et al., 2019; Jing et al., 2020; O'Keefe et al., 2013) composed basically of organic components (macerals) and, to a much minor extent, inorganic minerals (Kossovich et al., 2020; Onifade et al., 2021; Prasanta and Patrick, 1993; Ward, 2016).

Coal formation is the result of a mixture of biological and geological processes working on plant remains over a long period (Orem and Finkelman, 2003). The process of coal formation can be summarised in two steps, Figure 1.1:

i) Peatification: Peat formation is initiated by the accumulation of plant remains, suffering decomposition and biodegradation under anaerobic conditions (Clymo, 1983; Moore, 1987; Stach et al., 1982; Swaine, 1990).

ii) Coalification: The progressive effects of pressure and temperature are mainly responsible for developing peat into coals of increasing rank from primary brown coals (lignite and subbituminous) to hard coals (bituminous, and anthracite) as shown in Figures 1.1 and 1.2 (Bielowicz, 2013; Chaudhuri, 2016; Diessel, 1992; Flores, 2013; O'Keefe et al., 2013; Stach et al., 1982; Suárez-Ruiz and Crelling, 2008; Swaine, 1990).

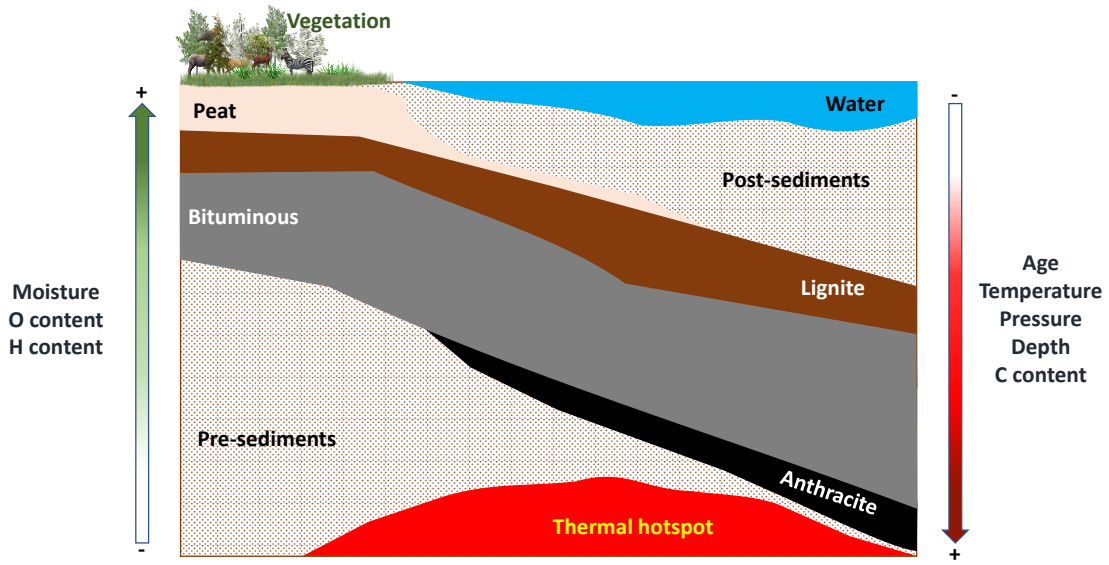

Figure 1.1. *Schematic representation of coal formation over time.*

Coal rank is determined by specific proximate and ultimate analysis, Figure 1.2, such as those of total organic carbon, volatile matter, calorific value, vitrinite or huminite reflectance and moisture content (Bielowicz, 2013; Chelgani et al., 2010; Suárez-Ruiz and Crelling, 2008; Vassilev et al., 1996; H. Wang et al., 2014).

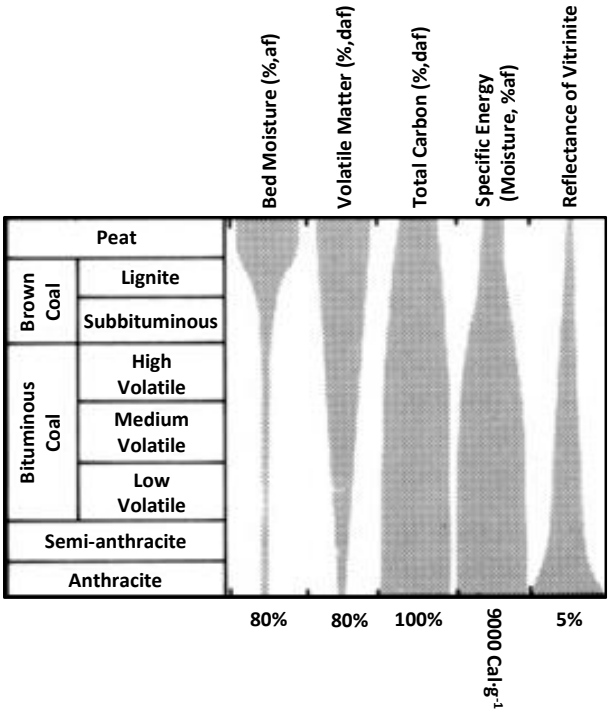

Figure 1.2. *Variation in proximate and ultimate compositions depending on coal rank advance (modified from Ward, 1984). af, ash free; daf, dry ash free.*

1.2. Coal geochemistry

The main component of coal is organic matter, which, in turn, is made of macerals. Macerals are derived from plant material which have been transformed under significant conditions during peatification and coalification (Stach et al., 1982; Swaine, 1990; Teichmüller, 1989; Yürüm, 1988), and accordingly evolved as a function of the coal rank or degree of coal maturity (Barnwal et al., 2000; Scott, 2002; Swaine, 1990; Teng et al., 2017). The macerals are homogeneous aggregates (Spackman, 1958), conventionally classified into three major groups: vitrinite, liptinite, and inertite (Cardott and Curtis, 2018; Dyrkacz and Horwitz, 1982; Lei et al., 2021; Potter et al., 1998; Stach et al., 1982).

The other major component of coal is the inorganic fraction, which also decisively influences coal quality and use, and can also provide useful information regarding coal's geologic evolution (Ward, 2016). The chemistry of this inorganic fraction is influenced by the diverse stages and processes of coal formation as outlined below (Cecil et al., 1982; Cobb and Cecil, 1993; Mraw et al., 1983; Stach et al., 1982; Swaine, 1990; Ward, 2016):

i) Plants need elements for their development and growth. These elements later become incorporated and distributed in the coals during the biological, chemical, or physical processes of peat formation.

ii) Elements might be incorporated into peat, trapped under anoxic condition by the organic matter and microorganisms.

iii) In the early stages of peat formation, there can be contributions to the inorganic fraction due to influx of sediment such as detrital mud and sand, volcanic ash, windborne dust, and salts provided by seawater or underground waters.

iv) Diagenetic contribution of inorganic material resulting from mineral precipitation, including sulphides, silicates or carbonates, or those trapped by the organic matrix.

v) Mineralisation due to the movement of hydrothermal fluids through the carbonaceous sediment, especially if driven by faulting or igneous heat sources.

1.3. Coal as a source of world energy

Coal is the most abundant fossil fuel in the world, it is well distributed globally, it is relatively cheap and is therefore a traditional energy source (Finkelman et al., 2021; Wang et al., 2020). It is estimated that the current global coal reserves reach around 1,100,000 Mt, with 43 % in the Asia Pacific, 24 % in North America, 18 % in the Commonwealth of Independent States (CIS), 13 % in Europe, and 2 % in the rest of the world (Africa, South, and Central America), Figure 1.3 (BP, 2021).

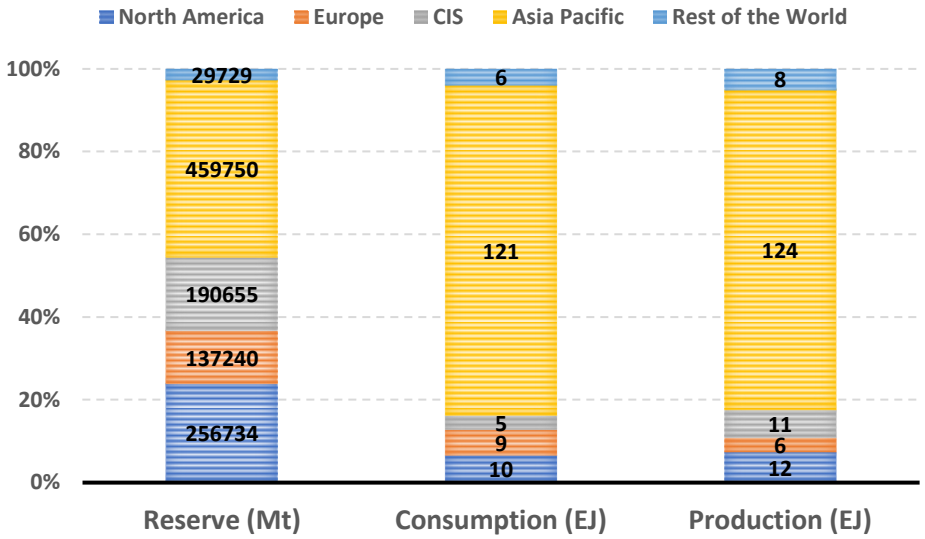

Figure 1.3. *Global coal reserves distribution from world regions, shown in percentages, including consumption and production figures in 2020 (BP, 2021). The numbers on the graph indicate the real values of reserves, consumption and production of coal of each region. Mt, Million tonnes; EJ, Exajoules.*

Coal is still the second most important source of energy around the world, behind oil followed by natural gas (BP, 2021). Global primary energy consumption of fuels are: oil 31 %, coal 27 %, natural gas 25 %, hydroelectricity 7 %, renewables 6 % and nuclear energy 4 % (Figure 1.4, BP, 2021). Coal worldwide consumption is still rising, with the high coal demand of Asia Pacific being the major cause of this increase (BP, 2021).

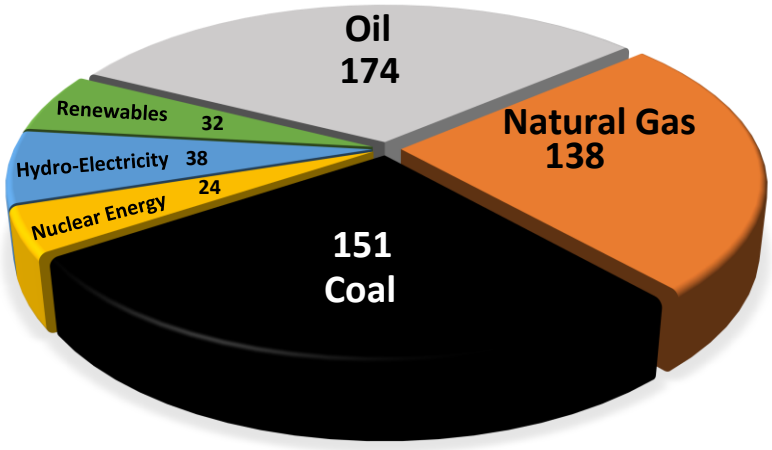

Figure 1.4. *Global primary energy consumption of different fuels in 2020, shown in percentages (BP, 2021). The numbers of the graph indicate the real values of global consumption. EJ, Exajoules.*

Thus, coal continues to be an important fossil fuel for power generation and metallurgy, including manufacturing of chemical products, its capacity for in-situ methane absorption and also its potential as an alternative hydrocarbon source (Ozbayoglu, 2018; Ward, 2016).

According to current forecasts, coal-fired power plants will continue to be one of the most important sources of electrical generation for the foreseeable future (BP, 2021). For example, in China it is estimated that around 60-70 % of total energy consumption is provided by coal (Dong

et al., 2017; Eguchi et al., 2021; IEA, 2020; Peng et al., 2018; Qiao et al., 2019) and China and Southeast Asia are still building new coal-fired power plants (Clark et al., 2020; IEA, 2020). According to IEO (2021) coal consumption in China and worldwide will remain broadly constant, or show a slight increase, over the next three decades (Figure 1.5).

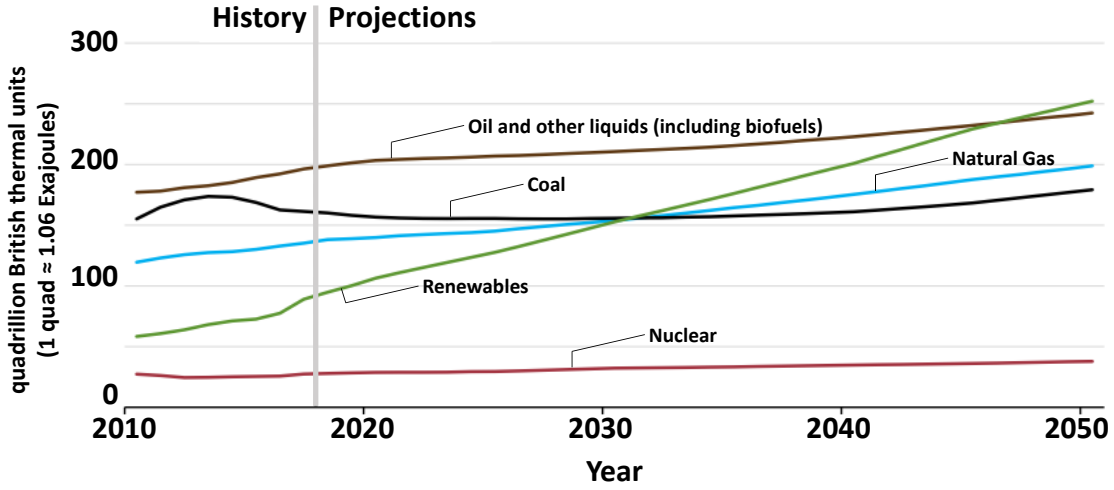

Figure 1.5. *Projections of primary energy consumption by fuel in worldwide during the next three decades (modified from IEO 2021).*

Despite concerns about global air pollution, greenhouse gas emissions and the Paris Agreement signed in 2016, coal will therefore likely remain as one of the most important fossil fuels for decades to come. The projections for a low-carbon transition scenario indicate that shares of energy production and power generation from coal will still be important during the first half of the 21st century (BP, 2021; IEA, 2020; WCA, 2020). While Europe and North America are changing their direction in terms of coal consumption, there are other zones, such as the Asia Pacific and Africa, that remain focused on coal consumption (BP, 2021; Koplitz et al., 2017; Kurniawan and Managi, 2018; Lin and Raza, 2020; McCunney et al., 2009; Oskarsson et al., 2021; Wang and Ge, 2020; Wang and Song, 2021; WCA, 2020).

An elevated level of coal production requires continued large-scale extraction, as well as a large workforce. It is estimated that around 6.5 million people currently work in coal mining, processing and delivery (WCA, 2020). Moreover, 2.5 million people work in associated coal jobs, such as power stations, in addition to the millions of people who work in coal-related industries (WCA, 2020).

1.4. Coal working methods and coal mine dust

Coal is worked by two mining methods, surface mining and underground mining, depending on several factors, such as topographical features, accessibility, overburden extent and ground water presence (Lee, 1990).

Strip mining and open-pit mining are the two principal surface mining methods, depending on the depth of the coal. Strip mining is the technique carried out when coal is very near to the surface, whereas open-pit mining is chosen when coal seams are relatively deep, but still workable by surface mining. Surface mining techniques are potentially more efficient than

underground mining; recovering up to 90 %, in comparison to the usual 60 % obtained by the method of underground mining. This is due to the use of more efficient machinery in surface mining and the possibility of working significantly large thicknesses, as opposed to underground mining which is limited to mine shafts (Lee, 1990; Zendehboudi and Bahadori, 2017).

In underground coal mining, mine dust emissions are much higher in the working front (WF) galleries, where coal is being worked via shearers, drilling and other mining operations. In spite of the ventilation systems and the common use of water spraying, high levels of dust are very frequently present in these WFs, and workers should always use protective measures (masks) (Han et al., 2019; NIOSH, 2010). Dust levels decrease from the WFs to the coal extraction (with continuous belts) and access galleries. Other sources of underground airborne dust include the wear of the mining machinery (including coal and gangue extraction belts and worker transport systems) and the resuspension of deposited coal dust during ventilation. Furthermore, once on the surface, coal milling and handling, and the transport and disposal of coal and gangue can be significant sources of dust if dust-control measures are not properly implemented.

In open-pit coal mines, many of the above sources of coal mine dust are present; however, compared to underground coal mines, there is a higher dispersion and particle dilution. On the other hand, this advantage is commonly offset by much higher volumes of coal and gangue (and accordingly higher emissions) and the large number of heavy trucks that induce widespread resuspension and exhaust emissions. Another air pollution source associated with mining is occasional coal or waste fires, which occur more often in open-pits and waste dumps, and much less frequently in underground mines (Haibin and Zhenling, 2010; Pallarés et al., 2017; Querol et al., 2008). These burning events can create significant emissions of suspended particulate matter (PM) and gaseous pollutants (Jiang et al., 2014; Kim, 2004; O'Keefe et al., 2010; Querol et al., 2011).

The continuous improvement in coal mining technology and advances in coal mine structures and coal extraction have improved both coal production and mining efficiency (Fan et al., 2018; Q. Ma et al., 2020). However, these developments, coupled with an increase in coal production, have also brought a marked increase of coal dust emitted by mine activities, which, in turn, has increased the average exposure levels to coal dust for mine workers. This has contributed to an increased risk for coal workers in currently registered occupational hazard diseases (Johann-Essex et al., 2017; Leonard et al., 2020; Perret et al., 2017). Therefore, studies on environmental conditions of different sections of coal mines where workers can be exposed to high levels of coal dust, along with the related risk of fire and explosion, continue to be highly relevant to coal miner health issues.

1.5. Coal dust

The most common hazardous product generated during coal mining, handling and transportation is coal dust. Coal dust is a complex and heterogeneous mixture of airborne particles made of coaly components and minerals (including crystalline silica, sulphides, silicates, and carbonates) with a wide particle size distribution (PSD) (Caballero-Gallardo and Olivero-Verbel, 2016; Dalal et al., 1995; Liu et al., 2005; Pedroso-Fidelis et al., 2020). The occurrence and levels of these components, including not only major components, but also the trace elements, are dependent on the properties of the parent coal and gangue and the different mining

activities of the coal mines (Azam et al., 2019; Dalal et al., 1995; Ishtiaq et al., 2018; Kizil and Donoghue, 2002; Li et al., 2021; Sharma et al., 2009; P. Wang et al., 2019; Xi et al., 2014).

High exposure levels of coal dust present several high occupational risks, mostly in underground coal mines, but also in open-pits (Castranova and Vallyathan, 2000; Finkelman et al., 2002; Landen et al., 2011; Liu et al., 2020; Masto et al., 2017; Zazouli et al., 2021). Another risk associated with coal dust is its impact on ecological and environmental pollution, affecting communities and ecosystems surrounding coal mining activities (Ishtiaq et al., 2018; Lashgari and Kecojevic, 2016; Masto et al., 2017; Sharma et al., 2009; Tang et al., 2017). Moreover, high contents of coal dust exposure can lead to spontaneous combustion, mostly in underground coal mines (Li et al., 2021; Liu et al., 2010, 2020; D. Ma et al., 2020; Shimura and Matsuo, 2019).

1.5.1. Coal dust exposure and human health

The key reasons for the epidemiological downturn in the health prospects of modern coal miners are as yet unclear and they likely involve a combination of changes in mining targets, methods and mine employment practices. There is evidence, for example, to indicate that miners working in smaller mines, who spend longer hours specifically at the coalface, are at greater risk of developing rapidly progressive coal workers' pneumoconiosis (CWP) (Antao et al., 2005; Kenny et al., 2002; Seaton et al., 1981). Another consideration is that modern, commonly diesel-powered, mining equipment, whilst more efficient at coal production, may create higher levels of PM underground and that this dust may be different in character to that produced by more traditional mining methods (Petsonk et al., 2013). Comparisons between ambient coal mine dust produced in the 1920's and that produced this century, for example, suggest that airborne PM underground has become finer over time (Sapko et al., 2007).

The potential impact of coal and gangue dust on human health can vary widely according to the grain size and mineralogical and chemical composition (Borm, 1997; Li et al., 2017; Sarver et al., 2019). As stated above, coal dust is a complex mixture of particles with a wide range of physical and compositional patterns. Several of these properties of coal dust have been directly related to different human diseases (Erol et al., 2013; Gautam et al., 2016; Xu et al., 2017; Zazouli et al., 2021; Zhang et al., 2021). Thus, chronic inhalation of respirable (< 4 µm in size) coal dust particles is directly responsible for the increased possibility of several lung diseases (Cohn et al., 2006a, 2006b; Qian et al., 2016; Schins and Borm, 1999; H. Wang et al., 2017). The processes by which coal mine dust causes lung diseases have been analysed using toxicology approaches, mostly cytotoxicity, genotoxicity, oxidative stress and reactive oxygen species (ROS), and DNA damage techniques (Cohn et al., 2006b; Pedroso-Fidelis et al., 2020; Tirado-Ballestas et al., 2020).

The finer the dust, the deeper it can penetrate into the respiratory system. Therefore, the higher these fractions are in the coal dust, the higher the potential impact on health and the ecosystem (Brown et al., 2013; Gustafsson et al., 2018; Johann-Essex et al., 2017). Furthermore, finer particles can also be weathered, and their components leached at a higher intensity than coarser particles.

According to ISO 7708:1995 and UNE-EN 481 1995 particles can penetrate human bodies in different ways, depending on the particle size of the coal dust analysed, which is attributed to their mass median diameter (D_{50}) as shown Figure 1.6 (Brown et al., 2013; CEN, 1992; Sánchez Jiménez et al., 2011):

i) Inhalable fraction: mass fraction of total airborne particles which is inhaled through the nose and mouth. This fraction is attributed to total dust suspended particles (TSP).

ii) Thoracic fraction: mass fraction of inhaled particles penetrating beyond the larynx. This fraction is attributed to coal dust particles <10 µm mass median diameter (D_{50} = 10 µm, PM_{10}).

iii) Respirable fraction: mass fraction of inhaled particles penetrating to the unciliated airways. This fraction is attributed to dust particles <4 µm mass median diameter (D_{50} = 4 µm). In outdoor ambient air studies, the respirable fraction of particles with <2.5 µm mass median diameter (D_{50} = 2.5 µm, $PM_{2.5}$) is used.

iv) Ultrafine particles (UFP) particles are those <0.1 µm in diameter and are usually measured in number concentration, instead of mass concentration.

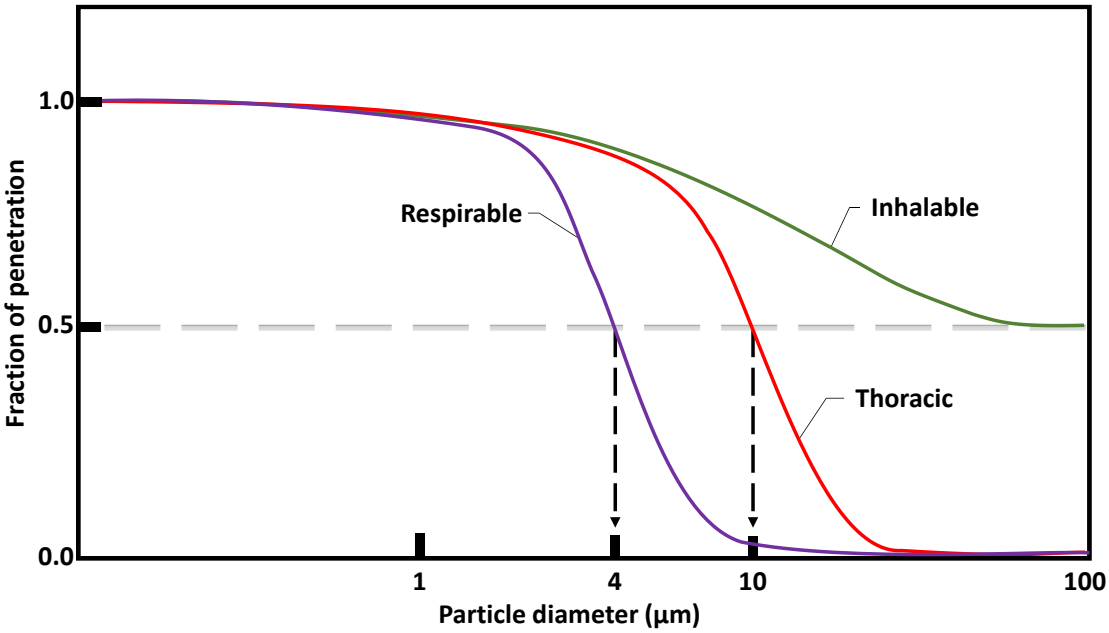

Figure 1.6. *Possibility of particle penetration as a role of aerodynamic diameter, worldwide approved by CEN/ISO/ACGHI. Modified from Sánchez Jiménez et al. (2011).*

1.5.2. Occupational coal health effects

Coal dust represents a serious concern for occupational health (WHO, 1999). Workers with long term exposure are at risk of developing lung diseases, including CWP, progressive massive fibrosis (PMF), lung function loss and emphysema (Harrison et al., 1997; Schins and Borm, 1999).

The recent resurgence of coal mine dust lung diseases (CMDLD) has surprised many in the scientific community. After several decades of substantial improvement in, for example, North American and Australian mines, the incidence of CWP is again increasing (Cohen and Velho, 2002). CWP is a disease that can intensify into its most pernicious, incurable and potentially fatal form, known as progressive PMF. Medical surveys are further revealing that relatively young miners are being affected, even though they have been working under modern dust control regulations (Graber et al., 2017; Perret et al., 2017). Doctors and researchers, who had thought that the increasing incidence of the more serious forms of CMDLD, such as rapidly progressive CWP, was the result of a poorly regulated past, have reacted with concern: *"It is unacceptable*

that new cases of pneumoconiosis should be occurring in the 21st Century at a time when the knowledge regarding prevention of such a disease is excellent. Lessons learned from the past seem to have been buried in the dusts of time" (Yates et al., 2016; see also Cohen et al., 2016).

The pathology is reminiscent of the classic "*U-shaped curve of concern*" identified Reichman (1991) regarding the late 20th Century return of tuberculosis (Petsonk et al., 2013). It is serious enough to warrant the status of an Occupational Sentinel Health Event (Antao et al., 2005; Rutstein et al., 1984), whereby the emergence (or, as in this case, re-emergence) of a preventable workplace disease provides a clear warning signal that new studies on the origin, control and prevention of the problem are required.

Although the problem of coal dust exposure has existed since the start of the coal industry, it was not until 1969 that legislation regarding coal dust was applied by the Coal Mine Health and Safety Act. Before this, coal miners were exposed without regulation. The permissible exposure limit of coal dust applied from 1970 to 1973 was 3.0 mg m^{-3} and, after 1973, was 2.0 mg m^{-3}. In 1995, after several global discussions concerning severe respiratory coal miners' diseases, the National Institute for Occupational Safety and Health (NIOSH) recommended an exposure limit of 1.0 mg m^{-3}, based on an average of 10 h per day or 40 h per week. However, as with many recommendations, this was not implemented as an enforceable standard (R. Cohen et al., 2008; Cohen and Velho, 2002; Liu and Liu, 2020; NIOSH, 1995).

1.5.2.1. Coal workers' pneumoconiosis

The first case of CWP was reported in British coal miners (Gregory, 1831). Originally, coal dust was considered harmless and CWP pathologies were considered as simple silicosis, due to similarities in their chest radiographies indicating black lungs. However, over time and through medical advances, CWP pathologies were distinguished from other similar diseases (Castranova and Vallyathan, 2000).

CWP is only one of the typical diseases occurred in the coal miners community and has been defined as an extremely severe occupational lung disease, Figure 1.7 (Castranova and Vallyathan, 2000; Han et al., 2017), including two forms, simple and complicated. With constant coal dust exposure and without medical intervention, simple CWP could develop into complicated CWP (Castranova and Vallyathan, 2000; Reichert and Bensadoun, 2009; Zosky et al., 2016).

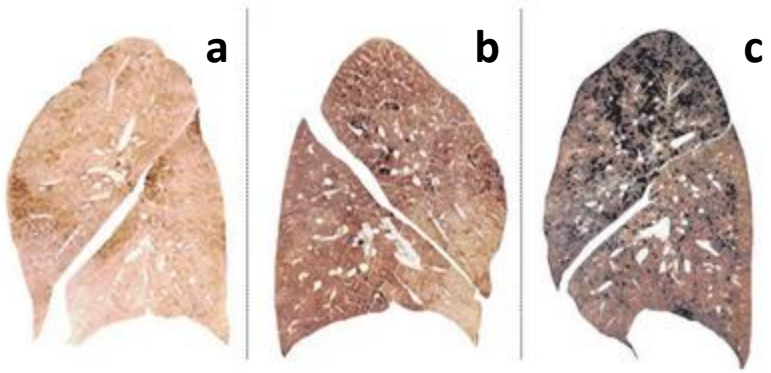

Figure 1.7. *Process of lung tissues of coal miners' during their working life in coal mining. A) healthy lung tissue; b) lung after approximately 10 years; c) lung after approximately 20 to 30 years (modified from Lungs at work, 2015).*

Simple CWP diagnosis consists basically of exploration of the lung by radiography and observation of black coal dust spots (called macules) on respiratory bronchioles (Barber and Fishwick, 2020; Castranova and Vallyathan, 2000; Han et al., 2017; Reichert and Bensadoun, 2009; Zosky et al., 2016). When observed under a microscope, macules have coal dust-laden macrophages with a fine net of reticulin and diverse collagen fibres. These pathologies are associated with pulmonary system deficiencies (Barber and Fishwick, 2020; Castranova and Vallyathan, 2000; Zosky et al., 2016). Coal dust spots are irregular in size, with those ranging below 1 cm diameter considered simple CWP injuries. After that, with continuous chronic coal dust exposure and without treatment, they could develop into more severe CWP disease, with spots greater than 1 cm diameter, causing complicated CWP, as shown in Figure 1.8 (Castranova and Vallyathan, 2000; Reichert and Bensadoun, 2009; Zhang et al., 2017)

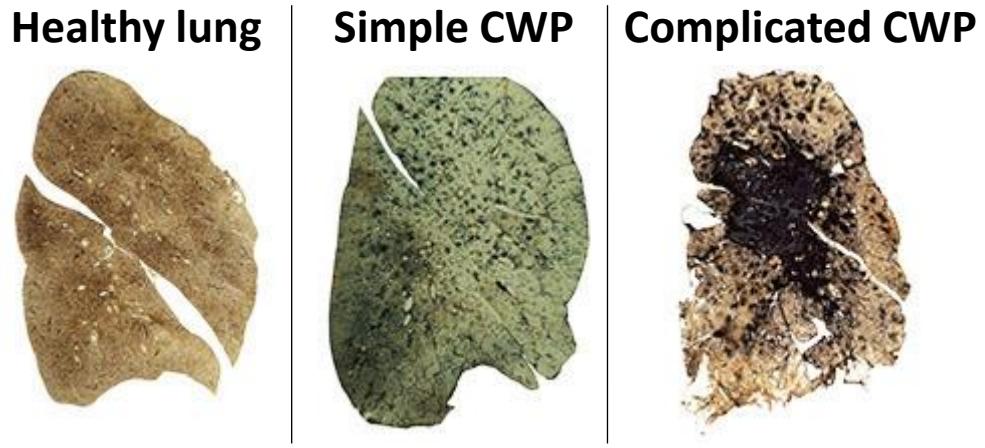

Figure 1.8. *CWP disease advancing, health lung, simple CWP and complicated CWP stages, caused by inhaling coal mine dust (modified from Hurt et al., 2012).*

In recent years, it has been noticed that CWP incidences have increased despite advances in coal mining techniques and implementation of stringent health and safety rules, as shown in Figure 1.9. As stated above, this could be attributed to a considerable increase in production, efficiency and capacity of coal mining activity, which produces smaller sized particles of coal dust and higher concentrations (Blackley et al., 2018; Laney and Attfield, 2010; Petsonk et al., 2013; Suarthana et al., 2011; Wang et al., 2020; Zosky et al., 2016).

Moreover, the other problem attributed to CWP is that this pathology is being detected in younger patients more frequently, as shown in Figure 1.9 (Blackley et al., 2018; Harris et al., 2020), resulting in greater health impacts and associated costs (Han et al., 2017; Liu and Liu, 2020; P. Wang et al., 2019; Wang et al., 2020).

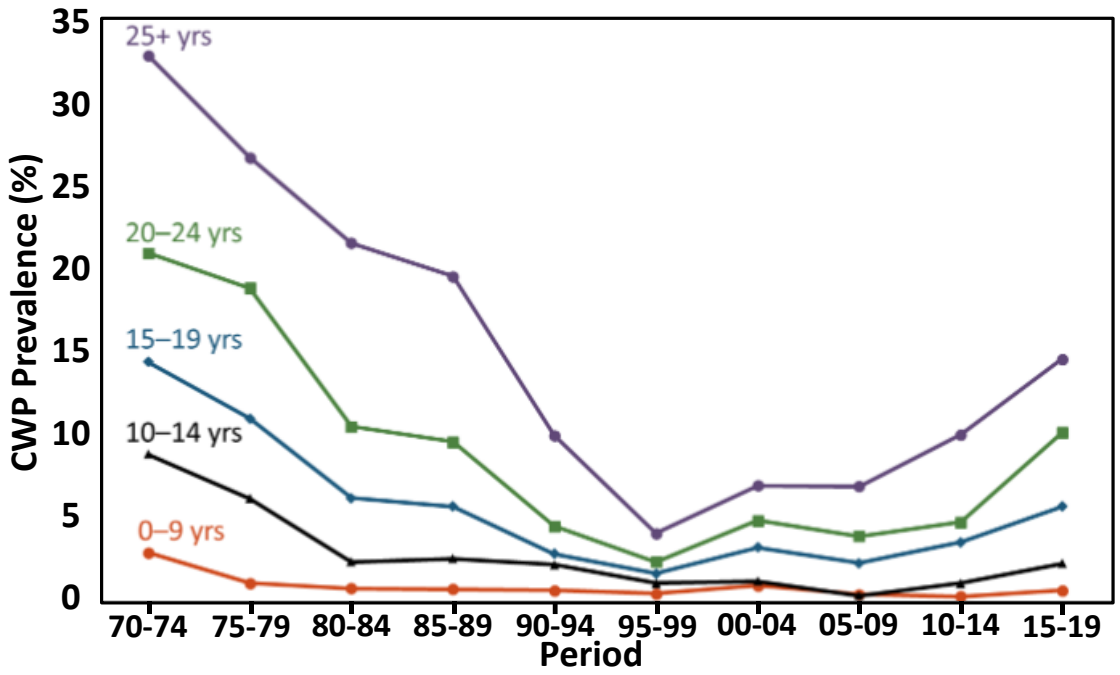

Figure 1.9. *Trends in CWP prevalence among examinees employed at underground coal mines by years of experience (tenure) (modified from NIOSH, 2021).*

The National Occupational Disease Report, released by the National Health Commission of the People's Republic of China (PRC), cited 27,992 and 22,701 CWP cases in 2016 and 2017 respectively. This also reported that there have been more than 20,000 cases per year during the last decade. It is estimated that 90 % of occupational coal workers' diseases reported in China are CWP (Han et al., 2019; Jin et al., 2018; Wang et al., 2020; Yuan et al., 2017). The National Health Commission of the PRC states that it endeavours to prevent and reduce occupational diseases of dust for people who have worked in hazardous environments for less than five years by 2022 and to maintain that downward trend to 2030 (National Health Commission of China). However, it is widely known that there exists a serious problem with the prevalence and treatment of CWP in China (Liu et al., 2016; P. Wang et al., 2019; Wang et al., 2020).

Moreover, CWP cases reported in US during the period of 1970-2017 indicated a slight decrease between 1970-2000, but the rate began to rise again from 2000 (Liu and Liu, 2020). Furthermore, according to de Matteis et al. (2017) and Tomášková et al. (2017), the same phenomenon is occurring in Eastern European countries, including Poland and the Czech Republic, where coal power generation has a significant share in national power generation.

1.5.2.2. Reactive oxygen species

It has been observed that the lung-damaging mechanism produced by the respirable fraction of coal dust can induce macrophage activation and the attachment of polymorphonuclear cells. This cell activation generates inflammatory indicators in the lung, defined as ROS (Pinho et al., 2004). As several authors had predicted in the past, ROS pathologies are important because they are capable of inducing or accelerating serious illnesses in coal miners, such as CWP (Dalal et al.,

1995; Huang et al., 1993). Thus, high ROS can be a marker for potential pneumoconiosis development.

ROS are chemical substances that contain radicals, molecules, ions, or atoms of oxygen, such as superoxide anions (O_2^-), hydroxyl radicals (-OH), and hydrogen peroxide (H_2O_2), among others, which are involved in many natural biochemical processes (Phaniendra et al., 2015). For this reason, they are continuously reacting across natural environments and within organisms, such as human bodies (Lu et al., 2006; D. Wang et al., 2014; Yu and Zhao, 2021; Zhang et al., 2018). ROS processes occur in cells, playing an important role in their survival, proliferation, differentiation and apoptosis (D'Autréaux and Toledano, 2007; Lou et al., 2015; Zhang et al., 2018; Zhou et al., 2021). Depending on several parameters, including concentration, locations, production, degradation and diffusion, it is possible to attribute the biological and chemical process of ROS to critical issues. Furthermore, ROS inform physiological and pathological diagnosis and further understanding of biological processes in the organism. For this reason, it is important to develop sensitive and selective methods for the detection of ROS in biochemical systems (Lou et al., 2015; Zhou et al., 2021; Zielonka and Kalyanaraman, 2018).

1.5.2.3. Oxidative stress, and oxidative potential

Oxidative stress is one state of ROS where free radicals, such as -OH, containing oxygen species are active in biological processes. Oxidative stress is manifested when the production of free radicals is greater than antioxidant activity, damaging proteins, nucleic acids and cells. In other words, when the equilibrium between oxidants and antioxidants in tissue or organ is disturbed in favour of oxidants (Betteridge, 2000; Finaud et al., 2006; MacNee and Rahman, 2001; Pizzino et al., 2017; Sies et al., 2017; Storz and Imlayt, 1999). These conditions produce a biological response in the organism that can be associated with the development of several diseases (Storz and Imlayt, 1999). Moreover, the relation between the lung immune system and oxidative stress can be linked to the advance of numerous lung illnesses (MacNee and Rahman, 2001; Pinho et al., 2004). Several authors have stated that chronic exposure to coal dust particles and suspended PM causes oxidative stress, producing health effects such as respiratory infections, lung cancers and chronic cardiopulmonary diseases (Janssen et al., 2014; Kelly, 2003; Li et al., 2020; MacNee, 2001).

The oxidative potential (OP) is defined as the capacity of particles to oxidise target molecules or the ability to consume antioxidants, generating ROS. This potential has been proposed as a measurement closely related to the biological response effect of occupational exposure particles, especially PM (Borm et al., 2007; Calas et al., 2018; Fang et al., 2017; Janssen et al., 2014). Although, OP is not commonly used yet as a standard response to coal dust analysis, it could be an attractive option since it integrates various biologically-relevant properties, including size, surface, mineralogical and chemical composition (Ayres et al., 2008; Janssen et al., 2014). Several methods for measuring OP have been developed, but no agreement has been reached as to which analysis should be recommended (Ayres et al., 2008; Calas et al., 2018; Moreno et al., 2017).

One of the most interesting points of OP analysis is the ability that occupational dust exposure or PM exposure has to deplete antioxidants, such as ascorbic acid (AA), glutathione (GSH) and dithiothreitol (DTT). These reactions are based on a-cellular redox-activated compounds which

are able to transfer electrons from AA, GSH and DTT to oxygen (Cho et al., 2005; Janssen et al., 2014; Mudway et al., 2004). Moreover, these indicators are important because AA is a physiological antioxidant present in the lung, and GSH and DTT are used as chemical surrogates of antioxidants (Fang et al., 2017). OP analysis uses a synthetic human respiratory tract lining fluid (RTLF) system to quantify occupational particles exposure which could induce specific ROS, such as $^{\cdot}OH$ radicals (Calas et al., 2018). Thus, OP could identify which properties, after coal dust exposure, could be harmful to human health.

1.5.3. Coal dust ecological and environmental pollution

Another concern about the high emission of coal dust is its ecological and environmental impact. Several studies have focussed on the physicochemical dust properties emitted from coal mining that could produce environmental damage, human health risks and ecological hazards in surrounding areas (Guerrero-Castilla et al., 2019; Li and Hu, 2017; Tang et al., 2017). The generation of polluted soils, groundwater, and air around coal mines and their consequent impact on flora and fauna have thus become a major cause of concern (Ahern et al., 2011; Alcala-Orozco et al., 2020; Benitez-Polo and Velasco, 2020; Berry et al., 2017; Johnson and Bustin, 2006; León-Mejía et al., 2011, 2007; Liao et al., 2010).

1.5.4. Coal mine dust controls

Mine developers are continuously trying to resolve coal mining concerns to minimise damage to mine workers' health, improve safety, and progress in structural design and engineering. This effort has resulted in an increase in studies on coal dust over the last decade (Fan et al., 2018; Wu et al., 2019). As an example, Więckol-Ryk et al. (2018) recommends new and improved filtering materials and respiratory protection equipment to safeguard the health of workers in the mining industry to reduce the hazardous coal dust produced.

Several methods can be applied with regard to dust control in coal mines These include wetting systems acting on coal dust surface particles, or spraying systems, using surfactant aqueous solutions (foam-sol), applying chemical suppressants for dust control, and improving ventilation systems in coal mine (Fang et al., 2020; Li et al., 2013; Liao et al., 2018; Ma et al., 2018; Marmur, n.d.; NIOSH, 2010; Ren et al., 2012; X. Wang et al., 2019; Xi et al., 2014; Xiu et al., 2020; Xu et al., 2017). These approaches need to consider the different locations throughout the mines, including coal working fronts (CWF), transportation, galleries, continuous mining, surface mining, among others, particularly in underground mines, where coal dust has greater concentrations.

1.6. Chemical and mineralogical patterns of coal dust and health effects

There is still discussion concerning old arguments about whether CMDLD risk is primarily a question of dust concentration and length of exposure (combined with influencing factors such as smoking habits and genetic predisposition), or whether the mineralogy and geochemistry of the PM inhaled is creating an important additional health issue (Laney and Weissman, 2014; Perret et al., 2017; Petsonk et al., 2013). In this context, the inability of researchers to identify a clear inorganic indicator, in the form of a specific dust component that can be proved to induce CWP, has generated uncertainty. For example, although regulations have focused on respirable

quartz, which is primarily responsible for silicosis and capable of inducing PMF (NIOSH, 2002), doubts remain as to whether this mineral is also a major influence on CWP (Beer et al., 2017; Lapp and Castranova, 1993). On the other hand, coal rank has been positively correlated with CWP (Attfield and Morring, 1992) but negatively correlated with quartz content (Harrison et al., 1997). Furthermore, specific studies concluded that "*quartz is not the predominant factor in the development of CWP*" (McCunney et al., 2009). Changing work practices underground, however, such as the mining of thinner coal seams with the consequent release of silica dust from adjacent rocks, may be inducing symptoms more allied to silicosis than "*traditional*" CWP, adding further confusion to the evaluation of newly emerging disease patterns (Cohen et al., 2016).

To summarise, the importance of chronic exposure to silica and respirable crystalline silica (RCS) for human health is well known in the coal community. However, more studies are needed on the relationship of other dust components (such as Fe, As, sulphides or sulphates minerals) or patterns (coal rank and particle size) and the possible development of hazardous health diseases, increasing typical CMDLD, or accelerating CWP or PMF, among others.

1.6.1. Silica in coal dust

Silica (silicon dioxide, SiO_2) is a crystalline solid. Quartz is the main silica mineral, and accordingly the main species of RCS. In coal dust, concentrations of RCS reach on average 5-6 %, and rarely exceed 10 % (WHO, 1986).

As stated above, high occupational exposure to inhalable silica is associated with the development of fibrotic reaction in the lungs, CWP and silicosis (Cohen and Velho, 2002; R. A. C. Cohen et al., 2008; WHO, 1986).

It was not until 1996 that the International Agency for Research on Cancer (IARC) considered RCS as a human carcinogen (NIOSH, 2002). Before this, coal miners were not protected by any standardised control of silica dust concentrations in coal dust exposure. However, after 1996, levels of RCS exposure in coal dust began to be controlled and exposure limitations were established (Borm, 1997).

1.6.2. Other minerals in coal dust

It is clearly not enough to focus entirely on a specific mineral, such as RCS, as a generic causative agent of negative health effects induced by coal dust, especially given the chemical complexity of particulate materials breathed in the mines. Coal dust mineral composition is dominated by silica (mostly quartz), clay minerals (mostly illite, kaolinite-clinochlore, montmorillonite and palygorskite), carbonate minerals (typically siderite, ankerite, dolomite and calcite), sulphides (mostly pyrite, marcasite and sphalerite), sulphates (a large variety of these, with gypsum as the prevailing one), feldspars (microcline, albite and anorthite) and anatase (titanium dioxide) (Ward, 2002). In short, many minerals found in coal dust can potentially affect human health.

Pyrite in coal dust has been identified also as a matter of concern in promoting CWP pathogenesis (Cohn et al., 2006c). Regular exposure to high-pyrite coal dust contributes to promoting a chronic level of inflammation, developing hydrogen peroxide and ferrous iron, which produce highly reactive hydroxyl radicals, contributing to the pathogenesis of CWP (Cohn et al., 2006c; Harrington et al., 2012). Furthermore, several studies link pyrite contents in coal

and coal dust with ROS generation, ROS in cells and a potential role in the pathogenesis of CWP (Castranova, 2000; Cohn et al., 2006c; Harrington et al., 2012; Huang and Finkelman, 2008; Liu and Liu, 2020; Murphy and Strongin, 2009; Zosky et al., 2016).

Sulphate in coal can occur naturally or also through the oxidation of sulphide minerals due to coal mining (J. Wang et al., 2017). Liu and Liu (2020) stated that respirable sulphate in the mining environment can cause depression of pulmonary particle clearance and asthma, due to the high biological activity. Schins and Borm (1999) suggested that the sulphate content of coal dust could play a dominant role in antiprotease inactivation. In addition, Gilmour et al. (2004) cited sulphate as an important toxicity factor. Furthermore, sulphate radicals are highly reactive species (Tsitonaki et al., 2010).

The toxicity of inhaled fine anatase particles is well documented as a precursor of lung inflammation (Hamilton et al., 2009; Oberdörster et al., 1992; Schins and Borm, 1999; Silva et al., 2021a). In addition, long exposure to clay minerals could cause diverse pathologies in lung systems, such as cancer, mesothelioma or pneumoconiosis (Carretero et al., 2006; Guthrie, 1992).

On the other hand, negative impacts on human health have not been documented for a number of coal dust minerals. Huang et al. (1993, 1998, 2006) and Zhang et al. (2002) stated that coals more likely to induce CWP contain less calcite, due to its buffering capacity for acidic species, which could reduce the presence of bioavailable Fe.

1.6.3. Metals in coal dust

As stated above, both the organic and mineral fractions of coal dust might house a wide range of metals known to be potentially capable of inducing health problems after inhalation (Finkelman et al., 2021). In general, there is a lack of information on the patterns of the materials being inhaled in mine dust, and most papers considering coal trace element geochemistry focus on toxic emissions and waste produced during combustion. However, several authors have stated that elevated chronic exposure to metals, such as Fe and Ni, could produce unfavourable human health effects, including significant influences on the incidence of CWP (Christian et al., 1979; Cohen et al., 2016; Harrington et al., 2012; Huang et al., 2005, 1998; McCunney et al., 2009).

In addition to this, several authors state that various metals in dust, including Cu, V, Cr, Fe, Mn, Pt, Zn, Ni, Mo, Co, V and Pb, could be responsible for the production of ROS, which in turn, lead to atherosclerosis, cancer and neurodegenerative diseases and also, in some cases, can be directly linked with CWP formation (Aruoma, 1998; Cohn et al., 2006b, 2005, 2004; Fu et al., 2014; Ghio and Quigley, 1994; Huang et al., 2002, 2005, 1998; Latvala et al., 2016; Lighty et al., 2000; Liu and Liu, 2020; Lloyd and Phillips, 1999; Shi et al., 1992; Shi and Dalal, 1992; Stohs and Bagchi, 1995; Strlič et al., 2003; Valko et al., 2005).

Furthermore, it is well known that ferruginous particles can remain in the deepest part of the lung over a long time (Harrington et al., 2012). Fe particles are present in a different range of concentrations in coal dust. Normally coming from clay, carbonate, sulphide and sulphate minerals, as well as bound to the coal macerals (Finkelman et al., 2018), but in coal dust these can also be from mining machinery wear and salts from acidic mine drainage (AMD).

Additionally, Fe-rich particles in dust can also be carriers of other hazardous trace elements, such as As, Cu, Ni, Co, Pb, Mo, Zn, Sb, and Se, in different concentration ranges (Gregory et al., 2015; Kolker, 2012).

Potentially hazardous trace elements in coal include Sb, As, B, Be, Cd, Cr, Co, Pb, Mn, Ni and U (Finkelman, 1999, 1994; Huggins, 2002; Wagner and Hlatshwayo, 2005). As is one of the most hazardous elements. Prolonged chronic exposure to As could result in the development of skin, lung, liver and lymph cancers, diabetes, stroke and several heart diseases (Singh et al., 2015; J. Wang et al., 2017). V could be toxic when inhaled in a high concentration (WHO, 2000). Furthermore, Cr is another important toxin that may induce developing pneumoconiosis and lung cancers (Finkelman et al., 2018; WHO, 2000). In addition, elevated exposure to Pb particles could develop neurological toxins (Finkelman et al., 2018). Although Mn is an essential element for natural organisms, high occupational exposure to it could damage the human nervous system (Apostoli et al., 2000; Myers et al., 2003). It is also well documented that inhalation of U particles may increase premature mortality from lung and lymph hematopoietic diseases and is associated with a risk of circulatory diseases (Canu et al., 2012, 2011; Zablotska et al., 2013; Zhivin et al., 2014). Sb long chronic exposure could develop several lung, heart, and gastrointestinal diseases, as well as pneumoconiosis (Cooper and Harrison, 2009; McCallum, 2005; Sundar and Chakravarty, 2010). Additionally, Cd exposure is associated with renal dysfunction and bone disease outcomes, with chronic exposure linked to lung cancer diseases (Järup, 2002; Nawrot et al., 2010; Stayner et al., 1992).

1.6.4. Other important coal dust patterns for health effects

Particle size distribution is also an important parameter of coal dust regarding sedimentation, solubility and human health effects (Liu and Liu, 2020; Marsalek and Sassikova, 2016; Plumlee and Morman, 2011). In this context the particle size of dust may have a great influence on the release of metals from inhaled coal dust (Silva et al., 2021b), playing an important role in the developing CWP (Liu and Liu, 2020).

As mentioned before, water spraying in coal mines is commonly used to abate coal dust exposure (Ajrash et al., 2017; Azam et al., 2019; Kuai et al., 2012; Küçük et al., 2003; Woskoboenko, 1988; Yuan et al., 2014). However, an excess of moisture in coal dust can develop ROS by promoting the oxidation of sulphides, which can contribute to CWP diseases (Allardice et al., 2003; Bailey-Serres and Voesenek, 2008; Choi et al., 2011; Mira et al., 2021; Wang et al., 2003; Xu et al., 2017). Moreover, the adsorption of moisture can soften and lubricate the microstructures, weakening mechanical coal matrix properties, favouring an easier release of minerals and metals embedded in the coal matrix (Ahamed et al., 2019; Ren et al., 2021).

Another relevant parameter is AMD, a process that usually occurs when sulphide minerals in coal or gangue materials, are continuously exposed to water and oxygen in atmospheric conditions (Akcil and Koldas, 2006; Pandey et al., 2021; Simate and Ndlovu, 2014; Skousen et al., 2015). This involves the oxidation of sulphide minerals to sulphate minerals generating acidity in coal dust, as well as an enrichment in bioavailable hazardous elements, since sulphate salts are enriched in specific hazardous elements, such as Pb, Zn, Cd and As (Alcobé et al., 2001; Hudson-Edwards et al., 2008; Kerolli-Mustafa et al., 2015; Kolitsch and Pking, 2001; Smith et al., 2006).

This PhD thesis focuses on the characterisation of PM breathed by coal miners, identifying the main parameters likely to be of concern in coal mine dusts, and presenting pilot case studies that link mining operations with coal dust features, and coal dust patterns with OP. For this a variety of coals (mostly from China) presenting a broad range of geochemical patterns has been evaluated in terms of finding possible links between OP and coal geochemistry.

Chapter 2

SCOPE, OBJECTIVES AND STRUCTURE

2. SCOPE, OBJECTIVES AND STRUCTURE

2.1. Scope

Coal has been a comprehensively studied subject, as a mineral and energy source, and also in regard to problems directly associated with coal use. Moreover, as described in the introductory chapter, coal dust has equally been a focus of research, particularly coal dust effects on occupational health and environmental pollution. There have been extensive examinations of specific effects on human health of minerals, such as silica or pyrite, some metals such as Fe or Si, and proximate analysis, such as coal ash, moisture or coal rank characteristics. Furthermore, several studies have encompassed occupational illnesses produced by coal dust, including lung cancer, PMF or CWP. It is interesting to note that coal dust studies have increased in the last decade, coinciding with the increase of coal-related illnesses. Studies on coal dust for different types of mining methods, such as underground and open-pit coal mines, and comparison of coal dust patterns from these are scarce. Also studies on coal dust comparing dust patterns from a wide variety of coals having different geochemical patterns are missing.

The possibility of sampling in coal mines is very limited as they have crucial, strict safety restrictions, an example being the limitation of extensive use of sampling or monitoring devices due to explosive issues, especially in underground mines. Additionally, coal mines are continuously working. So, hours of stopping machines to collect samples result in income and productivity losses. For these reasons, a protocol was developed to generate a large geochemical and mineralogical dataset of respirable coal dust equivalent samples from a wide variety of coals in China and Central Eastern Europe, including those representatives of coal dust produced from different coal mining activities.

These concerns inspired the present PhD thesis in terms of coal dust characterisation, relationship with the emission sources and indicators of potential health effects (OP, in this case). For this it is not of crucial importance if a component is hazardous in itself but, rather, to find links between dust patterns and emission sources and OP. Thus, the analyses are not done for specific dust components, as in most studies, but instead implementing these with a holistic focus. PSD, mineralogy, major and trace elements, ultimate analysis and OP are jointly evaluated, and datasets analysed to identify links of coal dust patterns and OP.

2.2. Objectives

The main objective of this PhD thesis is the study of major coal mine dust patterns from different types of mining operations and different types of coals with a wide range of geochemical patterns. Once coal dust was characterised, a wide selection of samples were selected to determine the OP in order to analyse possible links between geochemical, particle size, coal quality and coal rank parameters with the OP. Because of the difficulty sampling actual respirable coal mine dust in a large number of mines, and sites inside the mines, to cover all the above possibilities respirable coal mine dust in this study was extracted from:

i) Deposited coal mine dust collected in and around different parts and activities of underground and open-pit coal mines.

ii) Powdered coal samples from channel profile (CP) sampling at a wide variety of coal mines.

To fulfil the general objective, the following specific objectives were set up:

i) To perform a detailed analysis of deposited coal dust composition in several coal mines in order to find links between major dust geochemical parameters and mining activities (as emission sources). To this end, the first objective was to separate the respirable fraction from the sampled deposited coal dust, analysing in detail coal dust patterns from different zones of the coal mines and identifying sources of relevant dust components. Accordingly, coal dust composition was analysed from different zones of coal mines where diverse activities were carried out. This type of detailed sampling was carried out in underground coal mines from Central Eastern Europe (Slovenia and Poland, Articles #1 and #2), in a Northwest China open-pit coal mine, and in North, South and Southwestern China underground coal mines (Articles #3 and #4).

ii) To evaluate the relationship between major physical and geochemical patterns of respirable coal dust and OP. To this end, regression analysis was carried out with the datasets obtained on compositional and OP patterns to identify major drivers of OP. First, links between OP and major patterns of respirable coal dust samples obtained from deposited mine dust samples were analysed independently for an open-pit and an underground coal mine in China, using AA and GSH indicators (Articles #3 and #4). Subsequently, the analysis was applied to the respirable fractions obtained from a wide variety of powdered coal samples covering diverse coal geochemistry characteristics from different regions of China, using AA, GSH and DTT as OP tracers (Article #5). Finally, the analysis was repeated by including both respirable fractions from deposited coal mine dust and from powdered coal samples (Article #5).

iii) To include in the methodology the setting up and validation of the methods used for extracting the respirable fractions of deposited coal mine dust and powdered coal samples, the analysis of the dry PSD and the calibration of the mineralogical analysis.

Furthermore, measurements of the occupational coal dust concentrations (PM) in several coal mines were carried out. Firstly, in a number of Central Eastern European underground mines (Slovenia and Poland; Article #2), in a Southwest China underground coal mine and in a Northwest China open-pit coal mine (Articles #3 and #4). An online sampling ambient measurement was taken in the open-pit mine in China to evaluate the ambient PM concentrations during different mining activities.

2.3. Structure

This PhD thesis is presented as a compendium of articles with the following structure:

Chapter 1 is an introductory section on coal, coal dust, potential health effects and major patterns potentially governing these effects.

Chapter 2 describes the major objectives and structure of the PhD thesis, including the list of articles included.

Chapter 3 gives an overview of the sampling and key methods implemented that are not described in detail in the articles.

Chapter 4 includes the following five articles of the compendium:

i) *Trace element fractionation between PM_{10} and $PM_{2.5}$ in coal mine dust: Implications for occupational respiratory health.* Teresa Moreno, **Pedro Trechera**, Xavier Querol, Robert Lah, Diane Johnson, Aleksander Wrana, Ben Williamson. 2019. *International Journal of Coal Geology,* 203, 52-59. DOI: 10.1016/j.coal.2019.01.006. This includes a pilot study of coal dust fractionable sample separation of metallic composition in a Velenje coal mine (Slovenia) and a summary of potential concern of some metallic elements in coal mines.

ii) *Chemistry and particle size distribution of respirable coal dust in underground mines in Central Eastern Europe.* **Pedro Trechera**, Xavier Querol, Robert Lah, Diane Johnson, Aleksander Wrana, Ben Williamson, Teresa Moreno. Accepted. *International Journal of Coal Science and Technology*. This consists of a detailed analysis of particle size, geochemistry and occupational concentration of diverse coal dust samples from different mining activities in Central Eastern European undergrounds coal mines.

iii) *Mineralogy, geochemistry and toxicity of size-segregated respirable deposited dust in underground coal mines.* **Pedro Trechera**, Teresa Moreno, Patricia Córdoba, Natalia Moreno, Xinguo Zhuang, Baoqing Li, Jing Li, Yunfei Shangguan, Konrad Kandler, Ana Oliete Dominguez, Frank Kelly, Xavier Querol. 2020. *Journal of Hazardous Materials*, 399, 122935. DOI: 10.1016/j.jhazmat.2020.122935. Detailed analysis of mineralogy, geochemistry, particle size, occupational concentration and OP of diverse coal dust samples from different mining activities in Chinese underground coal mines.

iv) *Comprehensive evaluation of potential coal mine dust emissions in an open-pit coal mine in Northwest China.* **Pedro Trechera**, Teresa Moreno, Patricia Córdoba, Natalia Moreno, Xinguo Zhuang, Baoqing Li, Jing Li, Yunfei Shangguan, Ana Oliete Dominguez, Frank Kelly, Xavier Querol. 2021. *International Journal of Coal Geology*, 235, 103677. DOI: 10.1016/j.coal.2021.103677. This contains a detailed analysis of mineralogy, geochemistry, particle size and OP of coal dust samples from different mining activities in a Chinese open-pit coal mine. Including measurements online of environmental ambient and occupational coal dust concentrations.

v) *Geochemistry and oxidative potential of the respirable fraction of powdered mined Chinese coals.* **Pedro Trechera**, Teresa Moreno, Patricia Córdoba, Natalia Moreno, Fulvio Amato, Joaquim Cortés, Xinguo Zhuang, Baoqing Li, Jing Li, Yunfei Shangguan, Ana Oliete Dominguez, Frank Kelly, Takoua Mhadhbi, Jean Luc Jaffrezo, Gaelle Uzu, Xavier Querol. 2021. *Science of the Total Environment*, 800, 149486. DOI: 10.1016/j.scitotenv.2021.149486. This consists of a detailed analysis of mineralogy, geochemistry and OP of the respirable fraction of powdered coal samples from different zones of China; including a detailed joint analysis of the results from the respirable coal dust samples from the two previous articles.

Chapter 5 contains a joint discussion of the results from the five articles of the compendium.

Chapter 6 summarises major conclusions obtained.

Chapter 7 provides recommendations for further research on the study field based on the results obtained.

Chapter 8 includes the references.

Annex includes supporting information.

Chapter 3

METHODOLOGY

3. METHODOLOGY

This chapter describes the actual sampling and only the specific key protocols on sample treatment and analyses that required particular procedures and validations for this PhD thesis. Most of the methodology is reported in the specific articles.

3.1. Methodological approach

Figure 3.1 summarises the methodological strategy followed in this PhD thesis. Basically, this consisted in the sampling of coal mine deposited dust (DD) and CP samples from specific coal seams, for subsequent characterisation and sample treatment for extraction of the respirable fraction of DD or the powdered CP coal samples (RDD or CP_4, respectively). After a detailed physical, chemical and mineralogical characterisation, results were obtained on the origin of major RDD components and on those governing the OP. Furthermore, as shown in Figure 3.2, measurements of occupational exposure were carried out with different approaches in open-pit and underground mines due to the different limitations of mining safety in these two environments.

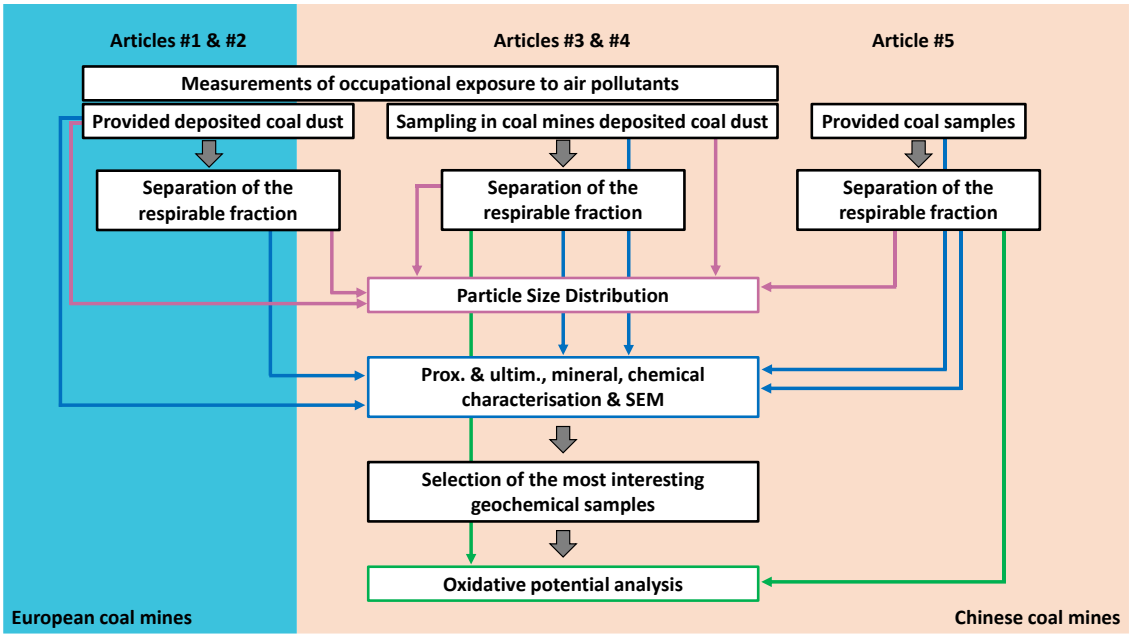

Figure 3.1. *Methodological approach used in the study for sampling and characterisation of respirable dust as a function of the regional origin of samples, methods applied and articles of the compendium. Prox. & ultim.; Proximate and ultimate analyses; SEM, scanning electron microscopy.*

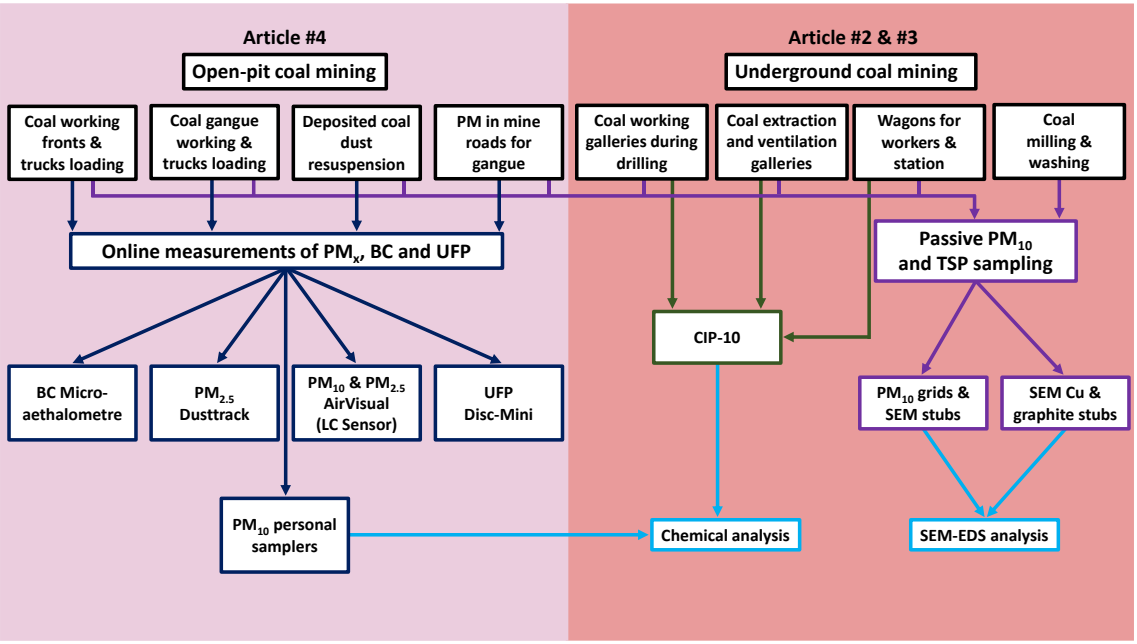

Figure 3.2. *Methodological approach used in the study for characterising the occupational PM exposure in surface and underground mines. PM_x, particulate matter; BC, black carbon; UFP, ultrafine particles; TSP, total suspended particles; CIP-10, PM_{10} individual dust sampler; SEM, scanning electron microscopy; EDS, energy dispersive spectroscopy.*

3.2. Samples received and sampling

The selection of the sampling areas was driven by two major factors:

i) First, samples of DD and PM were received within the activities of a European research project (ROCD, *Reducing risks from Occupational exposure to Coal Dust*) from the WFs of mines from the Upper Silesian Coal Basin (USCB) and Velenje Coal Basin (VCB), as indicated in blue in Figure 3.3.

ii) Furthermore, a detailed sampling was carried out in Chinese mines (where access permission for sampling was given) to evaluate the changes of levels, composition and OP of RDD and PM around specific mining activities, and the OP of dust from a wide variety of coals with different geochemical patterns. Thus, DD (from different activities carried out in two underground and one surface mining in North, South and Southwestern China) and powdered coal samples (having very different geochemical patterns and from different coal basins across China) from Chinese coal mines were collected (green and red in Figure 3.3).

The collection procedures were similar in both European and Chinese coal mines. In short, a large number of DD samples, including coal samples and occupational dust exposure samples were received and also analysed. Moreover, the USCB samples were collected in mines in close proximity to the WFs, allowing their comparison between different USCB mines. On the other hand, the samples collection from VCB were only obtained from one mine, where the distribution and separation between zone collections in the mine were markedly more clearly defined than in USCB mines. In the Chinese underground and surface mines, sampling was carried out in and around different coal mining operations (WFs and distances to these, drilling, transport, gangue, milling and other operations). The selection of the powdered coal samples to

extract the respirable fraction and determine OP levels followed the criteria of covering a wide of geochemical patterns, such as low and high ash, S, moisture, volatile matter, and contents of specific metals (i.e., As, Mo, U, Sb, W, V).

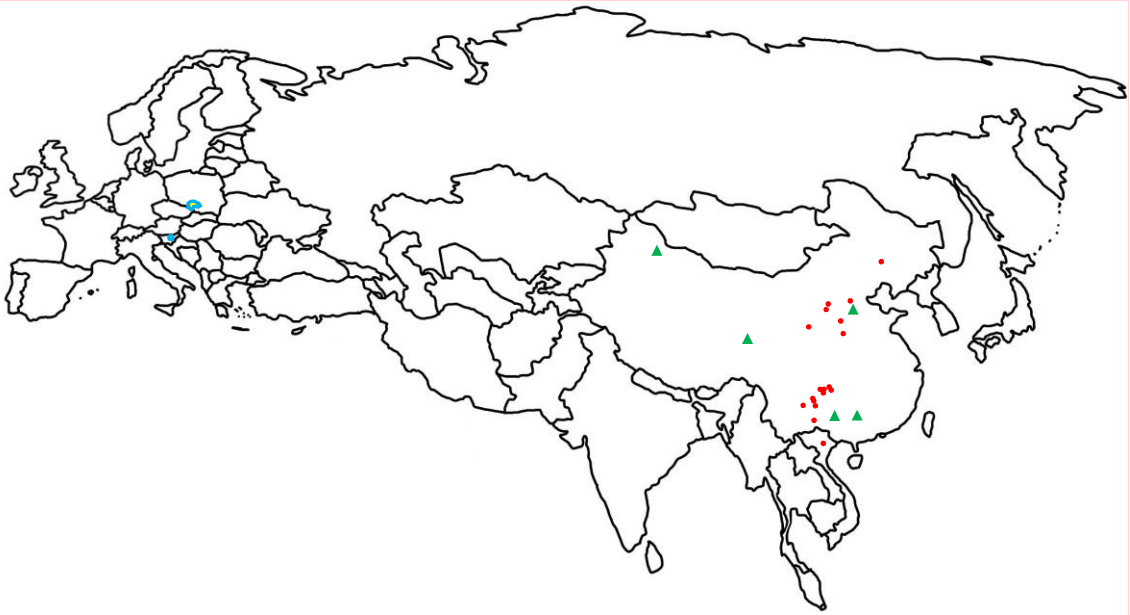

Figure 3.3. *Location of the samples of this study. In blue, samples of DD and PM received from Central Eastern European coal mines; in green, DD and PM samples obtained in Chinese mines; in red, powdered coal CP samples from worked coal seams from different Chinese coal basins.*

3.2.1. European coal dust mine samples

The collection of samples was focussed on Central Eastern Europe, specifically mines from Poland and Slovenia. Diverse DD and PM samples were received from the Premogovnik Velenje (PV) underground coal mine, situated in VCB, Slovenia. In addition, DD samples from different Polish underground coal mines situated in the USCB were also received. Two large Polish mining companies, Jastrzębska Spółka Węglowa SA (JSW) and Polska Grupa Górnicza SA (PGG), sampled and provided the samples.

3.2.2. Chinese samples

3.2.2.1. Underground coal mines working bituminous and subbituminous coals

The Wang Jiazhao underground coal mine (BWC, Bituminous Southwest China) works bituminous coals, and it is located in Liupanshui, Western Guizhou Province in Southwestern China. It started operations in 1965 and works Late Permian coal seams. According to the mining company, the annual production reaches 2.7 Mt yr^{-1} of middle-bituminous coal with 0.50-1.0 % S content, and a high ash yield (35-40 %). After coal washing, ash yields are largely reduced to around 10 %. Four workable coal seams (galleries #1, #7, #8, #11) were mined in 2018 but, during sampling, mining operations were active only for #7 and #11 coals. Mining is envisaged to continue at least another 59 years, according to the estimation of recoverable coal resources,

approximately around 160 Mt. The coal mine operates down to 500-600 m, using long galleries protected with several hydraulic jacks, called shields, and shearers.

The Heshan (Sankuang or Shicun #2 coal mine) and Baise (Donghuai Sankuang coal mine) mines (BSC, Bituminous South China and SSC, Subbituminous South China, respectively) underground mines, are located in the Central and Southwestern Guangxi Province (South China). According to the mining companies, these reach an annual production of 0.9 and 1.5 Mt yr^{-1} of bituminous coals and subbituminous, respectively.

The Heshan coal field is part of the late Permian epicontinental basin of South China (Li et al., 1999, 1990), which is located in the southeastern margin of the basin. The major coal-bearing strata were developed in the late Permian Heshan Formation, and are divided into upper and the lower units (Zeng et al., 2005). There are six coal seams (Dai et al., 2013) (5, 4L, 4U, 3L, 3U, and 2), and the main mineable coal seams are 3L, 3U, 4L, and 4U, of which 4U is the coal studied in this PhD thesis. The coal seam thickness is 2.3 m, which covers carbonaceous mudstone (floor) and underlies limestone (roof), resulting in a final thickness of 0.65 m carbonaceous mudstone (parting). Heshan coal is characterised by high ash yields and sulphurs contents, with a 5.6 % of total sulphur (0.59 % pyrite sulphur, 0.12 % sulphate sulphur and 4.9 % organic sulphur) (Zeng et al., 2005).

The Baise Coalfield is located in the Baise basin, which is developed on a Mesozoic basement and filled with Paleogene terrestrial sediments from a narrow, fault-bounded basin. The Eocene Nadu Formation is the major coal-bearing strata (Shao et al., 1998; Yan et al., 2019). There are ten coal seams (A, B, C, D, E1, E2, and H coal seams). The D coal worked in this PhD thesis contains a thickness of 2.3 m, with a relatively reduced thickness of 0.65 m, developed in two carbonaceous mudstone partings. Both roof and floor are carbonaceous mudstone. According to Zeng et al. (2005) and the mining company, Donghuai coal's mean values are 1.7 % moisture content, 43 % ash yield, 21 % volatile matter and 5.8 % total S.

3.2.2.2. Underground coal mine working anthracite

The Hecheng underground coal mine (ANC, Anthracite North China) is located in the Xinmi city, Hunan Province, North China. This mine is working Early Permian coal seams. Sampling was carried out in the vicinity of the WF of coal seam #2-1. According to data from the mining company, the mine is working an anthracite seam, with 18 % ash yield, 1.9 % moisture content, 9.1 % volatile matter and 0.30 % S content. The production reaches 0.5 Mt yr^{-1}. The workable face reaches a thickness ranging from 0.5 to 13 m, with an average of 4 m. A DD sample was collected from an air return conduit in the underground coal mine, close to an air shaft.

3.2.2.3. Bituminous open-pit coal mine

The Wucaiwan open-pit coal mine (BNW, Bituminous Northwest China) is located in Jimusaer County, Xinjiang Province, Northwester China. The open-pit covers approximately 24 km^2 and contains recoverable coal reserves of approximately 1,700 Mt. According to the mining company the production reaches 20 Mt yr^{-1}. This coal mine has been open since 2006, with an estimation of 63 years of life. The worked coal of this Middle Jurassic Eastern Junggar coalfield is a high-volatile bituminous coal with low ash yield (6.0 %), and low S content (0.40 %).

3.2.3. Sampling in the Chinese coal mines

3.2.3.1. Underground coal mines

Conditions for sampling in underground coal mines are extremely restrictive. The potentially explosive environments and related safety regulations as well as, reduced space and time limitations for sampling, restricted the sampling of DD in these environments and especially few samples of PM exposure. The following areas in the mines were sampled:

Access and ventilation galleries. Good ventilation in the underground coal mines is a key factor to abate occupational dust exposure, although maintaining clean air inside the underground mine is a difficult task, requiring a complex system of ventilation. Furthermore, ventilation also causes resuspension of coal dust inside the mine and through lines. Shotcrete is a technique commonly used in galleries to cover their walls and prevent large amounts of dust or collapses. For this reason, samples were collected from the galleries, including the galleries of the ventilation system of the underground coal mine.

Coal milling and gangue. Coal milling is another process that generates dust. The coal milling device, when grinding the worked coal, emits a large volume of dust that increases occupational exposure to PM. Another process emitting dust is the extraction and handling of coal gangue (the reject from coal mining). The process of piling and handling coal mine waste is a considerable source of dust, and workers are exposed to it. For these reasons, samples were collected from coal gangue dumps around the underground mine and the coal milling process, as is shown in Figure 3.4.

Figure 3.4. *a and b) Coal gangue piles around the underground coal mine sampling; c) coal discharge from the conveyor belt system.*

Coal working fronts and extraction galleries. The WF is a small gallery where fresh coal is worked and extracted. The friction of the shearers, the frequent drilling, and the poor ventilation cause extremely high dust concentration. On other hand, the zone is considerably unstable because of the temporary hydraulic jacks and the wall of the front. In addition to this, the routes to the CWF also reach high concentrations of dust, depending on the function of the ventilation system. However, the length of time that dust remains deposited in the tunnel, in combination with other processes, such as AMD or humidity, could modify the geochemical and morphological compositions of the dust, changing it completely from its origin. For this reason, samples were collected from these zones, in WFs and the tunnels to reach them.

Wagons and station. Train wagons are taken every day by the coal mine workers, a minimum of two, twice per day. They spend a certain amount of time in the carriage of the electric mining

train. The maximum capacity of the full metallic wagon is four miners. Workers carry dust that is deposited in the wagons and resuspended. In conclusion, vibrations, poor ventilation, dust and friction dust might emit a large volume of dust in carriages, wagons and stations. For this reason, a sample from the wagon and another from the underground station were collected.

3.2.3.2. Open-pit mine

Here the restrictions for sampling are much less intensive when compared with underground mines. However, as with underground, there is still a time limitation and elevated safety procedures. Therefore, a wide variety of working operations were sampled, but also online measurements of exposure were allowed.

Tailings handling (TH). Another process emitting a large volume of dust is the extraction and handling of coal gangue. The process of piling and handling coal mine waste produces great quantities of dust, to which workers are exposed to. In these areas, dust sampling and online measurements were carried out around a coal gangue handling, shown in Figure 3.5. Another mining task emitting dust in open-pit coal mines is the exploration and working drilling. So, for these reason, dust sampling and online measurements were also carried out around these locations, as illustrated in Figure 3.5.

Figure 3.5. *TH examples. A) Loading truck after exploration and drilling overburden zones; b) controlled explosion at coal face; c) handling coal gangue; d) coal gangue dust.*

Coal working fronts. Coal in these open-pit coal mines is worked by giant excavators that rip the coal seam walls. Worked coal is loaded into large mine trucks that are constantly moving in and out the mine. Both coal working and transport generate large volumes of dust emissions. Moreover, working and transport of coal fronts generate an intensive resuspension of previously deposited coal dust. Resuspension of dust was collected at the WF, in addition to the corresponding online measurements. Examples are shown in Figure 3.6.

Figure 3.6. *a) Resuspension of coal dust at CWFs, due to the transportation of coal; b) dust emitted due to handle coal, uploading coal after drilling the coal face.*

Mine roads traffic (RT). Major unpaved roads around the open-pit are used for the transportation of coal and gangue from the mine, with heavy truck traffic. Wetting of the surface of the unpaved roads is frequent in the mine, but both resuspension and vehicle exhaust could increase PM levels around these major heavily-trafficked arteries of the mine. A sampling location in the vicinity of one of these roads was selected for dust sampling, using the same protocols described for the other emission hotspots (Figure 3.7).

Figure 3.7. *Sampling of dust emitted from mine RT in the open-pit coal mine.*

Online measurements in the open-pit. As stated above, online measurements of PM, UFP and black carbon (BC) levels close to different mining operations were possible only in the open-pit mine. Thus, for all the coal mining processes reported above for the open-pit coal mine, sampling was accompanied by analysis in real time of air pollutants with portable devices (Figure 3.8).

Figure 3.8. *Online measurement examples during different activities carried out at the open-pit mine. See the results chapter for equipment descriptions.*

3.2.4. Chinese powdered coal samples

Years of collaboration between IDAEA-CSIC and the China University of Geosciences in Wuhan (CUG), particularly with the Key Laboratory of Tectonics and Petroleum Resources department (which started with the geochemical study of the Fuxin Coal Deposit in 1995), allowed the geochemical characterisation of numerous coal basins in China and the collation of a large archive of coal samples. The metal content of these coal samples varies considerably according to the geochemical settings of the specific coal basins. Based on the joint IDAEA-CUG geochemical database and sample compilation, 22 coal samples with specific geochemical patterns, coal rank and ash yield were selected for this study.

3.3. Specific key methodological protocols

This section will outline only specific protocols with particular procedures to be implemented in this PhD thesis for the extraction of respirable dust fractions, dry PSD analysis and quantitative mineralogy analyses. Other sample treatment and analytical methods are reported in the five articles of the compendium (chapter on results).

3.3.1. Particle size separation

With the purpose of obtaining respirable coal dust, RDD from DD, and respirable powdered coal samples, CP_4 from CP, two protocol have been optimized by using two different separator devices: i) the PM_4 and $PM_{2.5}$ separator (Moreno et al., 2005); and ii) the mobile chamber resuspension device (Amato et al., 2009).

3.3.1.1. PM_4 and $PM_{2.5}$ separator

This separator is shown in Figure 3.9 and comprises a small resuspension cylindrical chamber (4697 cm^2 by 17 cm diameter) of methacrylate, within which the DD or any other powdered sample is placed and is then subjected to slow rotation (1.5 rpm). This slow rotation causes a slight resuspension of particles in an air parcel sampled by a vacuum pump (5 or 25 L min^{-1} depending on the particle size to be separated), which are deposited firstly in a smaller chamber where coarse PM is deposited, and secondly, in a PM cut off inlet of PM_4. After the PM_4 or $PM_{2.5}$ separation, particles are retained on a polycarbonate filter.

In this case, the separator was fed with the bulk mine dust sample without any prior treatment, approximately 100 g (depending on availability of sample). During the development of the separation protocol, different flow-rates (15, 20, 25, 30 L min^{-1}, among others) and filter types (Polytetrafluoroethylene, Polycarbonate and Nylon) were tried, in order to determine the optimum conditions for sample collection. As a result of this experimentation, 25 L min^{-1} for PM_4 and 5 L min^{-1} for $PM_{2.5}$ were selected as optimal flow-rates. These are regulated using an in-situ flowmeter and the efficiency of separation has been verified using a Malvern Mastersizer 2000, coupled to the Malvern HydroG 2000 extension. Figure 3.10 shows the PSD of the PM_4 and $PM_{2.5}$ fractions extracted from the coal dust sample ROCD_PV_DD_001, using the optimized method described above. Separation time needed to obtain 1.5 g $PM_{2.5}$ varied from 4 to 16 days, and 1 to 3 days for PM_4.

PM_4 (RDD) and $PM_{2.5}$ dust were retained on 0.60 µm (pore) polycarbonate filters of 47 mm. This type of filter is strong enough, does not contaminate the sample and allows for a relatively easy extraction of the dust in comparison to the other filters tested. Such filters are available in different porosities, and further experimentation has demonstrated that, for PM_4 and $PM_{2.5}$ samples, a porosity of 0.60 µm was good for the analyses.

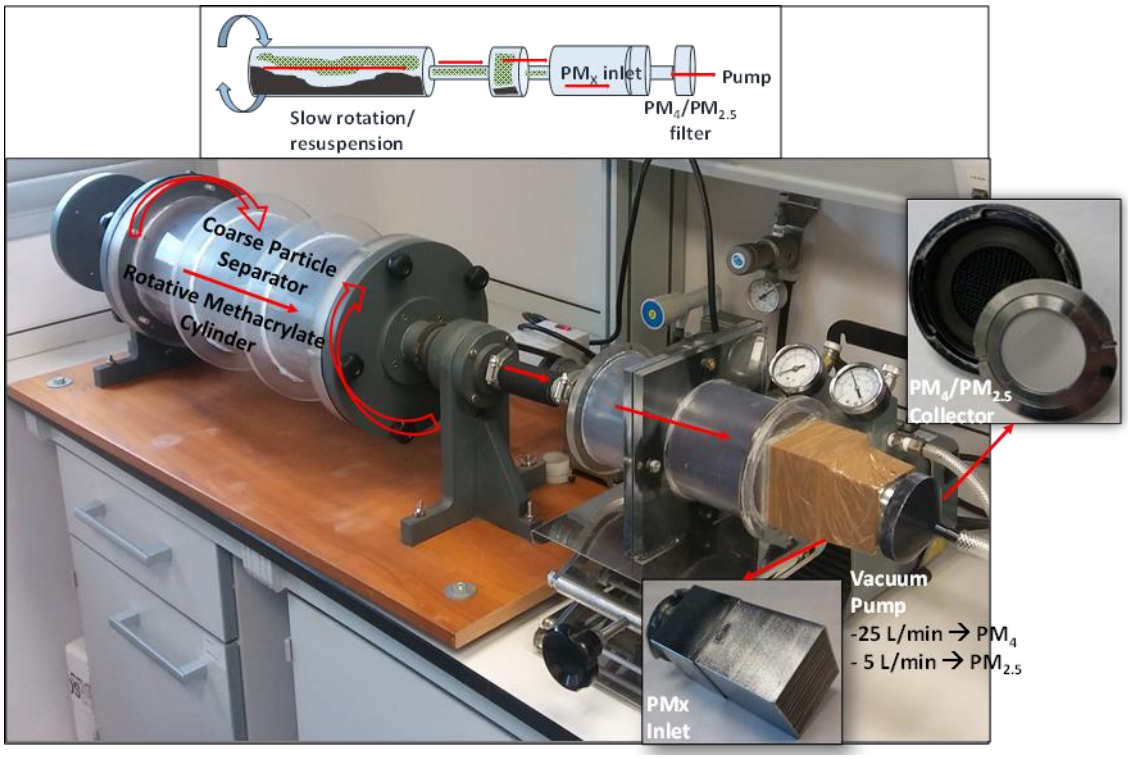

Figure 3.9. *Details of the PM_4 and $PM_{2.5}$ separator employed in this study.*

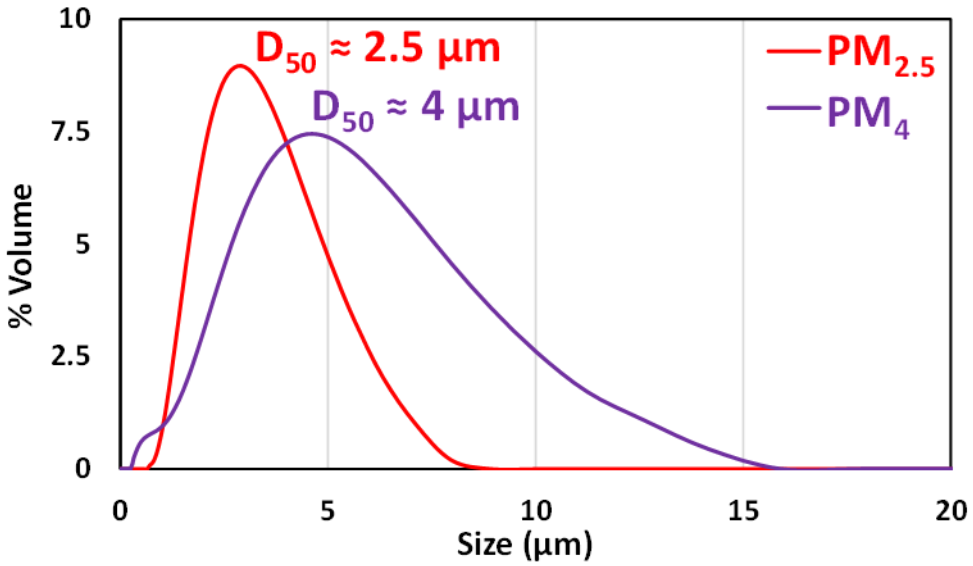

Figure 3.10. *Example of the PSD of the PM_4 and $PM_{2.5}$ fractions obtained from a DD sample using the separator shown in previous figure.*

3.3.1.2. Mobile chamber resuspension separator

This was used to separate the respirable fraction of the coal channel powdered samples to reduce the time of separation and apply this consistently to the 22 samples selected. First, coal samples were milled with a mortar Agatha Grinder RM in automatic mode for exactly 2 min. Following this, and extending the powder over clean surfaces, the chamber resuspension mobile separator (Figure 3.11) was used with the aim of separating the PM_4 fraction of the coal samples (CP_4). To this end, approximately 5.0 g of the freshly milled coal samples were spread on the surface of a large glass container, in order to create a thin layer of coal particles for a better aspiration. After that, the vacuum pump was started with a flow rate of 30 L min^{-1} in order to collect CP_4 particles on the surface of the polycarbonate filter.

The mobile chamber resuspension device consists of a portable device that suctions the dust required. A non-stick particle tube is placed in the chamber inlet hole to draw in the coal powder. Subsequently, the coal powder goes towards a methacrylate chamber, aided by the applied airflow. The sample advances through a <4 µm inlet and finally the CP_4 sample is deposited on the surface of a polycarbonate filter with 47 mm diameter and 0.6 µm pore size.

The sample deposited in the methacrylate chamber was collected, spread on a glass tray surface again and the CP_4 separation procedure was repeated. Finally, the sample collected on the filter surface was around 300-400 mg. The duration of each completed analysis was approximately 30 min.

The size cut off depends on the flow, therefore experiments were carried out to find the optimal flow for the separation of CP_4, resulting in the choice of 30 L min^{-1}. This was regulated using an in-situ flowmeter and the efficiency of separation was again verified using a Malvern Mastersizer 2000, coupled to the Malvern Scirocco 2000 extension, as is shown in Figure 3.12.

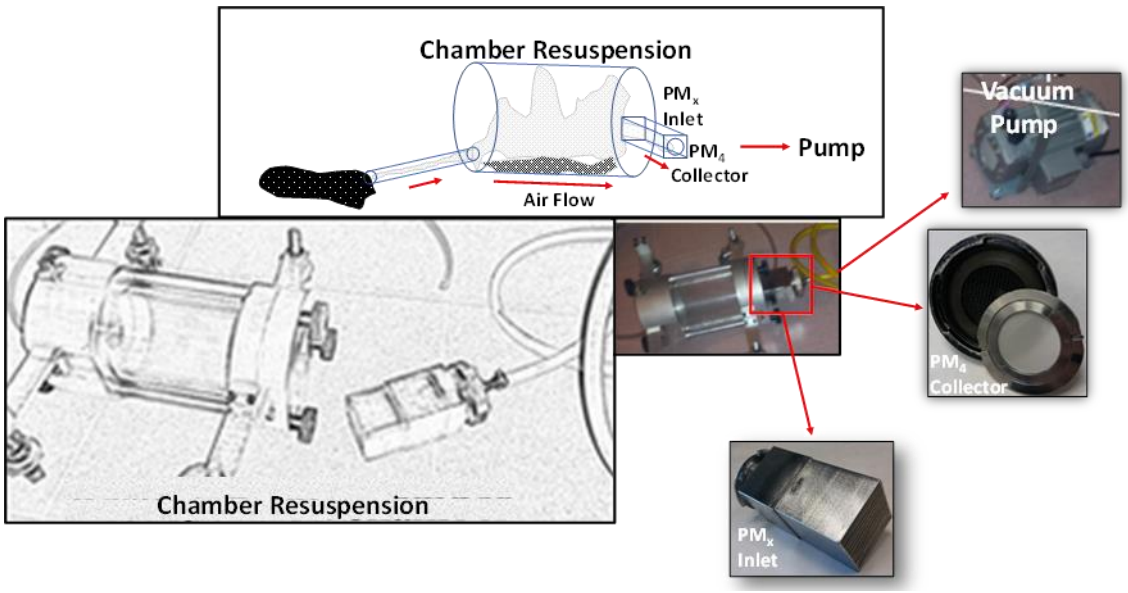

Figure 3.11. *Mobile chamber resuspension separator employed in this study.*

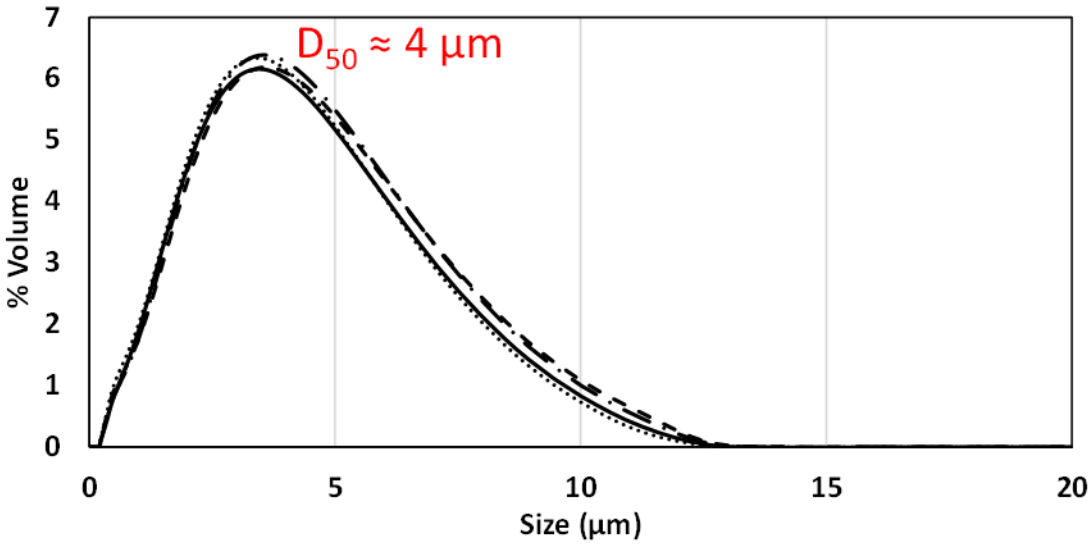

Figure 3.12. *Example of CP_4 fractions obtained from different powdered coal samples with this separator.*

3.3.2. Particle size distribution analysis

The Malvern Mastersizer 2000 was used to verify and confirm the clear separation of coal and coal dust samples and also to analyse the PSD of coal dust samples. The Malvern Mastersizer 2000 is a laser diffraction device that records PSD by measuring the angular variation in the intensity of light scattered as a laser beam passes through a dispersed particulate. Depending on whether the particles were analysed wet or dry, different coupled extensions were added, Malvern HydroG 2000 or Malvern Scirocco 2000, respectively.

3.3.2.1. Malvern Mastersizer coupled to Hydro G 2000

The Malvern 2000 Hydro G (Figure 3.13) is an ideal device for analysing the particle size of respirable fraction because, frequently, the shortage of sample creates difficulty in the particle size analysis. In order to follow the same structure for analysing the distribution of size particle coal dust samples, a standard protocol has been developed, based on Sperazza et al. (2004).

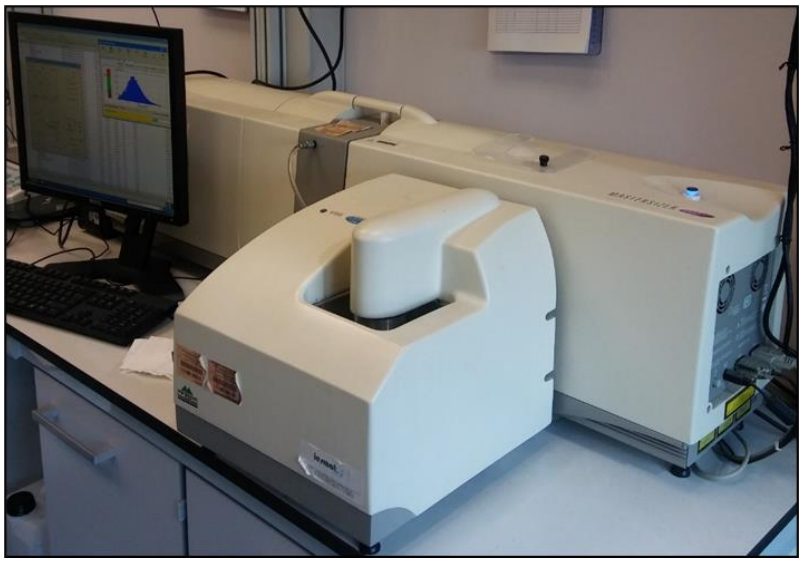

Figure 3.13. *Laser diffraction analyser for wet PSD Malvern HydroG 2000.*

The objective was always to analyse different samples in the same way to facilitate comparison. To develop the Malvern HydroG 2000 protocol, the same samples have been analysed under different parameters for physical conditions such as absorption, pump revolutions, stirrer velocity, or chemical conditions, including concentrations, shaking time and solvent type. This protocol has identified the optimal conditions for analysing the PSD in coal dust samples.

Firstly, a solution of 55 g L^{-1} of sodium polyphosphate ($(NaPO_3)_n$) was prepared. After this, the solution was left in a shaker with a slow rotation over 4 h. After this 100 mL of 55 g L^{-1} ($(NaPO_3)_n$) solution was transferred to a plastic container, to which the sample was added. A light sonication was applied for 30 s and, after this, the solution was left in a shaker for a further 12 h, with a slow rotation.

Ideally, sample weight for each analysis is approximately 0.25 g, although the amount of sample for each analysis depends on the quantity of sample available. The ideal quantity was estimated by obtaining the minimal value of weight residual (WR), since the Malvern HydroG 2000 can interpret the data values regardless of whether the amount of sample is either too small or too large.

The conditions of the analysis are adjusted according to the values shown in Table 3.1. Before doing the analysis, the Malvern HydroG 2000 needs to perform an auto-zero and a background analysis, both with the same blank suspension used for the analysis, in this case, 5.5 g L^{-1} of $(NaPO_3)_n$. Then, 100 mL of the first solution (55 g L^{-1} $(NaPO_3)_n$) and 900 mL of MilliQ water are added to obtain the final suspension. The analyses of the background should be repeated after 10-15 analyses have been made.

Table 3.1. *Conditions for the analysis of coal and coal dust samples by the Malvern HydroG 2000.*

Conditions	
Absorption	1
Stirrer	500 rpm
Index refraction	2.42
Index dispersion	1.33
Pump speed	800 rpm
Mixing	12 h
Density	1 g cm^{-3}
Sonication	60 s before analysis; 30 s at the beginning

Once the auto-zero and background have been done, 100 mL of the suspension containing the sample and 900 mL of MilliQ water are added to the Malvern HydroG 2000 container to obtain a final solution of 5.5 g L^{-1} of $(NaPO_3)_n$. The stirrer and pump are then turned on for approximately two min, followed by 60 s of sonication, before the analysis is ready to be carried out. The Malvern 2000 Hydro G does the analysis in triplicate and calculates their mean.

3.3.2.2. Malvern Mastersizer coupled to Scirocco 2000

The Malvern Sirocco 2000 (Figure 3.14) is an ideal device to analyse dust PSD in a dry procedure, which means that the sample was always introduced and analysed without any previous treatment, conserving its integrity. Furthermore, it is ideal to analyse coal dust samples that could contain larger particles to avoid agglomerations that could appear in wet analysis conditions.

The methodology of Malvern Sirocco 2000 involved adding the dust sample in an aluminium tray. This tray is placed in a closed vacuum, where vibration and air pressure are applied at the moment of the analysis. The dust sample is moved firstly to a mesh and ball system, across a gate, to deagglomerate the sample, and finally is directed towards an impactor, which spreads the particles. After this, the dust sample is aspirated by a vacuum pump, through to the laser diffraction detector, for analysis. The dust sample is destroyed, without recuperation and the analysis performed does not contain repetitions.

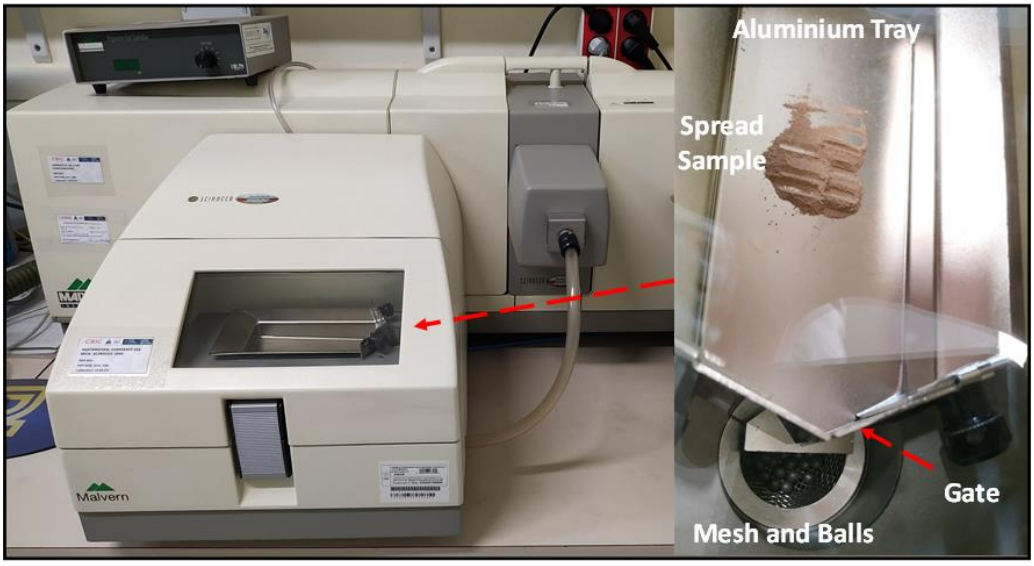

Figure 3.14. *Laser diffraction analyser for dry PSD Malvern Scirocco 2000.*

With the aim of using the minimal amount of sample as possible, the optimal conditions of the Malvern Sirocco 2000 were a key factor for PSD analysis, as is reflected in Table 3.2. These conditions included the tray aperture gate, analysis time, air pressure, tray vibration, dust sample collocation and particle absorption. Moreover, in order to obtain the ideal amount of sample for the analysis and to reduce the WR of the analysis, several amounts of sample were tested, resulting in the best quantity for the analysis being between 0.3 and 0.5 g.

Table 3.2. Conditions for analysis of coal and coal dust samples by the Malvern Scirocco 2000.

Conditions	
Absorption	1
Gate aperture	3.5 mm
Analysis time	12 s
Air pressure	3 bars
Tray vibration	75 %
Sample vollocation	Middle tray
Sample distribution	Large spread

3.3.3. Quantitative x-ray diffraction analysis

This technique gives the mineralogical composition of the coal dust and coal samples, including the possible silica components present in the coal dust and coal samples. The powder X-Ray Diffraction (XRD) data was collected by a Bruker D8 A25 Advance (Figure 3.15), θ-θ diffractometer, with CuKα1 radiation, Bragg-Brentano geometry, and a position sensitive LynxEyeXE detector. The diffractograms were obtained at 40 kV and 40 mA, scanning from 4º to 60º of 2θ with a step size of 0.019º and a counting time of 0.1 s $step^{-1}$, maintaining the sample in rotation (15 min). The crystalline phase identification was carried out using the EVA software package (Bruker), which utilised the ICDD (International Centre for Diffraction Data) database.

The normal weight to carry out the XRD analysis was in the range of 0.1-1.0 g. Although several XRD methods were tested, such as Rietveld and RIR (Reference Intensity Ratio), semi-quantitative XRD analysis was performed, using the method devised by Chung (1974) for the quantitative analysis of multi-component systems, using quartz as an internal reference.

Chung's method, in difference with the others, was completely suitable for the theoretical XRD results adjusted to coal and coal dust, being very appropriate for quantitative analysis of the mineralogy of coal and coal dust samples, since it indicates how the response of the mineral phases interacts, requiring binary mixtures for determining the constant of the interaction between phases.

$$\frac{C_i}{C_q} = K_i \frac{I_{XRDi}}{I_{XRDq}} \qquad \text{Equation 1}$$

C is the concentration of one mineral phase (i and q) into the sample, K_i is the constant between the two phases, and I is the peak intensity of every mineral phase. However, K_i can change with the type of the samples. For this reason, different mixtures were obtained to validate the semi-quantitative protocol, using mineral powdered reference materials and coal with very low ash, as is shown in Figure 3.16.

Figure 3.15. *XRD Bruker D8 A25 Advance used for XRD quantitative analyses.*

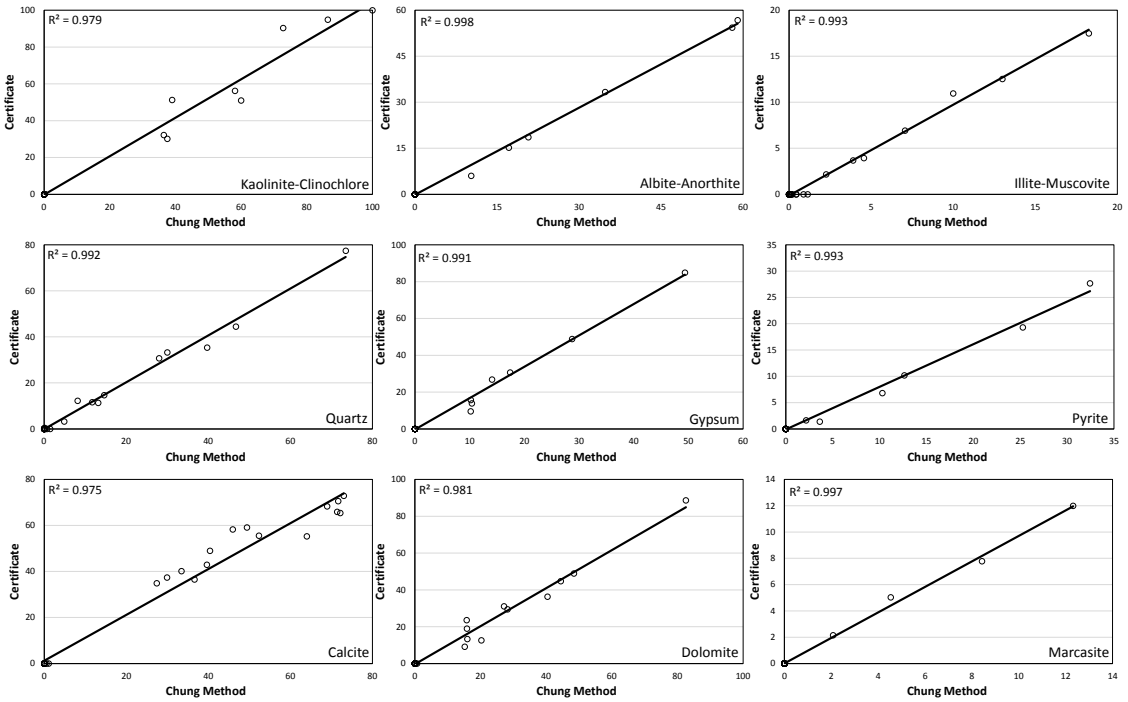

Figure 3.16. *Validation of semi-quantitative XRD analysis using mixtures of mineral reference materials and low ash coal, comparing it with Chung (1974) method.*

Chapter 4

RESULTS

4. RESULTS

Article #1 contains a review of major health-relevant coal dust geochemical patterns. Articles #2 to #4 show results from the sampling of deposited coal dust in a number of underground coal mines (China and Europe) and in an open-pit coal mine (China), and on the separation and characterisation of the respirable fractions. The samples were collected from different zones of the coal mines in order to cover the most relevant mining operations undertaken. In addition, in Article #5, powdered coal seam samples, covering a wide range of geochemical patterns from China, are used to separate and deeply characterise their respective respirable fractions.

In Articles #3 to #5 the respirable coal dust samples were selected (according to size and geochemical patterns) to evaluate the relationships among OP markers (AA, GSH and DTT) with the major physical and geochemical patterns by executing cross-correlation and multilinear regression analyses for underground mines dust samples (Article #3), open-pit mine samples (Article #4), and powdered coal samples (Article #5). Finally, the analysis was repeated by including both respirable fractions from deposited coal mine dust and from powdered coal samples (Article #5).

Moreover, suspended coal dust (PM) measurements were carried out in Articles #2 to #4 (Europe and China), including the online ambient measurement of $PM_{2.5}$, PM_{10}, BC and UFP around several mining operations in the open-pit mine (Article #4).

4.1. Article #1

Trace element fractionation between PM_{10} and $PM_{2.5}$ in coal mine dust: Implications for occupational respiratory health

Authors:

Teresa Moreno[a], **Pedro Trechera[a,b]**, Xavier Querol[a], Robert Lah[c], Diane Johnson[d], Aleksander Wrana[e], Ben Williamson[d].

a) Instituto de Diagnóstico Ambiental y Estudios del Agua, Consejo Superior de Investigaciones Científicas (IDAEA-CSIC), C/Jordi Girona 18–26, 08034 Barcelona, Spain.
b) Department of Natural Resources and Environment, Industrial and TIC Engineering (EMIT), Universitat Politécnica de Catalunya (UPC), 08242 Manresa, Spain.
c) Premogovnik Velenje d.d, Partizanskacesta 78, 3320 Velenje, Slovenia.
d) Camborne School of Mines, University of Exeter, Penryn, Cornwall TR10 9FE, UK.
e) Department of Extraction Technology and Mining Support, Central Mining Institute (GIG), 40–166 Katowice, PlacGwarkow 1, Poland.

Published in:

International Journal of Coal Geology, 203, 52-59

DOI: 10.1016/j.coal.2019.01.006

Accepted date:

Accepted 18 January 2019 (Open access)

Impact factor/Quartile

6.806/Q1

International Journal of Coal Geology 203 (2019) 52–59

Contents lists available at ScienceDirect

International Journal of Coal Geology

journal homepage: www.elsevier.com/locate/coal

Trace element fractionation between PM_{10} and $PM_{2.5}$ in coal mine dust: Implications for occupational respiratory health

Teresa Moreno[a,*], Pedro Trechera[a], Xavier Querol[a], Robert Lah[b], Diane Johnson[c], Aleksander Wrana[d], Ben Williamson[c]

[a] Instituto de Diagnóstico Ambiental y Estudios del Agua, Consejo Superior de Investigaciones Científicas (IDAEA-CSIC), C/Jordi Girona 18-26, 08034 Barcelona, Spain
[b] Premogovnik Velenje d.d, Partizanskacesta 78, 3320 Velenje, Slovenia
[c] Camborne School of Mines, University of Exeter, Penryn, Cornwall TR10 9FE, UK
[d] Department of Extraction Technology and Mining Support, Central Mining Institute (GIG), 40-166 Katowice, PlacGwarkow 1, Poland

ARTICLE INFO

Keywords:
Coal mine dust
Metals
Metalloids
Chemical fractionation
$PM_{2.5}$
PM_{10}

ABSTRACT

Investigations into the respiratory health impacts of coal mine particulate matter (PM) face the challenge of understanding its chemical complexity. This includes highly variable concentrations of trace metals and metalloids such as Fe, Ti, Mn, Zn, Ni, V, Cr, Cu, Pb, Cd, Sb, As and Sn, which may be capable of inducing cell damage. Analysis of PM_{10} and $PM_{2.5}$ samples size-separated from deposited coal mine dusts collected on PVC flat surfaces at a height of 1.5-2 m inside the second level in the Velenje lignite mine, Slovenia, demonstrates that some of these metallic elements (in this case Cu, Sb, Sn, Pb, Zn, As, Ni) can be concentrated in $PM_{2.5}$, the most deeply inhalable and therefore potentially most bioreactive size fraction. These elements are likely to be mainly present in silicates, oxides, and perhaps antimonides and arsenides, rather than in the calcareous, carbonaceous or sulphide components which show no obvious affinity for $PM_{2.5}$. Whereas in the Velenje lignites concentrations of these metallic elements are low and so do not present any obvious extra health risk to the miners, this is unlikely to be the case in mines where unusually metal-enriched coals are being excavated. We therefore recommend that levels of potentially toxic elements in $PM_{2.5}$ should be assessed where metal- and metalloid-rich coals are being mined worldwide, especially given uncertainties relating to the efficiency of current dust suppression and respiratory protective equipment for such fine particle sizes.

1. Introduction

The recent resurgence of coal mine dust lung disease (CMDLD) has caught many in the scientific community by surprise. After several decades of substantial improvement in, for example, North American and Australian mines, coal miners are once again suffering in increasing numbers from coal workers' pneumoconiosis (CWP), a condition that can intensify into its most pernicious, incurable and potentially fatal form known as progressive massive fibrosis (PMF) (Johan-Essex et al., 2017; Perret et al., 2017). Medical surveys are further revealing that relatively young miners are being affected, even though they have spent their whole working lives to date under modern dust control regulations (Perret et al., 2017; Graber et al., 2017). Doctors and researchers who thought that the more serious forms of CMDLD belonged to the poorly regulated past have reacted with consternation: "It is unacceptable that new cases of pneumoconiosis should be occurring in the 21st century at a time when the knowledge regarding prevention of such a disease is excellent. Lessons learned from the past seem to have been buried in the dusts of time" (Yates et al., 2016; see also Cohen et al., 2016). The pathology is reminiscent of the classic "U-shaped curve of concern" identified by Reichmann (1991) regarding the late 20th century return of tuberculosis (Petsonk et al., 2013). It is serious enough to warrant the status of an Occupational Sentinel Health Event (Rutstein et al., 1983; Antao et al., 2005), whereby the emergence (or, as in this case, re-emergence) of a preventable workplace disease provides a clear warning signal that new studies on the origin, control and prevention of the problem are required.

The key reasons for this epidemiological downturn in the health prospects of modern coal miners are as yet unclear and likely involve some combination of changes in mining targets, methods, and employment practices underground. There is evidence, for example, to indicate that miners working in smaller mines and spending longer hours specifically at the coalface are at enhanced risk of developing rapidly progressive CWP (Seaton et al., 1981; Kenny et al., 2002; Antao

* Corresponding author.
E-mail address: teresa.moreno@idaea.csic.es (T. Moreno).

https://doi.org/10.1016/j.coal.2019.01.006
Received 31 August 2018; Received in revised form 18 January 2019; Accepted 18 January 2019
Available online 26 January 2019

et al., 2005). Another consideration is that modern, commonly diesel-powered mining equipment, whilst more efficient at coal production, may create higher levels of PM underground, and that this dust may be different in character to that produced by more traditional mining methods (Petsonk et al., 2013). Comparisons between ambient coal mine dust produced in the 1920's and that produced this century, for example, suggest that the airborne particulate matter (PM) underground has become finer with time (Sapko et al., 2007). A complicating factor is the observation that the specific nature of new CMDLD cases seems to vary between regions and countries, for example between traditional CWP or more silicosis-like patterns (e.g Blackley et al., 2018; Cohen et al., 2016).

The current situation described above also revives old arguments about whether CMDLD risk is primarily simply a question of dust concentration and length of exposure (combined with influencing factors such as smoking habits and genetic predisposition), or whether the mineralogy and geochemistry of the PM being inhaled are additional factors. In this context the inability of research workers to identify a clear inorganic "smoking gun", in the form of a specific mineral that can be proven to induce CWP, has generated uncertainty. For example, although regulations have focused on respirable quartz, which is primarily responsible for silicosis and capable of inducing pulmonary fibrosis (NIOSH, 2002), doubt remains as to whether this mineral is also a major influence on CWP (Lapp and Castranova, 1993; Beer et al., 2017). Thus CWP has been positively correlated with coal rank (Attfield and Morring, 1992) but negatively correlated with quartz content (Harrison et al., 1997); some authors have concluded that "quartz is not the predominant factor in the development of CWP" (Mccunney et al., 2009). Changing work practices underground, however, such as the mining of thinner coal seams with the consequent release of siliceous dust from adjacent rocks, may be inducing symptoms more allied to silicosis than "traditional" CWP, adding further confusion to the evaluation of newly emerging disease patterns (Cohen et al., 2016).

It is clearly not enough to focus entirely on specific minerals such as quartz, or other components, as a generic causative agent of negative health effects induced by coal mine dust, especially given the chemical complexity of particulate materials potentially inhaled in mines. Whereas coal mine dust typically has a simple inorganic mineralogy dominated by silica (mostly quartz), phyllosilicates (mostly illite, kaolinite and/or montmorillonite), carbonates (typically siderite, ankerite and calcite) and sulphides (mostly pyrite) (Riley et al., 2012), it has a much more complex organic and trace element geochemistry. Of relevance here is the fact that both the organic (macerals) and inorganic (mineral) components of coal mine dust house a wide range of metallic elements known to be potentially capable of inducing cell damage after inhalation. Such elements may accumulate within the millimetric-sized dark carbonaceous dust-rich lesions known as "macules" that characteristically develop around the respiratory bronchioles of coal miners with CWP. Some researchers have already implicated transition metals such as bioavailable Fe or Ni to be significant influences on the incidence of CWP (Christian et al., 1979; Huang et al., 2002; Mccunney et al., 2009; Harrington et al., 2012), but there remains in general a lack of information about the exact character of the materials being inhaled in the mine dust because most papers dealing with coal trace element geochemistry focus on toxic emissions and wastes produced during combustion. In this paper therefore we refocus on the PM breathed by miners, identifying the main metallic elements likely to be of concern in these coal mine dusts, and presenting an exploratory pilot case study that demonstrates how dust chemistry, and especially metal and metalloid contents, can change as particle size decreases and the materials become more deeply inhalable.

2. Metallic elements of potential concern in coal mine dust

The inflammatory mechanisms likely involved in CWP are well documented and will not be repeated in detail here (see for example the review by Schins and Borm, 1999). Essentially, the deposition of abundant coal mine dust particles deep in the lung encourages the overproduction of reactive oxygen species (ROS) and other compounds that challenge and can overwhelm the antioxidant defence systems of cells. The coal mine dust can be directly cytotoxic, especially if particles are rich in bioreactive surface radicals, but it can also induce cell damage indirectly by activating alveolar macrophages to release ROS and proteins that escalate the inflammation around the macule site. The process will be facilitated by the presence of redox-active metals such as Fe, Mn, Cu, V and Cr which contribute to ROS production via Fenton-type reactions, although even redox-inactive metallic elements such as Pb, Cd, Hg and As can also produce ROS by acting directly on cellular molecules (Ercal et al., 2001; Birben et al., 2012; Valko et al., 2016; Ghio and Madden, 2017).

We identify a shortlist of metallic elements of potential concern in coal mine dust with respect to CWP, all of which have been shown to be capable of involvement in ROS production and cell damage. The concentration hierarchy of these metallic elements in world coals (Ketris and Yudovich, 2009) using arithmetic means is as follows: Fe (< 50,000 ppm), Ti (< 1,000 ppm), Mn (< 100 ppm), Zn, V (< 50 ppm), Ni, Cr, Cu (< 20 ppm), Pb, As, Se, Sb and Sn (< 10 ppm). These average concentrations obscure wide regional variations in coal geochemistry so that mean Cr contents for Chinese coals (32 ppm), for example, are much richer than for "world coals" (Yan et al., 2014). Furthermore, at a local level certain elements can become unusually enriched, with metal concentrations in some coals reaching > 14 wt% Fe, > 1.5 wt% Zn, > 8,000 ppm Mn, > 2,000 ppm As, > 1,900 ppm Pb, > 1,400 ppm V, > 900 ppm Cr, and > 300 ppm Ni and Cu (Dai et al., 2012). The "top ten" metallic elements ranked broadly in terms of their average concentrations in coal-derived mine dusts are therefore Fe, Ti, Mn, V, Zn, Cr, Cu, Ni, Pb and As. The occurrence modes of each of these metallic elements in coal-derived mine dust is briefly summarized below.

Iron is ubiquitously present in coal mine dust although its concentration varies greatly between different coals. It occurs in silicate (e.g. clay minerals), carbonate (e.g. siderite and ankerite), sulphide (e.g. pyrite) and sulphate particles, as well as bound to the coal macerals (Finkelman et al., 2018). Pyrite and marcasite are the commonest ferruginous sulphide minerals in coal and typically contains As, Cu, Ni, Co and Pb at concentrations of 100-1000 ppm, as well as a range of other trace elements such as Mo, Zn, Sb, and Se at lower concentrations (Kolker, 2012; Gregory et al., 2015). These trace elements may be concentrated within embedded microinclusions (such as is commonly the case with Zn and Cd in tiny sphalerite crystals) or be distributed more evenly through the pyrite structure (more typical, for example, of As: Gregory et al., 2015). Ferruginous particles can be biopersistent: it has been calculated that an inhaled 1 μm-sized pyrite crystal is likely to remain in the lung for over a year as it slowly dissolves, promoting the formation of ROS within cells and potentially contributing to the pathogenesis of CWP (Harrington et al., 2012). In addition, some of the iron in coal mine dust will be present in bioavailable forms within the carbonaceous humic substances that have also been signalled as likely involved in ROS generation and cell damage (Ghio and Quigley, 1994). A strong case has been made for bioavailable iron (BAI) to be closely linked to CWP pathology, more so than quartz or coal rank (Huang et al., 2002, 2005).

Titanium is the second most abundant transition metal in coals and occurs both in tetravalent isomorphous substitution for silicon in quartz as well as in oxide form (Rakov, 2006). Inhalable-sized microcrystals of the oxides rutile and anatase (TiO_2) of detrital origin are commonly visible embedded in coal mine dust clays and organic materials (Steinmetz et al., 1988). Titanium can also be sorbed onto clay minerals such as kaolinite (and also probably illite) or occur as fine-grained anatase within the kaolinite (Dai et al., 2015), or can occur in sulphides such as pyrite, and may be present to a limited extent in the organic fraction (Finkelman et al., 2018). Titanium oxides are relatively

chemically inert and poorly soluble, and so would be expected to be biopersistent in the lung environment. Involvement of such particles in ROS generation and cell damage is more likely to be due to their physical form rather than chemistry. In this context, for example, there is increasing concern over anthropogenic TiO_2 nanoparticle toxicity, especially when such particles possess shapes (such as highly elongated) that phagocytic cells have difficulty in processing (Hamilton et al., 2009).

Manganese in coal mine dust usually occurs in carbonates (substituting for Fe in ankerite and siderite), but it can also be found in trace amounts within clay minerals, sulphides, oxides and in the organic fraction (Finkelman et al., 1994; 2018). Manganese inhaled in unusually high concentrations is known to be toxic (Moreno et al., 2011), although given Mn concentrations typical of most coals (< 100 ppm: Finkelman et al., 2018) within the underground mine environment, any risk associated with Mn inhalation is likely to be very low.

Zinc and cadmium in coal most commonly occur in sphalerite (ZnS), although they can also be associated with clay minerals (notably illite) or present in oxide form (Finkelman et al., 2018). Coals that are unusually enriched in Zn typically contain sphalerite precipitated from zinc-bearing brines under sulphur-rich reducing conditions during coalification (Swaine, 1994). The sphalerite, which commonly contains trace amounts of Cd and Se, can occur associated with pyrite as well as with galena in mineralised veins and cleats (joints). Although Zn is known to be capable of involvement in ROS generation and cytotoxicity, especially in nanoparticulate form (e.g. Fu et al., 2014), it is unlikely that significant amounts of bioavailable Zn are inhaled by coal miners in a mine lacking abnormal concentrations of this metal. However, note that where high levels of Zn do occur then elevated levels of Cd are also likely in ambient dust.

Nickel in coals is likely to reside mostly in the sulphides and bound to organic compounds, although the metal also shows affinities with selenides, antimonides and arsenides (Finkelman et al., 2018). Nickel can thus occur as discrete minerals such as millerite (NiS), linnaeite ($(CoNi)_3S_4$), ullmannite (NiSbS), and clausthalite (PbSe), or as substitutions and microcrystals in sulphides (such as galena, sphalerite, and pyrite) and silicates (notably adsorbed to clay minerals) (Hower and Robertson, 2003; Dai et al., 2015b). As described above for zinc, nickel has been shown to be capable of ROS generation and cytotoxicity, although interestingly there is evidence to suggest that micron-sized rather than nanometric Ni PM are more bioreactive (Latvala et al., 2016).

Vanadium in coals is associated with both inorganic (mostly phyllosilicates, especially at higher coal ranks) and organic materials (especially at lower coal ranks such as lignite) (Liu et al., 2016). Although on average V is depleted in coals with respect to continental crust, striking exceptions occur across large parts of Southern China where concentrations of this metal can reach 8,000 ppm in Palaeozoic carbonaceous shales known as “stone coals” (Jiang et al., 1994), or in coals derived from the Kangdian Upland mafic sediment source region (Dai et al., 2014). The V enrichment is typically accompanied by significant enhancements in Mo, Ni, U, P, Cd, as well as enhanced levels of Au, Ag, Cu, Co, Zn, Se, Ga, Ge, Sc, Ti, REE, and Y (Dai et al., 2018). These coals have resulted from a combination of a chemically distinctive sediment source (e.g. erosion of V-enriched basalts) with a sulphurous black shale depositional environment concentrating V under anoxic conditions (Liu et al., 2016). In some areas the V enrichments have been enhanced by hydrothermal fluids that can result in the crystallisation of vanadinite ($Pb_5(VO_4)_3Cl$), but V usually occurs as organic matter and, to a lesser extent, associated with clay minerals (Liu et al., 2015; Dai et al., 2008). Although V is toxic when inhaled at high concentrations (WHO, 2000), it is not considered to be a metallic element of concern to most miners. It is likely, however, that this conclusion does not apply in the exceptional case of the Chinese V-rich stone coal mines, this being especially relevant given the increasing interest in expanding the exploitation of this important strategic resource.

Chromium in coal mine dust is likely to be mostly bound to organics as well as associated with silicates (notably in phyllosilicates such as illite), with lesser amounts occurring within sulphides, carbonates and oxides (Liu et al., 2015; Dai et al., 2008; Finkelman et al., 2018). This metal may also be present in microcrystals of chemically resistant minerals such as spinel, corundum, beryl and tourmaline; coals exceptionally enriched in Cr (> 500 ppm) can display crystals of chromite ($FeCr_2O_4$). Available evidence indicates that Cr in coal is present in the trivalent (Finkelman et al., 2018) rather than the much more toxic hexavalent form which is a known lung carcinogen. Although pneumoconiosis and cancer has been documented from the lungs of chromium mineral workers (WHO, 2000), we are not aware of any evidence to suggest that this metal represents a significant health threat to coal miners.

Copper in coals is distributed between the sulphide, selenide, carbonate, silicate and organic fractions (Riley et al., 2012; Dai et al., 2015; Finkelman et al., 2018). Crystals of chalcopyrite, commonly associated with galena, can be found filling voids within coalified peat (Finkelman et al., 2018). In exceptional cases, coal can contain > 400 ppm Cu, although average levels in coal are < 20 ppm making this metal unlikely to accumulate to high concentration levels in the total suspended particulate loading typical of the coal mine atmosphere.

Lead is primarily present in coals as galena (PbS), although it can also be found as the selenide clausthalite (PbSe) which occurs in solid solution with the sulphide (Hower and Robertson, 2003; Dai et al., 2006). Galena can occur commonly with other sulphides as relatively large epigenetic crystals filling fractures in the coal, but also as microcrystals inside pyrite and disseminated within the organic materials (Swaine, 1994; (Finkelman et al., 2018)). Although a well-documented neurological toxin, lead is normally present in very low levels within coal-bearing strata unless there has been significant late mineralisation.

Arsenic is widely distributed in coals, variously occurring in sulphides, silicates (mostly clays: kaolinite, smectite, illite), phosphates, carbonates, sulphates and arsenates, as well as organically bound. It is a common (up to 10 wt%) substitute for Fe in both finely dispersed syngenetic pyrite and epigenetic pyrite veins and cleats, and can occur as arsenopyrite (FeAsS), although Finkelman (1994) has correctly argued that this occurrence has been exaggerated. Whereas the As content of most coals is low (World Average 9 ppm: Ketris and Yudovich, 2009) and poses no obvious risk to coal miners, some deposits are spectacularly As-rich (such as the 35,000 ppm As-bearing coal reported from Guizhou Province in China by Finkelman et al., 2002). As with V, these natural As enrichments typically owe their origin to some combination of distinctive sediment source and later hydrothermal fluid movement. Most notorious are coals in parts of China, for example around Guizhou, where As poisoning due to domestic coal combustion is well documented (Belkin et al., 2008; Tian et al., 2013; and references therein). The effects of inhaling dust from the mines sourcing these coals does not appear to have been investigated, although a link between lung cancer and As inhalation in hard rock mines has been demonstrated (Taylor et al., 1989). The extreme toxicity of inorganic As and its proven role in ROS production and carcinogenesis within the lung (WHO, 2000) provides obvious cause for concern for miners working with high-As coals.

3. Pilot study: fractionation of metallic elements in Velenje mine coal dust

3.1. Methods

Given the overview presented above, we now consider the presence and distribution of metallic elements in coal mine dust in the light of the recently launched European ROCD Project (*Reducing risks from Occupational exposure to Coal Dust, 2017–2020*) which has reopened investigation into the mineralogical and chemical composition of airborne particles in underground coal mines. Part of the work schedule

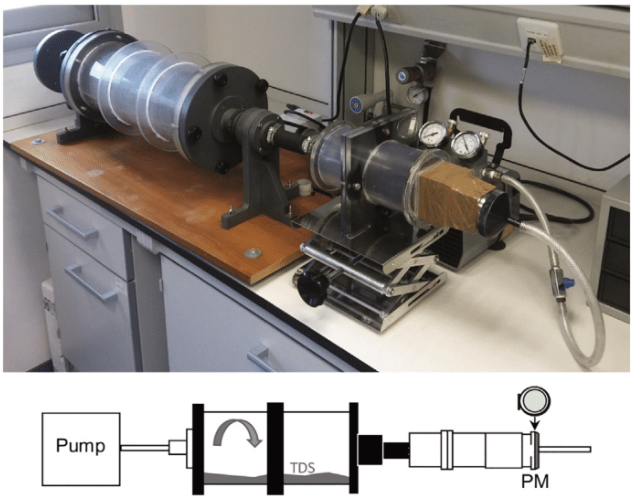

Fig. 1. Rotating cylinder device used to separate the inhalable particulate matter present in coal dust. TDS: Total Deposited Sample, PM: Particulate Matter.

for this project is to obtain a large chemical database on coal mine dusts separated into different size fractions. In order to achieve this, a protocol has been developed to allow the separation and comprehensive chemical analysis of inhalable and respirable PM fractions from coal dust collected inside mines. The method uses a specially designed and patented (Patent No. 201131895) particle size separation device (Fig. 1) comprising a rotating 17 cm diameter methacrylate cylinder which is attached at one end to a filter sampling head through which air is drawn by a pump. The cylinder is continuously rotated to resuspend PM which is then collected on a 0.60 μm pore size polycarbonate filter, at an air flow rate of 25 l min^{-1} or 5 l min^{-1} to collect PM_{10} and $PM_{2.5}$, respectively. Two hundred grams of each total deposited particle (TDP) sample collected in the Velenje mine were introduced in the cylinder in order to obtain 1.7 and 1.6 g of PM_{10} and $PM_{2.5}$ respectively for each sample after 8 and 32 h rotating for PM_{10} and $PM_{2.5}$ samples respectively. Approximatly 0.1 g of each sample were used for chemical analysis.

Chemical analysis of the PM_{10} and $PM_{2.5}$ samples involves using ICP-MS and ICP-AES, using a two-step acid digestion method devised to retain volatile elements (Querol et al., 1997). In order to obtain detailed (low detection limit), accurate and precise major and trace element data for coal dust samples we applied a tried-and-tested standard acid digestion technique involving the use of 60 ml PFA bombs. The method is summarized as follows: 2.5 ml of concentrated MERC supra-pure nitric acid (65%) is added to 0.1 g of coal sample and heated to 90 °C in a closed bomb for 4 h. After water addition (MilliQ, 18.2 MI~ − cm), the mixture is centrifuged and the solution obtained transferred to a volumetric flask (100 ml). The residue is water washed and centrifuged twice before adding the washing solution to the graduated flask. The residue is then transferred to the PFA bomb again and 7.5 ml of MERC supra-pure hydrofluoric acid (40%) and 2.5 ml of concentrated MERC supra-pure nitric acid (65%) added; the closed bomb is heated at 90 °C for 4 h 2.5 ml of MERC supra-pure perchloric acid (60%) is added and the mixture then heated at 250 °C to dryness. After that, when the sample is dry, add 1 ml of MERC supra-pure nitric acid (65%) to fix the sample and wait for it to evaporate. Once total dryness is reached, 2.5 ml of MERC supra-pure nitric acid (65%) is added and the solution transferred to a graduated flask (with the solutions obtained from the first stage) to make a volume of 100 ml. The final acid concentration is 2.5% nitric acid. The resulting solutions are then analysed by inductively-coupled plasma atomic-emission spectrometry (ICP-AES) for major and selected trace elements and by inductively-coupled plasma mass spectrometry (ICP-MS) for most trace elements. In order to check accuracy, the international coal reference material (SARM-19) and blanks were digested and analysed following the same procedure. Analytical errors were estimated at < 3% for most of the elements and around 10% for Cd, Mo, and P.

3.2. Regional setting

We applied this ROCD extraction-and-analysis protocol to samples of deposited coal dust collected inside the underground Velenje lignite coal mine located in the Šaleška valley, Slovenia. The Velenje Coal Mine is one of the largest and most modern deep coal mining sites in Europe operating on the largest Slovenian coal deposit and on one of the thickest known coal layers in the world (Markič, 2009; Markič and Sachsenhofer, 2010). The mining method used is known as Velenje Mining Method (VMM). The coal seam is 8.3 km long and up to 2.5 km wide at a depth between 200 and 500 m. Its average thickness is 60 m, with maximum values reaching up to 170 m. The area of exploitation extends above a hydraulic shield support which dynamic stresses cause breaking and crushing of the coal in upper excavation section (without blasting). In the lower excavation part, 3-4 m high protected with hydraulic shield support, the extraction of coal is achieved using a shearer. The mine ventilation system consists of over 60 km of roadways and other structures, with two surface ventilation stations exiting mine air, with total continuous airflow between 21,000 m^3/min and 25,000 m^3/min (Uranjek et al., 2013).

3.3. Results

The total deposited particle (TDP) samples obtained from the Velenje mine comprised ambient airborne dust collected passively over 24 h on PVC flat surfaces located at a height of 1.5-2 m inside the second mine level 20 m away from the longwall air outlet at the time excavation was taking place. Samples were collected from the same place using a brush (sample ROCD_1) or (three months later) a metal rule (sample ROCD_2) to scrape the sample into PVC sample pot, and then sent to Barcelona for size fractionation and analysis. The use of the metal tool for the ROCD_2 sample collection did not produce any obvious metallic contamination in the dust sample (as observed in the chemical results). The results from this pilot study provide a concise demonstration of how the metallic content of coal mine dust can change as the dust becomes finer and more deeply inhalable.

Table 1 presents results from the analysis of TDP samples collected in the underground Velenje mine and of PM_{10} and $PM_{2.5}$ separated from them. Results are shown as dry basis given the fact that the sample moisture is likely to change during transport and sample processing in the laboratory (in our case from 19 to 20 wt% at the sampling site to 10–13 wt% in the laboratory). In terms of major elements, all samples demonstrate their similar source by showing broad chemical similarities, with Ca, Al and Fe together comprising around 10 wt% of the particle mass, sulphur having values of 1.5-3 wt%, and Mg, K, and Na comprising 1-2 wt%. However, there are clear differences between TDP and the finer fractions (Fig. 2). In the coarser TDP, Ca is the most common cation but decreases in concentration in the finer fractions and can be overtaken in mass by Al which consistently increases from TDP through PM_{10} to $PM_{2.5}$. Most of the other major elements exhibit a similar behaviour to Al, with Fe, Mg, and especially K and Na all attaining highest levels in the $PM_{2.5}$. SEM-EDS analysis of the samples suggests that the main source of S in the samples is in the form of pyrite particles, and X-ray diffraction of the samples confirms the presence of quartz, illite, pyrite, calcite, and gypsum. Although we do not have analyses of the parent lignites directly sourcing our dust samples, Table 1 includes a column showing average compositions of 24 Velenje lignite borehole samples analysed by Markič (2009). The average lignite and our TDP samples show similar C and S concentrations, but all other elements analysed have higher concentrations in the TDP samples

Table 1
Major and trace element concentrations determined by ICP-AES and MS. TDP = Total Deposited Particulate (i.e. passively deposited coal mine dust). Moisture (M), Ash content (HTA) and % concentrations of C, N, and H. ar = as received basis, db = dry basis. Velenje lignite data recalculated from Markič (2009): average of 24 ICP-AES and ICP-MS analyses from successive samples 95CK to 43CK obtained in vertical structural borehole P-9 k/92 (drilled perpendicularly from the seam roof to a depth of 81 m).

		Velenje lignite	ROCD_1			ROCD_2		
	Unit		TDP	PM_{10}	$PM_{2.5}$	TDP	PM_{10}	$PM_{2.5}$
M	%ar		13.26	1.62	1.36	10.06	2.82	2.78
HTA	%db		33.79	34.23	37.94	29.67	31.06	32.65
C	%db	44.98	43.08	40.89	37.85	46.54	43.00	41.18
N	%db		0.91	0.82	0.80	1.08	0.99	0.99
H	%db		3.98	3.27	3.10	3.94	3.49	3.32
Al	%db	1.72	3.39	3.58	3.90	2.70	2.78	3.11
Ca	%db	2.56	4.14	3.64	3.70	4.25	3.74	3.85
Fe	%db	1.66	3.16	3.24	3.60	2.68	3.15	3.24
K	%db	0.27	0.63	0.75	0.84	0.50	0.58	0.64
Mg	%db	0.27	0.56	0.57	0.61	0.47	0.48	0.51
Na	%db	0.10	0.27	0.34	0.37	0.23	0.28	0.31
P	%db	0.03	0.06	0.06	0.07	0.05	0.06	0.06
S	%db	2.28	2.51	2.36	2.41	2.84	2.65	2.88
Li	mg/kg db		14	15	17	10	10	12
Be	mg/kg db		0.7	< 0.1	< 0.1	< 0.1	< 0.1	< 0.1
Sc	mg/kg db		4.7	4.5	4.8	2.9	< 0.1	2.9
Ti	mg/kg db	640	1191	1175	1291	875	961	953
V	mg/kg db	28	47	44	57	36	38	42
Cr	mg/kg db		32	35	42	23	31	34
Mn	mg/kg db	542	724	707	730	790	849	833
Co	mg/kg db	2.6	4.7	5.9	6.6	3.4	5.8	5.8
Ni	mg/kg db	8.6	19	30	32	17	30	42
Cu	mg/kg db	8.6	17	35	44	14	31	65
Zn	mg/kg db	22	69	119	139	55	103	125
Ga	mg/kg db	4.6	6.7	8.2	9.5	4.8	6.4	7.3
Ge	mg/kg db		< 0.1	< 0.1	< 0.1	< 0.1	< 0.1	< 0.1
As	mg/kg db	8.2	13	19	25	10	19	20
Rb	mg/kg db	21	38	46	51	28	37	38
Sr	mg/kg db	94	137	131	139	110	112	117
Y	mg/kg db	5.8	8.9	8.9	9.4	6.5	6.6	7.4
Zr	mg/kg db	16	25	26	26	18	16	20
Nb	mg/kg db	1.8	4.7	4.6	5.1	3.3	2.7	3.5
Mo	mg/kg db	10	22	25	27	20	16	26
Cd	mg/kg db	0.2	< 0.1	< 0.1	< 0.1	< 0.1	0.5	< 0.1
Sn	mg/kg db	1.2	1.5	3.5	5.1	1.1	2.4	5.0
Sb	mg/kg db	0.4	2.0	5.8	7.0	1.5	5.7	6.2
Cs	mg/kg db	2.1	3.6	4.5	5.1	2.5	3.7	3.5
Ba	mg/kg db	78	154	172	195	115	144	146
La	mg/kg db	6.9	12	12	13	8.8	10	10
Ce	mg/kg db	12	21	21	24	16	20	19
Pr	mg/kg db	1.5	2.6	2.7	3.0	1.9	2.4	2.3
Nd	mg/kg db	6.6	9.8	10	11	7.4	8.8	9.0
Sm	mg/kg db	1.2	2.0	2.1	2.3	1.5	1.8	1.7
Gd	mg/kg db	1.1	1.8	1.7	2.0	1.3	1.6	1.4
Dy	mg/kg db	0.9	1.6	1.6	1.7	1.2	1.4	1.3
Er	mg/kg db	0.5	0.8	0.8	0.9	< 0.1	< 0.1	< 0.1
W	mg/kg db	0.6	0.8	1.1	1.4	< 0.1	0.9	0.9
Pb	mg/kg db	8.7	16	28	35	13	42	33
Bi	mg/kg db	0.2	< 0.1	< 0.1	< 0.1	< 0.1	0.2	< 0.1
Th	mg/kg db	2.5	3.7	3.9	4.3	2.8	3.1	3.3
U	mg/kg db	9.5	13	14	15	10	9.2	12

(commonly 2 or 3 times higher), suggesting the trace element fractionation observed in the inhalable dusts has also operated in the initial release of PM during mining of the parent coals.

This preference for the finer dust fractions is also demonstrated by many of the trace elements presented in Table 1. The concentration hierarchy of trace elements in the TDP samples from highest to lowest is as follows: Ba, Sr, Zn, V, Rb, Cr, Zr, Ni, Cu, Mo, Pb, Li, U, As, La, Y, Ga, Sc, Co, Nb, Th, Cs, Pr, Sm, Sb, Gd, Dy and Sn. However, in the PM_{10} and even more so in $PM_{2.5}$ samples extracted from the TDP samples, this hierarchy is disrupted by several elements leapfrogging to higher positions. Those elements showing the least tendency to concentrate in the finer fractions are Sr, Zr, Y, Sc, Nb, Sm, Gd, and Dy. In contrast Ba, V, Rb, Cr, Mo, Li, Ga, Co, and Cs all increase moderately from TDP to $PM_{2.5}$. The most extreme preferences for the finer PM fraction however are exhibited by Zn, Ni, Pb, As, and especially by Cu, Sb and Sn (Fig. 3). In most cases these seven metallic elements more than double in concentration from TDP to $PM_{2.5}$ (Table 1).

4. Discussion and conclusions

The lignites mined at Velenje lie within the normal range of chemical compositions for coal worldwide (Ketris and Yudovich, 2009; Swaine, 1990, Fig. 4) and do not stand out as being exceptionally enriched in any element except Mn (compare for example Markič, 2009 with Yan et al., 2014). It is all the more interesting therefore that such a chemically unexceptional lignite shows significant enrichments of metallic elements in the more deeply inhalable fraction of coal dust present in the mine air. It is well established that many metallic particles

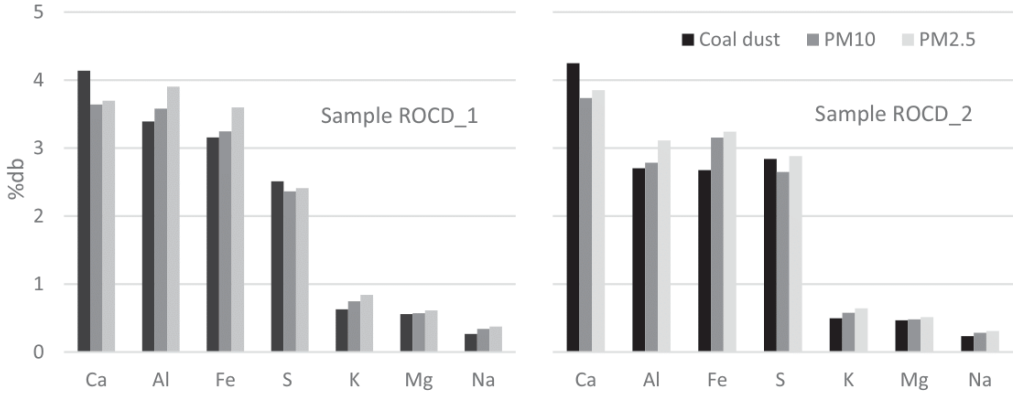

Fig. 2. Concentrations of principal major elements in the TDP (coal mine dust), PM_{10} and $PM_{2.5}$ fractions of the samples analysed.

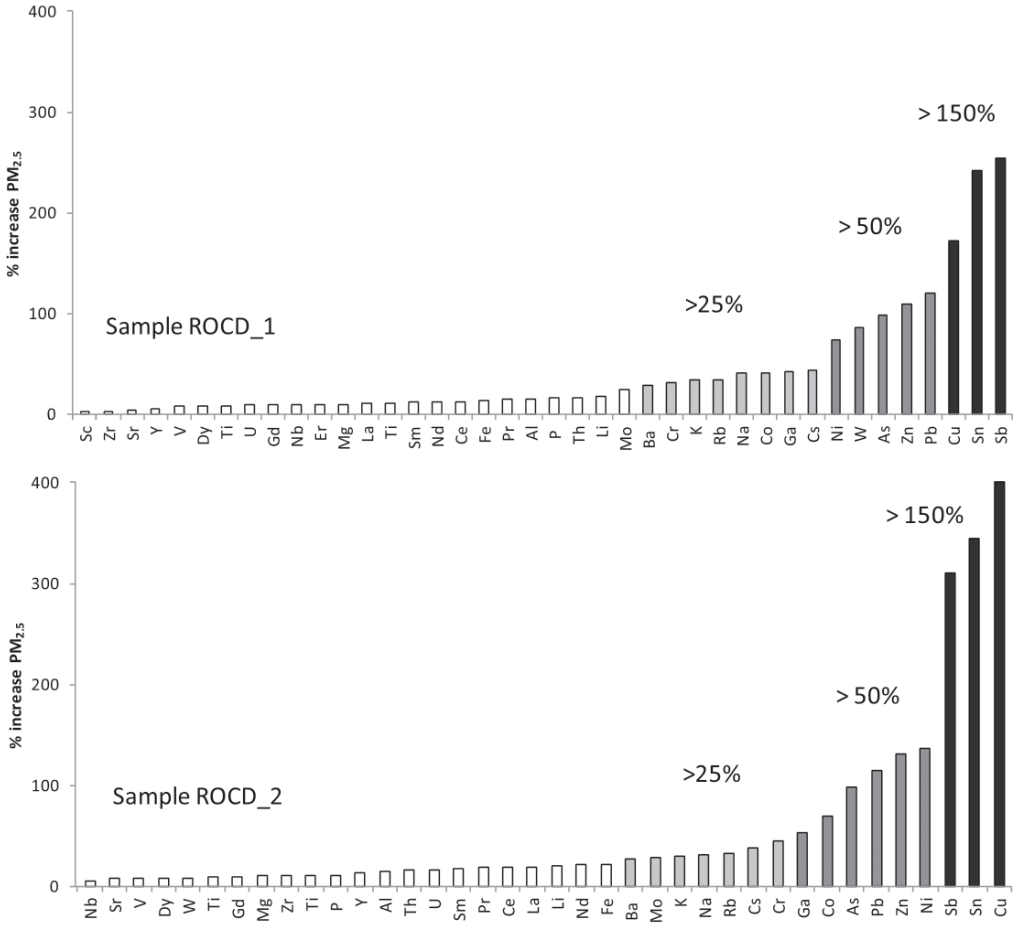

Fig. 3. Percentage enrichment in different elements between $PM_{2.5}$ and TDP.

tend to fractionate into fine size fractions ($PM_{2.5}$, and ultrafine), whereas mineral particles are coarser and predominate in the PM_{10} fraction (Williams et al., 1994; Moreno et al., 2006; NIOSH, 2010; Kollipara et al., 2014). At Velenje, for example, Cu concentrations in lignites with > 45% carbon average below 10 ppm (Markič, 2009), which is well below world average levels (Yan et al., 2014). Given our observation that Cu$PM_{2.5}$ concentration extracted from the Velenje TDP samples can reach 65 ppm, with $PM_{2.5}$/TDP increasing by > 400%, there exists the possibility for extremely high Cu-PM concentrations in the ambient air of mines excavating unusually Cu-rich coals, such as the Jungar coalfield of inner Mongolia, Northwestern China where individual coal seams can average 55 ppm Cu (Liu et al., 2018).

A similar argument applies to the other six metallic elements identified in our study as capable of strong enrichment in the inhalable fraction of coal mine dust, namely Sb, Sn, Pb, Zn, As and Ni. In the case of Sb, for example, enrichments measured in $PM_{2.5}$ samples are seven times higher than the average levels reported from the parent lignite (Markič, 2009). Either an additional source of this element is contributing to the ambient $PM_{2.5}$, or much of the Sb in the lignite is present in very fine particles (Dai et al., 2015). In the case of Velenje,

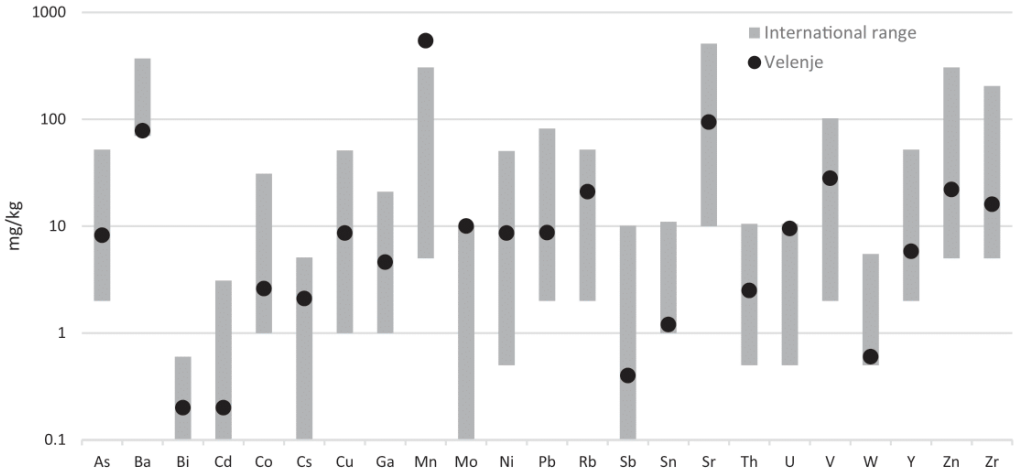

Fig. 4. Comparison of trace element Velenje coal composition with the coal world range from Swaine (1990).

the low levels (just 7 ppm Sb-$PM_{2.5}$) are of little concern, but some mines extract coal extremely enriched in Sb associated with the activity of carlin-type ore-forming fluids (Dai et al., 2012). It would be of interest to know ambient inhalable SbPM concentrations in coal mine dust from, for example, the Gokler Coalfield of western Turkey where coals contain on average 134 ppm Sb (and 833 ppm As: Karayigita et al., 2000), or the anthracites from Xingren, Guizhou, Southwest China, recorded as containing up to 3860 ppm Sb and 2226 ppm As (Dai et al., 2006).

Comparison of Ca and C concentrations in the TDP and extracted PM fractions indicate that in the Velenje mine at least it is not the calcareous or carbonaceous components of the airborne coal mine dust that are concentrating in the most inhalable particles (Table 1). Instead, the increasing levels of the cations Al, Fe, Mg, K and Na suggest the presence of fine silicate particles and oxides (and perhaps antimonides and arsenides) in the $PM_{2.5}$, rather than carbonates. This conclusion offers a hypothesis that can be tested by using other analytical methods such as scanning electron microscopy and invites a closer characterisation of the particulate matter forming these coal mine dusts.

We realise that other possible sources of particulates can contaminate passively collected coal mine dust samples, such as PM generated by machines cutting the coal strata, and especially by the involvement of siliciclastic sediments interlayered with the carbonaceous deposits. However, in our case the Velenje lignite was selected for its unusual thickness and relative chemical homogeneity (Table 1), and no diesel equipment is used in the mining operations that could emit metals in the $PM_{2.5}$ fraction. However, a limestone dusting product is applied to mitigate explosion hazards, and this could be influencing the different fractionating behaviour shown by Ca compared to other major cations.

Finally, we return to the initial topic of this paper, that of coal miner health. In this paper we identify seven metallic elements that, in our study at least, can become strongly concentrated into the finer, more inhalable fraction of airborne coal mine dust. These metals and metalloids are Cu, Sb, Sn, Pb, Zn, As and Ni. All of these metallic elements are known to be capable of inducing negative health effects in humans and therefore are of concern in situations where they become unusually concentrated. In the case of the Velenje coal mine, their concentrations are very low in the parent coal (compared with coals worldwide) and therefore are not excessively present in the ambient air. However, it is well known that coal is chemically extremely complex and highly variable in composition. Published concentrations of these seven elements in coals worldwide can reach hundreds and, in the case of Zn, Mn, As and Sb, thousands of ppm. We predict from our study of the Velenje lignite dust that the inhalable content of these seven metallic elements in coal mine air may be much higher than concentrations measured in TDP passive aerosol samplers, and very much higher than in analyses of the parent coals. Future research considering the possible health effects of coal mine dust would do well to focus specifically on the fine, inhalable fraction as our study demonstrates that this is chemically very different from the coarser airborne materials present in mine air.

Acknowledgements

This work forms part of the 'Reducing risks from Occupational exposure to Coal Dust" (ROCD) project which is supported by the European Commission Research Fund for Coal and Steel; Grant Agreement Number - 754205. Thanks to all partners in the ROCD project for their assistance in this study; see partner list at: http://emps.exeter.ac.uk/csm/rocd/. Support is also acknowledged from AGAUR SGR44.

References

Antao, V.C., Petsonk, E.L., Sokolow, L.Z., Wolfe, A.L., Pinheiro, G.A., Hale, J.M., Attfield, M.D., 2005. Rapidly progressive coal workers' pneumoconiosis in the United States: geographic clustering and other factors. Occup. Environ. Med. 62, 670–674.

Attfield, M.D., Morring, K., 1992. An investigation into the relationship between coal workers' pneumoconiosis and dust exposure in U.S. coal miners. Am. Ind. Hyg. Assoc. J. 53 (8), 486–492.

Beer, C., Kolstad, H.A., Søndergaard, K., Bendstrup, E., Heederik, D., Olsen, K.E., Omland, Ø., Petsonk, E., Sigsgaard, T., Sherson, D.L., Schlünssen, V., 2017. A systematic review of occupational exposure to coal dust and the risk of interstitial lung diseases. Eur. Clin. Respir. J. 4. https://doi.org/10.1080/20018525.2017.1264711.

Belkin, H., Zheng, B., Zhou, D., Finkelman, R., 2008. Chronic arsenic poisoning from domestic combustion of coal in rural China. A case study of the relationship between earth materials and human health. Environ. Geochem. https://doi.org/10.1016/B978-0-444-53159-9.00017-6.

Birben, E., Murat, U., Md, S., Sackesen, C., Erzurum, S., Kalayci, O., 2012. Oxidative stress and antioxidant defense. World Allergy Organ. J. 5, 9–19.

Blackley, D., Halldin, C., Laney, S., 2018. Continued increase in prevalence of coal workers' pneumoconiosis in the United States, 1970–2017. Am. J. Public Health 108 (9), e1–e3. https://doi.org/10.2105/AJPH.2018.304517.

Christian, R., Nelson, J., Cody, T., Larson, E., Bingham, E., 1979. Coal workers' pneumoconiosis: in vitro study of the chemical composition and particle size as causes of the toxic effects of coal. Environ. Res. 20, 358–365.

Cohen, R.A., Petsonk, E.L., Rose, C., Young, B., Regier, M., Najmuddin, A., Abraham, J.L., Churg, A., Green, F.H., 2016. Lung pathology in U.S. coal workers with rapidly progressive pneumoconiosis implicates silica and silicates. Am. J. Respir. Crit. Care Med. 193 (6), 673–680.

Dai, S., Zeng, R., Sun, Y., 2006. Enrichment of arsenic, antimony, mercury, and thallium in a late Permian anthracite from Xingren, Guizhou, Southwest China. Int. J. Coal Geol. 66, 217–226.

Dai, S., Ren, D., Zhou, Y., Chou, C., Wang, X., Zhao, L., Zhu, X., 2008. Mineralogy and geochemistry of a superhigh-organic-sulfur coal, Yanshan Coalfield, Yunnan, China: evidence for a volcanic ash component and influence by submarine exhalation. Chem.

Geol. 255, 182–194.
Dai, S., Ren, D., Chou, C.-L., Finkelman, R.B., Seredin, V.V., Zhou, Y., 2012. Geochemistry of trace elements in Chinese coals: a review of abundances, genetic types, impacts on human health, and industrial utilization. Int. J. Coal Geol. 94, 3–21.
Dai, S., Li, T., Seredin, V.V., Ward, C.R., Hower, J.C., Zhou, Y., Zhang, M., Song, X., Song, W., Zhao, C., 2014. Origin of minerals and elements in the late Permian coals, tonsteins, and host rocks of the Xinde Mine, Xuanwei, eastern Yunnan, China. Int. J. Coal Geol. 121, 53–78.
Dai, S., Li, T., Jiang, Y., Ward, C., Hower, J., Sun, J., Liu, J., Song, H., Wei, J., Li, Q., Xie, P., Huang, Q., 2015. Mineralogical and geochemical compositions of the Pennsylvanian coal in the Hailiushu Mine, Daqingshan Coalfield, Inner Mongolia, China: implications of sediment-source region and acid hydrothermal solutions. Int. J. Coal Geol. 137, 92–110.
Dai, S., Yang, J., Ward, C.R., Hower, J.C., Liu, H., Garrison, T.M., French, D., O'Keefe, J.M.K., 2015b. Geochemical and mineralogical evidence for a coal-hosted uranium deposit in the Yili Basin, Xinjiang, northwestern China. Ore Geol. Rev. 70, 1–30.
Dai, S., Zheng, X., Wang, X., Finkelman, R.B., Jiang, Y., Ren, D., Yan, X., Zhou, Y., 2018. Stone coal in China: a review. Int. Geol. Rev. 60, 736–753.
Ercal, N., Gurer-Orhan, H., Aykin-Burns, N., 2001. Toxic metals and oxidative stress part I: mechanisms involved in metal induced oxidative damage. Curr. Top. Med. Chem. 1 (6), 529–539.
Finkelman, R.B., 1994. Modes of occurrences of potential hazardous elements in coal, level of confidence. Fuel Process. Technol. 39, 21–34.
Finkelman, R.B., Orem, W., Castranova, V., Tatu, C.A., Belkin, H.E., Zheng, B., Lerch, H.E., Maharaj, S.V., Bates, A.L., 2002. Health impacts of coal and coal use: possible solutions. Int. J. Coal Geol. 50, 425–443.
Finkelman, R.B., Palmer, C., Wang, P., 2018. Quantification of modes of occurrence of 42 elements in coal. Int. J. Coal Geol. 185, 138–160.
Fu, P.P., Xia, Q., Hwang, H.-M., Ray, P.C., Yu, H., 2014. Mechanisms of nanotoxicity: generation of reactive oxygen species. J. Food Drug Anal. 22, 64–75.
Ghio, A.J., Madden, M.C., 2017. Human lung injury following exposure to humic substances and humic-like substances. Environ. Geochem. Health 1, 1–11.
Ghio, A.J., Quigley, D.R., 1994. Complexation of iron by humic-like substances in lung tissue: role in coal workers' pneumoconiosis. Am. J. Phys. 267, 173–179.
Graber, J.M., Harris, G., Almberg, K.S., Rose, C.S., Petsonk, E.L., Cohen, R.A., 2017. Increasing severity of pneumoconiosis among younger former US coal miners working exclusively under modern dust-control regulations. J. Occup. Environ. Med. 59, 105–111.
Gregory, D.D., Large, R.R., Halpin, J.A., Baturina, E., Lyons, T., Wu, S., Danyushevsky, L., Sack, P., Chappaz, A., Maslennikov, V., Bull, S., 2015. Trace element content of sedimentary pyrite in black shales. Econ. Geol. 110 (6), 1389–1410.
Hamilton, R.F., Wu, N., Porter, D., Buford, M., Wolfarth, M., Holian, A., 2009. Particle length-dependent titanium dioxide nanomaterials toxicity and bioactivity. Part. Fibre Toxicol. 6 (1), 35.
Harrington, A.D., Hylton, S., Schoonen, M.A.A., 2012. Pyrite-driven reactive oxygen species formation in simulated lung fluid: Implications for coal workers' pneumoconiosis. Environ. Geochem. Health 34, 527–538.
Harrison, J.C., Brower, P.S., Attfield, M.D., Doak, C., Keane, M., Grayson, R., Wallace, W., 1997. Surface composition of respirable silica particles in a set of US anthracite and bituminous coal mine dusts. J. Aerosol Sci. 28, 689–696.
Hower, J., Robertson, D., 2003. Clausthalite in coal. Int. J. Coal Geol. 53, 219–225.
Huang, C., Li, J., Zhang, Q., Huang, X., 2002. Role of bioavailable iron in coal dust-induced activation of activator protein-1 and nuclear factor of activated T cells: Difference between Pennsylvania and Utah coal dusts. Am. J. Respir. Cell Mol. Biol. 27, 568–574.
Huang, X., Li, W., Attfield, M.D., Nádas, A., Frenkel, K., Finkelman, R.B., 2005. Mapping and prediction of coal workers' pneumoconiosis with bioavailable iron content in the bituminous coals. Environ. Health Perspect. 113, 964–968.
Jiang, Y., Yue, W., Ye, Z., 1994. Characteristics, sedimentary environment and origin of the lower Cambrian stone-like coal in southern China. Coal Geol. China 6, 26–31 (in Chinese with English abstract).
Johan-Essex, V., Keles, C., Rezaee, M., Scaggs-Witte, M., Sarver, E., 2017. Respirable coal mine dust characteristics in samples collected in central and northern Appalachia. Int. J. Coal Geol. 182, 85–93.
Karayigita, A., Spears, D., Booth, C., 2000. Antimony and arsenic anomalies in the coal seams from the Gokler coalfield, Gediz, Turkey. Int. J. Coal Geol. 44, 1–17.
Kenny, L.C., Hurley, F., Warren, N.D., 2002. Estimation of the risk of contracting pneumoconiosis in the UK coal mining industry. Ann. Occup. Hyg. 46, 257–260.
Ketris, M.P., Yudovich, Ya.E., 2009. Estimations of clarkes for carbonaceous biolithes: world averages for trace element contents in black shales and coals. Int. J. Coal Geol. 78, 135–148.
Kolker, A., 2012. Minor element distribution in iron disulfides in coal: a geochemical review. Int. J. Coal Geol. 94, 32–43.
Kollipara, V., Chugh, Y., Mondal, K., 2014. Physical, mineralogical and wetting characteristics of dusts from interior basin coal mines. Int. J. Coal Geol. 127, 75–87.
Lapp, N.L., Castranova, V., 1993. How silicosis and coal workers' pneumoconiosis develop–a cellular assessment. Occup. Med. (Chic Ill) 8, 35–56.
Latvala, S., Hedberg, J., Di Bucchianico, S., Möller, L., Wallinder, I., Elihn, K., Karlsson, H., 2016. Nickel release, ROS generation and toxicity of Ni and NiO micro- and nanoparticles. PLoS One 11, 1–20.
Liu, J., Yang, Z., Yan, X., Ji, D., Yang, Y., Hu, L., 2015. Modes of occurrence of highly-elevated trace elements in superhigh-organic-sulfur coals. Fuel 156, 190–197.
Liu, Y., Liu, G., Qu, Q., Qi, C., Sun, R., Liu, H., 2016. Geochemistry of vanadium (V) in Chinese coals. Environ. Geochem. Health 39, 1–20.
Liu, D., Zhou, A., Zeng, F., Zhao, F., Zou, Y., 2018. The petrography, mineralogy and geochemistry of some Cu- and Pb-enriched coals from jungar coalfield, Northwestern China. Fortschr. Mineral. 8, 5.
Markič, M., 2009. Petrology and Genesis of the Velenje Lignite. PhD Thesis. University of Ljubljana (208 pp).
Markič, M., Sachsenhofer, R.F., 2010. The Velenje Lignite – Its Petrology and Genesis. Geološki zavod Slovenije/Geological Survey of Slovenia, Ljubljana, pp. 218. http://www.geo-zs.si/PDF/Monografije/Velenje%20lignite_14.pdf, Accessed date: 16 January 2019.
Mccunney, R.J., Morfeld, P., Payne, S., 2009. What component of coal causes coal workers' pneumoconiosis? J. Occup. Environ. Med. 51, 462–471.
Moreno, T., Querol, X., Alastuey, A., Viana, M., Salvador, P., Sánchez De La Campa, A., Artiñano, B., De La Rosa, J., Gibbons, W., 2006. Variations in atmospheric PM trace metal content in Spanish towns: illustrating the chemical complexity of the inorganic urban aerosol cocktail. Atmos. Environ. 40, 6791–6803.
Moreno, T., Pandolfi, M., Querol, X., Lavin, J., Alastuey, A., Viana, M., Gibbons, W., 2011. Manganese in the urban atmosphere: Identifying anomalous concentrations and sources. Environ. Sci. Pollut. Res. 18, 173–183.
NIOSH, 2002. Health Effects of Occupational Exposure to Respirable Crystalline Silica. DHHS Publ. No 2002–129. April 145.
NIOSH, 2010. Best Practices for Dust Control in Coal Mining. DHHS (NIOSH) Publication No. 2010–110 (January 2010).
Perret, J., Plush, B., Lachapelle, P., Hinks, T.S.C., Walter, C., Clarke, P., Irving, L., Brady, P., Dharmage, S.C., Stewart, A., 2017. Coal mine dust lung disease in the modern era. Respirology 22, 662–670.
Petsonk, E.L., Rose, C., Cohen, R., 2013. Coal mine dust lung disease: New lessons from an old exposure. Am. J. Respir. Crit. Care Med. 187, 1178–1185.
Querol, X., Whateley, M.K.G., Fernandez-Turiel, J.L., Tuncali, E., 1997. Geological controls on the mineralogy and geochemistry of the Beypazari lignite, Central Anatolia, Turkey. Int. J. Coal Geol. 33, 255–271.
Rakov, L.T., 2006. Mechanisms of isomorphic substitution in quartz. Geochem. Int. 44, 1004–1014.
Reichmann, L., 1991. The U-shaped curve of concern. Am. Rev. Respir. Dis. 144, 741–742.
Riley, K.W., French, D.H., Farrell, O.P., Wood, R.A., Huggins, F.E., 2012. Modes of occurrence of trace and minor elements in some Australian coals. Int. J. Coal Geol. 94, 214–224.
Rutstein, D.D., Mullan, R.J., Frazier, T.M., Halperin, W.E., Melius, J.M., Sestito, J.P., 1983. Sentinel health events (occupational): a basis for physician recognition and public health surveillance. Am. J. Pub. Health 73, 1054–1062.
Sapko, M.J., Cashdollar, K.L., Green, G.M., 2007. Coal dust particle size survey of US mines. J. Loss Prev. Process Ind. 20, 616–620.
Schins, R.P.F., Borm, P.J.A., 1999. Mechanisms and mediators in coal dust induced toxicity: a review. Ann. Occup. Hyg. 43, 7–33.
Seaton, A., Dodgson, J., Dick, J.A., Jacobsen, M., 1981. Quartz and Pneumoconiosis in Coalminers. Lancet 318, 1272–1275.
Steinmetz, G.L., Mohan, M.S., Zingaro, R.A., 1988. Characterization of titanium in United States coals. Energy Fuel 2, 684–692.
Swaine, D.J., 1990. Trace Elements in Coal. Butterworth & Co. Publ, London (278 pp).
Swaine, D.J., 1994. Galena and sphalerite associated with coal seams. In: Fontboté, L., Boni, M. (Eds.), Sediment-Hosted Zn-Pb Ores. Special Publication of the Society for Geology Applied to Mineral Deposits, vol. 10 Springer, Berlin, Heidelberg.
Taylor, P.R., Qiao, Y., Schatzkin, A., Yao, S., Lubin, J., Mao, B., Rao, J., McAdams, M., Xuan, X., Li, J., 1989. Relations of arsenic exposure to lung cancer among tin miners in Yunnan Province, China. Br. J. Ind. Med. 46, 881–886.
Tian, H.Z., Lu, L., Hao, J.M., Gao, J., Cheng, K., Liu, K., Qiu, P., Zhu, C., 2013. A review of key hazardous trace elements in Chinese coals: Abundance, occurrence, behavior during coal combustion and their environmental impacts. Energy Fuels 27, 601–614.
Uranjek, G., Zavšek, S., Pohorec, I., Golob, L., 2013. Odour emissions from the technological processes of coal extraction in Coal Mine Velenje. RMZ M&G 60, 131–142.
Valko, M., Jomova, K., Rhodes, C.J., Kuča, K., Musílek, K., 2016. Redox- and non-redox-metal-induced formation of free radicals and their role in human disease. Arch. Toxicol. 90, 1–37.
WHO, 2000. WHO Air Quality Guidelines, Second ed. WHO Regional Office for Europe, Copenhagen, Denmark.
Williams, K.L., Dobroski, H., Cantrell, B.K., 1994. Technologies for continuously monitoring respirable coal mine dust. In: 12th WVU International Mining Electrotechnology Conference, https://doi.org/10.1109/IMEC.1994.714367.
Yan, Z., Liu, G., Sun, R., Wu, D., Wu, B., Zhou, C., Tang, Q., Chen, J., 2014. Geochemistry of trace elements in coals from the Huainan Coalfield, Anhui, China. Geochem. J. 48, 331–344.
Yates, D.H., Gibson, P.G., Hoy, R., Zosky, G., Miles, S., Johnson, A.R., Silverstone, E., Brims, F., 2016. Down under in the coal mines. Am. J. Respir. Crit. Care Med. 194, 772–773.

International Journal of Coal Geology 219 (2020) 103392

Contents lists available at ScienceDirect

International Journal of Coal Geology

journal homepage: www.elsevier.com/locate/coal

Corrigendum

Corrigendum to Trace element fractionation between PM10 and PM2.5 in coal mine dust: Implications for occupational respiratory health' [Journal of Coal Geology 203 (2019) 52–59]

Teresa Moreno[a,*], Pedro Trechera[a], Xavier Querol[a], Robert Lah[b], Diane Johnson[c], Aleksander Wrana[d], Ben Williamson[c]

[a] *Instituto de Diagnóstico Ambiental y Estudios del Agua, Consejo Superior de Investigaciones Científicas (IDAEA-CSIC), C/Jordi Girona 18–26, 08034 Barcelona, Spain*
[b] *Premogovnik Velenje d.d, Partizanskacesta 78, 3320 Velenje, Slovenia*
[c] *Camborne School of Mines, University of Exeter, Penryn, Cornwall TR10 9FE, UK*
[d] *Department of Extraction Technology and Mining Support, Central Mining Institute (GIG), 40–166 Katowice, PlacGwarkow 1, Poland*

The authors regret to inform that the correct address of Pedro Trechera is as follows:

Pedro Trechera [a, e]

[a] Instituto de Diagnóstico Ambiental y Estudios del Agua, Consejo Superior de Investigaciones Científicas (IDAEA-CSIC), C/Jordi Girona 18–26, 08034 Barcelona, Spain.

[e] Department of Natural Resources and Environment, Industrial and TIC Engineering (EMIT), Universitat Politécnica de Catalunya (UPC), 08242 Manresa, Spain.

The authors would like to apologise for any inconvenience caused.

DOI of original article: https://doi.org/10.1016/j.coal.2019.01.006
* Corresponding author.
E-mail address: teresa.moreno@idaea.csic.es (T. Moreno).

https://doi.org/10.1016/j.coal.2020.103392

Available online 14 January 2020

4.2. Article #2

Chemistry and particle size distribution of respirable coal dust in underground mines in Central Eastern Europe

Authors:

Pedro Trechera[a, b], Xavier Querol[a], Robert Lah[c], Diane Johnson[d], Aleksander Wrana[e], Ben Williamson[d], Teresa Moreno[a]

a) Instituto de Diagnóstico Ambiental y Estudios del Agua, Consejo Superior de Investigaciones Científicas, (IDAEA-CSIC), C/Jordi Girona 18-26, 08034 Barcelona, Spain.
b) Department of Natural Resources and Environment, Industrial and TIC Engineering (EMIT-UPC), 08242 Manresa, Spain
c) Premogovnik Velenje d.d., Partizanskacesta 78, 3320 Velenje, Slovenia.
d) Camborne School of Mines, University of Exeter, Penryn, Cornwall TR10 9FE, UK.
e) Department of Extraction Technology and Mining Support, Central Mining Institute (GIG), 40-166 Katowice, PlacGwarkow 1, Poland.

Published in:

International Journal of Coal Science & Technology

Accepted:

In press (Open access)

Impact factor/Quartile

3.417/Q1

Chemistry and particle size distribution of respirable coal dust in underground mines in Central Eastern Europe

Pedro Trechera[a, b, *], Xavier Querol[a], Robert Lah[c], Diane Johnson[d], Aleksander Wrana[e], Ben Williamson[d], Teresa Moreno[a]

[a] *Instituto de Diagnóstico Ambiental y Estudios del Agua, Consejo Superior de Investigaciones Científicas, (IDAEA-CSIC), C/Jordi Girona 18-26, 08034 Barcelona, Spain.*
[b] *Department of Natural Resources and Environment, Industrial and TIC Engineering (EMIT-UPC), 08242 Manresa, Spain*
[c] *Premogovnik Velenje d.d., Partizanskacesta 78, 3320 Velenje, Slovenia.*
[d] *Camborne School of Mines, University of Exeter, Penryn, Cornwall TR10 9FE, UK.*
[e] *Department of Extraction Technology and Mining Support, Central Mining Institute (GIG), 40-166 Katowice, PlacGwarkow 1, Poland.*

** Corresponding author. E mail address: pedro.trechera@idaea.csic.es (P. Trechera)*

Abstract

Despite international efforts to limit worker exposure to coal dust, it continues to impact the health of thousands of miners across Europe. Airborne coal dust has been studied to improve risk models and its control to protect workers. Particle size distribution analyses shows that using spraying systems to suppress airborne dusts can reduce particulate matter concentrations and that coals with higher ash yields produce finer dust. There are marked chemical differences between parent coals and relatively coarse deposited dusts (up to 500 µm, DD_{500}). Enrichments in Ca, K, Ba, Se, Pb, Cr, Mo, Ni and especially As, Sn, Cu, Zn and Sb in the finest respirable dust fractions could originate from: i) mechanical machinery wear; ii) variations in coal mineralogy; iii) coal fly ash used in shotcrete, and carbonates used to reduce the risk of explosions. Unusual enrichments in Ca in mine dusts are attributed to the use of such concrete, and elevated K to raised levels of phyllosilicate mineral matter. Sulphur concentrations are higher in the parent coal than in the DD_{500}, probably due to relatively lower levels of organic matter. Mass concentrations of all elements observed in this study remained below occupational exposure limits.

Keywords: Coal dust, deposited dust, respirable dust, particle size distribution, dust chemistry, PM_{10} coal dust exposure.

1. Introduction

Around 66 % and 57 % of current European coal production and demand respectively is restricted to central-eastern countries such as Poland, Germany, Czech Republic and Ukraine (BP 2020). In this region, existing coal reserves comprise a total of 53,383 Mt of anthracite and bituminous reserves and 56,945 Mt of sub-bituminous and lignite reserves, which together account for 82% of European Union and around 11% of worldwide coal reserves (BP 2020). Given the continued importance of this industry in eastern Europe, and although coal mining activity in Europe has been steadily decreasing during the last few years (Jonek-Kowalska 2018), the environmental impact of coal mining on workers' health remains a matter of concern (Więckol-Ryk et al. 2018; Song et al. 2020). Of particular relevance is the amount and chemistry of the coal dust produced in underground coal mines. Coal dust is a chemically heterogeneous mixture of carbonaceous matter, with a variable mineral content (e.g. quartz, sulphates and sulphides),

and has distinctive major (Fe, Si, S) and trace element (As, Pb, Cr, Mn, U) signatures which may be linked to classic coal worker diseases such as pneumoconiosis (CWP) or progressive massive fibrosis (PMF) (Dalal et al. 1995; Liu et al. 2005; Cohen et al. 2008; Li et al. 2013; Caballero-Gallardo and Olivero-Verbel 2016; Fang et al. 2020; Pedroso-Fidelis et al. 2020; Jin et al. 2021). In recent years, the use of improved technologies has generally increased mine output but has also, in some cases, produced higher concentrations of dust (Perret et al. 2017; Johann-Essex et al. 2017; Leonard et al. 2020; Fan and Liu 2021). This may have been a factor in the resurgence of coal mining-related respiratory diseases in some mines (e.g. Fan et al., 2018; Wu et al., 2019). For this reason, dust monitoring control during the handling of different mining technologies requires extensive investigation, including information on the physicochemical characteristics of the deeply inhalable (particle size below 10 μm) and respirable fractions (particle size below 4 μm and 2.5 μm), both of which could be a key factor in the prevention of coal dust problems in mining, such as diverse authors are contributing (Zhang et al. 2020; Szkudlarek and Janas 2021; Jiang and Luo 2021; Liu et al. 2021; Reed et al. 2021).

In this study, as part of the European ROCD project (Reducing risks from Occupational exposure to Coal Dust), we focussed on the chemical characterisation of coarse (<500 μm) and respirable (<4 and <2.5 μm) coal dusts and their parent coals from underground mines in Central-Eastern Europe. This included determining the nature and origins of chemical fractionation of major and trace elements between different size fractions of dust. In addition, samples of mine airborne particulate matter below 10 μm (PM_{10}), emitted during different coal mining activities, were also obtained and analysed to evaluate possible chemical differences and the efficiency of ventilation and air suppression systems.

2. Geological Settings

A total of 16 underground coal mines have been sampled for this study (Table S1), all of them located in two coal mining areas of Central-Eastern Europe: Upper Silesian Coal Basin (USCB, 15 mines) and Velenje Coal Basin (VCB, 1 mine).

Upper Silesian Coal Basin

The USCB, which is one of the major coal basins in Europe, covers an area of around 7500 km^2 (5800 km^2 in Poland and 1600 km^2 in the Czech Republic, Figure 1a); only 30 % of its exploitable coal resources have been worked (Kotarba 2001; Kusiak et al. 2006; Stępniewska et al. 2014; Vaněk et al. 2017). It is a basin of polygenetic origin: the lower part (Namurian A) consists of an Upper Carboniferous coal-bearing lithostratigraphic sequence deposited in a paralic environment, whereas the upper part (Namurian B to Wesphalian D) is of purely continental origin (Kotas and Porzycki 1984; Kotas et al. 1994; Kotarba 2001; Kusiak et al. 2006).

The USCB hosts a wide range of coal types, from low-rank (sub-bituminous), high- to low-volatile rank (bituminous) to high-rank (anthracite) (Kotarba 2001; Kusiak et al. 2006; Kędzior 2009). Only the bituminous and sub-bituminous coals are mined and used in power stations (EPA 1995; Kedzior 2015). On average, USCB coals contain 0.9-2 % sulphur, have an ash yield of 11-16 % and calorific values ranging from 29 to 32 MJ/kg (EPA 1995).

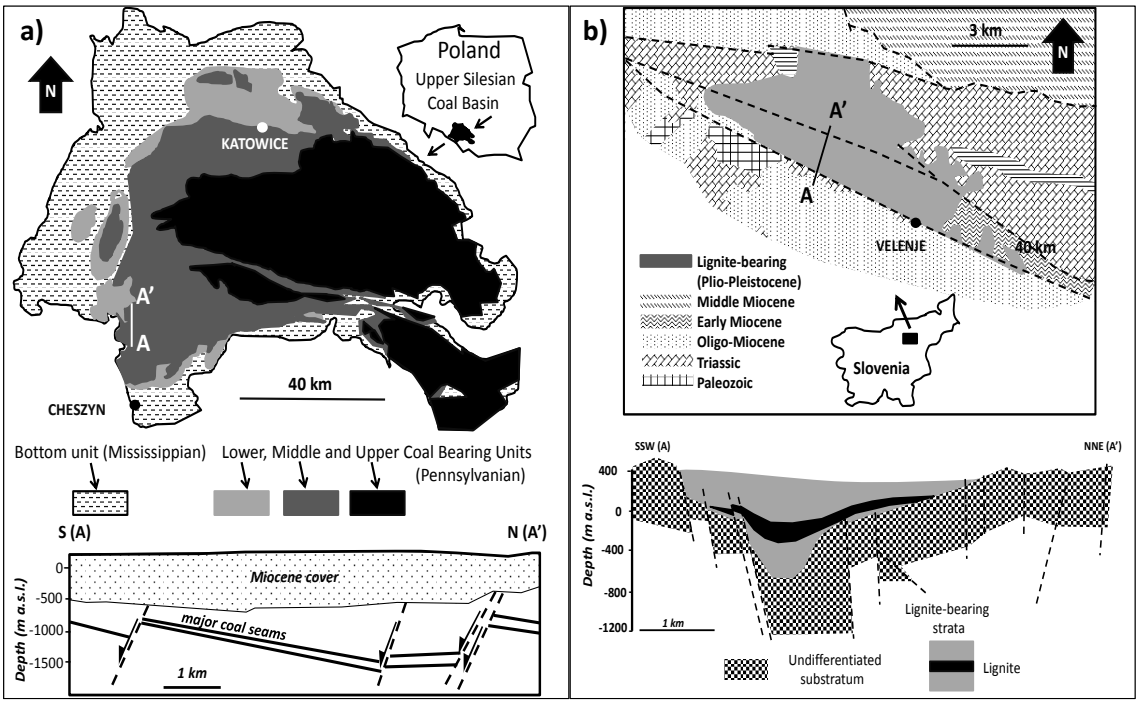

Figure 1. *a) Upper: Geological map of the Upper Silesian Coal Basin in Southern Poland. A-A' indicates the location of the geological cross section (lower figure). Modified from Kędzior (2019). B) Upper: Geological map of the Velenje Coal Basin area. Lower: Schematic geological cross-section of the Velenje Basin. For location of A – B cross-section see upper map. Adapted from Brezigar et al. (1987).*

Velenje Coal Basin

The VCB is located in NE Slovenia, at the SE end of the Alps, 70 km NE of Ljubljana (Figure 1b). The coal has an average calorific value of 8-13 MJ/kg, an ash yield of 5-40 % db, a moisture content of 15-45 % and sulphur content of 0.5-2 % db (Markič and Sachsenhofer 2010). The lignite-bearing Pliocene to Early Quaternary sediments accumulated in a 12 km long and 4 km wide WNW-ESE trending, fault bounded, depression. The mainly clastic basin fill is up to 1000 m thick, and contains a lenticular 10 km long, 3 km wide and up to 160 m thick lignite seam of Pliocene age (Brezigar 1987; Markic and Sachsenhofer 1997; Kędzior 2019).

3. Methodology

3.1. Mine sampling

A total of 91 deposited dust (DD) samples were collected manually inside the mines using two different methods. The most common method involved using a brush and a hermetic-sterilised plastic bag. Additionally, some coal DD samples were collected, using a plastic tray left in a specific workplace within the underground mine for 24-48 h, before being stored in a sterilised container. These two different coal dust collection methods offered the opportunity to compare relatively "aged" dust (which accumulated over an unknown time period, collected using a brush) with fresh DD on trays. In addition, given the likelihood that dust-generating activities carried out in the underground mines is related to the coal seam being worked, 16 rock samples of 'parent' coals were collected (Table S2). See sampling details in Tables S3, S4 and S5. Parent coals were coal samples extracted from the coal seam exploited during the DD sampling collection. They were used for checking the DD composition and for examining any possible

change in comparison with DD chemical concentration. Parent coals could provide information about DD chemical enrichments or decreases and identifying their possible origin.

3.2. Sample analysis

3.2.1. Sample pre-treatment

Figure 2 provides an overview of the analytical procedures undertaken: i) DD samples were sieved to <500 µm (DD_{500}) for the determination of particle size distribution (PSD), proximate, ultimate and geochemical composition; ii) a small (riffle-split) portion (100 g) of these DD samples (as received) was size separated using a special PM_4 or $PM_{2.5}$ separator/collection device to produce a respirable DD fraction (RDD, dust finer than 4 µm or 2.5 µm, RDD_4 or $RDD_{2.5}$, respectively); iii) parent coal rock samples were homogenised by crushing (using a hammer), mixing, and milling (using a Mortar Agatha Grinder RM 200 device in an automatic mode), prior to proximate and geochemical analysis.

In detail, to obtain the RDD_4 or $RDD_{2.5}$ samples, a separator was used following the protocols previously detailed by Amato et al. (2009)a and Moreno et al. (2019). The sieved coal DD_{500} samples were placed within the separator (which comprises a methacrylate chamber which has a volume of 4697 cm^2 by 17 cm of diameter) and subjected to mild resuspension as a result of slow rotation (1.5 rpm). The resuspended particles were sampled by drawing air, at a rate of 5 or 25 L/min for $RDD_{2.5}$ and RDD_4 respectively, through a size-selective inlet head which deposits PM_4 or $PM_{2.5}$ on to a 0.60 µm pore size, 47 mm diameter polycarbonate filter. This type of filter is strong enough, does not contaminate the sample, and allows for a relatively easy extraction from its surface. After that, the RDD samples were ready for chemical analysis.

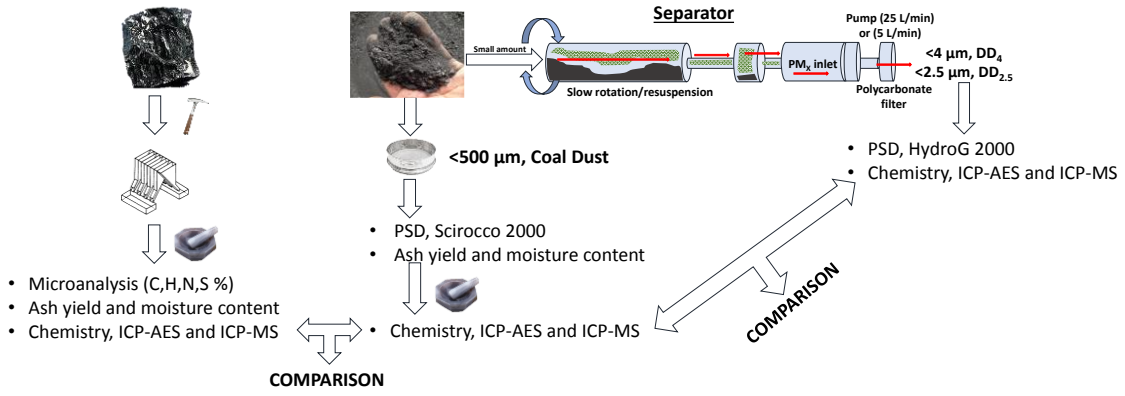

Figure 2. *Schematic of the sampling procedures used for parent coal, deposited dust and separation of the respirable deposited dust, and subsequent analyses.*

3.2.2. Particle Size distribution

The PSD of DD and RDD samples was determined using a Malvern Mastersizer device. For DD samples, a Scirocco 2000 unit was coupled to this device in order to disperse and separate the particulate in an air stream ready for laser diffraction size determination. For RDD samples (with very low sample volumes) PSD was obtained using a wet (water-polyphosphate RDD suspension) HydroG 2000 coupled unit to verify their RDD_4 size separation (Sperazza et al. 2004).

3.2.3. Proximate, ultimate and chemical characterization.

Coal sample proximate and ultimate analyses were done following ISO and ASTM procedures (ISO-589, 1981, ISO-1171, 1976, ISO-562, 1974, ASTM D-3286, D-3302M, D3174-12), with moisture (M) and ash yields (HTA) obtained at 105 and 750 ^{o}C.

Prior to geochemical analysis, coal, DD_{500} and RDD samples were HF-HNO_3-$HClO_4$ acid digested following the method of Querol et al. (1997; 1992) to retain potentially volatile elements, such as As and Se. The resulting sample solutions were analysed for major and trace elements by Inductively-Coupled Plasma Atomic-Emission Spectrometry for major elements (ICP-AES, Iris Advantage Radial ER/S device from Thermo Jarrell-Ash) and Inductively-Coupled Plasma Mass Spectrometry for trace elements (ICP-MS, X-SERIES II Thermo Fisher Scientific, Bremen, Germany). International reference materials SARM19 and NIST SRM 1633b, and blanks were treated in the same way. After thirteen analyses of the above reference materials, analytical errors and relative standard deviations (RSDVs) were included in the table S6.

3.2.4. PM_{10} measurements

The use of most electrical PM monitoring and collection devices in underground coal mines is not possible due to the risk of coal dust explosion. For this reason, only ATEX-certified instruments are permitted. In this study, a TECORA-CIP10 thoracic PM sampler (CIP10), designed for operation in explosive environments, was used to determine PM_{10} ambient concentrations during specific coal mining activities. The sampler, which operates at a flow rate of 10 L/min, has a PM_{10}-selective inlet that retains the >10 μm PM on an impaction surface and collects the PM_{10} onto a polyurethane foam.

The lack of amount sample retained in the filter foam makes sometimes impossible for their digestions, for this reason, some filter collection keeping always same conditions were occasionally combined. The mass of airborne PM_{10} per volume of air is calculated from the weight of the two fractions divided by the volume sampled. The CIP10 samplers were mainly operated for a period of 80-135 min, or, in a few cases, for 60-160 min.

The PM_{10} fractions retained in the polyurethane foam were subject to acid digestion using a mixture of HF, HNO_3 and $HClO_4$, following the method previously discussed in the section 3.2.3. The whole foam was digested. However, in this case 10 mL of HNO_3 was used in the first step, instead of 2.5 mL, and then all of the HNO_3 was evaporated off to eliminate the organic excess part of the foam (polyurethane) and avoid combustion in the second acid digestion step. Finally, all sample digested was recovered in the final of the second step ready for ICP-MS and ICP-AES analysis. Blank foams were digested using the same protocol and their contained concentrations of different elements then subtracted from the measured concentrations in the samples.

4. Results and discussion

4.1. Particle Size Distribution

A total of 91 coal DD samples from both coal basins and 2 Dust samples from VCB warehouse (Malta and Calplex, dust samples used in some places of the underground mine for security, preventing ignitions or collapses) were analysed for their PSD, moisture content (%M, air dried, ad) and ash yield (%HTA, dry bases, db) (Tables S7 and S8). Mean contents of the <500 (DD_{500}), <10 (DD_{10}), <4 (DD_4), and <2.5 μm ($DD_{2.5}$) in DD from both coal basins reached 98, 17, 6.0 and 3.3 % volume (%v), respectively, for VCB samples, and 98, 35, 16 and 10 %v, respectively, for

USCB. Thus, the proportions of DD_{10}, DD_4 and $DD_{2.5}$ in the DD samples from USCB were more than double those from the VCB. In contrast, mean moisture contents were higher in the VCB samples (12 %ad VCB vs 1.0 %ad USCB), and ash yield means were similar (36 % for VCB and 38 % for USCB).

The markedly higher moisture and lower DD_{10}, DD_4 and $DD_{2.5}$ proportions in the VCB DD_{500} are probably due to wetting of airborne and deposited coal dust in the underground mines and not to differences in coal rank. If that is the case, then it is likely that it has reduced markedly the proportion of finer particle sizes by agglomeration of particles. Thus, in the VCB underground mine, PSD analysis of very low moisture dust samples yield $DD_{2.5}$ fractions reaching up to 23 % DD_{500}. The efficiency of wetting DD in reducing coal mine worker exposure to dust, as well as in preventing coal dust explosions, is very well documented (Woskoboenko 1988; Küçük et al. 2003; Kuai et al. 2012; Yuan et al. 2014; Ajrash et al. 2017; Azam et al. 2019; Hu et al. 2021; Zhang et al. 2021). Küçük et al. (2003) and Yuan et al. (2014) found that a decrease in the dust fraction below <125 µm can be achieved by increasing the moisture content of deposited coal dust. These studies emphasise the importance of keeping a minimum moisture content in DD to prevent explosions. There is a balance to be found, however, as maintaining relatively low ambient humidity levels in underground mines provides a more comfortable working environment (Sunkpal et al. 2017) which improves work-place productivity.

When moisture contents of DD_{500} and then DD_{10}, DD_4 and $DD_{2.5}$ were determined independently for each of the two basins, some significant correlations were found for samples from the VCB mine (Eq.1-9); no such correlation was found in the USCB samples. This is probably because the moisture contents are very low (0.2 to 5.4 %ad) in USCB, compared to VCB (5.5 to 27 %ad) samples. On the other hand, systematic correlations between size fraction and HTA yields were only significant in the USCB DD samples, where a wider range of HTA yields of DD_{500} were obtained (8.2 to 79 %ad in USCB, compared with 19 to 47 %ad in VCB).

Another plausible explanation to account for the negative correlation between moisture content and fine DD_{500} fractions, different to the abatement of the fine dust fraction caused by the wetting of dust, is that the moisture content in DD_{500} from VCB increases with the coal content of the dust. An elevated coal matrix content in dust can yield to coarser dust, as well as higher moisture content (because this a lignite and accordingly moisture increases with the increase of the organic content), without the need of increasing moisture content by wetting DD. However, we do not believe this is the case because of the lack of correlation between ash yields and the fine fractions of DD_{500} in VCB. Thus, we point to the different degrees of wetting of the DD_{500} samples to account for the different concentrations of the fine fractions. On the other hand, this wetting may be hiding possible correlations between ash yields and fine fraction sizes, as found for the low moisture dust from USCB.

In the case of the DD collected at the VCB mine, these included fresh DD deposited on a plastic tray (24-48h collection time, 9 samples) and aged DD brushed from surfaces (9 samples). There were therefore a total of 18 of the 21 samples analysed (3 samples were considered outliers due to problems in their collection or store). Results for the different methods of collection are shown below to evaluate possible differences in the PSD of DD samples collected with the two methods.

Velenje Coal Basin samples

Fresh DD samples (n = 9/10)

$DD_{2.5}$ (%v) = -0.285 %M,ad + 7.328 R^2 = 0.746 **(Eq.1)**
DD_4 (%v) = -0.407 %M,ad + 11.887 R^2 = 0.677 **(Eq.2)**
DD_{10} (%v) = -1.087 %M,ad + 32.201 R^2 = 0.667 **(Eq.3)**

Aged DD samples (n = 9/11)

$DD_{2.5}$ (%v) = -0.229 %M,ad + 6.170 R^2 = 0.779 **(Eq.4)**
DD_4 (%v) = -0.329 %M,ad + 10.176 R^2 = 0.707 **(Eq.5)**
DD_{10} (%v) = -0.905 %M,ad + 28.276 R^2 = 0.639 **(Eq.6)**

All DD samples (n = 18/21)

$DD_{2.5}$ (%v) = -0.250 %M,ad + 6.680 R^2 = 0.754 **(Eq.7)**
DD_4 (%v) = -0.359 %M,ad + 10.948 R^2 = 0.688 **(Eq.8)**
DD_{10} (%v) = -0.975 %M,ad + 30.030 R^2 = 0.648 **(Eq.9)**

Very similar results were obtained for the two types of DD samples, showing that the DD sampling protocols collect dust with similar PSDs. Also, when the two warehouse samples are added, the correlation between moisture and particle size increases, presumably because warehouse samples (Malta and Calplex) have much lower moisture contents and much higher HTA yields (0.4 and 0.6 %ad moisture and 98 and 62 %db HTA), and therefore contain more fine dust.

Upper Silesian Coal Basin samples

Marcel DD samples (n = 8/10)

$DD_{2.5}$ (%v) = 0.495 %HTA,db - 9.075 R^2 = 0.958 **(Eq.10)**
DD_4 (%v) = 0.664 %HTA,db - 10.416 R^2 = 0.977 **(Eq.11)**
DD_{10} (%v) = 0.949 %HTA,db - 10.502 R^2 = 0.982 **(Eq.12)**

Bielszowice DD samples (n = 16/16)

$DD_{2.5}$ (%v) = 0.422 %HTA,db - 3.131 R^2 = 0.856 **(Eq.13)**
DD_4 (%v) = 0.567 %HTA,db - 1.901 R^2 = 0.810 **(Eq.14)**
DD_{10} (%v) = 0.856 %HTA,db + 3.810 R^2 = 0.681 **(Eq.15)**

Pniowek DD samples (n = 14/15)

$DD_{2.5}$ (%v) = 0.214 %HTA,db + 2.504 R^2 = 0.780 **(Eq.16)**
DD_4 (%v) = 0.2.83 %HTA,db + 7.578 R^2 = 0.673 **(Eq.17)**
DD_{10} (%v) = 0.409 %HTA,db + 30.305 R^2 = 0.335 **(Eq.18)**

Rest USCB *DD samples (n= 23/28)*

$DD_{2.5}$ (%v) = 0.230 %HTA,db + 1.287 R^2 = 0.776 **(Eq.19)**
DD_4 (%v) = 0.378 %HTA,db + 4.196 R^2 = 0.728 **(Eq.20)**
DD_{10} (%v) = 0.494 %HTA,db + 20.191 R^2 = 0.433 **(Eq.21)**

All USCB *DD samples (n = 61/69)*

$DD_{2.5}$ (%v) = 0.310 %HTA,db - 0.610 R^2 = 0.759 **(Eq.22)**
DD_4 (%v) = 0.431 %HTA,db + 1.529 R^2 = 0.733 **(Eq.23)**
DD_{10} (%v) = 0.670 %HTA,db + 12.07 R^2 = 0.500 **(Eq.24)**

A correlation was found between the proportions of finer fractions in DD_{500} and the ash yield for the USCB samples. An increase in the HTA yield was positively correlated with levels of the finer PSD, which is most obvious for the $DD_{2.5}$ size fraction (8 samples of a total of 69 have not been considered in these calculations being outliers in data from each of the mines) (Eq.10-24). This fact makes sense because the coal matrix (organic fraction) breaks to give coarser dust particles than clay, quartz and other mineral species, which increases the ash yields. Furthermore, the very low moisture contents of these DD_{500} samples allow finding these ash and high loads of fine DD fractions (Palmer et al. 1990; Jiang and Sheng 2018; Trechera et al. 2020). Another possible reason for the correlation between particle size and ash content in the USCB, not related to moisture content, could be that, given the high ranks of these coals, moisture is associated with the inorganic part, namely mineral matter (Jiang and Sheng 2018). However, this seems not to be the case here because of the lack of correlation between moisture and ash yields in most mines from the USCB, and the negative correlations found in two of them (Marcel and Bobrek-Piekary, Table 2). It is important also to highlight that when considering samples from all the mines from the USCB, the marked positive correlation is still evident (R^2 = 0.76, 0.73 and 0.50 for $DD_{2.5}$, DD_4 and DD_{10}, Eq.22-24), suggesting a regional similarity across the entire USCB coal basin, independently of the 15 individual mines sampled.

A multilinear regression analysis was performed both between moisture and ash contents for each mine separately (in USCB), and by method of collection (in VCB). No correlations were observed showing that moisture content is not provided by the coal samples (with the exception of Marcel and Bobrek-Piekary mines, previously commented).

4.2. Geochemical characterisation

4.2.1. Velenje Coal Basin samples

The concentrations of different elements in the coal sample generally lie within the range for worldwide coals presented by Ketris and Yudovich (2009) (Table S9), with a few minor exceptions (Tables S10, S11 and S12) such as for P (higher by a factor of 1.2), Zn (1.4), U (1.6) and Mn (1.7).

Deposited Dust Samples (DD_{500})

Figures 3a and 3b show a comparison between major and trace element concentrations in coal dust and parent coal samples. Most of the major elements show higher (2x or more) concentrations in the coal dust, with the exception of S which is very similar. This could relate to either: i) a higher content in mineral matter, with elements such as Al, Na, P or K coming from the coal gangue; ii) the mixing of coal dust with coal fly ash (Malta fly ash is commonly used in the mines as backfill, and Calplex, a carbonate 'rock dust,' is used for fire hazard reduction), that is chemically enriched in Al, Mg, Fe, Ca, Na, P, and K compared to coal (Table S13); iii) machine wear, especially for elements such as Fe and Mg.

With regards to trace elements, again most of them are enriched in the coal dust compared with parent coal samples by 2x or more, except for Mo and Sr. The trace elements Sn, Se, Ni, Zr and Sb show the highest relative enrichments (>5x), that may be due to contamination from machinery (belts, extractors, drills etc.) in the underground mine. Another potential contaminant is again fly ash (Malta), especially in trace elements such as Cr, Y, Ni, Se and Zr (Table S14).

Figures 3c and 3d compare the trace element contents of DD_{500} versus those in the parent coal for samples obtained using different collection methods: on plastic trays (fresh) or for longer term (aged) samples deposited onto mine surfaces and collected using a brush. Major elements, and the majority of the trace elements, do not show any appreciable difference according to the coal dust collection method. In the exceptional case of Sb (Figure 3d), one might speculate that this could relate to the brushing collection method which may have picked up more brake-contaminated dust on the floor of the mine than that obtained from the collection plastic tray placed 1.5 m above ground level.

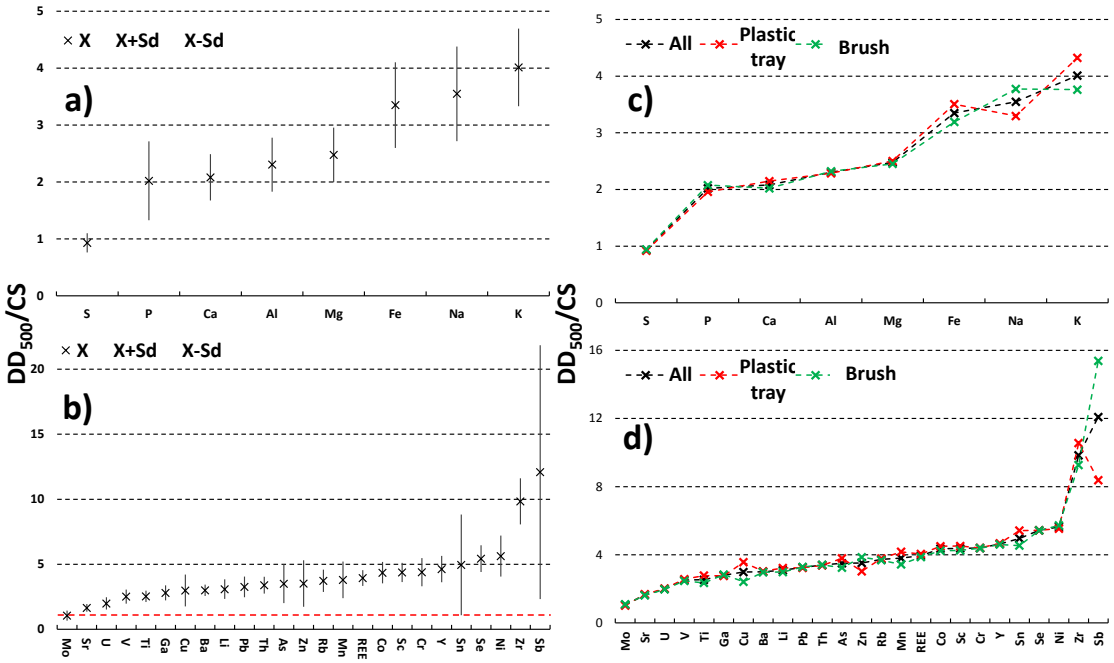

Figure 3. *Average deposited dust/parent coal elemental ratios for all dust fractions and standard deviation for the major (a) and trace (b) elements in the Velenje Coal Basin samples. Dashed red line represents ratio = 1. Average deposited dust/parent coal ratios from the different methods of collection ("fresh" plastic tray and "aged" mine surface deposits collected with a brush) for the major (c) and trace (d) elements in the Velenje Coal Basin. In black, average ratios from all deposited dust coal samples. In red, average ratios from all the "fresh" deposited dust. In green, average ratios from all the "aged" deposited dust.*

Finally, there are large variations in the elemental concentrations of some DD_{500} samples. This could be related to the types of mining activities carried out in the specific areas where sampling was carried out. Samples collected from the longwall k.-95/A-conveyor transfer point and longwall k.-95/B-conveyor transfer point present lower DD_{500} concentrations compared with DD samples from other locations. The sample ROCD_PV_002_4, collected from the longwall k.-95/A-conveyor transfer point, has the lowest element concentrations. This is probably because, in these zones, mining activity is less intense, and for this reason the levels of most elements (except Sb and U) decrease.

Respirable Deposited Dust (RDD_4 and $RDD_{2.5}$) Samples

The successful separation of the respirable fractions from the deposited coal dust (RDD_4 and $RDD_{2.5}$), using our particle size separator device, is demonstrated by the size distributions plotted on Figure S1 and shown in Table S15. Concentrations of major and trace elements (Tables S13

and S14) in these respirable (RDD_4 and $RDD_{2.5}$) samples, and the specific RDD_4/DD_{500} ratios are shown in Figure 4a, where major and trace elements (especially Ba, Se, Zn, Pb, As, Sn, Cu and Sb) are shown to be typically enriched in the finer dust fraction (ratios RDD_4/DD_{500} 1.2-1.4: Figure 4a).

Further fractionation into the $RDD_{2.5}$ size fraction is less apparent for the major elements (Figure 4b, top), but for the trace elements (Figure 4b, bottom) there are further enrichments in the metallic and metalloid elements, especially Ni, Sn and Cu. Common patterns were found concerning the elements enriched in the RDD fractions compared to the DD_{500}. This is mainly the case for Zn, Sb, As, Sn and Pb which were probably mostly sourced from the wear of mining machinery and from sulphide minerals in the coal. In contrast, Mn is the only trace element which decreases in its concentration in the finest fractions (RDD_4 and $RDD_{2.5}$) when compared to DD_{500} (Figure 4a and 4b, bottom). This result is linked to previous results of Trechera et al. (2020; 2021). Mn is probably joined with organic matter (producing coarser particles), which is commonly associated with carbonate minerals (Swaine 1990).

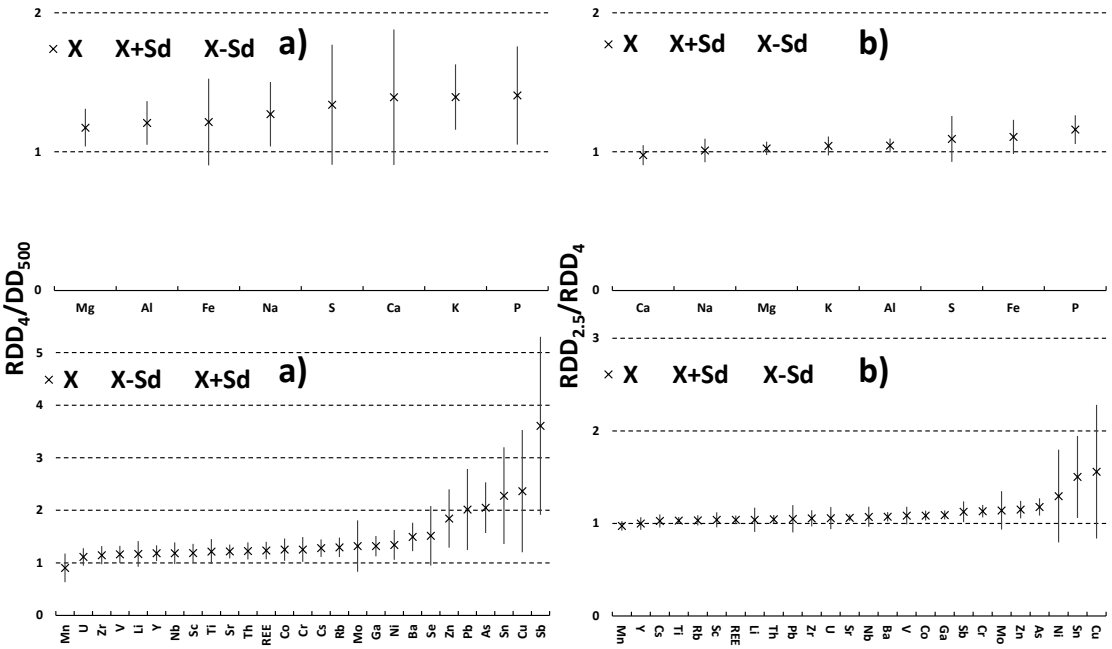

Figure 4. a) *Average RDD_4/DD_{500} major and trace element ratios and standard deviation for the Velenje Coal Basin samples.* ***B)*** *Average $RDD_{2.5}/RDD_4$ major and trace element ratios and standard deviation for the Velenje Coal Basin samples.*

4.2.2. Upper Silesian Coal Basin samples

Representative coal samples from five of the USCB mines (Pniowek, Jankowice, Marcel, Bielszowice and Murcki-Staszic) were analysed (Tables S10, S11 and S12). Elemental concentrations were generally <1.5x the average worldwide coal concentrations reported by Ketris and Yudovich (2009) (Table S9), although only Bielszowice mine samples meet the <1.5 factor for all elements. Other exceptions are for Mn (1.5x in the Marcel mine), Zn, Pb and Co (1.6x, 1.8x, and 2.8x respectively in Jankowice mine), Y (1.8x), Zn (2.1x), Sr (2.6x), Ba (2.8x), Sn (3.2x) and P (6.7x) in the Pniowek mine, and Ba (1.5x), Co (1.5-1.7x), W (1.6x), Cu (2.0x), Sb (2.2x), Pb (1.8-4.9x), Zn (6.4x) and Mn (5.0-12x) in Murcki-Staszic.

Deposited Dust Samples (DD_{500})

When DD_{500} samples (Table S16 and S17) are compared with their parent coals, most major elements in all USCB DD_{500} samples had increased concentrations, by at least 2.0x, when compared with parent coals, with the exception of S, and P (in Pniowek), which reached 0.4-1.4x, and 0.9x, respectively.

In the case of S, its content in coal dusts was lower than (or similar) to the parent coal in all USCB mines. This is likely related to S mostly occurring in the coal matrix and therefore coming from the organic part of the DD_{500}, and accordingly these (enriched in mineral matter) contain lower S than the parent coals. The content in pyrite in these coal dusts is presumably minimal due to their low S loads (Kotarba 2001). Ca shows a strongly increased concentration in the DD_{500} samples when compared to the parent coals (20-300x). This effect is attributed to the walls of these USCB mines being shotcrete with concrete to prevent collapses, although additional input of calcium carbonate from the coal gangue cannot be excluded. In addition to this, carbonate 'rock dust' is spread in some parts of the underground mines to prevent explosions. Also K concentrations are markedly higher (4x) in the DD_{500} compared with their parent coals in all USCB underground mines, with the exception of the Jankowice mine. This observation is attributed to the higher mineral matter loads in the dust.

With regard to trace element concentrations, most trace element concentrations were higher or very similar in DD_{500} than in the parent coal, with the exceptions of As, Co, Pb, Mn and Ge in the Murcki-Staszic mine; Co and Ni in the Marcel mine and As, Co, Mo and Ni in the Jankowice mine.

Respirable Deposited Dust Samples (RDD_4)

Average concentrations of major elements in RDD_4 and DD_{500} samples again show a marked enrichment in Al, Ca, Na, K, P in the RDD_4 fraction (Tables S16 to S19), with the exception of S, Fe and Mg which are enriched in the DD_{500}, and accordingly in the coarser fractions (Figure 5a). Thus, in 13 (S), 11 (Fe) and 10 (Mg) out of 15 USCB mines, RDD_4/DD_{500} ratios are <1 (Figure 5b). In contrast, Al ratio generally slightly exceeds 1, and this ratio is even >2 in some cases for Ca, Na, K and P.

RDD_4/DD_{500} ratios for trace element concentrations are shown in Figures 5c and 5d, with considerable variations, but a clear trend towards the enrichment of metals in the RDD_4. Elements such as Cu, Sn, Zn and As are concentrated by 1.5-1.7x, but it is the metalloid Sb that is most enriched (2.5x). However, Figure 5c also highlights major geochemical variations (high standard deviations) for average dusts. The least fractionated metallic element is Mn, with enrichments >1x in only five mines (Marcel, Chwalowice, Pniowek, Jankowice, and Jastrzebie). In contrast, Zr, Se and Ti reach RDD_4/DD_{500} ratios >2 in some cases; and Cu, Sn, Zn, As and Sb often reach >3.

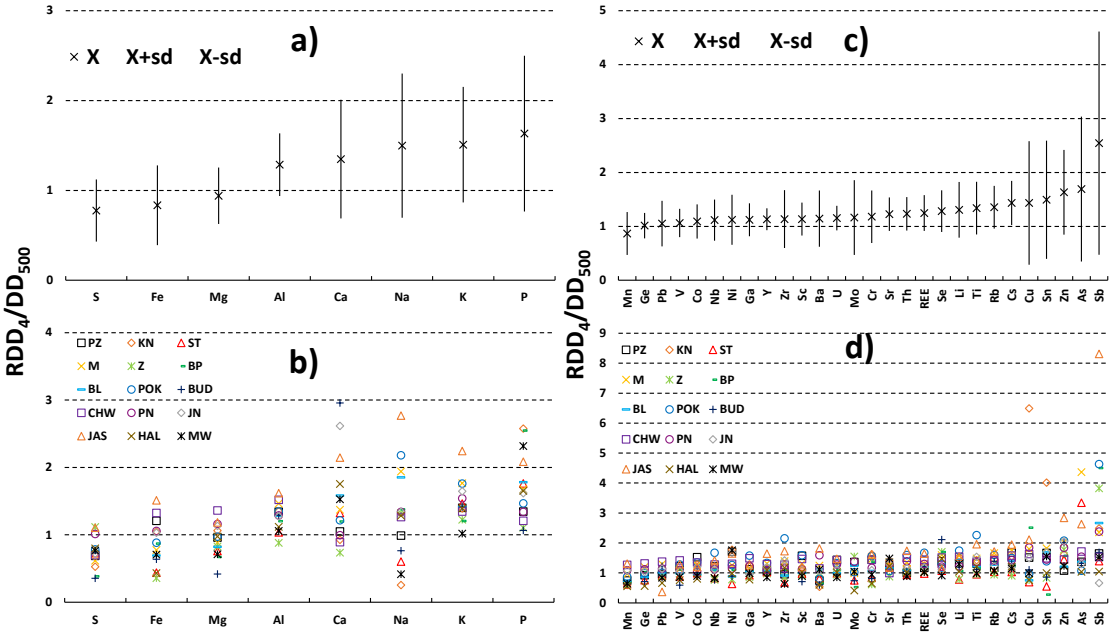

Figure 5. a) *Averaged major element RDD_4/DD_{500} ratios for all samples from the Upper Silesian Coal Basin.* ***B)*** *Averaged major element RDD_4/DD_{500} ratios for samples from individual mines in the Upper Silesian Coal Basin.* ***C)*** *Averaged trace element RDD_4/DD_{500} ratios for all samples from Upper Silesian Coal Basin.* ***D)*** *Averaged trace element RDD_4/DD_{500} ratios for samples from individual mines in the Upper Silesian Coal Basin. PZ, Piast-Ziemowit; KN, Knurów; ST, Murcki-Staszic; M, Marcel; Z, Zofiowka; BP, Bobrek-Piekary; BL, Bielszowice; POK, Pokój; BUD, Budryk; CHW, Chwalowice; PN, Pniowek; JN, Jankowice; JAS, Jastrzebie; HAL, Halemba; MW, Myslowice-Wesola.*

In summary, the results show that neither the parent coal, nor the DD_{500} have geochemical patterns reproducing those of the respirable dust (RDD_4), specially for some metals.

4.3. PM_{10} measurements

Velenje Coal Basin PM_{10} concentrations

PM_{10} airborne concentrations in the VCB mine were measured during coal working using CIP10 samplers at different distances from long-wall shearer operations (50, 100, 150 and 200 m). Here, the shearer moves along to cut a section of the coal seam then is progressed forwards by large hydraulic push rams, attached to roof supports, to cut the next section (Reid et al. 2006).

No reference on occupational exposure limits was found for ambient concentrations of metals in Slovenia. According to the occupational exposure limits for airborne toxic substances from Poland (Basic Legal Act in Poland 2010), measured elemental concentrations did not exceed the respective limit values.

As was expected, ambient PM_{10} concentrations progressively decreased with increasing distance from the long-wall shearer operations (Table 1). The general tendency was for constant element concentrations in PM_{10} in the VCB mine at a distance of 150 m from the shearer. At a distance of 200 m there was a slight decrease in their concentrations which is likely to have been due to the effectiveness of the long-wall "U-type" ventilation system, with a flow of new air coming into the workings (McPherson 1993; Smith et al. 1994; Marts et al. 2015), as well as the shearer spraying system reducing airborne dust concentrations (Colinet et al. 2010). There were a few

exceptions to this such as for Li and Zn (50 m away) and Cr, Ni and Cu (150 m away) where there were large increases in concentrations, with no clear explanation.

Table 1. *PM_{10} levels and major element oxide and trace element concentrations in PM_{10} per m^3 of air in the Velenje Coal Basin mine during shearer-longwall operations at a T-junction (exhaust air from longwall face), longwall k-95.*

Activity distance	**0 m**	**50 m**	**100 m**	**150 m**	**200 m**
PM_{10} (µg/m³)	5410	5135	4814	4994	3500
Sampling minutes	105	100	95	83	155
	µg/m³	**µg/m³**	**µg/m³**	**µg/m³**	**µg/m³**
Coal	1400	1317	1280	1242	878
SiO_2	167	167	174	169	119
Al_2O_3	112	111	116	113	79
CaO	100	88	97	97	62
Fe_2O_3	132	125	134	123	95
K_2O	94	67	13	13	8.4
MgO	18	16	18	17	11
Na_2O	31	37	31	38	25
S	120	117	124	115	85
TiO_2	4.7	4.4	5.1	4.3	3.1
	ng/m³	**ng/m³**	**ng/m³**	**ng/m³**	**ng/m³**
Li	35	49	29	36	26
Sc	<2	<2	<2	<2	<2
V	85	79	84	80	59
Cr	132	125	145	222	95
Mn	839	780	800	745	553
Co	11	9.9	10	9.9	8.0
Ni	20	14	18	127	18
Cu	124	156	171	245	140
Zn	1026	1871	1009	1042	902
Ga	18	17	18	18	13
As	35	41	38	41	29
Rb	91	88	88	83	65
Sr	443	379	377	441	280
Y	15	14	15	14	9.8
Zr	76	50	51	46	42
Nb	10	<2	<2	<2	6.5
Mo	74	70	73	66	56
Sb	636	655	642	578	621
Cs	<2	<2	<2	<2	6.8
Ba	296	286	330	293	221
Pb	83	72	53	76	52
Th	<2	<2	<2	<2	<2
U	28	26	29	25	19
REE	90	89	94	91	68

Another interesting pattern is the higher ambient concentrations of Mn and Fe_2O_3 in comparison with similar studies carried out in Chinese underground coal mines (Trechera et al. 2020, 2021), which are possibly from machine wear or from higher Mn and Fe contents in the Slovenian coals.

Upper Silesian Coal Basin PM_{10} concentrations

Ambient PM_{10} concentrations in the different USCB underground coal mines were measured during two different coal mining activities: i) Shearer cutting during long-wall excavations (as for the VCB mine), ii) Roadway drivage, which consists of cutting the coal and rock using a road-header, loading and transportation of the excavated material and the installing of underground supports.

Tables 2 to 4 show PM_{10} concentrations in the Knurów, Murcki-Staszic, Pnioweck, Marcel, and Bielszowice underground coal mines. Ambient concentrations of all determined elements are lower than the Polish recommended maximum values for occupational environments (Basic Legal Act in Poland 2010). However, ambient PM_{10} concentrations should not exceed 4.0 mg/m^3 where the coal contains 2-10 % of SiO_2 , or 2.0 mg/m^3 with 10-50 % of SiO_2 over a period of 8h. PM_{10} concentrations measured in various of the studied mines were above these values, such as in the Pniowek mine (9.8 to 12 mg/m^3 coal dust concentration in zone 'b', 4.7 to 6.0 mg/m^3 in zone 'a' and 14 to 24 mg/m^3 in zone 'c', Table 3), Marcel mine (8.3 to 9.6 mg/m^3 in zone 'a', and 12 to 13 mg/m^3 in zone 'b'), Knurów mine (7.7 to 14 mg/m^3, Table 2),) and Bielszowice mine (3.3 to 6.1 mg/m^3, Tables 3 and 4). However, these concentrations were measured over periods shorter than 8 h, and therefore are not comparable with the occupational standard. In any case, these short time high concentrations reinforced the importance of the protocols applied by mining companies to protect coal workers with sophisticated personal protective equipment and coal dust abatement controls.

As expected, PM_{10} concentrations are mostly higher closer to mine machine operations (Tables 2 to 4), with the exception of the Pniowek mine zone 'a', where measurements took place during a maintenance shift when mine machinery was switched off but the ventilation system continued to operate.

Comparing the two activities studied in all mines, shearer cutting during long-wall excavations emitted less PM_{10} coal dust than the roadway drivage operations. Mn concentrations were also clearly higher during roadway drivage. When comparing the different coal mines, lower PM_{10} concentrations were recorded in three mines, Murcki-Staszic, Pniowek zone 'b' and Bielszowice. In contrast, in the Knurów mine, concentrations of Al_2O_3, CaO, Fe_2O_3, K_2O, MgO, Na_2O, as well as metals such as Pb and Cr, were higher in comparison with other mines from this and other studies (Trechera et al. 2020, 2021).

When PM_{10} levels produced by each mining activity are compared, elevated levels of As (2.2x), Ba (1.5x), and Li (2.2x) are evidenced in the Pniowek zone 'c', and Zn (1.7-2.3x, Ba (1.5x) and Cu (2x) in the Marcel mine (zones 'a' and 'b'). The elevated levels of these metals were likely derived from a mix of sources including machine wear (Cu, Zn, Ba), resuspension of DD from the floor and walls (As, Ba, Li), and PM brought from other zones of the mine by the ventilation system.

4.4. PM_{10} and RDD_4 comparison

The aim of comparing PM_{10} and RDD_4 concentrations was to find the possible sources of each particle size fraction to clarify the dominant type of particle present in underground coal mine air, always in a qualitative way. The comparison was performed by calculating the difference in PM_{10} concentrations (Tables 3 to 6) of major and trace elements.

In the VCB underground mine, all element concentrations in PM_{10} were lower than in the RDD_4. Some elements, such as K, Cu, Zn, and Mo, were similar in both PM_{10} and RDD_4 samples, whereas Na and Sb show higher concentrations in PM_{10} from all sampling locations (1.3-2.0x Na and 7.1-12x higher Sb).

Table 2. *PM_{10} levels and major element oxide and trace element concentrations during roadway drivage technique in Knurów mine (exhaust air from roadway face; 5b, seam 404/1) and shearer cutting- longwall advance in Murcki-Staszic mine at the T-junction (exhaust air from longwall face 03/seam 510) from the Upper Silesian Coal Basin.*

Mine	Knurów	Knurów	Knurów	Murcki-Staszic	Murcki-Staszic	Murcki-Staszic	Murcki-Staszic	Murcki-Staszic
Activity distance	20-50 m	100-140 m	220-280 m	0 m	50 m	190 m	280 m	350 m
PM_{10} (µg/m³)	14025	15000	7702	11905	7833	14969	6578	7963
Sampling minutes	80	80	95	95	87	97	94	99
	µg/m³	**µg/m³**	**µg/m³**	**µg/m³**	**µg/m³**	**µg/m³**	**µg/m³**	**µg/m³**
Coal	6221	6086	3299	613	538	843	672	486
SiO_2	2669	2404	927	151	117	228	125	106
Al_2O_3	1780	1603	618	101	78	152	83	71
CaO	296	751	1128	272	217	331	388	214
Fe_2O_3	712	651	272	74	79	106	50	66
K_2O	273	250	93	5.6	8.1	13	10	13
MgO	180	151	69	32	32	44	27	22
Na_2O	146	121	96	57	55	86	61	52
S	49	48	53	47	61	54	54	41
TiO_2	89	82	32	7.1	5.5	9.7	8.1	5.1
	ng/m³	**ng/m³**	**ng/m³**	**ng/m³**	**ng/m³**	**ng/m³**	**ng/m³**	**ng/m³**
Li	575	566	206	99	74	91	50	79
Sc	168	150	50	<2	<2	<2	<2	<2
V	1048	979	345	58	40	83	46	37
Cr	1243	1130	426	75	89	654	80	78
Mn	10646	9736	3593	511	467	748	421	455
Co	176	156	55	<2	<2	17	9.7	6.9
Ni	446	375	152	<2	6.87	553	<2	<2
Cu	398	547	374	<2	848	93	81	31
Zn	1569	1419	1020	488	1611	2179	4686	1366
Ga	242	225	75	<2	12	21	13	10
As	51	46	25	<2	2.2	143	<2	<2
Rb	1206	1086	384	36	33	62	37	29
Sr	1248	1532	1277	509	1021	764	589	426
Y	243	228	83	<2	<2	<2	11	10
Zr	1111	871	296	38	44	64	43	32
Nb	137	122	44	<2	<2	<2	<2	<2
Mo	<2	<2	<2	<2	<2	<2	12	<2
Sb	133	245	246	626	965	897	393	738
Cs	73	65	25	<2	<2	<2	<2	<2
Ba	4368	3949	1555	806	829	1358	9778	1089
Pb	277	247	142	10	70	157	113	46
Th	124	121	42	<2	<2	<2	<2	<2
U	41	38	16	<2	<2	<2	<2	<2
REE	1724	1562	588	68	67	130	71	66

Table 3. *PM_{10} levels and major element oxide and trace element concentrations in the Pnioweck mine from the Upper Silesian Coal Basin. Zone a) Roadway drivage technique (exhaust air from roadway face PW-1, seam 358/16). Zone b) Shearer cutting – longwall advance at the T-junction (exhaust air from longwall face B-4, seam 404/2). Zone c) Roadway drivage technique (exhaust air from roadway face seam K-9, seam 363 362/3).*

Zone	a	a	a	b	b	b	b	c	c	c	c	c
Activity distance	60 m	120 m	180 m	0 m	50 m	100 m	150 m	0 m	50 m	100 m	150 m	200 m
PM_{10} (µg/m³)	4669	4602	5975	10544	11464	10325	9843	24343	10474	17480	17710	13405
Sampling minutes	96	93	85	125	125	120	115	105	103	70	60	83
	µg/m³	**µg/m³**	**µg/m³**	**µg/m³**	**µg/m³**	**µg/m³**	**µg/m³**	**µg/m³**	**µg/m³**	**µg/m³**	**µg/m³**	**µg/m³**
Coal	1794	1721	2193	2346	2136	2975	3145	9245	5919	7052	7589	6329
SiO_2	809	783	1013	566	534	834	861	1969	1247	1493	1603	1317
Al_2O_3	539	522	675	377	356	556	574	1312	831	995	1068	878
CaO	194	154	168	230	197	156	187	243	164	182	179	177
Fe_2O_3	184	186	250	68	70	111	106	353	212	266	294	239
K_2O	79	75	99	84	44	68	72	179	109	138	148	119
MgO	41	35	56	18	17	19	27	81	49	51	62	57
Na_2O	50	56	62	38	40	30	48	71	66	74	89	77
S	44	49	46	49	44	41	41	98	80	88	98	86
TiO_2	27	27	34	25	22	29	34	61	37	44	46	40
	ng/m³	**ng/m³**	**ng/m³**	**ng/m³**	**ng/m³**	**ng/m³**	**ng/m³**	**ng/m³**	**ng/m³**	**ng/m³**	**ng/m³**	**ng/m³**
Li	264	266	350	238	221	335	318	859	607	695	699	672
Sc	48	47	61	38	37	53	52	136	79	102	104	82
V	405	410	509	572	525	554	559	1307	827	974	995	822
Cr	372	351	597	436	359	414	441	957	605	710	770	619
Mn	2012	2098	3036	483	471	780	752	3654	1997	2555	2827	2262
Co	57	55	74	92	89	75	80	169	107	126	136	111
Ni	235	69	316	288	172	205	197	542	348	382	416	305
Cu	125	10	1104	178	70	115	149	295	178	176	82	101
Zn	1187	828	1389	1136	321	268	706	2156	1801	2744	1845	2217
Ga	77	80	98	64	62	85	86	198	122	147	155	129
As	40	17	84	72	7.5	10	34	311	110	154	141	84
Rb	403	391	514	275	253	415	405	1066	635	779	818	677
Sr	660	597	726	718	694	683	754	1798	1223	1416	1509	1277
Y	73	70	96	53	54	69	73	204	130	149	161	130
Zr	373	343	493	188	189	265	489	816	479	547	591	480
Nb	46	44	57	45	42	53	65	121	72	82	88	72
Mo	<2	<2	<2	<2	<2	<2	<2	32	9	<2	<2	<2
Sb	296	265	305	340	358	258	318	888	634	606	584	682
Cs	41	42	51	34	31	48	45	104	67	79	86	69
Ba	1816	1765	2354	1977	1961	2196	2243	5695	3489	4064	4239	3590
Pb	116	148	291	240	109	99	145	232	140	141	184	125
Th	43	42	46	25	27	36	56	101	64	71	80	65
U	15	<2	19	<2	<2	<2	<2	42	27	32	35	13
REE	609	562	799	415	404	576	586	1537	941	1130	1131	959

Table 4. *PM_{10} levels and major element oxide and trace element concentrations in different zones of Marcel (M) and Bielszowice (BL) mines from the Upper Silesian Coal Basin. M zone a: Shearer cutting – longwall advance at the T-junction (exhaust air from longwall face W-7, seam 505); M zone b): Roadway drivage technique (exhaust air from roadway face C3, seam 507); and BL: Roadway drivage technique (exhaust air from roadway face 4az, seam 510wd).*

Mine-Zone	M-a	M-a	M-a	M-b	M-b	M-b	M-b	BL	BL	BL
Location	20 m	70 m	120 m	10 m	40 m	60 m	80 m	15 m	40 m	60 m
Concentration ($\mu g/m^3$)	9590	8300	8255	12181	12960	12505	12242	6116	5627	3320
Sampling minutes	160	150	140	105	100	95	95	155	150	140
	µg/m³	**µg/m³**	**µg/m³**	**µg/m³**	**µg/m³**	**µg/m³**	**µg/m³**	**µg/m³**	**µg/m³**	**µg/m³**
Coal	2018	1788	1814	4514	4812	4347	4678	1757	3492	1214
SiO_2	450	396	398	1502	1625	1440	1548	425	853	811
Al_2O_3	300	264	265	1001	1083	960	1032	283	569	541
CaO	153	128	124	221	230	226	264	132	213	192
Fe_2O_3	105	100	107	344	339	325	337	65	134	128
K_2O	29	30	28	111	114	103	110	28	52	50
MgO	30	26	25	74	80	72	79	11	34	31
Na_2O	59	53	58	24	26	31	29	6.1	17	13
S	64	56	64	20	20	20	21	<2	20	21
TiO_2	13	12	12	42	45	40	43	16	29	28
	ng/m³	**ng/m³**	**ng/m³**	**ng/m³**	**ng/m³**	**ng/m³**	**ng/m³**	**ng/m³**	**ng/m³**	**ng/m³**
Li	91	81	64	495	420	310	399	119	187	156
Sc	24	19	20	87	87	80	86	22	45	39
V	196	177	176	648	670	593	642	194	302	285
Cr	229	225	214	625	684	595	622	97	306	277
Mn	951	927	946	2548	2544	2373	2544	598	1154	1082
Co	31	27	26	82	79	74	80	59	126	118
Ni	132	130	222	263	259	245	247	11	150	114
Cu	96	640	108	572	629	573	520	<2	147	148
Zn	4584	4817	4600	3482	3497	3211	3625	478	1248	1101
Ga	43	39	41	128	144	120	130	40	76	70
As	33	100	52	34	48.7	39	38	25	161	62
Rb	171	150	151	569	593	525	570	117	212	202
Sr	675	550	534	896	941	896	911	346	602	548
Y	46	41	43	113	125	110	119	33	53	49
Zr	142	139	128	499	533	463	503	118	252	248
Nb	22	21	20	65	71	62	67	22	42	39
Mo	17	21	17	<2	<2	<2	<2	<2	<2	<2
Sb	2292	2030	2361	1539	1311	1279	1467	204	616	611
Cs	24	21	21	71	75	65	71	<2	15	14
Ba	1477	1302	1301	4011	4037	4022	3458	917	1400	1320
Pb	67	164	57	114	132	97	104	7.3	85	86
Th	21	21	18	50	58	53	55	24	38	37
U	16	14	14	32	33	30	32	<2	17	15
REE	310	269	270	897	962	861	912	371	625	592

In the case of the USCB mines, most elements in the Knurów mine show lower concentrations in the PM_{10} samples compared to RDD_4, with the exception of Ti, V, Mn, Cr, Co, Mg, Ca and REE in some specific locations. The Murcki-Staszic mine also showed most elements to be enriched in the RDD_4 samples, except for Sb, Na, and S with higher concentrations in the PM_{10} samples in all locations (1.7 to 4.0x for Sb, 1.4 to 2.8x for Na and 1.7 to 4.0x for S). PM_{10}/RDD_4 ratios in the Pniowek mine zone were normally between 1.0 to 2.0, with the exception of Ba, Sr, Ca, Sb and Co that had a ratio <1.0, and S, Mn and Na with ratios >2.0 (1.7 to 2.4, 2.3 to 2.8, 3.3 to 3.9, respectively). In zone 'b', all PM_{10}/RDD_4 ratios were below or close to 1 and in zone 'c' Ni, Cu, Zn, As, Sr Mo, Pb, U and Ca concentrations were lower in the PM_{10} than RDD_4.

In the Marcel mine zone 'a', only Zn (3.9 to 4.7), Sb (6.9 to 8.2) and Na (4.4 to 5.0) were markedly higher in the PM_{10} than RDD_4, whereas Li, V, Cr, Mn, Cu, As, Sr, Y, Mo and Pb were enriched in the RDD_4 samples. In contrast, in Marcel mine zone 'b', a large number of elements such as Li, Sc, Ti, Ga Rb, Zr, Nb, Cs, Ba, Al, K and Sb, show PM_{10}/RDD_4 ratios higher than 2.5, especially in the case of Sb which had ratios of 3.5 to 4.4. Finally, in Bielszowice, most elements showed higher concentrations in the PM_{10} samples compared to their respective RDD_4 sample, with the exception of Ca, Mg, Na, Sr and Pb.

In summary, some elements such as Sb, Zn, Mn, Na, and S showed elevated concentrations in PM_{10} samples compared with their respective RDD_4. Firstly, maybe all particle size of these elements are coarser, for this reason their concentrations would be higher in PM_{10}. Moreover, the presence of airborne Sb, Zn and Mn could be directly related to wear in machinery used in the underground mines. Amato et al. 2009a; 2009b, among others, show Sb, Mn and Zn in atmospheric PM from abrasion sources (i.e. brake pads or tyres in vehicles) have generally a coarser size ($PM_{2.5-10}$) than resuspension. If this is the case in our studies (machinery wear sources), higher PM_{10} than DD_4 levels might be expected for them. On the other hand, Na and S are directly related to coal handling activities because these elements are coming from their organic matter. Furthermore, a multi regression analysis was performed to correlate average S content in PM_{10} with S in parent coal from each coal mine. The high correlation ($R^2 = 0.98$, $P = 0.0001$) indicates that S emissions related to PM_{10} ambient concentrations in the underground coal mine are directly related to coal handling and manipulation (drilling, extraction, transportation).

5. Conclusions

The analysis of the particle size distribution (PSD) of deposited dust (DD) finer than 500 µm (DD_{500}) in underground mines confirms the need to wet airborne coal dust and DD. In the Velenje Coal Basin (VCB) underground mine, DD_{500} is wetted which reduces the load of respirable DD (RDD), and accordingly the potential for miners to inhale coal dusts and for coal dust explosions. In contrast, in the Upper Silesian Coal Basin (USCB) underground mines, the combination of low moisture in the DD_{500} and a high ash yield doubles the relative load of RDD in DD_{500} when compared with VCB.

The geochemical composition of aged (collected over long time periods onto existing surfaces; sampled with a brush) and fresh (deposited on PVC trays over short time periods) DD coal samples from the same locations did not show major differences with the exception of Sb which was enriched in the aged DD, probably due to a relatively higher component of dust from brake-wear.

A comparison of geochemical compositions of parent coals and DD_{500} revealed very important differences, with relatively high levels of most major and trace elements in the DD_{500} for the VCB underground mine, especially for Ni, Zr and Sb. This can be attributed to an increased contribution to DD_{500} from particulate matter (PM) emitted from the wear of mine machinery (e.g. drills, excavators and belts, coal gangue, and from coal fly ash (called Malta D) and carbonate 'rock dust' (called Calplex) commonly used as backfill and fire hazard reduction respectively in this mine. The chemical composition of RDD (deposited dust finer than 4 and 2.5 µm, RDD_4 and $RDD_{2.5}$) samples extracted in the laboratory from DD_{500} reveals frequent

enrichments of metals and metalloids in the RDD. In the VCB mine these include Ba, Se, Zn, Pb, As, Cr, Mo, and especially Ni, Sn, Cu, and Sb.

Similar results were obtained for the USCB mines, where DD_{500} samples were also markedly enriched in Ca and K compared with parent coals. The enrichment in Ca is attributed to dusts from concrete gunite used behind mine supports, whereas K is attributed to dust contributions from coal gangue. An enrichment in Rb, Zr, Sb, Zn, Cr, V, Ti, Mn and Sn in the DD_{500} compared with the parent coal was evidenced. In contrast, S contents were higher in the parent coals probably due to the major association of S with the coal matrix (reduced in DD with respect the coal seam).

The USCB mines also showed a marked enrichment in metals and metalloids in RDD_4 compared with DD_{500}, especially for Cu, Sn, Zn, As and Sb (>1.5 fold higher than in the DD_{500}). In contrast, Mn was reduced in the RDD_4 samples compared to DD_{500} in all samples from both VCB and USCB mines.

According to the above results, we conclude that the geochemical composition of the RDD is markedly different to that of DD and the parent coals, and that the method we have used allows extracting RDD from DD sampling for further PSD, chemical and mineralogical analyses.

Airborne PM_{10} concentrations were below established occupational exposure limits. Long-wall shearer excavations produce lower PM coal dust concentrations than roadway drivage operations. Higher PM_{10} concentrations were observed in some USCB underground mine sections related to different mechanical tasks being conducted in the mines. However, these concentration peaks were present only transiently (typically over 80-135 minutes) and thus are not directly applicable to the 8h period legislated for occupation exposure.

Concentrations of metals and metalloids in PM_{10} were normally lower than in the RDD_4 samples, with the exception of Sb, Zn, Mn, Na, and S in some mines, that they could be present in the coarser particles. The presence of Sb, Zn, and Mn in PM_{10} may be attributed to machine wear. In contrast, S and Na may be attributed to the organic matter of coal. Moreover, S concentrations are directly correlated with coal handling manipulation in the underground coal mines ($R^2 = 0.98$, $P < 0.05$).

Considering the possible health implications of inhaling some of these metals and metalloids, further studies on the oxidative potential and cellular toxicology of coal dust samples should be carried out (Birch and Scollen 2003; Moreno et al. 2008; Colinet et al. 2010). Concentrations of such metals, and of coal dusts in general, should be kept at a minimum when working in underground mines. The studies carried out within the ROCD project aim to be the seed of future activities necessary to achieve better working conditions in this environment, especially given that global coal production may grow over the next few decades (BP 2020).

Acknowledgements

This work forms part of the 'Reducing risks from Occupational exposure to Coal Dust" (ROCD) project which is supported by the European Commission Research Fund for Coal and Steel; Grant Agreement Number – 754205 and the Generalitat de Catalunya (SGR41). Thanks to all partners in the ROCD project for their assistance in this study; see partner list at: http://emps.exeter.ac.uk/csm/rocd/. IDAEA-CSIC is a Centre of Excellence Severo Ochoa

(Spanish Ministry of Science and Innovation, Project CEX2018-000794-S). Malvern Mastersizer Scirocco 2000 extension measurements were performed at the ICTS NANBIOSIS by the Nanostructured Liquids Unit (U12) of the CIBER in Bioengineering, Biomaterials & Nanomedicine (CIBER-BBN), located at the IQAC-CSIC (Barcelona, Spain).

References

Ajrash MJ, Zanganeh J, Moghtaderi B (2017) The effects of coal dust concentrations and particle sizes on the minimum auto-ignition temperature of a coal dust cloud. Fire Mater 41:908–915. https://doi.org/10.1002/fam.2437

Amato F, Pandolfi M, Escrig A, et al (2009a) Quantifying road dust resuspension in urban environment by Multilinear Engine: A comparison with PMF2. Atmos Environ 43:2770–2780. https://doi.org/10.1016/j.atmosenv.2009.02.039

Amato F, Querol X, Alastuey A, et al (2009b) Evaluating urban PM10 pollution benefit induced by street cleaning activities. Atmos Environ 43:4472–4480. https://doi.org/10.1016/j.atmosenv.2009.06.037

Azam S, Mishra DP, Wang X, et al (2019) Synergistic effect of surfactant compounding on improving dust suppression in a coal mine in Erdos, China. Process Saf Environ Prot 344:35–43. https://doi.org/10.1016/j.powtec.2018.12.061

Basic Legal Act in Poland (2010) OCCUPATIONAL EXPOSURE LIMITS FOR AIRBORNE TOXIC SUBSTANCES. Basic Legal Act in Poland.

Birch GF, Scollen A (2003) Heavy metals in road dust, gully pots and parkland soils in a highly urbanised sub-catchment of Port Jackson, Australia. Aust J Soil Res 41:1329–1342. https://doi.org/10.1071/SR02147

BP (2020) bp Statistical Review of World Energy 2020

Brezigar A (1987) Geologic setting of the Pre-Pliocene basement of the Velenje depression and its surroundings. Geologija 30:31–65

Caballero-Gallardo K, Olivero-Verbel J (2016) Mice housed on coal dust-contaminated sand: A model to evaluate the impacts of coal mining on health. Toxicol Appl Pharmacol 294:11–20. https://doi.org/10.1016/j.taap.2016.01.009

Cohen RAC, Patel A, Green FHY (2008) Lung disease caused by exposure to coal mine and silica dust. Semin. Respir. Crit. Care Med. 29:651–661

Colinet JF;, James P. R, Jeffrey M. L, et al (2010) Best Practices for Dust Control in Coal Mining. Centers Dis Control Prev Natl Inst Occup Saf Heal 01:17–36

Dalal NARS, Newman J, Pack D, et al (1995) Original Contribution. 18:11–20

EPA (1995) Reducing Methane Emissions from Coal Mines in Poland : A Handbook for Expanding. Atmos Pollut Prev Div US Environ Prot AGENCY

Fan L, Liu S (2021) Respirable nano-particulate generations and their pathogenesis in mining workplaces: a review. Int J Coal Sci Technol 1–20. https://doi.org/10.1007/s40789-021-00412-w

Fan T, Zhou G, Wang J (2018) Preparation and characterization of a wetting-agglomeration-based hybrid coal dust suppressant. Process Saf Environ Prot 113:282–291. https://doi.org/10.1016/j.psep.2017.10.023

Fang X, Yuan L, Jiang B, et al (2020) Effect of water–fog particle size on dust fall efficiency of mechanized excavation face in coal mines. J Clean Prod 254:120146. https://doi.org/10.1016/j.jclepro.2020.120146

Hu S, Gao Y, Feng G, et al (2021) Experimental study of the dust-removal performance of a wet scrubber. Int J Coal Sci Technol 8:228–239. https://doi.org/10.1007/s40789-021-00410-y

Jiang H, Luo Y (2021) Development of a roof bolter drilling control process to reduce the generation of respirable dust. Int J Coal Sci Technol 8:199–204. https://doi.org/10.1007/s40789-021-00413-9

Jiang L, Sheng C (2018) Correlation of the Sub-micrometer Ash Yield from Pulverized Coal Combustion with Coal Ash Composition. Energy and Fuels 32:9961–9970. https://doi.org/10.1021/acs.energyfuels.8b02098

Jin L, Liu J, Guo J, et al (2021) Physicochemical factors affecting the wettability of copper mine blasting dust. Int J Coal Sci Technol 8:265–273. https://doi.org/10.1007/s40789-021-00411-x

Johann-Essex V, Keles C, Rezaee M, et al (2017) Respirable coal mine dust characteristics in samples collected in central and northern Appalachia. Int J Coal Geol 182:85–93. https://doi.org/10.1016/j.coal.2017.09.010

Jonek-Kowalska I (2018) How do turbulent sectoral conditions sector influence the value of coal mining enterprises? Perspectives from the Central-Eastern Europe coal mining industry. Resour Policy 55:103–112. https://doi.org/10.1016/j.resourpol.2017.11.003

Kedzior S (2015) Methane contents and coal-rank variability in the Upper Silesian Coal Basin, Poland. Int J Coal Geol 139:152–164. https://doi.org/10.1016/j.coal.2014.09.009

Kędzior S (2009) Accumulation of coal-bed methane in the south-west part of the Upper Silesian Coal Basin (southern Poland). Int J Coal Geol 80:20–34. https://doi.org/10.1016/j.coal.2009.08.003

Kędzior S (2019) Distribution of methane contents and coal rank in the profiles of deep boreholes in the Upper Silesian Coal Basin, Poland. Int J Coal Geol 202:190–208. https://doi.org/10.1016/j.coal.2018.12.010

Ketris MP, Yudovich YE (2009) Estimations of Clarkes for Carbonaceous biolithes: World averages for trace element contents in black shales and coals. Int J Coal Geol 78:135–148. https://doi.org/10.1016/j.coal.2009.01.002

Kotarba MJ (2001) Composition and origin of coalbed gases in the Upper Silesian and Lublin basins, Poland. Org

Geochem 32:163–180. https://doi.org/10.1016/S0146-6380(00)00134-0
Kotas A, Koniela Z, Wojcik A, et al (1994) Coal-bed methane potential of the Upper Silesian Coal Basin, Poland. Coal-bed methane potential Up Silesian Coal Basin, Pol 142:
Kotas A, Porzycki J (1984) Major features of Carboniferous coal basins in Poland. Przegląd Geol 32:268–280
Kuai N, Huang W, Yuan J, et al (2012) Experimental investigations of coal dust-inertant mixture explosion behaviors. Procedia Eng 26:1337–1345. https://doi.org/10.1016/j.proeng.2011.11.2309
Küçük A, Kadioğlu Y, Gülaboğlu MŞ (2003) A study of spontaneous combustion characteristics of a Turkish lignite: Particle size, moisture of coal, humidity of air. Combust Flame 133:255–261. https://doi.org/10.1016/S0010-2180(02)00553-9
Kusiak MA, Kedzior A, Paszkowski M, et al (2006) Provenance implications of Th-U-Pb electron microprobe ages from detrital monazite in the Carboniferous Upper Silesia Coal Basin, Poland. Lithos 88:56–71. https://doi.org/10.1016/j.lithos.2005.08.004
Leonard R, Zulfikar R, Stansbury R (2020) Coal mining and lung disease in the 21st century. Curr Opin Pulm Med 26:135–141. https://doi.org/10.1097/MCP.0000000000000653
Li Q, Lin B, Zhao S, Dai H (2013) Surface physical properties and its effects on the wetting behaviors of respirable coal mine dust. Powder Technol 233:137–145. https://doi.org/10.1016/j.powtec.2012.08.023
Liu G, Vassilev S V., Gao L, et al (2005) Mineral and chemical composition and some trace element contents in coals and coal ashes from Huaibei coal field, China. Energy Convers Manag. https://doi.org/10.1016/j.enconman.2004.11.002
Liu J, Wang S, Jin L, et al (2021) Water-retaining properties of NCZ composite dust suppressant and its wetting ability to hydrophobic coal dust. Int J Coal Sci Technol 8:240–247. https://doi.org/10.1007/s40789-020-00385-2
Markic M, Sachsenhofer RF (1997) Petrographic composition and depositional environments of the Pliocene Velenje lignite seam (Slovenia). Int J Coal Geol 33:229–254. https://doi.org/10.1016/S0166-5162(96)00043-2
Markič M, Sachsenhofer RF (2010) THE VELENJE LIGNITE Its Petrology and Genesis
Marts JA, Gilmore RC, Brune JF, et al (2015) Optimizing nitrogen injection for progessively sealed panels. 2015 SME Annu Conf Expo C 117th Natl West Min Conf – Min Navig Glob Waters 447–450
McPherson MJ (1993) Subsurface ventilation systems. In: Subsurface Ventilation and Environmental Engineering. Springer Netherlands, pp 91–133
Moreno T, Amato F, Querol X, et al (2008) Trace element fractionation processes in resuspended mineral aerosols extracted from Australian continental surface materials. Soil Res 46:128. https://doi.org/10.1071/SR07121
Moreno T, Trechera P, Querol X, et al (2019) Trace element fractionation between PM10 and PM2.5 in coal mine dust: Implications for occupational respiratory health. Int J Coal Geol 203:52–59. https://doi.org/10.1016/j.coal.2019.01.006
Palmer AD, Cheng M, Goulet JC, Furimsky E (1990) Relation between particle size and properties of some bituminous coals. Fuel 69:183–188. https://doi.org/10.1016/0016-2361(90)90171-L
Pedroso-Fidelis G dos S, Farias HR, Mastella GA, et al (2020) Pulmonary oxidative stress in wild bats exposed to coal dust: A model to evaluate the impact of coal mining on health. Ecotoxicol Environ Saf 191:. https://doi.org/10.1016/j.ecoenv.2020.110211
Perret JL, Plush B, Lachapelle P, et al (2017) Coal mine dust lung disease in the modern era. Respirology 22:662–670. https://doi.org/10.1111/resp.13034
Querol X, Fernandez Turiel JL, Lopez Soler A, Duran ME (1992) Trace elements in high-S subbituminous coals from the teruel Mining District, northeast Spain. Appl Geochemistry 7:547–561. https://doi.org/10.1016/0883-2927(92)90070-J
Querol X, Whateley MKG, Fernández-Turiel JL, Tuncali E (1997) Geological controls on the mineralogy and geochemistry of the Beypazari lignite, central Anatolia, Turkey. Int J Coal Geol 33:255–271. https://doi.org/10.1016/S0166-5162(96)00044-4
Reed WR, Shahan MR, Zheng Y, Mazzella A (2021) Laboratory results of foam application testing for longwall shield dust control in a simulated environment. Int J Coal Sci Technol 8:217–227. https://doi.org/10.1007/s40789-021-00414-8
Reid DC, Hainsworth DW, Ralston JC, McPhee RJ (2006) Shearer guidance: A major advance in longwall mining. Springer Tracts Adv Robot 24:469–476. https://doi.org/10.1007/10991459_45
Smith A 6, Diamond WP, Mucho TP, Organiscak A (1994) Bleederless Ventilation Systems as a Spontaneous Combustion Control Measure in U.S. Coal Mines UNITED STATES DEPARTMENT OF THE INTERIOR
Song Z, Konietzky H, Herbst M (2020) Drawing mechanism of fractured top coal in longwall top coal caving. Int J Rock Mech Min Sci 130:104329. https://doi.org/10.1016/j.ijrmms.2020.104329
Sperazza M, Moore JN, Hendrix MS (2004) High-Resolution Particle Size Analysis of Naturally Occurring Very Fine-Grained Sediment Through Laser Diffractometry. J Sediment Res 74:736–743. https://doi.org/10.1306/031104740736
Stępniewska Z, Pytlak A, Kuźniar A (2014) Distribution of the methanotrophic bacteria in the Western part of the Upper Silesian Coal Basin (Borynia-Zofiówka and Budryk coal mines). Int J Coal Geol 130:70–78. https://doi.org/10.1016/j.coal.2014.05.003
Sunkpal M, Roghanchi P, Kocsis KC (2017) A Method to Protect Mine Workers in Hot and Humid Environments. Saf Health Work 9:149–158. https://doi.org/10.1016/j.shaw.2017.06.011

Swaine DJ (1990) Trace elements in coal. Butterworth
Szkudlarek Z, Janas S (2021) Active protection of work area against explosion of dust–gas mixture. Int J Coal Sci Technol 1–11. https://doi.org/10.1007/s40789-020-00387-0
Trechera P, Moreno T, Córdoba P, et al (2020) Mineralogy, geochemistry and toxicity of size-segregated respirable deposited dust in underground coal mines. J Hazard Mater 399:122935. https://doi.org/10.1016/j.jhazmat.2020.122935
Trechera P, Moreno T, Córdoba P, et al (2021) Comprehensive evaluation of potential coal mine dust emissions in an open-pit coal mine in Northwest China. Int J Coal Geol 235:103677. https://doi.org/10.1016/j.coal.2021.103677
Vaněk M, Bora P, Maruszewska EW, Kašparková A (2017) Benchmarking of mining companies extracting hard coal in the Upper Silesian Coal Basin. Resour Policy 53:378–383. https://doi.org/10.1016/j.resourpol.2017.07.010
Więckol-Ryk A, Krzemień A, Sánchez Lasheras F (2018) Assessing the breathing resistance of filtering-facepiece respirators in Polish coal mines: A survey and laboratory study. Int J Ind Ergon 68:101–109. https://doi.org/10.1016/j.ergon.2018.07.001
Woskoboenko F (1988) Explosibility of Victorian brown coal dust. Fuel 67:1062–1068. https://doi.org/10.1016/0016-2361(88)90371-7
Wu Q, Han L, Xu M, et al (2019) Effects of occupational exposure to dust on chest radiograph, pulmonary function, blood pressure and electrocardiogram among coal miners in an eastern province, China. BMC Public Health 19:1229. https://doi.org/10.1186/s12889-019-7568-5
Yuan J, Wei W, Huang W, et al (2014) Experimental investigations on the roles of moisture in coal dust explosion. J Taiwan Inst Chem Eng 45:2325–2333. https://doi.org/10.1016/j.jtice.2014.05.022
Zhang Q, Chen X, Wang H, Xu C (2021) Exploration on molecular dynamics simulation methods of microscopic wetting process for coal dust. Int J Coal Sci Technol 8:205–216. https://doi.org/10.1007/s40789-021-00415-7
Zhang T, Jing D, Ge S, et al (2020) Numerical simulation of the dimensional transformation of atomization in a supersonic aerodynamic atomization dust-removing nozzle based on transonic speed compressible flow. Int J Coal Sci Technol 7:597–610. https://doi.org/10.1007/s40789-020-00314-3

4.3. Article #3

Mineralogy, geochemistry and toxicity of size-segregated respirable deposited dust in underground coal mines

Authors:

Pedro Trechera[a, b], Teresa Moreno[a], Patricia Córdoba[a], Natalia Moreno[a], Xinguo Zhuang[c], Baoqing Li[c], Jing Li[c], Yunfei Shangguan[c], Konrad Kandler[d], Ana Oliete Dominguez[e], Frank Kelly[e], Xavier Querol[a,c]

a) Institute of Environmental Assessment and Water Research (IDAEA-CSIC), 08034 Barcelona, Spain.
b) Department of Natural Resources and Environment, Industrial and TIC Engineering (EMIT-UPC), 08242 Manresa, Spain.
c) Key Laboratory of Tectonics and Petroleum Resources, China University of Geosciences, Ministry of Education, Wuhan 430074, China.
d) Institute of Applied Geosciences, Technical University Darmstadt, 64287 Darmstadt, Germany.
e) MRC-PHE Centre for Environment and Health, King's College London, London SE1 9NH, UK.

Published in:

Journal of Hazardous Materials, 399, 122935

DOI: 10.1016/j.jhazmat.2020.122935

Accepted date:

Accepted 11 May 2020 (Open access)

Impact factor/Quartile

10.588/Q1

Journal of Hazardous Materials 399 (2020) 122935

Contents lists available at ScienceDirect

Journal of Hazardous Materials

journal homepage: www.elsevier.com/locate/jhazmat

Mineralogy, geochemistry and toxicity of size-segregated respirable deposited dust in underground coal mines

Pedro Trechera[a,b,*], Teresa Moreno[a], Patricia Córdoba[a], Natalia Moreno[a], Xinguo Zhuang[c], Baoqing Li[c], Jing Li[c], Yunfei Shangguan[c], Konrad Kandler[d], Ana Oliete Dominguez[e], Frank Kelly[e], Xavier Querol[a,c]

[a] Institute of Environmental Assessment and Water Research (IDAEA-CSIC), 08034 Barcelona, Spain
[b] Department of Natural Resources and Environment, Industrial and TIC Engineering (EMIT-UPC), 08242, Manresa, Spain
[c] Key Laboratory of Tectonics and Petroleum Resources, China University of Geosciences, Ministry of Education, Wuhan, 430074, China
[d] Institute of Applied Geosciences, Technical University Darmstadt, 64287, Darmstadt, Germany
[e] MRC-PHE Centre for Environment and Health, King's College London, London, SE1 9NH, UK

GRAPHICAL ABSTRACT

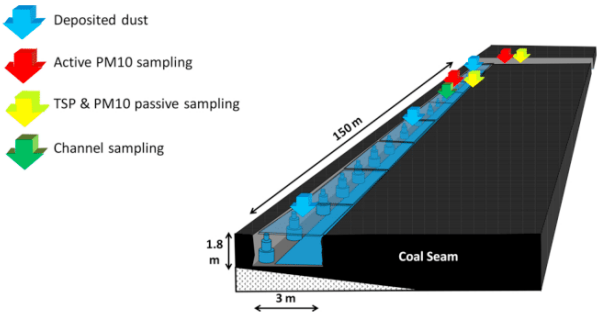

ARTICLE INFO

Editor: Rinklebe Jörg

Keywords:
Coal mining dust
Occupational exposure
Toxicology
Chemistry
China

ABSTRACT

We focus on a comparison of the geochemistry and mineralogy patterns found in coal, deposited dust (DD), respirable deposited dust (RDD) and inhalable suspended dust (PM10) from a number of underground mines located in China, with an emphasis on potential occupational health relevance. After obtaining the RDD from DD, a toxicological analysis (oxidative potential, OP) was carried out and compared with their geochemical patterns. The results demonstrate: i) a dependence of RDD/DD on the moisture content for high rank coals that does not exist for low rank coals; ii) RDD enrichment in a number of minerals and/or elements related to the parent coal, the wear on mining machinery, lime gunited walls and acid mine drainage; and iii) the geochemical patterns of RDD obtained from DD can be compared with PM10 with relatively good agreement, demonstrating that the characterization of DD and RDD can be used as a proxy to help evaluate the geochemical patterns of suspended PM10. With regards to the toxicological properties of RDD, the Fe content and other by-products of pyrite oxidation, as well as that of anatase, along with Si, Mn and Ba, and particle size (among others), were highly correlated with Ascorbic Acid and/or Glutathione OP.

* Corresponding author.
E-mail address: pedro.trechera@idaea.csic.es (P. Trechera).

https://doi.org/10.1016/j.jhazmat.2020.122935
Received 19 December 2019; Received in revised form 14 April 2020; Accepted 11 May 2020
Available online 25 May 2020

1. Introduction

Coal mining and its associated environmental impact, including exposure to coal mine dust, remain high on the list of global health issues to be ameliorated. The main impacts of coal mining activities result from emissions of atmospheric pollutants, with implications for both climate change and air quality. While the climatic effects arise from the increased emissions of greenhouse pollutants associated with mining activities and deforestation, the problems linked to air quality are largely associated with the local dust emissions created by mining work, waste disposal, coal/waste fires, the transport and handling of coal and the increases in population and industry around mining areas (Aneja et al., 2012; Duarte et al., 2019; Fabiano et al., 2014; Ghose and Majee, 2007; Hendryx et al., 2008; Patra et al., 2016; Petavratzi et al., 2005; Rout et al., 2014; Tang et al., 2017; Visser, 1992).

In underground coal mining, dust emissions are much higher in the working front (WF) galleries, where coal is being worked via shearers, drilling and other mining operations, despite the ventilation systems and the common use of water spraying (Colinet et al., 2010; Li et al., 2019; Moreno et al., 2019). Dust levels decrease from the WFs to the coal extraction galleries (with continuous belts) and access galleries (usually much better ventilated). Other sources of underground dust include the resuspension of deposited coal dust and wear on machinery (mining machinery, coal and gangue extraction belts and worker transport systems) during ventilation. Furthermore, on the surface, waste disposal, coal milling and handling, and the transport of coal and gangue can be significant sources of dust if containment measures are not properly implemented.

In open pit coal mines, many of the same sources of coal mine dust are present; however, compared to underground coal mines, there is higher dispersion, which is commonly offset by much higher volumes of coal and gangue (and accordingly higher emissions) and the large number of heavy trucks that enhance widespread resuspension and contribute exhaust emissions. Another air quality hazard associated with mining is occasional coal or waste fires, which can occur in open pits, underground mines and waste dumps (Haibin and Zhenling, 2010; Pallarés et al., 2017; Querol et al., 2008) and produce significant amounts of associated PM and gaseous pollutant emissions (Jiang et al., 2014; Kim, 2004; O'Keefe et al., 2010; Querol et al., 2011).

The potential impact of coal and gangue dust on human health and ecosystems can vary widely according to the grain size and mineralogical and chemical composition (Borm, 1997; Li et al., 2017; Sarver et al., 2019) of the particulates being inhaled. Obviously, the finer the dust, the deeper it can penetrate into the respiratory system, with the $< 4\,\mu m$ dust fraction accepted widely as the respirable dust fraction (Brown et al., 2013; Gustafsson et al., 2018; Johann-Essex et al., 2017). The higher this fraction is in the coal dust, especially if rich in crystalline silica and/or metals, the higher the potential cell inflammation and consequent health damage (Brodny and Tutak, 2018; Castranova, 2000; Cohen et al., 2008; Ercal et al., 2001; Ghio and Madden, 2017; Niosh, 2002; Schins and Borm, 1999; Valko et al., 2016).

Research from last decades on the toxicology of air pollution has identified oxidative stress as a unifying feature underlying the toxic actions of the air pollutants that cause concern (Kelly, 2003). Thus, it is now well accepted that pulmonary inflammation caused by exposure to air pollution is induced via oxidant signalling pathways. Classical studies on residual oil fly ash and urban PM evidenced that a high concentration of metals, such as, Fe, Ni, and V, can lead to aldehyde generation, pulmonary inflammation and oxidative stress, which correlates with the Fe content of these particles (Costa and Dreher, 1997; Kadiiska et al., 1997). Newer studies on Fe-ore PM also point to the high impact of Fe in the oxidative potential (OP) of PM (Soltani et al., 2018), with exceptions, such as subway PM (Moreno et al., 2017). Thus, the mode of occurrence of Fe and other metals in PM also seems to have a large impact on the OP. Furthermore, organic pollutants, such as PAH, might contribute significantly to increasing this oxidative stress (Chuang et al. (2013) and Kelly (2003), among others).Although much has been written on the problem of worker exposure to coal dust, there remain few data on the mineralogy, chemistry and toxicology of inhalable-sized dust samples collected directly from inside mines. In this context, the purpose of this study is to characterize coal mine dust from diverse areas in four different underground coal mines located in Southwest, South and North China, with the aim of evaluating dust particle sizes, mineralogical and geochemical patterns and their potential impacts on health, as well as to identify source origins by combining geochemical, mineralogical and toxicological tools. We also investigate how dust deposited in coal mines can be used to predict the mineralogical and chemical patterns of respirable dust in the mine. We adopt a novel approach involving separating out the respirable component present in deposited dust and comparing compositional patterns in samples of total suspended ambient particles (TSP) and PM10 (Particulate Matter finer than 10 μm in diameter).

2. Methodology

2.1. Sampling

Fig. 1 and S1 to S4 and Tables 1 and 2 show the regional location, map of the mines and type and number of coal mine dust samples collected in an Anthracite North China (ANC), a Bituminous South China (BSC), a Bituminous South-West China (BWC) and a Sub-bituminous (SSC) underground mines. In the case of the ANC mine (Figs. 1 and S1), coal seam #2-1 (4.1 m thick), was being worked at the time of sampling. In the BSC mine (Figs. 1 and S2), coal seam #4-1 (1.2 m thick) was being worked, but the dust was collected in a WF that had been inactive for 2 years. In the case of the BWC mine (Figs. 1 and S3), coals seams #7 (1.8 m thick) and #11 (2.2 m thick) were being worked during our sampling campaign. Finally, in the case of the SSC mine (Figs. 1 and S4), coal seam D-3 (2.0 m thick) was being worked. In all cases, deposited dust (DD) was collected in different parts of each mine, and worked coal was also sampled by means of channel profile (CP) samples at the WF galleries in order to compare the chemical compositions of the dust and parent coal in the same WF.

The majority of samples analysed in this study consist of DD in different locations in the coal mines (Figs S1–S4). The sampling time was limited to around 4 – 6 h, although for logistic reasons this was reduced to just 1.5 h in the seam head face. Deposited dust was collected either in plastic trays (left for 1 – 2 hours in zones of high concentrations such as WF galleries) or, more commonly, using brushes, and later stored in plastic bags. In addition, in the BWC mine we collected underground ambient PM samples finer than 10 μm and in the

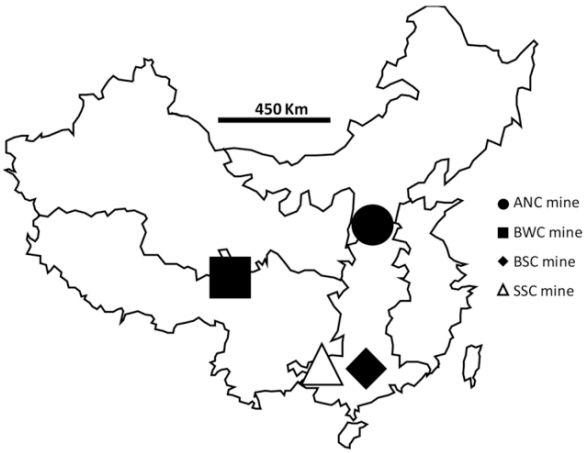

Fig. 1. Location of all the underground coal mines sampled in Democratic Republic of China.

Table 1
Samples of deposited dust on the ground (DD) and respirable deposited dust (RDD, < 4 µm) from the four underground mines. WF, Working front; GW, Gunited walls; FTW, Floor of train wagons.

Mine	Location	Type of sample
Bituminous South-West	GW #7	DD
Bituminous South-West	GW #7	DD
Bituminous South-West	GW #11	DD
Bituminous South-West	GW #11	DD
Bituminous South-West	1000 m WF #7	DD
Bituminous South-West	900 m WF #7	DD
Bituminous South-West	300 m WF #7	DD
Bituminous South-West	200 m WF #7	DD
Bituminous South-West	100 m WF #7	DD
Bituminous South-West	50 m WF #7	DD
Bituminous South-West	15 m WF #7	DD
Bituminous South-West	Workers rest #7	DD
Bituminous South-West	WF #7	DD
Bituminous South-West	WF #7	DD
Bituminous South-West	WF #11	DD
Bituminous South-West	WF #11	DD
Bituminous South-West	Wall drilling front #11	DD
Bituminous South-West	Wall drilling front #11	DD
Bituminous South-West	FTW	DD
Bituminous South-West	Coal mill	DD
Bituminous South-West	Coal mill	DD
Bituminous South-West	Coal gangue	DD
Bituminous South-West	Coal gangue	DD
Bituminous South-West	Production coal	DD
Bituminous South-West	GW #7	RDD
Bituminous South-West	300 m WF #7	RDD
Bituminous South-West	100 m WF #7	RDD
Bituminous South-West	50 m WF #7	RDD
Bituminous South-West	WF #7	RDD
Bituminous South-West	WF #11	RDD
Bituminous South-West	Floor train wagons	RDD
Subbituminous South	2000 m D-3	DD
Subbituminous South	100 m D-3	DD
Subbituminous South	25 m D-3	DD
Subbituminous South	50 m D-3	DD
Subbituminous South	WF D-3	DD
Subbituminous South	Coal belt	DD
Subbituminous South	Coal mill	DD
Subbituminous South	2000 m D-3	RDD
Subbituminous South	100 m D-3	RDD
Subbituminous South	WF D-3	RDD
Subbituminous South	Coal mill	RDD
Bituminous South	100 m WF #4-1	DD
Bituminous South	50 m WF #4-1	DD
Bituminous South	100 m WF #4-1	RDD
Bituminous South	50 m WF #4-1	RDD
Anthracite North	Air shaft #2-1	DD
Anthracite North	Air shaft #2-1	RDD
Anthracite North	Air shaft #2-1	RDD

10–200 µm range (PM10 and PM10 − 200, respectively), using two CIP-10 Thoracic (CIP-10T) instruments. This device is used for the evaluation of risks associated with the exposure to hazardous environments where batteries cannot be used, such as underground coal mines, and to collect ambient dust at a rate of 7 L/min. The CIP-10T allows the collection of both PM10 coal dust on polyurethane foams, with a coarser dust fraction being brushed into the impactor zone. The third sampling method, also conducted in the BWC mine, involved using standard electron microscopy aluminium stubs covered with copper foil, which was then covered with glue. These were distributed at different locations within the mine (Fig. S3) to obtain suspended dust samples via dry deposition for scanning electron microscopy purposes. Finally, coal samples were collected at the coal face as primary source materials to allow comparisons with the deposited airborne dust samples obtained elsewhere in the mine.

Table 2
Samples from channel profiles (CP) collected at the working fronts of the different mines, suspended PM10 and PM10-200 from the BWC mine, and of suspended dust (SD) and respirable deposited dust (RDD) for Scanning Electron Microscope (SEM).

Mine	Location	Type of sample
Bituminous South-West	1.8 m profile #7	CP
Bituminous South-West	2.2 m profile #11	CP
Subbituminous South	2.3 m profile D-3	CP
Bituminous South	1.2 m profile #4 − 1	CP
Anthracite North	4.1 m profile #2 − 1	CP
Bituminous South-West	Train station to WF #7	SD CIP PM10
Bituminous South-West	Train station to WF #11	SD CIP PM10
Bituminous South-West	Train station to WF #7	SD CIP PM10 − 200
Bituminous South-West	Train station to WF #11	SD CIP PM10 − 200
Bituminous South-West	WF #7	CP_SEM
Subbituminous South	WF D-3	CP_SEM
Bituminous South-West	WF#7	SD_SEM
Bituminous South-West	WF#11	SD_SEM
Bituminous South-West	Gallery #7	SD_SEM
Subbituminous South	Gallery D-3	RDD_SEM

2.2. Particle size

A total of 34 deposited dust samples and five CP samples belonging to the four underground coal mines in China were analysed in order to characterize the underground coal dust patterns and interpret composition and origin. All deposited dust samples were sieved at 500 µm (to obtain DD samples, or deposited dust < 500 µm). The respirable deposited dust (RDD) samples were separated from a selection of 16 bulk DD samples using a PM2.5 and PM10 separator device (Moreno et al., 2005) that allows the collection of samples on 47 mm polycarbonate filters (0.60 µm pore size).

Particle size distributions of both DD and RDD samples were obtained using a Malvern Mastersizer. For DD samples, a Scirocco 2000 unit was coupled to get the particle sizes in dry conditions. Samples moved along the Scirocco 2000 system on a tray as oscillation and air pressure forced them to scatter into individual grains, getting them ready for sizing via laser diffraction. RDD samples (with very low sample volumes) particle size distribution was obtained using a wet (water-Polyphosphate RDD suspension) HydroG 2000 coupled unit (Sperazza et al., 2004).

2.3. Mineralogical and morphological characterization

The mineralogical analyses of CP, DD and RDD samples were performed using a X-Ray Diffraction (XRD) Bruker D8 A25 Advance, θ-θ diffractometer with $CuK_{\alpha}1$ radiation, Bragg-Brentano geometry and a position-sensitive LynxEye detector. The diffractograms were obtained at 40 kV and 40 mA while scanning from 4° to 60° of 2θ, with a step size of 0.019° and a counting time of 0.1 s/step maintaining the sample's rotation (15/min). The crystalline phase identification was carried out using the EVA software package (Bruker), which uses the ICDD (International Centre for Diffraction Data) database. Semi-quantitative XRD analysis was performed via the method devised by Chung (1974) for the quantitative analysis of multi-component systems.

The scanning electron microscopes JEOL JSM-7001F and Quanta 400F ESEM with Oxford X-Max 150 EDX detector, both with secondary and backscattered electron detectors, at the University of Barcelona and Technical University of Darmstadt, respectively, were used to analyse samples prepared on copper-glue surfaces.

2.4. Proximate, ultimate and chemical characterization

Proximate and ultimate analyses of the CP and DD samples were performed using the ISO and ASTM recommendations (ISO-589, 1981; ISO-1171, 1976; ISO-562, 1974; ASTM D-3286, 1996). In order

Table 3
Size distribution and moisture (% air dried, ad) of all deposited dust (DD) samples in %wt (weight) and %v (volume). WF, Working front; GW, Gunited walls; FTW, Floor of train wagons. BWC, Bituminous South-West China; SSC, Subbituminous South China; BSC, Bituminous South China; and ANC, Anthracite North China.

Mine	Location	< 500 µm (%wt)	< 10 µm (%v)	< 4 µm (%v)	< 2.5 µm (%v)	M (%ad)
BWC	GW #7	80.62	23.30	13.07	7.96	0.87
BWC	GW #7	40.42	6.90	3.30	1.58	1.71
BWC	1000 m WF #7	48.05	11.97	4.67	2.22	0.74
BWC	GW #11	75.51	21.88	9.98	4.90	1.03
BWC	GW #11	89.00	26.86	13.55	7.51	1.03
BWC	1000 m WF #7	33.50	4.80	1.80	0.70	1.36
BWC	50 m WF #7	57.00	18.20	7.20	3.50	1.19
BWC	25 m WF #7	74.70	26.30	11.20	5.50	0.75
BWC	15 m WF #7	76.80	26.90	11.30	5.60	0.39
BWC	WF #7	92.50	30.60	12.80	6.20	0.38
BWC	WF #7	92.13	24.91	10.69	5.23	0.38
BWC	WF #11	94.76	29.19	12.50	6.05	0.21
BWC	WF #11	94.93	29.87	12.95	6.28	1.30
BWC	FTW	71.03	11.99	6.16	3.01	0.41
BWC	Coal mill	61.77	10.67	5.05	2.33	0.79
SSC	2000 m WF D-3	88.70	65.60	32.80	19.50	2.90
SSC	100 m WF D-3	84.70	57.50	32.60	20.30	1.86
SSC	50 m WF D-3	80.60	51.90	28.80	18.10	1.63
SSC	25 m WF D-3	79.50	46.50	25.00	15.70	1.41
SSC	WF D-3	87.90	38.70	21.20	13.50	1.67
SSC	Coal belt	29.70	12.00	6.70	4.40	1.94
SSC	Coal mill	87.00	21.80	10.80	6.70	2.40
BSC	50 m WF #4 − 1	96.10	53.20	25.30	14.70	0.98
BSC	100 m WF #4 − 1	95.70	57.70	27.70	16.10	0.64
ANC	Air shaft #2-1	77.68	43.76	19.10	9.52	0.97

determine moisture (M, at 105 °C) and ash yield (HTA, at 750 °C), the standard procedures, i.e., ASTM D3302M-17 for M and ASTM D3174-12 for HTA, were followed.

For CP, DD, RDD and PM10 (collected in the polyurethane foam provided in the CIP-10T devices) sample chemical analysis, a dried portion of the sample was acid-digested using a special two-step digestion method devised by Querol (1993) and Querol et al. (1997) to retain volatile elements. The concentrations of major elements in the acid digests were determined using Inductively-Coupled Plasma Atomic-Emission Spectrometry (ICP-AES, Iris Advantage Radial ER/S device from Thermo Jarrell-Ash). Trace elements were analysed by Inductively-Coupled Plasma Mass Spectrometry (ICP-MS, X-SERIES II Thermo Fisher Scientific, Bremen, Germany). Digestion of international reference materials (SARM19 and NIST SRM 1633b) and blanks were prepared following the same procedure.

After eleven repetitions of the analysis of the above reference materials, analytical errors were estimated to be within ± 1% of 7% for most major elements in both the SARM19 coal and NIST-1633b fly ash reference materials, with the exceptions of P in SARM19 (29%) and Na in the latter (10%, with relative standard deviations (RSDVs) ranging from 2% to 7%). The trace elements errors were in the range of ± 0 − 5% for Co (7%), U (7%), Cs (8%), Cu (10%), Zn (41%), Zr (31%) and Hf (14%) in SARM19 coal and ± 0 − 4% for all certified and 'for reference' elements in NIST-1633b-fly ash, with the exception of Sc (11%) and Ta (12%). The RSDVs were < 10% for most elements, with the exception of Li, Be, Sc, Cu, Se and Mo (11 − 20%) and Zr, Cd and Ta (21–58%) for SARM19 and < 10% for all elements, with the exception of Mo (14%), and Ta, Zr and Be (24–26%), for NIST-1633b. Because Si is lost during HF evaporation during the digestion of the samples during ICP-AES and ICP-MS analyses, 3 mg of each RDD and DD sample was loaded on Teflon© 47 mm filters using ethanol suspensions to determine the Si/Al concentrations by means of X Ray Fluorescence (XRF, Thermo Scientific ARL QUANT'X Energy-Dispersive X-Ray Fluorescence (EDXRF)). Subsequently, this Si/Al ratio was applied to the Al (ICP-AES determined) concentrations measured for each sample to obtain the Si concentrations. The above reference materials were also used to determine the accuracy of the Si/Al ratios.

2.5. Respirable crystalline silica (RCS)

In order to determine the RCS content in the RDD fractions, an RCS reference material (certified reference material BCR-066, quartz) was added in two rounds (to obtain three measurements of the quartz XRD intensity, the original was used, followed by the ones formed by the two additions) to a 0.1 g sub-sample of each RDD sample to determine RCS content by the addition method. This content was evaluated by means of the correlation between the concentration added and the intensity area obtained from the strongest quartz peak when using XRD.

2.6. Toxicology tests: oxidative potential (OP)

The oxidative stress of the RDD samples was determined via the OP method, which is based on the consumption of ascorbic acid (AA), urate (UA) and glutathione (GSH) antioxidants, as described in detail by Soltani et al. (2018). The OP method involves the resuspension of each RDD sample in ethanol and a 4 h incubation with a synthetic solution containing equi-molar concentrations of AA, UA and GSH. The consumption of AA, UA and GSH is determined by following the methodology developed by Baker et al. (1990) and Iriyama et al. (1984). In-house controls of PM-free, negative PM (M120, Cabot Corporation, USA) and positive PM (NIST1648a, urban particulate from NIST, USA) followed the same protocol for control purposes. The OP of the RDD samples was expressed as the percentage of consumption of each antioxidant with reference to the in-house, particle-free control. To obtain a metric for the oxidative potential, the data was expressed as OP per µg of PM (OP^{AA}/µg PM and OP^{GSH}/µg PM). Data for the individual antioxidants was also combined to provide a total OP value (OP^{TOTAL}/µg). All data obtained were correlated with elemental and mineral concentrations using the software StataCorp LLC (College Station, Texas, USA) version Stata/SE 15.1.

3. Results and discussion

3.1. Particle size

Table 3 and Fig. 2 demonstrate that the finest size distribution

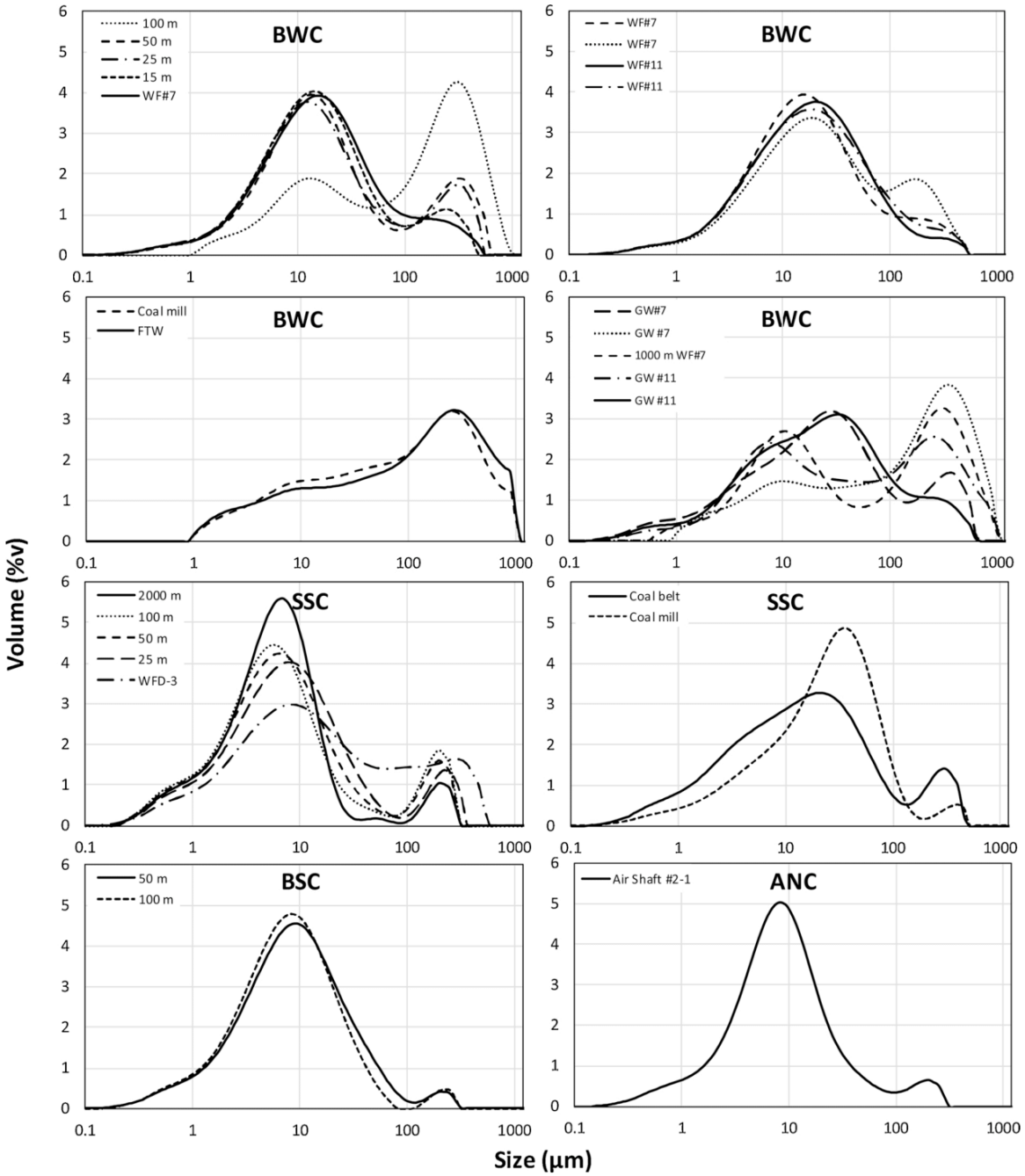

Fig. 2. Particle size distribution of the < 500 µm fraction of the deposited dust (DD) samples collected in the different underground coal mines. WF: Working front.

occurred in WFs samples (#7 and #11) which have 92–95%wt in the < 500 µm, and 25–31%v and 5–6%v in the < 10 µm and < 2.5 µm fractions, respectively. In the access galleries (1000m WF#7), an increase in the grain size was clearly evident within 15–100 m from the WF (95%wt to 28%wt, 27%v to 3%v and 4%v to 0.1%v for the above three fractions, respectively).

A number of galleries with walls covered in lime mortar (gunited walls) had a visually moderate level (markedly higher than the other access galleries but much lower than the WFs) of deposited fine dust (40–89%wt, 7–27%v, 3–14%v and 2–8%v for < 500 µm, < 10 µm, < 4 µm and 2.5 µm fractions, respectively).

The transition from the fine grain sizes in the WF and lime gunited galleries to the coarser grain sizes in the access galleries, train and coal mill is demonstrated clearly in the dry laser size distribution analyses presented in Fig. 2. In contrast, the particle size patterns of the DD from the underground subbituminous coal belonging to the SSC mine are characterised by an increase in the relative proportion allocated to the finest fractions as the distance to the WF increases, from 88%wt, 39%v and 14%v for the < 500 µm, < 10 µm and < 2.5 µm fractions at the WF, respectively, to 89%wt, 66%v and 20%v at a 2000 m distance. This change is attributed to the fact that close to the main emission sources (WF), the emissions of coarser particles are higher, and the finer fractions are transported further through the galleries. Obviously, the absolute concentrations of PM2.5 and PM10 are much higher closer to the

WF, but the relative contributions of these particles to the dust increase with the distance from the source. Furthermore, the DD close to the WF from the inactive BSC mine is characterised by a very high proportion of the finer fraction due to the lack of activity, reaching at 50 − 100 m from the WF 96%wt, 53 − 58%v and 15–16%v for the < 500 μm, < 10 μm and < 2.5 μm fractions, respectively.

The dust from the floor of train wagons and coal mills at the BWC mine is characterised by intermediate-sized particles (62–71%wt, 11–13%v and 2–3%v for < 500 μm, < 10 μm and < 2.5 μm fractions, respectively). As a comparison, the DD from the coal milling area at the SSC mine presents 87%wt, 22%v and 7%v for the < 500 μm, < 10 μm and < 2.5 μm fractions, respectively. The differences exhibited in these size proportions for the DDs from the mills, as suggested by visual observations, might be related to the high and low dust abatement control present in the BWC and SSC coal mills, respectively. Finally, the DD sample from the air shaft (air return) of the ANC mine is characterised by a fine particle size distribution, with 78%wt, 44%v and 10%v for the < 500 μm, < 10 μm, and < 2.5 μm fractions, respectively.

In the WFs of the mines, in addition to having much higher levels of DD (unquantified in our study, but visually very evident), the DD is markedly finer, with 11–13%v being in the respirable fraction (< 4 μm) in the BWC mine and 21%v being in that fraction in the SSC mine. Moving away from the WF, the rate of dust deposition decreases drastically in the BWC mine, and the respirable fraction reaches up to 7%v at 50 m. In the SSC mine, however, the respirable fraction increases to 29%v. In the case of the inactive BSC mine, the respirable fraction of the DD reaches up to 25–28%v at 50-100 m from the WF, while, in the coal mills, it accounts for 6–11%v (BWC and SSC, respectively, with high and low dust abatement controls). Dust from the floor of the wagons in the BWC mine contains a 5%v respirable fraction. In addition, the respirable size fraction distribution in the air return gallery of the ANC mine was 19%v.

In the case of the bituminous coal and anthracite DD samples (BWC and ANC mines), the particle size and the moisture content of the dust are markedly anti-correlated, even if moisture varied within a narrow range. Thus, the following regression equations were expressed for the three major size fractions (DD < 500 μm, < 10 μm and < 2.5 μm) based on 13 DD samples out of a total of 17 samples collected at both the ANC and BWC mines (most of the excluded samples are those from lime gunited galleries and train wagons):

$$DD500\ (\%wt < 500\,\mu m) = -37.75*Moisture\ (\%ad) + 97.26\ (R^2 = 0.79) \quad (1)$$

$$DD10\ (\%vol < 10\,\mu m) = -18.57*Moisture\ (\%ad) + 35.62\ (R^2 = 0.74) \quad (2)$$

$$DD2.5\ (\%vol < 2.5\,\mu m) = -4.18*Moisture\ (\%ad) + 7.67\ (R^2 = 0.73) \quad (3)$$

The correlations did not increase when the moist ash free basis was used (M,%maf, R^2 = 0.70, 0.67 and 0.66 for the three DD fractions, respectively) instead of the air dried moisture (M,%ad); no correlation was found between the fine dust proportions and ash yields (R^2 = 0.31, 0.19, 0.23, respectively, for DD500, DD10 and DD2.5).

In the active SSC coal mine, the anti-correlation between the moisture and the DD500, DD10 and DD2.5 fractions seen above is not apparent (Eqs. (4)–(6)), possibly due to the fact that in the ANC and BWC mines, the anthracite and bituminous ranks account for the low moisture in the coal or the total moisture might be highly influenced by condensation, while, in the subbituminous coal rank of the SSC, the moisture content of the dust seems to be dominated by the coal moisture. In this mine, it was observed that the ash content increases inversely with the moisture and the finer fractions of the DD, which should mean that, with a low correlation, the fine dust fractions decrease with increasing mineral matter in the dust. Thus, the following regression equations were obtained for the three major size fractions based on five of the seven samples collected:

$$DD500\ (\%wt < 500\,\mu m) = +5.06*Moisture\ (\%ad) + 74.68\ (R^2 = 0.51) \quad (4)$$

$$DD10\ (\%vol < 10\,\mu m) = +13.98*Moisture\ (\%ad) + 25.50\ (R^2 = 0.63) \quad (5)$$

$$DD2.5\ (\%vol < 2.5\,\mu m) = +2.51*Moisture\ (\%ad) + 12.66\ (R^2 = 0.28) \quad (6)$$

$$DD500\ (\%wt < 500\,\mu m) = -0.23*Ash\ yield\ (\%db) + 99.69\ (R^2 = 0.25) \quad (7)$$

$$DD10\ (\%vol < 10\,\mu m) = -0.80*Ash\ yield\ (\%db) + 106.29\ (R^2 = 0.52) \quad (8)$$

$$DD2.5\ (\%vol < 2.5\,\mu m) = -0.12*Ash\ yield\ (\%db) + 25.21\ (R^2 = 0.15) \quad (9)$$

No correlation analysis was performed with the DD samples since the BSC coal mine from which these samples came is abandoned, which could lead to uncertainties in relation to the moisture patterns of the other DD samples.

3.2. Mineralogy of deposited dust (DD)

Tables S1 and S2 list the mineralogical composition of all the samples collected in this study. The mineral compositions of the < 500 μm fractions of the DD samples from the BWC mine's WFs #7 and #11 are very different from each other but, as expected, very similar to those of their parent coal seams. The minerals present in the DD from WF #7 are clay minerals (19–23%, kaolinite-clinochlore, muscovite-illite), quartz (18–24%), carbonates (9–15%, calcite, siderite and ankerite), anatase (3 − 5%), pyrite (3–4%) and gypsum (< 1%). The parent coal is characterised by a lower mineral content: clay minerals (10%, kaolinite-clinochlore), quartz (13%), carbonates (4%, calcite and ankerite), anatase (2%), pyrite (2%) and feldspar (< 0.1%, albite-anorthite).

The DD from WF #11 is markedly lower in mineral matter, especially in quartz and pyrite, with 11–13% in clay minerals (muscovite-illite and kaolinite-clinochlore), 3–4% in carbonates (calcite and siderite) and 1% in quartz. The parent coal has a very similar composition, with 12% in clay minerals (muscovite-illite and kaolinite-clinochlore), 3% in carbonates (calcite and siderite), < 0.1% in anatase and < 0.1% in pyrite.

The DD from the SSC mine's WF is markedly different from that from the BWC mine, with higher contents of quartz (34%) and clays (37%, kaolinite-clinochlore and muscovite-illite), traces of feldspar (< 0.5%, albite-anorthite and microcline), anatase (< 0.5%), calcite (< 0.5%), gypsum (< 0.5%) and pyrite (< 1%). The CP of the coal seam worked at the SSC mine has a lower quartz content (12%) and a higher amount of clay (48%, kaolinite-clinochlore and muscovite-illite) than that of the DD collected in the WF.

In the inactive BSC mine, the DD samples collected only at 50 and 100 m from the WF had very similar mineralogy, with 30–33% clays (muscovite-illite and kaolinite-clinochlore), 5–6% quartz, 1–4% calcite, 3% gypsum and traces of pyrite, feldspar (albite-anorthite and microcline) and anatase. The worked coal seam here has slightly higher clay content (45%), plus trace calcite, anatase, pyrite, gypsum and quartz.

Deposited dust from the access galleries for the WFs #7 and #11 is characterised by the occurrence of gypsum and jarosite-alunite (up to 20% and 1%, respectively). These minerals usually occur in coal mining as weathering products of Fe-sulphides such as alunite (Cogram, 2018; Murphy et al., 2009; Welch et al., 2008) and might imply the enrichment of dust in hazardous elements, such as Pb, Zn, Cd and As, trapped by these minerals during their precipitation in acid mine drainages (AMDs), which might affect miners' exposure to toxic metals (Alcobe et al., 2001; Hudson-Edwards et al., 2008; Kerolli-Mustafa et al., 2015;

Kolitsch and Pring, 2001; Smith et al., 2006). In contrast, the galleries leading out from #7 and #11 that had walls gunited with lime mortar were characterised by very high calcite content (40–82%), probably due to the carbonation of lime (CaO), plus clays (2–24%, kaolinite-clinochlore and muscovite-illite), quartz (3–30%), anatase (< 1–6%) and sulphides (1–3%; pyrite). Moreover, the DD from the SSC access gallery (25 − 100 m from the WF) has a similar mineralogy to that of the WF DD, dominated by clays (28–41 vs. 37%) and quartz (30–38 vs 34%). The sample from the access gallery at 2000 m had somehow lower quartz content (19%) and a slightly higher content of gypsum (1%) when compared with the DD from the WF.

The DD from the BWC train wagons is characterised by high calcite (35%), whereas in the coal and gangue belts of the SSC mine is characterised by a high quartz content (40%) and low clay content (17%). On the other hand, the DD samples from coal milling have a slightly higher clay content (17% in the BWC mine, 24% in the SSC mine) and a slightly lower quartz content (9% in the BWC mine) than their respective coal CPs.

Finally, the DD from the ANC air shaft is highly enriched in calcite (27%), probably from lime gunited walls, with lower clay content (9%) (muscovite-illite and kaolinite-clinochlore), quartz (7%) and traces of pyrite and gypsum. This DD is characterised by the highest coal and lowest mineral content of all the samples analysed.

In the BWC mine, the occurrence of jarosite-alunite in the DD from the non-gunited access galleries and of gypsum in the gunited ones is very interesting. In coal mining, jarosite-alunite sulphates arise from coal-pyrite weathering, which produces sulphuric (H_2SO_4) acid and Fe^{2+} that subsequently yield to the jarosite-alunite precipitation at pHs below 3.7 (Murphy et al., 2009; Welch et al., 2008). In addition, the interaction of acidic sulphate with lime and/or calcite leads to the formation of gypsum. Fig. 3 summarises the relevant formation stages yielding the jarosite-alunite in mine dust in the access galleries (mechanism i). Thus, in the first formation pathway, the original gallery is cut into the fresh coal seam, inducing cracks and fractures in the coal seam and coal-bearing strata (Fig. 3a and b). Hence, the underground water can then access these seams via this fissure system, causing the weathering of the sulphide minerals and producing acidic acid mine waters that drain towards the surface of the gallery walls (Fig. 3c), where water evaporation causes the precipitation of jarosite-alunite crusts (in non- gunited galleries) or gypsum (in the lime gunited galleries) (Fig. 3d or e). Next, air flows from ventilation cause the break-up and airborne suspension of jarosite-alunite and/or gypsum-rich particles, which are subsequently deposited (Fig. 3f or g). Other possible mechanisms for the occurrence of jarosite-alunite in the mine dust include: ii) AMD solutions reach the roofs and walls of the galleries and produce a kind of acid rain that results in the formation of jarosite-alunite from the weathering of the pyrite of the DD; iii) water from the roofs and walls and from condensation causes the oxidation of DD containing pyrite, generating jarosite-alunite; and iv) the coal seam being worked is partially weathered and contains previously existing jarosite-alunite from epigenetic reactions of acid or from the weathering favoured by the local tectonic setting. The geochemical analyses (see below) should help to elucidate the main mechanism of jarosite-alunite formation. If jarosite-alunite-enriched metals (As, Sb) are also enriched in the DD, the formation mechanism illustrated in Fig. 3 is likely to prevail because these metals are usually enriched in AMD waters (He et al., 2019; Madzivire et al., 2019; Mohanty et al., 2018).

3.3. Geochemistry of coal and deposited dust (DD)

Table 4 compares the contents of major and trace elements in the coal CPs sampled in our study with Chinese coals and worldwide

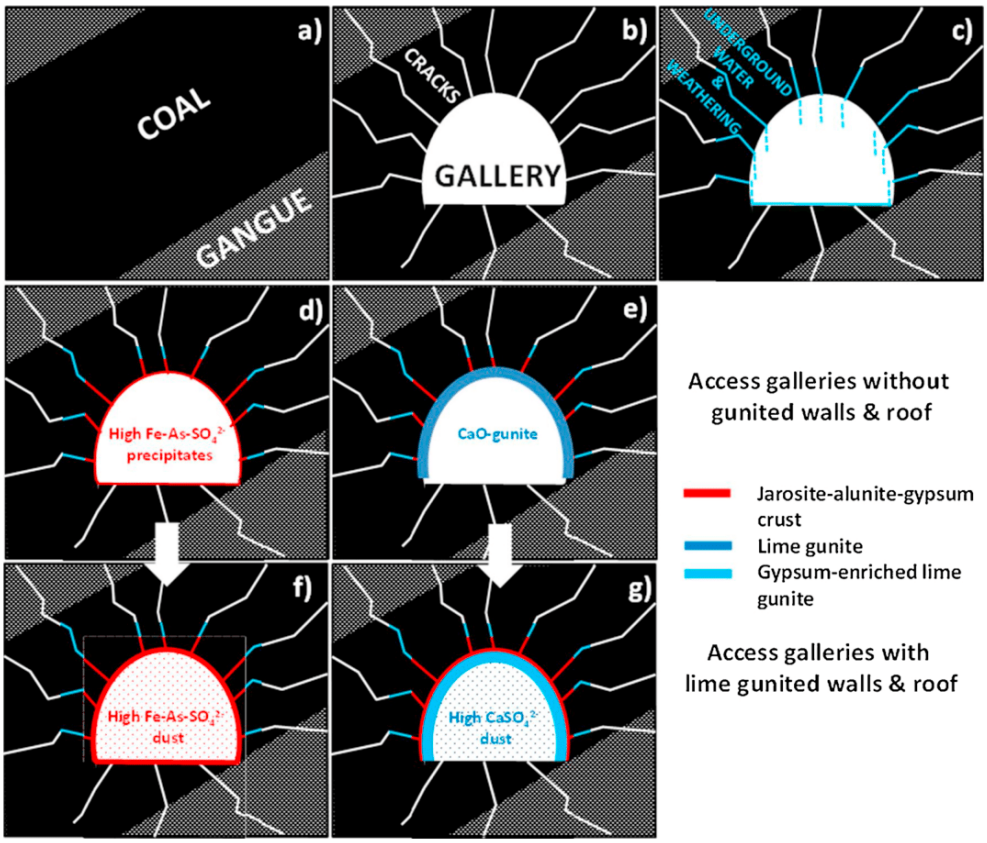

Fig. 3. Conceptual model for the emission of alunite-jarosite and gypsum dust in underground mines with and without gunited walls. a) to g) indicate the time sequence.

Table 4
Major and trace element contents in the coal seams worked (CP, average of channel profiles of the different seams) at the study underground mines and comparison with the respective China and Worldwide averaged concentrations (a. Dai et al., 2007, 2008; b. Ketris and Yudovich, 2009, respectively). Average coals of China and around the world, and all the coals channel profiles collected in the four undergrounds mines. BWC, Bituminous South-West China; SSC, Subbituminous South China; BSC, Bituminous South China; and ANC, Anthracite North China.

Element	CHINA[a]	WORLD[b]			BWC		SSC	BSC	ANC
		Brown	*Hard*	*All*	*CP #7*	*CP #11*	*CP D-3*	*CP #4−1*	*CP#2−1*
	%	%	%	%	%	%	%	%	%
Moisture	–	–	–	–	0.86	0.69	3.14	0.74	2.22
Ash yield	–	–	–	–	30.71	15.18	62.41	46.32	13.10
C	–	–	–	–	60.05	73.92	22.80	39.04	79.03
H	–	–	–	–	3.59	4.37	2.35	2.20	2.76
N	–	–	–	–	0.98	1.32	0.82	0.36	0.99
S	–	–	–	–	2.00	0.78	1.93	3.34	0.17
Ca	0.88	–	–	–	0.88	0.97	0.20	0.23	0.81
K	0.16	–	–	–	0.26	0.03	1.51	0.58	0.27
Fe	3.39	–	–	–	2.02	0.75	2.04	0.39	0.55
Mg	0.13	–	–	–	0.18	0.05	0.29	0.14	0.09
Na	0.12	–	–	–	0.05	0.03	0.24	0.12	0.23
Al	3.32	–	–	–	3.21	2.70	9.69	8.92	3.40
	mg/kg	mg/kg	mg/kg	mg/kg	mg/kg	mg/kg	mg/kg	mg/kg	mg/kg
Ti	1978	720 ± 40	890 ± 40	800	3900	1026	2627	2963	2972
Mn	116	100 ± 6	71 ± 5	86	201	19	80	16	78
P	402	200 ± 30	250 ± 10	230	72	503	380	708	501
Li	32	10 ± 1	14 ± 1	12	32	23	81	213	48
Be	2.1	1.2 ± 0.1	2.0 ± 0 .1	1.6	1.7	1.4	2.5	2.0	0.42
Sc	4.4	4.1 ± 0.2	3.7 ± 0.2	3.9	7.3	4.3	19	19	8.4
V	35	22 ± 2	28 ± 1	25	184	89	172	84	56
Cr	15	15 ± 1	17 ± 1	16	38	13	100	51	30
Co	7.1	4.2 ± 0.3	6.0 ± 0.2	5.1	11	11	13	3.9	22
Ni	14	9.0 ± 0.9	17 ± 1	13	28	16	44	17	23
Cu	18	15 ± 1	16 ± 1	16	85	35	51	25	22
Zn	41	18 ± 1	28 ± 2	23	27	35	74	23	44
Ga	6.6	5.5 ± 0.3	6.0 ± 0.2	5.8	12	8.5	27	27	13
Ge	2.8	2.0 ± 0.1	2.4 ± 0.2	2.2	3.8	2.2	3.2	2.3	1.5
As	3.8	7.6 ± 1.3	9.0 ± 0.7	8.3	3.4	4.3	12	6.5	3.0
Se	2.5	1.0 ± 0.15	1.6 ± 0.1	1.3	3.3	2.6	4.0	8.7	4.5
Rb	9.3	10 ± 0.9	18 ± 1	14	9.8	1.6	133	13	8.3
Sr	140	120 ± 10	100 ± 7	110	109	96	85	118	129
Y	18	8.6 ± 0.4	8.2 ± 0.5	8.4	19	19	24	46	16
Zr	90	35 ± 2	36 ± 3	36	82	45	121	231	145
Nb	9.4	3.3 ± 0.3	4.0 ± 0.4	3.7	15	7.4	9.6	16	15
Mo	3.1	2.2 ± 0.2	2.1 ± 0.1	2.2	0.25	0.27	9.5	9.0	11
Cd	0.25	0.24 ± 0.04	0.20 ± 0.04	0.22	< 0.1	< 0.1	0.15	0.32	< 0.1
Sn	2.1	0.79 ± 0.09	1.4 ± 0.1	1.1	2.9	2.2	3.4	4.2	2.8
Sb	0.84	0.84 ± 0.09	1.00 ± 0.09	0.92	< 0.1	0.41	3.0	0.51	0.23
Cs	1.1	0.98 ± 0.10	1.1 ± 0.12	1	0.61	< 0.1	14	4.5	0.39
Ba	159	150 ± 20	150 ± 10	150	112	84	300	27	107
La	23	10 ± 0.5	11 ± 1	11	26	21	29	52	24
Ce	47	22 ± 1	23 ± 1	23	52	41	57	106	51
Pr	6.4	3.5 ± 0.3	3.4 ± 0.2	3.5	6.3	4.9	7.8	12	6.0
Nd	22	11 ± 1	12 ± 1	12	23	18	25	41	24
Sm	4.1	1.9 ± 0.1	2.2 ± 0.1	2	5.1	4.1	6.0	9.5	6.0
Eu	0.84	0.50 ± 0.02	0.43 ± 0.02	0.47	0.68	< 0.1	1.0	1.4	0.61
Gd	4.7	2.6 ± 0.2	2.7 ± 0.2	2.7	3.9	3.2	4.0	7.0	3.8
Tb	0.62	0.32 ± 0.03	0.31 ± 0.02	0.32	0.29	< 0.1	0.31	1.1	0.43
Dy	3.7	2.0 ± 0.1	2.1 ± 0.1	2.1	4.1	3.4	4.7	9.3	3.7
Ho	0.96	0.50 ± 0.05	0.57 ± 0.04	0.54	0.32	0.52	0.89	2.0	0.50
Er	1.8	0.85 ± 0.08	1.0 ± 0.1	0.93	1.9	1.9	2.7	4.9	1.0
Tm	0.64	0.31 ± 0.02	0.30 ± 0.02	0.31	< 0.1	< 0.1	0.22	1.2	0.27
Yb	2.1	1.0 ± 0.1	1.0 ± 0.06	1	1.9	2.0	2.6	5.1	1.3
Lu	0.38	0.19 ± 0.02	0.20 ± 0.01	0.2	< 0.1	< 0.1	< 0.1	0.45	0.17
Hf	3.7	1.2 ± 0.1	1.2 ± 0.1	1.2	4.0	2.5	4.2	7.4	4.3
Ta	0.62	0.26 ± 0.03	0.30 ± 0.02	0.28	0.41	0.26	0.20	0.22	0.52
W	1.1	1.2 ± 0.2	0.99 ± 0.11	1.1	0.36	< 0.1	1.3	2.3	0.89
Tl	0.47	0.68 ± 0.07	0.58 ± 0.04	0.63	< 0.1	< 0.1	1.0	< 0.1	< 0.1
Pb	15	6.6 ± 0.4	9.0 ± 0.7	7.8	13	11	31	38	31
Bi	0.79	0.84 ± 0.09	1.1 ± 0.1	0.97	< 0.1	< 0.1	0.29	0.82	0.38
Th	5.8	3.3 ± 0.2	3.2 ± 0.1	3.3	6.9	6.0	15	22	17
U	2.4	2.9 ± 0.3	1.9 ± 0.1	2.4	2.5	1.7	7	10	3.3

averages (Dai et al., 2008, 2007; Ketris and Yudovich, 2009). Although most of the major and trace elements in the coals sampled fall within the usual range described for Chinese coals, several relevant differences are reported below:

i) BWC mine: Concentration coefficient (CC, the ratio of the concentration in the coal divided by the reference concentration) of V reaches 2.5, and those of Mo, W, Cs, Bi, Mn, Rb, K, Tl Fe, Na, Mg, Cd and Ta vary across a range from 0.1 to 0.4. Furthermore, in coal #7,

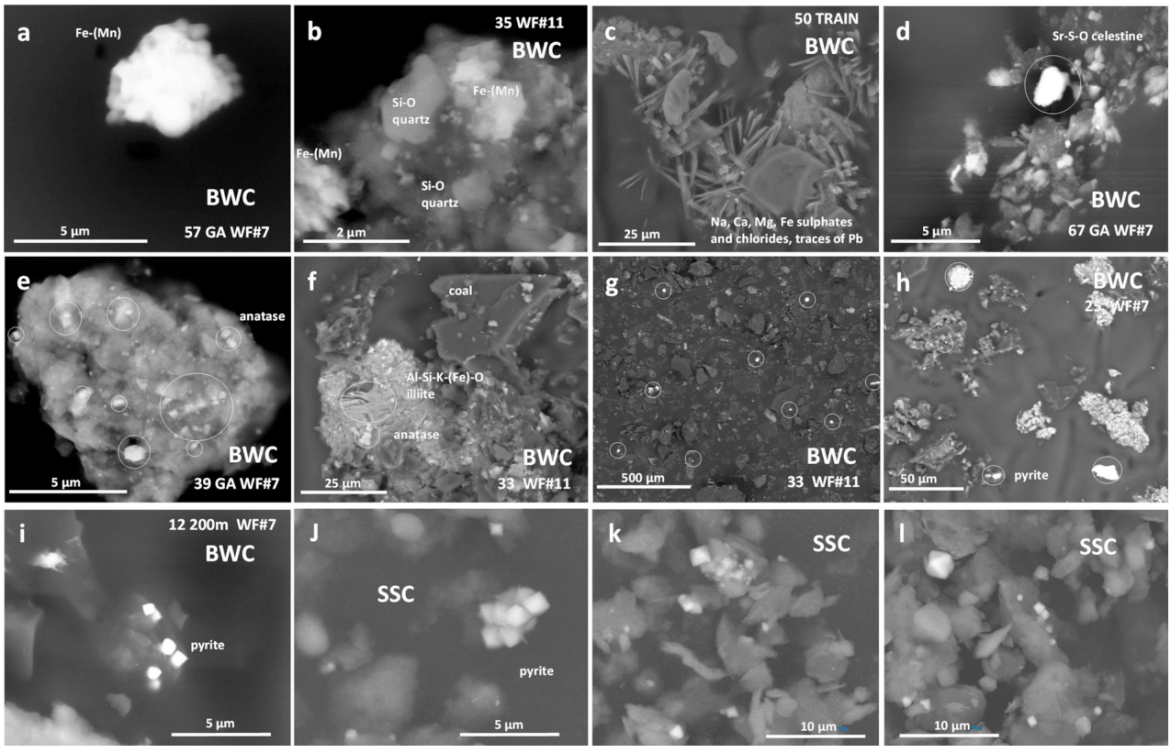

Fig. 4. Scanning electron microscopy (SEM) images showing diverse aspects redacted in all of this study. (a–b) shows the occurrence of metallic Fe-Mn particles in the suspended dust sampled at WF #7 and #11, c-d) shows the occurrence of Ca-Na sulphates and celestine in suspended dust from BWC, (e–f) shows the occurrence of anatase in very fine crystal aggregates, (g–i) shows the occurrence of pyrite in suspended dust from the BWC mine present as isolated particles, and (j–l) shows the occurrence of isolated pyrite crystals in the RDD from the SSC D3 and BWC #7 coals. In the first case the framboidal pyrite aggregates are embedded into a kaolinite matrix while in the second these are into the maceral matrix.

the CCs of Ti, Ni, Cr, Cu and V reach from 2.0–5.3 and from 0.1 to 0.4 for Mo, Sb, Bi, P, Tl, W, Cd and Na.

ii) SSC mine: Subbituminous coal highly enriched in Na, Pb, Mg, Tl, Li, Th, Cu, U, Al, Mo, As, Ni, Sb, Ga, Sc, V, Cr, K, Cs, and Rb with CCs from 2.0–14.3, and depleted in only Ca, Ta and Bi (0.2 − 0.4).

iii) ANC mine: Anthracite highly enriched in Pb, Th, Co and Mo (CCs = 2.0–3.6) and depleted in Fe, Be, Tl, Sb, Cs and Cd (0.2 − 0.4) when compared with the Chinese coal averages.

iv) BSC mine: Bituminous coal highly enriched in a large number of elements. Thus, CC values reach 2.0–6.6 for Sn, Hf, W, REE's, V, Pb, Zr, Y, Al, Mo, Cr, Se, K, Th, Cs, Ga, U, Sc and Li, and 0.1 − 0.4 for Fe, Mn, Ba, Tl, Ca and Ta.

The DD samples from the ANC, BWC, BSC and SSC mines are geochemically similar to the parent coals described above. Relevant differences are discussed below (Tables S4 and S5).

BWC mine:

i) Relative to the DD from WF #11, the WF #7 DD is enriched in most major and trace elements associated with aluminium-silicate and sulphide and phosphate minerals due to its higher ash yields. Dust from #11 is only enriched vs #7 in Zn, which is usually associated with sulphide in coal.

ii) With respect to the CP (DD/CP = 7.0), WF #7 DD is highly enriched in P, which could be associated with the higher phosphate mineral content in the DD. Furthermore, it is also enriched in Ca, Fe, Ti, Cr, Co, As, Cs, Zn, Sr, Mg, Mn, Ta, Ba K, Na Rb and Ni (DD/CP = 1.5–3.0). The same applies for Mn in #11 (DD/CP = 5.1) as well as Mg, V, Cr, K, Rb, Ti and Zn (1.5–2.5).

iii) The DD in the access galleries is highly enriched in Fe, As, Sb and S compared to samples from the WFs, in parallel with the jarosite-alunite enrichment.

iv) The galleries with lime gunited walls are highly enriched in Ca, Zn and S. In line with the foregoing discussion, the AMD reaching the lime gunited walls can be considered to be the source of the water with high sulphate content that generates gypsum when interacting with lime. This gypsum can be emitted from the walls and deposited with the dust.

v) The DD on the floor of the wagons (worker transport) is enriched in Ca, Fe, Mn, Cr, Zn, As, Sr, Sb and Pb with respect to the DD samples from WFs #7 and #11, maybe related to wear from mining machinery in the WF, which could emit metals such as Mn, V, Cr, Fe, Ni, Co and Zn.

vi) Lastly, the DD from the coal mill has similar major and trace element content to that of the CPs, with slightly higher concentrations of Zn, As and Pb. In contrast, the Mn concentration in the coal mill is lower than that in the DD collected in the WFs.

SSC mine:

i) The DD from the WF is highly enriched (compared to the CP) in Sb (DD/CP = 16), and, to a lesser extent, in Mn and Zn (5.0), and also in Ge, Co, Fe, Bi, Ca, As, Cu, Cd and Ta (1.5–3.7).

ii) The DD from the access gallery has similar or slightly lower concentrations of most elements (Tables S4 and S5), except for Fe, Mn, As, Sn, Sb and Pb, and especially Zn. Concentrations of Zn in the DD increase as a function of the distance from the WF, e.g. 25 m out (524 mg/kg), 50 m out (2734 mg/kg) and 100 m out (4893 mg/kg), when starting at 385 mg/kg in the DD in the WF.

iii) The DD sample of a gallery with a coal and gangue belt is characterised by a much lower Mn content and higher Na, Pb, and especially As (x2) than the corresponding contents in the WF.

iv) Lastly, the coal mill DD is characterised by slightly low contents of most elements but higher P and S (Tables S4 and S5).

BSC mine:

i) In this inactive mine, elements with a high DD/CP rate include Ca and As (10 and 13), Zn (50) and Sb (175) but also Cu, V, U, Co, Mg, Cr, Ba, Mo, Cd, Sr, Ta, Mn, W and Fe (1.5–5.5).
ii) Concentrations of most major and trace elements in the DD samples from the access gallery and the WF are very similar, with the exception of Ca and Sr (probably from the lime gunited walls, higher in the 50 m than the 100 m DD samples; Zn (x10)), As and Sb (much higher in the 100 m dust sample than in the 50 m one).

ANC mine

i) The chemical composition of the DD sample from the return air shaft, compared with that of the CP showed a DD enrichment in Ca, As (9) and Sb (53) but also in Ba, Zn, Ta, S, Sr, Na, W, Pb, Be, Fe, K, Mg, Rb, Cs and Mg (DD/CP from 1.5 to 5).

In terms of a general pattern for most mines, it is worth noting that the DD/coal enrichment of a number of elements is potentially associated with the wear on mining machinery (Fe, Mn, V, W, Cr, Ni, Co, depending on the mine). Fig. 4 shows the occurrence of different minerals under the scanning electron microscope including metallic Fe-Mn particles in the DD sampled at WFs #7 and #11 (Fig. 4a and b). Elements associated with salts (such as gypsum, jarosite and alunite) from AMD (Fe, As, Sb, Zn, Pb, Mn, Mg, and Na, also depending on the mine) also have high DD/coal enrichment. The latter suggests the emission of jarosite-alunite, usually enriched in As, Sb, Pb, Cd, Zn and Ba, among others, either from the walls of the galleries or from process (i) described in the prior section. In any case, As and Sb arise from AMD; therefore, guniting the walls of the galleries might therefore reduce As and Sb content in the dust from these areas. On the other hand, the significant of Zn, especially in the access galleries of the BSC and SSC mines, might be ascribed to wear emissions from the metallic cylinders of the mine belts.

The DD sample taken on the floor of the train in the BWC mine is enriched in a large number of elements compared to the DD samples from WFs #7 and #11, which is probably due to the contributions of the gunited lime walls (Ca and Sr), rails and brakes (Fe, Mn, Cr, Zn, Sb and Pb (Font et al., 2019; Moreno et al., 2015) and jarosite dust (Fe, Sb, As, Pb).

3.4. Mineralogy and composition of the respirable fraction of deposited dust (RDD)

Table 5 shows the 25th (D25), 50th (D50), 75th (D75), and 90th (D90) percentiles of the size distributions of the RDD samples. All RDD samples have D50 s in the range of 3 − 5 μm, with most concentrating around 4 μm, confirming that we succeeded in separating the respirable fraction from the DD samples. On the other hand, the D90 values are in the 6 − 10 μm size range, which indicates that RDD samples separated by the PM10 and PM2.5 device have grain sizes < 10 μm.

Fig. 5 (top) shows the RDD/DD ratios for the mineral content in the samples. The results demonstrate a depletion of quartz (RDD/DD = 0.6 ± 0.2) and carbonate minerals (0.6 ± 0.3) as well as lower proportions of feldspars (0.8 ± 0.4), sulphides (0.8 ± 0.5) and sulphates (0.8 ± 0.5) in the RDD (< 4 μm) but very similar contents of anatase (1.0 ± 0.7) and clay minerals (1.1 ± 0.1) compared with the DD (< 500 μm). Accordingly, the results show that, on average, the mineralogy of the RDD is similar to that of the DD, with a constantly higher content of quartz (RCS) and carbonate minerals. However, the variability among samples might be high (e.g. 68% relative standard deviations for quartz and anatase).

Table 5
Percentile 25, 50, 75 and 90 (D25, D50, D75 and D90, in μm) of the grain size distribution of the respirable deposited dust (RDD). WF, Working front; GW, Gunited walls; FTW, Floor of train wagons.

Mine	Location	D25	D50	D75	D90
Bituminous South-West	GW #7	3.37	4.93	6.99	9.74
Bituminous South-West	300 m WF #7	3.25	4.40	7.58	9.66
Bituminous South-West	100 m WF #7	3.39	4.45	7.37	9.20
Bituminous South-West	50 m WF #7	3.25	4.68	6.58	9.11
Bituminous South-West	WF #7	2.91	4.25	5.97	8.23
Bituminous South-West	WF #11	3.06	4.42	6.16	8.42
Bituminous South-West	FTW	2.49	3.85	5.47	7.57
Subbituminous South	2000 m WF D-3	2.48	3.99	5.87	8.37
Subbituminous South	100 m WF D-3	2.38	3.70	5.27	7.30
Subbituminous South	WF D-3	1.64	3.14	4.41	5.92
Subbituminous South	Coal mill	2.45	3.87	5.61	7.91
Bituminous South	100 m WF #4 − 1	2.77	4.24	6.26	9.17
Bituminous South	50 m WF #4 − 1	2.50	3.90	5.64	7.94
Anthracite North	Air shaft #2 − 1	2.63	4.61	7.75	10.11
Anthracite North	Air shaft #2 − 1	2.39	4.20	7.89	9.32

Same ratio but for each mine is shown in Fig. 5 (bottom). Low RDD/DD ratios in 3 mines (bituminous coal and anthracite, usually < 1 and, in most cases, < 0.75) reveal a general depletion of most minerals in hard coals, with the exception of anatase (1.4) in the BSC mine and clay minerals (1.4, and especially 1.8 kaolinite-clinochlore) in the ANC mine. However, for the subbituminous coal (SSC mine), there are a number of minerals with significant RDD/DD enrichment such as the sulphate and sulphide minerals and feldspars (1.2 − 1.7). It is interesting to note a constantly low RDD/DD for quartz in all mines.

Thus, it seems that quartz (RCS) and carbonate minerals are depleted in most RDD samples when compared with the DD samples. For the other minerals, a high variability was found, most likely due to differences in the size occurrence modes of the minerals in the parent coal and the mining operation patterns. It is also evident that hard coals are more depleted in RDD/DD for most minerals compared with the soft coal studied.

Table 6 shows that the RCS content is markedly higher in the SSC RDD samples (from a coal with very high ash yield), with concentrations ranging from 9.6–19.7% in the RDD, while, in most RDD samples from the BWC, BSC and ANC mines, the RCS content reaches up to 1.4–7.5%, with one BWC sample at < 0.1%. When we refer these RCS contents to the basis of the DD (i.e. deposited dust < 500 μm), these concentrations reach 1.8–6.5% for SSC and 0.1 to 0.8% for all the other samples, with the exception of 2.2% in a BSC sample and < 0.1% in one BWC sample.

Fig. 6 (top) shows the RDD/DD ratios for the major elements, with ratios from 0.6 to 0.8 for Fe (0.6 ± 0.3), Ca (0.8 ± 0.3) and Mg (0.8 ± 0.3) (usually with Fe-sulphide and/or carbonate affinity in our samples) and from 0.9 to 1.1 for the other major elements (with sulphide, sulphate, aluminium-silicate, anatase or phosphate affinities). Thus, indicating once again a decrease in carbonate-associated elements in the RDD compared to the DD and a similar content in the case of the aluminium-silicate fractions. In spite of this general trend, Fig. 6 (bottom) shows, as described above for most minerals, that for hard coals, the RDD/DD values are < 1 for most elements and samples, while, for the soft coal, there is an opposite trend.

For trace elements (Fig. 7, top), Mo, Mn, Be, and Nb have average RDD/DDs from 0.7 to 0.8, whereas W, Se, Cs, Cd, Sb and As reach values from 1.2 to 1.4, with all other elements showing very similar contents in RDD and DD. Again these averaged patterns might be quite different from those from the individual mines (Fig. 7 bottom), depending on the mode of occurrence of these trace elements, the size of the minerals containing them in the parent coal seams, and the specific operating patterns of the mine.

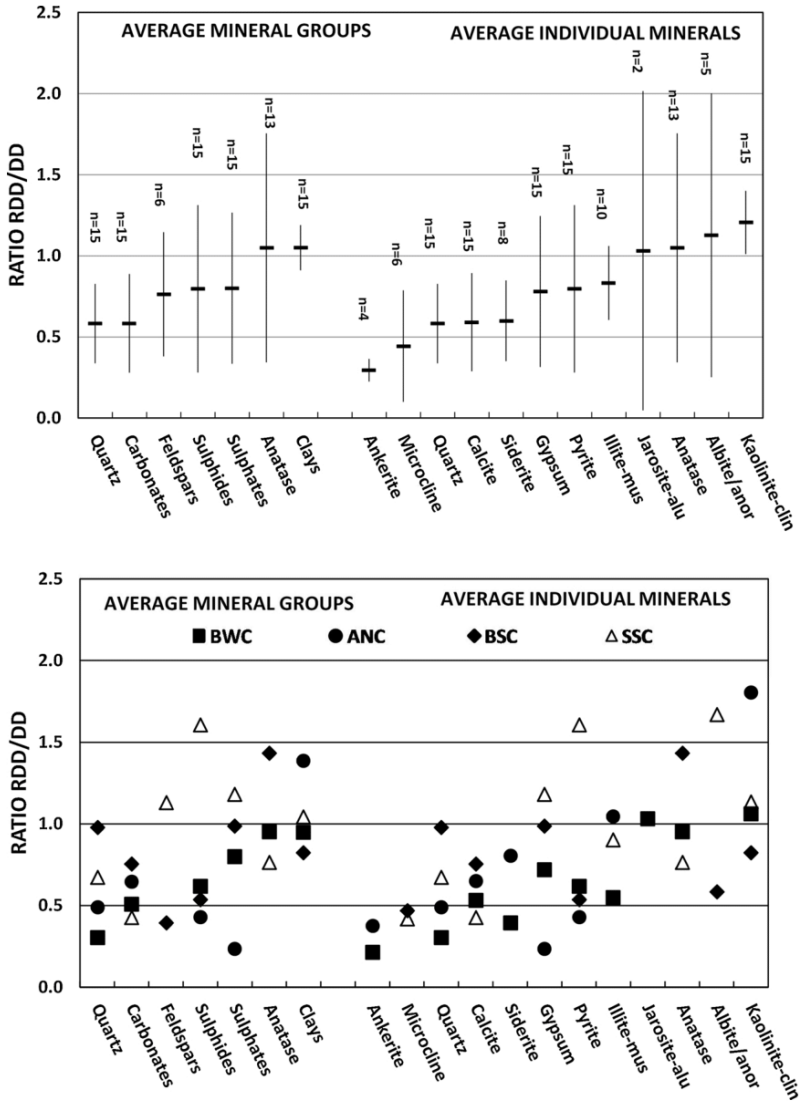

Fig. 5. Ratio of mineral contents determined by XRD analysis in the respirable deposited dust (RDD) and the parent deposited dust (DD < 500 µm) (RDD/DD). Top: Average ratios ± SDV for the 4 mines; bottom: average for each mine.

Table 6
Content of respirable crystalline silica (RCS,%) in the respirable deposited dust (RDD) and re-calculated content with the basis of RCS content in the respective deposited dust finer than 500 µm (DD). WF, Working front; GW, Gunited walls; FTW, Floor of train wagons.

Mine	Location	RCS in RDD	RCS in DD
Bituminous South-West	GW #7	1.4	0.2
Bituminous South-West	300 m WF #7	4.6	0.8
Bituminous South-West	100 m WF #7	4.7	0.2
Bituminous South-West	50 m WF #7	4.6	0.6
Bituminous South-West	WF #7	4.0	0.6
Bituminous South-West	WF #11	< 0.1	< 0.1
Bituminous South-West	FTW	3.3	0.3
Subbituminous South	2000 m WF D-3	9.6	3.6
Subbituminous South	100 m WF D-3	16.9	6.5
Subbituminous South	WF D-3	19.7	4.2
Subbituminous South	Coal mill	14.6	1.8
Bituminous South	100 m WF #4 – 1	7.5	2.2
Bituminous South	50 m WF #4 – 1	3.2	0.8
Anthracite North	Air shaft #2 – 1	3.2	0.8

3.5. CIP-10T analysis

Two CIP-10T samples were taken in the BWC mine, one on the way to WF #7 (from the railway station to the WF, 1 h in the WF and back, with a total duration of the sampling of 5.3 h), and the second one on the way to WF #11 (similar to path taken in WF #7 but with a duration of 3.6 h). The PM10 averaged levels during this time period (5.3 and 3.6 h, of which 1.5 h was spent in the respective WF) reached 3204 and 4,578 µg/m^3 for WF #7 and WF #11, respectively, and PM10 – 200 levels of 5,442 and 14,618 µg/m^3 were sampled, respectively, which is equivalent to a total suspended particle (TSP) concentrations of 8646 and 16,671 µg/m^3, respectively. The higher average levels for the WF #11 sample are probably due to the higher relative weight of the 1.5 h sampling in the WF (1.5/3.6 h) on the bulk sampling compared to the one from WF #7 (1.5/5.3 h). In fact, TSP concentrations measured at 5 min intervals with an optical device by the security staff of the BWC mine reached 14,000–76,000 µg/m^3 in WF #11 and 8100 – 57,700 µg/m^3 in WF #7.

Table 7 shows the occupational levels of major and trace elements in the PM10 and PM10 – 200 measured in the BWC mine when

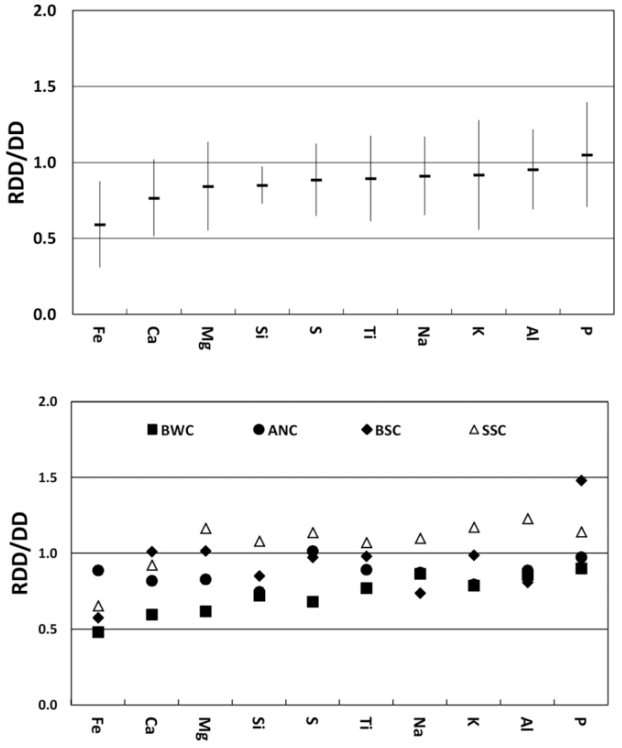

Fig. 6. Ratio of major element contents in the respirable deposited dust (RDD) and the parent deposited dust (DD < 500 µm) (RDD/DD). Top: Average ratios ± SDV for the 4 mines; bottom: average for each mine.

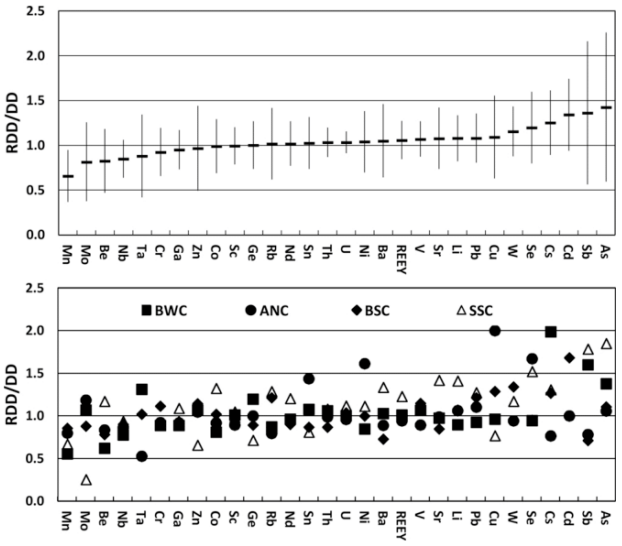

Fig. 7. Ratio of trace element contents in the respirable deposited dust (RDD) and the parent deposited dust (DD < 500 µm) (RDD/DD). Top: Average ratios ± SDV for the 4 mines; bottom: average for each mine.

travelling in and out and working at WFs #7 and #11. As would be expected from the high dust concentrations, the levels are very high, and the sum of all the components reaches around 15–17% of the PM10 and PM10 – 200 levels, which is close to the 11 – 23% ash yields obtained for the DD samples. We evaluated the major and trace elements in the occupational PM10 (sampled using the CIP-PM10 samplers) with those in two composite RDD chemical profiles created from the access and WF gallery results and modulated by the relative time spent in each

Table 7
Levels of major and trace elements in PM10 and PM10-200 occupational exposure samples collected in the Bituminous South-West China (BWC) underground mine.

	PM10 #7	PM10 – 200 #7	PM10 #11	PM10 – 200 #11
	(µg/m^3)	**(µg/m^3)**	**(µg/m^3)**	**(µg/m^3)**
PM10 – 200	–	7973	–	9977
PM10	3204	–	4578	–
CO_3^{2-}	87	142	92	186
SiO_2	212	529	258	803
Al_2O_3	104	203	134	336
Fe	15	123	68	60
S	34	66	43	109
Ca	35	57	37	75
MgO	3.3	41	15	9.3
MnO	0.26	3.3	1.4	0.78
TiO_2	7.5	42	23	22
K_2O	8.0	17	10	28
Na_2O	5.2	10	6.7	17
P_2O_5	1.6	3.2	2.1	5.3
	(ng/m^3)	**(ng/m^3)**	**(ng/m^3)**	**(ng/m^3)**
Li	92	61	72	154
Sc	19	47	23	53
V	261	600	501	1163
Cr	49	980	134	2487
Co	36	102	42	106
Ni	47	533	106	1453
Cu	288	525	210	1007
Ga	31	63	34	78
Rb	15	132	46	22
Sr	471	919	521	928
Y	66	74	54	167
Zr	226	727	352	854
Ba	204	717	405	391
As	153	369	684	181
La	88	166	93	245
Ce	166	355	200	455
Nb	18	88	37	63
Pr	20	40	22	52
Nd	69	144	80	183
Sm	16	28	17	39
Gd	12	19	< 0.1	28
Dy	13	18	< 0.1	33

of them (Table S3). It should be noted that the RDD is equivalent to PM4 and not PM10, but it was not possible to sample PM4 with the CIP instrumentation. In the case of the WF #11 trip, the CIP-PM10/RDD ratios for most major (0.9–1.4) and trace (0.7–1.4) elements is small, with the exception of Ca (0.4) and As (2.6). In the case of WF #7, the CIP-PM10 concentrations of major and trace elements are in many cases lower than those found in the RDD, with CIP-PM10/RDD ratios from 0.3 to 0.5 for most major elements, with the exception of Al (0.8), and between 0.7 and 1.4 for most trace elements, except for As (2.6) and Ti, V, Cr, Mn, Ni, Rb, Nb and Ba (0.3 – 0.6). Accordingly, our results reveal that the composition of the occupational PM10 is quite close to the RDD composition indicated by the CIP-PM10 for WF #11, but is reduced by around 50% for most major and trace elements in the case of the CIP-PM10 for WF #7. We do not have an obvious explanation for this difference because we followed the same protocol in both cases, with the main difference being that during sampling with the CIP-PM10, WF #11 remained active at all times, but WF #7 remained active during only one third of the sampling time.

China's Occupational Exposure Limit (OEL) for time-weighted average exposure value (TWA) for over 8 h of As is fixed at 10 µg/m^3 (Liang et al., 2006), whereas in the BWC mine, 0.1 and 0.7 µg/m^3 were reached. Moreover, also in China, for coal dust with < 10% crystalline silica, the TWA OELs for TSP and respirable fractions (PM4) are fixed at 4,000 and 2,500 µg/m^3, respectively, while, for coal dust with 10–50% crystalline silica, these values are fixed at 1000 and 700 µg/m^3, respectively (Liang et al., 2006). In this study the occupational exposure concentrations reached 11,177 and 15,555 µg/m^3 for TSP and 3204 and

Table 8
Oxidation potential (OP) for Ascorbic Acid (AA), glutathione (GSH) and total (TOT) obtained for the samples of respirable deposited dust (RDD) from the different underground coal mines. WF, Working front; GW, Gunited walls; FTW, Floor of train wagons.

Mine	Location	OP^{AA}%/μg	± SD	OP^{GSH}%/μg	± SD	OP^{TOT}%/μg
Bituminous South-West	GW #7	0.7	0.05	0.5	0.00	1.2
Bituminous South-West	300 m WF #7	1.2	0.01	< 0.1	–	1.1
Bituminous South-West	100 m WF #7	2.0	0.00	0.2	0.06	2.2
Bituminous South-West	50 m WF #7	0.9	0.08	< 0.1	–	0.9
Bituminous South-West	WF #7	0.8	0.06	0.1	0.02	0.9
Bituminous South-West	WF #11	0.1	0.04	0.0	0.05	0.1
Bituminous South-West	FTW	0.2	0.00	0.0	0.01	0.2
Subbituminous South	2000 m WF D-3	0.6	0.04	0.0	0.03	0.6
Subbituminous South	100 m WF D-3	0.5	0.02	0.1	0.02	0.6
Subbituminous South	WF D-3	0.5	0.01	0.2	0.07	0.6
Subbituminous South	Coal mill	0.4	0.03	0.1	0.07	0.5
Bituminous South	100 m WF #4 – 1	0.5	0.04	0.1	0.07	0.6
Bituminous South	50 m WF #4 – 1	0.7	0.03	0.1	0.08	0.7

4,578 μg/m^3 for the inhalable fraction (PM10) for WF #7 and WF #11, respectively, but at 5.3 – 3.6 h, respectively, as opposed to the 8 h required for the TWA.

3.6. Toxicology: oxidative potential (OP)

As far as we know our study presents the first data on OP^{AA} and OP^{GSH} of coal mine dust. The analysed samples display a negligible amount of oxidation towards urate. Past experience with a variety of PM samples has shown that urate is not usually susceptible to oxidisation by PM (Soltani et al., 2018), and, in fact, it is used as a control for the experiment. AA and GSH are both important antioxidants with low molecular weight found within the respiratory tract lining fluid (RTLF) (Kelly, 2003). Their depletion by PM indicates that they play a protective role against PM when it enters the airways, as they have a suicidal reaction, i.e. they react with oxidants present (or generated) on the PM to decrease the OP of the PM, thus reducing its ability to cause harmful oxidative reactions when it reaches the lung surface. As shown in Table 8, the five RDD samples from the BWC mine's WF #7, especially the one collected 50 m away from the WF, stand out from the rest with regards to oxidant activity towards OP^{AA}. These samples were collected in the same area nearby WF #7, but no trend between OP^{AA} and the distance to this WF is observed. The sample collected at the BWC mine in the lime gunited gallery close to WF #7 is again the most active against GSH (OP^{GSH}), followed by the BWC sample 50 m away from this WF, and a SSC mine sample from the WF. Thus, in the same BWC mine, the RDD from WFs #7 and #11 yield very different values for OP^{AA}, with the highest OP^{AA} concentration in the RDD sample with higher ash yields and metal content.

The NIST1648a control yielded 35% of AA consumption, compared to 35–100% for all BWC WF #7 samples, < 10% for all BWC WF #11 samples, and 20–30% for samples from the SSC and BSC mines. In terms of GSH consumption, the NIST control reached 15% OP^{GSH}, while 25% was attained by the lime gunited gallery RDD from WF #7 in the BWC mine, and < 10% was obtained by all the other samples.

Fig. 8 compares the normalised OP^{TOT} ($OP^{AA} + OP^{GSH}$, in %consumption/μg) of the RDD samples from our study with both the NIST control, and equivalent results from the Chamonix Valley in summer and winter (the latter with high PM contributions from biomass burning) (Calas et al., 2018) as well as subway PM from six stations in Barcelona (Moreno et al., 2017) and PMs from indoor and outdoor locations around a Fe-ore facility in Iran (Soltani et al., 2018). As shown in this figure, the average RDD OP^{TOT} for the three coal mines is 6.9-fold lower than Chamonix-winter PM (probably due to the high content of PAHs from biomass burning) and 1.6–2.3-fold lower than the NIST urban, Fe-ore, Chamonix-summer and Barcelona subway PM. However, values obtained for the WF #7 RDD are relatively higher and similar to those found for the NIST urban, Fe-ore and Chamonix-summer PM and

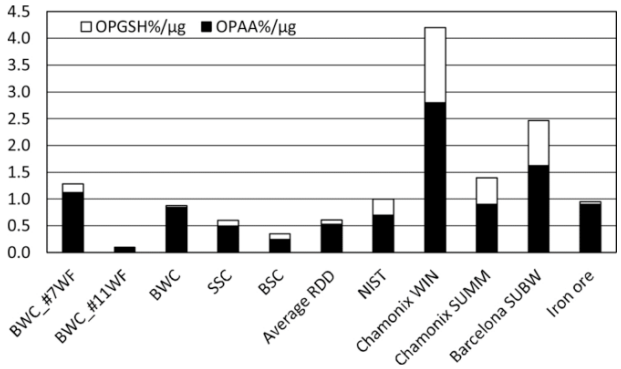

Fig. 8. Normalised total oxidative potential ($OP^{TOT} = OP^{AA} + OP^{GSH}$, in %consumption/μg) of the respirable deposited dust (RDD) samples from our study with the NIST urban particles, and results from the Chamonix Valley in summer and winter (the latter with high biomass burning PM contributions) (Calas et al., 2018); subway PM from six stations in Barcelona (Moreno et al., 2017), and PM from indoor and outdoor around Fe-ore facility in Iran (Soltani et al., 2018).

1.9–3.3 fold lower than those found for the Barcelona subway and Chamonix-winter PM. Another contrasting piece of evidence is the < 0.1 rate obtained for OP^{GSH}/OP^{AA} for the RDD from the coal mines and Fe-ore PM, while, for the urban, subway and Chamonix Valley PM, this ratio reaches 0.4 – 0.6, most likely due to the higher relative influence of Fe on the OP of the samples in the RDD and Fe-ore PM, with more influence on the OP^{AA} than the OP^{GSH} (see below). The mode of occurrence of Fe and probably its oxidation state, however, must play a key role since the subway study found extremely high Fe levels but relatively low OP.

A cross correlation analysis of the OP^{AA} and OP^{GSH} of the RDD samples with their respective content of major and trace elements and mineral contents, as well as the particle size distribution, was carried out to identify major drivers of the OP. Most RDD components did not show correlation with OP values, but a reduced number of them accounted for a high proportion of the OP variance.

For RDD samples from BWC mine, excluding the one from the wagon's floor, OP^{AA} was markedly and positively correlated ($p < 0.05$) with the contents of Mo ($R^2 = 0.67$), S (0.78) and Fe (0.98); and with quartz (0.60), sulphates (0.70), pyrite (0.82), and anatase (0.94). Furthermore, OP^{GSH} values correlated positively with the contents of Mg, K, Cr, Pb ($R^2 = 0.74 - 0.79$), calcite, Zn, Rb, Sb, As, Cs, Ba, Ca, Na (0.81 – 0.88) and Sr (0.95).

When RDD from the two bituminous coal mines (BWC and BSC, excluding again the one of wagon from BWC) were considered, OP^{AA} was highly and positively correlated ($p < 0.05$) with Fe ($R^2 = 0.97$),

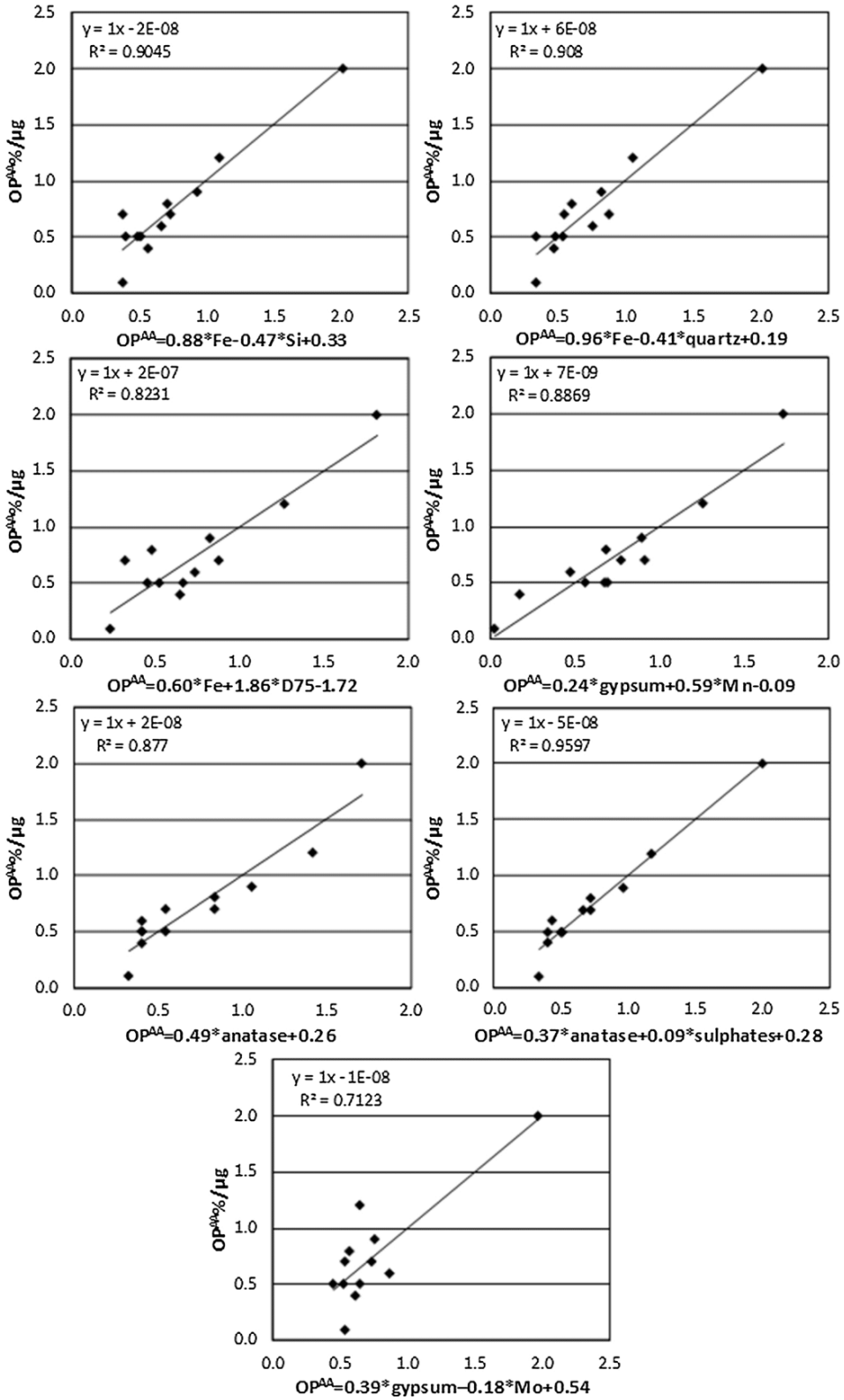

Fig. 9. Cross correlation plots of total Ascorbic Acid (OP^{AA}) in %consumption of antioxidant/µg of the respirable deposited dust (RDD) and the normalised content of specific elements and minerals. All RDD samples from all mines included, with the exception of the one from the floor of the train wagons of BWC.

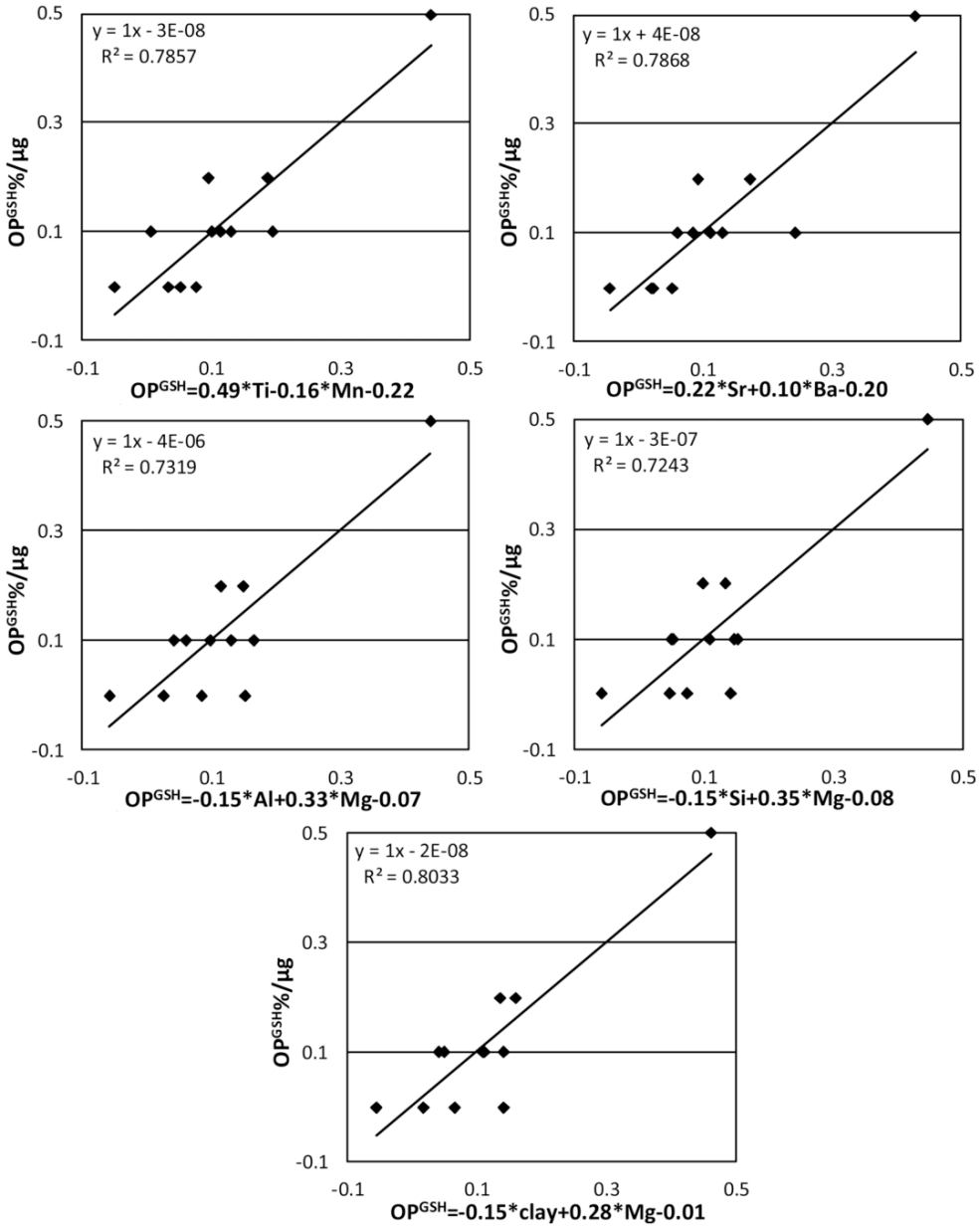

Fig. 10. Cross correlation plots of (top) the total glutathione (OP^{GSH} in %consumption of antioxidant/µg of the respirable deposited dust, RDD) and the normalised content of specific elements. All RDD samples from BWC and BSC mines included, with the exception of the one from the floor of the train wagons of BWC.

and also with sulphate minerals (0.62), pyrite (0.71) and anatase (0.89); and OP^{GSH} with Ba, Mg, Sr (0.64 − 0.69), calcite, Ca and Na (0.80 − 0.85).

In the case of the RDD from the subbituminous coal mine (SSC), OP^{AA} values correlated ($p < 0.05$) only with contents of Ca ($R^2 = 0.94$); and the OP^{GSH} ones with those of Cu, quartz, Cs and Ba (0.87 − 0.99).

A light positive correlation ($R^2 = 0.45$, $p = 0.07$) between particle size (D75) and OP^{AA} for the RDD of the two bituminous coal mines was found, and no correlation for the subbituminous coal RDD.

A multilinear regression analysis was carried out to identify the major RDD components governing the OP^{AA} (Fig. 9) and OP^{GSH} (Fig. 10) variability of RDD. Again all samples were included in the analysis with the exception of the one from the wagon of the BWC mine. To this end the concentration of each element and mineral was normalised with respect to the average concentrations of the 12 RRD samples. The main multivariate relationships found with a high statistical significance ($p < 0.05$) for slopes and constants of the regression equations were:

$$OP^{AA} = 0.88*Fe - 0.47*Si + 0.33 \ (R^2 = 0.91) \quad (10)$$

$$OP^{AA} = 0.96*Fe - 0.41*quartz + 0.19 \ (R^2 = 0.91) \quad (11)$$

$$OP^{AA} = 0.60*Fe + 1.86*D75 - 1.72 \ (R^2 = 0.82) \quad (12)$$

$$OP^{AA} = 0.24*gypsum + 0.59*Mn - 0.09 \ (R^2 = 0.89) \quad (13)$$

$$OP^{AA} = 0.49*anatase + 0.26 \ (R^2 = 0.88) \quad (14)$$

$$OP^{AA} = 0.37*anatase + 0.09*sulphate\ minerals + 0.28 \ (R^2 = 0.96) \quad (15)$$

$$OP^{AA} = 0.39*gypsum - 0.18*Mo + 0.54 \ (R^2 = 0.96) \quad (16)$$

$$OP^{GSH} = 0.49*Ti - 0.16*Mn - 0.22 \ (R^2 = 0.79) \quad (17)$$

$$OP^{GSH} = 0.22*Sr + 0.10*Ba - 0.20 \ (R^2 = 0.79) \quad (18)$$

$$OP^{GSH} = -0.15*Al + 0.33*Mg - 0.07 \ (R^2 = 0.73) \quad (19)$$

$$OP^{GSH} = -0.15*Si + 0.35*Mg - 0.08 \ (R^2 = 0.72) \quad (20)$$

$$OP^{GSH} = -0.15*clay + 0.28*Mg - 0.01 \ (R^2 = 0.80) \quad (21)$$

Where the OP^{AA} or OP^{GSH} values are given in % consumption AA or GSH/μg; and the elements and minerals, the normalised concentration versus the respective average contents of the 12 RDD samples.

According to the results, OP^{AA} in RDD from the 2 bituminous coal mines is markedly driven by Fe content. Huang et al. (1998) defined bioavailable Fe (BAI) in coal as the free-Fe released in a 10 mM phosphate solution, pH 4.5 which is the pH of the phagolysosomes of lung's macrophages. They hypothesised that the prevalence of CWP may be higher in coal workers exposed to coal dust with high acid-soluble Fe^{2+} and low buffering capacity (low carbonate minerals in coal) than in workers exposed to coal with low acid-soluble Fe^{2+} and high buffering capacity. Huang et al. (2005) found a high correlation (R = 0.94) of BAI values of bituminous coal with CWP cases in coal mining areas of the United States, as well as with the content of sulphate and pyrite sulphur (R = 0.91). Indeed, the low OP^{AA} for the wagon's floor dust and the lack of correlation with pyrite and Fe might be due to the low content of pyrite (0.3%) and the high buffering effect of calcite (38%) of this specific sample, although this buffering does still not account for the absence of correlation of OP^{AA} and pyrite content in the subbituminous coal samples (SSC mine). Similarly, Gilmour et al. (2004) found that high-sulphur (bituminous) coal produces more toxic RDD emissions than low-sulphur subbituminous coal and lignite. Cohn et al. (2006) suggested that the toxicity of coal dust may be in part explained by the occurrence of pyrite, and Moreno et al. (2019) reported that pyrite particles might remain for an entire year in the lungs, promoting the formation of reactive oxygen species (ROS) within cells, and potentially contributing to the pathogenesis of CWP.

The mineralogical analysis shows that the dominant mode of occurrence of Fe in the BWC, BSC and SSC RDD samples is as pyrite. Thus, using all samples from the BWC and BSC mines, with the exception of the train floor sample from the BWC mine, it can be concluded that the pyrite contents in RDD and OP^{AA} are highly correlated (R^2 = 0.71). Pyrite is easily oxidised into sulphuric acid and Fe-oxide, and it usually contains relevant proportions of Mn and Mo (also found to be correlated with OP^{AA}). In addition, the products of pyrite oxidation include gypsum, alunite, jarosite, tenardite, celestine and barite. Mg, Ca, Na, K, Cu, Mo, Cr, Pb, Zn, As, Ba, Rb, Sb, Cs and Sr can occur in coal within these sulphates (see Fig. 4c and d for the occurrence of Ca-Na sulphates and celestine in suspended dust from the BWC mine), as well as in other minerals such as molybdates and chromates, are correlated with OP^{AA} or OP^{GSH} and can produce oxidative reactions in the lung cells. Using other indicators Gilmour et al. (2004) also observed a contribution to toxicity from sulphates, and Schins and Borm (1999) reported that sulphates have also been suggested to play a dominant role in antiprotease inactivation. Most of the above listed elements in other types of dust have been identified as OP-relevant by Godri et al. (2011); Janssen et al. (2014); Pant et al. (2015); Moreno et al. (2017) and Soltani et al. (2018) using the same OP technique.

Titanium content is also highly correlated with OP^{GSH} (Fig. 10) for the RDD from the bituminous coal mines. This correlation increases notably for OP^{AA} if the anatase (TiO_2 analysed by XRD) is considered instead of Ti (Fig. 9). As shown in Fig. 11, the anatase and Ti contents have a low correlation (R^2 = 0.21) because a significant proportion of Ti probably occurs in aluminium silicate minerals substituting for other elements, whereas anatase usually occurs in very fine crystal aggregates, mostly mixed with clay mineral assemblages (Fig. 4e and f).

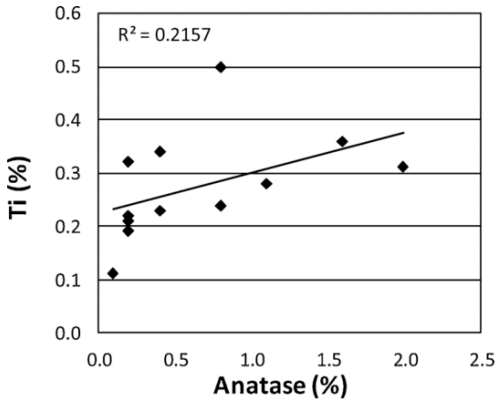

Fig. 11. Cross correlation plots of the the Ti (%) and anatase (%) contents.

Oberdöster et al. (1992) found that TiO_2 particles could produce significantly inflammation and interstitial translocation in the lung, with higher effects for ultrafine-TiO_2 than for the fine size fractions. Schins and Borm (1999) found also a significant role of TiO_2 for increasing 8-oxodG/dG ratios in toxicity. Hamilton et al. (2009) demonstrated that alteration of anatase TiO_2 nanomaterial into a fibre structure of greater than 15 μm creates a highly toxic particle and initiates an inflammatory response by alveolar macrophages.

Various workers have demonstrated the combined role of both size and chemical composition of dust in producing ROS (Schins and Borm, 1999; Borm, 2002; Li et al. (2003, 2008; Gilmour et al., 2004). In our study we did not find a negative correlation of Fe and size, probably because we already evaluated respirable dust with D50 close to 4 μm. Conversely, when considering the RDD but a positive size-OP^{AA} relationship was found in the multilinear regression. This might be due to the fact that, when considering this fine PM, pyrite is associated with the coal organic matrix, being enriched in the coarser sizes compared with clays.

The above evaluation of the correlation of OP with the chemical and mineralogical patterns of RDD is based on the samples from the mines working bituminous coal (BWC and BSC mines). Excluding the case of anatase, when adding the four samples from subbituminous coal (SSC samples), the correlation with Fe decreases markedly. Furthermore, the OP^{TOT} values reached for these four RDD SSC mine samples are not as high as the values seen in the bituminous coal mine samples, which might be due in part to the very high clay mineral content (24–41%db), as compared with the other RDD samples (3–28% db). In this context it has been reported that the toxicity of RCS decreases when the quartz crystals are coated with clay minerals (Pavan et al., 2019; Pavan and Fubini, 2017; Turci et al., 2015). Thus, if pyrite crystals are embedded with clay mineral aggregates or the coal matrix, then their toxicity might be decreased. As shown in Fig. 4, the SEM-EDX analysis demonstrates that the pyrite in the suspended dust from both the BWC (Fig. 4g to i) and SSC (Fig. 4j to l) mines is mostly present as isolated particles or aggregates. However, when using the SEM-EDX to analyse the samples from the coal seams (Fig. S5), it was shown that pyrite is embedded in the coal matrix in BWC mine dust, while it occurs in the clay matrix in the SSC mine. Other causes, such as the different OP, might account for the different toxicological effects.

Finally, it is important to note the low OP values obtained for the RDD sampled from the floor of the BWC mine train wagons, despite the fact that this dust has a similar mineral and chemical composition to other samples from the BWC mine with higher OP yields. One possible cause for this is the fact that this DD is quite old when compared with the other DD samples since there is evidence that the ageing of the

surface of the RCS particles can decrease their toxicological effect markedly (Turci et al., 2015).

4. Conclusions

In this study, we aimed to characterize underground coal mine dust evaluating particle sizes, mineralogical and geochemical patterns and their potential impacts on health, identifying their source origins using combined geochemical, mineralogical, and toxicological tools. We also investigated how DD finer than 500 µm in coal mines may be used to deduce the mineralogical and chemical patterns of respirable dust in the mine. We adopted a novel approach by separating the respirable component present in DD (RDD) and comparing its compositional patterns with samples of total suspended ambient PM (TSP) and PM10 (PM finer than 10 µm).

Deposited dust (DD) within coal mines contains a higher relative proportion of the finest fractions as the distance from the WFs increases, which is attributed to the fact that emissions of coarser particles are higher close to the main emission sources (WF), with only the finer fractions being transported longer distances through the galleries. Obviously, the absolute concentrations of PM2.5 and PM10 are much higher closer to the WF, but the relative contributions of the finer fraction increase with distance from the source.

In the WFs, the RDD fraction of the DD varied from up to 11–13%v in the BWC mine to 29%v in the SSC mine. At the ANC and BWC mines, we demonstrated a negative correlation between moisture in the DD and its proportion of RDD, but this same correlation was not observed in the SSC mine, possibly due to the fact that in the ANC and BWC mines, the anthracite and bituminous ranks result in lower moisture in the coal. In addition, the total moisture present might be highly influenced by water condensation, whereas in the subbituminous coal the moisture content of the dust seems to be dominated by the coal moisture, not by the condensation that may agglomerate dust.

In general, the DD mineralogy of the access gallery or WF is characterised by an ash yield when compared with its parent coal channel profile. In contrast, clay minerals tend to increase in the parent coal. AMD solutions reach the roof and walls of the galleries and give rise to the formation of sulphate minerals such as jarosite-alunite and gypsum. The dust arising from the emission of these sulphate-crusted minerals is highly loaded with potentially toxic trace metals/metalloids such as As, Pb, Zn, Sb, Cd. Gunited walls in the galleries might prevent, or at least lessen, the emission of high jarosite dust from the walls.

When compared with the parent coal, DD is enriched in a number of metals potentially associated with wear from mining machinery (Fe, Mn, V, W, Cr, Ni and Co, depending on the mine), elements associated with sulphates from AMD (Fe, As, Sb, Zn, Pb, Mn, Mg and Na, also depending on the mine), and Zn, probably due to emissions from the wear on the cylinders of the mine belts (especially in the galleries of the BSC and SSC mines).

The percentage of RCS was always higher in the vicinities of the WFs (in the cases of the SSC was higher by up to 20%) than farther away; however, when calculating the RCS on the basis of the DD (deposited dust < 500 µm), these contents were quite reduced in all mines (the highest content was 6.5% in the SSC mine).

In the case of RDD samples quartz and carbonate minerals decrease markedly (by 40%, on average) compared to DD, while the content of the other minerals is broadly similar, as demonstrated by the major element content. However, some potentially hazardous trace elements increased in RDD (As, Cd, Sb and Se).

Finally, the evaluation of the correlations of the mineral and elemental contents of RDD with the respective Oxidative Potential showed that OP^{AA} and OP^{TOT} highly correlated with Fe, Si, Mn and Ba, and Ba, Sr, Na and Ti with OP^{GSH}. The results demonstrate that Fe is the element with the highest OP^{TOT} and OP^{AA} impact in most RDD samples from the BWC and SSC mines, probably due to the oxidation of pyrite in these mines, supporting the findings by Huang et al. (1998, and 2005) on the high impact of acidic components from pyrite oxidation on the coal workers' pneumoconiosis (CWP) injuries. In the case of the SSC mine, with even higher pyrite content, the OP is much lower, probably due to the fact that pyrite occurs embedded in clay minerals or is less easily oxidised than in the other dust samples. The buffering of the acidic species by calcite is not enough to account for the low OP of these samples. A number of elements and minerals potentially arising from direct pyrite oxidation or acid mine drainage (sulphate minerals, As, Ba, Cr, Mo, Mn, Pb, Sr, Zn, among others) contributed also to increase OP values. To conclude, we found anatase (TiO_2) highly correlated with OP^{TOT} and OP^{AA} when using all samples from all mines. However, anatase and Ti contents have a low correlation (R^2 =0.21), probably due to Ti being predominantly in aluminium silicate minerals (substituting other elements), whereas anatase occurs in fine crystal aggregates in the mineral matter of dust. To conclude, we found anatase (TiO_2) highly correlated with OP^{TOT} and OP^{AA} when using all samples from all mines. However, anatase and Ti contents have a low correlation (R^2 = 0.21), probably due to Ti being predominantly in aluminium silicate minerals (substituting other elements), whereas anatase occurs in fine crystal aggregates in the mineral matter of dust.

Credits of authors

The corresponding author, Pedro Trechera, is responsible for ensuring that the descriptions are accurate and agreed by all authors, did the sampling and most of the analyses and most of writing.

Xavier Querol participated in the sampling and analysis, discussed results, also wrote some sections and reviewed the manuscript.

Zhuang Xinguo, Baoqing Li, Jing Li, Yunfei Shangguan and Patricia Córdoba, participated in the sampling of different mines, discussed results and reviewed the manuscript.

Ana Oliete and Frank Kelly did the OP analysis, wrote a section and reviewed the manuscript.

Teresa Moreno, Natalia Moreno, Konrad Kandler performed SEM and DRX analyses, discussed results and reviewed the manuscript.

Declaration of Competing Interest

The authors declare that they have no known competing financial interests or personal relationships that could have appeared to influence the work reported in this paper.

Acknowledgements

This study was supported by Generalitat de Catalunya (AGAUR 2017 SGR41), Spain; by the National Science Foundation of China (grant 41972180); the Program of Introducing Talents of Discipline to Universities (grant B14031) and Overseas Top Scholars Program for the Recruitment of Global Experts, China; the Deutsche Forschungsgemeinschaft (DFG, German Research Foundation, grant4 16816480) and by the Spanish Ministry of Science and Innovation (Excelencia Severo Ochoa, Project CEX2018-000794-S). Pedro Trechera is contracted by the ROCD (Reducing risks from Occupational exposure to Coal Dust) project supported by the European Commission Research Fund for Coal and Steel; Grant Agreement Number 754205.

Appendix A. Supplementary data

Supplementary material related to this article can be found, in the online version, at doi:https://doi.org/10.1016/j.jhazmat.2020.122935.

References

Alcobe, X., Bassa, J., Tarruella, I., Roca, A., Vinals, J., 2001. Structural characterization of synthetic Beudantite-type phases by Rietveld refinement. Mater. Sci. Forum 378–383, 671–676.

Aneja, V.P., Isherwood, A., Morgan, P., 2012. Characterization of particulate matter (PM10) related to surface coal mining operations in Appalachia. Atmos. Environ. 54, 496–501. https://doi.org/10.1016/j.atmosenv.2012.02.063.
Baker, M.A., Cerniglia, G.J., Zaman, A., 1990. Microtiter plate assay for the measurement of glutathione and glutathione disulfide in large numbers of biological samples. Anal. Biochem. 190, 360–365. https://doi.org/10.1016/0003-2697(90)90208-Q.
Borm, Pa.J.A., 1997. Toxicity and occupational fealth hazards of coal fly ash (CFA). A Review of Data and Comparison to Coal Mine Dust. Ann. Occup. Hyg 41. https://doi.org/10.1093/annhyg/41.6.659.
Borm, P.J.A., 2002. Particle toxicology: from coal mining to nanotechnology. Inhal. Toxicol. 14, 311–324. https://doi.org/10.1080/08958370252809086.
Brodny, J., Tutak, M., 2018. Exposure to harmful dusts on fully powered longwall coal mines in Poland. Int. J. Environ. Res. Public Health 15, 1846. https://doi.org/10.3390/ijerph15091846.
Brown, J.S., Gordon, T., Price, O., Asgharian, B., 2013. Thoracic and respirable particle definitions for human health risk assessment. Part. Fibre Toxicol. 10, 12. https://doi.org/10.1186/1743-8977-10-12.
Calas, A., Uzu, G., Kelly, F.J., Houdier, S., Martins, J.M.F., Thomas, F., Molton, F., Charron, A., Dunster, C., Oliete, A., Jacob, V., Besombes, J.L., Chevrier, F., Jaffrezo, J.L., 2018. Comparison between five acellular oxidative potential measurement assays performed with detailed chemistry on PM10 samples from the city of Chamonix (France). Atmos. Chem. Phys. 18, 7863–7875. https://doi.org/10.5194/acp-18-7863-2018.
Castranova, V., 2000. From coal mine dust to quartz: mechanisms of pulmonary pathogenicity. Inhal. Toxicol. 12, 7–14. https://doi.org/10.1080/08958378.2000.11463226.
Chuang, H.-C., BéruBé, K., Lung, S.-C.C., Bai, K.-J., Jones, T., 2013. Investigation into the oxidative potential generated by the formation of particulate matter from incense combustion. J. Hazard. Mater. 244–245, 142–150. https://doi.org/10.1016/j.jhazmat.2012.11.034.
Chung, F.H., 1974. Quantitative interpretation of X-ray diffraction patterns of mixtures. I. Matrix-flushing method for quantitative multicomponent analysis. J. Appl. Crystallogr. 7 (6), 519–525. https://doi.org/10.1107/S0021889874010375.
Cogram, P., 2018. Jarosite. Reference Module in Earth Systems and Environmental Sciences. Elsevierhttps://doi.org/10.1016/B978-0-12-409548-9.10960-1.
Cohen, R., Patel, A., Green, F., 2008. Lung disease caused by exposure to coal mine and silica dust. Semin. Respir. Crit. Care Med. 29, 651–661. https://doi.org/10.1055/s-0028-1101275.
Cohn, C.A., Laffers, R., Simon, S.R., O'Riordan, T., Schoonen, M.A.A., 2006. Role of pyrite in formation of hydroxyl radicals in coal: possible implications for human health. Part. Fibre Toxicol. 3, 16. https://doi.org/10.1186/1743-8977-3-16.
Colinet, J.F., Rider, J.P., Listak, J.M., Organiscak, J.A., Wolfe, A.L., 2010. Best practices for dust control in coal mining. IC 9517 Inf. Circ. Best Pract. Dust Control Coal Min. 01, 17–36.
Costa, D.L., Dreher, K.L., 1997. Bioavailable transition metals in particulate matter mediate cardiopulmonary injury in healthy and compromised animal models. Environ. Health Perspect. 105, 1053–1060. https://doi.org/10.1289/ehp.97105s51053.
Dai, S., Zhou, Y., Ren, D., Wang, X., Li, D., Zhao, L., 2007. Geochemistry and mineralogy of the Late Permian coals from the Songzo Coalfield, Chongqing, southwestern China. Sci. China Ser. D Earth Sci. 50, 678–688. https://doi.org/10.1007/s11430-007-0001-4.
Dai, S., Ren, D., Zhou, Y., Chou, C.-L., Wang, X., Zhao, L., Zhu, X., 2008. Mineralogy and geochemistry of a superhigh-organic-sulfur coal, Yanshan Coalfield, Yunnan, China: evidence for a volcanic ash component and influence by submarine exhalation. Chem. Geol. 255, 182–194. https://doi.org/10.1016/J.CHEMGEO.2008.06.030.
Duarte, A.L., DaBoit, K., Oliveira, M.L.S., Teixeira, E.C., Schneider, I.L., Silva, L.F.O., 2019. Hazardous elements and amorphous nanoparticles in historical estuary coal mining area. Geosci. Front. 10, 927–939. https://doi.org/10.1016/j.gsf.2018.05.005.
Ercal, N., Gurer-Orhan, H., Aykin-Burns, N., 2001. Toxic metals and oxidative stress part I: mechanisms involved in me-tal induced oxidative damage. Curr. Top. Med. Chem. 1, 529–539.
Fabiano, B., Currò, F., Reverberi, A.P., Palazzi, E., 2014. Coal dust emissions: from environmental control to risk minimization by underground transport. An applicative case-study. Process Saf. Environ. Prot. 92, 150–159. https://doi.org/10.1016/j.psep.2013.01.002.
Font, O., Moreno, T., Querol, X., Martins, V., Sánchez Rodas, D., de Miguel, E., Capdevila, M., 2019. Origin and speciation of major and trace PM elements in the Barcelona subway system. Transp. Res. Part D Transp. Environ. 72, 17–35. https://doi.org/10.1016/j.trd.2019.03.007.
Ghio, A.J., Madden, M.C., 2017. Human lung injury following exposure to humic substances and humic-like substances. Environ. Geochem. Health 1–11. https://doi.org/10.1007/s10653-017-0008-5.
Ghose, M.K., Majee, S.R., 2007. Characteristics of hazardous airborne dust around an indian surface coal mining area. Environ. Monit. Assess. 130, 17–25. https://doi.org/10.1007/s10661-006-9448-6.
Gilmour, M.I., O'Connor, S., Dick, C.A.J., Miller, C.A., Linak, W.P., 2004. Differential pulmonary inflammation and in vitro cytotoxicity of size-fractionated fly ash particles from pulverized coal combustion. J. Air Waste Manag. Assoc. 54 (3), 286–295. https://doi.org/10.1080/10473289.2004.10470906.
Godri, K.J., Harrison, R.M., Evans, T., Baker, T., Dunster, C., Mudway, I.S., Kelly, F.J., 2011. Increased oxidative burden associated with traffic component of ambient particulate matter at roadside and urban background schools sites in London. PLoS One 7, e21961. https://doi.org/10.1371/journal.pone.0021961.
Gustafsson, Å., Krais, A.M., Gorzsás, A., Lundh, T., Gerde, P., 2018. Isolation and characterization of a respirable particle fraction from residential house-dust. Environ. Res. 161, 284–290. https://doi.org/10.1016/J.ENVRES.2017.10.049.
Haibin, L., Zhenling, L., 2010. Recycling utilization patterns of coal mining waste in China. Resour. Conserv. Recycl. 54, 1331–1340. https://doi.org/10.1016/j.resconrec.2010.05.005.
Hamilton, R.F.Jr., Wu, N., Porter, D., Buford, M., Wolfarth, M., Holian, A., 2009. Particle length-dependent titanium dioxide nanomaterials toxicity and bioactivity. Part. Fibre Toxicol. 6, 35. https://doi.org/10.1186/1743-8977-6-35.
He, J., Li, W., Liu, J., Chen, S., Frost, R.L., 2019. Investigation of mineralogical and bacteria diversity in Nanxi River affected by acid mine drainage from the closed coal mine: Implications for characterizing natural attenuation process. Spectrochim. Acta Part A Mol. Biomol. Spectrosc. 217, 263–270. https://doi.org/10.1016/J.SAA.2019.03.069.
Hendryx, M., O'Donnell, K., Horn, K., 2008. Lung cancer mortality is elevated in coal-mining areas of Appalachia. Lung Cancer 62, 1–7. https://doi.org/10.1016/j.lungcan.2008.02.004.
Huang, X., Fournier, J., Koenig, K., Chen, L.C., 1998. Buffering capacity of coal and its acid-soluble Fe^{2+} content: possible role in coal workers' pneumoconiosis. Chem. Res. Toxicol. 11, 722–729. https://doi.org/10.1021/tx970151o.
Huang, X., Li, W., Attfield, M.D., Nádas, A., Frenkel, K., Finkelman, R.B., 2005. Mapping and prediction of Coal Workers' Pneumoconiosis with bioavailable iron content in the bituminous coals. Environ. Health Perspect. 113, 964–968. https://doi.org/10.1289/ehp.7679.
Hudson-Edwards, K.A., Smith, A.M.L.D., Bennett, A.J., Murphy, P.J., Wright, K., 2008. Comparison of the structures of natural and synthetic Pb-Cu-jarosite-type compounds. Eur. J. Mineral. 20, 241–252. https://doi.org/10.1127/0935-1221/2008/0020-1788.
Iriyama, K., Yoshiura, M., Iwamoto, T., Ozaki, Y., 1984. Simultaneous determination of uric and ascorbic acids in human serum by reversed-phase high-performance liquid chromatography with electrochemical detection. Anal. Biochem. 141, 238–243. https://doi.org/10.1016/0003-2697(84)90451-2.
Janssen, N.A.H., Yang, A., Strak, M., Steenhof, M., Hellack, B., Gerlofs-Nijland, M.E., Kuhlbusch, T., Kelly, F., Harrison, R., Brunekreef, B., Hoek, G., Cassee, F., 2014. Oxidative potential of particulate matter collected at sites withdifferent source characteristics. Sci. Total Environ. 472, 572–581. https://doi.org/10.1016/j.scitotenv.2013.11.099.
Jiang, X., Lu, W.X., Zhao, H.Q., Yang, Q.C., Yang, Z.P., 2014. Potential ecological risk assessment and prediction of soil heavy-metal pollution around coal gangue dump. Nat. Hazards Earth Syst. Sci. Discuss. 14, 1599–1610. https://doi.org/10.5194/nhess-14-1599-2014.
Johann-Essex, V., Keles, C., Rezaee, M., Scaggs-Witte, M., Sarver, E., 2017. Respirable coal mine dust characteristics in samples collected in central and northern Appalachia. Int. J. Coal Geol. 182, 85–93. https://doi.org/10.1016/J.COAL.2017.09.010.
Kadiiska, M.B., Mason, R.P., Dreher, K.L., Costa, D.L., Ghio, A.J., 1997. In vivo evidence of free radical formation in the rat lung after exposure to an emission source air pollution particle †. Chem. Res. Toxicol. 10, 1104–1108. https://doi.org/10.1021/tx970049r.
Kelly, F.J., 2003. Oxidative stress: its role in air pollution and adverse health effects. Occup. Environ. Med. 60, 612–616. https://doi.org/10.1136/oem.60.8.612.
Kerolli–Mustafa, M., Fajković, H., Rončević, S., Ćurković, L., 2015. Assessment of metal risks from different depths of jarosite tailing waste of Trepça Zinc Industry, Kosovo based on BCR procedure. J. Geochemical Explor. 148, 161–168. https://doi.org/10.1016/J.GEXPLO.2014.09.001.
Ketris, M.P., Yudovich, Y.E., 2009. Estimations of Clarkes for Carbonaceous biolithes: world averages for trace element contents in black shales and coals. Int. J. Coal Geol. 78, 135–148. https://doi.org/10.1016/J.COAL.2009.01.002.
Kim, A.G., 2004. Locating fires in abandoned underground coal mines. Int. J. Coal Geol. 59, 49–62. https://doi.org/10.1016/j.coal.2003.11.003.
Kolitsch, U., Pring, A., 2001. Crystal chemistry of the crandallite, beudantite and alunite groups: a review and evaluation of the suitability as storage materials for toxic metals. J. Mineral. Petrol. Sci. 96, 67–78. https://doi.org/10.2465/jmps.96.67.
Li, N., Sioutas, C., Cho, A., Schmitz, D., Misra, C., Sempf, J., Wang, M., Oberley, T., Froines, J., Nel, A., 2003. Ultrafine particulate pollutants induce oxidative stress and mitochondrial damage. Environ. Health Perspect. 111, 455–460. https://doi.org/10.1289/ehp.6000.
Li, N., Xia, T., Nel, A.E., 2008. The role of oxidative stress in ambient particulate matter-induced lung diseases and its implications in the toxicity of engineered nanoparticles. Free Radical Bio Med. 44, 1689–1699. https://doi.org/10.1016/j.freeradbiomed.2008.01.028.
Li, H., Ji, H., Shi, C., Gao, Y., Zhang, Y., Xu, X., Ding, H., Tang, L., Xing, Y., 2017. Distribution of heavy metals and metalloids in bulk and particle size fractions of soils from coal-mine brownfield and implications on human health. Chemosphere 172, 505–515. https://doi.org/10.1016/J.CHEMOSPHERE.2017.01.021.
Li, S., Xie, B., Hu, S., Jin, H., Liu, H., Tan, X., Zhou, F., 2019. Removal of dust produced in the roadway of coal mine using a mining dust filtration system. Adv. Powder Technol. 30, 911–919. https://doi.org/10.1016/J.APT.2019.02.005.
Liang, Y., Wong, O., Yang, L., Li, T., Su, Z., 2006. The development and regulation of occupational exposure limits in China. Regul. Toxicol. Pharmacol. 46, 107–113. https://doi.org/10.1016/j.yrtph.2006.02.007.
Madzivire, G., Maleka, R.M., Tekere, M., Petrik, L.F., 2019. Cradle to cradle solution to problematic waste materials from mine and coal power station: acid mine drainage, coal fly ash and carbon dioxide. J. Water Process Eng. 30, 100474. https://doi.org/10.1016/j.jwpe.2017.08.012.
Mohanty, A.K., Lingaswamy, M., Rao, V.G., Sankaran, S., 2018. Impact of acid mine drainage and hydrogeochemical studies in a part of Rajrappa coal mining area of Ramgarh District, Jharkhand State of India. Groundw. Sustain. Dev. 7, 164–175.

https://doi.org/10.1016/J.GSD.2018.05.005.
Moreno, T., Higueras, P., Jones, T., McDonald, I., Gibbons, W., 2005. Size fractionation in mercury-bearing airborne particles (HgPM10) at Almadén, Spain: implications for inhalation hazards around old mines. Atmos. Environ. 39, 6409–6419. https://doi.org/10.1016/j.atmosenv.2005.07.024.
Moreno, T., Martins, V., Querol, X., Jones, T., BéruBé, K., Minguillón, M.C., Amato, F., Capdevila, M., de Miguel, E., Centelles, S., Gibbons, W., 2015. A new look at inhalable metalliferous airborne particles on rail subway platforms. Sci. Total Environ. 505, 367–375. https://doi.org/10.1016/J.SCITOTENV.2014.10.013.
Moreno, T., Kelly, F.J., Dunster, C., Oliete, A., Martins, V., Reche, C., Minguillón, M.C., Amato, F., Capdevila, M., de Miguel, E., Querol, X., 2017. Oxidative potential of subway PM2.5. Atmos. Environ. 148, 230–238. https://doi.org/10.1016/J.ATMOSENV.2016.10.045.
Moreno, T., Trechera, P., Querol, X., Lah, R., Johnson, D., Wrana, A., Williamson, B., 2019. Trace element fractionation between PM10 and PM2.5 in coal mine dust: implications for occupational respiratory health. Int. J. Coal Geol. 203, 52–59. https://doi.org/10.1016/j.coal.2019.01.006.
Murphy, P.J., Smith, A.M.L., Hudson-Edwards, K.A., Dubbin, W.E., Wright, K., 2009. Raman and IR spectroscopic studies of Alunite-supergroup compounds containing Al, Cr^{3+}, Fe^{3+} and V^{3+} at the B Site. Can. Mineral. 47, 663–681. https://doi.org/10.3749/canmin.47.3.663.
Niosh, 2002. Health effects of occupational exposure to respirable crystalline silica. DHHS Publ. No. 2002-129 145, 127 https://doi.org/2002-129.
O'Keefe, J.M.K., Henke, K.R., Hower, J.C., Engle, M.A., Stracher, G.B., Stucker, J.D., Drew, J.W., Staggs, W.D., Murray, T.M., Hammond, M.L., Adkins, K.D., Mullins, B.J., Lemley, E.W., 2010. CO_2, CO, and Hg emissions from the Truman Shepherd and Ruth Mullins coal fires, eastern Kentucky. USA. Sci. Total Environ. 408, 1628–1633. https://doi.org/10.1016/J.SCITOTENV.2009.12.005.
Oberdöster, G., Ferin, J., Lehnert, B.E., 1992. Correlation between particle size, in vivo particle persistence, and lung injury. Environ. Health Perspect. 102, 173–179. https://doi.org/10.1289/ehp.102-1567252.
Pallarés, J., Herce, C., Bartolomé, C., Peña, B., 2017. Investigation on co-firing of coal mine waste residues in pulverized coal combustion systems. Energy 140, 58–68. https://doi.org/10.1016/J.ENERGY.2017.07.174.
Pant, P., Baker, S.J., Shukla, A., Maikawa, C., Godri Pollit, K.J., Harrison, R.M., 2015. The PM10 fraction of road dust in the UK and India: characterization, source profiles and oxidative potential. Sci. Total Environ. 530-531, 445–452. https://doi.org/10.1016/j.scitotenv.2015.05.084.
Patra, A.K., Gautam, S., Kumar, P., 2016. Emissions and human health impact of particulate matter from surface mining operation-A review. Environ. Technol. Innov. 5, 233–249. https://doi.org/10.1016/j.eti.2016.04.002.
Pavan, C., Fubini, B., 2017. Unveiling the variability of "Quartz hazard" in light of recent toxicological findings. Chem. Res. Toxicol. 30, 469–485. https://doi.org/10.1021/acs.chemrestox.6b00409.
Pavan, C., Delle Piane, M., Gullo, M., Filippi, F., Fubini, B., Hoet, P., Horwell, C.J., Huaux, F., Lison, D., Lo Giudice, C., Martra, G., Montfort, E., Schins, R., Sulpizi, M., Wegner, K., Wyart-Remy, M., Ziemann, C., Turci, F., 2019. The puzzling issue of silica toxicity: are silanols bridging the gaps between surface states and pathogenicity? Part. Fibre Toxicol. 16, 32. https://doi.org/10.1186/s12989-019-0315-3.
Petavratzi, E., Kingman, S., Lowndes, I., 2005. Particulates from mining operations: a review of sources, effects and regulations. Miner. Eng. 18, 1183–1199. https://doi.org/10.1016/j.mineng.2005.06.017.
Querol, X., 1993. The Occurrence and Distribution of Trace Elements in the Teruel Mining District Coals and Their Behaviour During Coal Combustion. European Coal and Steel Community Project 7220/ED/014.
Querol, X., Whateley, M.K.G., Fernández-Turiel, J.L., Tuncali, E., 1997. Geological controls on the mineralogy and geochemistry of the Beypazari lignite, central Anatolia. Turkey. Int. J. Coal Geol. 33, 255–271. https://doi.org/10.1016/S0166-5162(96)00044-4.
Querol, X., Izquierdo, M., Monfort, E., Alvarez, E., Font, O., Moreno, T., Alastuey, A., Zhuang, X., Lu, W., Wang, Y., 2008. Environmental characterization of burnt coal gangue banks at Yangquan, Shanxi Province. China. Int. J. Coal Geol. 75, 93–104. https://doi.org/10.1016/J.COAL.2008.04.003.
Querol, X., Zhuang, X., Font, O., Izquierdo, M., Alastuey, A., Castro, I., van Drooge, B.L., Moreno, T., Grimalt, J.O., Elvira, J., Cabañas, M., Bartroli, R., Hower, J.C., Ayora, C., Plana, F., López-Soler, A., 2011. Influence of soil cover on reducing the environmental impact of spontaneous coal combustion in coal waste gobs: a review and new experimental data. Int. J. Coal Geol. 85, 2–22. https://doi.org/10.1016/j.coal.2010.09.002.
Rout, T.K., Masto, R.E., Padhy, P.K., George, J., Ram, L.C., Maity, S., 2014. Dust fall and elemental flux in a coal mining area. J. Geochemical Explor. 144, 443–455. https://doi.org/10.1016/J.GEXPLO.2014.04.003.
Sarver, E., Keles, C., Rezaee, M., 2019. Beyond conventional metrics: comprehensive characterization of respirable coal mine dust. Int. J. Coal Geol. 207, 84–95. https://doi.org/10.1016/j.coal.2019.03.015.
Schins, R.P.F., Borm, Pa.J.A., 1999. Mechanisms and mediators in coal dust InducedToxicity: a review. Ann. Occup. Hyg. 43, 7–33. https://doi.org/10.1016/S0003-4878(98)00069-6.
Smith, A.M.L., Hudson-Edwards, K.A., Dubbin, W.E., Wright, K., 2006. Dissolution of jarosite [KFe3(SO4)2(OH)6] at pH 2 and 8: insights from batch experiments and computational modelling. Geochim. Cosmochim. Acta 70, 608–621. https://doi.org/10.1016/J.GCA.2005.09.024.
Soltani, N., Keshavarzi, B., Sorooshian, A., Moore, F., Dunster, C., Dominguez, A.O., Kelly, F.J., Dhakal, P., Ahmadi, M.R., Asadi, S., 2018. Oxidative potential (OP) and mineralogy of iron ore particulate matter at the Gol-E-Gohar Mining and Industrial Facility (Iran). Environ. Geochem. Health 40, 1785–1802. https://doi.org/10.1007/s10653-017-9926-5.
Sperazza, M., Moore, J.N., Hendrix, M.S., 2004. High-resolution particle size analysis of naturally occurring very fine-grained sediment through laser diffractometry. J. Sediment. Res. A Sediment. Petrol. Process. 74, 736–743. https://doi.org/10.1306/031104740736.
Tang, Z., Chai, M., Cheng, J., Jin, J., Yang, Y., Nie, Z., Huang, Q., Li, Y., 2017. Contamination and health risks of heavy metals in street dust from a coal-mining city in eastern China. Ecotoxicol. Environ. Saf. 138, 83–91. https://doi.org/10.1016/j.ecoenv.2016.11.003.
Turci, F., Pavan, C., Leinardi, R., Tomatis, M., Pastero, L., Garry, D., Anguissola, S., Lison, D., Fubini, B., 2015. Revisiting the paradigm of silica pathogenicity with synthetic quartz crystals: the role of crystallinity and surface disorder. Part. Fibre Toxicol. 13, 32. https://doi.org/10.1186/s12989-016-0136-6.
Valko, M., Jomova, K., Rhodes, C.J., Kuča, K., Musílek, K., 2016. Redox- and non-redox-metal-induced formation of free radicals and their role in human disease. Arch. Toxicol. https://doi.org/10.1007/s00204-015-1579-5.
Visser, G.T., 1992. A wind-tunnel study of the dust emissions from the continuous dumping of coal. Atmos. Environ. Part A. Gen. Top. 26, 1453–1460. https://doi.org/10.1016/0960-1686(92)90130-D.
Welch, S.A., Kirste, D., Christy, A.G., Beavis, F.R., Beavis, S.G., 2008. Jarosite dissolution II—reaction kinetics, stoichiometry and acid flux. Chem. Geol. 254, 73–86. https://doi.org/10.1016/j.chemgeo.2008.06.010.

4.4. Article #4

Comprehensive evaluation of potential coal mine dust emissions in an open-pit coal mine in Northwest China

Authors:

Pedro Trechera[a, b], Teresa Moreno[a], Patricia Córdoba[a], Natalia Moreno[a], Xinguo Zhuang[c], Baoqing Li[c], Jing Li[c], Yunfei Shangguan[c], Ana Oliete Dominguez[d], Frank Kelly[d], Xavier Querol[a,c]

a) Institute of Environmental Assessment and Water Research (IDAEA-CSIC), 08034 Barcelona, Spain.
b) Department of Natural Resources and Environment, Industrial and TIC Engineering (EMIT-UPC), 08242 Manresa, Spain.
c) Key Laboratory of Tectonics and Petroleum Resources, China University of Geosciences, Ministry of Education, Wuhan 430074, China.
d) MRC-PHE Centre for Environment and Health, King's College London, London SE1 9NH, UK.

Published in:

International Journal of Coal Geology, 235, 103677

DOI: 10.1016/j.coal.2021.103677

Accepted date:

1 January 2021 (Open access)

Impact factor/Quartile

6.806/Q1

International Journal of Coal Geology 235 (2021) 103677

Contents lists available at ScienceDirect

International Journal of Coal Geology

journal homepage: www.elsevier.com/locate/coal

Comprehensive evaluation of potential coal mine dust emissions in an open-pit coal mine in Northwest China

Pedro Trechera [a,b,*], Teresa Moreno [a], Patricia Córdoba [a], Natalia Moreno [a], Xinguo Zhuang [c], Baoqing Li [c], Jing Li [c], Yunfei Shangguan [c], Ana Oliete Dominguez [d], Frank Kelly [d], Xavier Querol [a,c]

[a] Institute of Environmental Assessment and Water Research (IDAEA-CSIC), 08034 Barcelona, Spain
[b] Department of Natural Resources and Environment, Industrial and TIC Engineering (EMIT-UPC), 08242 Manresa, Spain
[c] Key Laboratory of Tectonics and Petroleum Resources, China University of Geosciences, Ministry of Education, Wuhan 430074, China
[d] MRC-PHE Centre for Environment and Health, King's College London, London SE1 9NH, UK

ARTICLE INFO

Keywords:
Coal mine dust
Oxidative potential
Tailings
Mineralogy
Particle size
Geochemistry
Respirable dust fraction

ABSTRACT

Coal mining in China is continually increasing, and the associated emitted coal mine dust is of growing environmental and occupational concern. In this study, deposited coal mine dust (DD) was analysed in three different regions of an active, highly-volatile bituminous open-pit coal mine in the Xingjian Province, Northwest of China: coal working fronts, tailings handling sites, and road traffic sites. Samples were analysed for particle size, and geochemical and mineralogical patterns, and then compared with the respirable DD fractions (RDDs, <4 μm) separated from DD samples. Online measurements of ambient air concentrations of particulate matter (PM_{10} and $PM_{2.5}$), black carbon (BC) and ultrafine particles (UFP) were performed in the same mine zones where DD was sampled.

Furthermore, the RDD samples were subjected to analysis of specific biological response or toxicological indicators (oxidative potential, OP). The results demonstrated: i) large differences in particle size and composition among DD from tailings handling, road traffic and coal working front sites, ii) a strong influence of the DD moisture contents and ash yields on particle size, and, accordingly, on the potential dust emissions, iii) an enrichment of multiple elements (such as Nb, Th, Cr, Sr, Li, As, Pb, Cu, Zr and Ni) in the RDD from coal working fronts compared with their contents in the worked parent coal seams, mostly attributed to mining machinery, tyre and brake wear emissions and to deposition of dust emitted from gangue working zones, iv) low OP values of the RDD emitted from the studied mine, which works a high-quality coal, with OP being influenced by Mn, sulphate and anatase (TiO_2) contents, and v) the impact of specific mining operations and mine areas on the levels of air pollutants, such as high PM from tailings handling in the upper parts of the mine or the high UFP levels in the bottom of the mine (due to vehicle and machinery emissions and lower dispersive conditions). The data presented here demonstrate the necessity of extracting the more deeply respirable size fraction of coal mine dusts in future studies on the health effects of these materials because this finer fraction is mineralogically and geochemically different from the parent rocks.

1. Introduction

Coal represents the second most consumed energy source worldwide, accounting for 27.2% of the total, less only than oil (33.6%) (BP, 2019). Even though consumption of coal is decreasing in some regions, such as Europe and North America, coal consumption will continue to increase during the next two decades according to the International Energy Agency (IEA), World Coal Association (WCA) and British Petroleum (BP) (BP, 2019; IEA, 2019; WCA, 2020). The Asiatic Pacific region will be principally responsible for this increase, as increased demand and extraction of coal are expected there in the near future. The primary demand originates mainly from China, where coal is the main energy source (58.2% of total energies consumed). This makes it the principal country consumer of coal (50.5%), followed by India and USA (12.0%

* Corresponding author at: Institute of Environmental Assessment and Water Research (IDAEA-CSIC), 08034 Barcelona, Spain.
E-mail address: pedro.trechera@idaea.csic.es (P. Trechera).

https://doi.org/10.1016/j.coal.2021.103677
Received 29 July 2020; Received in revised form 23 December 2020; Accepted 1 January 2021
Available online 8 January 2021

and 8.4%, respectively)(BP, 2019).

Coal can be extracted by two mining methods, surface mining and underground mining, both depending on topographical features, accessibility, overburden thickness, and groundwater presence, among other factors (Lee, 1990). In open-pit coal mining, dust produced during coal extraction is a ubiquitous health concern, but other related processes can also produce dust. So, in open-pit coal mines, multiple activities must be taken into account when analysing the environmental conditions in the different sections to ensure safety for the workers and other individuals surrounding the mine. These activities include: i) drilling and extraction of rocks and sand necessary to find the coal seam, ii) explosion control to remove rocks in the area of interest, iii) coal mine dust gangue manipulation, extraction and transportation, iv) use of different diesel and gasoline transportation machinery (trucks, drillers, washers, excavators, and others), and v) coal extraction and transportation.

Coal mine dust is a common hazard generated during coal production. This is a complex and heterogeneous mixture composed of particles of different sizes and compositions from a variety of minerals, organic compounds and coal species (Caballero-Gallardo and Olivero-Verbel, 2016; Dalal et al., 1995; Liu et al., 2005; Pedroso-Fidelis et al., 2020). All these characteristics depend on the properties of the parent coal and gangue, and the different mining activities conducted in the coal mines (Dalal et al., 1995). It is important to consider the suspended respirable fraction (particle size <4 μm) of coal mine dust produced during coal activities, since it is primarily responsible for coal workers' pneumoconiosis (CWP) and silicosis (Cheng et al., 2016; Erol et al., 2013; Shi et al., 2019). Moreover, high levels of coal mine dust can present a significant risk of spontaneous combustion in (mostly underground) coal mines (Liu et al., 2010; Ma et al., 2020; Shimura and Matsuo, 2019). Furthermore, coal and coal gangue fires might occur in open-pits, which would result in the emission of both particulate and gaseous pollutants.

Due to technical improvements, finer coal milling products, and increased efficiencies for coal extraction are occurring in coal mines, and accordingly coal mine (finer) dust emissions have increased. Simultaneously, CWP injuries have also risen (Gamble, 2012; Johann-Essex et al., 2017; Sarver et al., 2019; Suarthana et al., 2011), influenced by these and possibly other factors such as the size of the mine, the miners' tasks and type of coal could also affect the increase in CWP (Sarver et al., 2019; Suarthana et al., 2011).

One of the major concerns regarding occupational health relevance is the particle size of suspended coal mine dust, sensu *lato,* which originates from the above multiple mining activities and emission sources (Richardson et al., 2018), including also soot from vehicles and machinery or coal self-combustion.

Coal mine dust is generally coarse in size, with its suspended mass being coarser than the respirable particulate matter (PM) fraction PM_4 (<4 μm). Thus, studies carried out along coal conveys into mines have measured low (4–13%) contents of respirable dust in ambient bulk coal dust, defined as coal dust particles with a diameter ≤ 74 μm (Shahan et al., 2017). On the other hand, atmospheric PM emissions from exhaust and spontaneous coal burns would be expected to have a dominantly ultrafine particle (UFP) size (< 0.1 μm) (Dias et al., 2014; Kurth et al., 2014). These two types of ambient suspended particles (PM_4 and UFP) likely have different occupational health effects. The former are retained in the alveoli and thus may damage mainly the respiratory systems (WHO, 2013), whereas the latter are potentially capable of passing through the lung to enter the circulatory system, to be translocated to other organs of the body (Cassee et al., 2019, 2011; Heusinkveld et al., 2016).

The presence of respirable crystalline silica (RCS) in coal mine dust is extremely important as this is known to be responsible for CWP injuries and lung cancer (Brodny and Tutak, 2018; Castranova, 2000; Cohen et al., 2008; NIOSH, 2002). Furthermore, the elevated content of metals and/or some organic pollutants in the dust could substantially increase the oxidative stress caused by mining dust, thus also increasing potential precursors of some injuries (Birben et al., 2012; Ghio and Madden, 2018; Ercal et al., 2005; Schins and Borm, 1999; Valko et al., 2016). Some metals and metalloids (Fe, Ti, Mn, Cu, Sb, Sn, Pb, Zn, Cr, V, As and Ni) present in the respirable fraction in high concentrations can produce negative health effects in humans (Dai et al., 2014; Dai and Finkelman, 2018; Finkelman, 1994; Fu et al., 2014; Hower and Robertson, 2003; Latvala et al., 2016; Moreno et al., 2019; Riley et al., 2012).

The aim of the present work is to evaluate the potential dust emissions in an open-pit coal mine working high-quality Jurassic coal in the Xinjiang Province, Northwest of China. To this end, a detailed study of the open-pit mine was carried out, where mining dust generated different activities and sources were measured, sampled and analysed. The analyses include particle size, morphology, chemistry, mineralogy and oxidative stress of deposited dust (DD) and the respirable DD fraction (RDD) separated from the DD which was collected in multiple dust hotspots in the mine. The parent coal was analysed for comparison purposes with the DD and RDD from the working front. Furthermore, online exposure measurements for PM finer than 2.5 and 10 μm ($PM_{2.5}$ and PM_{10}), black carbon (BC), and UFP, were also included for comparison of the impact of different mining activities on exposure to these pollutants.

2. Geological setting

Wucaiwan open-pit coal mine is located in Jimusaer County, Xinjiang Province, Northwest of China (Fig. 1A). The open-pit covers approximately 24 km^2 and contains recoverable coal reserves of approximately 1.7 billion tones. The annual production capacity of coal mine is 20 million tonnes in 2017. This coal mine was opened since 2006, with an estimation of 63 years of life.

The Wucaiwan open-pit coal mine is located in the Western margin of Eastern Junggar Coalfield (Fig. 1B), where the Jurassic Badaowan, Sangonghe, and Xishanyao Formations are the coal-bearing strata (Fig. 1C). Among these, the Middle Jurassic Xishanyao Formation is the predominant coal-bearing unit, and, it is made up by finely grained sandstone, with coal seams, and minor siltstone and carbonaceous mudstone (Fig. 1D). The Xishanyao Formation conformably overlies the Early Jurassic Sangonghe Formation and conformably underlies the Late Jurassic Shishugou Formation (Fig. 1D). Based on the coal exploration data of Eastern Junggar Coalfield, the thickness of the Xishanyao Formation in the Wucaiwan open-pit coal mine ranges from 37 m to 198 m with an average of 136 m; it contains one workable coal seams, and, its average thickness is 60 m.

Previous coal exploration data of Eastern Junggar Coalfield show that the Middle Jurassic mineable coal seam is high-volatile bituminous and contains medium moisture content (≈13%), low ash yield (≈6%), and low sulphur content (≈0.4%). The coal quality is discussed in detail in previously published papers (Li et al., 2012; Zhou et al., 2010).

3. Methodology

3.1. Sampling

A total of seven tailing and coal working zones were examined in the Wucaiwan open-pit coal mine over two working days. These sample locations were selected to characterise dust from most mining activities in the open-pit. These included coal extraction (coal front), coal transportation, drilling, truck traffic and tailings handling. Fig. 1C shows a simplified map of the open-pit mine and the investigated zones. Dust from coal working front was studied in the C and D zones, where, in addition, two-parent coal channel profiles (CPs) were sampled.

Table S1 summarises the location and origin of the thirteen DD samples collected (six in coal fronts and seven in tailing-related activities). DD samples were collected using plastic trays and brushes, and, kept in sealed plastic bags until analysis. Trays were left in the vicinity of the specific operations for approximately thirty minutes, until DD mass

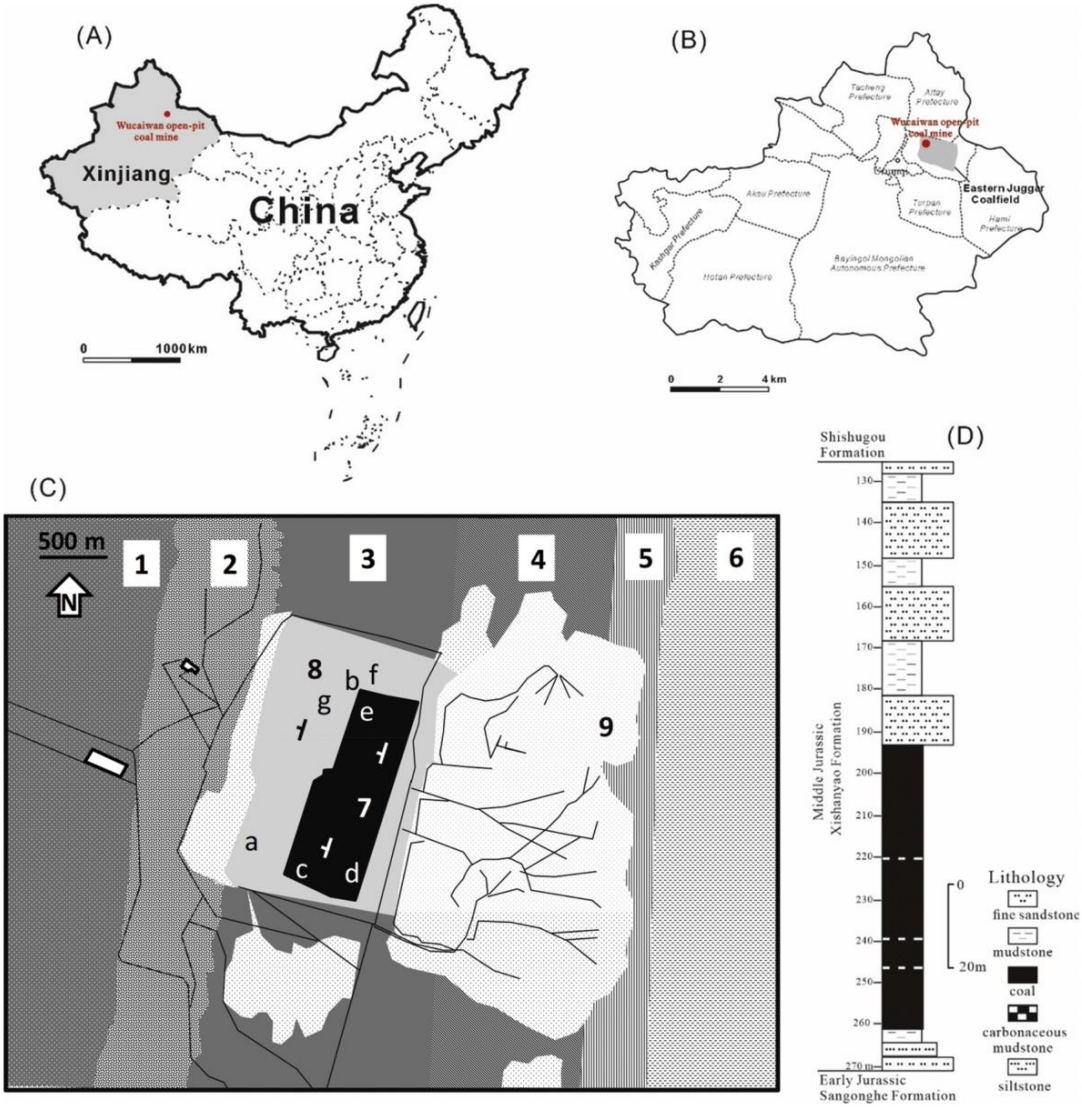

Fig. 1. Location of Wucaiwan open-pit coal mine in China (A), and, in Xinjiang Province, Northwest of China (B). Geological map of the Wucaiwan open-pit coal mine with the working areas where measurements of meteorological parameters, BC, UFP, PM_{10}, $PM_{2.5}$ and sampling of PM, deposited dust and coal channel profiles were carried out (C). Stratigraphic series of Wucaiwan open-pit (D). *a/b-TH, Tailings handling; c/d/e- CWF, Coal working front; f-TH; g-RT, Road traffic into a mine road for tailings. Legend: 1-Quaternary; 2-Middle-Late Jurassic Shishugou group; 3-Middle Jurassic Xishanyao formation; 4-Early Jurassic Sangonghe formation; 5-Early Jurassic Badaowan formation; 6-Middle-Late Triassic Xiaoquangou group; 7-Worked coal outcrops; 8-Tailings disposal into the pit; 9-Tailings disposal outside the pit.*

(around 200–500 g) was enough for subsequent analysis. Samples were stored without light, hermetically closed and at room temperature to prevent oxidation processes. Passive stubs for scanning electron microscopy with energy dispersion spectroscopy (SEM-EDS) analyses with graphite label surfaces were placed in all zones for 1-h collection of ambient air samples. Finally, real-time measurements of ambient concentrations of suspended PM, BC and UFP, as well as meteorological parameters, and sampling of PM_{10} were carried out at the above seven locations where DD was sampled, Tables S2 and S3.

Ambient air PM_{10}, PM_4, or $PM_{2.5}$ were generally not sampled because the sampling work was allowed inside the mine for only one day and a half. Given this time constraint, collecting DD and extracting from it RDD (at the laboratory) allowed the sampling of different areas and operations. Thus, a limitation of the study is that RDD was not air sampled but obtained from DD. This study does not take into account how, for example, the intensity of different mining activities might change over time, or how varying meteorological conditions might affect dust loading. However, sampling in numerous locations provided very valuable information. In any case this is an arid region and relative humidity (RH) is normally low and similar to that one measured during sampling campaign. Finally, one clear advantage was that the whole sampling campaign was carried out while the coal mine workers were performing their daily work operations with total normality, thus allowing us to capture a representative snapshot of a typically working day in the open-pit mine.

3.2. Analysis

3.2.1. Sample pre-treatment and particle size

Before analysis, all DD samples collected were sieved <500 μm (with only a very minor amount being >500 μm). After this point DD will be refer to this <500 μm DD fraction. Then, DD samples were riffled to obtain two sub-samples of 100 g, from one of which 50 g were used for RDD extraction. Sub-samples of 0.10 to 2.0 g were obtained from the DD

and RDD for the different analyses. A total of thirteen DD (Table S1) and two CP samples were collected from open-pit coal mine areas where most dust emitting mining activities were conducted, and these were compared with the parent coal. A mechanical dust size-separator device (Moreno et al., 2005) was used in the laboratory to separate the RDD from the DD samples. Since obtaining RDD from DD is a laborious task, eight from the thirteen DD samples were selected to this end, based on the similarity of particle size distribution (PSD), mineral and chemical compositions and covering all the locations sampled. Thus, four DD samples were selected from the coal working and four from tailings handling. Around 50 g of untreated DD samples were introduced into the PM separator to be mechanically re-suspended in a rotator and a pump at 25 L·min^{-1} to separate the RDD fraction on polycarbonate filters (47 mm diameter, 0.60 μm pore size). The size distribution of each collected RDD was measured to confirm their respirable size (<4 μm).

A Malvern Mastersizer was used for PSD analysis of DD and RDD samples, 1.0 g and 0.25 g respectively. A Scirocco 2000 extension was used to analyse the particle size in dry conditions when a large sample volume was available, and a HydroG 2000 extension was used for low sample volumes, following the method of Sperazza et al. (2004) based on suspension in a Na polyphosphate solution. Malvern Mastersizer Scirocco 2000 extension measurements were performed at the ICTS NANBIOSIS by the Nanostructured Liquids Unit (U12) of the CIBER in Bioengineering, Biomaterials & Nanomedicine (CIBER-BBN), located at the IQAC-CSIC (Barcelona, Spain).

3.2.2. Mineralogical and morphological characterisation

Mineralogical characterisation of 1.0 g of CP and DD, and 0.30 g of RDD samples were conducted by powder X-ray diffraction (XRD). A Bruker D8 Advance A25, θ-θ diffractometer with CuKα1 radiation, Bragg-Brentano geometry, and a position-sensitive Lynx Eye detector, was used for these analyses. Diffractograms at 40 kV and 40 mA, scanning from 4 to 60° of 2 θ with a step size of 0.019° and a counting time of 0.10 s·step^{-1} maintaining the sample in rotation (15 min^{-1}) were performed. The crystalline phase identification was conducted using the EVA software package (Bruker), which utilised the ICDD (International Centre for Diffraction Data) database. Semi-quantitative XRD analysis was performed using the method devised by Chung (1974) for the quantitative analysis of multi-component systems, using quartz as an internal reference. Mixtures were obtained using powdered mineral reference materials and coal with very low ash to validate the semi-quantitative protocol (Fig. S1).

Scanning electron microscope JEOL JSM-7001F SEM-EDX with secondary and backscattered electron detectors from the Scientific-Technical Services of the University of Barcelona was used for morphological and chemical analysis of single particles deposited on the graphite surface of the passive samplers. To this end gold coating was used to qualitatively analyse the occurrence of specific RDD components of interest according the correlation of oxidative potential (OP) and mineral and elemental compositions.

3.2.3. Proximate, ultimate and chemical characterisation

Proximate and ultimate analyses followed ISO and ASTM procedures (ISO-589, 1981, ISO-1171, 1976, ISO-562, 1974, ASTM D-3286, D-3302M, D3174-12), with moisture and ash yields obtained at 150 °C and 750 °C, respectively. The amount of sample used was always around 0.50 g.

Before geochemical analysis, 0.10 g of samples were digested in HF-HNO_3-$HClO_4$ acid following the method by Querol et al. (1997, 1992) to retain potentially volatile elements, such as As and Se. The resulting acidic digestions were analysed for major and trace elements by using inductively-coupled plasma atomic-emission spectrometry (ICP-AES, Iris Advantage Radial ER/S device from Thermo Jarrell-Ash) and inductively-coupled plasma mass spectrometry (ICP-MS, X-SERIES II Thermo Fisher Scientific, Bremen, Germany). International reference materials SARM19 and NIST SRM 1633b, and blanks were treated in the same way. Because Si is lost during HF digestion, its content in DD and RDD samples was determined by X-ray fluorescence (XRF, Thermo Scientific ARL QUANT'X Energy-Dispersive X-ray fluorescence spectrometer) loading Teflon© 47 mm filters with 3.0 mg of the sample using an ethanol suspension. XRF Si/Al ratios obtained were applied to the Al determined by ICP-AES analysis of each sample. This method was validated using the above reference materials.

After five repetitions of the analysis of the above reference materials, analytical errors were estimated at ±1–6% for most major elements in both the SARM19 coal and NIST-1633b fly ash reference materials, with the exceptions of P in SARM19 (16%) and Na in the latter (10%, with relative standard deviations [RSDVs] ranging from 1 to 8%, with P exception in NIST-1633b-fly ash, 10%). Most of trace element errors for all certified and 'for reference' elements in SARM19 coal were in the range of ±0–5%, with the exception of Li, Sc, Ni, Cu, Zn, Y, Sn, Gd, Pb (±6–10%); Be, Se, Lu, Hf, W (±11–20%); Zr (27%), Cd (29%), Tm (31%), Sb (80%) and ± 0–5% for all certified and 'for reference' elements in NIST-1633b-fly ash, with the exception of Sc, Cu, Zn, Ge, Nb, Sn, Eu (6–10%); Be, Mo, Cd, Gd, Lu, Hf, Bi (11–20%); and Zr (21%), Tm (28%), Ta (30%) with RSDV <10% for most elements, with the exception of Y(11%), W (14%), Gd (15%), Sn (18%), Hf (18%), Li (20%), Tb (22%), Sb (23%), Zr (29%), Cd (46%), Zn (50%), Ta (52%) and Se (60%) for SARM19 and < 10% for all elements, with the exception of Lu (13%), Gd, Tm, Ta (29%) for NIST-1633b.

3.3. PM_{10} measurements

Ambient air PM_{10} in the mine was measured and collected using personal environmental monitoring (PEM) samplers equipped with Leland Pumps (10 L·min^{-1}) on PAL high purity 37 mm quartz microfibre filters of 2.0 μm pore size. Table S2 provides the location and duration of the four PEM samplings. Filters were weighed before and after sampling previous equilibrium over 48 h at 50% RH and 20 °C.

The PM_{10} filters were acid (HF-HNO_3-$HClO_4$) digested following the method by Querol et al. (2001). The resulting acidic digestions were analysed for major and trace elements using the above ICP-AES and ICP-MS instrumentation. These quartz filters have very low contents of major and trace elements and are widely used in air quality studies, but in any case, blank digestions and analyses were carried out and the blank concentrations for each element analysed subtracted of each sample.

3.4. Online measurements

To measure real-time ambient concentrations of suspended PM in emission hotspots in the open-pit, three real-time monitors were used in seven locations from zones A to G (Fig. 1C). For $PM_{2.5}$ and PM_{10} mass concentrations (in μg·m^{-3}), a Dust-track-TSI and an AirVisual Pro were used in all the zones of the mine, with a 30 s resolution. The latter also measured temperature (°C), RH (%) and CO_2 concentrations (ppm). For BC (μg·m^{-3}) and UFPs number concentration (#cm^{-3}), mainly influenced by the exhaust emissions of on-road and off-road vehicles/machinery, a microAeth® AE51 (zones A, C, D) and DiSCmini (zones A, C, D) monitors were used with a 10 and 60 s resolution. Table S3 summarises the relevant details of these measurements. Prior to use, instruments were compared with reference instruments: a GRIMM 1108 optical counter for Airvisual Pro (IQAir) and Dust-track, a CPC-TSI for Disc-mini, and a MAAP-Thermo for microAeth® AE51 (Fig. S2). Online measurements were always carried out close to the DD sample collection point of each zone, with the procedure in each case being: i) switching online measurements and PM sampling, ii) collecting DD samples, and iii) finishing online measurements and PM sampling.

3.5. Oxidative potential test

Oxidative potential was determined using a synthetic respiratory tract lining fluid (RTLF) validated by Mudway et al. (2004) and Zielinski

et al. (1999) containing the toxicological indicators, such as ascorbate (AA), urate (UA) and reduced glutathione (GSH) found in the surface of the lung. This is widely used to characterise the OP of atmospheric particles (Kelly, 2003, and references therein). When the particles are added to a solution of these tracers, the oxidation of AA, UA and GSH might occur as a function of their composition and size.

The oxidative stress of the RDD samples was evaluated by measuring the OP based on the consumption of the antioxidants AA, UA and GSH, according to the methodology by Soltani et al. (2018). This technique involves the resuspension of mg of each RDD in ethanol followed by a 4 h incubation with a synthetic solution containing equimolar concentrations of AA, UA and GSH. The consumption of AA, UA and GSH was determined by previously published methodology (Baker et al., 1990; Iriyama et al., 1984). In-house controls of PM-free, negative (M120, Cabot Corporation, USA) and positive PM (NIST1648a, urban particulate from NIST, USA) followed the same protocol for control purposes. The OP is expressed as the percentage of consumption of each antioxidant with reference to the in-house particle-free control. To obtain a metric for OP, the data was expressed as OP·μg^{-1} of PM (OP^{AA}·μg^{-1} PM and OP^{GSH}·μg^{-1} PM). Data for the individual antioxidants were also combined to provide a total OP value (OP^{TOTAL}·μg^{-1}).

4. Results

Sampling and measurements focused on three major activities: coal working fronts, tailings handling, and road traffic in the open-pit. Major patterns of DD samples and variability of ambient air levels of the studied pollutants in relation to these zones are described, with the intention of characterising dust from different activities and sources and identifying potential dust hazards for each activity. The section on results is divided into two parts, the first dealing with DD, RDD and OP, and a second on atmospheric measurements.

4.1. Deposited dust and respirable deposited dust

4.1.1. Particle size

Table 1 shows the analysed PSD patterns of DD samples using the dry method, as well as the respective moisture contents and ash yields. Fig. 2 compares data from the three mining activities listed above.

At the coal working fronts, DD was markedly coarser than at both tailings handling and road traffic sites, where DD had higher ash yields and lower moisture contents. The coal working fronts DD fractions <500 (DD500), <10 (DD10), <4 (DD4), and < 2.5 μm (DD2.5) reached 19–32, 9–15 and 5–9%volume (%vol), respectively, which were considerably lower than those of tailings handling (18–55, 11–38 and 6–27%vol), and road traffic (36, 23 and 15%vol), respectively. The moisture content of DD has been reported as a major driver of resuspension (Amato et al., 2010; Colinet et al., 2010; Medeiros et al., 2012; Xi et al., 2014). Eqs. (1) to (4) and fig. S3 (1–4) show the cross-correlation, using Pearson's correlation coefficients (r), of moisture contents with the proportion of the <500, <10, <4, and < 2.5 μm fractions of DD samples from the coal working fronts.

4.1.1.1. Coal working front

$$\mathrm{DD500}\ (\%\mathrm{vol} < 500\ \mu\mathrm{m}) = -1.84{*}\mathrm{Moisture}\ (\%\mathrm{ad}) + 107.18\ (\mathrm{r} = -0.60) \quad (1)$$

$$\mathrm{DD10}\ (\%\mathrm{vol} < 10\ \mu\mathrm{m}) = -0.77{*}\mathrm{Moisture}\ (\%\mathrm{ad}) + 32.98\ (\mathrm{r} = -0.66) \quad (2)$$

$$\mathrm{DD4}\ (\%\mathrm{vol} < 4\ \mu m) = -0.37{*}\mathrm{Moisture}\ (\%\mathrm{ad}) + 15.92\ (\mathrm{r} = -0.71) \quad (3)$$

$$\mathrm{DD2.5}\ (\%\mathrm{vol} < 2.5\ \mu\mathrm{m}) = -0.43{*}\mathrm{Moisture}\ (\%\mathrm{ad}) + 10.71\ (\mathrm{r} = -0.92) \quad (4)$$

The results indicate a clear (r = −0.92) decrease of the DD2.5 fraction with increasing moisture. In the case of the coarser fractions, the negative correlation persists but with lower significance (r = −0.60 to −0.71). This indicates that lower DD2.5 was available for resuspension in moistened DD. As it might be expected, high moisture in DD reduces the occurrence of DD2.5 due to the agglomeration effect caused by water. Sprayed water is frequently applied to the coal working fronts and unpaved mine roads to reduce re-suspension (Zhang et al., 2012). As shown in Table 1, coal working front DD samples reached the highest moisture contents due to the greater coal content in DD, but also because of the frequent wetting of the coal mine dust surfaces.

No correlation was found between DD and moisture in the tailings handling zone, probably because water is not spread in these areas of tailings disposal and moisture contents are very low. In this area some samples, usually located at the high-altitude zones of the pit, the RDD reached very high proportions of 20–38%vol of DD (samples BNW_DD_001, 008 and 009), much higher than in the wetter and coaly DD from the working front. This dry tailing DD has accordingly an increased resuspension potential during windy episodes and during transport of tailings, compared to DD from the coal fronts.

Eqs. (5)–(8) and fig. S3 (5–8) show the same regressions as above, but in this case, between the ash yields (% dry basis, db) from the coal working fronts. A clear positive correlation can be observed, (even higher than those for moisture contents), especially for DD2.5 ($r = 0.99$, excluding BNW_DD_013) with the ash yields (%db). Coals containing an elevated mineral content, usually fine clays and quartz, yield to a greater proportion of DD2.5 in DD than more low-ash yield varieties, the organic matrix of which produces coarser grains when breaking up into particles (Rosita et al., 2020; Sevim and Demir, 2019; Yang et al., 2019).

4.1.1.2. Coal working front

$$\mathrm{DD500}\ (\%\mathrm{vol} < 500\ \mu\mathrm{m}) = 1.13{*}\mathrm{Ash\ yield}\ (\%\mathrm{db}) + 74.36\ (\mathrm{r} = 0.67) \quad (5)$$

Table 1
Particle size distribution and results of proximate analysis of deposited dust (DD, <500 μm) samples. *TH, Tailings handling; CWF, Coal working front; RT, Road traffic into a mine road for tailings. M, moisture, HTA, Ash yield.*

Sample	Location	<500 μm (%wt)	<10 μm (%v)	<4 μm (%v)	<2.5 μm (%v)	M (%ad)	HTA (%db)
BNW_DD_002	C –CWF	99.03	30.25	14.02	8.70	5.50	24.78
BNW_DD_012	C –CWF	99.53	25.27	11.86	7.25	5.52	16.50
BNW_DD_005	C –CWF	63.89	18.63	12.80	4.86	12.47	5.84
BNW_DD_006	D –CWF	86.98	20.92	9.39	4.58	13.62	7.53
BNW_DD_013	D –CWF	94.20	31.57	15.16	8.73	7.40	7.22
BNW_DD_007	E –CWF	89.71	25.01	9.91	4.61	15.20	4.75
BNW_DD_001	A –TH	97.65	55.25	38.02	26.53	0.80	90.49
BNW_DD_010	B –TH	96.47	28.30	18.64	12.87	0.57	90.03
BNW_DD_011	B –TH	91.38	18.39	10.47	5.63	2.51	94.05
BNW_DD_003	B –TH	80.17	18.45	11.35	5.61	2.44	93.11
BNW_DD_004	B –TH	92.13	23.70	13.89	8.31	2.25	93.08
BNW_DD_008	F–TH	94.54	32.22	20.84	13.41	3.70	90.95
BNW_DD_009	G–RT	96.45	36.12	23.29	15.20	2.17	92.82

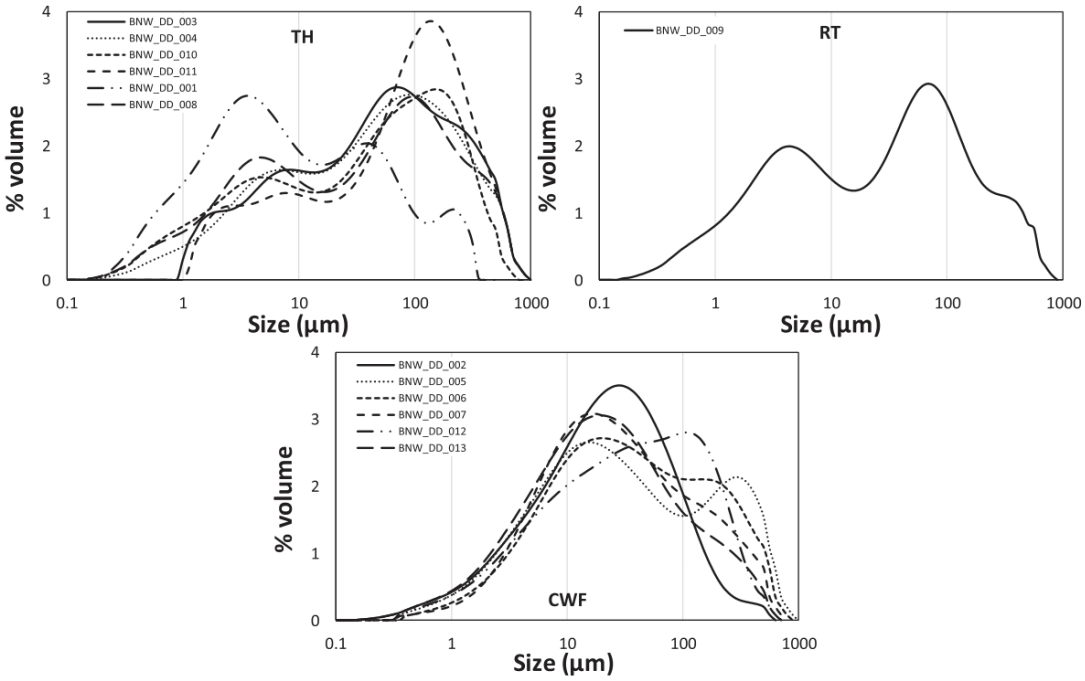

Fig. 2. Particle size distribution of deposited dust (DD, <500 μm) samples from the open-pit coal mine split by the three type of activities. *TH, Tailings handling; CWF, Coal working front; RT, Road traffic into a mine road for tailings.*

$$\text{DD10 (\%vol} < 10\ \mu\text{m)} = 0.43\text{*Ash yield (\%db)} + 18.96\ (r = 0.82) \quad (6)$$

$$\text{DD4 (\%vol} < 4\ \mu\text{m)} = 0.16\text{*Ash yield (\%db)} + 9.70\ (r = 0.70) \quad (7)$$

$$\text{DD2.5 (\%vol} < 2.5\ \mu\text{m)} = 0.22\text{*Ash yield (\%db)} + 3.43\ (r = 0.99) \quad (8)$$

In contrast, the very high ash yields of DD from tailings handling (Eqs. (9)–(12) and fig. S3, 9–12) are negatively correlated with the proportions of DD10, DD4 and DD2.5 ($r = -0.86$ to -0.94, excluding BNW_DD_001). Because all DD samples from tailings handling had very low coal content (< 5%), the changes in the proportions of the fine fraction in DD due to elevated coal contents (low ash yield) cannot be evaluated. However, the fine fraction of DD increases as carbonate minerals decrease, and clay and quartz increase.

4.1.1.3. Tailings handling

$$\text{DD500 (\%vol} < 500\ \mu\text{m)} = -2.17\text{*Ash yield (\%db)} + 290.68\ (r = -0.57) \quad (9)$$

$$\text{DD10 (\%vol} < 10\ \mu\text{m)} = -3.13\text{*Ash yield (\%db)} + 312.87\ (r = -0.86) \quad (10)$$

Table 2
Mineral contents in deposited dust (DD, <500 μm) and channel profile (CP) samples. Values in %wt. Gypsum (Gp), Qtz (Quartz), Anatase (Ant), Calcite (Cal), Microcline (Mc), Albite/Anorthite (Ab/An), Illite/Muscovite (Ilt/Ms), Kaolinite/Clinochlore (Kln/Clc). *TH, Tailings handling; CWF, Coal working front; RT, Road traffic into a mine road for tailings.*

Sample	Zone	Ilt/Ms	Kln/Clc	Qtz	Ab/An	Mc	Cal	Gp	Ant	Total
BNW_DD_002_CWF	C	0	8.9	15	0	0	0	0.5	0	25
BNW_DD_012_CWF	C	0	6.3	8.4	1.1	0	0	0.7	0	17
BNW_DD_005_CWF	C	0	3	2.2	0	0	0	0.6	0	5.8
BNW_DD_006_CWF	D	0	3.1	1.4	0	0	0	3.1	0	7.5
BNW_DD_013_CWF	D	0	1.8	4.1	0	0	0	1.3	0	7.2
BNW_DD_007_CWF	E	0	0	1.1	0	0	0	3.7	0.3	5.1
BNW_DD_001_TH	A	8.6	56	33	0.3	0	0.8	0.4	0.6	100
BNW_DD_010_TH	B	1.4	8.1	40	16	0.6	34	0	0.5	100
BNW_DD_011_TH	B	2.2	9.6	78	8	1.2	0	0	0.9	100
BNW_DD_003_TH	B	2.8	19	61	8	1.5	7	0	1.1	100
BNW_DD_004_TH	B	5.6	25	60	3.8	1.4	3.7	0	0.7	100
BNW_DD_008_TH	F	2.1	29	64	2.5	0.9	0	0.3	0.7	100
BNW_DD_009_RT	G	1.9	12	71	12	1.2	0	1	0.8	100
BNW_CP_001	C	0	2.6	1	0	0	0	0	0	3.6
BNW_CP_002	D	0	3.2	0	0	0	0	0	0	3.2
BNW_RDD_002_CWF	C	0	12	12	0	0	0	0.2	0	25
BNW_RDD_005_CWF	C	0	3.8	1.7	0	0	0	0.4	0	5.8
BNW_RDD_006_CWF	D	0	4.5	0.4	0	0	0	2.7	0	7.5
BNW_RDD_007_CWF	E	0	0	1.8	0	0	0	3.0	0.3	5.1
BNW_RDD_001_TH	A	9.7	74	15	0.3	0	0.6	0.3	0.3	100
BNW_RDD_003_TH	B	3.5	25	56	1.6	0.9	12	0	1.1	100
BNW_RDD_008_TH	F	2.5	30	64	0.9	1.5	0	0.8	0.6	100
BNW_RDD_009_RT	G	2.4	13	82	1.2	0.6	0	0.6	0.3	100

$$\text{DD4 } (\%\text{vol} < 4\ \mu\text{m}) = -2.47\text{*Ash yield } (\%\text{db}) + 242.93\ (r = -0.91) \quad (11)$$

$$\text{DD2.5 } (\%\text{vol} < 2.5\ \mu\text{m}) = -2.12\text{*Ash yield } (\%\text{db}) + 204.41\ (r = -0.94) \quad (12)$$

4.1.2. Mineralogy

The worked coal is a high quality one, with very low yields, due to low content of kaolinite (3%weight, %wt) and quartz (1%wt) identified by XRD (Table 2), and low S contents (Tables 3 and S4 and fig. S4, a–b). As expected, the mineral contents of coal working front DD samples increased (up to 9%wt kaolinite/clinochlore, 1–15%wt quartz, and with up to 3.7%wt gypsum, and traces, < 1.0%wt, of albite/anorthite, and anatase) compared to the parent coal. All coal working front DD samples were collected close to the main 72 m-thick very low-ash coal seam. Thus, the elevated mineral content of the DD compared with the parent coal is attributed to dust deposition from the tailings handling operations, the occurrence of partings in the coal seam (not sampled in the channel sampling profile of this work), the emissions of dust deposited on trucks, drilling and mine explosions, and the contributions of external windblown dust.

Also as expected, the mineral composition of DD samples from tailings handling and road traffic is entirely different from the one from the coal working fronts, showing greater clay and quartz contents, with illite/muscovite being the major minerals (10–65 and 14%wt clays and 34–78 and 71%wt quartz, respectively, Table 2). Furthermore, calcite content in some of the tailings handling DD samples reached up to 34% wt, and feldspars and anatase 0.3–16 and 0.5–1.1%wt respectively, in both tailings handling and road traffic DD (Table 2). Conversely, gypsum contents decreased with respect to DD from the coal working front. The slight increase in gypsum content in the latter is suggested to be due to the excess of humidity resulting from the spreading of water containing dissolved sulphate, favouring the oxidation of sulphides from DD. The occurrence of trace amounts of pyrite in coal and the high humidity might cause the oxidation of this mineral and the generation of gypsum (Akinwekomi et al., 2020). In contrast, in the tailing and road truck zones, the lack of humidity, and probably the lower content of pyrite, might have reduced the formation of gypsum (Akinwekomi et al., 2020; Gomo, 2018; Madzivire et al., 2010). On the other hand, the reducing environments during peat deposition, combined with the effects of the interaction between dissolved Fe and H_2S cause enrichment of pyrite in coal, due to their bacterial reduction of sulphate ion (Casagrande, 1987; Dai et al., 2020; Querol et al., 1989) compared with more oxidising sedimentary environments, producing the pink to beige sediments converted into tailings. Road traffic and tailings handling DD samples had a very similar mineral composition because the road traffic site sampled is used for extraction of tailings.

4.1.3. Geochemistry

Major and trace element concentrations of DD and CPs are reported in Tables 3 and 4. The comparison of the concentrations of major and trace elements in the parent coal with the Chinese (Dai et al., 2008, 2007) and the worldwide (Ketris and Yudovich, 2009) averaged coal contents shows that the coal analysed in this study was depleted in most elements, with only Mg and Ba (1.1–1.5) and Sr and Na (1.6–2.0) having higher concentrations. The majority of the elements are enriched in the DD of the coal working front compared with the parent coal, an exception being in samples from zone B. The concentrations of most major and trace elements in the DD from tailings handling and road traffic were similarly higher than those from the coal working front. Mn is the only element with clearly different concentrations (488 $\mu g \cdot g^{-1}$ in tailings handling and 250 $\mu g \cdot g^{-1}$ in road traffic). Conversely, S, B and Sr were present in greater concentrations in the coal working front, and Ba in similarly elevated concentrations in all three types of DD.

Multiple potentially hazardous elements, such as Mn, Co, Ni, Zn, As and Cr (Finkelman, 1994), occurred in much larger concentrations in DD than in the parent coal, presumably due to dust deposition from the tailings handling zones, mining machinery and truck wear (Chen et al., 2015; Munir et al., 2020; Xu et al., 2017).

4.1.4. Respirable deposited dust

Table 5 shows the RDD particle size data (D50 and D90, median and percentile 90) separated from the DD by the PM separator. PSD analyses revealed that all RDD samples had a D50 in the range of 3–4 μm, which represent the respirable fraction. However, D90 values varied more widely depending on the type of DD. In the case of coal working front RDD, D90 reached 7–8 μm size but 4–5 μm in the tailings handling locations, making the RDD samples finer. As mentioned above, this might be due to the finer PSD of clay and quartz compared to the higher coarse coaly matrix proportion in the coal working front. In any case, the increased metal load and finer size patterns of the tailings handlings

Table 3
Major element contents in the deposited dust (DD, < 500 μm) and channel profile (CP) samples. Values in %wt. *TH, Tailings handling; CWF, Coal working front; RT, Road traffic into a mine road for tailings.*

Sample	Zone	Al	Si	Ca	Fe	K	Mg	Na	P	S
BNW_DD_002_CWF	C	2.32	5.23	1.08	0.52	0.31	0.27	0.59	0.01	0.44
BNW_DD_012_CWF	C	1.41	3.42	0.83	0.32	0.21	0.18	0.48	0.01	0.45
BNW_DD_005_CWF	C	0.27	0.53	0.73	0.08	0.04	0.29	0.37	<0.01	0.37
BNW_DD_006_CWF	D	0.19	0.29	1.21	0.07	0.03	0.21	0.83	<0.01	0.88
BNW_DD_013_CWF	D	0.37	0.79	0.77	0.09	0.04	0.33	0.56	<0.01	0.43
BNW_DD_007_CWF	E	0.19	0.3	0.71	0.09	0.01	0.13	0.48	<0.01	0.4
BNW_DD_001_TH	A	12.03	21.66	0.24	0.53	1.11	0.20	0.11	0.01	0.27
BNW_DD_010_TH	B	6.06	21.64	6.17	1.93	1.30	0.49	1.54	0.01	0.02
BNW_DD_011_TH	B	8.72	24.5	0.99	3.4	1.65	0.50	1.00	0.03	0.03
BNW_DD_003_TH	B	8.29	22.67	1.36	3.55	1.50	0.47	1.02	0.03	0.03
BNW_DD_004_TH	B	8.55	22.27	1.22	3.92	1.46	0.49	0.92	0.04	0.03
BNW_DD_008_TH	F	9.00	23.44	0.35	2.18	1.51	0.43	0.51	0.05	0.28
BNW_DD_009_RT	G	8.59	24.94	0.66	2.93	1.63	0.46	1.26	0.03	0.20
BNW_CP_001	C	0.10	0.20	0.79	0.05	0.02	0.17	0.23	<0.01	0.34
BNW_CP_002	D	0.07	0.11	0.63	0.06	0.01	0.18	0.25	<0.01	0.37
BNW_RDD_002_CWF	C	2.48	5.09	1.02	0.44	0.28	0.32	0.47	0.02	0.32
BNW_RDD_005_CWF	C	0.44	0.69	0.80	0.06	0.03	0.36	0.44	<0.01	0.35
BNW_RDD_006_CWF	D	0.40	0.47	1.82	0.03	0.04	0.27	0.89	0.01	1.32
BNW_RDD_007_CWF	E	0.21	0.22	0.67	0.10	0.01	0.17	0.57	0.01	0.32
BNW_RDD_001_TH	A	16.22	21.50	0.24	0.51	1.29	0.23	0.16	0.02	0.18
BNW_RDD_003_TH	B	9.80	28.71	2.18	4.62	1.59	0.60	0.77	0.05	0.16
BNW_RDD_008_TH	F	9.42	22.50	0.63	1.66	1.63	0.36	0.37	0.06	0.54
BNW_RDD_009_RT	G	9.71	22.77	0.67	3.43	1.63	0.52	0.70	0.03	0.27

Table 4
Trace element contents in deposited dust (DD, <500 μm) and channel profile (CP) samples. Values in $\mu g \cdot g^{-1}$. Mo, Cd, Ta, Tl and Bi were found in concentrations lower than detection limit (<dl). *TH, Tailings handling; CWF, Coal working front; RT, Road traffic into a mine road for tailings.*

Sample	Zone	Li	Be	B	Sc	Ti	V	Cr	Mn	Co	Ni	Cu	Zn	Ga	Ge	As	Se	Rb	Sr	Y	Zr	Nb	Sn	Sb	Cs	Ba	Hf	W	Pb	Th	U	REE
BNW_DD_002_CWF	C	8.0	<dl	55	5.2	1265	42	20	86	4.7	10	22	100	6.1	1.1	3.6	2.0	15	320	12	30	2.2	1.1	<dl	1.3	397	1.4	<dl	6.6	1.7	1.2	60
BNW_DD_012_CWF	C	4.6	<dl	39	2.1	794	16	10	66	2.9	8.7	7.7	34	3.1	<dl	1.9	<dl	8.9	190	4.5	18	1.6	0.77	<dl	0.74	344	0.86	<dl	2.7	1.0	3.2	21
BNW_DD_005_CWF	C	1.1	<dl	64	<dl	138	2.5	2.2	17	<dl	2.0	3.0	25	<dl	<dl	<dl	<dl	1.4	413	0.92	3.1	<dl	<dl	<dl	<dl	349	<dl	<dl	<dl	<dl	<dl	4.0
BNW_DD_006_CWF	D	1.5	<dl	54	<dl	64	1.2	1.2	31	<dl	1.7	2.8	27	<dl	<dl	<dl	<dl	<dl	289	<dl	1.7	<dl	<dl	<dl	<dl	1022	<dl	<dl	<dl	<dl	<dl	1.6
BNW_DD_013_CWF	D	2.6	<dl	61	<dl	196	3.9	2.7	22	<dl	2.8	5.1	22	0.86	<dl	<dl	<dl	2.1	398	1.3	3.8	<dl	<dl	<dl	<dl	406	<dl	<dl	1.0	<dl	<dl	5.2
BNW_DD_007_CWF	E	0.78	<dl	58	<dl	89	2.7	1.7	282	<dl	2.0	3.2	21	<dl	<dl	0.90	0.81	<dl	82	1.1	2.0	<dl	<dl	<dl	<dl	420	<dl	<dl	0.91	<dl	2.1	2.5
BNW_DD_001_TH	A	23	1.1	29	16	7735	158	108	65	40	80	53	116	27	2.6	6.3	3.4	62	88	19	172	19	4.3	1.5	5.5	328	8.1	1.7	24	14	4.4	135
BNW_DD_010_TH	B	17	0.76	11	9.5	3755	69	49	1448	13	22	17	80	13	2.2	3.0	4.5	44	320	25	82	6.0	1.6	<dl	2.1	447	4.2	<dl	9.3	3.9	1.4	130
BNW_DD_011_TH	B	30	1.7	25	15	5300	112	68	307	14	32	36	93	19	2.5	5.9	3.1	75	130	28	115	8.8	2.4	0.82	5.2	499	5.8	<dl	12	6.1	2.1	146
BNW_DD_003_TH	B	29	1.6	12	14	5566	108	80	427	14	38	27	95	18	2.3	10	3.6	66	111	28	112	8.7	2.2	0.82	4.4	470	5.6	<dl	11	5.6	1.6	139
BNW_DD_004_TH	B	32	1.6	14	14	5254	111	82	463	14	36	28	94	19	2.4	10	4.3	66	108	28	113	6.7	2.2	<dl	4.5	358	5.4	<dl	11	5.8	1.7	141
BNW_DD_008_TH	F	22	1.5	133	17	5613	125	69	217	28	55	43	112	20	3.2	16	4.1	71	327	30	124	9.8	2.7	1.1	5.7	495	6.0	0.73	19	6.3	2.2	148
BNW_DD_009_RT	G	25	2.1	30	14	5253	109	66	250	14	31	32	102	19	2.8	8.6	3.1	72	166	28	114	9.2	2.4	0.9	4.8	466	5.6	<dl	13	6.0	2.9	138
BNW_CP_001	C	1.2	<dl	67	<dl	59	1.3	1.8	26	<dl	1.9	2.6	20	0.38	<dl	<dl	<dl	<dl	223	<dl	1.2	<dl	0.44	<dl	<dl	280	<dl	<dl	<dl	<dl	<dl	1.4
BNW_CP_002	D	<dl	<dl	56	<dl	31	<dl	0.86	19	<dl	1.9	2.2	17	<dl	<dl	0.49	<dl	<dl	238	<dl	0.69	<dl	<dl	<dl	<dl	106	<dl	<dl	<dl	<dl	<dl	<dl
BNW_RDD_002_CWF	C	6.6	1.9	25	5.4	1150	35	16	66	4.4	7.8	17	34	5.7	<dl	2.8	1.3	14	316	10	42	3.1	0.95	<dl	1.3	105	<dl	<dl	4.5	2.4	1.2	63
BNW_RDD_005_CWF	C	2.3	<dl	62	<dl	180	4.2	3.1	19	<dl	3.7	3.1	17	<dl	<dl	1.8	<dl	2.1	886	1.2	7.1	<dl	<dl	<dl	<dl	59	<dl	<dl	1.20	<dl	<dl	5.3
BNW_RDD_006_CWF	D	2.1	<dl	53	<dl	58	1.3	1.9	33	<dl	1.9	2.6	18	<dl	<dl	7.1	<dl	<dl	319	<dl	1.2	<dl	<dl	<dl	<dl	39	<dl	<dl	1.30	<dl	<dl	1.9
BNW_RDD_007_CWF	E	<dl	<dl	76	<dl	99	3.1	2.5	380	<dl	4.8	15	39	<dl	<dl	1.7	<dl	<dl	91	1.3	4.0	<dl	<dl	<dl	<dl	17	<dl	<dl	2.7	<dl	2.4	4.2
BNW_RDD_001_TH	A	29	1.2	369	19	7323	194	112	52	44	85	52	139	30	1.9	7.8	1.3	76	87	16	262	16	4.1	1.3	6.6	246	7.7	2.1	33	14	5.1	120
BNW_RDD_003_TH	B	35	<dl	57	17	5842	142	80	531	18	59	35	118	20	2.8	13	3.7	75	155	31	173	6.5	3.2	1.5	5.1	464	4.8	<dl	17	6.5	1.8	148
BNW_RDD_008_TH	F	20	1.7	69	14	5457	138	62	138	27	56	64	108	21	2.2	29	3.6	71	405	26	156	9.5	3.9	3.4	5.5	456	4.3	0.92	21	6.6	2.2	140
BNW_RDD_009_RT	G	30	<dl	<dl	16	5549	130	73	198	16	34	55	174	20	2.3	9.5	3.9	73	162	25	144	8.2	7.5	26	5.7	326	3.9	<dl	19	5.6	3.6	131

Table 5
50 and 90 percentile values (D50 and D90, in μm) of the grain size distribution of the respirable deposited dust (RDD). *TH, Tailings handling; CWF, Coal working front; RT, Road traffic into a mine road for tailings.* ** Not enough sample to complete the analysis.

Name	Zone	Activity	D50	D90
BNW_RDD_002	C	CWF bottom open-pit (DD on car)	3.3	7.3
BNW_RDD_005	C	CWF bottom open-pit (extraction coal & truck uploading by excavator)	3.5	7.7
BNW_RDD_006	D	CWF bottom open-pit (extraction coal & truck uploading by excavator)	3.1	7.3
BNW_RDD_007	E	CWF bottom open-pit (truck uploading by excavator)	4.0	7.5
BNW_RDD_001	A	TH, gangue (truck uploading by excavator)	2.2	4.4
BNW_RDD_003	B	TH, drilling into gangue	3.2	4.5
BNW_RDD_008	F	TH, gangue dust	**	**
BNW_RDD_009	G	RT, trucks in a gangue extraction road	**	**

samples make them potentially more hazardous for the coal workers (Borm, 2002; Gilmour et al., 2004; Li et al., 2008, 2003; Oberdörster et al., 1992).

Tables 2 to 4 summarise the results of the mineralogical and geochemical characterisation of RDD samples. The concentration of minerals and elements is compared using the RDD/DD ratio. Clays and calcite are consistently enriched in the finer DD fraction (RDD/DD 1.1–1.4), similar to the quartz in the road traffic and gypsum, and microcline in the tailings handling (1.1, 1.6 and 1.1 respectively) (Fig. 3). Anatase, plagioclase, and quartz in the coal working front and tailings handling, and gypsum in the coal working front and road traffic RDD were consistently coarser (RDD/DD 0.1–0.9) (Fig. 3). Similar results were obtained by Johann-Essex et al. (2017), who analysed respirable dust samples from different underground coal mines and their mineral content increase with the distance to the coal working front.

For major elements, most RDD/DD values lay within the range of 0.8–1.2 (Fig. 4). However, in the coal working front zone, relative Fe content decreased in the RDD (<0.8) whereas Mg, Al, and P (all occurring mostly in phosphates and clay minerals) increased (>1.2), similar to Ca and P in the tailings handling zone (Fig. 4). In the road traffic zone, Na content decreased in the RDD (<0.6). For trace elements, RDD/DD ratios >1.2 were found for Nb, Th, Cr, Sr, Li, As, Pb, Cu, Zr and Ni in the coal working front, whereas ratios were < 0.8 for Se, Hf and Ba (Fig. 5). The finer character of the first group of elements is likely

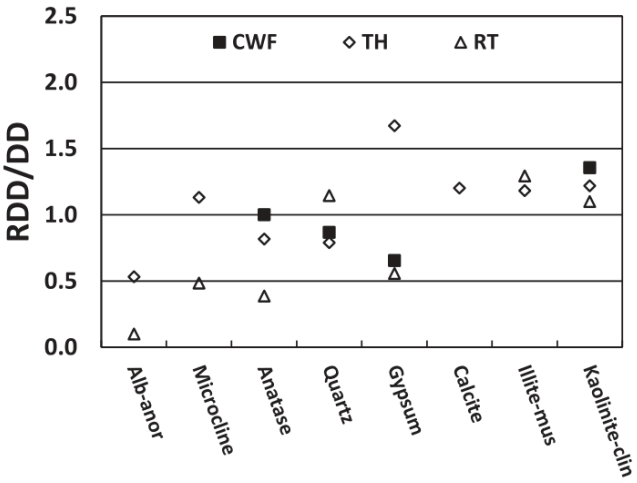

Fig. 3. Ratio of mineral contents determined by XRD analysis in the respirable deposited dust (RDD) and their parent deposited dust (DD, <500 μm) (RDD/DD). Average for each type of DD: *TH, tailings handling; CWF, Coal working front; RT, Road traffic into a mine road for tailings*. Values used are shown in Table S1.

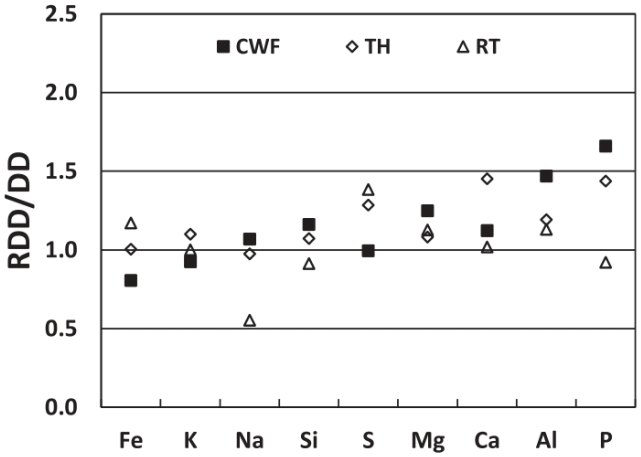

Fig. 4. Ratio of major element contents in the respirable deposited dust (RDD) and their parent deposited dust (DD, <500 μm) (RDD/DD). Average for each type of DD: *TH, Tailings handling; CWF, Coal working front; RT, Road traffic into a mine road for tailings*. Values used are shown in Table S2.

attributed to their association with clays and carbonates and perhaps with mining machinery wear (Fig. S4 c) (Azam and Mishra, 2019; Moreno et al., 2019; Querol et al., 2007). In contrast, the coarser Ba pattern might be due to the occurrence of fine barite ($BaSO_4$) crystals embedded in the coaly matrix (evidenced by fig. S4 d) (Gürdal, 2008; Zhao et al., 2014). Notables are the contrasting size patterns of Zr and Hf, which is attributed to the presence of both geogenic zircon (coarser, enriched in Hf) and contamination from the wear of drilling and other mining machinery (finer and poorer in Hf: fig. S4, e-f). For the tailings handling RDD samples, RDD/DD ratios were > 1.2 for W, As, Zr, Sn, Cu and Sb and < 0.8 for Ge, Se and B and the road traffic RDD Cu, Sn, Pb, Zr, Sb, Zn and Se, and Ba and Hf, respectively (Figs. 5, S4, f-h).

An enrichment (not extraordinarily high but clearly evident) of elements of potential concern in the RDD versus the parent materials (represented by DD in coal working fronts and tailings handling operations) was evident. Accordingly, RDD constituents and health effects might be quite different to what would be expected if the constituents and related effects from the parent materials are simply extrapolated without considering the effects of mineral fractionation within the dusts released during the coal mining process.

4.1.5. *Oxidative potential of the respirable deposited dust*

Oxidative potential is suggested to be one of the most relevant indicators of PM toxicity. The OP values obtained for the RDD samples (Table 6) were relatively low compared to those obtained in a prior study of RDD originating from underground mines of other coal mining districts with substantially higher pyrite contents (Trechera et al., 2020). Thus, OP^{AA} in this study ranged from 0.1–0.5% AA consumption·μg^{-1} RDD, while in the referred study, 0.4–2.0%·μg^{-1} was reached in 11 out of 13 RDD samples (Table 6). For OP^{GSH}, the results were the opposite, with 0.2–0.4%·μg^{-1} in this study and 0.0–0.2%·μg^{-1} in the underground mines (Table 6). Furthermore, in this study, 27–63% of the OP^{TOT} was supplied by the OP^{AA}, while this contribution in RDD samples from underground mines reached 80–100%.

The OP^{TOT} (OP^{AA} + OP^{GSH}) potential obtained for RDD in this study (0.34 to 0.80 OP^{TOT} %·μg^{-1}) is slightly lower or similar to urban dust (NIST control 1.0 OP^{TOT} %·μg^{-1}) and from indoor and outdoor locations around a Fe-ore facility in Iran (0.9 OP^{TOT} %·μg^{-1}, Soltani et al., 2018). However, it is much lower than those obtained for PM from the Chamonix Valley (France) in summer (1.4 OP^{TOT} %·μg^{-1}) and winter (4.1 OP^{TOT}%·μg^{-1}) (the latter with PM contributions from biomass burning) (Calas et al., 2018) and PM from subway platforms from Barcelona (2.5 OP^{TOT} %·μg^{-1}, Moreno et al., 2017).

A cross-correlation analysis using r coefficients was carried out using the OP^{AA} and OP^{GSH} values of each RDD sample with the content of major and trace elements and minerals in the respective samples (Fig. 6). When using the 8 RDD samples from the open-pit (Fig. 6a), it was shown that the contents of Mn, followed by those of anatase and calcite, drove the OP^{AA} (group I in the figure and r = 0.8–0.9 with OP^{AA}). Those of gypsum and moisture and a relatively coarse 10 percentile of the PSD drove the OP^{GSH} (r = 0.5–0.7, group II in the figure).

When considering only the RDD samples from the coal working front (Fig. 6), a marked correlation between OP^{AA} and OP^{GSH} was obtained (r = 0.8). In this case, moisture (Fig. 6b) and gypsum contents drove OP^{AA} (r = 0.5–0.6, group I) and Ni and Pb concentrations drove OP^{GSH} (r = 0.7–0.8, group II). Furthermore, a coarser 25 percentile of the PSD and the contents of anatase, Mn, U, Zn and Cu drove both OP^{AA} and OP^{GSH} (r = 0.6–1.0, group III). Conversely, elevated contents of Mg, Sr and Ca were associated with a decrease in both types of OP (r = −0.5 to −0.8 with both OP types, group IV). Despite these high r coefficients, average OP^{AA} values of the coal working front RDD samples were low (0.2%·μg^{-1}), compared to the tailings handling and road traffic RDD samples (0.3%·μg^{-1}, and much lower than those of the RDD from underground coal mines (0.70%·μg^{-1}, Trechera et al., 2020) with much greater pyrite contents. For OP^{GSH} the situation was reversed, with samples yielding 0.3, 0.2 and 0.1%·μg^{-1}, respectively.

The RDD from tailings handling and road traffic, also with relatively low OP^{AA}, was driven by the contents of multiple silicate- and calcite-associated elements, Mn and anatase, and a finer 25 percentile of the PSD (r = 0.6–1.0 and − 0.8 for the latter, group I in Fig. 6c). For OP^{GSH}, contents of As, Bi, Be, Sr, S and moisture were found to be positively

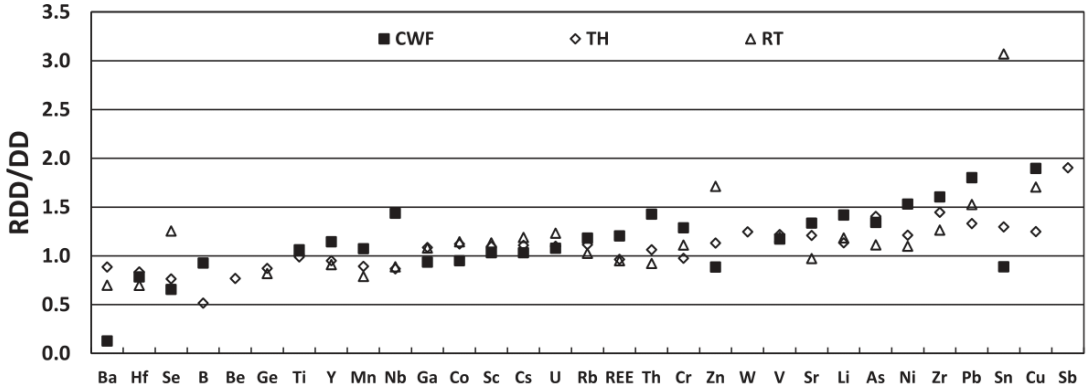

Fig. 5. Ratio of trace element contents in the respirable deposited dust (RDD) and their parent deposited dust (DD, <500 μm) (RDD/DD). Average for each type of DD: *TH, tailings handling; CWF, Coal working front; RT, Road traffic into a mine road for tailings*. Values used are shown in Table S3.

Table 6
Oxidative potential (OP) values of respirable deposited dust (RDD) in %consumption·μg^{-1} for Ascorbic Acid (OP^{AA}), Glutathione (OP^{GSH}) and Total oxidative potential (OP^{TOT} = OP^{AA} + OP^{GSH}). *TH, Tailings handling; CWF, Coal working front; RT, Road traffic into a mine road for tailings*. On the bottom, results of previous studies from different underground coal mines in China (Trechera et al., 2020).

Name	Zone	Activity	OP^{AA}	OP^{GSH}	OP^{TOT}
BNW_RDD_002	C	CWF bottom open-pit (DD on car)	0.13	0.35	0.48
BNW_RDD_005	C	CWF bottom open-pit (extraction coal & truck uploading by excavator)	0.10	0.20	0.40
BNW_RDD_006	D	CWF bottom open-pit (extraction coal & truck uploading by excavator)	0.11	0.23	0.34
BNW_RDD_007	E	CWF bottom open-pit (truck uploading by excavator)	0.40	0.40	0.80
BNW_RDD_001	A	TH, gangue (truck uploading by excavator)	0.20	0.20	0.40
BNW_RDD_003	B	TH, drilling into gangue	0.50	0.20	0.80
BNW_RDD_008	F	TH, gangue dust	0.23	0.24	0.47
BNW_RDD_009	G	RT, trucks in a gangue extraction road	0.18	0.17	0.35
Underground mines (Trechera et al., 2020)					
BCC_RDD_011	Mine 1	300 m CWF#7	1.2	0.0	1.2
BCC_RDD_009	Mine 1	100 m CWF#7	2.0	0.2	2.2
BCC_RDD_008	Mine 1	50 m CWF#7	0.9	0.0	0.9
BCC_RDD_005	Mine 1	CWF#7	0.8	0.1	0.9
BCC_RDD_014	Mine 1	CWF#11	0.1	0.0	0.1
BCC_RDD_001	Mine 1	Gallery close CWF#7 (cemented)	0.7	0.5	1.2
BCC_RDD_015	Mine 1	Floor train wagons	0.2	0.0	0.2
SCC_RDD_001	Mine 2	2000 m CWF	0.6	0.0	0.6
SCC_RDD_004	Mine 2	100 m CWF	0.5	0.1	0.6
SCC_RDD_005	Mine 2	CWF	0.5	0.2	0.6
SCC_RDD_007	Mine 2	Coal milling	0.4	0.1	0.5
BSC_RDD_001	Mine 3	Abandoned mine 30 m CWF	0.7	0.1	0.7
BSC_RDD_002	Mine 3	Abandoned mine 90 m CWF	0.5	0.1	0.6

correlated (r = 0.6–0.9, group II). Those of Ba and P were correlated with both OP types (group III, r = 0.5–0.7), and Zn, Sb, Sn and U were negatively correlated ($r = -0.4$-0.9, group IV).

According to the results, Mn and anatase were found to be major drivers of OP^{AA}, and OP^{GSH} in the RDD from the coal working front, while for tailings handling-road traffic a finer particle size was associated with a high OP^{AA}. In the first case, Mn and anatase occur in this type of RDD, mostly embedded in the coal matrix (Fig. S4, f, j–l), and this might cause enrichment in the coarser dust particles compared to the finer ones.

The OP^{GSH} of the tailings handling-road traffic RDD samples was found to be driven by moisture and elements usually associated with sulphate minerals from the weathering of sulphides (As, S, Ba, Sr) and, in the coal working front, by some heavy metals and U (in addition to Mn and anatase). Thus, in the case of DD from the coal front, the impact of Mn and anatase on both OP^{AA} and OP^{GSH} was implicated in the correlation between both OPs, but this was not the case for the samples from tailings handling-road traffic.

Fig. 6d shows the above mentioned OP^{AA} and OP^{GSH} cross-correlation analysis for a set of 21 RDD samples, 8 from the coal open-pit mine of this study and 13 from three underground mines by Trechera et al. (2020). This analysis shows that OP^{AA} was clearly driven by contents of Fe-sulphates, other sulphates and anatase, as well as by a slightly coarser PSD (probably favoured by the occurrence of Fe-sulphates) (group I and r = 0.7–0.9). Because of the high quality of the coal mined in the open-pit, the low content of pyrite might account for lower Fe-sulphates, oxides and metal contents in RDD, and accordingly for the lower OP compared with the other RDD samples from other mines. Fe-oxides and sulphates derived from the oxidation of pyrite were suggested as significant drivers of OP in coal mine dust, and probably contributing to CWP injuries in coal mine workers (Huang et al., 2005). Also, as stated by Trechera et al. (2020), acid mine drainage favoured by underground mining might also favour the oxidation of sulphides. The presence of anatase was a major OP^{AA} driver in this study: the lung-inflammation-related toxicity of inhaled TiO_2 particles is well documented (Oberdörster et al., 1992; Schins and Borm, 1999).

On the other hand, OP^{GSH} is moderately driven by moisture, Ca and Na contents (r = 0.5), probably representing the amount of coaly matrix and sulphate and carbonate minerals. The very low ash yield and the relatively high Mn contents of the coals of this study might account for an increased OP^{GSH,} compared to the underground RDD samples.

Based on these results, a multilinear-regression analysis was applied to the 21 RDD data set using the above OP drivers and represented the OP^{AA} and OP^{GSH} according to Eqs. (13) and (14).

$$\mathrm{OP}^{AA}\ (\%\mu g^{-1}) = 0.211{*}\mathrm{anatase}\ (\%db) + 0.055{*}\mathrm{sulphate}\textit{minerals}\ (\%db) + 0.147\ (r = 0.93 p = 0.00) \quad (13)$$

$$\mathrm{OP}^{GSH}\ (\%{\cdot}\mu g^{-1}) = 0.066{*}\mathrm{moisture}\ (\%ad) + 0.026{*}\mathrm{Ca}\ (\%db) + 0.067\ (r = 0.70, p = 0.00) \quad (14)$$

Fig. 7 shows the outputs of the multilinear regression with the differentiation of mines from which RDD samples were obtained. The role of drivers of OP in specific RDD samples (such as Mn in this study) with a specific composition (low metal and sulphur sediments in this study) is diluted when compiling data from different mines where drivers such as pyrite oxidation products and anatase seem to prevail.

4.2. Online and offline air quality measurements in the open mine pit

4.2.1. Online measurements of air quality

As stated in the methodology section, levels of PM_{10}, $PM_{2.5}$, BC and UFP were measured near specific mining activities, where, in addition, DD was simultaneously sampled.

4.2.1.1. Tailings handling. In zone A, air quality around coal gangue uploaded on a truck with an excavator was monitored (16/10/2018, 11:45–12:55 h LT). Here, the impact of emissions from the loading of tailings on trucks and the exhaust emissions from diesel excavators and natural compressed gas trucks on UFP, BC and PM levels and DD were evaluated. This zone was located at a relatively high altitude in the upper banks at the SW of the open mine pit (Fig. 1C). There, because few operations take place, wetting of the surfaces or other dust abatement controls were not implemented. The gangue loaded was a clear pale beige clay-rich material, probably transported to processing plants to be used in the ceramic industry. The very clear colour indicates a minimal amount of coaly material, meaning that absorbance from the BC was hardly influenced by dust. The RDD fraction from this operation (BNW_RDD_001_TH, Table 2) was composed of 74, 9.7, 15, 0.3, 0.6, 0.3, 0.3% clay minerals kaolinite/clinochlore, illite/muscovite, quartz, albite/anorthite, calcite, gypsum and anatase, respectively. The DD sampled was very fine with 55, 38 and 26% of DD10, DD4 and DD2.5 in DD500, and 98% of DD500 in DD.

Fig. 8a shows the time series of 1 min concentrations of $PM_{2.5}$, BC

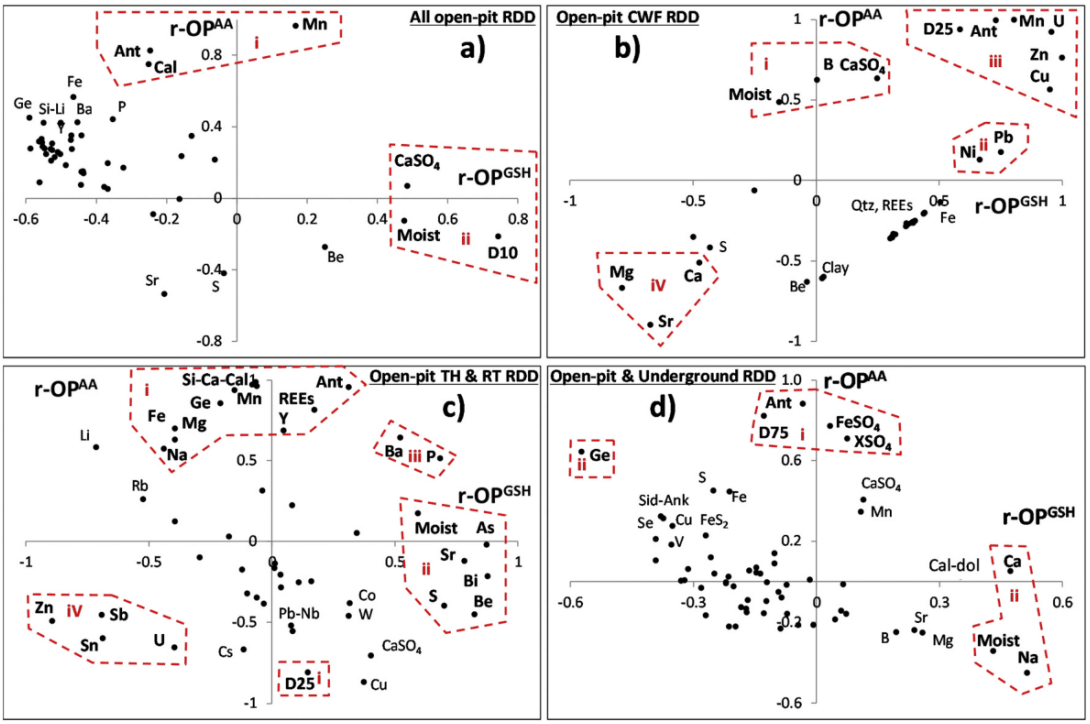

Fig. 6. Cross correlation plots between the Pearson's correlation coefficients of the normalised (concentration/average concentration) concentrations of the elements and minerals contents in the respirable deposited dust (RDD) samples and their respective OP^{AA} and OP^{GSH} values using; a) Eight RDD samples from the open-pit coal mine; b) Four CWF RDD samples from the open-pit coal mine; c) Three TH RDD samples and one RT RDD sample from the open-pit coal mine; and d) Data from this study and 13 additional RDD samples from underground mining by Trechera et al. (2020) previous study. *TH, tailings handling; CWF, Coal working front; RT, Road traffic into a mine road for tailings.*

and UFP recorded at this site (with ambient conditions of 21 °C, RH 33%, and CO_2 428 ppm). Very elevated levels of PM_{10} and $PM_{2.5}$ (1 h average values of 3652 and 354 $\mu g \cdot m^{-3}$ for the personal PM_{10} PEM samplers, and $PM_{2.5}$-Dusttrack, respectively) were reached, with $PM_{2.5}/PM_{10}$ of 0.24. However, levels of UFP were relatively low, reaching an average of 4475 $\#cm^{-3}$, typical from a regional background or low polluted urban sites according to Cassee et al. (2011) and Morawska et al. (2008). Levels of BC (11 $\mu g \cdot m^{-3}$) can be considered moderate compared with typical concentrations measured in European, Middle East and Asian urban road traffic sites (maxima annual or seasonal averages of 8–18 $\mu g \cdot m^{-3}$, Hung et al., 2014; Hussein et al., 2019; Reche et al., 2011), especially given the fact that in this study measurements were collected near two large operating mining motor engines.

Emissions of PM_x mainly occurred during the loading of the excavator (with 1 min levels up to 1080 $\mu g \cdot m^{-3}$ $PM_{2.5}$). These are clearly correlated with BC peaks and, accordingly, are attributed to the engine of the excavator. However, UFP particles were completely decoupled from BC and PM, and peak concentrations are attributed to the exhaust emissions of the truck. Regardless, UFP peaks reached up to 11,000 $\#cm^{-3}$, which are relatively low considering the proximity to the truck, the low rpm of the stopped truck, and the fact that usually UFP averages reported for urban zones (Cassee et al., 2019; Morawska et al., 2008) are of the same order of the UFP peaks recorded at this mine site.

The impact of emissions from the drilling and working tailings with diesel excavators on levels of UFP, BC and PM and DD were also evaluated. Measurements were also performed close to drilling (16/10/2018, 12:28–13:40 h LT, 17 °C, RH 42%, CO_2 410 ppm) and excavator (17/10/2018, 12:28–13:40 h LT, 12 °C, RH 54%, CO_2 412 ppm) operations in zone B (Fig. S5a and b), also at the high altitude zones, but in this case at the N sector of the pit (12 °C, RH 54%, CO_2 412 ppm), and with no dust abatement measures implemented. There PM_{10} and $PM_{2.5}$ levels were reduced in relation to Zone A (1 h averages of 549 and 127, and 723 and 167 $\mu g \cdot m^{-3}$, respectively), with a similar $PM_{2.5}/PM_{10}$ ratio (0.23 in both cases). At that site, the mineral composition of the gangue RDD was 28, 56, 2.5, 12 and 1.1% clay minerals (74% of Kln/Clc and 10% of Ilt/Ms), quartz, feldspars, calcite and anatase. In this case, DD was much coarser than for the loading of gangue at A, with 18–28, 11–18 and 6–13% of DD10, DD4 and DD2.5 in DD500 and 80–97% of DD500 in DD.

4.2.1.2. Coal working fronts. Measurements and sampling were conducted in the coal working fronts at the bottom of the open-pit, where coal was worked and loaded onto trucks by excavators at zones C (S sector) and D (SE). These were also carried out at a mid-altitude sector E (central area), where coal was worked with excavators without loading onto trucks. At these sites wetting of the surface was frequently applied to abate dust resuspension. Here, the impact of emissions from coal working with diesel excavators, the loading of coal on trucks, the emissions from resuspension of dust by trucks accessing and leaving the front, and the exhaust emissions of excavators and trucks on UFP, BC and PM levels and DD were evaluated.

During coal work and loading, RDD sampled at these three sites was found to be greatly enriched in the organic coal matrix (75–95, 0–12, 0.5–12, 0–3, 0.3% coal, clay minerals, quartz, gypsum and anatase, respectively), as the coal worked is very low in ash yields. The DD of the three positions is markedly coarser (probably due to the low ash yields) than the one from the gangue, with DD10, DD4, DD2.5 accounting for 19–32, 9–15 and 5–9% of DD500, and DD500 for 64–100% of DD.

At the working front sites (zone C and D), where coal is extracted and loaded, sampling and measurements were performed on 16/10/2018 at 14:06–15:45 h LT, in sector C, and, 16:27 to 17:32, sector D, under environmental conditions of 19 °C, RH 44%, and CO_2 450 ppm. Average PM_{10} and $PM_{2.5}$ levels reached 1535 and 98 $\mu g \cdot m^{-3}$, respectively, at site C, and, 264 $\mu g \cdot m^{-3}$ $PM_{2.5}$ at site D. The $PM_{2.5}/PM_{10}$ ratios were very low

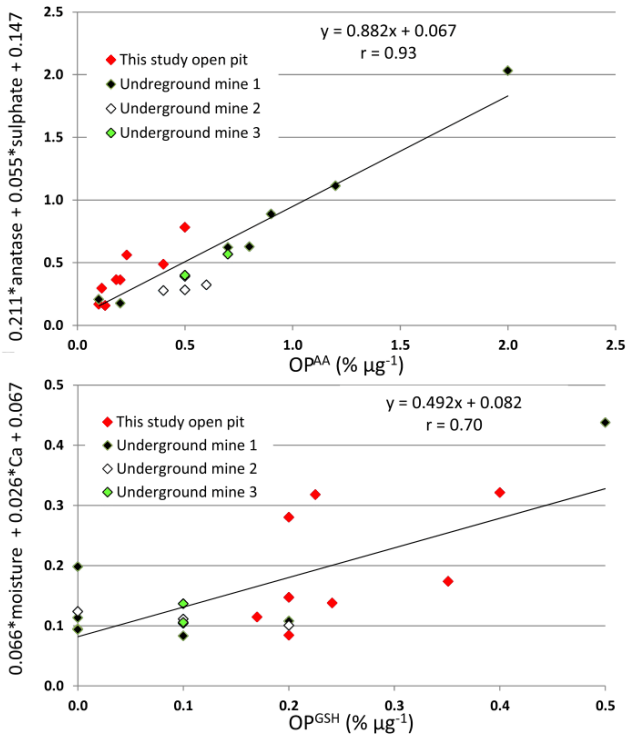

Fig. 7. Cross correlation plots between OP^{AA} and OP^{GSH} multilinear regression with their respective geochemical drivers, combined with underground mine data on RDD (mines 1 to 3) from previous study by Trechera et al. (2020).

(0.06). Levels of BC were moderate (22 and 9 $\mu g \cdot m^{-3}$ for C and D sites, respectively) considering the number of trucks and excavators and the potential influence of coal mine dust on absorbance measurements of BC. However, levels of UFP, similarly high at the C and D positions, reached average concentrations of 31,682 and 25,735 $\#cm^{-3}$, respectively. These are typical values of urban traffic sites (Morawska et al., 2008), but unexpectedly low for this busy mining environment. Regardless, UFP were markedly higher than those recorded at the highest altitude sectors of the mine where the work was done with tailings. This is attributed to the elevated truck traffic and excavator density and lower dispersion (because sectors C and D are at the bottom of the large open-pit). Thus, as shown in Fig. 8b and c, background and peak levels reached 11,000–17,000 $\#cm^{-3}$, and up to 111,300 $\#cm^{-3}$, one order of magnitude greater than at zone A (close to the top of the open-pit). Also, as shown in the figure, PM and BC peaks again coincided due to the impact of the emissions from the engines of the excavators (BC) and those during loading. However, UFP peaks were closely related to the Liquefied-Natural-Gas fuelled truck exhaust emissions.

At the mid-altitude coal working front area with no truck loading activity (zone E), measurements around coal works with an excavator (17/10/2018, 10 °C, RH 64%, CO_2 395 ppm), yielded moderately low PM_{10} and $PM_{2.5}$ levels (68 and 28 $\mu g \cdot m^{-3}$, respectively), and high $PM_{2.5}/PM_{10}$ ratios (0.37) (Fig. S5 c).

4.2.1.3. Truck traffic into the open-pit. At the border of mine track located at a relatively high altitude, on 17/10/2018, 11:32 to 12:46 h LT, with ambient conditions of 12 °C, RH 55%, CO_2 391 ppm. In this track, there was frequent wetting of the surface to abate resuspension of dust by truck movement. Here, the impact of emissions from the loss of bulk material from trucks, the road dust resuspension, and the exhaust emissions from loaded trucks on UFP, BC and PM levels and DD were evaluated.

Respirable deposited dust sampled at this site was composed of 16, 82, 2, 1 and 0.3% of clay minerals, quartz, feldspar, gypsum and anatase, 36, 23 and 15% DD10, DD4 and DD2.5 in DD500, and 97% of DD is DD500. Thus, this dust, compared to that from coal front or tailings areas, is intermediate in size and greatly enriched in quartz. Fig. 8c shows that levels of BC (9 $\mu g \cdot m^{-3}$) and $PM_{2.5}$ (264 $\mu g \cdot m^{-3}$) were moderate-low compared to those at other sites due to the intermittent emissions and the relatively high dispersive conditions that prevail at the site. Trucks are fuelled with Liquefied-Natural-Gas, and very low BC levels, but relatively high UFP concentrations (22,775 $\#cm^{-3}$) were recorded, although values were still moderate compared to traffic sites. Relevant UFP emissions are supported by a previous study that examined the UFP emissions from natural gas-fuelled heavy-duty vehicles (Giechaskiel, 2018). These results are very close to the ones by Kurth et al. (2014) in coal mining areas influenced by emissions from machinery and trucks (mostly 5000 to 10,000 $\#cm^{-3}$, but reaching 30,000 $\#cm^{-3}$ in some of them).

The high quartz content and RDD contents measured at the border site of a mine track suggest the possibility of quite hazardous exposure in this area. However, workers rarely are exposed to these conditions because only trucks and excavators work there, and these are indoor ventilated with filtered air. Also, the DD loads are visibly lower than in other locations.

The bottom of the open-pit, where coal is primarily worked, had moderate-high PM levels probably due to the application of control measures (surface wetting). The PM at this site was coarser than in other locations because the coal mined is of high quality (low S and ash yield) and coal fragments are coarser than the mineral ones. Peak concentrations of BC seem to be associated with those of PM but not to UFP. This evidence suggests that the exhaust of the excavators extracting and loading coal is the main source of BC, but mean levels are typical of those from high-traffic sites in busy cities (Reche et al., 2011). The tailings are disposed of in the upper parts of the open-pit but, in some cases, these are discarded with no control measures, and high levels of PM were measured when loading high clay materials. The ambient air in the mine track for extraction of tailings in the upper part of the pit was characterised by low BC, moderate PM and high UFP concentrations, due to the high ventilation and the fact that trucks are fuelled with natural gas (Fig. 8c). Notably, at the bottom of the mine, due to heightened excavator and truck density but lower atmospheric dispersion, UFP levels are one order of magnitude higher than at the top of the pit. These are also above the highest PM levels recorded close to the handling of tailings at the banks in that location.

4.2.2. PM_{10} levels and composition

Sampling of PM_{10} was carried out in some of the locations simultaneously with the sampling of DD. Table 7 summarises the ambient air PM_{10} concentrations of major and trace elements (in $\mu g \cdot m^{-3}$ and $ng \cdot m^{-3}$, respectively), and, Table S2 shows the ambient air PM_{10} details of collection from the different zones of the open-pit mine.

The coal working front PM_{10} contained a markedly elevated proportion of coal (90–95%), much higher than road traffic and tailings handling PM_{10} samples (10–35%). Comparing the PM_{10} compositions with those of RDD obtained from DD co-collected at the same zones, and, taking into account that the first refers to PM with at least 50% <10 µm and the second to <4 µm, remarkable similarities were found. This result is notable because DD is much easier and cheaper to sample than PM_{10}. However, remarkable PM_{10}/RDD differences were found in the road traffic only for Zn, Cu, As, Cd and Sn, whose contents were much higher in PM_{10} than in RDD. These differences might be due to the high machinery and brake and tyre wear emissions at road traffic, as these elements in PM_{10} are usually attributed to these specific emission sources (Amato et al., 2009). However, due to their relatively fine size, their deposition rate is low and accordingly depleted in RDD compared with PM_{10}. Moreover, Liang et al. (2006) show China occupational exposure limits (OELs) for permissible concentration-short term exposure limit (PC-STEL) for coal dust with less content of 10% in SiO_2 (3.5 $mg \cdot m^{-3}$)

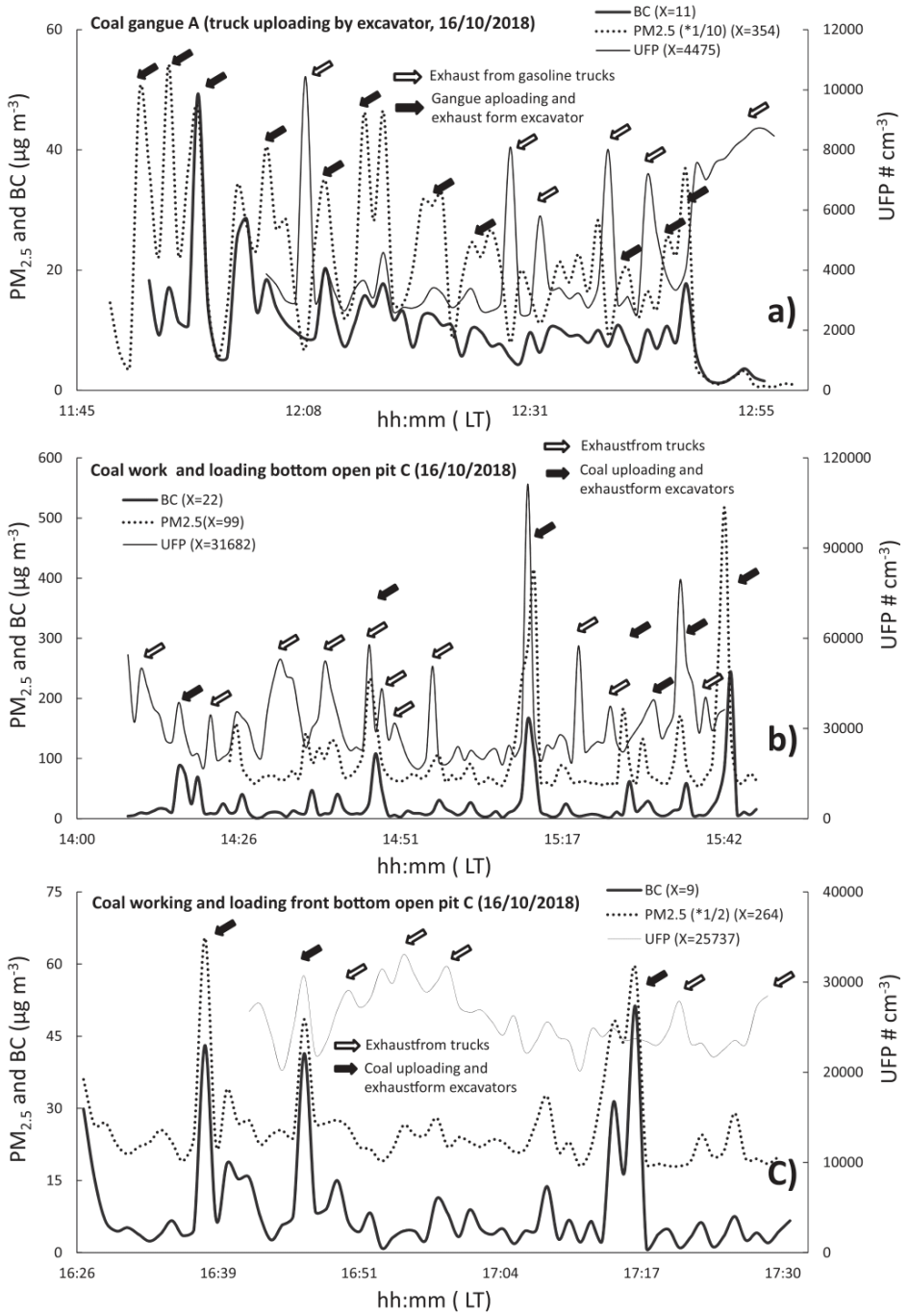

Fig. 8. Ambient concentrations of BC, $PM_{2.5}$ and UFP measured in the vicinity of tailings handling, coal working front and road traffic into a mine road for tailings.

and for the content between 10 and 50% in SiO_2 (1.0 mg·m^{-3}). In the coal working front measurements recorded a concentration of 1.4 mg·m^{-3} with less 10% content of SiO_2. In the tailings handling and road traffic concentration values were 2.7 and 0.1 mg·m^{-3} respectively (10–50% content of SiO_2).

5. Discussion and conclusions

In this study the mineralogy and geochemistry of deposited dust (DD) coal mine samples were examined, and their respirable DD (RDD) size fraction (<4 μm), collected from three different regions of an active, highly volatile bituminous open-pit coal mine. The areas of collection were coal working fronts, tailings handling sites, and road traffic sites. Online measurements of ambient air concentrations of particulate matter (PM_{10} and $PM_{2.5}$), black carbon (BC) and ultrafine particle numbers (UFP) were performed in the three mine zones. The respirable fraction samples were subjected to analysis of specific biological response or toxicological indicators (Oxidative Potential, OP). The results demonstrated i) a notable difference in particle size and chemical composition of DD from the different sampling areas, ii) a noticeable effect of moisture content and ash yield of DD on the particle size distribution (PSD), and, accordingly, on the potential emissions of the finer,

Table 7
Major and trace elements concentrations of coal dust exposure in open-pit coal mine. *TH, Tailings handling; CWF, Coal working front; RT, Road traffic into a mine road for tailings.* See Table S2 for sampling explanation.

Sample	CHI_1	CHI_2	CHI_4	CHI_6
Location	TH	CWF	CWF	RT
Zone	A	C	D	G
Concentration (ug/m^3)	3652	1535	29,179	257
	ug·m^{-3}	ug·m^{-3}	ug·m^{-3}	ug·m^{-3}
Tot	2719	1444	22,816	117
Coal	272	1335	21,104	41
Sum	2447	108	1711	76
SiO_2	1353	32	623	30
Al_2O_3	902	18	268	15
CaO	33	32	363	17
Fe_2O_3	29	4.4	44	5.5
K_2O	53	2.2	24	2.2
MgO	16	6.2	227	2.6
Na_2O	1.1	0.33	1.4	0.47
P_2O_5	1.9	0.57	2.3	0.80
S	15	10	123	0.54
TiO_2	39	0.82	12	1.1
	ng·m^{-3}	**ng·m^{-3}**	**ng·m^{-3}**	**ng·m^{-3}**
Li	71	6.6	58	1.0
V	587	16	159	20
Cr	337	17	77	1.0
Mn	196	89	705	29
Co	147	5.9	28	1.0
Ni	326	19	28	1.0
Cu	126	1.0	63	483
Zn	1081	103	1302	671
Ga	101	2.8	29	2.2
As	1.0	1.0	9.1	30
Rb	208	9.2	84	12
Sr	320	294	14,891	33
Zr	1111	276	692	279
Nb	50	1.0	18	1.0
Cd	1.0	1.0	1.0	108
Sn	53	19	101	96
Cs	19	1.0	8.3	1.0
Ba	673	124	4919	33
REE	424	22	240	14
Hf	39	13	25	13
Pb	114	31	64	31
Th	45	1.0	15	1.0
U	15	1.2	6.2	1.0

RDD fraction, iii) an enrichment of multiple elements (such as Nb, Th, Cr, Sr, Li, As, Pb, Cu, Zr and Ni) in this RDD fraction, attributed, at least in part, to mining machinery, tyre and brake wear emissions, iv) a major impact from specific mining operations and mine areas on the levels of air pollutants (such as high PM from tailings handling in the upper parts of the mine or the high UFP levels in the lower parts of the mine due to vehicle and machinery emissions and low dispersive conditions), v) the predicted low OP of the RDD fraction in a mine working with high-quality coal, with OP within the RDD fraction seemingly influenced by Mn, sulphates and anatase contents, as suggested by previous studies.

These results provide insight into the mineralogical and chemical variations present within inhalable size fractions of coal mine dust collected from differing localities within coal mines. The results show how, at the coal working front, the contents of mineral silicates in the inhalable fraction extracted from DD are much higher than in the parent coal. As would be expected from what is known about mineral matter in coals (e.g., Finkelman et al., 2019), the mineral silicates identified in this dust analysis at the coal working front are dominated by phyllosilicates (kaolinite/clinochlore) and quartz. In addition to which are sulphates (mostly gypsum) and very minor amounts of plagioclase feldspars and titanium oxide polymorphs such as anatase.

Perhaps the most important conclusion within this context is the fact that the data presented demonstrate that coals containing a greater content of fine aluminosilicates and silica impurities produce an elevated loading of finer, more deeply inhalable particles ($PM_{2.5}$) in resulting mine dust emissions than more carbonaceous samples, sourced from purer coals. Given the health concerns over the presence of siliceous particles in mine dust, it was observed that these can be preferentially fractionated into deeply inhalable size-fractions of PM, relevant to safe work practices. It follows that precautions for dust suppression and inhalation should be taken by miners working on coals with higher silicate impurity contents.

The mineralogy of dust generated at the coal working front is clearly quite different from that inhaled in the tailings handling and road traffic areas sampled. In these latter two environments, ambient dust contains a much higher concentration of silicates (quartz, feldspars, and clay minerals, with the phyllosilicate content including a significant quantity of illite-muscovite), plus notable amounts of carbonate and Ti-oxide (TiO_2), but much less sulphate. These mineralogical differences are reflected in the trace element content of the DDs, presumably reflecting the fact that most such elements are typically concentrated within phyllosilicates which are more abundantly present in the more felsic geochemistry of the tailings and road samples. Thus, the coal working front samples are depleted in most trace elements, notably Ti, V, Cr, Co, Ni, Ga, Ge, Se, Rb, Zr, Nb, Sn, Cs, Hf, Pb, Th, U, and REE. Such observations underline how coal mine dust has its own distinctive mineralogical, and therefore, geochemical signature, which is likely to be different from ambient PM encountered elsewhere in the mine.

From an exposure point of view, it is relevant to note that, in the coal working fronts, some elements (Nb, Th, Cr, Sr, Li, As, Pb, Cu, Zr and Ni) of the RDD were found at higher levels in the finer fraction than in the DD. This is possibly related to the mineralogy of the samples, since these elements are associated with clay and carbonate minerals, and also potentially with mining machinery wear. In contrast, the high levels of coarser Ba in DD might be due to the occurrence of fine barite ($BaSO_4$) crystals embedded in the coaly matrix.

Size patterns of Zr and Hf are also interesting, with 2 types of zircon likely present: the coarser (geogenic origin and enriched in Hf) and the finer (originating from the wear of the drilling and other mining machinery, lower in Hf). On the other hand, in tailings handling and road traffic, some elements (Cu, Sn, Pb, Sb and Zn) were associated with the RDD fraction and possibly produced from tyre and brake wear. Given the likelihood of enrichment of trace elements of potential concern in the finer, RDD fraction of the DD, when compared to the parent materials, it is necessary to emphasise the potential importance of size fractionation in mine dusts. It is not unreasonable to suspect that the health effects on mine workers breathing these particulate materials might be different to what would be expected if the composition of the dust derived from the parent materials was simply extrapolated, without considering the effects of mineral size fractionation in the dust released during the coal mining process.

When looking at the oxidative stress results obtained from the samples measured, the high coal quality of the open-pit coal mine, with its low pyrite and quartz contents (and therefore less potential risk of silicosis), appears to have minimised any obvious association of OP with acid mine drainage products. In particular, manganese and anatase were correlated with OP^{AA} and OP^{GSH} at the coal working front. In contrast, in the tailings handling and road traffic sampling areas, particle size was associated with OP^{AA}, which was negatively-correlated with the coal working front. This is due to the elements being likely embedded in the coal matrix, yielding slightly coarser particles. A clear correlation for RDD samples with sulphates and anatase was found in OP^{AA} and, to a lesser extent, with PSD. Also, a slight correlation was found between OP^{GSH} and Ca and Na contents, representing the amount of coaly matrix and sulphate and carbonate minerals.

Finally, these different approaches to mine dust indicated in this study demonstrate, as far as the study's researchers are aware, for the first time, the necessity of extracting the more deeply respirable size fraction of coal mine dusts in future studies on the health effects of such materials. This respirable fraction is geochemically different from the

parent materials, not only from the actual coal (and related sediments) being mined, but also from the coarser-grained passively-DDs found around the mine.

Authors statements

The corresponding author, Pedro Trechera, is responsible for ensuring that the descriptions are accurate and agreed by all authors, did the sampling and most of the analyses and most of writing.

Xavier Querol participated in the sampling and analysis, discussed results, also wrote some sections and reviewed the manuscript.

Zhuang Xinguo, Baoqing Li, Jing Li, Yunfei Shangguan and Patricia Córdoba, participated in the sampling of different mines, discussed results and reviewed the manuscript.

Ana Oliete and Frank Kelly did the OP analysis, wrote a section and reviewed the manuscript.

Teresa Moreno and Natalia Moreno performed SEM and DRX analyses, discussed results and reviewed the manuscript.

Declaration of Competing Interest

The authors declare that they have no known competing financial interests or personal relationships that could have appeared to influence the work reported in this paper.

Acknowledgements

This study was supported by Generalitat de Catalunya (AGAUR 2017 SGR41), Spain; by the National Science Foundation of China (grant 41972180); the Program of Introducing Talents of Discipline to Universities (grant B14031) and Overseas Top Scholars Program for the Recruitment of Global Experts, China and by the Spanish Ministry of Science and Innovation (Excelencia Severo Ochoa, Project CEX2018-000794-S). Pedro Trechera is contracted by the ROCD (Reducing risks from Occupational exposure to Coal Dust) project supported by the European Commission Research Fund for Coal and Steel; Grant Agreement Number-754205.

Appendix A. Supplementary data

Supplementary data to this article can be found online at https://doi.org/10.1016/j.coal.2021.103677.

References

Akinwekomi, V., Maree, J.P., Masindi, V., Zvinowanda, C., Osman, M.S., Foteinis, S., Mpenyana-Monyatsi, L., Chatzisymeon, E., 2020. Beneficiation of acid mine drainage (AMD): a viable option for the synthesis of goethite, hematite, magnetite, and gypsum – Gearing towards a circular economy concept. Miner. Eng. 148, 106204. https://doi.org/10.1016/J.MINENG.2020.106204.

Amato, F., Querol, X., Alastuey, A., Pandolfi, M., Moreno, T., Gracia, J., Rodriguez, P., 2009. Evaluating urban PM10 pollution benefit induced by street cleaning activities. Atmos. Environ. 43, 4472–4480. https://doi.org/10.1016/j.atmosenv.2009.06.037.

Amato, F., Querol, X., Johansson, C., Nagl, C., Alastuey, A., 2010. A review on the effectiveness of street sweeping, washing and dust suppressants as urban PM control methods. Sci. Total Environ. 408, 3070–3084. https://doi.org/10.1016/j.scitotenv.2010.04.025.

Azam, S., Mishra, D.P., 2019. Effects of particle size, dust concentration and dust-dispersion-air pressure on rock dust inertant requirement for coal dust explosion suppression in underground coal mines. Process. Saf. Environ. Prot. 126, 35–43. https://doi.org/10.1016/j.psep.2019.03.030.

Baker, M.A., Cerniglia, G.J., Zaman, A., 1990. Microtiter plate assay for the measurement of glutathione and glutathione disulfide in large numbers of biological samples. Anal. Biochem. 190, 360–365. https://doi.org/10.1016/0003-2697(90)90208-Q.

Birben, E., Sahiner, U.M., Sackesen, C., Erzurum, S., Kalayci, O., 2012. Oxidative stress and antioxidant defense. World Allergy Organ. J. 5, 9–19. https://doi.org/10.1097/WOX.0b013e3182439613.

Borm, P.J.A., 2002. Particle toxicology: from coal mining to nanotechnology. Inhal. Toxicol. 14, 311–324. https://doi.org/10.1080/08958370252809086.

BP (Ed.), 2019. 2019. BP Statistical Review of World Energy Statistical Review of World, pp. 1–69. Ed. BP Stat. Rev. World Energy.

Brodny, J., Tutak, M., 2018. Exposure to harmful dusts on fully powered longwall coal mines in Poland. Int. J. Environ. Res. Public Health 15. https://doi.org/10.3390/ijerph15091846.

Caballero-Gallardo, K., Olivero-Verbel, J., 2016. Mice housed on coal dust-contaminated sand: a model to evaluate the impacts of coal mining on health. Toxicol. Appl. Pharmacol. 294, 11–20. https://doi.org/10.1016/j.taap.2016.01.009.

Calas, A., Uzu, G., Kelly, F.J., Houdier, S., Martins, J.M.F., Thomas, F., Molton, F., Charron, A., Dunster, C., Oliete, A., Jacob, V., Besombes, J.-L., Chevrier, F., Jaffrezo, J.-L., 2018. Comparison between five acellular oxidative potential measurement assays performed with detailed chemistry on PM₁₀ samples from the city of Chamonix (France). Atmos. Chem. Phys. 18, 7863–7875. https://doi.org/10.5194/acp-18-7863-2018.

Casagrande, D.J., 1987. Sulphur in peat and coal. Geol. Soc. Spec. Publ. 32, 87–105. https://doi.org/10.1144/GSL.SP.1987.032.01.07.

Cassee, F.R., Mills, N.L., Newby, D. (Eds.), 2011. Cardiovascular Effects of Inhaled Ultrafine and Nanosized Particles, Cardiovascular Effects of Inhaled Ultrafine and Nanosized Particles. John Wiley & Sons, Inc., Hoboken, NJ, USA https://doi.org/10.1002/9780470910917.

Cassee, F.R., Morawska, L., Peters, A., 2019. Ambient Ultrafine Particles : Evidence for Policy Makers.

Castranova, V., 2000. From Coal Mine Dust to Quartz: Mechanisms of Pulmonary Pathogenicity. Inhal. Toxicol. 12, 7–14. https://doi.org/10.1080/08958378.2000.11463226.

Chen, F., Wang, S., Mou, S., Azimuddin, I., Zhang, D., Pan, X., Al-Misned, F.A., Mortuza, M.G., 2015. Physiological responses and accumulation of heavy metals and arsenic of Medicago sativa L. growing on acidic copper mine tailings in arid lands. J. Geochemical Explor. 157, 27–35. https://doi.org/10.1016/J.GEXPLO.2015.05.011.

Cheng, W., Yu, H., Zhou, G., Nie, W., 2016. The diffusion and pollution mechanisms of airborne dusts in fully-mechanized excavation face at mesoscopic scale based on CFD-DEM. Process. Saf. Environ. Prot. 104, 240–253. https://doi.org/10.1016/j.psep.2016.09.004.

Chung, F.H., 1974. Quantitative interpretation of X-ray diffraction patterns of mixtures. I. Matrix-flushing method for quantitative multicomponent analysis. J. Appl. Crystallogr. 7, 519–525. https://doi.org/10.1107/s0021889874010375.

Cohen, R.A.C., Patel, A., Green, F.H.Y., 2008. Lung disease caused by exposure to coal mine and silica dust. Semin. Respir. Crit. Care Med. https://doi.org/10.1055/s-0028-1101275.

Colinet, J.F., James, P.R., Jeffrey, M.L., John, A.O., Anita, L.W., 2010. Best Practices for Dust Control in Coal Mining. Centers Dis. Control Prev. Natl. Inst. Occup. Saf. Heal. 01, 17–36.

Dai, S., Finkelman, R.B., 2018. Coal as a promising source of critical elements: Progress and future prospects. Int. J. Coal Geol. 186, 155–164. https://doi.org/10.1016/j.coal.2017.06.005.

Dai, S.F., Zhou, Y.P., Ren, D.Y., Wang, X.B., Li, D., Zhao, L., 2007. Geochemistry and mineralogy of the late Permian coals from the Songzo Coalfield, Chongqing, southwestern China. Sci. China Ser. D Earth Sci. 50, 678–688. https://doi.org/10.1007/s11430-007-0001-4.

Dai, S., Ren, D., Zhou, Y., Chou, C.L., Wang, X., Zhao, L., Zhu, X., 2008. Mineralogy and geochemistry of a superhigh-organic-sulfur coal, Yanshan Coalfield, Yunnan, China: evidence for a volcanic ash component and influence by submarine exhalation. Chem. Geol. 255, 182–194. https://doi.org/10.1016/j.chemgeo.2008.06.030.

Dai, S., Li, T., Seredin, V.V., Ward, C.R., Hower, J.C., Zhou, Y., Zhang, M., Song, X., Song, W., Zhao, C., 2014. Origin of minerals and elements in the late Permian coals, tonsteins, and host rocks of the Xinde Mine, Xuanwei, eastern Yunnan, China. Int. J. Coal Geol. 121, 53–78. https://doi.org/10.1016/j.coal.2013.11.001.

Dai, S., Bechtel, A., Eble, C.F., Flores, R.M., French, D., Graham, I.T., Hood, M.M., Hower, J.C., Korasidis, V.A., Moore, T.A., Püttmann, W., Wei, Q., Zhao, L., O'Keefe, J.M.K., 2020. Recognition of peat depositional environments in coal: a review. Int. J. Coal Geol. https://doi.org/10.1016/j.coal.2019.103383.

Dalal, N.A.R.S., Newman, J., Pack, D., Leonard, S., Vallyathan, V.A.L., 1995. Original Contribution, 18, pp. 11–20.

Dias, C.L., Oliveira, M.L.S., Hower, J.C., Taffarel, S.R., Kautzmann, R.M., Silva, L.F.O., 2014. Nanominerals and ultrafine particles from coal fires from Santa Catarina, South Brazil. Int. J. Coal Geol. 122, 50–60. https://doi.org/10.1016/j.coal.2013.12.011.

Ercal, N.B.S.P., Hande Gurer-Orhan, B.S.P., Nukhet Aykin-Burns, B.S.P., 2005. Toxic Metals and Oxidative stress part I: mechanisms involved in Me-tal induced oxidative damage. Curr. Top. Med. Chem. 1, 529–539. https://doi.org/10.2174/1568026013394831.

Erol, I., Aydin, H., Didari, V., Ural, S., 2013. Pneumoconiosis and quartz content of respirable dusts in the coal mines in Zonguldak, Turkey. Int. J. Coal Geol. 116–117, 26–35. https://doi.org/10.1016/j.coal.2013.05.008.

Finkelman, R.B., 1994. Modes of occurrence of potentially hazardous elements in coal: levels of confidence. Fuel Process. Technol. 39, 21–34. https://doi.org/10.1016/0378-3820(94)90169-4.

Finkelman, R.B., Dai, S., French, D., 2019. The importance of minerals in coal as the hosts of chemical elements: a review. Int. J. Coal Geol. 212, 103251.

Fu, P.P., Xia, Q., Hwang, H.M., Ray, P.C., Yu, H., 2014. Mechanisms of nanotoxicity: generation of reactive oxygen species. J. Food Drug Anal. 22, 64–75. https://doi.org/10.1016/j.jfda.2014.01.005.

Gamble, F.J., 2012. Rapidly progressing coal workers pneumoconiosis as a confounding risk factor in assessing coal mine dust safe exposure levels. J. Clin. Toxicol. 01 https://doi.org/10.4172/2161-0495.s1-003.

Ghio, A.J., Madden, M.C., 2018. Human lung injury following exposure to humic substances and humic-like substances. Environ. Geochem. Health 40, 571–581. https://doi.org/10.1007/s10653-017-0008-5.

Giechaskiel, B., 2018. Solid particle number emission factors of euro vi heavy-duty vehicles on the road and in the laboratory. Int. J. Environ. Res. Public Health 15. https://doi.org/10.3390/ijerph15020304.
Gilmour, M.I., O'Connor, S., Dick, C.A.J., Miller, C.A., Linak, W.P., 2004. Differential pulmonary inflammation and in vitro cytotoxicity of size-fractionated fly ash particles from pulverized coal combustion. J. Air Waste Manage. Assoc. 54, 286–295. https://doi.org/10.1080/10473289.2004.10470906.
Gomo, M., 2018. Conceptual hydrogeochemical characteristics of a calcite and dolomite acid mine drainage neutralised circumneutral groundwater system. Water Sci. 32, 355–361. https://doi.org/10.1016/J.WSJ.2018.05.004.
Gürdal, G., 2008. Geochemistry of trace elements in Çan coal (Miocene), Çanakkale. Turkey. Int. J. Coal Geol. 74, 28–40. https://doi.org/10.1016/J.COAL.2007.09.004.
Heusinkveld, H.J., Wahle, T., Campbell, A., Westerink, R.H.S., Tran, L., Johnston, H., Stone, V., Cassee, F.R., Schins, R.P.F., 2016. Neurodegenerative and neurological disorders by small inhaled particles. Neurotoxicology 56, 94–106. https://doi.org/10.1016/j.neuro.2016.07.007.
Hower, J.C., Robertson, J.D., 2003. Clausthalite in coal. Int. J. Coal Geol. 53, 219–225. https://doi.org/10.1016/S0166-5162(03)00022-3.
Huang, X., Li, W., Attfield, M.D., Nádas, A., Frenkel, K., Finkelman, R.B., 2005. Mapping and prediction of coal Workers' Pneumoconiosis with bioavailable iron content in the bituminous coals. Environ. Health Perspect. 113, 964–968. https://doi.org/10.1289/ehp.7679.
Hung, N.T.Q., Lee, S.B., Hang, N.T., Kongpran, J., Kim Oanh, N.T., Shim, S.G., Bae, G.N., 2014. Characterization of black carbon at roadside sites and along vehicle roadways in the Bangkok Metropolitan Region. Atmos. Environ. 92, 231–239. https://doi.org/10.1016/j.atmosenv.2014.04.011.
Hussein, T., Saleh, S., dos Santos, V., Abdullah, H., Boor, B., 2019. Black carbon and particulate matter concentrations in eastern mediterranean urban conditions: an assessment based on integrated stationary and mobile observations. Atmosphere (Basel). 10, 323. https://doi.org/10.3390/atmos10060323.
IEA, 2019. World Energy Outlook 2019. IEA, Paris [WWW Document].
Iriyama, K., Yoshiura, M., Iwamoto, T., Ozaki, Y., 1984. Simultaneous determination of uric and ascorbic acids in human serum by reversed-phase high-performance liquid chromatography with electrochemical detection. Anal. Biochem. 141, 238–243. https://doi.org/10.1016/0003-2697(84)90451-2.
Johann-Essex, V., Keles, C., Rezaee, M., Scaggs-Witte, M., Sarver, E., 2017. Respirable coal mine dust characteristics in samples collected in central and northern Appalachia. Int. J. Coal Geol. 182, 85–93. https://doi.org/10.1016/j.coal.2017.09.010.
Kelly, F.J., 2003. Oxidative stress: its role in air pollution and adverse health effects. Occup. Environ. Med. 60, 612–616. https://doi.org/10.1136/oem.60.8.612.
Ketris, M.P., Yudovich, Y.E., 2009. Estimations of Clarkes for Carbonaceous biolithes: World averages for trace element contents in black shales and coals. Int. J. Coal Geol. 78, 135–148. https://doi.org/10.1016/j.coal.2009.01.002.
Kurth, L.M., McCawley, M., Hendryx, M., Lusk, S., 2014. Atmospheric particulate matter size distribution and concentration in West Virginia coal mining and non-mining areas. Mod. Pathol. 27, 405–411. https://doi.org/10.1038/jes.2014.2.
Latvala, S., Hedberg, J., Di Bucchianico, S., Möller, L., Wallinder, I.O., Elihn, K., Karlsson, H.L., 2016. Nickel release, ROS generation and toxicity of Ni and NiO micro- and nanoparticles. PLoS One 11, 1–20. https://doi.org/10.1371/journal.pone.0159684.
Lee, S., 1990. Oil Shale Technology, p. 280.
Li, N., Sioutas, C., Cho, A., Schmitz, D., Misra, C., Sempf, J., Wang, M., Oberley, T., Froines, J., Nel, A., 2003. Ultrafine particulate pollutants induce oxidative stress and mitochondrial damage. Environ. Health Perspect. 111, 455–460. https://doi.org/10.1289/ehp.6000.
Li, N., Xia, T., Nel, A.E., 2008. The role of oxidative stress in ambient particulate matter-induced lung diseases and its implications in the toxicity of engineered nanoparticles. Free Radic. Biol. Med. 44, 1689–1699. https://doi.org/10.1016/j.freeradbiomed.2008.01.028.
Li, J., Zhuang, X., Querol, X., Font, O., Moreno, N., Zhou, J., Lei, G., 2012. High quality of Jurassic Coals in the Southern and Eastern Junggar Coalfields, Xinjiang, NW China: Geochemical and mineralogical characteristics. Int. J. Coal Geol. 99, 1–15. https://doi.org/10.1016/j.coal.2012.05.003.
Liang, Y., Wong, O., Yang, L., Li, T., Su, Z., 2006. The development and regulation of occupational exposure limits in China. Regul. Toxicol. Pharmacol. 46, 107–113. https://doi.org/10.1016/j.yrtph.2006.02.007.
Liu, G., Vassilev, S.V., Gao, L., Zheng, L., Peng, Z., 2005. Mineral and chemical composition and some trace element contents in coals and coal ashes from Huaibei coal field, China. Energy Convers. Manag. https://doi.org/10.1016/j.enconman.2004.11.002.
Liu, Q., Bai, C., Li, X., Jiang, L., Dai, W., 2010. Coal dust/air explosions in a large-scale tube. Fuel 89, 329–335. https://doi.org/10.1016/j.fuel.2009.07.010.
Ma, D., Qin, B., Gao, Y., Jiang, J., Feng, B., 2020. Study on the explosion characteristics of methane–air with coal dust originating from low-temperature oxidation of coal. Fuel 260, 116304. https://doi.org/10.1016/j.fuel.2019.116304.
Madzivire, G., Petrik, L.F., Gitari, W.M., Ojumu, T.V., Balfour, G., 2010. Application of coal fly ash to circumneutral mine waters for the removal of sulphates as gypsum and ettringite. Miner. Eng. 23, 252–257. https://doi.org/10.1016/J.MINENG.2009.12.004.
Medeiros, M.A., Leite, C.M.M., Lago, R.M., 2012. Use of glycerol by-product of biodiesel to produce an efficient dust suppressant. Chem. Eng. J. 180, 364–369. https://doi.org/10.1016/j.cej.2011.11.056.
Morawska, L., Ristovski, Z., Jayaratne, E.R., Keogh, D.U., Ling, X., 2008. Ambient nano and ultrafine particles from motor vehicle emissions: Characteristics, ambient processing and implications on human exposure. Atmos. Environ. https://doi.org/10.1016/j.atmosenv.2008.07.050.
Moreno, T., Higueras, P., Jones, T., McDonald, I., Gibbons, W., 2005. Size fractionation in mercury-bearing airborne particles (HgPM 10) at Almadén, Spain: Implications for inhalation hazards around old mines. Atmos. Environ. 39, 6409–6419. https://doi.org/10.1016/j.atmosenv.2005.07.024.
Moreno, T., Kelly, F.J., Dunster, C., Oliete, A., Martins, V., Reche, C., Minguillón, M.C., Amato, F., Capdevila, M., de Miguel, E., Querol, X., 2017. Oxidative potential of subway PM2.5. Atmos. Environ. 148, 230–238. https://doi.org/10.1016/j.atmosenv.2016.10.045.
Moreno, T., Trechera, P., Querol, X., Lah, R., Johnson, D., Wrana, A., Williamson, B., 2019. Trace element fractionation between PM10 and PM2.5 in coal mine dust: Implications for occupational respiratory health. Int. J. Coal Geol. 203, 52–59. https://doi.org/10.1016/j.coal.2019.01.006.
Mudway, I.S., Stenfors, N., Duggan, S.T., Roxborough, H., Zielinski, H., Marklund, S.L., Blomberg, A., Frew, A.J., Sandström, T., Kelly, F.J., 2004. An in vitro and in vivo investigation of the effects of diesel exhaust on human airway lining fluid antioxidants. Arch. Biochem. Biophys. 423, 200–212. https://doi.org/10.1016/j.abb.2003.12.018.
Munir, M.A.M., Liu, G., Yousaf, B., Mian, M.M., Ali, M.U., Ahmed, R., Cheema, A.I., Naushad, M., 2020. Contrasting effects of biochar and hydrothermally treated coal gangue on leachability, bioavailability, speciation and accumulation of heavy metals by rapeseed in copper mine tailings. Ecotoxicol. Environ. Saf. 191, 110244. https://doi.org/10.1016/J.ECOENV.2020.110244.
NIOSH, 2002. Health effects of occupational exposure to respirable crystalline silica. NIOSH Hazard Rev. 145 doi:2002–129.
Oberdörster, G., Ferin, J., Lehnert, B.E., 1992. Correlation between particle size, in vivo particle persistence, and lung injury. Environ. Health Perspect. 102, 173–179. https://doi.org/10.1289/ehp.102-1567252.
Pedroso-Fidelis, G. Dos S., Farias, H.R., Mastella, G.A., Boufleur-Niekraszewicz, L.A., Dias, J.F., Alves, M.C., Silveira, P.C.L., Nesi, R.T., Carvalho, F., Zocche, J.J., Pinho, R.A., 2020. Pulmonary oxidative stress in wild bats exposed to coal dust: a model to evaluate the impact of coal mining on health. Ecotoxicol. Environ. Saf. 191, 110211. https://doi.org/10.1016/J.ECOENV.2020.110211.
Querol, X., Chinchon, S., Lopez-Soler, A., 1989. Iron sulfide precipitation sequence in Albian coals from the Maestrazgo Basin, southeastern Iberian Range, northeastern Spain. Int. J. Coal Geol. 11, 171–189. https://doi.org/10.1016/0166-5162(89)90004-9.
Querol, X., Fernandez Turiel, J.L., Lopez Soler, A., Duran, M.E., 1992. Trace elements in high-S subbituminous coals from the Teruel Mining District, Northeast Spain. Appl. Geochem. 7, 547–561. https://doi.org/10.1016/0883-2927(92)90070-J.
Querol, X., Whateley, M.K.G., Fernández-Turiel, J.L., Tuncali, E., 1997. Geological controls on the mineralogy and geochemistry of the Beypazari lignite, Central Anatolia, Turkey. Int. J. Coal Geol. 33, 255–271. https://doi.org/10.1016/S0166-5162(96)00044-4.
Querol, X., Alastuey, A., Rodriguez, S., Plana, F., Mantilla, E., Ruiz, C.R., 2001. Monitoring of PM10 and PM2.5 around primary particulate anthropogenic emission sources. Atmos. Environ. 35, 845–858. https://doi.org/10.1016/S1352-2310(00)00387-3.
Querol, X., Viana, M., Alastuey, A., Amato, F., Moreno, T., Castillo, S., Pey, J., de la Rosa, J., Sánchez de la Campa, A., Artíñano, B., Salvador, P., García Dos Santos, S., Fernández-Patier, R., Moreno-Grau, S., Negral, L., Minguillón, M.C., Monfort, E., Gil, J.I., Inza, A., Ortega, L.A., Santamaría, J.M., Zabalza, J., 2007. Source origin of trace elements in PM from regional background, urban and industrial sites of Spain. Atmos. Environ. 41, 7219–7231. https://doi.org/10.1016/J.ATMOSENV.2007.05.022.
Reche, C., Querol, X., Alastuey, A., Viana, M., Pey, J., Moreno, T., Rodríguez, S., González, Y., Fernández-Camacho, R., de la Rosa, J., Dall Osto, M., Prévôt, A.S.H., Hueglin, C., Harrison, R.M., Quincey, P., 2011. New considerations for PM, Black Carbon and particle number concentration for air quality monitoring across different European cities. Atmos. Chem. Phys. 11, 6207–6227. https://doi.org/10.5194/acp-11-6207-2011.
Richardson, C., Rutherford, S., Agranovski, I., 2018. Characterization of particulate emissions from Australian open-cut coal mines: toward improved emission estimates. J. Air Waste Manage. Assoc. 68, 598–607. https://doi.org/10.1080/10962247.2017.1415236.
Riley, K.W., French, D.H., Farrell, O.P., Wood, R.A., Huggins, F.E., 2012. Modes of occurrence of trace and minor elements in some Australian coals. Int. J. Coal Geol. 94, 214–224. https://doi.org/10.1016/j.coal.2011.06.011.
Rosita, W., Bendiyasa, I.M., Perdana, I., Anggara, F., 2020. Sequential particle-size and magnetic separation for enrichment of rare-earth elements and yttrium in Indonesia coal fly ash. J. Environ. Chem. Eng. 8, 103575. https://doi.org/10.1016/j.jece.2019.103575.
Sarver, E., Keles, C., Rezaee, M., 2019. Beyond conventional metrics: Comprehensive characterization of respirable coal mine dust. Int. J. Coal Geol. 207, 84–95. https://doi.org/10.1016/j.coal.2019.03.015.
Schins, R.P.F., Borm, P.J.A., 1999. Mechanisms and mediators in coal dust induced toxicity: a review. Ann. Occup. Hyg. 43, 7–33. https://doi.org/10.1016/S0003-4878(98)00069-6.
Sevim, Ö., Demir, İ., 2019. Optimization of fly ash particle size distribution for cementitious systems with high compactness. Constr. Build. Mater. 195, 104–114. https://doi.org/10.1016/j.conbuildmat.2018.11.080.
Shahan, M.R., Seaman, C.E., Beck, T.W., Colinet, J.F., Mischler, S.E., 2017. Characterization of airborne float coal dust emitted during continuous mining, longwall mining and belt transport. Min. Eng. 69, 61–66 doi:10.19150/me.7746.

Shi, G.Q., Han, C., Wang, Y. Ming, Wang, H.T., 2019. Experimental study on synergistic wetting of a coal dust with dust suppressant compounded with noncationic surfactants and its mechanism analysis. Powder Technol. 356, 1077–1086. https://doi.org/10.1016/j.powtec.2019.09.040.

Shimura, K., Matsuo, A., 2019. Using an extended CFD-DEM for the two-dimensional simulation of shock-induced layered coal-dust combustion in a narrow channel. Proc. Combust. Inst. 37, 3677–3684. https://doi.org/10.1016/j.proci.2018.07.066.

Soltani, N., Keshavarzi, B., Sorooshian, A., Moore, F., Dunster, C., Dominguez, A.O., Kelly, F.J., Dhakal, P., Ahmadi, M.R., Asadi, S., 2018. Oxidative potential (OP) and mineralogy of iron ore particulate matter at the Gol-E-Gohar Mining and Industrial Facility (Iran). Environ. Geochem. Health 40, 1785–1802. https://doi.org/10.1007/s10653-017-9926-5.

Sperazza, M., Moore, J.N., Hendrix, M.S., 2004. High-resolution particle size analysis of naturally occurring very fine-grained sediment through laser diffractometry. J. Sediment. Res. 74, 736–743. https://doi.org/10.1306/031104740736.

Suarthana, E., Laney, A.S., Storey, E., Hale, J.M., Attfield, M.D., 2011. Coal workers' pneumoconiosis in the United States: Regional differences 40 years after implementation of the 1969 Federal Coal Mine Health and Safety Act. Occup. Environ. Med. 68, 908–913. https://doi.org/10.1136/oem.2010.063594.

Trechera, P., Moreno, T., Córdoba, P., Moreno, N., Zhuang, X., Li, B., Li, J., Shangguan, Y., Kandler, K., Dominguez, A.O., Kelly, F., Querol, X., 2020. Mineralogy, geochemistry and toxicity of size-segregated respirable deposited dust in underground coal mines. J. Hazard. Mater. 399, 122935. https://doi.org/10.1016/j.jhazmat.2020.122935.

Valko, M., Jomova, K., Rhodes, C.J., Kuča, K., Musílek, K., 2016. Redox- and non-redox-metal-induced formation of free radicals and their role in human disease. Arch. Toxicol. https://doi.org/10.1007/s00204-015-1579-5.

WCA, 2020. World Coal Association [WWW Document]. URL. https://www.worldcoal.org/.

WHO, 2013. Review of Evidence on Health Aspects of Air Pollution – REVIHAAP Project Technical Report. World Health Organization. https://doi.org/10.1007/BF00379640.

Xi, Z., Jiang, M., Yang, J., Tu, X., 2014. Experimental study on advantages of foam–sol in coal dust control. Process. Saf. Environ. Prot. 92, 637–644. https://doi.org/10.1016/j.psep.2013.11.004.

Xu, C., Wang, D., Wang, H., Xin, H., Ma, L., Zhu, X., Zhang, Y., Wang, Q., 2017. Effects of chemical properties of coal dust on its wettability. Powder Technol. 318, 33–39. https://doi.org/10.1016/j.powtec.2017.05.028.

Yang, L., Zhu, Z., Li, D., Yan, X., Zhang, H., 2019. Effects of particle size on the flotation behavior of coal fly ash. Waste Manag. 85, 490–497. https://doi.org/10.1016/j.wasman.2019.01.017.

Zhang, X., Chen, W., Ma, C., Zhan, S., 2012. Modeling the effect of humidity on the threshold friction velocity of coal particles. Atmos. Environ. 56, 154–160. https://doi.org/10.1016/j.atmosenv.2012.04.015.

Zhao, C.L., Sun, Y.Z., Xiao, L., Qin, S.J., Wang, J.X., Duan, D.J., 2014. The occurrence of barium in a Jurassic coal in the Huangling 2 Mine, Ordos Basin, northern China. Fuel 128, 428–432. https://doi.org/10.1016/J.FUEL.2014.03.040.

Zhou, J., Zhuang, X., Alastuey, A., Querol, X., Li, J., 2010. Geochemistry and mineralogy of coal in the recently explored Zhundong large coal field in the Junggar basin, Xinjiang province, China. Int. J. Coal Geol. 82, 51–67. https://doi.org/10.1016/j.coal.2009.12.015.

Zielinski, H., Mudway, I.S., Bérubé, K.A., Murphy, S., Richards, R., Kelly, F.J., 1999. Modeling the interactions of particulates with epithelial lining fluid antioxidants. Am. J. Phys. Lung Cell. Mol. Phys. 277, 719–726. https://doi.org/10.1152/ajplung.1999.277.4.l719.

4.5. Article #5

Geochemistry and oxidative potential of the respirable fraction of powdered mined Chinese coals

Authors:

Pedro Trechera[a, b], Teresa Moreno[a], Patricia Córdoba[a], Natalia Moreno[a], Fulvio Amato[a], Joaquim Cortés[a], Xinguo Zhuang[c], Baoqing Li[c], Jing Li[c], Yunfei Shangguan[c], Ana Oliete Dominguez[d], Frank Kelly[d], Takoua Mhadhbi[e], Jean Luc Jaffrezo[e], Gaelle Uzu[e], Xavier Querol[a,c]

a) Institute of Environmental Assessment and Water Research (IDAEA-CSIC), 08034 Barcelona, Spain.
b) Department of Natural Resources and Environment, Industrial and TIC Engineering (EMIT-UPC), 08242 Manresa, Spain.
c) Key Laboratory of Tectonics and Petroleum Resources, China University of Geosciences, Ministry of Education, Wuhan 430074, China.
d) MRC-PHE Centre for Environment and Health, King's College London, London SE1 9NH, UK.
e) Univ. Grenoble Alpes, IRD, CNRS, Grenoble INP, IGE (UMR 5001), 38000, Grenoble, France.

Published in:

Science of The Total Environment, 800, 149486

DOI: 10.1016/j.scitotenv.2021.149486

Accepted date:

2 August 2021 (Open access)

Impact factor/Quartile

7.963/Q1

Science of the Total Environment 800 (2021) 149486

Contents lists available at ScienceDirect

Science of the Total Environment

journal homepage: www.elsevier.com/locate/scitotenv

Geochemistry and oxidative potential of the respirable fraction of powdered mined Chinese coals

Pedro Trechera [a,b], Teresa Moreno [a], Patricia Córdoba [a], Natalia Moreno [a], Fulvio Amato [a], Joaquim Cortés [a], Xinguo Zhuang [c], Baoqing Li [c], Jing Li [c], Yunfei Shangguan [c], Ana Oliete Dominguez [d], Frank Kelly [d], Takoua Mhadhbi [e], Jean Luc Jaffrezo [e], Gaelle Uzu [e], Xavier Querol [a,c,*]

[a] Institute of Environmental Assessment and Water Research (IDAEA), Spanish Research Council (CSIC), 08034 Barcelona, Spain
[b] Department of Natural Resources and Environment, Industrial and TIC Engineering (EMIT-UPC), 08242 Manresa, Spain
[c] Key Laboratory of Tectonics and Petroleum Resources, China University of Geosciences, Ministry of Education, Wuhan 430074, China
[d] MRC-PHE Centre for Environment and Health, King's College London, London SE1 9NH, UK
[e] Univ. Grenoble Alpes, IRD, CNRS, Grenoble INP, IGE (UMR 5001), 38000 Grenoble, France

HIGHLIGHTS

- Mo, Mn, Hf and Ge decrease in respirable fractions and Cs, W, Zn and Zr increase.
- AA is associated with inorganic matter, GSH and DTT with organic matter.
- OP^{AA} was clearly linked with Fe ($r = 0.83$) and pyrite ($r = 0.66$).
- OP^{GSH} was associated with moisture ($r = 0.73$), Na ($r = 0.56$) and B ($r = 0.51$).
- OP^{DTT} was highly correlated with Mg ($r = 0.70$), Na ($r = 0.59$) and B ($r = 0.47$).

GRAPHICAL ABSTRACT

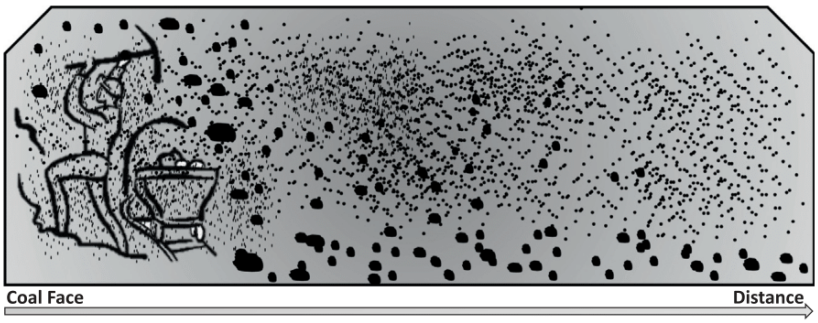

ARTICLE INFO

Article history:
Received 17 June 2021
Received in revised form 29 July 2021
Accepted 2 August 2021
Available online 5 August 2021

Editor: Pavlos Kassomenos

Keywords:
Chinese coal
Respirable dust
Oxidative potential
Coal dust
Coal geochemistry

ABSTRACT

This study evaluates geochemical and oxidative potential (OP) properties of the respirable (finer than 4 μm) fractions of 22 powdered coal samples from channel profiles (CP_4) in Chinese mined coals. The CP_4 fractions extracted from milled samples of 22 different coals were mineralogically and geochemically analysed and the relationships with the OP evaluated. The evaluation between CP_4/CP demonstrated that CP_4 increased concentrations of anatase, Cs, W, Zn and Zr, whereas sulphates, Fe, S, Mo, Mn, Hf and Ge decreased their CP_4 concentrations. OP results from ascorbic acid (AA), glutathione (GSH) and dithiothreitol (DTT) tests evidenced a clear link between specific inorganic components of CP_4 with OP^{AA} and the organic fraction of OP^{GSH} and OP^{DTT}. Correlation analyses were performed for OP indicators and the geochemical patterns of CP_4. These were compared with respirable dust samples from prior studies. They indicate that Fe ($r = 0.83$), pyrite ($r = 0.66$) and sulphate minerals ($r = 0.42$) (tracing acidic species from pyrite oxidation), followed by S ($r = 0.50$) and ash yield ($r = 0.46$), and, to a much lesser extent, Ti, anatase, U, Mo, V and Pb, are clearly linked with OP^{AA}. Moreover, OP^{GSH} correlation was identified by organic matter, as moisture ($r = 0.73$), Na ($r = 0.56$) and B ($r = 0.51$), and to a lesser extent by the coarse particle size, Ca and carbonate minerals. In addition, Mg ($r = 0.70$), B ($r = 0.47$), Na ($r = 0.59$), Mn, Ba, quartz, particle size and Sr regulate OP^{DTT} correlations. These became more noticeable when the analysis was done for samples of the same type of coal rank, in this case, bituminous.

* Corresponding author at: Institute of Environmental Assessment and Water Research (IDAEA), Spanish Research Council (CSIC), 08034 Barcelona, Spain.
E-mail addresses: xavier.querol@idaea.csic.es (X. Querol), pedro.trechera@idaea.csic.es (P. Trechera).

https://doi.org/10.1016/j.scitotenv.2021.149486

1. Introduction

1.1. Chinese coal and coal geochemistry

The use of coal in Chinese society can be traced back, with references to coal mining 3490 years ago (Dodson et al., 2014). Early documents refer to the use of Chinese coal for heating, cooking and smelting steel dating from 300 BCE (Gelegdorj et al., 2007; Li and Lu, 1995).

Nowadays, China is the greatest worldwide coal producer and consumer, with over half of the world's total consumption (BP, 2020; IEA, 2020; WCA, 2020). This situation will remain unchanged over the next few decades (Fan and Xia, 2012; Li et al., 2017; Wang et al., 2011; Yang et al., 2016).

Therefore, coal is the main source of energy production, representing 70% of the primary energy supply in China (Jie et al., 2020; J. Li et al., 2019; Qiao et al., 2019; Yuan, 2018). Some Chinese industrial sectors are directly dependent on coal for producing raw materials, such as steel, glass, cement or fertilizers (Lin and Tan, 2017; Wei et al., 2020).

China's coal resources have reached 13% of the global share (142 billion tonnes, BP, 2020), which account for 92–94% of the Chinese fossil fuel resources (Han et al., 2018; J. Li et al., 2019; Mao and Tong, 2013). Therefore, the large amount of coal production also requires large numbers of workers, which in China is around 5.5 million coal miners, according to Chen et al. (2013). Coal resources are widespread across China, where a prevalence of high rank over low rank coals (11% anthracite, 6% semi-anthracite, 70% bituminous coal, and 13% sub-bituminous coal and lignite) have been noticed (Mao and Tong, 2013). In these resources, a wide range of coal qualities from a large variety of coal basins in different geochemical regions are found, also accompanied by geochemical anomalies. Thus, Chinese coal ranges from the high-quality enormous coal resources from the Xinjiang Province (Li et al., 2012, 2014; Zhuang et al., 2012) to coals that contain such a high content of metals that they can be considered a source for these metals (Dai et al., 2003, 2016).

Examples of geochemical anomalies in coals from Northern China include high enrichment in Mn, Mg, Bi, Be, Cd, Mo, REEs and Y in the Huainan coalfields (Munir et al., 2018). There is a considerable content of Li and Ga in coals from the Jungar Coalfield, Inner Mongolia (Dai et al., 2012; J. Li et al., 2016). An elevated concentration of Zn, Pb and Cr can be found in coals from Yuyang, Hengshan, Shenmu, Huangling and Lingwu regions (Wang et al., 2014). Coals high in Mn, Nb and Ta have been extracted from the Jimunai depression (B. Li et al., 2019a). Coals with elevated concentration of REEs, Y, Nb, Ta, Zr, Hf, Ga, Th, and U have originated from the Qiandongbei coalfield (B. Li et al., 2020). The Gemudi mine contains coals with higher levels of V (Du et al., 2021) and coals with greater levels of As have been located in Southwestern China (Guo et al., 2017). Additionally high As, Ge, and U coals have been found in Shengli (Liu et al., 2021; Zhuang et al., 2006). This list of anomalies is not comprehensive (Dai et al., 2003, 2016; Tian et al., 2013; Yuzhuang et al., 2015).

Furthermore, some mineralogical enrichments have also been described for specific Chinese coals. In the Yueliangtian coal mining district, in Southwestern China, Wang et al. (2016) reported elevated concentrations of quartz in coal, due to precipitated siliceous solutions from the weathering of the Emeishan basalt. In northern China, Dai et al. (2010) reported high pyrite contents in #12 coal in the Songzao Coalfield, originating from a synsedimentary marine transgression over peat deposits and high Fe derived mainly from the mafic tuffs.

1.2. Coal geochemistry and mining occupational health

The high geochemical anomalies in coals in relation to some strategic elements such as Li, Ga or REEs, are very relevant from the point of view of their potential benefits (Qin et al., 2015; Zhang et al., 2015, 2020) but, in some cases, these might also be relevant from environmental and occupational points of view. Environmentally potentially hazardous elements can be directly emitted during coal use, extraction or transport of coal, the disposal of coal mining wastes and coal combustion by-products (Izquierdo and Querol, 2012).

High coal dust exposure levels is a matter of concern as may increase the occupational health risk (Landen et al., 2011; Liu et al., 2020; Masto et al., 2017; Zazouli et al., 2021) according to specific geochemical anomalies of coals (Fan and Xu, 2021; Liu and Liu, 2020; Moreno et al., 2019). There are several occupational diseases known to derive from coal handling, including lung diseases caused by excessive respirable crystalline silica (RCS). Intensive research has been carried out on the occupational health impacts of coal dust associated with coal workers' pneumoconiosis (CWP), silicosis and the possibility of pulmonary fibrosis (Mo et al., 2014; NIOSH, 2002). Specific studies concluded that "quartz is not the predominant factor in the development of CWP" (McCunney et al., 2009); and others have implicated transition metals, such as bioavailable Fe or Ni, as relevant contributors to the development of CWP (Christian et al., 1979; Harrington et al., 2012; Huang et al., 2002, 2005; McCunney et al., 2009).

Although, CWP is one of the most common disease in occupational coal mining, other pathologies can be linked to high levels of coal dust exposure (Ávila Júnior et al., 2009; Pedroso-Fidelis et al., 2020; Wilhelm Filho et al., 2010; Yu et al., 2020, among others). Nardi et al. (2018) indicated that inflammatory and oxidative stress parameters are potential early biomarkers for silicosis.

Frequent exposure to respirable pyrite particles in coal dust over time promotes a chronic level of inflammation, developing hydrogen peroxide and ferrous Fe, which produce highly reactive hydroxyl radicals, contributing to the pathogenesis of CWP (Cohn et al., 2006b; Harrington et al., 2012). Furthermore, several studies link pyrite contents in coal and coal dust with reactive oxygen species (ROS) generation, ROS in cells and a potential role in the pathogenesis of CWP (Castranova, 2000; Cohn et al., 2006a; Harrington et al., 2012; Huang and Finkelman, 2008; Liu and Liu, 2020; Moreno et al., 2019; Murphy and Strongin, 2009; Zosky et al., 2021).

In coal, sulphate can occur naturally or also through the oxidation of sulphide minerals during mining (Wang et al., 2017). Liu and Liu (2020) evidenced that sulphate nanoparticles exist in the mining environment, which can cause depression of pulmonary particle clearance and asthma due to the high biological activity.

There is considerable research on the production of ROS through increased concentrations of various metallic elements in dust, including Cu, V, Cr, Fe, Mn, Pt, Zn, Ni, Mo, Co, V and Pb (Cohn et al., 2006a; Fu et al., 2014; Huang et al., 2005; Latvala et al., 2016; Liu and Liu, 2020; Valko et al., 2005, among others). Moreover, Cr could be related to lung cancer in coal mine workers (WHO, 2000), and elevated exposure to Pb could be linked to the development of neurological toxins (Moreno et al., 2019). All in all, due to the widely different and heterogeneous compositions of coal, different diseases through exposure to coal mining and handling can potentially be developed by coal workers. Finkelman et al. (2002) gave an overview of possible health effects of coal and coal use.

Another risk associated with coal dust is its impact on ecological and environmental pollution, affecting communities in areas surrounding coal mining activities (Ishtiaq et al., 2018; Lashgari and Kecojevic, 2016; Masto et al., 2017; Tang et al., 2017). Moreover, high underground coal dust concentrations may lead to spontaneous combustion (Li et al., 2021; Liu et al., 2020; Ma et al., 2020; Querol et al., 2011; Shimura and Matsuo, 2019).

This study aims to evaluate the relationships between a variety of coal geochemical and mineralogical anomalies in a wide variety of mined Chinese coals with oxidative potential (OP), focusing on the respirable coal dust fraction (occupational exposure), by extracting and characterising the respirable fractions of the selected powdered coal samples. Respirable dust is the mass fraction of inhaled particles that are able to penetrate the respiratory tract and reach the non-ciliated, gas exchange, alveolar region of the lung. This fraction is attributed to

coal dust particles <4 μm mass median diameter (D_{50} = 4 μm) (Brown et al., 2013; European Committee for Standardization, 1992; Sánchez Jiménez et al., 2011).

To validate the method used, the analyses were repeated by including more results, namely those obtained by Trechera et al. (2020, 2021) on recently coal mine dust samples.

2. Methodology

2.1. Selection of coal samples: geological and geochemical settings

Twenty coal channel profile (CP) samples from six Chinese provinces were selected in this study (Fig. 1). These include fifteen underground coal mines, one open-pit coal mine and two coal exploration boreholes. Additionally, two Vietnamese coal samples (CP_21 and CP_22, not included in Fig. 1), were also selected. This selection was based on geochemically anomalous coals previously studied by the authors and sample availability. The reasons for sample selection and a brief description of their origin are summarised below:

- CP_01 and CP_02 were collected from underground coalfaces of the #11 and #5 coals, respectively, from the Sangshuping coal mine (Southeastern Shaanxi Province). These Late Carboniferous (Taiyuan Formation) coals have different geochemical patterns and coal rank (#11 is a low-volatile, LV, bituminous according to ASTM D388-12 and #5 coal a semi-anthracite). The first is a high organic S coal, with relatively low pyrite content, while the second is a low S and middle ash yield coal (J. Li et al., 2020).
- CP_03 was collected from underground coalfaces of the #5 coal from the Yongming coal mine (Northern Shaanxi Province). This is a Late Triassic (Wayaobao Formation) high-volatile (HV) bituminous coal. This is a high Sr coal (authors' unpublished data).
- CP_04 and CP_05 were collected from the high-Ge Wulantuga open-pit coal mine in the Shengli Coalfield, Northeastern Inner Mongolia. This #6 coal seam, Early Cretaceous Shengli Formation, reaches the sub-bituminous coal rank. These are coals with high Ge, As and W contents (Li et al., 2011).
- CP_06 and CP_07 were collected from #6 coal seam from the Junggur Coalfield, in the Buertaohai-Tianjiashipan coal mining district (Inner Mongolia) in two exploration boreholes (Borehole ZK43-25 and ZK17-15, respectively). This is a Late Carboniferous (Taiyuan Formation) HV bituminous coal. The first was selected for its high Pb content, and the second for the slight enrichment in Th (J. Li et al., 2016).
- CP_08 coal was collected from the underground working face of #4 coal from the Chunlei coal mine (Northeastern Guizhou) working Late Permian (Wujiaping Formation) medium-volatile (MV)

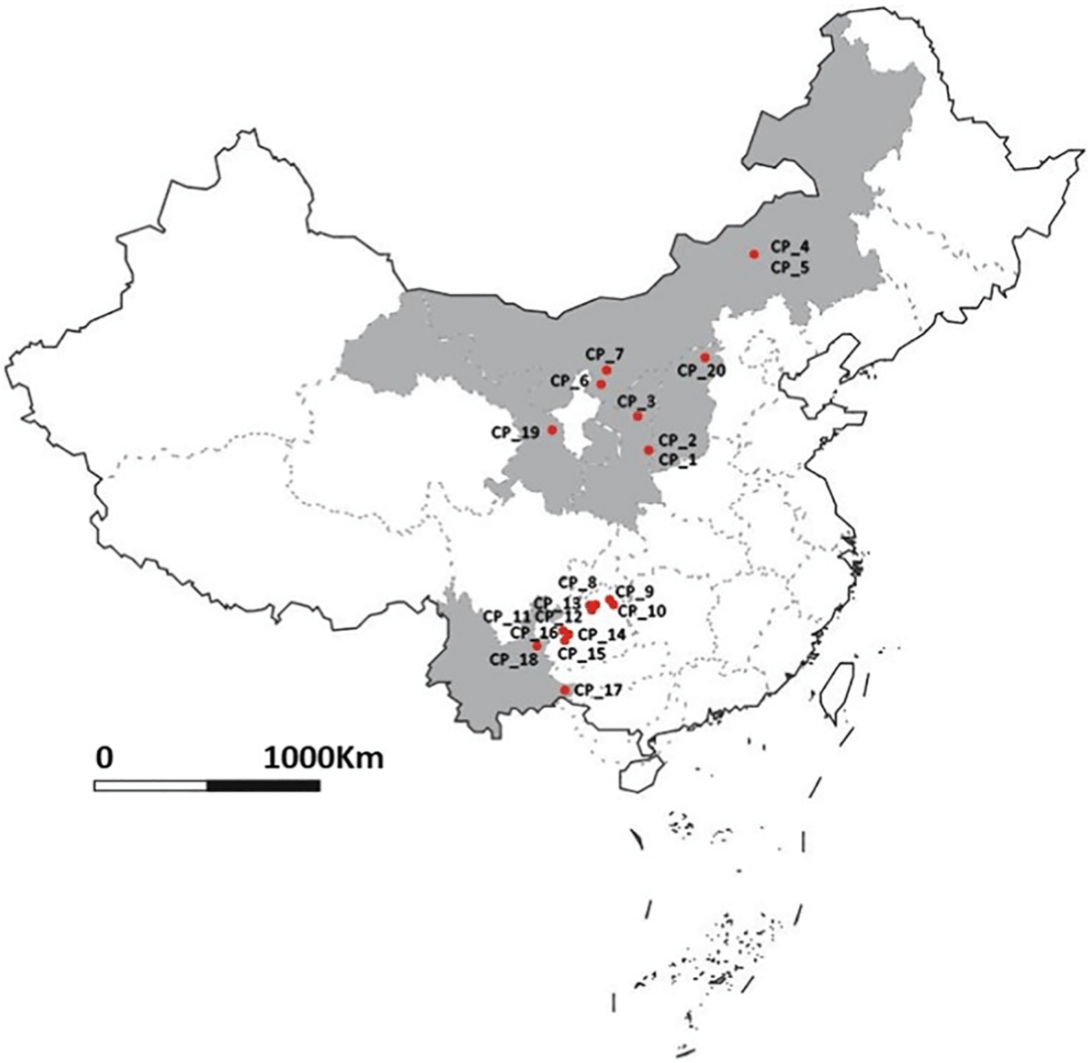

Fig. 1. Location of the 20 coal samples collected from different coal mines in China. Two Vietnamese coal samples, CP_21 and CP_22, not included in the figure.

bituminous coals. This coal has a high ash yield, pyrite and metals (Zn, Zr, REEs, Y, Nb, Pb, Cd, Ni, Cr, As, Se) (B. Li et al., 2019b).

- CP_09 and CP_10 were also obtained from the Late Permian (Wujiaping Formation) coals but, in this case, from the Jinqi and Yudai underground mines in the Qiandongbei Coalfield (Northeastern Guizhou), working MV and LV bituminous coals, respectively. Geochemically these are very different coals. The first is a high ash yield, pyrite and metals (V, Mo, Cr, U, As) coal, while the second is also a high pyrite coal but enriched in other metals (Pb, As, Se, Y, Nb, REEs) (B. Li et al., 2020).
- CP_11 and CP_12 were also collected from the Late Permian (Wujiaping Formation); in this case, from the underground working face of the LV bituminous C4 coal from the Chalinbao coal mine in the Tongzi Coalfield (Northeastern Guizhou). The first is a high Sr middle ash yield coal, and the second a high P and very high Sr coal (B. Li et al., 2019b).
- CP_13 was collected from C2 coal seam in Tiedingyan underground coal mine (Northeastern Guizhou), mining also Late Permian (Wujiaping Formation) LV bituminous coal. This is a very high Ti coal with moderate enrichments in Th, Y, Zr and REE (authors' unpublished data).
- CP_14 and CP_16 were obtained from the Late Permian (Longtan Formation) anthracite coals in the Fenghuangshan and Wenjiaba underground coal mines of the China Coalfield (Western Guizhou). The first is a middle ash yield and S coal enriched in Mo, V and U, and the second a middle ash yield coal enriched in Li (Li et al., 2017).
- CP_15 was obtained from the Late Permian (Longtan Formation) LV bituminous coal, worked in the Liulong underground mine of the Liuzhi coalfield (Guizhou Province). This is a High Sr and Mn coal (B. Li et al., 2016).
- CP_17 was collected from the Puyang underground coal mine (Southeastern Yunnan), working Tertiary (Xiaolongtan Formation) lignite. This is a high ash yield, moderately enriched in aluminium-silicate associated metals (Cr, Rb, Cu and Ni) (authors' unpublished data).
- CP_18 was collected from the Quqing underground coal mine (Eastern Yunnan), working Late Permian (Longtan Formation) HV bituminous coals. This is a high carbonate minerals coal enriched in Sr and Mn (authors' unpublished data).
- CP_19 was taken from the Wangjiashan underground coal mine (Central Gansu), working Jurassic (Yaojie Formation) HV bituminous coal. This is a low ash yield coal, moderately enriched in B (authors' unpublished data).
- CP_20 was obtained from the HV bituminous Early Permian coal worked (Shanxi Formation) in the Datong coal mine (Shaanxi province). This is a low ash yield and high Sr coal (authors' unpublished data).
- CP_21 and CP_22 were obtained from the Nui Houg Late Triassic coal mine, in Thai Nguyen Province of Vietnam. These coals are highly enriched in As, Mo, Sb, U and Tl (authors' unpublished data).

2.2. Sample treatment and analyses

In order to obtain a precise representation of the coal seam, the samples were collected using the CP approach, vertically across the coal seams, and stored in plastic bags to avoid oxidation. Samples were first analysed for bulk mineralogical and geochemical characterisation of the parent coal. Subsequently, a riffled fraction of the sample was milled using the same automatic agate mortar and time, and the resulting powdered coal sub-samples used to extract the respirable fraction (<4 μm, CP_4). Afterwards, a complete particle size distribution (PSD), mineralogical and geochemical characterisation was obtained from each CP_4. In parallel, OP analyses were also performed for each CP_4 with the aim of evaluating links between geochemical patterns and ROS. Finally, this link was evaluated again including data from recently coal mine dust collected (Trechera et al., 2020, 2021). This was performed in order to validate the results obtained using the laboratory protocol explained in this study to obtain samples representing respirable coal dust from powdered coal samples.

2.2.1. Sample pre-treatment

In order to separate the respirable fraction of coal powder samples, a special chamber resuspension device was used, due to the small amount of powdered sample available. Furthermore, the efficiency of technique was tested before analysis, using different coal ranks, changing the filter collector and optimising the best flow-rates.

A total of twenty-two coal samples (twelve bituminous, five semi-anthracites, three sub-bituminous/lignite and two anthracite) were analysed. First, 5.0 g of each sample were milled with a Mortar Agatha Grinder RM 200 in an automatic mode for exactly 2 min. Second, using a mobile chamber resuspension device separator, the CP_4 fraction was obtained from a riffled sub-sample of each powdered coal using a laboratory particulate matter (PM), PM_{10}-$PM_{2.5}$ powdered dust sampler (Moreno et al., 2008). Briefly, the coal powder was spread onto a glass tray surface and, with the corresponding vacuum (30 $L \cdot min^{-1}$ of airflow), the sample was suctioned into a methacrylate chamber. The sample was advanced through a <4 μm inlet and finally the CP_4 sample was deposited on the surface of a polycarbonate filter with 47 mm diameter and 0.6 size porosity. The size cut off depends on the flow, therefore experiments were carried out to find the optimal flow for <4 μm. The sample deposited into a methacrylate chamber was recollected, spread onto a glass tray surface again and repeated the CP_4 separation procedure. Finally, the sample collected, around 300–400 mg, on the filter surface was brushed prudently and ready for the subsequent analysis.

2.2.2. Dry particle size distribution

With the aim to confirm that the respirable fraction was separated from the powdered CP sample, Malvern Scirocco 2000 analyses were performed for each CP_4 sample.

A Malvern Mastersizer, coupled to a Scirocco 2000 extension, was used to analyse the dry PSD and confirm that the median particle diameter (D_{50}) of each CP_4 was close to 4 μm as required to be 'respirable'. Furthermore, for each CP_4 sample D_{10}, D_{25} and D_{75} values were obtained for evaluating the potential links between PSD and OP for CP_4 samples.

2.2.3. Mineralogical analysis

In order to analyse the mineralogical characterisation of parent bulk coal and the respective CP_4 samples, a powder X-ray diffraction (XRD) was used with A Bruker D8 Advance A25, θ-θ diffractometer with CuKα1 radiation, Bragg-Brentano geometry, and a position-sensitive Lynx Eye detector. Diffractograms at 40 kV and 40 mA, scanning from 4 to 60° of 2 θ with a step size of 0.019° and a counting time of 0.10 $s \cdot step^{-1}$ maintaining the sample in rotation (15 min) were performed. The crystalline phase identification was conducted using the EVA software package (Bruker), which utilised the ICDD (International Centre for Diffraction Data) database. Semi-quantitative XRD analysis was performed using the method devised by Chung (1974) for the quantitative analysis of multi-component systems, using quartz as an internal reference. Chung's method was used on mixtures, which were obtained from powdered mineral reference materials and coal with low ash to validate the semi-quantitative protocol, shown in Fig. S1.

2.2.4. Proximate, ultimate and chemical analyses

In order to evaluate the composition of CP and CP_4 several geochemical analyses were performed. Proximate and ultimate analyses followed ISO and ASTM procedures (ISO-589, 1981, ISO-1171, 1976, ISO-562, 1974, ASTM D-3286, D-3302M, D3174-12), with moisture and ash yield obtained at 150 °C and 750 °C, respectively.

Before major and trace element analyses, 0.10 g of samples of the parent coal and CP_4 samples were digested in HF-HNO_3-$HClO_4$ acid following the method by Querol et al. (1992, 1997) to retain potentially volatile elements, such as As and Se. The resulting acidic digestions were analysed for major and trace elements by using inductively-coupled plasma atomic-emission spectrometry (ICP-AES, Iris Advantage Radial ER/S device from Thermo Jarrell-Ash) and inductively-coupled plasma mass spectrometry (ICP-MS, X-SERIES II Thermo Fisher

Scientific, Bremen, Germany). International reference materials SARM19 and NIST SRM 1633b, and blanks were treated in the same way.

Using the same analytical approaches and type for coal and coal mine dust samples (Trechera et al., 2020, 2021), adding two more repetitions, elements analysed reported the analytical errors shown in Table S1.

Because Si is lost during HF digestion, its contents in coal samples and CP_4 were determined by X-ray fluorescence (XRF, Thermo Scientific ARL QUANT'X Energy-Dispersive X-ray fluorescence spectrometer) loading Teflon© 47 mm filters with 3.0 mg of the sample using an ethanol suspension. This method was validated using the above reference materials.

2.2.5. Oxidative potential

In order to evaluate the links between geochemical patterns of CP_4 and oxidative stress, an OP test was performed for each sample. OP is an indicator of the capacity to generate ROS in human bodies that may result in oxidative stress. Several studies have linked respiratory disorders and lung diseases to the ROS formation in cells (Imai et al., 2008; Kelly, 2003; Kim et al., 2018; Pietrogrande et al., 2021; Rahman and Adcock, 2006). In addition, oxidative stress plays a key role in understanding how atmospheric suspended PM affects health through respiratory inflammation, lung cancer, and chronic cardiopulmonary diseases, among others (Fang et al., 2019; Janssen et al., 2014; Kelly, 2003; Leni et al., 2020; MacNee, 2001; Y.J. Zhang et al., 2021).

The oxidative stress of the CP_4 samples was evaluated via the OP method in two different laboratories. Firstly, OP method was performed in King's College of London, which is based on the consumption of ascorbic acid (AA), urate (UA) and glutathione (GSH) antioxidants, as described in detail by Soltani et al. (2018). The OP analysis involves the resuspension of each CP_4 sample in ethanol and a 4 h incubation with a synthetic solution containing equi-molar concentrations of antioxidants. The consumption of these antioxidants is determined following the methodology by Baker et al. (1990) and Iriyama et al. (1984). In-house controls of PM-free, negative PM (M120, Cabot Corporation, USA) and positive PM (NIST1648a, urban particulate from NIST, USA) followed the same protocol for control purposes.

Secondly, OP analyses were also carried out in Grenoble Alpes University, this time based on the consumption of dithiothreitol (DTT) antioxidants, as described in detail by Calas et al. (2018). For each sample, 40 μL of PM suspension (in triplicate) with 205 μL of phosphate buffer (pH = 7.4) were incubated at 37 °C in 12.5 nmol of DTT (DTT solution in phosphate buffer). Reaction was stopped at 0, 15 and 30 min adding 50 nmol of 5,5′-dithiobis (2-nitrobenzoic acid) (DTNB in phosphate buffer). A solution of 40 μL of 1,4 naphtoquinone (1,4-NQ 24.7 μM) was used as positive control. DTT consumption by formation of DTT-disulfide form in presence of ROS (Yang et al., 2014) was measured at 412 nm using a plate-reader TECAN spectrophotometer Infinite® M 200 pro and 96 well CELLSTAR® plates. OP was obtained from the slope of the linear regression of the consumed DTT (corrected from blank measurements and from matrix absorbance from particles) normalized by the PM_{10} mass (nmol DTT min^{-1} μg^{-1}).

The OP of the CP_4 samples was expressed as the percentage of consumption of each antioxidant with reference to the in-house, particle-free control. To obtain a metric for the OP, the data were expressed as OP per μg ($OP^{AA}\mu g^{-1}$, $OP^{GSH}\mu g^{-1}$, $OP^{DTT}\mu g^{-1}$). Since AA and GSH were mixed in the same assay, individual antioxidant depletions were also combined to provide a total OP value (OP^{TOTAL}(OP^{AA+GSH}) μg^{-1}).

2.2.6. Data analysis

Data obtained from the PSD, mineralogical and geochemical characterisations were evaluated for correlation with OP patterns by using the software StataCorp LLC (College Station, Texas, USA) version Stata/SE 15.1.

2.3. Limitations of the methodology used

The present study was carried out through the selection of coal samples (CP), milling the samples and obtaining the respirable fraction (<4 μm) of each CP sample (CP_4). In addition, the subsequent evaluation took place under similar conditions (atmospheric particulate matter finer than 4 μm, PM_4) present in the coal mine from where the CP sample was collected. The conditions could not be fully replicated because, in the coal mine, sources of PM include not only the dust from the worked coal seam, but also from the other sediments where coal is interlayered, wear of machinery, salts and other components from precipitates of acidic mine drainage, among others (Trechera et al., 2020).

Furthermore, when working the coal seam, coal can be powdered in a very different way to a laboratory mill, with some coal components being enriched or depleted in the respirable fractions. However, collecting respirable dust samples in the numerous Chinese mines included in this study, would have required considerably more time and increased costs. Furthermore, the objective of this study is to analyse the geochemical patterns of coal that might enrich a given coal dust in specific elements and minerals and to evaluate the effect of these enrichments on OP of dust. Thus, it was considered that, in spite of the above limitations, this method is useful for the aims of this study.

To support this, at the end of the manuscript the results of the joint evaluation of OP and geochemical patterns for a compiled set of true respirable dust obtained from deposited coal mines, together with the 22 CP_4 samples is presented. If associations of elements, minerals and coal patterns with OP remain unchanged with respect to the single analysis of the CP_4 sets, this will support the applicability of the method.

3. Results and discussion

3.1. Mineralogy and geochemistry

Results from proximate and ultimate analyses of the coal samples are shown in Table 1, while Tables 2 and 3 illustrate mineral and elemental concentrations from all parent coal samples analysed in this study. Tables 4 and 5, following, show the same data for CP_4 samples.

3.1.1. Parent coals

Tables 1 and 2 show that samples CP_08, CP_09 and CP_17 (bituminous the first two and lignite the last) have a high mineral matter content, with ash yields of 32, 34, and 34% dry basis (db), respectively. Sample CP_17 contains a high quartz content (15% weight, % wt), and CP_08, CP_14 and CP_09 are high pyrite coals (6, 5 and 14% wt, respectively). Furthermore, CP_08 has a high carbonate minerals content (3 and 11% wt, ankerite and calcite, respectively,) as does CP_18 (1 and 12% wt, ankerite and calcite); while CP_09 and CP_10 contain a relatively high sulphate minerals content (4–5% wt), CP_21 high tobelite (13% wt, an illitic clay with NH_4^+ replacing K^+).

The major and trace element contents of the bulk CP parent coals were compared with their respective Chinese average concentrations, Table S2 (Dai et al., 2007, 2008) to evidence specific geochemical enrichments. The most relevant geochemical enrichments for each sample are summarised in Table 6, in comparison with Chinese geochemical averaged concentrations.

3.1.2. Geochemistry of the <4 μm fraction of the powdered coals

Fig. S2 and Table S3 show the PSD of CP_4 samples, with the percentiles of the diameter, and evidence the efficiency of the separation technique and procedure conducted during the analysis, because D_{50} of CP_4 are in all classes remarkably close to 4.0 μm.

Fig. 2 shows the average ratios of the mineral contents between the CP_4 samples and the respective bulk powdered parent coal (CP_4/CP). As expected, high similarities between CP_4 and CP mineralogy were found, with average ratios close to 1. However, several exceptions were detected, such as sulphate minerals, slightly depleted in CP_4 (ratios close

Table 1
Details of the origin of all coal channel profiles (CP) collected in mines across China for this study and data from proximate analysis. M, Moisture; ad, air dry; db, dry basis; VM, Volatile Matter; LV, Low-Volatile; HV, High-Volatile; MV, Medium-Volatile.

Sample	M (%ad)	Ash (%db)	VM (%)	Rank	Sampling location	Province	Geological age
CP_01	0.25	9.36	15.40	LV bituminous	Sangshuping Coal mine	Shaanxi Province, Southeastern China	Late Carboniferous, Taiyuan Formation
CP_02	0.19	7.97	13.70	Semi-anthracite	Sangshuping Coal mine	Shaanxi Province, Shoutheastern China	Late Carboniferous, Taiyuan Formation
CP_03	1.20	21.31	41.50	HV bituminous	Yongming Coal mine	Shaanxi Province, northwest China	Late Triassic, Wayaobao Formation
CP_04	8.31	7.51	51.20	Sub-bituminous	Wulantuga Coal mine	Inner Mongolia, northeastern China	Early Cretaceous, Shengli Formation
CP_05	9.73	9.39	46.12	Sub-bituminous	Wulantuga Coal mine	Inner Mongolia, northeastern China	Early Cretaceous, Shengli Formation
CP_06	2.51	16.74	36.80	HV bituminous	Junggur Coalfield Borehole	Inner Mongolia, northeastern China	Late Carboniferous, Taiyuan Formation
CP_07	4.16	16.05	37.50	HV bituminous	Junggur Coalfield Borehole	Inner Mongolia, northeastern China	Late Carboniferous, Taiyuan Formation
CP_08	0.99	32.33	26.84	MV bituminous	Chunlei Coal mine	Northeastern Guizhou Province, southwest China	Late Permian, Wujiaping Formation
CP_09	1.79	34.41	33.64	MV bituminous	Jinqi Coal mine	Northeastern Guizhou Province, southwest China	Late Permian, Wujiaping Formation
CP_10	2.95	22.48	21.46	LV bituminous	Yudai Coal mine	Northeastern Guizhou Province, southwest China	Late Permian, Wujiaping Formation
CP_11	0.49	10.81	13.80	Semi-anthracite	Chalinbao Coal mine	Northeastern Guizhou Province, southwest China	Late Permian, Wujiaping Formation
CP_12	0.49	17.28	14.65	Semi-anthracite	Chalinbao Coal mine	Northeastern Guizhou Province, southwest China	Late Permian, Wujiaping Formation
CP_13	0.49	22.98	20.99	LV bituminous	Tiedingyan Coal mine	Northeastern Guizhou Province, southwest China	Late Permian, Wujiaping Formation
CP_14	1.59	14.81	7.87	Anthracite	Fenghuangshan Coal mine	Western Guizhou Province, southwest China	Late Permian, Longtan Formation
CP_15	0.91	18.39	20.11	LV bituminous	Liulong Coal mine	Western Guizhou Province, southwest China	Late Permian, Longtan Formation
CP_16	1.29	10.65	7.45	Anthracite	Wenjiaba Coal mine	Western Guizhou Province, southwest China	Late Permian, Longtan Formation
CP_17	7.05	34.25	60.70	Lignite	Puyang Coal mine	Southeastern Yunnan Province, southwest China	Tertiary, Xiaolongtan Formation
CP_18	2.00	14.09	39.30	HV bituminous	Quqing Coal mine	Eastern Yunnan Province, southwest China	Late Permian, Longtan Formation
CP_19	7.47	2.76	37.90	HV bituminous	Wangjiashan Coal mine	Gansu Province, northwest China	Jurassic, Yaojie Formation
CP_20	8.28	4.51	39.40	HV bituminous	Datong Coal mine	Shaanxi Province, north China	Early Permian, Shanxi Formation
CP_21	1.06	20.17	8.19	Semi-anthracite	Nui Houg Coal mine	Thai Nguyen Province, Vietnam	Late Triassic
CP_22	1.55	11.70	8.75	Semi-anthracite	Nui Houg Coal mine	Thai Nguyen Province, Vietnam	Late Triassic

to 0.8, melanterite mineral being almost completely absent in CP_4 fractions), and anatase, with a marked increase in CP_4 (×2.7) in most samples. Sulphate minerals in coal and coal dust occur usually in large crystals, commonly much larger than the respirable particle size, while anatase occurs generally as exceptionally fine crystal aggregates dispersed in both the organic and clay matrixes (Figs. 4 and S4 of Trechera et al. (2020, 2021), respectively).

Sulphate CP_4/CP ratios are positively correlated ($r = 0.74$) with moisture (% air dried, ad). Moisture potentially accelerates the process of oxidation of sulphides in coals (Allardice et al., 2003; Choi et al., 2011; Wang et al., 2003), which usually have a relatively fine PSD. Moreover, the adsorption of moisture can soften and lubricate the microstructures, weakening mechanical coal matrix properties (Ahamed et al., 2019; Ren et al., 2021). The highest CP_4/CP for sulphate minerals is obtained for sub-bituminous coals, probably induced by a higher moisture content, which causes more intense oxidation. On the other hand, carbonate minerals (especially calcite), ratios are correlated with the volatile matter (% dry ash free, daf), thus increasing towards low rank coals ($r = 0.74$ and 0.90 respectively) pointing to a finer size of calcite in lower coal rank coals. In fact, the ratios followed this trend HV > MV > LV (from 1.7 to 0.2) in bituminous coal. This is probably due to the recrystallisation processes, which are more probable in higher rank coals.

Average CP_4/CP for major elements (Fig. 2) reach 0.7 and 0.8 for Fe and S; while the P, Al and Na averaged ratios reach 1.2, 1.3 and 1.5, respectively. No correlations were observed between CP_4/CP of major elements and coal rank when including all coals, but $r = 0.87$ and -0.70 are reached for Fe and K ratios and moisture when only bituminous coals are evaluated. Thus, and accordingly, volatile matter is marginally correlated with Fe ratios ($r = 0.70$) and noticeable negatively correlated with K ($r = -0.74$).

Furthermore, ash yields are negatively correlated with Fe ($r = -0.80$) and S ($r = -0.81$), ratios pointing that high ash yield coals contain coarser pyrite than low ash ones. In fact, ash yield is correlated with pyrite contents in bituminous samples ($r = 0.80$ for CP and $r = 0.71$ CP_4). Thus, higher pyrite coal might contain coarser pyrite. In contrast, in low pyrite coals, fine framboidal pyrite is the prevailing form of this mineral. Thus, the highest ratios are obtained for samples with pyrite content below the XRD detection limit (CP_4_19 and CP_4_20). In prior studies on Chinese and European bituminous coals, the concentrations of Fe and S also decreased in the respirable coal dust fraction compared with the parent bulk coal dust (Trechera et al., 2020, 2021).

Concerning the CP_4/CP ratios of trace elements, those for Mo, Mn, Hf and Ge are generally <1.0, ($n = 10, 21, 13, 18$, respectively), with only six samples with ratios slightly >1.0 (four in the case of Mn and two in the one of Ge). These results concur with those of Trechera et al. (2020, 2021), especially as far as Mn is concerned. On the other hand, elements such as Cs, W, Zn and Zr increase their concentration in CP_4. Usually Hf and Zr are associated with zircon (Zr-silicate) in coal (Swaine, 1990); however, in this study, it seems that Hf is particularly concentrated in the coarser zircon. Mo and Ge are usually associated with organic matter (yielding coarser particles), while Mn is usually associated with carbonate minerals (Swaine, 1990).

3.2. Oxidative potential

3.2.1. Oxidative potential of the <4 μm fraction of the powdered coal samples (CP_4)

The OP test is defined as a measure of the capacity of PM to oxidise target molecules. The outputs of the OP are used as a predictor of biological responses to PM toxicity and might yield more information on the potential health effects than PM mass or chemistry (Ayres et al., 2008; Borm et al., 2007; Daellenbach et al., 2020). Although the OP analyses are not commonly used yet to characterise standard responses of coal dust, it could be a valuable technique to evaluate potential occupational hazards, since it integrates various biologically-relevant dust properties, including size, surface and mineralogical and chemical composition (Ayres et al., 2008; Janssen et al., 2014). Several methods for measuring OP are available, and agreement has not been reached on recommending one of them (Ayres et al., 2008; Calas et al., 2018; Moreno et al., 2017). Different tests monitor specific oxidative processes caused by particular PM or dust component types. Commonly, OP^{AA}, OP^{GSH}, and OP^{DTT} assays are used for PM exposure, based on the facts that AA and GSH are physiological antioxidants present in the lung and DTT is a strong reducing agent, chemical surrogates of antioxidants (Fang et al., 2017).

In these samples, OP^{TOT} average values reached 1.16 (0.4–2.0) $\%OP^{TOT}\mu g^{-1}$ ($OP^{TOT} = OP^{AA} + OP^{GSH}$, in % consumption·$\mu g^{-1}$) (Table 7). These OP values fall in the range reported for a number of Chinese actual

Table 2
Mineral contents (% wt) of the bulk coal channel profile samples (CP). Qtz, Quartz; Ant, Anatase; Cb, Carbonates; Py, Pyrite; Sul, Sulphates; Ill-Ms, Illite-Muscovite; Mm, Montmorillonite; Kln-Clc, Kaolinite-Clinochlore; Tob, Tobelite; Ank, Ankerite; Cal, Calcite; Dol, Dolomite; Sid, Siderite; Gy, Gypsum; Jar, Jarosite; Szo, Szomolnokite; Roz, Rozenite; Mel, Melanterite.

Sample	CP_01	CP_02	CP_03	CP_04	CP_05	CP_06	CP_07	CP_08	CP_09	CP_10	CP_11	CP_12	CP_13	CP_14	CP_15	CP_16	CP_17	CP_18	CP_19	CP_20	CP_21	CP_22
Clays	4.4	4.5	12.2	<dl	3.9	14.9	13.2	10.7	13.0	11.2	9.2	12.9	13.1	5.4	<dl	9.3	17.3	0.4	1.1	<dl	13.0	8.0
Qtz	<dl	<dl	5.1	3.6	3.8	<dl	1.2	0.6	2.8	0.7	<dl	<dl	<dl	2.3	4.7	<dl	15.4	<dl	0.3	4.5	4.9	3.0
Ant	<dl	<dl	<dl	<dl	<dl	<dl	<dl	<dl	<dl	<dl	<dl	<dl	<dl	0.7	0.6	0.5	<dl	<dl	<dl	<dl	0.3	0.2
Cb	4.1	3.4	3.6	<dl	<dl	0.4	1.5	14.5	<dl	<dl	<dl	0.4	9.6	<dl	6.2	<dl	<dl	13.5	1.3	<dl	<dl	<dl
Py	0.6	0.1	0.3	2.7	0.9	0.6	<dl	5.6	14.1	4.1	1.7	3.5	0.3	5.3	4.7	0.9	1.6	0.1	<dl	<dl	2.0	0.6
Sul	0.2	<dl	<dl	1.2	0.7	0.9	<dl	0.9	4.5	6.4	<dl	0.4	<dl	1.1	2.2	<dl	<dl	<dl	<dl	<dl	<dl	<dl
Ill-Ms	<dl	<dl	<dl	<dl	<dl	<dl	<dl	<dl	<dl	<dl	<dl	<dl	<dl	<dl	<dl	1.2	3.8	<dl	<dl	<dl	<dl	<dl
Mm	<dl	<dl	<dl	<dl	<dl	<dl	<dl	<dl	<dl	<dl	<dl	<dl	<dl	2.5	<dl	<dl	<dl	<dl	<dl	<dl	<dl	<dl
Kln-Clc	1.9	2.9	12.2	<dl	3.9	14.9	13.2	10.7	13.0	11.2	2.4	2.4	13.1	<dl	<dl	8.2	13.5	0.4	1.1	<dl	<dl	<dl
Tob	2.5	1.6	<dl	<dl	<dl	<dl	<dl	<dl	<dl	<dl	6.8	10.5	<dl	2.9	<dl	<dl	<dl	<dl	<dl	<dl	13.0	8.0
Ank	<dl	0.2	0.5	<dl	<dl	<dl	<dl	3.4	<dl	<dl	<dl	<dl	<dl	<dl	<dl	<dl	<dl	1.3	<dl	<dl	<dl	<dl
Cal	4.1	3.2	2.7	<dl	<dl	<dl	1.5	10.7	<dl	<dl	<dl	<dl	9.5	<dl	6.2	<dl	<dl	11.9	1.3	<dl	<dl	<dl
Dol	<dl	<dl	<dl	<dl	<dl	<dl	<dl	<dl	<dl	<dl	<dl	<dl	0.1	<dl	<dl	<dl	<dl	<dl	<dl	<dl	<dl	<dl
Sid	<dl	<dl	0.4	<dl	<dl	0.4	<dl	0.4	<dl	<dl	<dl	0.4	<dl	<dl	<dl	<dl	<dl	0.3	<dl	<dl	<dl	<dl
Gy	0.2	<dl	<dl	1.2	0.7	<dl	<dl	0.5	<dl	0.4	<dl	<dl	<dl	<dl	<dl	<dl	<dl	<dl	<dl	<dl	<dl	<dl
Jar	<dl	<dl	<dl	<dl	<dl	<dl	<dl	<dl	<dl	<dl	<dl	0.4	<dl	<dl	<dl	<dl	<dl	<dl	<dl	<dl	<dl	<dl
Szo	<dl	<dl	<dl	<dl	<dl	<dl	<dl	<dl	2.7	1.2	<dl	<dl	<dl	<dl	2.2	<dl	<dl	<dl	<dl	<dl	<dl	<dl
Roz	<dl	<dl	<dl	<dl	<dl	<dl	<dl	<dl	1.8	2.8	<dl	<dl	<dl	1.1	<dl	<dl	<dl	<dl	<dl	<dl	<dl	<dl
Mel	<dl	<dl	<dl	<dl	<dl	0.9	<dl	0.5	<dl	2.1	<dl	<dl	<dl	<dl	<dl	<dl	<dl	<dl	<dl	<dl	<dl	<dl

respirable coal mine dust samples by Trechera et al. (2020, 2021), with 0.3–0.8%$OP^{TOT}\cdot\mu g^{-1}$ for coal open-pit mine dust from the Xingjian's high-quality coal, and 0.1–2.2%$OP^{TOT}\cdot\mu g^{-1}$ for similar samples from underground coal mines (working lower coal quality in Southern and Southwestern China). Moreover, some OP analysis from PM_4 by Zazouli et al. (2021) in Alborz Coal Basin underground coal mines show also low levels of OP^{TOT} (0.4–1.0%$OP^{TOT}\cdot\mu g^{-1}$ of PM_4). In accordance with Zazouli et al. (2021), which also collect their samples in eight different locations of underground coal mines, OP^{TOT} average reached 0.7%$OP^{TOT}\cdot\mu g^{-1}$ of PM_4 in their OP analyses, a value close to the averages of this study, open-pit coal mine study (Trechera et al., 2021), and underground coal mines study (Trechera et al., 2020), reaching 1.2, 0.5 and 0.8%$OP^{TOT}\cdot\mu g^{-1}$, respectively. Thus, the results are quite similar, even when the OP from Zazouli et al. (2021) was measured on true respirable coal dust in suspension (PM_4), the ones from Trechera et al. (2020 and 2021) were obtained in respirable fractions extracted from deposited coal dust, and the ones from this study are CP_4 samples.

All the above values can be considered as relatively low when compared with those reported for other PM types. Thus, Moreno et al. (2017) reported 2.5%$OP^{TOT}\cdot\mu g^{-1}$ as average values from $PM_{2.5}$ samples collected in the Barcelona subway system. Calas et al. (2018) reported 1.5 and 4.0%$OP^{TOT}\cdot\mu g^{-1}$, respectively, for PM from the Chamonix Valley in summer and winter (the latter with high PM contributions from biomass burning). Godri et al. (2011) and Soltani et al. (2018) reported 1.1 and 3.6%$OP^{TOT}\cdot\mu g^{-1}$ at the Iranian Gol-E-Gohar mining and industrial facility and London Roadside PM control, respectively. It is also very relevant that ROS levels measured for coal mine dust by means of OP tests are somewhat reduced when compared with atmospheric PM from most anthropogenic sources (Trechera et al., 2020, 2021).

When evaluating correlations of the particle size, geochemical and mineralogical patterns of the 22 CP_4 samples with OP^{AA} (Fig. 3), a positively correlation ($r = 0.69$) with Fe, and with anatase, S, pyrite, U, Mo, V and Ti ($r = 0.5–0.6$) was found, as well as with Ni, Cu, Pb, ash yield, Al and Si ($r = 0.4–0.5$). On the other hand, OP^{GSH} was correlated with moisture (% ad, $r = 0.67$), and with H (%), volatile matter (% daf) and quartz ($r = 0.4–0.5$). Furthermore, OP^{DTT} was correlated with moisture, B, Ge, As and W ($r = 0.5–0.6$) and less correlated with particle size, volatile matter, and Ca ($r = 0.4–0.5$), Fig. 3.

Fig. 4 shows the cross-correlation analysis for CP_4 from bituminous coals (twelve out of the twenty-two samples analysed). OP^{AA} correlation increased slightly for Fe ($r = 0.80$), ash yield ($r = 0.72$) and pyrite ($r = 0.70$), as well as with sulphates, As, K, S, Si, Al, V, and Cr ($r = 0.5–0.6$) and Pb, Cu, Ti, U, and Ni ($r = 0.4–0.5$). For OP^{GSH} the correlation with moisture again markedly increased ($r = 0.78$), as did that with H, particle size, Sb, Bi, Tl, volatile matter, B, Ge and C ($r = 0.3–0.5$). For OP^{DTT}, correlations also increased for particle size, Ca, Sr, and B ($r = 0.6–0.7$), and for Mg, Mn, and quartz ($r = 0.4–0.5$). However, the correlation with Ge, W, As, Be, moisture content and volatile matter were decreased (the two latter being low in bituminous coal).

Accordingly, both OP^{GSH} and OP^{DTT} seem to correlate with the organic matter content (traced by moisture, H, volatile matter and by some typically organic associated trace elements, such as B, Mo, W and Ge (Swaine, 1990), and coarser particle size). In contrast, Figs. 3 and 4 clearly illustrate the mineral components (inorganic fraction) are linked to OP^{AA} (conversely to OP^{GSH} and OP^{DTT}), especially pyrite, Fe, S, sulphate minerals (arising from pyrite oxidation), anatase, and a number of trace metals (U, Mo, V). Most of these correlations increase when considering only bituminous coals, since the regression scatter caused by the possible impact of coal rank-dependent parameters is reduced. Attfield and Morring (1992), Castranova and Vallyathan (2000), Huang et al. (2005), Maclaren et al. (1989) and Huang et al. (1998) have showed that coal rank plays an important role in developing coal miners' diseases, with CWP risk increasing with rank.

Table 3
Contents of major and trace elements in the bulk coal channel profile samples (CP). wt, weight.

Sample	CP_01	CP_02	CP_03	CP_04	CP_05	CP_06	CP_07	CP_08	CP_09	CP_10	CP_11	CP_12	CP_13	CP_14	CP_15	CP_16	CP_17	CP_18	CP_19	CP_20	CP_21	CP_22
% wt																						
Al	1.16	1.19	2.78	0.32	0.57	2.96	2.91	3.37	3.82	2.60	2.02	2.99	4.33	1.85	0.87	1.98	4.55	0.06	0.18	0.09	2.85	1.50
Ca	1.31	0.91	0.97	0.63	0.57	0.16	0.53	2.91	0.07	0.16	0.09	0.53	0.75	0.03	1.87	0.05	0.78	6.40	0.38	1.35	0.42	0.39
Fe	0.52	0.11	0.99	1.41	0.94	1.69	0.27	4.59	8.04	6.10	0.99	1.43	0.54	2.27	3.60	1.01	0.89	1.48	0.09	0.13	2.05	0.59
K	0.09	0.04	0.24	0.02	0.05	0.03	0.14	0.17	0.40	0.12	0.11	0.07	0.14	0.37	0.18	0.10	0.87	<0.01	<0.01	<0.01	0.17	0.06
Mg	0.02	0.05	0.17	0.13	0.14	0.02	0.03	0.39	0.12	0.05	0.04	0.03	0.10	0.05	0.09	0.06	0.34	0.31	0.07	0.18	0.12	0.03
Na	0.01	0.02	0.10	0.03	0.03	0.02	0.02	0.02	0.02	0.01	0.03	0.04	0.01	0.14	0.02	0.14	0.01	0.01	0.17	0.06	0.01	0.01
P	<0.01	0.05	0.02	<0.01	<0.01	<0.01	0.02	0.02	0.01	0.02	0.02	0.40	0.01	<0.01	<0.01	0.01	0.01	<0.01	<0.01	<0.01	0.12	0.08
S	4.87	0.36	0.63	1.72	1.21	1.61	0.55	4.93	10.11	7.10	2.66	3.08	1.80	2.90	4.22	1.14	1.38	0.24	0.11	0.11	5.51	3.37
$mg \cdot kg^{-1}$																						
Li	68	33	16	2.9	4.2	25	35	70	52	46	44	36	70	31	9.0	162	31	0.97	<dl	<dl	12	3.4
Be	1.4	<dl	1.0	17	11	6.0	2.1	6.3	3.6	16	4.1	5.6	17	2.5	1.5	0.81	2.0	<dl	<dl	2.4	0.89	0.20
B	4.1	24	<dl	51	65	1.9	12	14	27	<dl	34	16	<dl	3.5	<dl	<dl	<dl	32	126	52	43	6.3
Sc	1.6	1.1	3.5	1.0	0.90	5.0	6.2	26	5.4	6.2	2.7	1.8	15	3.3	2.5	3.4	8.2	<dl	<dl	<dl	3.2	<dl
Ti	328	371	986	156	358	1045	1807	1709	2589	2027	786	483	2791	1835	558	661	1625	14	48	45	1111	718
V	7.5	6.6	18	4.5	7.1	15	35	53	268	65	15	21	94	199	65	20	93	<dl	0.94	<dl	116	51
Cr	4.4	4.1	11	2.9	4.6	5.4	9.9	51	79	25	9.9	14	41	46	7.9	8.8	61	<dl	0.96	0.52	30	12
Mn	19	23	148	49	48	97	29	82	154	13	10	27	8.6	8.4	235	4.1	11	721	12	18	36	6.1
Co	1.6	2.5	4.4	0.92	1.0	8.3	2.8	9.0	10	12	3.3	14	6.6	7.1	6.4	5.4	6.6	<dl	1.5	8.7	2.7	<dl
Ni	2.2	7.4	11	2.5	2.2	13	4.3	69	33	16	8.2	16	36	22	12	11	32	0.56	4.3	5.1	22	20
Cu	4.5	6.8	16	3.0	4.5	16	17	55	22	39	13	24	52	54	30	21	43	<dl	0.64	1.2	20	19
Zn	8.9	22	21	6.9	13	24	26	2446	24	14	57	28	14	17	2.5	9.6	19	<dl	<dl	<dl	48	35
Ga	5.0	3.9	9.2	1.7	1.8	10	16	51	14	36	10	13	52	8.8	3.8	7.6	12	<dl	<dl	2.2	7.9	5.1
Ge	3.2	1.1	2.1	577	436	3.2	2.0	11	3.9	15	5.8	18	17	1.6	0.79	1.0	2.6	<dl	<dl	3.7	22	4.4
As	1.6	1.1	3.1	484	436	9.8	2.9	36	29	36	4.0	6.6	8.5	3.0	5.7	1.6	8.4	<dl	<dl	1.3	225	65
Se	0.64	1.2	1.8	<dl	<dl	2.2	2.5	21	6.0	17	2.8	8.5	16	2.2	1.9	1.8	2.5	<dl	<dl	<dl	5.4	5.0
Rb	3.9	0.89	16	1.4	3.6	0.92	5.5	4.6	10	3.4	2.7	2.5	3.8	15	3.9	3.2	89	<dl	<dl	<dl	38	10
Sr	63	239	432	51	47	33	185	149	138	81	358	3770	118	54	1014	90	25	792	95	532	98	23
Y	4.8	8.6	15	1.5	2.0	17	17	200	21	80	16	33	110	14	9.6	16	16	<dl	<dl	7.1	12	5.7
Zr	18	9.8	40	3.9	6.4	50	132	1888	122	296	69	91	735	100	14	22	38	<dl	1.3	1.1	24	19
Nb	1.8	1.8	6.4	0.75	1.2	5.3	7.7	144	24	54	18	25	90	23	2.2	3.1	5.9	<dl	<dl	<dl	3.5	5.0
Mo	1.8	<dl	<dl	<dl	<dl	<dl	2.2	8.2	160	16	2.7	3.3	2.7	122	7.2	<dl	<dl	<dl	<dl	<dl	138	402
Sn	0.48	<dl	1.3	<dl	<dl	1.4	1.4	5.8	3.2	3.6	1.2	1.3	11	1.4	0.39	0.80	1.8	<dl	<dl	<dl	<dl	<dl
Sb	<dl	<dl	1.1	27	20	<dl	<dl	8.8	1.9	0.65	<dl	<dl	0.95	<dl	<dl	<dl	14	<dl	<dl	4.4	29	7.6
Cs	<dl	<dl	2.2	4.6	5.2	<dl	<dl	0.81	0.84	<dl	<dl	<dl	<dl	<dl	<dl	<dl	13	<dl	<dl	<dl	49	23
Ba	1.7	37	151	26	21	21	39	8.0	25	6.0	18	34	8.8	90	33	31	146	5.4	23	6.4	170	37
Hf	0.94	<dl	2.1	<dl	<dl	2.6	5.9	47	5.2	12	2.9	4.0	25	4.0	<dl	1.2	2.0	<dl	<dl	<dl	<dl	<dl
W	1.2	<dl	0.58	461	447	5.1	1.7	0.79	1.1	0.94	<dl	1.1	0.66	0.99	<dl	<dl	0.72	<dl	<dl	<dl	9.6	1.5
Pb	3.1	8.6	16	0.43	0.67	112	22	95	25	155	3.4	3.9	17	8.4	1.9	4.8	15	<dl	<dl	<dl	15	13
Th	1.9	1.1	11	<dl	0.82	7.2	10	8.6	5.5	9.1	3.6	2.7	12	3.9	1.3	2.8	8.3	<dl	<dl	<dl	4.7	2.9
U	0.81	<dl	4.4	<dl	<dl	2.3	2.8	7.4	45	4.7	2.1	3.6	11	51	1.5	1.0	11	<dl	<dl	<dl	81	73
REE	28	88	104	8.0	10	91	116	991	189	760	203	311	629	85	51	88	73	1.2	1.0	17	54	33

Table 4
Mineral contents (%wt) in the fraction <4 μm of the powdered samples from the channel profiles (CP_4). Qtz, Quartz; Ant, Anatase; Cb, Carbonates; Py, Pyrite; Sul, Sulphates; Ill-Ms, Illite-Muscovite; Mm, Montmorillonite; Kln-Clc, Kaolinite-Clinochlore; Tob, Tobelite; Ank, Ankerite; Cal, Calcite; Dol, Dolomite; Sid, Siderite; Gy, Gypsum; Jar, Jarosite; Szo, Szomolnokite; Roz, Rozenite; Mel, Melanterite.

Sample	CP_4_01	CP_4_02	CP_4_03	CP_4_04	CP_4_05	CP_4_06	CP_4_07	CP_4_08	CP_4_09	CP_4_10	CP_4_11	CP_4_12	CP_4_13	CP_4_14	CP_4_15	CP_4_16	CP_4_17	CP_4_18	CP_4_19	CP_4_20	CP_4_21	CP_4_22
Clays	5.4	3.2	11.7	<dl	4.3	12.9	4.6	5.8	8.9	4.3	7.8	9.7	14.9	9.0	<dl	15.0	18.9	0.1	1.4	<dl	16.4	13.9
Qtz	<dl	<dl	7.2	4.0	3.2	<dl	1.3	0.6	1.7	0.1	<dl	<dl	<dl	2.4	2.2	<dl	29.6	<dl	0.5	11.9	8.3	7.7
Ant	<dl	<dl	<dl	<dl	<dl	<dl	<dl	<dl	<dl	<dl	<dl	<dl	<dl	0.9	0.5	0.9	<dl	<dl	<dl	<dl	1.1	0.8
Cb	1.3	2.1	5.2	<dl	<dl	1.1	2.1	9.2	<dl	<dl	<dl	0.2	1.7	<dl	3.2	<dl	<dl	14.4	2.0	<dl	<dl	<dl
Py	0.3	0.1	0.5	2.4	0.6	0.7	<dl	3.4	9.5	8.1	0.7	2.7	0.2	7.5	2.3	0.5	2.5	0.1	<dl	<dl	2.5	1.2
Sul	0.1	<dl	<dl	1.5	1.3	0.1	<dl	0.3	3.7	2.2	<dl	0.3	<dl	1.1	1.5	<dl	<dl	<dl	<dl	<dl	<dl	<dl
Ill-Ms	<dl	<dl	<dl	<dl	<dl	<dl	<dl	<dl	<dl	<dl	<dl	<dl	<dl	5.3	<dl	0.9	4.6	<dl	<dl	<dl	<dl	<dl
Mm	<dl	<dl	<dl	<dl	<dl	<dl	<dl	<dl	<dl	<dl	<dl	<dl	<dl	<dl	<dl	<dl	<dl	<dl	<dl	<dl	<dl	<dl
Kln-Clc	2.1	1.9	11.7	<dl	4.3	12.9	4.6	5.8	8.9	4.3	1.9	1.5	14.9	<dl	<dl	14.1	14.4	0.1	1.4	<dl	<dl	<dl
Tob	3.3	1.4	<dl	<dl	<dl	<dl	<dl	<dl	<dl	<dl	5.9	8.1	<dl	3.7	<dl	<dl	<dl	<dl	<dl	<dl	16.4	13.9
Ank	<dl	0.1	0.3	<dl	<dl	<dl	<dl	1.2	<dl	<dl	<dl	<dl	<dl	<dl	<dl	<dl	<dl	0.8	<dl	<dl	<dl	<dl
Cal	1.3	1.9	4.6	<dl	<dl	<dl	2.1	7.5	<dl	<dl	<dl	<dl	1.6	<dl	3.2	<dl	<dl	13.1	2.0	<dl	<dl	<dl
Dol	<dl	<dl	<dl	<dl	<dl	<dl	<dl	<dl	<dl	<dl	<dl	<dl	0.1	<dl	<dl	<dl	<dl	<dl	<dl	<dl	<dl	<dl
Sid	<dl	<dl	0.3	<dl	<dl	1.1	<dl	0.5	<dl	<dl	<dl	0.2	<dl	<dl	<dl	<dl	<dl	0.5	<dl	<dl	<dl	<dl
Gy	0.1	<dl	<dl	1.5	1.3	<dl	<dl	0.1	<dl	0.2	<dl	<dl	<dl	<dl	<dl	<dl	<dl	<dl	<dl	<dl	<dl	<dl
Jar	<dl	<dl	<dl	<dl	<dl	<dl	<dl	<dl	<dl	<dl	<dl	0.3	<dl	<dl	<dl	<dl	<dl	<dl	<dl	<dl	<dl	<dl
Szo	<dl	<dl	<dl	<dl	<dl	<dl	<dl	<dl	2.2	1.5	<dl	<dl	<dl	<dl	1.5	<dl	<dl	<dl	<dl	<dl	<dl	<dl
Roz	<dl	<dl	<dl	<dl	<dl	<dl	<dl	<dl	1.6	0.3	<dl	<dl	<dl	1.1	<dl	<dl	<dl	<dl	<dl	<dl	<dl	<dl
Mel	<dl	<dl	<dl	<dl	<dl	0.1	<dl	0.1	<dl	0.1	<dl	<dl	<dl	<dl	<dl	<dl	<dl	<dl	<dl	<dl	<dl	<dl

3.2.2. Correlation analysis of OP and geochemical patterns including CP_4 actual respirable coal mine dust samples

Figs. 5 and 6 show the results of the cross-correlation analysis of OP with geochemical, mineralogical and particle size of CP_4 samples but, in this case, adding recently respirable coal mine dust (RD) from Chinese mines, sampled and characterised using the same methodology by Trechera et al. (2020, 2021). The information on the origin and features of the RD samples included is supplied in Table S4. This re-analysis is done with the aim to validate the procedure to study the possible OP from mining dust of a given coal by sampling the coal seam, powdering the coal and extracting the CP_4. Thus, the main results obtained for CP_4, which remain valid in the re-analysis by including RD, will support the validation of the protocol used in this study.

There, again correlation was found for S, U, Mo and pyrite ($r = 0.6–0.5$) with OP^{AA} (Fig. 5). However, in spite of the correlation of OP^{AA} with pyrite, the OP^{AA}-Fe correlation markedly decreased ($r = 0.39$) when all samples were combined (CP_4 and RD). On the other hand, moisture ($r = 0.52$) and some elements and minerals, such as Ca, Na, carbonates ($r = 0.3–0.4$) and B ($r = 0.20$) correlated with OP^{GSH}. By including actual coal mine dust samples in the correlation analysis, some high calcite, Na and As dust from galleries with lime-gunited walls that interacted with acid drainage waters (Trechera et al., 2020) seem to increase correlation with OP^{GSH}; and Na and Mg ($r = 0.6–0.5$) and moisture ($r = 0.40$) with OP^{DTT} (Fig. 5). Furthermore, by including RD samples elements such as K, Si, Rb, Sb, Ge, W, As, and Ba markedly decreased their correlation with OP^{DTT}.

Again, OP correlations increased when the analysis focused only on bituminous coal and coal dust samples (Fig. 6). There, an increase was found for correlation of ash yield, sulphates, anatase, Ti, Ni, Co, V, Pb and REEs with OP^{AA}, but the most noticeable increase was found for Fe ($r = 0.83$) and pyrite ($r = 0.66$). Thus, Fe-OP^{AA} correlation is very high when CP_4 and RD are analysed together for bituminous coals. For OP^{GSH} and OP^{DTT}, elements such as Ca, Na, Mg, B, Bi, Tl, and Sr, PSD, moisture content and quartz mineral also increase correlations. Moisture-OP^{GSH} ($r = 0.73$) and Mg-OP^{DTT} ($r = 0.70$) markedly increased in this combined analysis. Conversely, U and Mo correlation with OP^{AA} decreased when only bituminous coal was considered.

According to this re-analysis, OP correlations remain or even increase when RD samples for Fe, pyrite, S, sulphates, moisture content or B are included, and also, to a lesser extent, with elements such as U, Mo, V, Ti, Ni, K, Si, Pb, Co, Sb, Bi, As, W, Ge, Ca, Na, Mg and Mn; and minerals such as anatase, quartz or carbonates, ash yield, and particle size.

The results obtained between the OP and respirable fractions from CP_4 analysis samples of given coal might yield information on the expected OP of the RD of the coal when some working operations are carried out in the coal mines. In conclusion, the evaluation of OP coal worked in coal mines could offer insight into which elements could be more problematic in coal mines or which parameters are more potentially hazardous in coal mines.

3.2.3. Multilinear regression analysis

Figs. S3 and S4 and Eqs. (1) to (22) summarise the results of the multilinear regression analysis performed for the OP^{AA}, OP^{GSH}, and OP^{DTT} with geochemical parameters for the combined CP_4 and RD dataset. It has to be pointed out that a number of components are included in the equations for OP^{AA}, OP^{GSH}, and OP^{DTT} although they have opposite effects.

All coal and dust samples ($n = 43$), Fig. S3

$$OP^{AA}\ (\%\cdot\mu g^{-1}) = 0.11 * \text{pyrite}\ (\%wt) + 0.09 * \text{sulphates}\ (\%wt) - 0.07 * \text{moisture content}\ (\%ad) + 0.74\ (r = 0.70; \rho < 0.0001) \quad (1)$$

Table 5
Contents of major and trace elements in the fraction <4 μm of the powdered samples of the coal channel profiles (CP_4). wt, weight.

Sample	CP_4_01	CP_4_02	CP_4_03	CP_4_04	CP_4_05	CP_4_06	CP_4_07	CP_4_08	CP_4_09	CP_4_10	CP_4_11	CP_4_12	CP_4_13	CP_4_14	CP_4_15	CP_4_16	CP_4_17	CP_4_18	CP_4_19	CP_4_20	CP_4_21	CP_4_22
% wt																						
Al	1.22	0.83	3.59	0.44	0.83	2.80	1.22	3.20	3.57	2.21	1.66	2.46	3.39	3.06	0.84	3.26	6.04	0.12	0.42	0.11	3.95	3.67
Si	1.18	0.82	5.60	0.86	1.90	2.90	1.33	3.73	4.51	2.47	1.85	2.46	3.84	4.02	1.62	3.38	9.44	0.10	0.43	0.14	7.07	5.35
Ca	0.47	0.57	0.72	0.71	0.76	0.13	0.43	1.06	0.14	0.24	0.07	0.38	0.24	0.21	0.95	0.08	0.83	6.76	0.41	1.43	0.52	0.36
Fe	0.27	0.04	1.10	0.76	0.88	1.08	0.18	1.05	4.08	2.55	0.18	0.32	0.19	3.30	1.61	0.75	0.94	1.25	0.11	0.13	2.36	0.58
K	0.09	0.04	0.37	0.02	0.06	<0.01	0.06	0.16	0.34	0.09	0.07	0.05	0.11	0.63	0.16	0.14	1.14	0.01	<0.01	<0.01	0.27	0.13
Mg	0.02	0.03	0.20	0.15	0.17	0.02	0.04	0.18	0.12	0.05	0.04	0.03	0.08	0.09	0.06	0.09	0.44	0.20	0.08	0.20	0.16	0.03
Na	0.03	0.02	0.13	0.05	0.04	0.02	0.02	0.02	0.03	0.02	0.03	0.04	0.02	0.22	0.03	0.21	0.03	0.02	0.15	0.06	0.03	0.01
P	<0.01	0.05	0.02	<0.01	<0.01	<0.01	0.01	0.02	0.02	0.01	0.02	0.31	0.01	0.01	<0.01	0.01	0.01	<0.01	<0.01	<0.01	0.13	0.09
S	5.30	0.35	0.70	1.00	1.07	1.05	2.55	1.46	6.22	4.78	1.62	2.02	1.50	3.68	2.71	0.74	1.25	0.25	0.10	0.12	5.45	1.34
$mg \cdot kg^{-1}$																						
Li	69	21	18	4.3	5.0	18	9.9	56	30	28	27	25	47	41	5.6	193	36	<dl	1.0	<dl	7.8	30
Be	1.0	<dl	<dl	16	17	5.7	2.3	5.8	4.3	5.2	1.6	3.6	12	2.5	<dl	0.89	2.6	<dl	<dl	2.2	2.0	0.89
B	24	27	3.3	47	36	19	12	18	64	7.8	8.1	18	<dl	<dl	7.3	<dl	<dl	32	73	45	23	11
Sc	1.6	1.2	4.2	0.91	1.0	6.1	5.6	27	6.2	6.0	2.5	1.6	14	4.2	2.5	3.7	9.3	<dl	<dl	<dl	5.0	3.8
Ti	287	398	992	163	337	854	1016	1702	2390	1687	608	425	2418	1603	518	645	1663	12	34	18	1289	1450
V	7.8	7.2	26	3.9	6.5	16	38	59	269	65	13	21	94	246	66	24	84	0.75	0.76	<dl	95	42
Cr	4.8	4.6	16	2.8	4.5	6.3	15	34	76	24	9.5	14	40	53	8.9	8.9	64	<dl	0.45	<dl	35	9.3
Mn	6.8	11	78	47	46	86	23	26	74	7.3	4.9	11	3.3	23	102	5.1	12	640	14	16	32	7.0
Co	1.5	2.4	5.1	0.88	0.94	7.1	2.6	7.0	9.7	6.4	2.0	11	5.5	10	5.3	5.1	5.1	<dl	1.7	9.6	4.1	3.4
Ni	1.2	7.2	14	1.2	1.4	11	4.8	55	34	8.5	4.2	13	33	38	6.5	5.7	30	<dl	2.5	3.5	21	22
Cu	4.1	4.1	20	3.2	5.8	12	12	34	15	18	6.1	11	31	63	24	20	41	3.1	2.5	2.6	21	20
Zn	19	38	48	14	17	18	26	526	40	27	28	27	29	33	23	15	24	10	16	12	45	37
Ga	5.4	3.3	9.8	1.3	1.6	8.7	13	43	9.6	24	7.4	9.2	41	14	3.5	10	14	<dl	<dl	1.5	9.3	7.0
Ge	2.7	0.85	1.9	315	211	2.2	19	11	3.2	6.4	3.8	14	12	2.0	<dl	1.2	1.8	<dl	<dl	1.4	20	1.8
As	1.8	3.5	3.5	389	495	12	14	18	18	24	3.1	22	5.8	5.7	7.5	1.8	7.7	0.53	0.47	1.3	249	58
Se	0.72	<dl	2.2	<dl	<dl	1.5	2.3	19	3.7	12	2.7	6.2	11	3.3	1.2	2.2	2.2	<dl	<dl	<dl	2.4	1.2
Rb	4.8	<dl	25	2.1	5.0	<dl	4.3	4.3	7.5	2.6	2.0	1.9	3.2	25	3.5	4.5	110	<dl	<dl	<dl	46	10
Sr	54	226	319	52	55	31	140	110	125	77	278	3308	104	127	499	163	30	767	92	500	124	156
Y	4.0	6.7	13	1.4	1.9	16	10	181	22	65	12	25	93	14	7.6	15	13	<dl	<dl	5.8	15	14
Zr	27	17	57	4.9	9.3	66	107	3335	184	512	97	132	1174	141	25	31	53	<dl	1.3	<dl	29	104
Nb	1.5	2.0	5.9	<dl	0.86	3.9	5.1	140	21	48	14	22	81	18	2.0	3.0	5.9	<dl	<dl	<dl	4.0	6.3
Mo	3.8	0.86	2.2	<dl	<dl	0.97	21	3.2	79	5.8	2.2	2.8	2.6	98	2.8	<dl	<dl	<dl	<dl	<dl	41	115
Sn	0.38	0.77	1.7	<dl	0.70	1.6	1.2	6.2	2.5	4.0	1.5	4.5	10	1.5	<dl	0.88	2.0	<dl	<dl	<dl	1.8	1.7
Sb	<dl	3.3	1.3	20	16	<dl	7.4	5.8	<dl	<dl	<dl	23	0.79	0.84	0.84	<dl	11	<dl	<dl	2.8	31	0.79
Cs	<dl	<dl	3.9	6.8	9.3	<dl	4.1	<dl	<dl	<dl	<dl	<dl	<dl	1.1	<dl	<dl	17	<dl	<dl	<dl	56	15
Ba	1.7	35	187	34	37	20	38	11	21	7.3	11	30	9.7	157	35	59	211	6.0	27	6.6	270	41
Hf	0.74	<dl	1.5	<dl	<dl	1.9	2.5	39	4.5	9.1	2.1	3.2	19	3.2	<dl	0.90	1	<dl	<dl	<dl	0.80	2.6
W	1.7	<dl	1.3	406	360	3.4	2.8	1.6	<dl	1.3	0.87	1.6	1.1	1.8	<dl	<dl	1.4	<dl	<dl	<dl	8.1	0.76
Pb	2.5	8.3	17	<dl	0.88	122	20	38	7.8	117	1.1	1.9	14	5.1	1.8	4.7	16	0.86	0.97	0.58	11	6.6
Th	2.1	1.3	13	<dl	0.99	8.1	9.4	7.2	5.2	7.0	3.7	2.6	9.7	5.0	1.5	3.8	11	<dl	<dl	<dl	5.0	6.2
U	0.91	<dl	5.4	<dl	<dl	2.4	5.8	8.6	48	5.1	2.0	4.2	12	99	2.0	1.3	10	<dl	<dl	<dl	79	59
REE	27	89	114	9.5	13	78	91	1026	158	552	171	275	530	153	44	111	82	2.0	1.0	17	75	74

Table 6
Most geochemical interesting and enrichments elements and high concentrations of bulk channel profile (CP) coals in comparison with Chinese geochemical averaged concentrations (Dai et al., 2007, 2008). LV, Low-Volatile; HV, High-Volatile; MV, Medium-Volatile.

Sample	Ash yield	Rank	Interesting elements	Trace elements ($mg \cdot kg^{-1}$)
CP_01	Medium	LV bituminous	High organic S, low Fe and pyrite	Low levels
CP_02	Medium	Semi-anthracite	Low S	Low levels
CP_03	High	HV bituminous		Sr (432), Th (11)
CP_04	Medium	Sub-bituminous		Ge (577), As (484), W (461), Sb (27), Be (17), Cs (5.2)
CP_05	Medium	Sub-bituminous		Ge (436), As (436), W (447), Sb (20), Be (11), Cs (5.2)
CP_06	High	HV bituminous		Pb (112), Be (6.0), As (9.8), W (5.1)
CP_07	High	HV bituminous	Anatase mineral detected by XRD (High Ti)	Th (10)
CP_08	High	MV bituminous	High pyrite	Zn (2446), Zr (1888), Cd, Pb, Cr, Ni, Cu, Ga (51–95), As (36) Se (21), Y (200), Nb (144), REE's (991)
CP_09	High	MV bituminous	High S, Fe and pyrite	V (268), Mo (160), Cr (79), U (45), As (29)
CP_10	High	LV bituminous	High S, Fe and pyrite; Anatase mineral detected by XRD (High Ti)	Pb (155), As (36), Se (17), Y (80), Nb (54), REE's (760)
CP_11	Medium	Semi-anthracite		Sr (358)
CP_12	High	Semi-anthracite	High P	Sr (3770)
CP_13	High	LV bituminous	Anatase mineral detected by XRD (High Ti)	Ti (2791), Y (110), Zr (735), REE (629), Th (12)
CP_14	Medium	Anthracite	Anatase mineral detected by XRD (High Ti)	Mo (122), V (199), U (51)
CP_15	High	LV bituminous		Sr (1014), Mn (235)
CP_16	Medium	Anthracite		Li (162)
CP_17	High	Lignite	High quartz, kaolinite-chlorite and illite minerals; Anatase mineral detected by XRD (High Ti)	Cr, Rb, Cu, Ni (32–89)
CP_18	Medium	HV bituminous	High Ca and carbonates minerals	Mn (721), Sr (792)
CP_19	Low	HV bituminous		B (126)
CP_20	Low	HV bituminous		Sr (532)
CP_21	High	Semi-anthracite	High organic S	As (225), Mo (138), Sb (29), U (81)
CP_22	Medium	Semi-anthracite	High organic S	As (65), Mo (402), Sb (7.6), U (73), Tl (25)

$$OP^{AA}\ (\%\cdot\mu g^{-1}) = 0.13 * S\ (\%wt) + 0.01 * Mo\left(mg\cdot kg^{-1}\right) - 0.05 * \text{moisture content}\ (\%ad) + 0.65\ (r = 0.69; \rho < 0.0001) \quad (2)$$

$$OP^{AA}\ (\%\cdot\mu g^{-1}) = 0.19 * Fe\ (\%wt) + 0.01 * U\left(mg\cdot kg^{-1}\right) - 1.22 * Na\ (\%wt) + 0.64\ (r = 0.70; \rho < 0.001) \quad (3)$$

$$OP^{AA}\ (\%\cdot\mu g^{-1}) = 0.12 * \text{pyrite}\ (\%wt) + 0.42 * \text{anatase}\ (\%wt) - 1.81 * Mg\ (\%wt) + 0.80\ (r = 0.73; \rho < 0.0001) \quad (4)$$

$$OP^{GSH}\ (\%\cdot\mu g^{-1}) = 0.02 * \text{moisture content}\ (\%ad) + 0.02 * Ca\ (\%wt) - 0.03 * D_{25}(\mu m) + 0.15\ (r = 0.71; \rho < 0.0001) \quad (5)$$

$$OP^{GSH}\ (\%\cdot\mu g^{-1}) = 0.02 * \text{moisture content}\ (\%ad) + 0.004 * \text{carbonates}\ (\%wt) + 0.09\ (r = 0.65; \rho < 0.0001) \quad (6)$$

$$OP^{DTT}\ (\%\cdot\mu g^{-1}) = 1.45 * Mg\ (\%wt) + 0.98 * Na\ (\%wt) + 0.002 * Ge\left(mg\cdot kg^{-1}\right) + 0.52\ (r = 0.71; \rho < 0.0001) \quad (7)$$

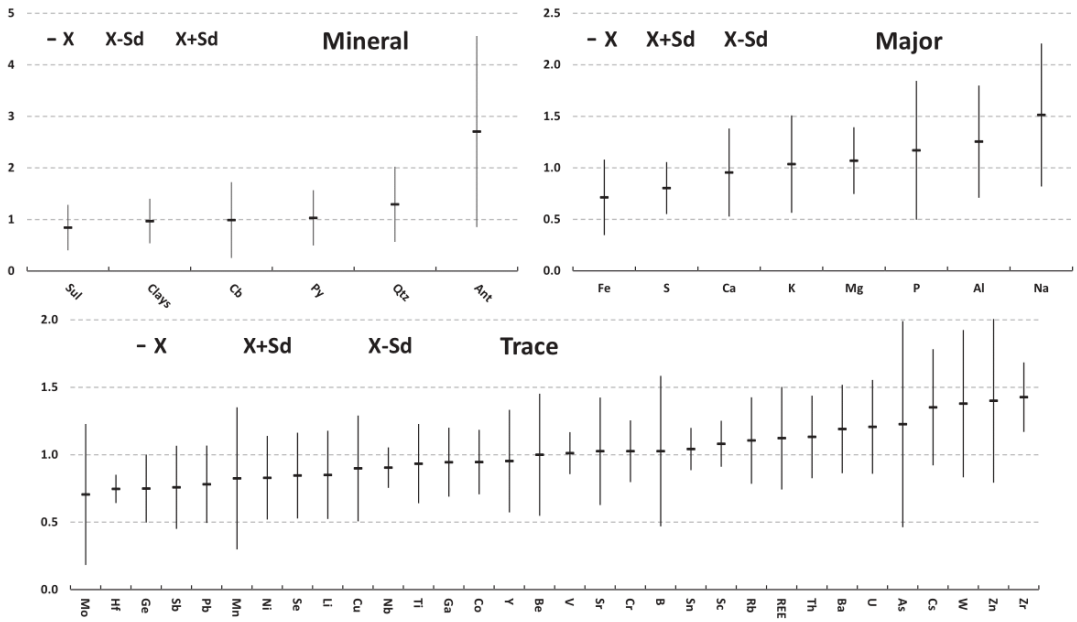

Fig. 2. Average ratio of mineral and major and trace element contents in the channel profile ⁻4 μm (CP_4) and bulk channel profile (CP) samples. Ratio average (X) = CP_4/CP; Sd, Standard Deviation; Sul, Sulphates; Cb, Carbonates; Py, Pyrite; Qtz, Quartz; Ant, Anatase.

Table 7
Oxidative potential (OP) of the fraction <4 μm of the powdered channel profile samples (CP_4). AA, Ascorbic Acid; Sd, Standard deviation; GSH, Glutathione; TOT = AA+GSH; DTT, Dithiothreitol; **, insufficient sample for OP analysis.

Sample	$\%OP^{AA}$ μg^{-1}	Sd^{AA}	$\%OP^{GSH}$ μg^{-1}	Sd^{GSH}	$\%OP^{TOT}$ μg^{-1}	$\%OP^{DTT}$ μg^{-1}	Sd^{DTT}
CP_4_01	0.99	0.04	0.10	0.08	1.09	0.71	0.00
CP_4_02	0.42	0.01	0.25	0.06	0.68	0.88	0.00
CP_4_03	1.27	0.02	0.03	0.04	1.30	0.22	0.00
CP_4_04	0.24	0.03	0.19	0.08	0.42	1.88	0.00
CP_4_05	0.31	0.01	0.24	0.02	0.55	0.90	0.00
CP_4_06	1.50	0.07	0.18	0.03	1.68	0.50	0.00
CP_4_07	0.34	0.01	0.26	0.01	0.60	0.22	0.00
CP_4_08	1.49	0.02	0.16	0.01	1.65	0.44	0.00
CP_4_09	1.86	0.00	0.03	0.02	1.89	**	**
CP_4_10	1.80	0.00	0.09	0.03	1.89	0.22	0.00
CP_4_11	0.79	0.01	0.12	0.04	0.91	0.76	0.00
CP_4_12	0.65	0.04	0.01	0.05	0.66	0.38	0.00
CP_4_13	0.62	0.01	0.15	0.06	0.77	0.50	0.00
CP_4_14	1.60	0.02	0.09	0.03	1.69	0.68	0.00
CP_4_15	1.75	0.03	0.06	0.02	1.81	0.54	0.00
CP_4_16	1.47	0.04	0.11	0.06	1.58	0.62	0.00
CP_4_17	0.19	0.01	0.28	0.08	0.47	0.77	0.00
CP_4_18	1.04	0.02	0.12	0.08	1.16	1.22	0.00
CP_4_19	0.16	0.09	0.27	0.15	0.43	0.85	0.00
CP_4_20	0.12	0.00	0.28	0.08	0.40	1.41	0.00
CP_4_21	1.90	0.02	0.11	0.04	2.00	0.82	0.00
CP_4_22	1.78	0.00	0.16	0.06	1.94	0.56	0.00

$$OP^{DTT}\ (\%\cdot\mu g^{-1}) = 1.43 * Mg\ (\%wt) + 0.96 * Na\ (\%wt) + 0.002 * W\left(mg\cdot kg^{-1}\right) + 0.54\ (r = 0.70; \rho<0.0001) \quad (8)$$

$$OP^{DTT}\ (\%\cdot\mu g^{-1}) = 0.002 * Ba\left(mg\cdot kg^{-1}\right) + 0.04 * \text{moisture content}\ (\%, ad) - 0.05 * Th\left(mg\cdot kg^{-1}\right) + 0.86\ (r = 0.68; \rho = 0.0001)$$

Bituminous coals and Bituminous coal dust (n = 23), Fig. S4

$$OP^{AA}\ (\%\cdot\mu g^{-1}) = 0.36 * \text{anatase}\ (\%wt) + 0.15 * \text{pyrite}\ (\%wt) - 0.05 * \text{moisture content}\ (\%ad) + 0.71\ (r = 0.83; \rho = 0.0001) \quad (10)$$

$$OP^{AA}\ (\%\cdot\mu g^{-1}) = 0.44 * Fe\ (\%wt) + 0.04 * \text{carbonates}\ (\%wt) - 1.81 * Mg\ (\%wt) + 0.55\ (r = 0.90; \rho<0.0001) \quad (11)$$

$$OP^{AA}\ (\%\cdot\mu g^{-1}) = 0.64 * Fe\ (\%wt) + 0.01 * Li\left(mg\cdot kg^{-1}\right) - 0.01 * V\left(mg\cdot kg^{-1}\right) + 0.28\ (r = 0.91; \rho<0.0001) \quad (12)$$

$$OP^{AA}\ (\%\cdot\mu g^{-1}) = 0.48 * Al\ (\%wt) + 0.0003 * Ti\left(mg\cdot kg^{-1}\right) - 0.11 * \text{clays}\ (\%wt) + 0.50\ (r = 0.80; \rho<0.0001) \quad (13)$$

$$OP^{AA}\ (\%\cdot\mu g^{-1}) = 0.15 * \text{pyrite}\ (\%wt) + 0.08 * \text{sulphate}\ (\%wt) - 0.01 * B\left(mg\cdot kg^{-1}\right) + 0.87\ (r = 0.83; \rho = 0.0001) \quad (14)$$

$$OP^{AA}\ (\%\cdot\mu g^{-1}) = 0.04 * \text{ash yield}\ (\%db) + 0.01 * Pb\left(mg\cdot kg^{-1}\right) - 0.07 * \text{clays}\ (\%wt) + 0.36\ (r = 0.81; \rho = 0.0001) \quad (15)$$

$$OP^{GSH}\ (\%\cdot\mu g^{-1}) = 0.027 * \text{moisture content}\ (\%ad)\ (r = 0.85; \rho<0.0001) \quad (16)$$

$$OP^{GSH}\ (\%\cdot\mu g^{-1}) = 0.003 * B\left(mg\cdot kg^{-1}\right) + 0.0001 * Ti\left(mg\cdot kg^{-1}\right) - 0.002 * V\left(mg\cdot kg^{-1}\right) + 0.092\ (r = 0.76; \rho = 0.001) \quad (17)$$

$$OP^{GSH}\ (\%\cdot\mu g^{-1}) = 0.020 * Bi\left(mg\cdot kg^{-1}\right) + 0.003 * B\left(mg\cdot kg^{-1}\right) - 0.003 * Mo\left(mg\cdot kg^{-1}\right) + 0.071\ (r = 0.76; \rho = 0.001) \quad (18)$$

$$OP^{DTT}\ (\%\cdot\mu g^{-1}) = 3.29 * Mg\ (\%wt) - 0.06 * Th\left(mg\cdot kg^{-1}\right) + 0.71\ (r = 0.85; \rho<0.0001) \quad (19)$$

$$OP^{DTT}\ (\%\cdot\mu g^{-1}) = 1.28 * Na\ (\%wt) + 0.06 * \text{quartz}\ (\%wt) + 0.001 * Mn\left(mg\cdot kg^{-1}\right) + 0.42\ (r = 0.85; \rho = 0.001) \quad (20)$$

$$OP^{DTT}\ (\%\cdot\mu g^{-1}) = 0.04 * \text{moisture content}\ (\%ad) + 0.09 * \text{quartz}\ (\%wt) - 0.13 * Cs\left(mg\cdot kg^{-1}\right) + 0.60\ (r = 0.75; \rho = 0.002) \quad (21)$$

$$OP^{DTT}\ (\%\cdot\mu g^{-1}) = 0.01 * B\left(mg\cdot kg^{-1}\right) + 0.07 * \text{quartz}\ (\%wt) - 0.03 * Mo\left(mg\cdot kg^{-1}\right) + 0.56\ (r = 0.76; \rho = 0.002) \quad (22)$$

Thus, as shown by these equations, Fig. S3 and Fig. S4, Fe, pyrite and sulphate minerals (indicating acidic species from pyrite oxidation), followed by anatase and, in a much lower proportion, U, Mo, V and Pb, clearly govern the OP^{AA}; while moisture content, Ca, carbonate minerals, coarse particle size and B control OP^{GSH}; whereas Mg, Na, quartz, B, moisture content and Ba regulate OP^{DTT}.

3.2.4. Interpretation of links between geochemical patterns of samples and oxidative potential

3.2.4.1. Ascorbic acid oxidative potential (OP^{AA}). As stated above, Fe and pyrite are most strongly linked to OP^{AA} in the CP_4 and RD samples studied, and this relationship increases when only bituminous coals rank species are evaluated. Cohn et al. (2006b), Liu and Liu (2020), and R. Zhang et al. (2021) found that ROS generation is strongly linked with Fe and pyrite contents in coal. Harrington et al. (2012) reported that pyrite particles may remain in the lungs for a year or more, generating ROS in cells and potentially contributing to the pathogenesis of CWP. Thus, the results indicate that special controls should be implemented for working and handling high pyrite coals to reduce the occupational health impacts.

Huang et al. (1998) defined bioavailable Fe (BAI) as free-Fe in a 10 mM phosphate solution, pH 4.5 - which is the pH of the phagolysosomes of lung macrophages. They proposed this BAI as a marker of the potential of the dust to induce CWP. Coal workers' exposure to coal dust that contains acid-soluble Fe with low buffering capacity coal (low carbonate minerals in coal) would be more likely to induce oxidative stress, leading to lung injury and CWP development. This is in contrast to high buffering capacity coal exposure, which renders the coal less hazardous. Huang et al. (2005) reported a strong correlation for BAI values and CWP cases for bituminous coal mining areas of the United States, as well as was the correlation with the content of sulphate and pyrite sulphur. Furthermore, Harrington et al. (2012) documented the role of inhaled pyrite particles in promoting CWP pathogenesis. Regular exposure to coal dust containing pyrite mineral is predicted to lead to a build-up of pyrite in the lung that will slowly disappear over a time

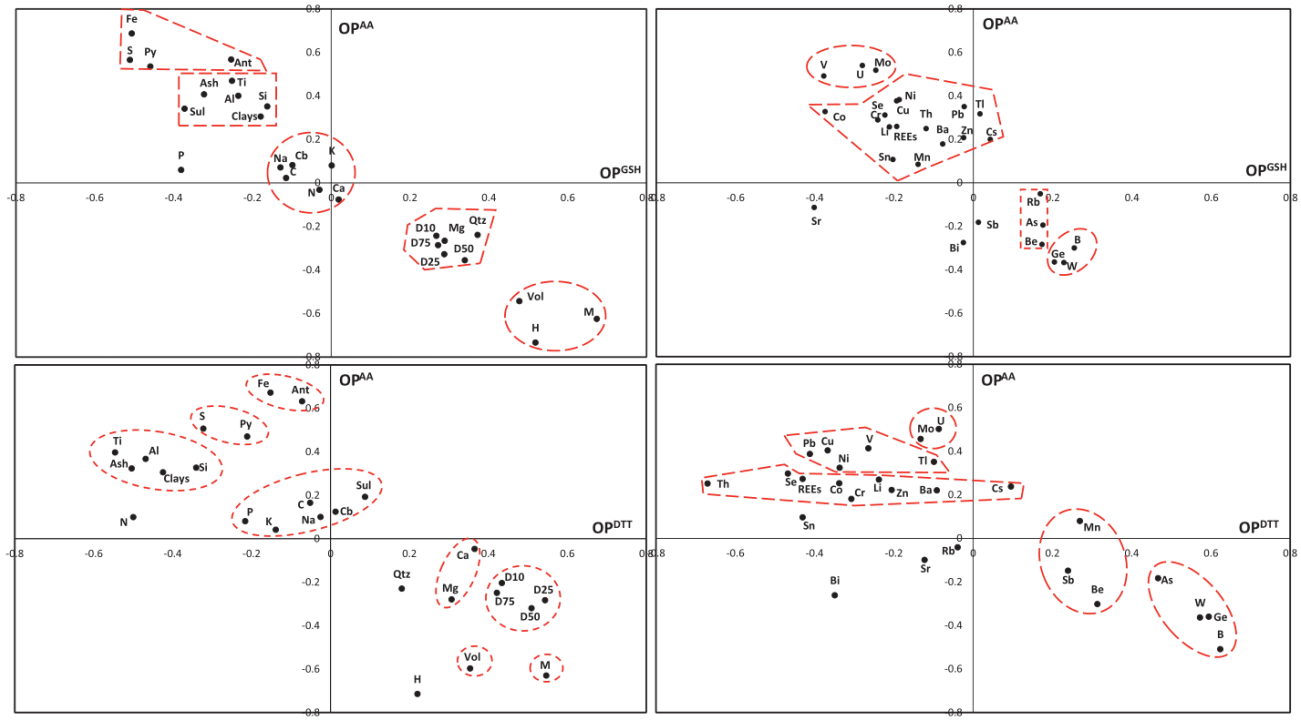

Fig. 3. Cross-correlation plots between the Pearson's correlation coefficients of geochemical parameters of all (22) channel profile samples <4 μm (CP_4) (mineralogy, chemistry, size, and proximate analysis) with their respective OP^{AA} vs OP^{GSH}, and OP^{AA} vs OP^{DTT}. Py, Pyrite; Ant, Anatase; Sul, Sulphates; Cb, Carbonates; Qtz, Quartz; D_{10}, D_{25}, D_{50}, D_{75}, percentiles 10, 25, 50 and 75 of the particle size in μm, respectively; Vol, Volatile Matter; M, Moisture.

scale of years. Moreover, frequent exposure to respirable pyrite particles in coal dust over years promotes a chronic level of inflammation, developing hydrogen peroxide and ferrous-Fe, which produce highly reactive hydroxyl radicals, potentially contributing to the pathogenesis of CWP (Cohn et al., 2006b; Harrington et al., 2012). In addition, other minerals in coal dust, such as quartz, have been shown to promote CWP pathogenesis, but none of these minerals could generate hydroxyl radicals at the same level as pyrite (Cohn et al., 2006a; Harrington et al., 2012). Moreover, Yu et al. (2020) state that several metals, including Fe, are correlated with intracellular ROS in alveolar macrophages, confirming that oxidative stress indicators of underground coal workers are correlated with the progression of CWP.

Summarising, extensive bibliography such as the results published in this work identify Fe and pyrite as potentially hazardous agents. They may promote oxidative stress and ROS and also could be involved in CWP injuries. In short, these components should be carefully monitored and controlled in coal mines due to their possible negative consequences.

Other transition metals, such as Ti, Cu, Ni, Mo, Co, Cr, and V may be agents in the formation and transformation of ROS (Aruoma, 1998; Lighty et al., 2000; Lloyd and Phillips, 1999; Shi et al., 1992; Shi and Dalal, 1992; Stohs and Bagchi, 1995; Strlič et al., 2003; Valko et al., 2005; Yu et al., 2020). Latvala et al. (2016) state the capability of Ni species to generate ROS. Moreno et al. (2019) suggest that redox-active elements, such as Cu, V and Cr, can contribute to ROS production; however, redox-inactive Pb can produce ROS by acting directly on cellular molecules. Yu et al. (2020) found that Mn, Cr, Ti, Fe, Cu, Zn, Ni, and Mo were correlated with ROS in non-small cell lung cancer cell lines. So, as previously indicated here, Cu, Ni, Mo, Co, Cr, Pb and V transition metals are related to OP and could develop ROS. In spite of the correlation of OP^{AA} with U, data on the OP of this metal was not found in the literature.

Moreover, sulphate, anatase and silica minerals results were linked to promoting ROS pathologies, as also indicated by the bibliography. Fang et al. (2017) also found a relevant correlation between sulphate contents in ambient PM and OP, and Gilmour et al. (2004), using other approaches, identified sulphate as an important factor of toxicity. Schins and Borm (1999) suggested that sulphate content in coal dust could play a dominant role in antiprotease inactivation. In addition, sulphate may also promote solubility, enhancing further the development of OP and ROS (Weber et al., 2016). Fubini and Hubbard (2003) reported in detail two main sources of ROS contributing to adverse reactions with silica: i) particle-generated free radicals and ROS (acting on cells); and ii) extracellular components and cell-generated ROS and reactive nitrogen species (RNS). Hamilton et al. (2009) demonstrated that anatase (TiO_2) could create an increase in toxic particles and produce an inflammatory response in lungs.

In addition to this, Zazouli et al. (2021) evaluated the cross correlation (r) between OP and PM_4 components from eight underground coal mines in Alborz Coal Basin. The results were in concordance with this study, with relatively high r values for elements such as Pb, Al, As, Cr or Co. Of special relevance are the similar results obtained for Fe in that and the present studies (r = 0.93 and 0.83, respectively).

3.2.4.2. Glutathione oxidative potential (OP^{GSH}). The moisture contents, and those of B and Na, are highly correlated with OP^{GSH} and, to a lesser degree, with the particle size, W and Ge. These associations could indirectly reflect the association of organic matter with OP^{GSH}. When an increase of coaly organic matter in dust occurs, the moisture content and the content of elements, typically associated with organic matter such as B, Ge and W (Swaine, 1990), also increase. Furthermore, the increase of organic matter in RD yields to a coarser particle size (Trechera et al., 2020, 2021). The association of organic matter-OP^{GSH} in these cases is probably related to specific patterns of radicals or organic components. Xu et al. (2017) demonstrate that the wettability of coal dust is closely related to the surface hydroxyl functional group, which, as previous commented, can contribute to the pathogenesis of CWP. This is relevant because moisture is an important parameter, among others, in defining

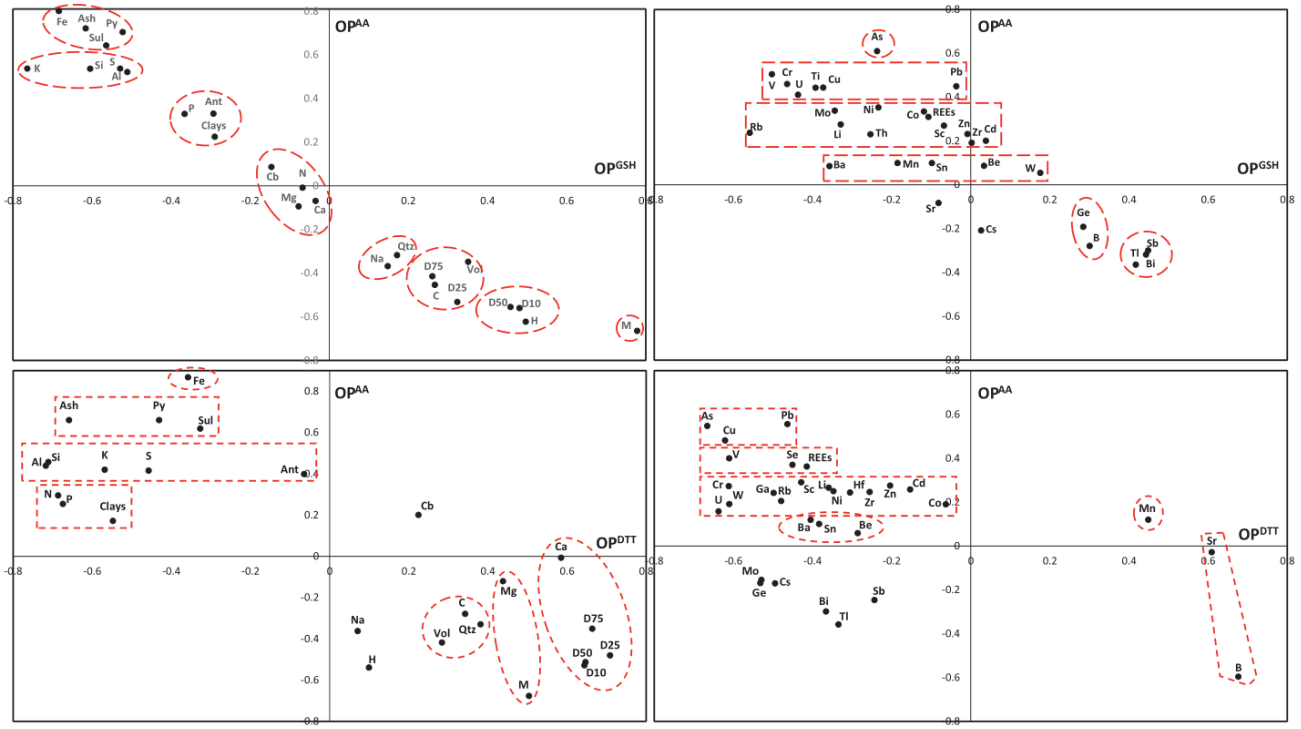

Fig. 4. Cross-correlation plots between the Pearson's correlation coefficients of geochemical parameters of all channel profile samples <4 μm (CP_4) (mineralogy, chemistry, size, and proximate analysis) from bituminous coals (12 of 22 samples) with their respective OP^{AA} vs OP^{GSH}, and OP^{AA} vs OP^{DTT}. Py, Pyrite; Ant, Anatase; Sul, Sulphates; Cb, Carbonates; Qtz, Quartz; D_{10}, D_{25}, D_{50}, D_{75}, percentiles 10, 25, 50 and 75 of the particle size in μm, respectively; Vol, Volatile Matter; M, Moisture.

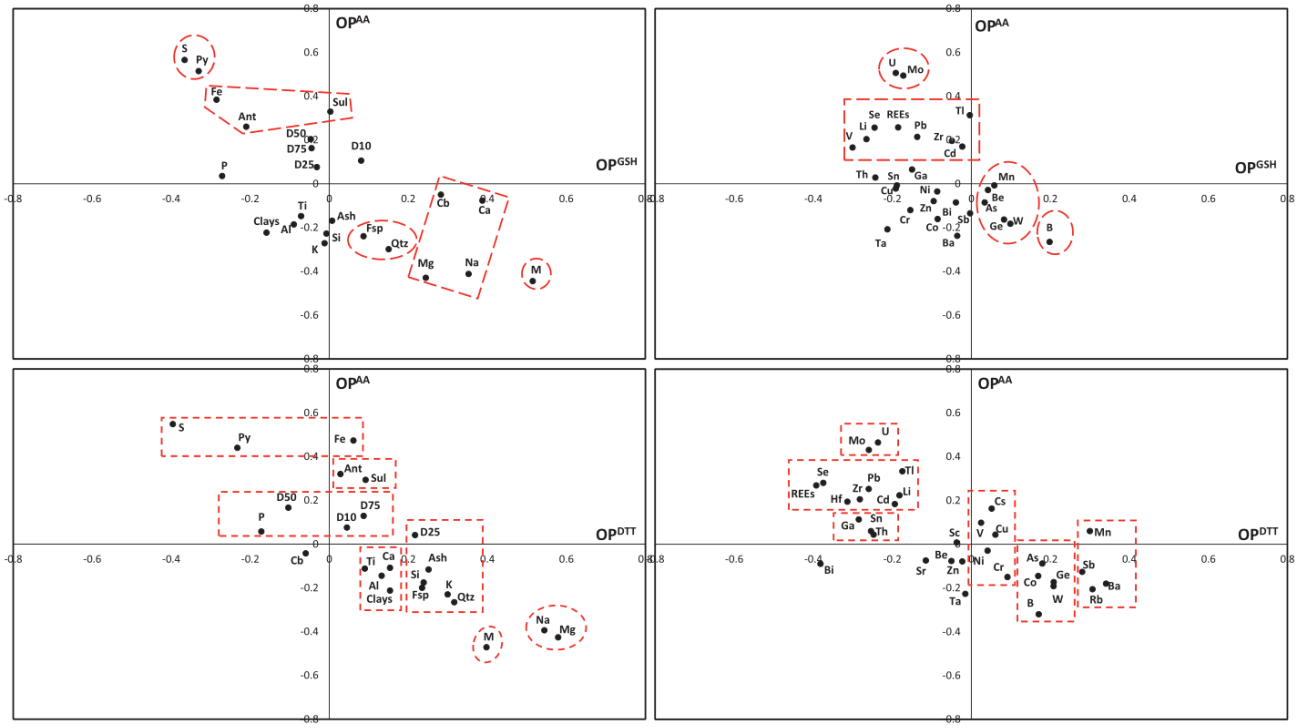

Fig. 5. Cross-correlation plots between the Pearson's correlation coefficients of geochemical parameters with their respective OP^{AA}, OP^{GSH}, and OP^{DTT}. All channel profile samples <4 μm (CP_4) and actual respirable coal mine dust samples showed in Table S4 are evaluated. Py, Pyrite; Ant, Anatase; Sul, Sulphates; Cb, Carbonates; Qtz, Quartz; Fsp, Feldspar; D_{10}, D_{25}, D_{50}, D_{75}, percentiles 10, 25, 50 and 75 of the particle size in μm, respectively; Vol, Volatile Matter; M, Moisture.

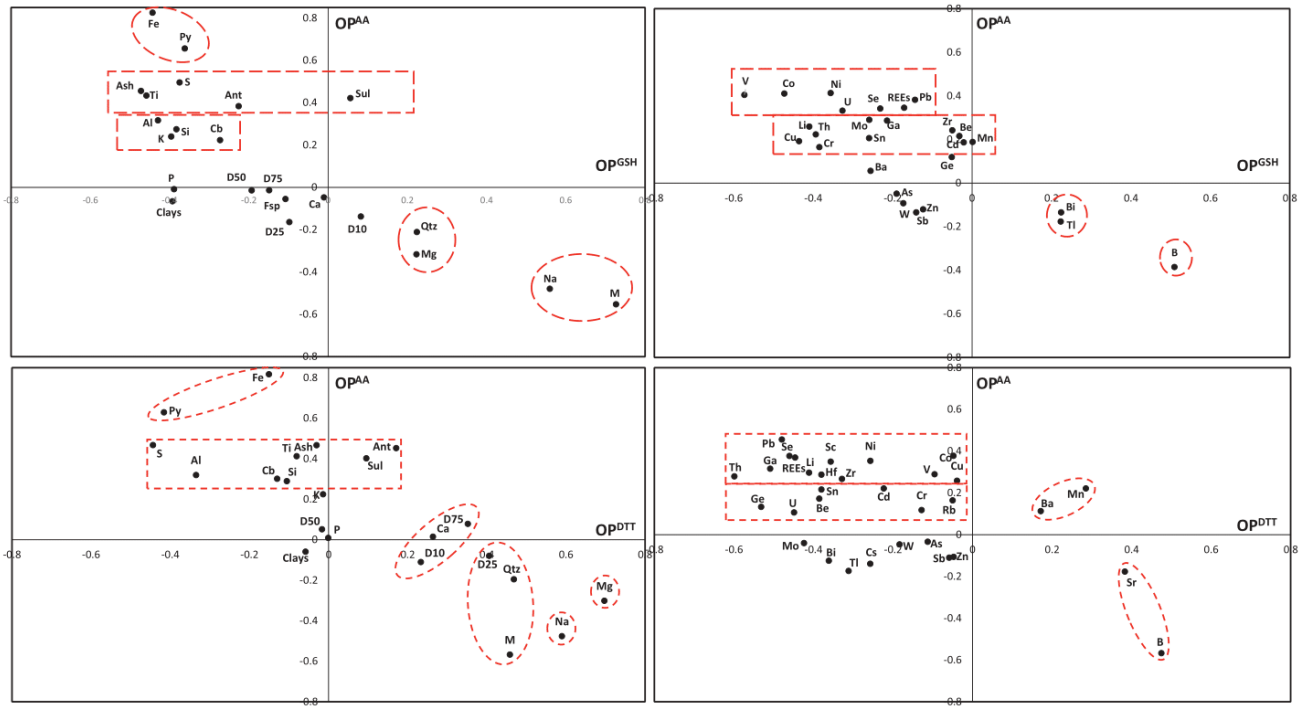

Fig. 6. Cross-correlation plots between the Pearson's correlation coefficients of geochemical parameters with their respective OP^{AA}, OP^{GSH}, and OP^{DTT}. Only the bituminous channel profile samples <4 μm (CP_4) and actual respirable coal mine dust samples showed in Table S4 are evaluated. Py, Pyrite; Ant, Anatase; Sul, Sulphates; Cb, Carbonates; Qtz, Quartz; Fsp, Feldspar; D_{10}, D_{25}, D_{50}, D_{75}, percentiles 10, 25, 50 and 75 of the particle size in μm, respectively; Vol, Volatile Matter; M, Moisture.

coal rank, decreasing as coal rank increases (Stach et al., 1982). However, Attfield and Morring (1992), Huang et al. (2005), Maclaren et al. (1989) and Huang et al. (1998) reported an increase of CWP with coal rank. The C content (% daf) in coal increases (by reducing H and O contents) as coal rank does (Stach et al., 1982), and this might increase specific surface and free radicals in the organic matrix, which could explain its higher cytotoxicity and pathogenicity (Castranova and Vallyathan, 2000; Dalal et al., 1995).

Furthermore, Pedroso-Fidelis et al. (2020) evaluated pulmonary oxidative stress in wild bats exposed to coal dust. They posited that, when Na concentration, among other metals, increased during coal dust exposure, an increased ROS was evident if compared with the control. Additionally, Alcala-Orozco et al. (2020) evidenced coal dust exposure generates a negative regulation in various genes, including GSH, which possibly develop oxidative stress. Moreover, Iram Batool et al. (2020) demonstrated that GSH levels are reduced in the coal miners with high exposure to coal dust, which reveals an elevated level of oxidative stress. They ordered in different levels the exposure of coal dust and the possible effect of workers (underground workers < surface workers < administrative group), supposing and recommending that workers with better health habits nutrition might cause an increase in antioxidant activity protecting the cell of the damage of the oxidative stress.

3.2.4.3. Dithiothreitol oxidative potential (OP^{DTT}). The main coal components showing correlation with OP^{DTT} in this study are Mg, B, moisture content and, to a lesser degree, particle size, quartz, Na, Ca, Mn, Sr, Ge, W, and Ba. As for OP^{GSH}, the results of correlation analysis for OP^{DTT} point to an association with the content of organic matter, as indicated by the correlation with moisture, B, W and Ge.

Furthermore, quartz, and carbonate minerals (traced by Ca, Mg, Sr, Mn) might also have an impact on OP^{DTT}. Mn was found to be associated with OP^{DTT} (Charrier and Anastasio, 2012; Cheng et al., 2021; Gao et al., 2020; Nishita-Hara et al., 2019; Yu et al., 2018). Nishita-Hara et al. (2019) demonstrated a correlation between Mg ($r = 0.56$) and Ba ($r = 0.61$) species with OP^{DTT} for PM from Asian dust events. Moreover, Gao et al. (2020) showed a correlation of Mg- and water insoluble-Mg and -Mn and water soluble-Ca with OP^{DTT}. No association has been identified in prior studies between quartz and OP^{DTT} as has been demonstrated in this study.

Finally, Barraza et al. (2020) found positive correlation between OP^{DTT} and Ba in the North Amazon Region in Ecuador, indicating that Ba is one of the main sources that is associated with ROS, after analysing the principals PM_{10} contributor of oil refining and industrial activities.

4. Conclusions and Recommendations

In this study, the respirable fraction (<4 μm, CP_4) from bulk powdered coal channel profile samples (CP) from various locations in China was obtained in the laboratory. The selection of coal samples was based on analysing a wide coverage of geochemical patterns (major and trace element contents and mineralogy) and coal ranks. As could be expected, CP_4/CP ratios for most elements and minerals were close to 1.0, with the exception of sulphate minerals, Fe, S, Mo, Ge, and Mn, with contents decreasing in CP_4 (CP_4/CP ratios between 0.6 and 0.8), and anatase, Na, Cs, W, Zn, and Zr, increasing in CP_4 (CP_4/CP ratios higher than 1.5).

Oxidative Potential (OP) tests, using Ascorbic Acid (AA) and Glutathione (GSH) as indicators, were performed for the CP_4 coals samples. The total OP ($OP^{TOT} = OP^{AA} + OP^{GSH}$) of CP_4 is relatively low (1.2%OP^{TOT}μg^{-1}) when compared with that reported for other particulate matter (PM), such as PM from subway systems (2.5%$OP^{TOT}\cdot\mu g^{-1}$), roadsides (3.6%$OP^{TOT}\cdot\mu g^{-1}$), or urban background pollution (1.5 to 4.0%$OP^{TOT}\cdot\mu g^{-1}$). The cross-correlation analysis shows that OP^{AA} is linked to specific inorganic components, whereas OP^{GSH} and dithiothreitol (OP^{DTT}) are related to organic components.

Furthermore, the OP correlation with specific components increases when the analysis is done for a specific coal rank (bituminous). Thus,

the correlation of Fe and pyrite with OP^{AA} reached r = 0.69 and 0.54, respectively, which increased to 0.80 and 0.70, respectively when only bituminous coals were considered. Moreover, their correlation remains, Fe (r = 0.83) and pyrite (r = 0.66) when only bituminous coals and coals dust are taken into account. This fact could demonstrate that bituminous coals contain more oxidising species of Fe and pyrite, which are more likely to generate reactive oxygen species (ROS) and are also transmitted to bituminous coal dust. However also that the scattering of the regression is smaller by reducing the potential effect of rank-related parameters on OP.

On the other hand, moisture content (as an indicator of the coaly organic matter content) is correlated with OP^{GSH} (r = 0.67), and these associations are stronger for bituminous coals (r = 0.78). Furthermore, moisture-OP^{GSH} correlation in bituminous coals and coal dust are also important, r = 0.73. This is the same with OP^{DTT} indicator, which shows an increased correlation with the parameters in bituminous coals for Mg and Na (ineffective in coal and bituminous coals), starting with low correlations of Mg (r = 0.31), increasing in bituminous coals, Mg (r = 0.44), and rising after bituminous coal and coal dust combinations, Mg (r = 0.70) and Na (r = 0.59).

To validate the method used (extraction of CP_4 to determine the OP of the derived respirable coal dust, RD) a correlation re-analysis was carried out by including actual RD and associated OP data from prior studies. This re-analysis conformed most of the results obtained for CP_4, especially when considering only bituminous coals. The results demonstrate that noticeable associations of Fe (r = 0.83) and pyrite (r = 0.66) are clearly linked with OP^{AA}. Organic matter, as identified by the parameters of moisture (r = 0.73), Na (r = 0.56) and B (r = 0.51) control OP^{GSH}, whereas Mg (r = 0.70) and Na (r = 0.59) are associated with OP^{DTT}.

A multilinear regression analysis allowed the geochemical associations with OP to be categorised. The results indicate that Fe, pyrite and sulphate minerals (indicating acidic species from pyrite oxidation) showing high correlation with elevated r (0.8–0.9), followed by anatase, and in a much lower proportion U, Mo, V and Pb, clearly govern the OP^{AA} of CP_4 and RD; while the contents of organic matter (traced by those of moisture, B and the coarse size, r = 0.85–0.75), Ca, carbonate minerals control OP^{GSH}; and those of Mg, Na, quartz, organic matter and Ba regulate OP^{DTT}, with r coefficients approximate to 0.7.

The results support the conclusions drawn from Harrington et al. (2012) and Huang et al. (2005) concerning the relevance of the Fe and pyrite contents in inhalable particles from coal dust ability to lead to oxidative stress, which, in turn, may lead to lung injury and coal workers' pneumoconiosis (CWP) development. Moreover, correlations obtained are in concordance with other similar studies (Zazouli et al., 2021). The results also show that the organic matter of coal can increase OP^{DTT} and OP^{GSH}. Thus, the results highlight the need to implement high efficiency primary and secondary coal dust abatement measures in coal mines, especially in the mining of high pyrite coals. As intensive coal mining in China will continue in the forthcoming decades and because the production has increased dramatically since 2000, a large number of miners are exposed to coal dust, and research on coal dust and occupational health and on coal dust abatement controls should be continuously supported.

Credit authorship contribution statement

The corresponding author, Pedro Trechera, is responsible for ensuring that the descriptions are accurate and agreed by all authors, participated in sampling, did analyses and writing.

Teresa Moreno discussed results, wrote some sections and reviewed manuscript.

Natalia Moreno did DRX analyses, discussed results and reviewed manuscript.

Joaquim Cortés did some chemical and separation analysis, discussed results and reviewed manuscript.

Fulvio Amato reviewed manuscript.

Zhuang Xinguo, Baoqing Li, Jing Li, Yunfei Shangguan and Patricia Córdoba, participated in sampling, discussed results and reviewed manuscript.

Ana Oliete and Frank Kelly did some OP analysis, wrote a section and reviewed manuscript.

Takoua Mhadhbi, Jean Luc Jaffrezo and Gaelle Uzu did some OP analysis, wrote a section and reviewed manuscript.

Xavier Querol participated in sampling, did some analysis, discussed results, wrote some sections and reviewed the manuscript.

Declaration of competing interest

The authors declare that they have no known competing financial interests or personal relationships that could have appeared to influence the work reported in this paper.

Acknowledgments

This study was supported by Generalitat de Catalunya (AGAUR 2017 SGR41), Spain; by the National Science Foundation of China (grant 41972180); the Program of Introducing Talents of Discipline to Universities (grant B14031) and Overseas Top Scholars Program for the Recruitment of Global Experts, China; and by the Spanish Ministry of Science and Innovation (Excelencia Severo Ochoa, Project CEX2018-000794-S). Malvern Mastersizer Scirocco 2000 extension measurements were performed at the ICTS NANBIOSIS by the Nanostructured Liquids Unit (U12) of the CIBER in Bioengineering, Biomaterials & Nanomedicine (CIBER-BBN), located at the IQAC-CSIC (Barcelona, Spain). Pedro Trechera is contracted by the ROCD (Reducing risks from Occupational exposure to Coal Dust) project supported by the European Commission Research Fund for Coal and Steel; Grant Agreement Number 754205.

Appendix A. Supplementary data

Supplementary data to this article can be found online at https://doi.org/10.1016/j.scitotenv.2021.149486.

References

Ahamed, M.A.A., Perera, M.S.A., Matthai, S.K., Ranjith, P.G., Dong-yin, L., 2019. Coal composition and structural variation with rank and its influence on the coal-moisture interactions under coal seam temperature conditions – a review article. J. Pet. Sci. Eng. https://doi.org/10.1016/j.petrol.2019.06.007.

Alcala-Orozco, M., Caballero-Gallardo, K., Olivero-Verbel, J., 2020. Intergenerational effects of coal dust on Tribolium castaneum. Herbst. Environ. Res. 182, 109055. https://doi.org/10.1016/j.envres.2019.109055.

Allardice, D.J., Clemow, L.M., Jackson, W.R., 2003. Determination of the acid distribution and total acidity of low-rank coals and coal-derived materials by an improved barium exchange technique. Fuel 82, 35–40. https://doi.org/10.1016/S0016-2361(02)00193-X.

Aruoma, O.I., 1998. Free radicals, oxidative stress, and antioxidants in human health and disease. J. Am. Oil Chem. Soc. 75, 199–212. https://doi.org/10.1007/s11746-998-0032-9.

Attfield, M.D., Morring, K., 1992. An investigation into the relationship between coal workers' pneumoconiosis and dust exposure in U.S. coal miners. Am. Ind. Hyg. Assoc. J. 53, 486–492. https://doi.org/10.1080/15298669291360012.

Ávila Júnior, S., Possamai, F.P., Budni, P., Backes, P., Parisotto, E.B., Rizelio, V.M., Torres, M.A., Colepicolo, P., Wilhelm Filho, D., 2009. Occupational airborne contamination in South Brazil: 1. oxidative stress detected in the blood of coal miners. Ecotoxicology 18, 1150–1157. https://doi.org/10.1007/s10646-009-0364-8.

Ayres, J.G., Borm, P., Cassee, F.R., Castranova, V., Donaldson, K., Ghio, A., Harrison, R.M., Hider, R., Kelly, F., Kooter, I.M., Marano, F., Maynard, R.L., Mudway, I., Nel, A., Sioutas, C., Smith, S., Baeza-Squiban, A., Cho, A., Duggan, S., Froines, J., 2008. Evaluating the toxicity of airborne particulate matter and nanoparticles by measuring oxidative stress potential - A workshop report and consensus statement. Inhalation Toxicology. Taylor & Francis, pp. 75–99 https://doi.org/10.1080/08958370701665517.

Baker, M.A., Cerniglia, G.J., Zaman, A., 1990. Microtiter plate assay for the measurement of glutathione and glutathione disulfide in large numbers of biological samples. Anal. Biochem. 190, 360–365. https://doi.org/10.1016/0003-2697(90)90208-Q.

Barraza, F., Uzu, G., Jaffrezo, J.-L., Schreck, E., Budzinski, H., Le Menach, K., Dévier, M.-H., Guyard, H., Calas, A., Perez, M.-I., Villacreces, L.-A., Maurice, L., 2020. Contrasts in chemical composition and oxidative potential in PM10 near flares in oil extraction

and refining areas in Ecuador. Atmos. Environ. 223, 117302. https://doi.org/10.1016/j.atmosenv.2020.117302.
Borm, P.J.A., Kelly, F., Künzli, N., Schins, R.P.F., Donaldson, K., 2007. Oxidant generation by particulate matter: from biologically effective dose to a promising, novel metric. Occup. Environ. Med. https://doi.org/10.1136/oem.2006.029090.
BP, 2020. BP Statistical Review of World Energy 2020.
Brown, J.S., Gordon, T., Price, O., Asgharian, B., 2013. Thoracic and respirable particle definitions for human health risk assessment. Part. Fibre Toxicol. 10, 12. https://doi.org/10.1186/1743-8977-10-12.
Calas, A., Uzu, G., Kelly, F.J., Houdier, S., Martins, J.M.F., Thomas, F., Molton, F., Charron, A., Dunster, C., Oliete, A., Jacob, V., Besombes, J.-L., Chevrier, F., Jaffrezo, J.-L., 2018. Comparison between five acellular oxidative potential measurement assays performed with detailed chemistry on PM₁₀ samples from the city of Chamonix (France). Atmos. Chem. Phys. 18, 7863–7875. https://doi.org/10.5194/acp-18-7863-2018.
Castranova, V., 2000. From coal mine dust to quartz: mechanisms of pulmonary pathogenicity. Inhal. Toxicol. 12, 7–14. https://doi.org/10.1080/08958378.2000.11463226.
Castranova, V., Vallyathan, V., 2000. Silicosis and coal workers' pneumoconiosis. Environ. Health Perspect. 108, 675–684. https://doi.org/10.1289/ehp.00108s4675.
Charrier, J.G., Anastasio, C., 2012. On dithiothreitol (DTT) as a measure of oxidative potential for ambient particles: evidence for the importance of soluble \newline transition metals. Atmos. Chem. Phys. 12, 9321–9333. https://doi.org/10.5194/acp-12-9321-2012.
Chen, H., Feng, Q., Long, R., Qi, H., 2013. Focusing on coal miners' occupational disease issues: a comparative analysis between China and the United States. Saf. Sci. 51, 217–222. https://doi.org/10.1016/j.ssci.2012.06.025.
Cheng, Y., Ma, Y., Dong, B., Qiu, X., Hu, D., 2021. Pollutants from primary sources dominate the oxidative potential of water-soluble PM2.5 in Hong Kong in terms of dithiothreitol (DTT) consumption and hydroxyl radical production. J. Hazard. Mater. 405, 124218. https://doi.org/10.1016/j.jhazmat.2020.124218.
Choi, H., Thiruppathiraja, C., Kim, S., Rhim, Y., Lim, J., Lee, S., 2011. Moisture readsorption and low temperature oxidation characteristics of upgraded low rank coal. Fuel Process. Technol. 92, 2005–2010. https://doi.org/10.1016/j.fuproc.2011.05.025.
Christian, R.T., Nelson, J.B., Cody, T.E., Larson, E., Bingham, E., 1979. Coal workers' pneumoconiosis: in vitro study of the chemical composition and particle size as causes of the toxic effects of coal. Environ. Res. 20, 358–365. https://doi.org/10.1016/0013-9351(79)90012-4.
Chung, F.H., 1974. Quantitative interpretation of X-ray diffraction patterns of mixtures. I. Matrix-flushing method for quantitative multicomponent analysis. J. Appl. Crystallogr. 7, 519–525. https://doi.org/10.1107/s0021889874010375.
Cohn, C.A., Laffers, R., Schoonen, M.A.A., 2006a. Using yeast RNA as a probe for generation of hydroxyl radicals by earth materials. Environ. Sci. Technol. 40, 2838–2843. https://doi.org/10.1021/es052301k.
Cohn, C.A., Laffers, R., Simon, S.R., O'riordan, T., Schoonen, M.A., 2006b. Role of Pyrite in Formation of Hydroxyl Radicals in Coal: Possible Implications for Human Health. https://doi.org/10.1186/1743-8977-3-16.
Daellenbach, K.R., Uzu, G., Jiang, J., Cassagnes, L.E., Leni, Z., Vlachou, A., Stefenelli, G., Canonaco, F., Weber, S., Segers, A., Kuenen, J.J.P., Schaap, M., Favez, O., Albinet, A., Aksoyoglu, S., Dommen, J., Baltensperger, U., Geiser, M., El Haddad, I., Jaffrezo, J.L., Prévôt, A.S.H., 2020. Sources of particulate-matter air pollution and its oxidative potential in Europe. Nature 587, 414–419. https://doi.org/10.1038/s41586-020-2902-8.
Dai, S., Ren, D., Hou, X., Shao, L., 2003. Geochemical and mineralogical anomalies of the late Permian coal in the Zhijin coalfield of Southwest China and their volcanic origin. Int. J. Coal Geol. 55, 117–138. https://doi.org/10.1016/S0166-5162(03)00083-1.
Dai, S.F., Zhou, Y.P., Ren, D.Y., Wang, X.B., Li, D., Zhao, L., 2007. Geochemistry and mineralogy of the Late Permian coals from the Songzo Coalfield, Chongqing, southwestern China. Sci. China Ser. D Earth Sci. 50, 678–688. https://doi.org/10.1007/s11430-007-0001-4.
Dai, S., Ren, D., Zhou, Y., Chou, C.L., Wang, X., Zhao, L., Zhu, X., 2008. Mineralogy and geochemistry of a superhigh-organic-sulfur coal, Yanshan Coalfield, Yunnan, China: evidence for a volcanic ash component and influence by submarine exhalation. Chem. Geol. 255, 182–194. https://doi.org/10.1016/j.chemgeo.2008.06.030.
Dai, S., Wang, X., Chen, W., Li, D., Chou, C.L., Zhou, Y., Zhu, C., Li, H., Zhu, X., Xing, Y., Zhang, W., Zou, J., 2010. A high-pyrite semianthracite of Late Permian age in the Songzao Coalfield, southwestern China: mineralogical and geochemical relations with underlying mafic tuffs. Int. J. Coal Geol. 83, 430–445. https://doi.org/10.1016/j.coal.2010.06.004.
Dai, S., Jiang, Y., Ward, C.R., Gu, L., Seredin, V.V., Liu, H., Zhou, D., Wang, X., Sun, Y., Zou, J., Ren, D., 2012. Mineralogical and geochemical compositions of the coal in the guanbanwusu mine, Inner Mongolia, China: further evidence for the existence of an Al (Ga and REE) ore deposit in the jungar coalfield. Int. J. Coal Geol. 98, 10–40. https://doi.org/10.1016/j.coal.2012.03.003.
Dai, S., Graham, I.T., Ward, C.R., 2016. A review of anomalous rare earth elements and yttrium in coal. Int. J. Coal Geol. 159, 82–95. https://doi.org/10.1016/j.coal.2016.04.005.
Dalal, N.S., Newman, J., Pack, D., Leonard, S., Vallyathan, V., 1995. Hydroxyl radical generation by coal mine dust: possible implication to coal workers' pneumoconiosis (CWP). Free Radic. Biol. Med. 18, 11–20. https://doi.org/10.1016/0891-5849(94)E0094-Y.
Dodson, J., Li, X., Sun, N., Atahan, P., Zhou, X., Liu, H., Zhao, K., Hu, S., Yang, Z., 2014. Use of coal in the Bronze Age in China. The Holocene 24, 525–530. https://doi.org/10.1177/0959683614523155.
Du, F., Qiao, J., Zhao, X., Tan, F., Li, C., Luo, Z., 2021. Enrichment of V in Late Permian coals in Gemudi Mine, Western Guizhou, SW China. J. Geochem. Explor. 221, 106701. https://doi.org/10.1016/j.gexplo.2020.106701.
European Committee for Standardization, 1992. Workplace Atmospheres: Size Fraction Definitions for Measurement of Airborne Particles in the Workplace, CEN - EN 481.
Fan, Y., Xia, Y., 2012. Exploring energy consumption and demand in China. Energy 40, 23–30. https://doi.org/10.1016/j.energy.2011.09.049.
Fan, Z., Xu, F., 2021. Health risks of occupational exposure to toxic chemicals in coal mine workplaces based on risk assessment mathematical model based on deep learning. Environ. Technol. Innov. 22, 101500. https://doi.org/10.1016/j.eti.2021.101500.
Fang, T., Guo, H., Zeng, L., Verma, V., Nenes, A., Weber, R.J., 2017. Highly acidic ambient particles, soluble metals, and oxidative potential: a link between sulfate and aerosol toxicity. Environ. Sci. Technol. 51, 40. https://doi.org/10.1021/acs.est.6b06151.
Fang, T., Lakey, P.S.J., Weber, R.J., Shiraiwa, M., 2019. Oxidative potential of particulate matter and generation of reactive oxygen species in epithelial lining fluid. Environ. Sci. Technol. 53, 12784–12792. https://doi.org/10.1021/acs.est.9b03823.
Finkelman, R.B., Orem, W., Castranova, V., Tatu, C.A., Belkin, H.E., Zheng, B., Lerch, H.E., Maharaj, S.V., Bates, A.L., 2002. Health impacts of coal and coal use: possible solutions. Int. J. Coal Geol. 50, 425–443. https://doi.org/10.1016/S0166-5162(02)00125-8.
Fu, P.P., Xia, Q., Hwang, H.M., Ray, P.C., Yu, H., 2014. Mechanisms of nanotoxicity: generation of reactive oxygen species. J. Food Drug Anal. 22, 64–75. https://doi.org/10.1016/j.jfda.2014.01.005.
Fubini, B., Hubbard, A., 2003. Reactive oxygen species (ROS) and reactive nitrogen species (RNS) generation by silica in inflammation and fibrosis. Free Radic. Biol. Med. https://doi.org/10.1016/S0891-5849(03)00149-7.
Gao, D., Mulholland, J.A., Russell, A.G., Weber, R.J., 2020. Characterization of water-insoluble oxidative potential of PM2.5 using the dithiothreitol assay. Atmos. Environ. 224, 117327. https://doi.org/10.1016/j.atmosenv.2020.117327.
Gelegdorj, E., Chunag, A., Gordon, R.B., Park, J.S., 2007. Transitions in cast iron technology of the nomads in Mongolia. J. Archaeol. Sci. 34, 1187–1196. https://doi.org/10.1016/j.jas.2006.10.007.
Gilmour, M.I., O'Connor, S., Dick, C.A.J., Miller, C.A., Linak, W.P., 2004. Differential pulmonary inflammation and in vitro cytotoxicity of size-fractionated fly ash particles from pulverized coal combustion. J. Air Waste Manage. Assoc. 54, 286–295. https://doi.org/10.1080/10473289.2004.10470906.
Godri, K.J., Harrison, R.M., Evans, T., Baker, T., Dunster, C., Mudway, I.S., Kelly, F.J., 2011. Increased oxidative burden associated with traffic component of ambient particulate matter at roadside and urban background schools sites in London. PLoS One 6, e21961. https://doi.org/10.1371/journal.pone.0021961.
Guo, J., Yao, D., Chen, P., Chen, J., Shi, F., 2017. Distribution, enrichment and modes of occurrence of arsenic in Chinese coals. Minerals 7. https://doi.org/10.3390/min7070114.
Hamilton, R.F., Wu, N., Porter, D., Buford, M., Wolfarth, M., Holian, A., 2009. Particle length-dependent titanium dioxide nanomaterials toxicity and bioactivity. Part. Fibre Toxicol. 6, 1–11. https://doi.org/10.1186/1743-8977-6-35.
Han, S., Chen, H., Long, R., Cui, X., 2018. Peak coal in China: a literature review. Resour. Conserv. Recycl. 129, 293–306. https://doi.org/10.1016/j.resconrec.2016.08.012.
Harrington, A.D., Hylton, S., Schoonen, M.A.A., 2012. Pyrite-driven reactive oxygen species formation in simulated lung fluid: implications for coal workers' pneumoconiosis. Environ. Geochem. Health 34, 527–538. https://doi.org/10.1007/s10653-011-9438-7.
Huang, X., Finkelman, R.B., 2008. Understanding the chemical properties of macerals and minerals in coal and its potential application for occupational lung disease prevention. J. Toxicol. Environ. Health - Part B Crit. Rev. https://doi.org/10.1080/10937400701600552.
Huang, X., Fournier, J., Koenig, K., Chen, L.C., 1998. Content: Possible Role in Coal Workers' Pneumoconiosis, pp. 722–729.
Huang, C., Li, J., Zhang, Q., Huang, X., 2002. Role of bioavailable iron in coal dust-induced activation of activator protein-1 and nuclear factor of activated T cells: difference between Pennsylvania and Utah coal dusts. Am. J. Respir. Cell Mol. Biol. 27, 568–574. https://doi.org/10.1165/rcmb.4821.
Huang, X., Li, W., Attfield, M.D., Nádas, A., Frenkel, K., Finkelman, R.B., 2005. Mapping and prediction of coal workers' pneumoconiosis with bioavailable iron content in the bituminous coals. Environ. Health Perspect. 113, 964–968. https://doi.org/10.1289/ehp.7679.
IEA, 2020. World Energy Outlook 2020. IEA, Paris, p. 124.
Imai, Y., Kuba, K., Neely, G.G., Yaghubian-Malhami, R., Perkmann, T., van Loo, G., Ermolaeva, M., Veldhuizen, R., Leung, Y.H.C., Wang, H., Liu, H., Sun, Y., Pasparakis, M., Kopf, M., Mech, C., Bavari, S., Peiris, J.S.M., Slutsky, A.S., Akira, S., Hultqvist, M., Holmdahl, R., Nicholls, J., Jiang, C., Binder, C.J., Penninger, J.M., 2008. Identification of oxidative stress and toll-like receptor 4 signaling as a key pathway of acute lung injury. Cell 133, 235–249. https://doi.org/10.1016/j.cell.2008.02.043.
Iram Batool, A., Huma Naveed, N., Aslam, M., da Silva, J., Rehman, M., 2020. Coal Dust-induced Systematic Hypoxia and Redox Imbalance Among Coal Mine Workers. https://doi.org/10.1021/acsomega.0c03977.
Iriyama, K., Yoshiura, M., Iwamoto, T., Ozaki, Y., 1984. Simultaneous determination of uric and ascorbic acids in human serum by reversed-phase high-performance liquid chromatography with electrochemical detection. Anal. Biochem. 141, 238–243. https://doi.org/10.1016/0003-2697(84)90451-2.
Ishtiaq, M., Jehan, N., Khan, S.A., Muhammad, S., Saddique, U., Iftikhar, B., Zahidullah, 2018. Potential harmful elements in coal dust and human health risk assessment near the mining areas in Cherat, Pakistan. Environ. Sci. Pollut. Res. 25, 14666–14673. https://doi.org/10.1007/s11356-018-1655-5.
Izquierdo, M., Querol, X., 2012. Leaching behaviour of elements from coal combustion fly ash: an overview. Int. J. Coal Geol. https://doi.org/10.1016/j.coal.2011.10.006.
Janssen, N.A.H., Yang, A., Strak, M., Steenhof, M., Hellack, B., Gerlofs-Nijland, M.E., Kuhlbusch, T., Kelly, F., Harrison, R., Brunekreef, B., Hoek, G., Cassee, F., 2014. Oxidative potential of particulate matter collected at sites with different source characteristics. Sci. Total Environ. 472, 572–581. https://doi.org/10.1016/j.scitotenv.2013.11.099.

Jie, D., Xu, X., Guo, F., 2020. The future of coal supply in China based on non-fossil energy development and carbon price strategies. Energy 220, 119644. https://doi.org/10.1016/j.energy.2020.119644.
Kelly, F.J., 2003. Oxidative stress: its role in air pollution and adverse health effects. Occup. Environ. Med. 60, 612–616. https://doi.org/10.1136/oem.60.8.612.
Kim, Y.H., Warren, S.H., Krantz, Q.T., King, C., Jaskot, R., Preston, W.T., George, B.J., Hays, M.D., Landis, M.S., Higuchi, M., DeMarini, D.M., Gilmour, M.I., 2018. Mutagenicity and lung toxicity of smoldering vs. flaming emissions from various biomass fuels: implications for health effects from wildland fires. Environ. Health Perspect. 126, 017011. https://doi.org/10.1289/EHP2200.
Landen, D.D., Wassell, J.T., McWilliams, L., Patel, A., 2011. Coal dust exposure and mortality from ischemic heart disease among a cohort of U.S. coal miners. Am. J. Ind. Med. 54, 727–733. https://doi.org/10.1002/ajim.20986.
Lashgari, A., Kecojevic, V., 2016. Comparative analysis of dust emission of digging and loading equipment in surface coal mining. Int. J. Mining Reclam. Environ. 30, 181–196. https://doi.org/10.1080/17480930.2015.1028516.
Latvala, S., Hedberg, J., Bucchianico, S.Di, Möller, L., Odnevall Wallinder, I., Elihn, K., Karlsson, H.L., 2016. Nickel Release, ROS Generation and Toxicity of Ni and NiO Micro-and Nanoparticles. https://doi.org/10.1371/journal.pone.0159684.
Leni, Z., Cassagnes, L.E., Daellenbach, K.R., Haddad, I.El, Vlachou, A., Uzu, G., Prévôt, A.S.H., Jaffrezo, J.L., Baumlin, N., Salathe, M., Baltensperger, U., Dommen, J., Geiser, M., 2020. Oxidative stress-induced inflammation in susceptible airways by anthropogenic aerosol. PLoS One 15, 1–17. https://doi.org/10.1371/journal.pone.0233425.
Li, W., Lu, D., 1995. Industrial Geography of China.
Li, J., Zhuang, X., Querol, X., 2011. Trace element affinities in two high-Ge coals from China. Fuel 90, 240–247. https://doi.org/10.1016/j.fuel.2010.08.011.
Li, J., Zhuang, X., Querol, X., Font, O., Moreno, N., Zhou, J., Lei, G., 2012. High quality of Jurassic coals in the Southern and Eastern Junggar Coalfields, Xinjiang, NW China: geochemical and mineralogical characteristics. Int. J. Coal Geol. 99, 1–15. https://doi.org/10.1016/j.coal.2012.05.003.
Li, B., Zhuang, X., Li, J., Zhao, S., 2014. Geological controls on coal quality of the Yili Basin, Xinjiang, Northwest China. Int. J. Coal Geol. 131, 186–199. https://doi.org/10.1016/j.coal.2014.06.013.
Li, B., Zhuang, X., Li, J., Querol, X., Font, O., Moreno, N., 2016. Geological controls on mineralogy and geochemistry of the Late Permian coals in the Liulong Mine of the Liuzhi Coalfield, Guizhou Province, Southwest China. Int. J. Coal Geol. 154–155, 1–15. https://doi.org/10.1016/j.coal.2015.12.003.
Li, J., Zhuang, X., Yuan, W., Liu, B., Querol, X., Font, O., Moreno, N., Li, Jianfu, Gang, T., Liang, G., 2016. Mineral composition and geochemical characteristics of the Li-Ga-rich coals in the Buertaohai-Tianjiashipan mining district, Jungar Coalfield, Inner Mongolia. Int. J. Coal Geol. 167, 157–175. https://doi.org/10.1016/j.coal.2016.09.018.
Li, B., Zhuang, X., Li, J., Querol, X., Font, O., Moreno, N., 2017. Enrichment and distribution of elements in the Late Permian coals from the Zhina Coalfield, Guizhou Province, Southwest China. Int. J. Coal Geol. 171, 111–129. https://doi.org/10.1016/j.coal.2017.01.003.
Li, B., Zhuang, X., Querol, X., Li, J., Moreno, N., Córdoba, P., Shangguan, Y., Zhou, J., Ma, X., Liu, S., 2019a. Geological controls on enrichment of Mn, Nb (Ta), Zr (Hf), and REY within the Early Permian coals of the Jimunai Depression, Xinjiang Province, NW China. Int. J. Coal Geol. 215, 103298. https://doi.org/10.1016/j.coal.2019.103298.
Li, B., Zhuang, X., Querol, X., Moreno, N., Yang, L., Shangguan, Y., Li, J., 2019b. Mineralogy and geochemistry of Late Permian coals within the Tongzi Coalfield in Guizhou Province, Southwest China. Minerals 10, 44. https://doi.org/10.3390/min10010044.
Li, J., Xie, C., Long, H., 2019. The roles of inter-fuel substitution and inter-market contagion in driving energy prices: evidences from China's coal market. Energy Econ. 84, 104525. https://doi.org/10.1016/j.eneco.2019.104525.
Li, B., Zhuang, X., Querol, X., Moreno, N., Córdoba, P., Shangguan, Y., Yang, L., Li, J., Zhang, F., 2020. Geological controls on the distribution of REY-Zr (Hf)-Nb (Ta) enrichment horizons in late Permian coals from the Qiandongbei Coalfield, Guizhou Province, SW China. Int. J. Coal Geol. 231, 103604. https://doi.org/10.1016/j.coal.2020.103604.
Li, J., Wu, P., Yang, G., Pan, L., Zhuang, X., Querol, X., Moreno, N., Li, B., Shangguan, Y., 2020. Enrichment of Li–Ga–Zr–Hf and Se–Mo–Cr–V–As–Pb assemblages in the No. 11 superhigh organic sulfur coal from the Sangshuping Coal Mine, Weibei Coalfield, Shaanxi, North China. Energies 13, 6660. https://doi.org/10.3390/en13246660.
Li, B., Liu, G., Bi, M.S., Li, Z.B., Han, B., Shu, C.M., 2021. Self-ignition risk classification for coal dust layers of three coal types on a hot surface. Energy 216, 119197. https://doi.org/10.1016/j.energy.2020.119197.
Lighty, J.S., Veranth, J.M., Sarofim, A.F., 2000. Combustion aerosols: factors governing their size and composition and implications to human health. J. Air Waste Manage. Assoc. 50, 1565–1618. https://doi.org/10.1080/10473289.2000.10464197.
Lin, B., Tan, R., 2017. Estimating energy conservation potential in China's energy intensive industries with rebound effect. J. Clean. Prod. 156, 899–910. https://doi.org/10.1016/j.jclepro.2017.04.100.
Liu, T., Liu, S., 2020. The impacts of coal dust on miners' health: a review. Environ. Res. https://doi.org/10.1016/j.envres.2020.109849.
Liu, R., Zhou, G., Wang, C., Jiang, W., Wei, X., 2020. Preparation and performance characteristics of an environmentally-friendly agglomerant to improve the dry dust removal effect for filter material. J. Hazard. Mater. 397, 122734. https://doi.org/10.1016/j.jhazmat.2020.122734.
Liu, J., Spiro, B.F., Dai, S., French, D., Graham, I.T., Wang, X., Zhao, L., Zhao, J., Zeng, R., 2021. Strontium isotopes in high- and low-Ge coals from the Shengli Coalfield, Inner Mongolia, northern China: new indicators for Ge source. Int. J. Coal Geol. 233, 103642. https://doi.org/10.1016/j.coal.2020.103642.
Lloyd, D.R., Phillips, D.H., 1999. Oxidative DNA damage mediated by copper(II), iron(II) and nickel(II) Fenton reactions: evidence for site-specific mechanisms in the formation of double-strand breaks, 8-hydroxydeoxyguanosine and putative intrastrand cross-links. Mutat. Res. - Fundam. Mol. Mech. Mutagen. 424, 23–36. https://doi.org/10.1016/S0027-5107(99)00005-6.
Ma, D., Qin, B., Gao, Y., Jiang, J., Feng, B., 2020. Study on the explosion characteristics of methane–air with coal dust originating from low-temperature oxidation of coal. Fuel 260, 116304. https://doi.org/10.1016/j.fuel.2019.116304.
Maclaren, W.M., Hurley, J.F., Collins, P.R., Cowie, A.J., 1989. Factors associated with the development of progressive massive fibrosis in British coalminers: a case-control study. Br. J. Ind. Med. 46, 597–607. https://doi.org/10.1136/oem.46.9.597.
MacNee, W., 2001. Oxidative stress and lung inflammation in airways disease. Eur. J. Pharmacol. https://doi.org/10.1016/S0014-2999(01)01320-6.
Mao, J.X., Tong, H.L., 2013. Coal resources, production and use in China. The Coal Handbook: Towards Cleaner Production. Elsevier Inc., pp. 220–234 https://doi.org/10.1533/9781782421177.2.220.
Masto, R.E., George, J., Rout, T.K., Ram, L.C., 2017. Multi element exposure risk from soil and dust in a coal industrial area. J. Geochem. Explor. 176, 100–107. https://doi.org/10.1016/j.gexplo.2015.12.009.
McCunney, R.J., Morfeld, P., Payne, S., 2009. What component of coal causes coal workers' pneumoconiosis? J. Occup. Environ. Med. 51, 462–471. https://doi.org/10.1097/JOM.0b013e3181a01ada.
Mo, J., Wang, L., Au, W., Su, M., 2014. Prevalence of coal workers' pneumoconiosis in China: a systematic analysis of 2001-2011 studies. Int. J. Hyg. Environ. Health https://doi.org/10.1016/j.ijheh.2013.03.006.
Moreno, T., Amato, F., Querol, X., Alastuey, A., Gibbons, W., 2008. Trace element fractionation processes in resuspended mineral aerosols extracted from australian continental surface materials. Soil Res. 46, 128. https://doi.org/10.1071/SR07121.
Moreno, T., Kelly, F.J., Dunster, C., Oliete, A., Martins, V., Reche, C., Minguillón, M.C., Amato, F., Capdevila, M., de Miguel, E., Querol, X., 2017. Oxidative potential of subway PM2.5. Atmos. Environ. 148, 230–238. https://doi.org/10.1016/j.atmosenv.2016.10.045.
Moreno, T., Trechera, P., Querol, X., Lah, R., Johnson, D., Wrana, A., Williamson, B., 2019. Trace element fractionation between PM10 and PM2.5 in coal mine dust: implications for occupational respiratory health. Int. J. Coal Geol. 203, 52–59. https://doi.org/10.1016/j.coal.2019.01.006.
Munir, M.A.M., Liu, G., Yousaf, B., Ali, M.U., Abbas, Q., Ullah, H., 2018. Enrichment of Bi-Be-Mo-Cd-Pb-Nb-Ga, REEs and Y in the Permian coals of the Huainan Coalfield, Anhui China. Ore Geol. Rev. 95, 431–455. https://doi.org/10.1016/j.oregeorev.2018.02.037.
Murphy, R., Strongin, D.R., 2009. Surface reactivity of pyrite and related sulfides. Surf. Sci. Rep. https://doi.org/10.1016/j.surfrep.2008.09.002.
Nardi, J., Nascimento, S., Göethel, G., Gauer, B., Sauer, E., Fão, N., Cestonaro, L., Peruzzi, C., Souza, J., Garcia, S.C., 2018. Inflammatory and oxidative stress parameters as potential early biomarkers for silicosis. Clin. Chim. Acta https://doi.org/10.1016/j.cca.2018.05.045.
NIOSH, 2002. Health Effects of Occupational Exposure to Respirable Crystalline Silica. Department of Health and Human Services, Centers for Disease Control and Prevention, National Institute for Occupational Safety and Health doi:2002-129.
Nishita-Hara, C., Hirabayashi, M., Hara, K., Yamazaki, A., Hayashi, M., 2019. Dithiothreitol-measured oxidative potential of size-segregated particulate matter in Fukuoka, Japan: effects of asian dust events. GeoHealth 3, 160–173. https://doi.org/10.1029/2019GH000189.
Pedroso-Fidelis, G. dos S., Farias, H.R., Mastella, G.A., Boufleur-Niekraszewicz, L.A., Dias, J.F., Alves, M.C., Silveira, P.C.L., Nesi, R.T., Carvalho, F., Zocche, J.J., Pinho, R.A., 2020. Pulmonary oxidative stress in wild bats exposed to coal dust: a model to evaluate the impact of coal mining on health. Ecotoxicol. Environ. Saf. 191. https://doi.org/10.1016/j.ecoenv.2020.110211.
Pietrogrande, M.C., Bertoli, I., Clauser, G., Dalpiaz, C., Dell'Anna, R., Lazzeri, P., Lenzi, W., Russo, M., 2021. Chemical composition and oxidative potential of atmospheric particles heavily impacted by residential wood burning in the Alpine region of Northern Italy. Atmos. Environ., 118360 https://doi.org/10.1016/j.atmosenv.2021.118360.
Qiao, H., Chen, S., Dong, X., Dong, K., 2019. Has China's coal consumption actually reached its peak? National and regional analysis considering cross-sectional dependence and heterogeneity. Energy Econ. 84, 104509. https://doi.org/10.1016/j.eneco.2019.104509.
Qin, S., Zhao, C., Li, Y., Zhang, Y., 2015. Review of coal as a promising source of lithium. Int. J. Oil, Gas Coal Technol. https://doi.org/10.1504/IJOGCT.2015.067490.
Querol, X., Fernandez Turiel, J.L., Lopez Soler, A., Duran, M.E., 1992. Trace elements in high-S subbituminous coals from the Teruel Mining District, northeast Spain. Appl. Geochem. 7, 547–561. https://doi.org/10.1016/0883-2927(92)90070-J.
Querol, X., Whateley, M.K.G., Fernández-Turiel, J.L., Tuncali, E., 1997. Geological controls on the mineralogy and geochemistry of the Beypazari lignite, central Anatolia, Turkey. Int. J. Coal Geol. 33, 255–271. https://doi.org/10.1016/S0166-5162(96)00044-4.
Querol, X., Zhuang, X., Font, O., Izquierdo, M., Alastuey, A., Castro, I., van Drooge, B.L., Moreno, T., Grimalt, J.O., Elvira, J., Cabañas, M., Bartroli, R., Hower, J.C., Ayora, C., Plana, F., López-Soler, A., 2011. Influence of soil cover on reducing the environmental impact of spontaneous coal combustion in coal waste gobs: a review and new experimental data. Int. J. Coal Geol. 85, 2–22. https://doi.org/10.1016/j.coal.2010.09.002.
Rahman, I., Adcock, I.M., 2006. Oxidative stress and redox regulation of lung inflammation in COPD. Eur. Respir. J. 28, 219–242. https://doi.org/10.1183/09031936.06.00053805.
Ren, Q., Zhang, Y., Arauzo, I., Shan, L., Xu, J., Wang, Y., Su, S., Hu, S., Xiang, J., 2021. Roles of moisture and cyclic loading in microstructures and their effects on mechanical properties for typical chinese bituminous coals. Fuel 293, 120408. https://doi.org/10.1016/j.fuel.2021.120408.
Sánchez Jiménez, A., Van Tongeren, M., Cherrie, J.W., 2011. A Review of Monitoring Methods for Inhalable Hardwood Dust. Inst. Occup. Med P937/1A.
Schins, R.P.F., Borm, P.J.A., 1999. Mechanisms and mediators in coal dust induced toxicity: a review. Ann. Occup. Hyg. 43, 7–33. https://doi.org/10.1016/S0003-4878(98)00069-6.

Shi, X., Dalal, N.S., 1992. The role of superoxide radical in chromium(VI)-generated hydroxyl radical: the Cr(VI) haber-weiss cycle. Arch. Biochem. Biophys. 292, 323–327. https://doi.org/10.1016/0003-9861(92)90085-B.

Shi, X., Dalal, N.S., Kasprzak, K.S., 1992. Generation of free radicals from lipid hydroperoxides by Ni2 in the presence of oligopeptides. Arch. Biochem. Biophys. 299, 154–162. https://doi.org/10.1016/0003-9861(92)90257-W.

Shimura, K., Matsuo, A., 2019. Using an extended CFD-DEM for the two-dimensional simulation of shock-induced layered coal-dust combustion in a narrow channel. Proc. Combust. Inst. 37, 3677–3684. https://doi.org/10.1016/j.proci.2018.07.066.

Soltani, N., Keshavarzi, B., Sorooshian, A., Moore, F., Dunster, C., Dominguez, A.O., Kelly, F.J., Dhakal, P., Ahmadi, M.R., Asadi, S., 2018. Oxidative potential (OP) and mineralogy of iron ore particulate matter at the Gol-E-Gohar Mining and Industrial Facility (Iran). Environ. Geochem. Health 40, 1785–1802. https://doi.org/10.1007/s10653-017-9926-5.

Stach, E., Mackowsky, M.-T., Teichmüller, M., Taylor, G.H., Chandra, D., Teichmüller, R., 1982. Stach's Textbook of Coal Petrology. Gebrüder Borntraeger Berlin Stuttgart, p. 535.

Stohs, S.J., Bagchi, D., 1995. Oxidative mechanisms in the toxicity of metal ions. Free Radic. Biol. Med. 18, 321–336. https://doi.org/10.1016/0891-5849(94)00159-H.

Strlič, M., Kolar, J., Šelih, V.S., Kocar, D., Pihlar, B., 2003. A comparative study of several transition metals in fenton-like reaction systems at circum-neutral pH. Acta Chim. Slov. 50, 619–632.

Swaine, D.J., 1990. Trace Elements in Coal. Butterworth.

Tang, Z., Chai, M., Cheng, J., Jin, J., Yang, Y., Nie, Z., Huang, Q., Li, Y., 2017. Contamination and health risks of heavy metals in street dust from a coal-mining city in eastern China. Ecotoxicol. Environ. Saf. 138, 83–91. https://doi.org/10.1016/j.ecoenv.2016.11.003.

Tian, H.Z., Lu, L., Hao, J.M., Gao, J.J., Cheng, K., Liu, K.Y., Qiu, P.P., Zhu, C.Y., 2013. A review of key hazardous trace elements in Chinese coals: abundance, occurrence, behavior during coal combustion and their environmental impacts. Energy Fuel 27, 601–614. https://doi.org/10.1021/ef3017305.

Trechera, P., Moreno, T., Córdoba, P., Moreno, N., Zhuang, X., Li, B., Li, J., Shangguan, Y., Kandler, K., Dominguez, A.O., Kelly, F., Querol, X., 2020. Mineralogy, geochemistry and toxicity of size-segregated respirable deposited dust in underground coal mines. J. Hazard. Mater. 399, 122935. https://doi.org/10.1016/j.jhazmat.2020.122935.

Trechera, P., Moreno, T., Córdoba, P., Moreno, N., Zhuang, X., Li, B., Li, J., Shangguan, Y., Dominguez, A.O., Kelly, F., Querol, X., 2021. Comprehensive evaluation of potential coal mine dust emissions in an open-pit coal mine in Northwest China. Int. J. Coal Geol. 235, 103677. https://doi.org/10.1016/j.coal.2021.103677.

Valko, M., Morris, H., Cronin, M.T.D., 2005. Metals, toxicity and oxidative stress. Curr. Med. Chem. 12, 1161–1208.

Wang, H., Dlugogorski, B.Z., Kennedy, E.M., 2003. Coal oxidation at low temperatures: oxygen consumption, oxidation products, reaction mechanism and kinetic modelling. Prog. Energy Combust. Sci. https://doi.org/10.1016/S0360-1285(03)00042-X.

Wang, Y., Gu, A., Zhang, A., 2011. Recent development of energy supply and demand in China, and energy sector prospects through 2030. Energy Policy 39, 6745–6759. https://doi.org/10.1016/j.enpol.2010.07.002.

Wang, H., Du, M.L., Zhang, G.T., 2014. Concentration and distribution of Cr, Pb and Zn in the Jurassic coals from northern Shaanxi and Ningxia, China. Adv. Mater. Res. 989–994, 1415–1418. https://doi.org/10.4028/www.scientific.net/AMR.989-994.1415.

Wang, P., Ji, D., Yang, Y., Zhao, L., 2016. Mineralogical compositions of Late Permian coals from the Yueliangtian mine, western Guizhou, China: comparison to coals from eastern Yunnan, with an emphasis on the origin of the minerals. Fuel 181, 859–869. https://doi.org/10.1016/j.fuel.2016.05.043.

Wang, H., Zhang, L., Wang, D., He, X., 2017. Experimental investigation on the wettability of respirable coal dust based on infrared spectroscopy and contact angle analysis. Adv. Powder Technol. 28, 3130–3139. https://doi.org/10.1016/j.apt.2017.09.018.

WCA, 2020. World Coal Association [WWW Document]. https://www.worldcoal.org/.

Weber, R.J., Guo, H., Russell, A.G., Nenes, A., 2016. High aerosol acidity despite declining atmospheric sulfate concentrations over the past 15 years. Nat. Geosci. 9, 282–285. https://doi.org/10.1038/ngeo2665.

Wei, W., Mushtaq, Z., Sharif, M., Zeng, X., Wan-Li, Z., Qaisrani, M.A., 2020. Evaluating the coal rebound effect in energy intensive industries of China. Energy 207, 118247. https://doi.org/10.1016/j.energy.2020.118247.

WHO, 2000. WHO Air Quality Guidelines [WWW Document]. Second ed. WHO Reg. Off. Eur. Copenhagen, Denmark.

Wilhelm Filho, D., Júnior, S.Á., Possamai, F.P., Parisotto, E.B., Moratelli, A.M., Garlet, T.R., Inácio, D.B., Torres, M.A., Colepicolo, P., Dal-Pizzol, F., 2010. Antioxidant therapy attenuates oxidative stress in the blood of subjects exposed to occupational airborne contamination from coal mining extraction and incineration of hospital residues. Ecotoxicology 19, 1193–1200. https://doi.org/10.1007/s10646-010-0503-2.

Xu, C., Wang, D., Wang, H., Xin, H., Ma, L., Zhu, X., Zhang, Y., Wang, Q., 2017. Effects of chemical properties of coal dust on its wettability. Powder Technol. 318, 33–39. https://doi.org/10.1016/j.powtec.2017.05.028.

Yang, A., Jedynska, A., Hellack, B., Kooter, I., Hoek, G., Brunekreef, B., Kuhlbusch, T.A.J., Cassee, F.R., Janssen, N.A.H., 2014. Measurement of the oxidative potential of PM2.5 and its constituents: the effect of extraction solvent and filter type. Atmos. Environ. 83, 35–42. https://doi.org/10.1016/j.atmosenv.2013.10.049.

Yang, J., Wu, Jingli, He, T., Li, L., Han, D., Wang, Z., Wu, Jinhu, 2016. Energy gases and related carbon emissions in China. Resour. Conserv. Recycl. 113, 140–148. https://doi.org/10.1016/j.resconrec.2016.06.016.

Yu, H., Wei, J., Cheng, Y., Subedi, K., Verma, V., 2018. Synergistic and antagonistic interactions among the particulate matter components in generating reactive oxygen species based on the dithiothreitol assay. Environ. Sci. Technol. 52, 2261–2270. https://doi.org/10.1021/acs.est.7b04261.

Yu, H., Gao, Y., Zhou, R., 2020. Oxidative stress from exposure to the underground space environment. Front. Public Health https://doi.org/10.3389/fpubh.2020.579634.

Yuan, J., 2018. The future of coal in China. Resour. Conserv. Recycl. https://doi.org/10.1016/j.resconrec.2016.12.006.

Yuzhuang, S., Cunliang, Z., Yanheng, L., Jinxi, W., 2015. Anomalous concentrations of rare metal elements, rare-scattered (dispersed) elements and rare earth elements in the coal from Iqe Coalfield, Qinghai Province, China. Acta Geol. Sin. Engl. Ed. 89, 229–241. https://doi.org/10.1111/1755-6724.12407.

Zazouli, M.A., Dehbandi, R., Mohammadyan, M., Aarabi, M., Dominguez, A.O., Kelly, F.J., Khodabakhshloo, N., Rahman, M.M., Naidu, R., 2021. Physico-chemical properties and reactive oxygen species generation by respirable coal dust: implication for human health risk assessment. J. Hazard. Mater. 405, 124185. https://doi.org/10.1016/j.jhazmat.2020.124185.

Zhang, W., Rezaee, M., Bhagavatula, A., Li, Y., Groppo, J., Honaker, R., 2015. A review of the occurrence and promising recovery methods of rare earth elements from coal and coal by-products. Int. J. Coal Prep. Util. 35, 295–330. https://doi.org/10.1080/19392699.2015.1033097.

Zhang, W., Noble, A., Yang, X., Honaker, R., 2020. Lithium leaching recovery and mechanisms from density fractions of an Illinois Basin bituminous coal. Fuel 268, 117319. https://doi.org/10.1016/j.fuel.2020.117319.

Zhang, R., Liu, S., Zheng, S., 2021. Characterization of nano-to-micron sized respirable coal dust: particle surface alteration and the health impact. J. Hazard. Mater. 413, 125447. https://doi.org/10.1016/j.jhazmat.2021.125447.

Zhang, Y.J., Huang, C., Lv, Y.S., Ma, S.X., Guo, Y., Zeng, E.Y., 2021. Polycyclic aromatic hydrocarbon exposure, oxidative potential in dust, and their relationships to oxidative stress in human body: a case study in the indoor environment of Guangzhou, South China. Environ. Int. 149, 106405. https://doi.org/10.1016/j.envint.2021.106405.

Zhuang, X., Querol, X., Alastuey, A., Juan, R., Plana, F., Lopez-Soler, A., Du, G., Martynov, V.V., 2006. Geochemistry and mineralogy of the Cretaceous Wulantuga high-germanium coal deposit in Shengli coal field, Inner Mongolia, Northeastern China. Int. J. Coal Geol. 66, 119–136. https://doi.org/10.1016/j.coal.2005.06.005.

Zhuang, X., Su, S., Xiao, M., Li, J., Alastuey, A., Querol, X., 2012. Mineralogy and geochemistry of the Late Permian coals in the Huayingshan coal-bearing area, Sichuan Province, China. Int. J. Coal Geol. 94, 271–282. https://doi.org/10.1016/j.coal.2012.01.002.

Zosky, G.R., Bennett, E.J., Pavez, M., Beamish, B.B., 2021. No association between pyrite content and lung cell responses to coal particles. Sci. Rep. 11, 8193. https://doi.org/10.1038/s41598-021-87517-z.

Chapter 5

DISCUSSION

5. DISCUSSION

The aim of this chapter is to combine discussions of the five articles featured in this PhD thesis to support the final conclusions. In conjunction with this, it also discusses the results of coal dust and powdered coal samples evaluated in this study.

This PhD thesis provides an exhaustive data analysis on particle size, geochemistry and mineralogy of coal dust in open-pit and underground coal mines and powdered coal samples from several regions of China and Central Eastern Europe, including an extensive analysis of the respirable coal and coal dust fractions. The link of these patterns with OP obtained for the individual samples is evaluated with cross-correlation and multilinear regression analyses. In specific coal mines, data on occupational exposure concentrations and online measurements of exposure to PM, BC and UFP was also obtained.

5.1. Factors controlling particle size of coal mine dust

As reported in prior chapters, PSD of coal mine dust is a key parameter to understand its potential health impacts (Andersen et al., 2008; Kurth et al., 2014; Shekarian et al., 2021). It has also been shown that a major reason for the sudden increase in recent CWP cases reported in coal mining might be linked to the more advanced and improved modern machinery which produces finer coal mine dust particles (Fan et al., 2018; Johann-Essex et al., 2017; Leonard et al., 2020; Q. Ma et al., 2020; Perret et al., 2017). For this reason, the PSD of coal mine dust from different operations is a key factor to be evaluated in the reduction of occupational exposure risks.

In this PhD thesis, three articles evaluate the PSD results of several DD samples. One analyses the PSD of coal mine dust from Central Eastern European coal (Article #2), and the other two from underground and open-pit Chinese coal mines (Articles #3 and #4, respectively). Table 5.1 shows the average results of DD_{500}, DD_{10}, DD_4 and $D_{2.5}$ (DD finer than 500, 10, 4 and 2.5 μm, respectively) for all articles, including their moisture content (%,air dried, ad) and their ash yield (%,dry basis, db).

5.1.1. Moisture content

According to Table 5.1 and Articles #2, #3 and #4, the moisture content is a key factor in controlling the PSD of coal mine dust. In mine locations where water spraying is implemented to abate resuspension or where underground water affects mine dust, the high moisture of the DD samples accounts for marked lower proportions of DD_{10}, DD_4 and $DD_{2.5}$, due to particle agglomeration (negative correlation of moisture contents with these proportions reaching R^2 = 0.73-0.74 in the Chinese underground mines of Article #3, and R^2 = 0.81-0.96 for samples of the Chinese open-pit CWF in Article #4).

When considering a single open-pit mine, comparing zones where water spraying is applied with others without this control measure, a large reduction of the fine fraction of DD is clearly evidenced in water spraying zones. However, DD from high quartz and clay gangue dumping is highly enriched in the fine fractions when compared with the coal dust from the CWF.

Table 5.1. *Average of PSD of DD samples for all results published in this PhD thesis. DD_{500}, DD_{10}, DD_4 and $DD_{2.5}$, deposited dust finer than 500, 10, 4 and 2.5 µm, respectively; %v, %volume; M, Moisture content; %ad, %air dried; HTA, Ash yield; %db, %dry basis; VCB, Velenje Coal Basin; USCB, Upper Silesian Coal Basin; BWC, Bituminous Southwest China; GW, Gallery walls; WF, Working Front; SSC and BSC, Subbituminous and Bituminous South China; ANC, Anthracite North China; CWF, Coal Working Front; TH, Tailing Handling; RT, mining Roads Traffic.*

Location	Coal Rank	DD_{500}	DD_{10}(%v)	DD_4(%v)	$DD_{2.5}$(%v)	M (%ad)	HTA (%db)
Article #2 – Central Eastern Europe							
VCB	Lignite	98 (%v)	17	6	3.3	12	36
USCB	Hard Coal	98 (%v)	35	16	10	1	38
Article #3 – underground mining China							
BWC (GW)	Bituminous	67 (%wt)	18	8.9	4.8	1.1	58
BWC (Tunnels WF#7)	Bituminous	61 (%wt)	19	7.9	3.8	0.92	43
BWC (WF)	Bituminous	94 (%wt)	29	12	5.9	0.57	30
BWC (Mill)	Bituminous	66 (%wt)	11	5.6	2.7	0.60	43
SSC (Tunnels WF)	Subbituminous	83 (%wt)	55	30	18	2.0	66
SSC (WF)	Subbituminous	88 (%wt)	39	21	14	1.7	73
SSC (Mill)	Subbituminous	58 (%wt)	17	8.8	5.6	2.2	51
BSC (100-50 m to WF)	Bituminous	96 (%wt)	55	27	15	0.81	43
ANC (Air Shaft)	Anthracite	78 (%wt)	44	19	9.5	0.97	43
Article #4 – open-pit mining China							
Open-pit (CWF)	Bituminous	89 (%wt)	25	12	6.5	10	11
Open-pit (TH)	Bituminous	92 (%wt)	29	19	12	2.0	92
Open-pit (RT)	Bituminous	96 (%wt)	36	23	15	2.2	93

In underground mines, DD can be wetted by underground water infiltration into galleries, but also some underground mines, such as USCB and VCB, are using wetting techniques to reduce occupational dust concentrations. Results showed that, only in the VCB underground mine, the increase of moisture markedly reduced the finer fraction of DD (negative correlation of moisture content with DD_{10}, DD_4 and $DD_{2.5}$, with R^2 = 0.65-0.75 in Article #2), probably because dust moisture is relatively high in underground coal mines, due to water infiltration and condensation.

Thus, as expected, an elevated moisture content (unrelated to the high moisture content of low coal rank, but with condensation and infiltration water) produces stronger agglomerations in the finer fractions of coal dust, proving that wetting systems are significantly efficient in reducing coal dust particle size. Not only is moisture content efficient in reducing re-suspension, but also in reducing the finer DD fractions.

Thus, sprayed water or wetting systems contributed to the reduction of coal mine dust emitted from WFs, the minimisation of coal dust resuspension and the prevention of spontaneous coal dust combustion (NIOSH, 2010). However, it is extremely important to control the accumulation of water in mining environments because an excess could cause problematic effects in coal workers, affecting the comfort of their environment, producing less workplace productivity and possibly increasing stress (Sunkpal et al., 2017), but also favouring oxidation of coal particles and potentially favouring spontaneous combustion in the long term (Querol et al., 2011).

5.1.2. Coal mine operations and distance to working fronts

Results from this PhD thesis have indicated significant effects of coal mine operations on PSD of DD collected from different parts of underground and open-pit coal mines. Thus, in the WFs of the underground mines, DD is markedly coarser due to the coarse dust produced in the vicinity

of the coal working. With coal mine ventilation, part of this emitted dust can be transported along galleries with a progressive enrichment of the finer fractions in the transported (and subsequently sedimented) dust (Article #2 and #3). Obviously, the absolute concentrations of suspended dust (PM) are much higher closer to the WF, but the relative contributions of fine particles to the dust increase with the distance from the source (Figure 5.1). The same effect was evidenced as the distance to the WF increase in the open-pit mine (Article #4).

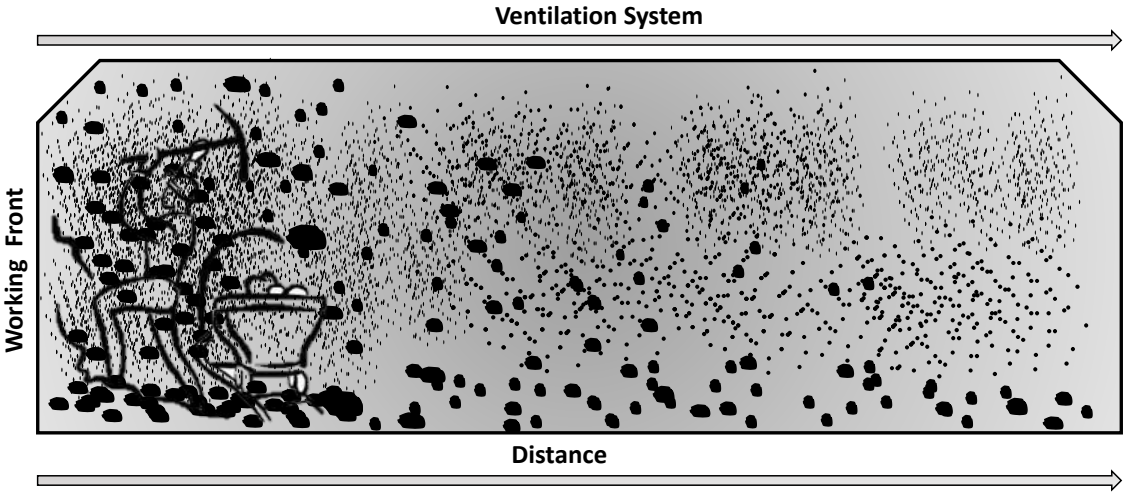

Figure 5.1. *Conceptual model for the dust particle size fractionation from the WF to access galleries.*

5.1.3. Coal mine dust composition

A marked positive correlation between ash yield and the increase of the finer DD fractions was observed in coal dust. This was particularly evidenced in Article #2 for USCB coal mine (positive correlation with R^2 = 0.70-0.99) and in Article #4 for the open-pit mine (r = 0.70- 0.99). Thus, coal mine dust containing high mineral contents, usually fine clays and quartz, is characterised by a much finer PSD, especially a higher proportion of finer fractions ($DD_{2.5}$) when compared to more low-ash yield coal mine dust. This is noticeably evident in the dust from coal gangue dumping in the open-pit of Article #4. The organic fraction of coal dust (coaly matrix) is much more fragile and/or rigid than the mineral one and, when worked, generates coarser dust grains (Rosita et al., 2020; Sevim and Demir, 2019; Yang et al., 2019). However, this effect is reversed in the results of SSC underground mine of Article #3. Here, ash yield of DD is negatively correlated with PSD, where the ash yield of all samples was extremely high and, in some cases, mineral dust largely originated from carbonate minerals not necessarily producing fine dust as clays and quartz. Thus, the higher ash yield does not always result in a finer coal mine dust, but it seems that the increase of clay and quartz contents might favour this finer PSD when comparing operations of the mine working or the handling of low and high clay-quartz materials. Furthermore, if the coal worked is a high ash coal, or a high calcite-dolomite coal, these differences are reduced.

Results also evidenced a higher positive correlation with ash yield and finer particle size of DD in samples from high coal rank mines (Article #3). The organic matrix from the high coal ranks (such as anthracite) tends to be more rigid and/or fragile than the one for brown coal ranks

(lignite and subbituminous), due to the much lower moisture and higher C contents in the high coal ranks. This might yield to coarser dust when the hard coals are worked.

5.2. Factors controlling mineralogy and chemical composition of deposited dust

Major dust emission sources in coal mines include working of coal, tunnelling, handling of coal and gangue, resuspension of dust by ventilation flows, abrasion of the machinery, milling, and dumping, among the most relevant. In the WFs, coal dust will have a close composition to that of the worked coal seam, probably with a relatively higher mineral content, possibly also with the influence of contributions from the machinery wear. However, in underground and open-pit mines the composition of coal mine dust changes dramatically in correlation to the distance to the WF because of the size fractionation of the WF dust and the higher relative relevance of the dust contribution of other emission sources.

Articles #1 to #4 produced results on the compositional patterns of coal mine dust that are summarised below:

i) As could be expected, the highest coal mine dust concentrations and DD occurs in the WF where coal is worked, reaching levels of tens of mg m^{-3}. DD samples collected in WF or closer to WF are markedly similar to their respective worked coal seam patterns, in regard to the mineral and chemical composition. However, higher concentrations of some elements and minerals were evidenced due to the contribution from roof and bottom of the coal seam (gangue), and the machinery wear, among other factors.

ii) Deposited dust with very high content of Ca, calcite ($CaCO_3$) and gypsum ($CaSO_4.2H_2O$), commonly originates from the gallery walls and roofs. A number of access galleries are gunited with lime (CaO) mortar. Lime is quickly hydrated into portlandite ($Ca(OH)_2$). The interaction of this with carbonate (CO_3^{2-}) and sulphate (SO_4^{2-}) in underground waters reaching the walls and roofs of galleries or CO_2 from the mine air, yield to the production of calcite and gypsum in the gunite material. When dried by ventilation flows, this might result in the emission of high calcite and gypsum dust. Because the underground waters reaching the gunited walls may be affected by AMD caused by oxidation of sulphide minerals, the waters can be enriched by a number of metals, such as As, Pb and Fe (Alcobé et al., 2001; Hudson-Edwards et al., 2008; Kerolli-Mustafa et al., 2015; Kolitsch and Pking, 2001; Smith et al., 2006), which are trapped by salts originated from the lime gunite, and then enrich dust in the elements outlined in the following paragraphs.

iii) In the access galleries, DD and suspended dust levels are orders of magnitude lower than in the WF. There, DD samples have a much higher ash yield than the ones from the WF. Furthermore, the variety of minerals and enriched elements is also higher. The fact that only a significantly small proportion of the finest transported dust from WF emission reaches these galleries, and the presence of DD from older emissions (tunnelling, gangue and coal handling, salts from AMD, machinery wear, among others) are the major causes of this increase. Moreover, old dust can be enriched in several potentially hazardous elements, such as Pb, Zn, Cd, and As from AMD (Cogram, 2018; Murphy et al., 2009; Welch et al., 2008). The

latter is clearly shown in Article #3, in which this source accounted for the highest levels of As in DD of a specific underground coal mine.

iv) Deposited dust samples collected around TH, mine RT, milling and workers transport systems have different compositions, but commonly have a higher mineral content, basically due to increased clay, calcite and quartz contents. This is due to the dilution of coal dust by the contributions of emissions from other sources. Thus, in Article #4, DD around tailings dumping and mine roads in the open-pit has negligible contents of coal dust, being entirely made up of mineral dust, completely different from that of the WF. In Article #3, DD in the wagons from the rail workers transport system into an underground mine, the mineral dust from the boots of the workers and the wear from friction of train wheels and rails yield to a markedly high content on Ca, Fe, Mn, Cr, Zn, As, Sr, Sb and Pb.

v) Sulphur content is reduced in most DD samples from Articles #2 to #4 where low S coals are worked. However, Article #3 showed clearly high S contents in DD, caused by enrichment of sulphate minerals, especially jarosite-alunite and gypsum, occurring in tunnels and access galleries containing non-gunited and gunited walls, respectively. As mentioned above, this is attributed to the common influence of AMD waters in underground mines. These acidic waters contain high sulphuric acid species (H_2SO_4), which also reacts with high Fe^{2+} (both from the oxidation of sulphide minerals) to produce jarosite-alunite (Murphy et al., 2009; Welch et al., 2008). Moreover, the interaction of acidic sulphate with lime mortars or calcite leads to the formation of gypsum. In both cases, this high sulphate dust is enriched in As, Sb, or Pb, also typically enriched by acid mine waters (He et al., 2019; Madzivire et al., 2019; Mohanty et al., 2018). In Article #3 a conceptual model for the generation of this high sulphate and metal mine dust is provided.

5.3. Factors controlling mineralogy and chemical composition of respirable dust

Sampling directly RDD requires the use of specific instrumentation reducing the risk of explosion by using batteries underground. Additionally, extended sampling periods inside a mine are required to obtain enough sample from different operations, and usually the sampling of suspended dust is for a given dust size cut-off, being necessary to simultaneously use several instruments with different cut-off inlets. In this study, access to the coal mines was given for a restricted period of time. In addition to this, the number of sampling instruments for respirable dust able to be used in underground high explosion risk coal mines was limited. The separation of the RDD from the DD was optimized and implemented to collect and characterise respirable coal mine dust from different sites within a mine and from different coal mines. This allowed the characterisation of different size fractions, such as DD_{10}, DD_4 and $DD_{2.5}$. This section is focused on the comparison of RDD (DD_4) with DD.

After the evaluation of DD in all the five articles featured in this PhD thesis, the compositions of RDD fractions were compared with the parent DD. After characterisation of RDD, OP analyses were implemented to evaluate the links between specific compositional and particle size patterns with OP. Furthermore, in Article #5, the CP_4 fraction was extracted from powdered samples of CP of coal seams from a variety of mines from all across China, covering a wide range

of geochemical and coal rank patterns. OP analyses were also implemented for these CP_4 samples.

5.3.1. Mineralogy

The RDD enrichments versus DD (RDD/DD ratios, Figure 5.2) for minerals in underground and open-pit coal mines from China (Articles #3 and #4) and the CP_4/CP ratios (Figure 5.2) were evaluated from around 20 powdered coal samples (Article #5). In both cases most of the ratios were <1.0 for most minerals. For sulphate minerals, pyrite or quartz, ratios were close to 1.0, and >1.0 for clay minerals and anatase.

The contents of feldspars and carbonate minerals are usually markedly lower in RDD when compared to the parent DD samples. For CP_4/CP, carbonate mineral contents increase compared to RDD/DD but are still in the range of 0.6-0.8. Thus, carbonate minerals and feldspars are enriched in DD compared to the parent coal seam but depleted in the RDD, compared to DD, due to the coarser particle size.

The RDD/DD ratios for sulphate, pyrite, quartz and anatase are close to 1 (0.8-1.0), with a wide standard deviation, as would be expected from the variety of modes of occurrence of these minerals in the coals studied (i.e., very fine framboidal pyrite disseminated in the coal matrix in some samples to millimetric massive pyrite mineralization in others). However, an increase in the average ratios of anatase was evidenced when CP_4/CP samples were included (1.4).

For clay minerals, RDD/DD reached a value of 1.2, with a lower standard deviation, but this was slightly reduced (1.1) and the standard deviation was greatly increased when CP_4/CP ratios were considered.

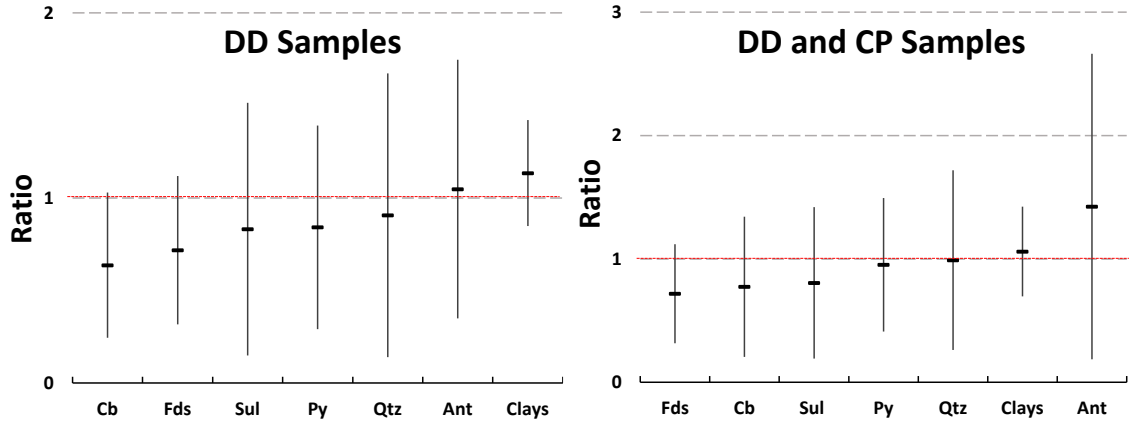

Figure 5.2. *Average values and standard deviations of RDD/DD and CP_4/CP ratios for mineral contents of samples analysed in Articles #3 to #5. Cb, Carbonates; Fds, Feldspar; Sul, Sulphates; Py, Pyrite; Qtz, Quartz; Ant, Anatase.*

Figure 5.3 shows the RDD/DD and CP_4/CP ratios for the mineral groups in the Articles #3, #4 and #5. It demonstrates markedly similar results in the three studies for feldspars, sulphate minerals, pyrite, clays and quartz, but different results in CP_4/CP (Article #5) for anatase and carbonate minerals in Article #3 (underground mine) are evidenced. In the latter, the effect of coarse carbonate minerals from gunited walls causes a depletion in the RDD. For anatase in CP_4, a large standard deviation was indicated, with some samples of powdered coal having coarse anatase and a few others having very fine anatase, with micronic and submicronic anatase being

detected frequently in these samples by scanning electron microscopy (some samples in Article #3). In the open-pit (Article #4) anatase was mostly present in RDD from TH and RT, not in coal, with noticeably coarse particle size. Supporting this is the fact that in the underground mines, (Article #3), low RDD/DD ratios were reached in the high ash subbituminous coal mine. Thus, anatase from high mineral dust samples has a coarser particle size.

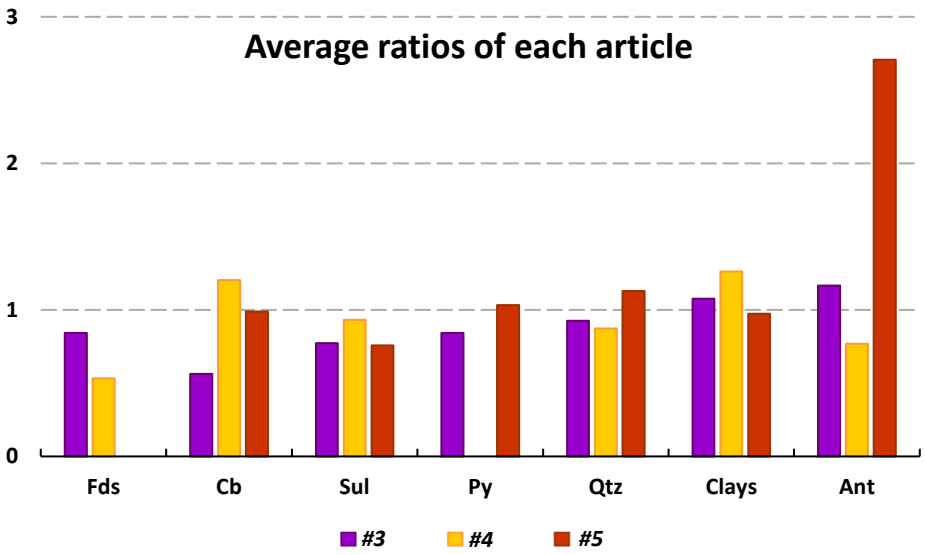

Figure 5.3. *Average values of RDD/DD and CP_4/CP ratios for mineral contents of samples shown individually for Articles #3 to #5. Cb, Carbonate minerals; Fds, Feldspars; Sul, Sulphates; Py, Pyrite; Qtz, Quartz; Ant, Anatase.*

5.3.2. Major elements

Average and standard deviation of RDD/DD and CP_4/CP values for major elements are shown in Figure 5.4. Ratios of Al, Ca, Na, K and P, in all cases, tend to reach 1.2-1.5, thus being enriched in the respirable fractions. Conversely, the ratios for Fe, S and Si tend to reach 0.8-0.9, thus slightly depleted in the fine fraction, as described for sulphate minerals, pyrite and quartz in prior sections. Pyrite (and derived sulphate minerals from its oxidation) tends to be enriched in coal, as opposed to the gangue and coal particles, which tend to yield coarser PSD than clays. This may explain the coarser mode of pyrite and sulphate minerals and the finer one of Al, Na and K.

In spite of these general trends, it is worth highlighting the elevated standard deviation for the ratios of some elements enriched in the RDD fraction (Ca, Na, K and P). However, this does not occur in the case of the Al, possibly indicating that most of it originates from the clay minerals, as in the previous section, increasing its concentration in the respirable fraction. In addition to this, clay minerals could provide most of the P and Al concentrations because, as is shown in Figure 5.4, most of their ratios in each article are higher than 1.0.

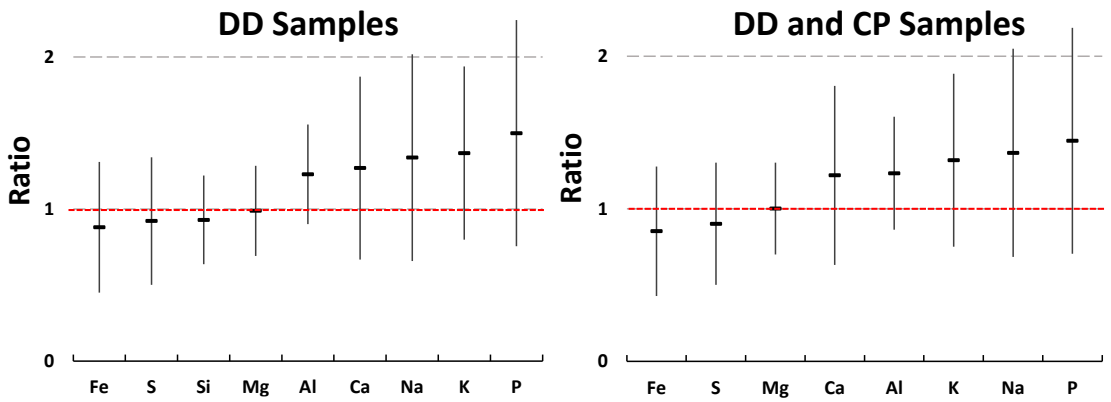

Figure 5.4. *Average values and standard deviations of RDD/DD and CP_4/CP ratios for major elements contents of samples from Articles #2 to #5.*

The RDD/DD values for the samples from the VCB underground coal mine (Article #2) exceed 1.0 for all major elements. Fly ash and carbonate dust were used for guniting walls in galleries, and for spraying the galleries to reduce the risk of spontaneous combustion, respectively and, due to their fine particle sizes in both cases and their enriched compositions in most of the major elements (shown in Article #2), promoted enrichment in the RDD (Figure 5.5). Furthermore, the RDD/DD of Ca increases in the USCB underground coal mine (Article #2) and in the Chinese open-pit (Article #4), in both cases, DD with particularly high mineral contents (Figure 5.5).

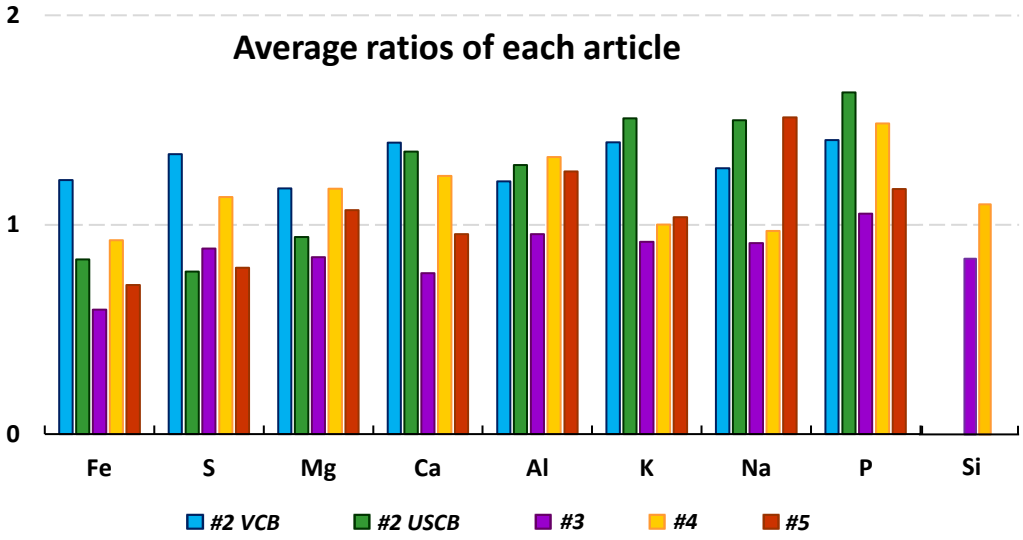

Figure 5.5. *Average values of RDD/DD and CP_4/CP ratios for major elements contents of samples shown individually* for Articles #2 to #5.

5.3.3. Trace elements

Average and standard deviation of RDD/DD and CP_4/CP values for trace elements are shown in Figure 5.6. These ratios reached values of 0.8-1.2 for most elements but an increase in the RDD was indicated for most of them. Thus, trace elements showing greater enrichments in RDD were Zn, Cu, Sn, As and Sb (ratios 1.3 to 2.7). As reported in Article #1, all of them are potentially hazardous for humans, specifically by elevating cell damage (which can be a precursor for

developing ROS), and generating chronic hazardous injuries, such as neurological toxins, PMF or CWP. It is also important to highlight that standard deviations are relatively small for most elements and, therefore, the results are potentially generalised. However, for a number of key hazardous elements such as Se, Ba, Mo, Pb, Zn, Sn, As, Cu and Sb, the standard deviations are significantly large (Figure 5.7), pointing to different scenarios concerning the size segregation of these metals, probably due to the different modes of occurrence in dust.

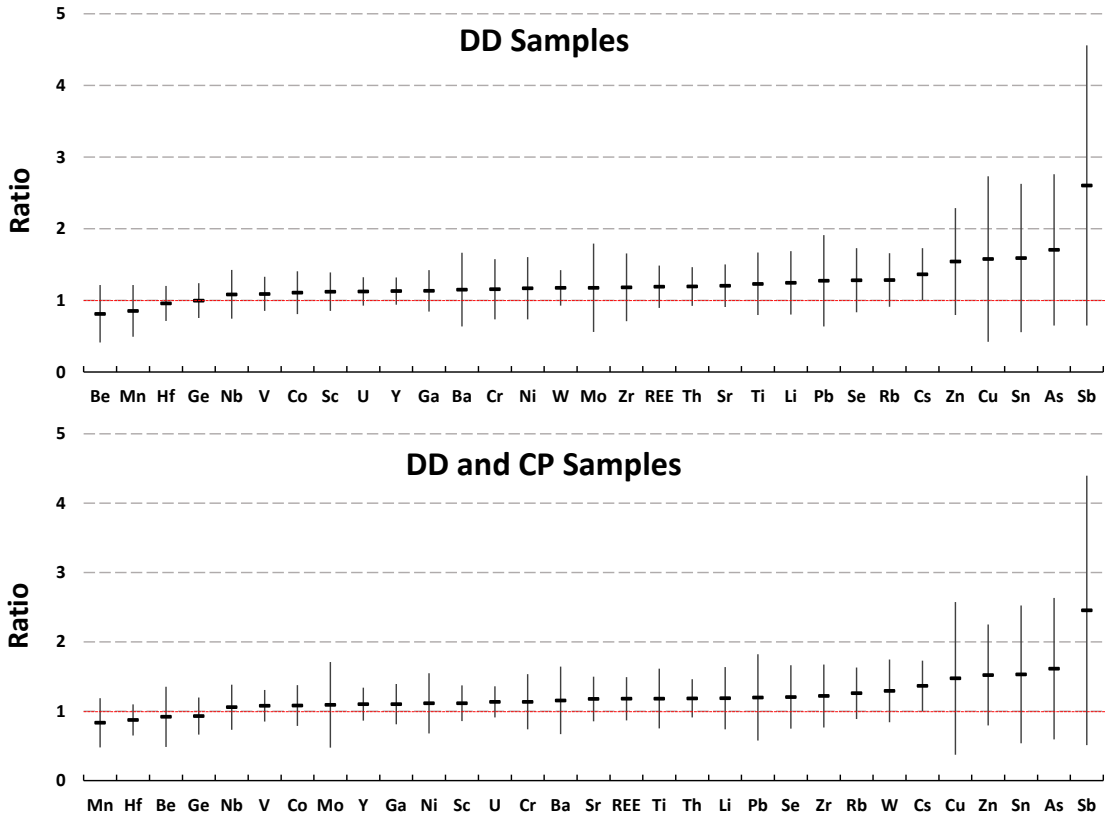

Figure 5.6. *Average values and standard deviations of RDD/DD and CP_4/CP ratios for trace elements content of samples from Articles #2 to #5.*

Interestingly there are a number of elements which are moderately to highly enriched in the RDD versus DD (Articles #2 to #4), including Se, Mo, Pb, Zn, Sn, As, Cu and Sb, as well as Ni, Co and Cr, and much less enriched in CP_4 versus CP (powdered coal samples, Article #5) (Figure 5.7). This might be attributed to the fact that, within the coal mine, it is not only coal dust that builds up the mine dust, but dust from other sources, such as machinery wear, belts and transportation and gangue dust, which contributes decisively to increase the contents of these elements in RDD and DD, while, in the CP samples, it is only the trace element content in the worked coals that contributes.

As for major elements, the higher RDD/DD values of specific trace elements, including Co, Mo, Ni, Ba, Pb, Cu, Zn, Sn, As and Sb, in samples from the underground VCB coal mine (Article #2) are attributed to the use of fly ash (with extremely fine particle size and enriched in these elements) for guniting galleries. Furthermore, in Article #2 also for VCB mine, it was evidenced that $DD_{2.5}$/DD vales for these elements were similar to RDD/DD.

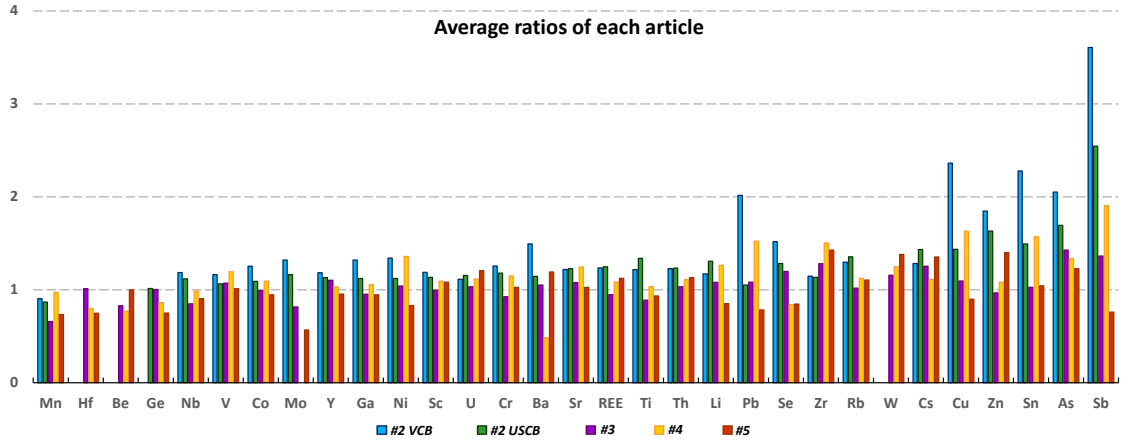

Figure 5.7. *Average values of RDD/DD and CP_4/CP ratios for trace elements contents of samples shown individually for Articles #2 to #5.*

5.4. Factors controlling the oxidative potential of coal mine dust

As reported in the introductory chapter, OP has rarely been used as an indicator of potential toxicity of coal dust samples. However OP is effective as an indicator of the capacity of PM to oxidise target molecules and as a predictor of biological responses to PM toxicity and might yield more information on the potential health effects than PM mass or chemistry (Ayres et al., 2008; Borm et al., 2007; Daellenbach et al., 2020). Thus, OP could be a good indicator of toxicity of the RDD in order to evaluate occupational hazards in coal mining, since it integrates various biologically-relevant dust properties, including size, surface and mineralogical and chemical composition (Ayres et al., 2008; Janssen et al., 2014).

In this PhD thesis, an evaluation of OP links with geochemical and particle size patterns of coal mine dust was one of the major objectives. Articles #3 to #5 indicated that pyrite and Fe, among others, could be a concern in coal dust because of their positive correlation with OP, other prior studies also support this hypothesis. Cohn et al. (2004; 2006c), Harrington et al. (2012), Huang et al. (2005) and Huang and Finkelman (2008), among others, obtained similar results, leading to the conclusion that quartz might not be the only mineral responsible for the principal occupational lung pathogenesis in coal miners, with other dust components contributing to the generation of ROS and accelerating the process of developing silicosis, CWP or PMF.

5.4.1. Oxidative potential values

Figure 5.8 summarises mean values of total OP (as OP^{TOT}, with OP^{TOT} = OP^{AA} + OP^{GSH}, in % consumption of anti-oxidants per µg of RDD or CP_4) from the data obtained in Articles #3 to #5, as well as the comparison with $\%OP^{TOT}\ \mu g^{-1}$ found in other studies for different types of PM (Calas et al., 2018; Godri et al., 2011; Moreno et al., 2017; Soltani et al., 2018), and coal dust, Zazouli et al. (2021), the only article focusing on OP of coal mine dust). This comparison shows that the OP^{TOT} values for RDD and CP_4 of this PhD thesis fall in the range of the underground respirable coal mine dust from Turkey (Zazouli et al., 2021), even though this study shows OP of respirable coal dust in suspension (PM_4) and not RDD, as in this PhD thesis, supporting the presence of RDD and CP_4. It is also evident that all these RDD, CP_4 and PM_4 OP^{TOT} values are considerably reduced

when compared with those reported for atmospheric PM from, for example, subways, urban background affected by winter domestic biomass burning or roadsides (Figure 5.8 bottom).

Figure 5.8 (Top) shows that, in this PhD thesis, the highest OP values were obtained for the underground BWC mine RDD (Article #3), probably due to the relatively high contributions of salts and metals from AMD to RDD of this mine, elevating its OP^{AA}. Conversely, the lowest OP^{TOT} values were obtained for RDD from the Chinese open-pit (Article #4) because of the extremely low contents of sulphides and most metals. The OP^{TOT} values obtained for CP_4 were very high, due to the powdered coal samples selected, some chosen because of the very high content of specific elements of minerals.

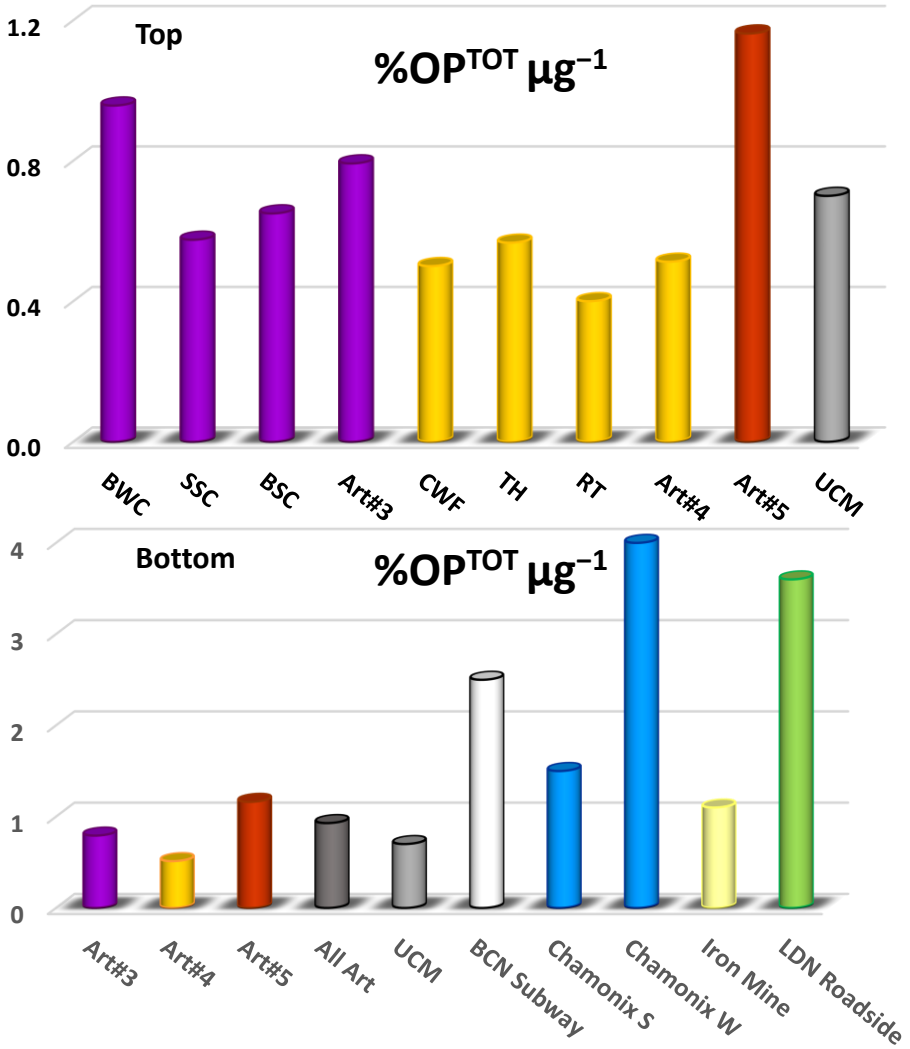

Figure 5.8. *%OP^{TOT} μg^{-1} averages. Top. Article #3: RDD from BWC (underground bituminous coal mine from Southwest China), SSC and BSC (underground subbituminous and bituminous coal mines from South China), Art#3 (average of data from Article #3). Article #4: RDD from an open-pit subbituminous coal mine in Northwest China, CWF (Coal Working Front), TH (Tailing Handling), RT (Roads Traffic), Art#4 (average of data from Article #4). Article #5: Art#5 (average of data from Article #5). UCM: PM_4 from an underground coal mine from Turkey* (Zazouli et al., 2021). *Bottom: OP^{TOT} averages for RDD from Articles #3 and #4, for CP_4 from Article #5, from all articles (#3 to #5), from PM_4 from UCM* (Zazouli et al., 2021), *from $PM_{2.5}$ from the Barcelona subway* (Moreno et al., 2017), *Chamonix Valley in summer (S) and winter (W) (Calas et al., 2018), from a Fe mine and industrial facility from Iran (Godri et al., 2011), and from a roadside in London (Soltani et al., 2018).*

5.4.2. Correlation of oxidative potential with compositional patterns of dust

5.4.2.1. Ascorbic acid, OP^{AA}

OP^{AA} contributed to most of the OP^{TOTAL} (0.93 $\%OP^{TOT}$ μg^{-1} as a mean for all RDD and CP_4 samples analysed) as also recently reported by Zazouli et al. (2021) for underground coal mine dust from Turkey.

The first OP^{AA} analyses for RDD samples were carried out for samples of two bituminous Chinese underground mines (Article #3), with the results showing a high correlation with quartz, sulphate minerals and pyrite (r = 0.8-0.9), increasing with anatase (r = 0.94) and Fe (r = 0.98). Additionally, a positive correlation was observed for D_{75} particle size (r = 0.7), and specially Mo and S (r = 0.8-0.9) for RDD from the underground mine influenced by AMD.

By contrast, in the case of the very high ash subbituminous coal Chinese mine (Article #3), OP^{AA} of RDD was highly correlated with Ca (r = 0.97) and, in the case of the open-pit mine (Article #4), with Mn, anatase and calcite (r = 0.8–0.9). However, when only the high coal CWF RDD samples of open-pit coal mine were analysed, OP^{AA} was correlated with moisture content, gypsum and B (r = 0.5-0.6) and, particularly, with D_{25}, anatase, Mn, U, Zn and Cu (r = 0.6–0.99); whereas, when only the high mineral RDD from TH and RT were analysed, OP^{AA} values were linked with silicate minerals and calcite associated elements, Mn, REEs, Y, Ba, Ge, Mg, Fe and Na (r = 0.6–0.99). Thus, very different OP^{AA} associations were found for the high coal matrix and high mineral content RDD samples, even in the same coal mine.

When considering data on OP^{AA} from all samples of RDD from Articles #3 and #4, the association of OP^{AA} with high contents of Fe-sulphates, other sulphate species and anatase, and a slightly coarser PSD (D_{25}) was indicated, thus pointing to salts from pyrite oxidation and to anatase as major general drivers.

Article #5 evidenced that OP^{AA} of CP_4 samples correlated positively (r= 0.7) with Fe, anatase, S, pyrite, U, Mo, V and Ti (r = 0.5–0.6). When only bituminous CP_4 samples were considered, OP^{AA} drivers were Fe (r = 0.8), ash yield and pyrite (r = 0.7), as well as sulphate minerals, As, K, S, Si, Al, V and Cr (r = 0.5–0.6).

When including all RDD and CP_4 samples from Articles #3 to #5 in the correlation analysis, results pointed to S, U, Mo and pyrite (r = 0.6–0.5) as major drivers of the OP^{AA}. There, OP^{AA}-Fe and OP^{AA}-pyrite had markedly decreased, possibly due to the high content of clay minerals in the subbituminous and lignite coals analysed. This is probably because Fe is present in some of the clay minerals and the fact that they aggregate in high ash coals embed pyrite assemblages, reducing their oxidation and the OP effects, as shown in Article #3 (Figure 4, j to l of this article). Again, the correlations increased with ash yield, sulphate mineral, anatase, S, Ti, Ni, Co, V, Pb and REEs (r=0.5-0.4), and particularly Fe (r = 0.8) and pyrite (r = 0.7), when only considering bituminous coals.

According to the above results, it seems that OP^{AA} of RDD and CP_4 is mostly driven by specific components of the inorganic matter of coal, especially Fe and pyrite. Moreover, sulphate minerals from the oxidation of pyrites, especially the Fe-sulphates species, as well as anatase, ash yield, quartz, S, Ti and various trace metals, such as Mn, Mo and U, seem also to increase

OP^{AA}. As stated above, prior studies found a high correlation between the contents of Fe species in PM and ROS generation in humans (Cohn et al., 2006b; Hamilton et al., 2009; Harrington et al., 2012; Liu and Liu, 2020; Zhang et al., 2021). In addition, Huang et al. (1998, 2005) reported a high correlation, in bituminous coal mining areas of the United States, between bioavailable Fe values and CWP cases. The evaluation of the effect of the other elements and minerals in coal mine dust analysed here with OP^{AA} has not been reported in the literature, other than the recent study by Zazouli et al. (2021).

5.4.2.2. Glutathione, OP^{GSH}

In Article #3, OP^{GSH} values for BWC mined RDD samples were correlated with the contents of Mg, K, Cr, Pb, calcite, Zn, Rb, Sb, As, Cs, Ba, Ca (r = 0.9), Na (r = 0.94) and Sr (r = 0.97). When samples from the BSC mine were added, the correlations decreased with Ba, Mg, Sr, calcite, Ca and Na (0.8−0.9). However, for RDD from the SSC mine, OP^{GSH} correlated with Cu, quartz, Cs and Ba contents (r = 0.94−0.99).

In Article #4, a slight correlation of OP^{GSH} with gypsum, moisture content and a D_{10} particle size was found (r = 0.5–0.7). For the high coal dust content from the CWF zone of this open-pit, correlations were evident for Ni and Pb (r = 0.7–0.8) and also with D_{25}, anatase, Mn, U, Zn and Cu (r = 0.6–0.99); whereas, when considering only the high mineral dust content of the same mine (TH and RT zones), the correlation was found for As, Bi, Be, Sr, P, and moisture content (r = 0.6-0.9).

When combining all RDD samples from Articles #3 and #4, OP^{GSH} was moderately correlated only with the contents of moisture, Ca and Na (r = 0.5), probably tracing the organic content of the RDD, with OP^{GSH} showing higher values for samples from Article #4 than from those of #3. This could probably be attributed to the very low ash yield and the relatively high Mn contents of the CWF RDD samples in the open-pit mine, which could account for an increased OP^{GSH}.

OP^{GSH} from all CP_4 samples of Article #5 correlated with moisture content (r = 0.7), again probably tracing OP caused by organic matrix of CP_4. For CP_4 from bituminous coals, OP^{GSH} correlation was markedly increased with moisture content (r = 0.8), as well as with H and D_{10} particle size (r = 0.6–0.5), indicating OP caused by the organic matrix.

When combining OP^{GSH} values from all three articles, a slight correlation with moisture content (r = 0.5) still persisted; and when focusing on bituminous coals OP^{GSH} correlation increased, with a higher driver in moisture content (r = 0.7).

According to the results, while OP^{AA} is mainly governed by specific minerals or elements, OP^{GSH} is mostly influenced by the organic matter of coal dust because moisture and elements such as H, B, and in some cases Ca, being associated with the organic matter content (Swaine, 1990), which, as already reported above, yields to a coarser dust when compared with high clay mineral matter, and then giving positive correlations of OP^{GSH} and particle size of RDD and CP_4 (Oberdörster et al., 2005). However, although the association between OP^{GSH} and moisture of PM was not directly referenced in bibliography, several authors outlined the possible contribution of moisture to developing ROS in studies where OP^{GHS} increased with coal rank, with decreasing moisture of coaly matrix (Attfield and Morring, 1992; Castranova and

Vallyathan, 2000; Dalal et al., 1995; Huang et al., 2005, 1998; Maclaren et al., 1989; Stach et al., 1982). Therefore, moisture derived from condensation and water spraying in coal mines (such as the open-pit of this PhD thesis) might also increase OP^{GSH}. Thus, wettability of coal and coal dust has been closely related to the surface hydroxyl functional group, which could contribute to the pathogenesis of CWP (Xu et al., 2017).

5.4.2.3. Dithiothreitol, OP^{DTT}

OP^{DTT} analyses were only implemented in Article #5 for both RDD and CP_4 samples, with a slight correlation found for Na and Mg (r = 0.6–0.5) and moisture content (r = 0.4). When evaluating the correlation only for bituminous coals, OP^{DTT} values were correlated for Na, B, Sr, and particle size (D_{25}), moisture content and quartz (r=0.6-0.4), and especially for Mg (r = 0.70).

As for OP^{GSH}, OP^{DTT} was found to be strongly linked with the content of organic matter of CP_4 (as traced by the correlation with moisture content and particle size), and the content of some organic-associated elements, such as B, Ge and W (Swaine, 1990, among others). Gao et al. (2020) and Nishita-Hara et al. (2019) found correlations between OP^{DTT} and Mg contents.

5.4.3. Multilinear regression analysis of the oxidative potential of coal dust

After the cross-correlation analyses presented in the prior section, multilinear regression analyses were carried out to simplify interpretations on the identification of the major drivers of OP for coal dust.

In Article #3, OP^{AA} drivers were Fe, anatase and sulphate minerals, while for $OP^{GSH,}$ the results were less robust, with Mg accounting for a fraction of this OP type in the RDD samples. In Article #4, anatase and sulphate minerals accounted for most of the OP^{AA}, while moisture and Ca accounted for most of OP^{GSH} when combining RDD samples from Articles #3 and #4.

In Article #5, OP^{AA} in the CP_4 samples was mostly accounted by the contents of Fe, pyrite, sulphates and anatase, while OP^{GSH} was mostly accounted by moisture contents and OP^{DTT} by contents Mg, Na and Ba. When focusing only to the bituminous coals Al contents were added to the above elements and minerals for OP^{AA}, and Ba was removed for OP^{DTT}.

According to the above results, OP^{AA} of RDD and CP_4 is mostly driven by the contents of Fe, pyrite, sulphate minerals from pyrite oxidation and anatase. The only case study of this PhD thesis where Fe and pyrite do not influence OP^{AA} is the open-pit mine of Article #4, because of the extremely low contents of Fe and pyrite in these samples. Several authors have already highlighted the relevant role in ROS generation of Fe, pyrite, anatase and sulphate in coal dust, with the potentially associated impact on coal miners' health (Cohn et al., 2006b; Fang et al., 2017; Fubini and Hubbard, 2003; Gilmour et al., 2004; Hamilton et al., 2009; Harrington et al., 2012; Huang et al., 2005, 1998; Liu and Liu, 2020; Schins and Borm, 1999; Weber et al., 2016; Zhang et al., 2021). On the other hand, OP^{GSH} and OP^{DTT} are driven by the contents of organic matter and, probably, water from condensation or spraying, Mg, Na and Ba. A number of studies are in accordance with prior studies which found a relevant role of organic matter and/or moisture Ca species, Mg, Na and Ba of dust in ROS generation (Alcala-Orozco et al., 2020; Attfield and Morring, 1992; Barraza et al., 2020; Castranova and Vallyathan, 2000; Charrier and Anastasio, 2012; Cheng et al., 2021; Dalal et al., 1995; Gao et al., 2020; Huang et al., 2005, 1998;

Iram Batool et al., 2020; Maclaren et al., 1989; Nishita-Hara et al., 2019; Pedroso-Fidelis et al., 2020; Xu et al., 2017; Yu et al., 2018).

5.5. Other results on coal mine dust

Concentrations of suspended dust exposure were measured in Articles #2, #3 and #4. In all cases, PM_{10} measurements and, in some cases, offline analysis of major and trace elements, were carried out in order to evaluate potential occupational exposure in different mines. Furthermore, in Article #4, real-time ambient concentrations of PM_{10}, $PM_{2.5}$, UFP and BC were measured in-situ around PM emission hotspots from different operations in the mine. This was done only in the open-pit mine because of the safety restrictions for operating these instruments using lithium batteries in high explosion risk environments, such as underground coal mines.

5.5.1. PM_{10} measurements

In China, for coal dust with < 10 %crystalline silica, the time-weighted average (TWA) occupational exposure limits (OELs) for TSP and respirable fractions (PM_4) are fixed at 4 and 2.5 mg m^{-3}, respectively, for 8 h means; while, for coal dust with 10–50 %crystalline silica, values are 1.0 and 0.7 mg m^{-3}, respectively (Liang et al., 2006). In Article #3, 11 and 16 mg m^{-3} were measured for TSP, and 3.2 and 4.6 mg m^{-3} PM_{10} for WF#7 and WF#11 respectively, but with a 5.3−3.6 h basis, thus not comparable with the 8 h TWA OELs. In the open–pit from China (Article #4) PM_{10} levels around TH and RT concentration reached 2.7 and 0.1 mg m^{-3}, respectively, for 0.5 h.

Occupational PM_{10} exposure levels in Poland are recommended not to exceed 4.0 or 2.0 mg m^{-3} over a period of 8h, where the coal dust contains 2-10 or 10-50 %crystalline silica, respectively (Basic Legal Act in Poland, 2010). In Article #2, PM_{10} concentrations measured in the Pniowek mine reached 9.8 to 12 mg m^{-3} in zone 'b', 4.7 to 6.0 mg m^{-3} in zone 'a', and 14 to 24 mg m^{-3} in zone 'c'. In the Marcel mine, these reached 8.3 to 9.6 mg m^{-3} in zone 'a', and 12 to 13 mg m^{-3} in zone 'b'. In the Knurów mine, these reached 7.7 to 14 mg m^{-3}, and 3.3 to 6.1 mg m^{-3} in the Bielszowice mine. All this data from Article #2 refers to average concentrations for periods ranging from 1 h to 1.7 h, thus not comparable with OELs. However, the high levels measured point to the need of implementing more effective dust abatement measures and protecting coal workers with sophisticated personal protective equipment correctly worn.

In Article #2, PM_{10} measurements were performed at different distances during coal working operations, using two methods, shearer cutting during long-wall excavations and roadway drivage. Shearer cutting during long-wall excavations (with water sprayer implemented) emitted less PM_{10} dust than the roadway drivage operations. Furthermore, as expected, PM_{10} concentrations were higher closer to the point operations of WFs, with a few exceptions, where effective coal mine ventilation was implemented at the WF. A number of studies have shown that, in addition to ventilation, the WF operations might drastically reduce dust concentrations using the spraying system methods (Marts et al., 2015; McPherson, 1993; NIOSH, 2010; Smith et al., 1994).

The concentrations of major and trace elements in RDD samples (DD_4) were, in specific cases in Articles #2, #3 and #4, compared with those from their respective contents of in-situ sampled

ambient PM_{10}. In the open-pits, higher concentrations were found for some elements, such as Sb, Zn, Mn, Cu, As, Cd and Sn. These elements are usually emitted by mining machinery wear, as well as by brake and tyre wear (Amato et al., 2010).

5.5.2. Real-time measurements in the open-pit mine

Levels of PM_{10}, $PM_{2.5}$, BC and UFP were measured in-situ near specific mining activities, in order to characterise their concentrations in different zones of the open-pit coal mine affected by different mining operations (Article #4).

At the bottom of the mine, PM emissions were moderately high in CWF, mostly due to low wind speeds and the implementation of frequent water spraying as a dust abatement measure. In addition, PM in CWF was coarser than in other parts of the mine, probably due to the very low ash coal dust (high content of low ash coal dust is coarser than high content clay gangue dust, dominating the other zones of the mine) and the agglomeration of particles by repeated water spraying.

Short-time (min) peak concentrations of BC seem to be associated with those of PM but not with those of UFP. This suggests that the exhaust of the excavators extracting and loading coal is the main source of BC. The mean BC levels reach those typically measured in high-traffic urban sites (Reche et al., 2011).

Around TH operations (downloading and uploading) water spraying was not applied because operations were sporadic and changing spatially. For this reason, and because the high content of clay minerals of the gangue, ambient PM levels measured were markedly high, although workers inside the trucks and excavators were protected from this dust. Furthermore, these areas, usually located in the top parts of the mine, were characterised by very low BC and short peaks of high UFP concentrations, due to the high ventilation and the fact that trucks are fuelled with Liquefied-Natural-Gas, with very low BC and PM emissions but high emissions of UFP (Giechaskiel, 2018).

Levels of UFP were higher, deeper into the open-pit mine, where ventilation is reduced, coal is worked and trucks traffic is dense. Again, the levels of UFP measured were close to those frequently measured in high-traffic urban sites (Cassee et al., 2019; Morawska et al., 2008).

Levels of PM, BC and UFP close to a mine road at the top of the mine, were moderate and comparable with data reported from other mining areas (Kurth et al., 2014).

Chapter 6

CONCLUSIONS

6. CONCLUSIONS

This PhD thesis has aimed to characterise underground and open-pit coal mine dust collected from different regions of active coal mines. It has evaluated particle sizes, mineralogical and geochemical patterns and their oxidative potential (OP) as indicator of specific potential health effects. This allowed characterising dust, source origins and identifying major factors controlling its OP. It has also investigated how deposited coal mine dust finer than 500 μm (DD) in coal mines may be used to deduce the mineralogical and chemical patterns of respirable dust in the mine. A novel approach was adopted by separating the respirable (DD < 4 μm) component present in DD (RDD) and comparing its compositional patterns with samples of PM_{10} (particulate matter < 10 μm). Moreover, the separation of powdered coal seam channel profile samples (CP) < 4 μm size (CP_4) was also studied. The main conclusions from this work are shown below.

6.1. Particle size of coal mine dust

i) **Particle size distribution** (PSD) in coal mine dust is a significant parameter for air quality which needs to be studied as it indicates the size of the dust particles, some of which could be harmful to human health when inhaled.

ii) **Moisture content** in RDD and DD plays a key role in controlling its size distribution. Moisture content of DD in a number of mines examined is negatively correlated with the proportion of finer coal dust. Effective use of wetting techniques and ventilation systems in coal mining spaces help not only to abate dust emissions by resuspension, but also to reduce the proportion of fine particles in dust due to the particle agglomeration produced by water. Moreover, water in coal mining also controls coal dust resuspension and the short-term prevention of spontaneous coal dust combustion. However, excessive use of water could lead to some negative outcomes, such as worsening coal workers environments and increasing spontaneous combustion (by inducing exothermic oxidations of specific minerals and organic matter).

iii) **Ash yields** of DD and RDD are positively correlated with the proportion of fine dust when samples from high rank coals are evaluated; in this study coinciding with these having relatively low ash yields. This indicates that, for these low ash high rank coals, when mineral matter (especially clay minerals) increases, dust is finer than when compared to the high coaly matrix dust from the working fronts (WFs). Only in one underground mine, working very high ash subbituminous, was this correlation not evident (Article #3) because all DD and RDD samples have high ash yield.

6.2. Mineralogy and chemical composition coal mine dust

i) **Deposited coal mine dust** decreases in levels and contains a higher relative proportion of the finest particles as the distance from the WFs increases. This is attributed to the higher dust emission levels of operations at the WFs and the deposition of coarser particles close to these, with only the finer fractions being transported longer distances through the galleries. The mineral content of DD samples is relatively higher than that of respective parental worked coal seams. This is as expected, because DD receive contributions from not only dust from the coal seam, but from the gangue, salts, machinery wear and gunited walls, as inferred from the mineralogy of DD from different zones of the mines.

ii) **The geochemical patterns of DD** are largely driven by the mining activity carried out in the sampling zones. High-ash DD are basically enriched in clay minerals, quartz and calcite. Those from access galleries contain higher Ca-bearing mineral species, due to dust emitted from lime mortar gunited galleries. These frequently experience the influence of infiltrated phreatic waters affected by acid mine drainage (AMD) that interact with the lime mortar and generate salts and fix metals; thus, the dust emitted from these guinted powder might contain also potentially hazardous dust components (such as sulphate species, As, Sb, among others). Samples of DD from access tunnels in underground coal mines are markedly different in regard to chemical composition, metal content and mineralogy, compared to those of the parent worked coal seams, because, as stated above, the numerous dust emission sources are different to the ones of WFs, where relative contributions to DD increase with the distance.

6.3. Mineralogy and chemical composition of respirable coal mine dust

i) **In RDD and DD sample comparisons**, most average mineral ratios (RDD/DD and CP_4/CP) < 1.0 indicate coarser modes of occurrence. However, ratios for clay minerals are very often > 1.0, especially for RDD/DD, due to their relative finer mode of occurrence. Concentration ratios for anatase are also high, but with a wide standard deviation, particularly for CP_4/CP, due to the wide variety of geochemical patterns included in the CP selection and the different ways that anatase occurs (coarse size in clay mineral assemblages or micronic particles spread in coaly matrices as shown by SEM-EDX in Article #3).
ii) Regarding the **ratios of elemental concentrations**, Zn, Cu, Sn, As and Sb markedly increase in the RDD fractions, something which is potentially problematic, as these elements might be hazardous for human health. Moreover, relatively high RDD/DD ratios were obtained for Se, Mo, Pb, Zn, Sn, As, Cu and Sb, as well as Ni, Co and Cr, while not for CP_4/CP, probably to the fact that the main source of these for RDD is not the worked coal dust but other dust sources, such as AMD-derived mine dust, gangue dust and machinery wear as supported by Articles #3 and #4.

6.4. Oxidative potential of respirable coal mine dust

i) In absolute values, **OP of RDD and CP_4** lie within the range of those reported for underground coal mine dust from a recent publication by Zazouli et al. (2021), as far as we know the only reporting data on this apart from Articles #3 to #5. However, these OP values are markedly lower (2 to 5-fold) than those reported from PM from subway systems, valleys with high domestic biomass burning or roadside sites.
ii) **Ascorbic acid OP (OP^{AA})** of RDD and CP_4 is mostly driven by specific inorganic species and elements. The main drivers are Fe, pyrite, sulphate minerals and anatase. Moreover, the correlations of the concentrations of these components of dust or coal with OP^{AA} increases further if only high rank coal or coal dust (mostly bituminous in this study) is evaluated. The strong correlations between Fe or pyrite with OP found here are in agreement with other studies supporting the relevance of the Fe and pyrite contents in inhalable particles from coal dust for oxidative stress (i.e. Cohn et al., 2006b; Liu and Liu, 2020; Yu et al., 2020; Zazouli et al., 2021; Zhang et al., 2021), which, in turn, may lead to lung injury and coal workers pneumoconiosis (CWP) development (Harrington et al., 2012; Huang et al., 2005).

iii) **Glutathione OP and dithiothreitol OP** (OP^{GSH} and OP^{DTT}, respectively) of RDD and CP_4 are found to be driven by the organic (coaly) part of coal and coal dust and moisture content, as well as by the content of Ca, Mg, Na and Ba, again with an increase in the correlations of OP and these components when only hard coals are considered. This is in accordance with prior studies supplying evidence for the associations of the generation of reactive oxidative species (ROS) and organic matter, water or Mg contents of dust (i.e. Gao et al., 2020; Nishita-Hara et al., 2019; Xu et al., 2017).

iv) If the **influence of coal geochemical patterns on OP** is evaluated (OP data of 22 CP_4 samples obtained from powdered coal, thus only varying the compositional patterns of coal), it is evident that OP^{AA} is driven by Fe, pyrite, anatase sulphate minerals. Moreover, coals with high As, K, S, Si, Al, and Cr, and especially U, Mo and V, are highly correlated, with OP^{AA}. For the OP^{GSH}, results are very similar to those from RDD, with a high role of organic matter, water and coarser particles and additionally for Na and Mg, in the case of OP^{DTT}.

6.5. Other conclusions on coal mine dust

i) Results of **PM_{10} ambient measurements** from coal mines evidence the importance of the effectiveness of methods used in underground coal mines in order to reduce airborne dust concentrations. In some cases, PM_{10} levels at the WFs were not the highest in the mine, due to the implementation of dust abatement measures and to the adequate ventilation. In other cases, PM_{10} occupational exposure limits (OEL) were exceeded, but concentrations were measured for periods (1 to 2.5 h) shorter than 8 h, as the OEL recommends, and therefore cannot be directly compared.

ii) When **comparing RDD and PM_{10}** sampled at the same locations at WFs, it becomes evident that, for most elements, contents similar or slightly lower are found in PM_{10}, when compared with RDD samples. However, for other elements, such as Sb, Zn, Mn, Cu, As, Cd and Sn, they are higher in PM_{10} samples. The latter is probably due to the higher impact of the working machinery (underground and open-pit mines) and brake and tyre wear from vehicles (open-pit mine) on PM_{10}, compared to RDD.

iii) **Online measurements of PM_{10}**, black carbon (BC) and ultrafine particles (UFP) in the open-pit coal mine indicate that the dust registered at the bottom of the open-pit mine was more concentrated than in the top mine zones, even though the wetting system was only used in the coal WF (bottom of the pit) and on mine roads, excluding tailings handling (TH) areas. This is due to the lack of air dispersion at the bottom of the mine in contrast with the top areas, and to the high machinery and truck density, reflecting again the importance of dust control and abatement within coal mines. Moreover, it would suggest that BC peaks measured were linked to exhaust emission of the excavators extracting and loading coal, whilst the principal source of UFP emissions was trucks fuelled with Liquefied-Natural-Gas. Also, very high PM_{10} levels were measured around the TH areas, where water flushing was not implemented.

iv) **These results highlight** the need to implement high efficiency primary and secondary coal dust abatement measures in coal mines, especially when mining high pyrite coals. As intensive coal mining in countries such as China will continue in the forthcoming decades (BP, 2021), large numbers of miners will continue to be exposed to coal dust (Han et al., 2019; Jin et al., 2018; NIOSH, 2010; Wang et al., 2020; Yuan et al., 2017). The occupational inhalation

of coal dust presents a problem that does not appear to have diminished in recent years, and there is a clear need for further research on coal dust and occupational health, and on coal dust abatement controls.

Chapter 7

LIMITATIONS AND FUTURE RESEARCH

7. LIMITATIONS AND FUTURE RESEARCH

The research described in this PhD thesis aims to promote a better understanding of the environmental and occupational characterisation of dusts produced during coal mining. It has centred on an intensive series of sampling campaigns carried out within mines and has produced a large amount of geochemical data, as well as data on toxicity indicators, giving to this research a different focus to that of previous coal mining studies.

7.1. Limitations

Although dedicated protocols were followed during the study, several limitations were identified after the sampling and analysing activities were completed. Firstly, it was assumed that an extensive occupational PM_4 sampling campaign would be more representative than extracting the RDD of DD or from powdered coal samples (CP_4). However, the cost, time and sampling limitation (i.e., time restrictions for sampling around several operations into the mine, the prohibition on using lithium batteries, mine safety rules, extreme sampling conditions and the reduction of coal mine productivity) in coal mines, made this task extremely difficult. The conditions could not be fully replicated, and it must be supposed that the respirable fraction of deposited dust is similar in composition to the one in suspension. However, the method allowed sampling around several operations in the coal mine affected by sources of PM, including not only the dust from the worked coal seam or the other sediments where coal is interlayered, but also the wear of machinery, salts and other components from precipitates of AMD, among others. For this reason, numerous DD samples were collected from diverse places of the coal mine and then the RDD fraction was separated in the laboratory in order to simulate the PM_4 fraction in coal mines.

In addition, occupational PM_{10} and RDD samples were difficult to collect to establish a comparative concentration with the RDD fraction and cover a wide variety of coal compositional properties. Thus, in order to have the larger possible number of samples, the study included samples sent by collaborators from Slovenia and Poland (PM_{10} and RDD) and China (22 powdered samples of channel coal seam profiles CP, from which the respirable fraction CP_4 was extracted), reducing time and cost but increasing the possible variances between sample way of collection. In the case of CP_4, this tries to simulate PM_4 dust produced from the working of the coal faces, but without the effect of the machinery wear and gangue dust.

Furthermore, in conjunction with the sampling limitations, the safety protocols used in coal mining are extremely strict, complicating even more data collection. In other less strict environments, a sampling procedure could have been designed differently, facilitating sample collection as well as monitoring measurements.

7.2. Future research

This study was focused on the environmental characterisation of coals and dust from coal mining of potential relevance to occupational exposure, which is an uncommon topic with a relatively sparse bibliography. In the light of the experience acquired during the study, along with the difficulties identified, methodological modifications should be employed in future similar investigations.

Firstly, a sampling campaign should ideally be carried out in underground mines using occupational PM samplers, specifically designed for use in this environment, in parallel with DD sample collection, in order to compare all contemporaneous data, avoiding possible errors and limitations produced in the DD sampling campaign. Moreover, occupational PM samplers should be used under OEL specifications.

Furthermore, in open-pit mines, an extensive coal, gangue and deposited dust sampling, as well as extensive online and PM occupational measurements in different zones affected by dust from diverse mining operations need to be evaluated. PM exposure of workers inside trucks and excavators should also be considered, as well as the PM in surrounding areas of the mine. Afterwards, sampling and measurements should be repeated in different open-pit mines to identify possible common patterns, including the different techniques carried out in each open-pit mine.

Moreover, other possible future works should focus on the geochemical fractionation of chemical elements in coal dust, analysing the different sizes of dust samples (PM_{10}, $PM_{2.5}$ and $PM_{0.1}$ at least) and identifying in which size fraction minerals and chemicals elements are concentrated. This could be done with a cascade impactor device.

Additionally, investigations into how dust control measures affect dust levels and properties and into the reduction of the health effects of various potentially hazardous elements/minerals such as Fe, pyrite, anatase or sulphates in coal and coal dust are necessary. For example Huang et al. (2005) explain that coals with carbonate minerals might reduce sulphate and pyrite effects in CWP injuries. Moreover, as Article #3 shows, pyrite is embedded in clay minerals reducing its possible health effects.

Finally, the OP measurements collected are useful indicators of potential toxicology effects. However, more studies on the direct toxicological analyses that could also relate coal dust effects to coal miners' injuries, using toxicological "in vitro" assays, pulmonary cells, DNA damage tests, or epidemiological studies, are necessary. Also, the use of other techniques that will complement OP analysis performed for coal and coal dust could help to identify potentially hazardous elements more easily. In short, the use of toxicological techniques is more related to human health than OP, because the latter does not imply a correlation between some health outcomes and diverse contaminants. However, it does suggest probable concerns in health outcomes.

Chapter 8

REFERENCES

8. REFERENCES

Ahamed, M.A.A., Perera, M.S.A., Matthai, S.K., Ranjith, P.G., Dong-yin, L., 2019. Coal composition and structural variation with rank and its influence on the coal-moisture interactions under coal seam temperature conditions – A review article. J. Pet. Sci. Eng. https://doi.org/10.1016/j.petrol.2019.06.007

Ahern, M.M., Hendryx, M., Conley, J., Fedorko, E., Ducatman, A., Zullig, K.J., 2011. The association between mountaintop mining and birth defects among live births in central Appalachia, 1996-2003. Environ. Res. 111, 838–846. https://doi.org/10.1016/j.envres.2011.05.019

Ajrash, M.J., Zanganeh, J., Moghtaderi, B., 2017. The effects of coal dust concentrations and particle sizes on the minimum auto-ignition temperature of a coal dust cloud. Fire Mater. 41, 908–915. https://doi.org/10.1002/fam.2437

Akcil, A., Koldas, S., 2006. Acid Mine Drainage (AMD): causes, treatment and case studies. J. Clean. Prod. 14, 1139–1145. https://doi.org/10.1016/j.jclepro.2004.09.006

Alcala-Orozco, M., Caballero-Gallardo, K., Olivero-Verbel, J., 2020. Intergenerational effects of coal dust on Tribolium castaneum, Herbst. Environ. Res. 182, 109055. https://doi.org/10.1016/j.envres.2019.109055

Alcobé, X., Bassas, J., Tarruella, I., Roca, A., Viñals, J., 2001. Structural characterization of synthetic beudantite-type phases by Rietveld refinement, in: Materials Science Forum. Trans Tech Publications Ltd, pp. 671–676. https://doi.org/10.4028/www.scientific.net/msf.378-381.671

Allardice, D.J., Clemow, L.M., Jackson, W.R., 2003. Determination of the acid distribution and total acidity of low-rank coals and coal-derived materials by an improved barium exchange technique. Fuel 82, 35–40. https://doi.org/10.1016/S0016-2361(02)00193-X

Amato, F., Pandolfi, M., Viana, M., Querol, X., Alastuey, A., Moreno, T., 2009. Spatial and chemical patterns of PM10 in road dust deposited in urban environment. Atmos. Environ. 43, 1650–1659. https://doi.org/10.1016/j.atmosenv.2008.12.009

Amato, F., Querol, X., Johansson, C., Nagl, C., Alastuey, A., 2010. A review on the effectiveness of street sweeping, washing and dust suppressants as urban PM control methods. Sci. Total Environ. 408, 3070–3084. https://doi.org/10.1016/j.scitotenv.2010.04.025

Andersen, Z J, Wahlin, P., Raaschou-Nielsen, O., Ketzel, M., Scheike, T., Loft, S., Andersen, Zorana J, 2008. Size distribution and total number concentration of ultrafine and accumulation mode particles and hospital admissions in children and the elderly in Copenhagen, Denmark. Occup Env. Med 65, 458–466. https://doi.org/10.1136/oem.2007.033290

Antao, V.C.D.S., Petsonk, E.L., Sokolow, L.Z., Wolfe, A.L., Pinheiro, G.A., Hale, J.M., Attfield, M.D., 2005. Rapidly progressive coal workers' pneumoconiosis in the United States: Geographic clustering and other factors. Occup. Environ. Med. 62, 670–674. https://doi.org/10.1136/oem.2004.019679

Apostoli, P., Lucchini, R., Alessio, L., 2000. Are current biomarkers suitable for the assessment of manganese exposure in individual workers? Am. J. Ind. Med. 37, 283–290. https://doi.org/10.1002/(SICI)1097-0274(200003)37:3<283::AID-AJIM6>3.0.CO;2-E

Aruoma, O.I., 1998. Free radicals, oxidative stress, and antioxidants in human health and disease. J. Am. Oil Chem. Soc. 75, 199–212. https://doi.org/10.1007/s11746-998-0032-9

Attfield, M.D., Morring, K., 1992. An investigation into the relationship between coal workers' pneumoconiosis and dust exposure in u.s. coal miners. Am. Ind. Hyg. Assoc. J. 53, 486–492. https://doi.org/10.1080/15298669291360012

Ayres, J.G., Borm, P., Cassee, F.R., Castranova, V., Donaldson, K., Ghio, A., Harrison, R.M., Hider, R., Kelly, F., Kooter, I.M., Marano, F., Maynard, R.L., Mudway, I., Nel, A., Sioutas, C., Smith, S., Baeza-Squiban, A., Cho, A., Duggan, S., Froines, J., 2008. Evaluating the toxicity of airborne particulate matter and nanoparticles by measuring oxidative stress potential - A workshop report and consensus statement, in: Inhalation Toxicology. Taylor & Francis, pp. 75–99. https://doi.org/10.1080/08958370701665517

Azam, S., Mishra, D.P., Wang, X., Yuan, S., Li, X., Jiang, B., 2019. Synergistic effect of surfactant compounding on improving dust suppression in a coal mine in Erdos, China. Process Saf. Environ. Prot. 344, 35–43. https://doi.org/10.1016/j.powtec.2018.12.061

Bailey-Serres, J., Voesenek, L.A.C.J., 2008. Flooding Stress: Acclimations and Genetic Diversity. https://doi.org/10.1146/annurev.arplant.59.032607.092752

Barber, C., Fishwick, D., 2020. Pneumoconiosis. Med. (United Kingdom). https://doi.org/10.1016/j.mpmed.2020.03.012

Barnwal, J.P., Patil, D.D., Rao, T.E., Kawatra, S.K., 2000. Enrichment of coal macerals using froth flotation. MIinerals Metall. Process. 17, 56–61. https://doi.org/10.1007/BF03402829

Barraza, F., Uzu, G., Jaffrezo, J.-L., Schreck, E., Budzinski, H., Le Menach, K., Dévier, M.-H., Guyard, H., Calas, A., Perez, M.-I., Villacreces, L.-A., Maurice, L., 2020. Contrasts in chemical composition and oxidative potential in PM10 near flares in oil extraction and refining areas in Ecuador. Atmos. Environ. 223, 117302. https://doi.org/10.1016/j.atmosenv.2020.117302

Basic Legal Act in Poland, 2010. OCCUPATIONAL EXPOSURE LIMITS FOR AIRBORNE TOXIC SUBSTANCES. Basic Legal Act in Poland. https://www.ilo.org/wcmsp5/groups/public/---ed_protect/---protrav/---safework/documents/legaldocument/wcms_151571.pdf

Beer, C., Kolstad, H.A., Søndergaard, K., Bendstrup, E., Heederik, D., Olsen, K.E., Omland, Ø., Petsonk, E., Sigsgaard, T., Sherson, D.L., Schlünssen, V., 2017. A systematic review of occupational exposure to coal dust and the risk of interstitial lung diseases. Eur. Clin. Respir. J. https://doi.org/10.1080/20018525.2017.1264711

Benitez-Polo, Z., Velasco, L.A., 2020. Effects of suspended mineral coal dust on the energetic physiology of the Caribbean scallop Argopecten nucleus (Born, 1778). Environ. Pollut. 260, 114000. https://doi.org/10.1016/j.envpol.2020.114000

Berry, K.L.E., Hoogenboom, M.O., Brinkman, D.L., Burns, K.A., Negri, A.P., 2017. Effects of coal

contamination on early life history processes of a reef-building coral, Acropora tenuis. Mar. Pollut. Bull. 114, 505–514. https://doi.org/10.1016/j.marpolbul.2016.10.011

Betteridge, D.J., 2000. What is oxidative stress? Metabolism. 49, 3–8. https://doi.org/10.1016/S0026-0495(00)80077-3

Bielowicz, B., 2013. Relationship between random reflectance of ulminite B/collotelinite and technological parameters of Polish low-rank coal. Fuel 111, 229–238. https://doi.org/10.1016/j.fuel.2013.04.034

Blackley, D.J., Halldin, C.N., Scott Laney, A., 2018. Continued increase in prevalence of coal workers' pneumoconiosis in the United States, 1970-2017. Am. J. Public Health 108, 1220–1222. https://doi.org/10.2105/AJPH.2018.304517

Borm, P.J.A., 1997. Toxicity and occupational health hazards of coal fly ash (CFA). A review of data and comparison to coal mine dust. Ann. Occup. Hyg. 41, 659–676. https://doi.org/10.1016/S0003-4878(97)00026-4

Borm, P.J.A., Kelly, F., Künzli, N., Schins, R.P.F., Donaldson, K., 2007. Oxidant generation by particulate matter: From biologically effective dose to a promising, novel metric. Occup. Environ. Med. https://doi.org/10.1136/oem.2006.029090

BP, 2021. Statistical Review of World Energy 2021. BP, 70. https://www.bp.com/content/dam/bp/business-sites/en/global/corporate/pdfs/energy-economics/statistical-review/bp-stats-review-2021-full-report.pdf.

Brown, J.S., Gordon, T., Price, O., Asgharian, B., 2013. Thoracic and respirable particle definitions for human health risk assessment. Part. Fibre Toxicol. 10, 12. https://doi.org/10.1186/1743-8977-10-12

Caballero-Gallardo, K., Olivero-Verbel, J., 2016. Mice housed on coal dust-contaminated sand: A model to evaluate the impacts of coal mining on health. Toxicol. Appl. Pharmacol. 294, 11–20. https://doi.org/10.1016/j.taap.2016.01.009

Calas, A., Uzu, G., Kelly, F.J., Houdier, S., Martins, J.M.F., Thomas, F., Molton, F., Charron, A., Dunster, C., Oliete, A., Jacob, V., Besombes, J.-L., Chevrier, F., Jaffrezo, J.-L., 2018. Comparison between five acellular oxidative potential measurement assays performed with detailed chemistry on PM₁₀ samples from the city of Chamonix (France). Atmos. Chem. Phys. 18, 7863–7875. https://doi.org/10.5194/acp-18-7863-2018

Canu, I.G., Garsi, J.P., Caër-Lorho, S., Jacob, S., Collomb, P., Acker, A., Laurier, D., 2012. Does uranium induce circulatory diseases? First results from a French cohort of uranium workers. Occup. Environ. Med. 69, 404–409. https://doi.org/10.1136/oemed-2011-100495

Canu, I.G., Jacob, S., Cardis, E., Wild, P., Caër, S., Auriol, B., Garsi, J.P., Tirmarche, M., Laurier, D., 2011. Uranium carcinogenicity in humans might depend on the physical and chemical nature of uranium and its isotopic composition: Results from pilot epidemiological study of French nuclear workers. Cancer Causes Control 22, 1563–1573.

https://doi.org/10.1007/s10552-011-9833-5

Cardott, B.J., Curtis, M.E., 2018. Identification and nanoporosity of macerals in coal by scanning electron microscopy. Int. J. Coal Geol. 190, 205–217. https://doi.org/10.1016/j.coal.2017.07.003

Carretero, M.I., Gomes, C.S.F., Tateo, F., 2006. Chapter 11.5 Clays and Human Health. Dev. Clay Sci. https://doi.org/10.1016/S1572-4352(05)01024-X

Cassee, F.R., Morawska, L., Peters, A., 2019. Ambient ultrafine particles : evidence for policy makers. https://efca.net/files/WHITE%20PAPER-UFP%20evidence%20for%20policy%20makers%20(25%20OCT).pdf

Castranova, V., 2000. From Coal Mine Dust To Quartz: Mechanisms of Pulmonary Pathogenicity. Inhal. Toxicol. 12, 7–14. https://doi.org/10.1080/08958378.2000.11463226

Castranova, V., Vallyathan, V., 2000. Silicosis and coal workers' pneumoconiosis. Environ. Health Perspect. 108, 675–684. https://doi.org/10.1289/ehp.00108s4675

Cecil, C.B., Stanton, R.W., Dulong, F.T., Renton, J.J., 1982. GEOLOGIC FACTORS THAT CONTROL MINERAL MATTER IN COAL, in: Plenum Press (Ed.), Atomic and Nuclear Methods in Fossil Energy Research. R. H. Filby et al. (eds.), New York, pp. 323–335.

CEN, E.C. for S., 1992. Workplace atmospheres: size fraction definitions for measurement of airborne particles in the workplace, CEN - EN 481.

Charrier, J.G., Anastasio, C., 2012. On dithiothreitol (DTT) as a measure of oxidative potential for ambient particles: Evidence for the importance of soluble \newline transition metals. Atmos. Chem. Phys. 12, 9321–9333. https://doi.org/10.5194/acp-12-9321-2012

Chaudhuri, S.N., 2016. Coalification, in: Encyclopedia of Mineral and Energy Policy. Springer Berlin Heidelberg, pp. 1–2. https://doi.org/10.1007/978-3-642-40871-7_92-1

Chelgani, S.C., Mesroghli, S., Hower, J.C., 2010. Simultaneous prediction of coal rank parameters based on ultimate analysis using regression and artificial neural network. Int. J. Coal Geol. 83, 31–34. https://doi.org/10.1016/j.coal.2010.03.004

Cheng, Y., Ma, Y., Dong, B., Qiu, X., Hu, D., 2021. Pollutants from primary sources dominate the oxidative potential of water-soluble PM2.5 in Hong Kong in terms of dithiothreitol (DTT) consumption and hydroxyl radical production. J. Hazard. Mater. 405, 124218. https://doi.org/10.1016/j.jhazmat.2020.124218

Cho, A.K., Sioutas, C., Miguel, A.H., Kumagai, Y., Schmitz, D.A., Singh, M., Eiguren-Fernandez, A., Froines, J.R., 2005. Redox activity of airborne particulate matter at different sites in the Los Angeles Basin. Environ. Res. 99, 40–47. https://doi.org/10.1016/j.envres.2005.01.003

Choi, H., Thiruppathiraja, C., Kim, S., Rhim, Y., Lim, J., Lee, S., 2011. Moisture readsorption and low temperature oxidation characteristics of upgraded low rank coal. Fuel Process. Technol. 92, 2005–2010. https://doi.org/10.1016/j.fuproc.2011.05.025

Christian, R.T., Nelson, J.B., Cody, T.E., Larson, E., Bingham, E., 1979. Coal Workers' Pneumoconiosis: In vitro study of the chemical composition and particle size as causes of

the toxic effects of coal. Environ. Res. 20, 358–365. https://doi.org/10.1016/0013-9351(79)90012-4

Chung, F.H., 1974. Quantitative interpretation of X-ray diffraction patterns of mixtures. I. Matrix-flushing method for quantitative multicomponent analysis. J. Appl. Crystallogr. 7, 519–525. https://doi.org/10.1107/s0021889874010375

Clark, R., Zucker, N., Urpelainen, J., 2020. The future of coal-fired power generation in Southeast Asia. Renew. Sustain. Energy Rev. 121, 109650. https://doi.org/10.1016/j.rser.2019.109650

Clymo, R.S., 1983. Ecosystems of the World, 4A: Mires: swamp, bog, fen and moor. Regional studies, Journal of Range Management. Elsevier, Amsterdam. https://doi.org/10.2307/3898373

Cobb, J.C., Cecil, C.B., 1993. Modern and Ancient Coal-Forming Environments. Geological Society of America. https://doi.org/10.1130/SPE286

Cogram, P., 2018. Jarosite, in: Reference Module in Earth Systems and Environmental Sciences. Elsevier. https://doi.org/10.1016/b978-0-12-409548-9.10960-1

Cohen, R., Patel, A., Green, F., 2008. Lung Disease Caused by Exposure to Coal Mine and Silica Dust. Semin. Respir. Crit. Care Med. 29, 651–661. https://doi.org/10.1055/s-0028-1101275

Cohen, R., Velho, V., 2002. Update on respiratory disease from coal mine and silica dust. Clin. Chest Med. 23, 811–826. https://doi.org/10.1016/S0272-5231(02)00026-6

Cohen, R.A., Petsonk, E.L., Rose, C., Young, B., Regier, M., Najmuddin, A., Abraham, J.L., Churg, A., Green, F.H.Y., 2016. Lung pathology in U.S. coal workers with rapidly progressive pneumoconiosis implicates silica and silicates. Am. J. Respir. Crit. Care Med. 193, 673–680. https://doi.org/10.1164/rccm.201505-1014OC

Cohen, R.A.C., Patel, A., Green, F.H.Y., 2008. Lung disease caused by exposure to coal mine and silica dust. Semin. Respir. Crit. Care Med. https://doi.org/10.1055/s-0028-1101275

Cohn, C.A., Borda, M.J., Schoonen, M.A.A., 2004. RNA decomposition by pyrite-induced radicals and possible role of lipids during the emergence of life. Earth Planet. Sci. Lett. 225, 271–278. https://doi.org/10.1016/j.epsl.2004.07.007

Cohn, C.A., Laffers, R., Schoonen, M.A.A., 2006a. Using Yeast RNA as a Probe for Generation of Hydroxyl Radicals by Earth Materials. Environ. Sci. Technol. 40, 2838–2843. https://doi.org/10.1021/es052301k

Cohn, C.A., Laffers, R., Simon, S.R., O'riordan, T., Schoonen, M.A., 2006b. Role of pyrite in formation of hydroxyl radicals in coal: possible implications for human health. https://doi.org/10.1186/1743-8977-3-16

Cohn, C.A., Mueller, S., Wimmer, E., Leifer, N., Greenbaum, S., Strongin, D.R., Schoonen, M.A.A., 2006c. Pyrite-induced hydroxyl radical formation and its effect on nucleic acids. Geochem. Trans. 7, 3. https://doi.org/10.1186/1467-4866-7-3

Cohn, C.A., Pak, A., Strongin, D., Schoonen, M.A., 2005. Quantifying hydrogen peroxide in iron-

containing solutions using leuco crystal violet. https://doi.org/10.1063/1.1935449

Cooper, R., Harrison, A., 2009. The exposure to and health effects of antimony. Indian J. Occup. Environ. Med. 13, 3–10. https://doi.org/10.4103/0019-5278.50716

D'Autréaux, B., Toledano, M.B., 2007. ROS as signalling molecules: Mechanisms that generate specificity in ROS homeostasis. Nat. Rev. Mol. Cell Biol. 8, 813–824. https://doi.org/10.1038/nrm2256

Daellenbach, K.R., Uzu, G., Jiang, J., Cassagnes, L.E., Leni, Z., Vlachou, A., Stefenelli, G., Canonaco, F., Weber, S., Segers, A., Kuenen, J.J.P., Schaap, M., Favez, O., Albinet, A., Aksoyoglu, S., Dommen, J., Baltensperger, U., Geiser, M., El Haddad, I., Jaffrezo, J.L., Prévôt, A.S.H., 2020. Sources of particulate-matter air pollution and its oxidative potential in Europe. Nature 587, 414–419. https://doi.org/10.1038/s41586-020-2902-8

Daemen, J.J.K., 2004. Coal Industry, History of. Encycl. Energy 1, 457–473. https://doi.org/10.1016/b0-12-176480-x/00043-7

Dai, S., Zhang, W., Seredin, V. V., Ward, C.R., Hower, J.C., Song, W., Wang, X., Li, X., Zhao, L., Kang, H., Zheng, L., Wang, P., Zhou, D., 2013. Factors controlling geochemical and mineralogical compositions of coals preserved within marine carbonate successions: A case study from the Heshan Coalfield, southern China. Int. J. Coal Geol. 109–110, 77–100. https://doi.org/10.1016/j.coal.2013.02.003

Dalal, N.S., Newman, J., Pack, D., Leonard, S., Vallyathan, V., 1995. Hydroxyl radical generation by coal mine dust: Possible implication to coal workers' pneumoconiosis (CWP). Free Radic. Biol. Med. 18, 11–20. https://doi.org/10.1016/0891-5849(94)E0094-Y

de Matteis, S., Heederik, D., Burdorf, A., Colosio, C., Cullinan, P., Henneberger, P.K., Olsson, A., Raynal, A., Rooijackers, J., Santonen, T., Sastre, J., Schlünssen, V., Tongeren, M. Van, Sigsgaard, T., 2017. Current and new challenges in occupational lung diseases. Eur. Respir. Rev. https://doi.org/10.1183/16000617.0080-2017

Diessel, C.F.K., 1992. Coal-Bearing Depositional Systems, Coal-Bearing Depositional Systems. https://doi.org/10.1007/978-3-642-75668-9

Dodson, J., Li, X., Sun, N., Atahan, P., Zhou, X., Liu, H., Zhao, K., Hu, S., Yang, Z., 2014. Use of coal in the Bronze Age in China. Holocene 24, 525–530. https://doi.org/10.1177/0959683614523155

Dong, K.-Y., Sun, R.-J., Li, H., Jiang, H.-D., 2017. A review of China's energy consumption structure and outlook based on a long-range energy alternatives modeling tool. Pet. Sci. 14, 214–227. https://doi.org/10.1007/s12182-016-0136-z

Dyrkacz, G.R., Horwitz, E.P., 1982. Separation of coal macerals. Fuel 61, 3–12. https://doi.org/10.1016/0016-2361(82)90285-X

Eguchi, S., Takayabu, H., Lin, C., 2021. Sources of inefficient power generation by coal-fired thermal power plants in China: A metafrontier DEA decomposition approach. Renew. Sustain. Energy Rev. 138, 110562. https://doi.org/10.1016/j.rser.2020.110562

Erol, I., Aydin, H., Didari, V., Ural, S., 2013. Pneumoconiosis and quartz content of respirable dusts in the coal mines in Zonguldak, Turkey. Int. J. Coal Geol. 116–117, 26–35. https://doi.org/10.1016/j.coal.2013.05.008

Fan, T., Zhou, G., Wang, J., 2018. Preparation and characterization of a wetting-agglomeration-based hybrid coal dust suppressant. Process Saf. Environ. Prot. 113, 282–291. https://doi.org/10.1016/j.psep.2017.10.023

Fang, T., Guo, H., Zeng, L., Verma, V., Nenes, A., Weber, R.J., 2017. Highly Acidic Ambient Particles, Soluble Metals, and Oxidative Potential: A Link between Sulfate and Aerosol Toxicity. Environ. Sci. Technol 51, 40. https://doi.org/10.1021/acs.est.6b06151

Fang, X., Yuan, L., Jiang, B., Zhu, W., Ren, B., Chen, M., Mu, M., Yu, G., Li, P., 2020. Effect of water–fog particle size on dust fall efficiency of mechanized excavation face in coal mines. J. Clean. Prod. 254, 120146. https://doi.org/10.1016/j.jclepro.2020.120146

Finaud, J., Lac, G., Filaire, E., 2006. Oxidative Stress. Sport. Med. 36, 327–358. https://doi.org/10.2165/00007256-200636040-00004

Finkelman, R.B., 1999. Trace Elements in Coal Environmental and Health Significance. Biol. Trace Elem. Res. 67, 197–204. https://doi.org/10.1007/BF02784420

Finkelman, R.B., 1994. Modes of occurrence of potentially hazardous elements in coal: levels of confidence. Fuel Process. Technol. 39, 21–34. https://doi.org/10.1016/0378-3820(94)90169-4

Finkelman, R.B., Dai, S., French, D., 2019. The importance of minerals in coal as the hosts of chemical elements: A review. Int. J. Coal Geol. 212, 103251. https://doi.org/10.1016/j.coal.2019.103251

Finkelman, R.B., Orem, W., Castranova, V., Tatu, C.A., Belkin, H.E., Zheng, B., Lerch, H.E., Maharaj, S. V., Bates, A.L., 2002. Health impacts of coal and coal use: Possible solutions. Int. J. Coal Geol. 50, 425–443. https://doi.org/10.1016/S0166-5162(02)00125-8

Finkelman, R.B., Palmer, C.A., Wang, P., 2018. Quantification of the modes of occurrence of 42 elements in coal. Int. J. Coal Geol. 185, 138–160. https://doi.org/10.1016/j.coal.2017.09.005

Finkelman, R.B., Wolfe, A., Hendryx, M.S., 2021. The future environmental and health impacts of coal. Energy Geosci. 2, 99–112. https://doi.org/10.1016/j.engeos.2020.11.001

Flores, R.M., 2013. Coal and Coalbed Gas: Fueling the Future, Coal and Coalbed Gas: Fueling the Future. Elsevier Inc. https://doi.org/10.1016/C2011-0-06861-8

Fu, P.P., Xia, Q., Hwang, H.M., Ray, P.C., Yu, H., 2014. Mechanisms of nanotoxicity: Generation of reactive oxygen species. J. Food Drug Anal. https://doi.org/10.1016/j.jfda.2014.01.005

Fubini, B., Hubbard, A., 2003. Reactive oxygen species (ROS) and reactive nitrogen species (RNS) generation by silica in inflammation and fibrosis. Free Radic. Biol. Med. https://doi.org/10.1016/S0891-5849(03)00149-7

Gao, D., Mulholland, J.A., Russell, A.G., Weber, R.J., 2020. Characterization of water-insoluble

oxidative potential of PM2.5 using the dithiothreitol assay. Atmos. Environ. 224, 117327. https://doi.org/10.1016/j.atmosenv.2020.117327

Gautam, S., Prasad, N., Patra, A.K., Prusty, B.K., Singh, P., Pipal, A.S., Saini, R., 2016. Characterization of PM2.5 generated from opencast coal mining operations: A case study of Sonepur Bazari Opencast Project of India. Environ. Technol. Innov. 6, 1–10. https://doi.org/10.1016/j.eti.2016.05.003

Gelegdorj, E., Chunag, A., Gordon, R.B., Park, J.S., 2007. Transitions in cast iron technology of the nomads in Mongolia. J. Archaeol. Sci. 34, 1187–1196. https://doi.org/10.1016/j.jas.2006.10.007

Ghio, A.J., Quigley, D.R., 1994. Complexation of iron by humic-like substances in lung tissue: Role in coal workers' pneumoconiosis. Am. J. Physiol. - Lung Cell. Mol. Physiol. 267. https://doi.org/10.1152/ajplung.1994.267.2.l173

Giechaskiel, B., 2018. Solid particle number emission factors of euro vi heavy-duty vehicles on the road and in the laboratory. Int. J. Environ. Res. Public Health 15. https://doi.org/10.3390/ijerph15020304

Gilmour, M.I., O'Connor, S., Dick, C.A.J., Miller, C.A., Linak, W.P., 2004. Differential Pulmonary Inflammation and In Vitro Cytotoxicity of Size-Fractionated Fly Ash Particles from Pulverized Coal Combustion. J. Air Waste Manage. Assoc. 54, 286–295. https://doi.org/10.1080/10473289.2004.10470906

Godri, K.J., Harrison, R.M., Evans, T., Baker, T., Dunster, C., Mudway, I.S., Kelly, F.J., 2011. Increased Oxidative Burden Associated with Traffic Component of Ambient Particulate Matter at Roadside and Urban Background Schools Sites in London. PLoS One 6, e21961. https://doi.org/10.1371/journal.pone.0021961

Graber, J.M., Harris, G., Almberg, K.S., Rose, C.S., Petsonk, E.L., Cohen, R.A., 2017. Increasing Severity of Pneumoconiosis Among Younger Former US Coal Miners Working Exclusively Under Modern Dust-Control Regulations. J. Occup. Environ. Med. 59, e105–e111. https://doi.org/10.1097/JOM.0000000000001048

Gregory, D.D., Large, R.R., Halpin, J.A., Baturina, E.L., Lyons, T.W., Wu, S., Danyushevsky, L., Sack, P.J., Chappaz, A., Maslennikov, V. V., Bull, S.W., 2015. Trace element content of sedimentary pyrite in black shales. Econ. Geol. 110, 1389–1410. https://doi.org/10.2113/econgeo.110.6.1389

Gregory, J.C., 1831. Case of Peculiar Black Infiltration of the Whole Lungs, Resembling Melanosis. Edinburgh Med. Surg. J. 36, 389–394.

Guerrero-Castilla, A., Olivero-Verbel, J., Sandoval, I.T., Jones, D.A., 2019. Toxic effects of a methanolic coal dust extract on fish early life stage. Chemosphere 227, 100–108. https://doi.org/10.1016/j.chemosphere.2019.04.012

Gustafsson, Å., Krais, A.M., Gorzsás, A., Lundh, T., Gerde, P., 2018. Isolation and characterization of a respirable particle fraction from residential house-dust. Environ. Res. 161, 284–290. https://doi.org/10.1016/j.envres.2017.10.049

Guthrie, G.D., 1992. Biological effects of inhaled minerals. Am. Mineral. 77, 225–243.

Haibin, L., Zhenling, L., 2010. Recycling utilization patterns of coal mining waste in China. Resour. Conserv. Recycl. 54, 1331–1340. https://doi.org/10.1016/j.resconrec.2010.05.005

Hamilton, R.F., Wu, N., Porter, D., Buford, M., Wolfarth, M., Holian, A., 2009. Particle length-dependent titanium dioxide nanomaterials toxicity and bioactivity. Part. Fibre Toxicol. 6, 1–11. https://doi.org/10.1186/1743-8977-6-35

Han, L., Gao, Q., Yang, J., Wu, Q., Zhu, B., Zhang, H., Ding, B., Ni, C., 2017. Survival Analysis of Coal Workers' Pneumoconiosis (CWP) Patients in a State-Owned Mine in the East of China from 1963 to 2014. Int. J. Environ. Res. Public Health 14, 489. https://doi.org/10.3390/ijerph14050489

Han, L., Yao, W., Bian, Z., Zhao, Y., Zhang, H., Ding, B., Shen, H., Li, P., Zhu, B., Ni, C., 2019. Characteristics and Trends of Pneumoconiosis in the Jiangsu Province, China, 2006–2017. Int. J. Environ. Res. Public Health 16, 437. https://doi.org/10.3390/ijerph16030437

Harrington, A.D., Hylton, S., Schoonen, M.A.A., 2012. Pyrite-driven reactive oxygen species formation in simulated lung fluid: Implications for coal workers' pneumoconiosis. Environ. Geochem. Health 34, 527–538. https://doi.org/10.1007/s10653-011-9438-7

Harris, D.A., Willis, J., Tomann, M., 2020. A new era of coal workers' pneumoconiosis: decades in mines may not be required. Lancet. https://doi.org/10.1016/S0140-6736(20)30731-5

Harrison, J.C., Brower, P.S., Attfield, M.D., Doak, C.B., Keane, M.J., Grayson, R.L., Wallace, W.E., 1997. Surface composition of respirable silica particles in a set of U.S. anthracite and bituminous coal mine dusts. J. Aerosol Sci. 28, 689–696. https://doi.org/10.1016/S0021-8502(96)00033-X

He, J., Li, W., Liu, J., Chen, S., Frost, R.L., 2019. Investigation of mineralogical and bacteria diversity in Nanxi River affected by acid mine drainage from the closed coal mine: Implications for characterizing natural attenuation process. Spectrochim. Acta - Part A Mol. Biomol. Spectrosc. 217, 263–270. https://doi.org/10.1016/j.saa.2019.03.069

Huang, C., Li, J., Zhang, Q., Huang, X., 2002. Role of bioavailable iron in coal dust-induced activation of activator protein-1 and nuclear factor of activated T cells: Difference between Pennsylvania and Utah coal dusts. Am. J. Respir. Cell Mol. Biol. 27, 568–574. https://doi.org/10.1165/rcmb.4821

Huang, X., Finkelman, R.B., 2008. Understanding the chemical properties of macerals and minerals in coal and its potential application for occupational lung disease prevention. J. Toxicol. Environ. Heal. - Part B Crit. Rev. https://doi.org/10.1080/10937400701600552

Huang, X., Fournier, J., Koenig, K., Chen, L.C., 1998. Buffering capacity of coal and its acid-soluble Fe2+ content : Possible Role in Coal Workers ' Pneumoconiosis. Chem Res Toxicol. 7, 722–729. https://doi.org/10.1021/tx970151o

Huang, X., Laurent, P.A., Zalma, R., Pezerat, H., 1993. Inactivation of α1-Antitrypsin by Aqueous Coal Solutions: Possible Relation to the Emphysema of Coal Workers. Chem. Res. Toxicol. 6, 452–458. https://doi.org/10.1021/tx00034a011

Huang, X., Li, W., Attfield, M.D., Nádas, A., Frenkel, K., Finkelman, R.B., 2005. Mapping and prediction of Coal Workers' Pneumoconiosis with bioavailable iron content in the bituminous coals. Environ. Health Perspect. 113, 964–968. https://doi.org/10.1289/ehp.7679

Hudson-Edwards, K.A., Smith, A.M.L.D., Bennett, A.J., Murphy, P.J., Wright, K., 2008. Comparison of the structures of natural and synthetic Pb-Cu-jarosite-type compounds. Eur. J. Mineral. 20, 241–252. https://doi.org/10.1127/0935-1221/2008/0020-1788

Huggins, F.E., 2002. Overview of analytical methods for inorganic constituents in coal. Int. J. Coal Geol. 50, 169–214. https://doi.org/10.1016/S0166-5162(02)00118-0

Hurt, A., Berkes, H., Cypress, A., 2012. What Is Black Lung? https://www.npr.org/2012/07/05/156302772/what-is-black-lung

IEA, 2020. World Energy Outlook 2020. IEA, Paris 124. https://iea.blob.core.windows.net/assets/a72d8abf-de08-4385-8711-b8a062d6124a/WEO2020.pdf

IEO, 2021. International Energy Outlook 2021, Energy Information Administration, US. https://www.eia.gov/outlooks/ieo/pdf/IEO2021_ReleasePresentation.pdf

Iram Batool, A., Huma Naveed, N., Aslam, M., da Silva, J., Fayyaz ur Rehman, M., 2020. Coal Dust-Induced Systematic Hypoxia and Redox Imbalance among Coal Mine Workers. https://doi.org/10.1021/acsomega.0c03977

Ishtiaq, M., Jehan, N., Khan, S.A., Muhammad, S., Saddique, U., Iftikhar, B., Zahidullah, 2018. Potential harmful elements in coal dust and human health risk assessment near the mining areas in Cherat, Pakistan. Environ. Sci. Pollut. Res. 25, 14666–14673. https://doi.org/10.1007/s11356-018-1655-5

Janssen, N.A.H., Yang, A., Strak, M., Steenhof, M., Hellack, B., Gerlofs-Nijland, M.E., Kuhlbusch, T., Kelly, F., Harrison, R., Brunekreef, B., Hoek, G., Cassee, F., 2014. Oxidative potential of particulate matter collected at sites with different source characteristics. Sci. Total Environ. 472, 572–581. https://doi.org/10.1016/j.scitotenv.2013.11.099

Järup, L., 2002. Cadmium overload and toxicity. Nephrol. Dial. Transplant. 17, 35–39. https://doi.org/10.1093/ndt/17.suppl_2.35

Jiang, X., Lu, W.X., Zhao, H.Q., Yang, Q.C., Yang, Z.P., 2014. Potential ecological risk assessment and prediction of soil heavy-metal pollution around coal gangue dump. Nat. Hazards Earth Syst. Sci. 14, 1599–1610. https://doi.org/10.5194/nhess-14-1599-2014

Jin, Y., Fan, J.G., Pang, J., Wen, K., Zhang, P.Y., Wang, H.Q., Li, T., 2018. Risk of Active Pulmonary Tuberculosis among Patients with Coal Workers' Pneumoconiosis: A Case-control Study in China. Biomed. Environ. Sci. 31, 448–453. https://doi.org/10.3967/bes2018.058

Jing, Y., Rabbani, A., Armstrong, R.T., Wang, J., Mostaghimi, P., 2020. A hybrid fracture-micropore network model for multiphysics gas flow in coal. Fuel 281, 118687. https://doi.org/10.1016/j.fuel.2020.118687

Johann-Essex, V., Keles, C., Rezaee, M., Scaggs-Witte, M., Sarver, E., 2017. Respirable coal mine dust characteristics in samples collected in central and northern Appalachia. Int. J. Coal Geol. 182, 85–93. https://doi.org/10.1016/j.coal.2017.09.010

Johnson, R., Bustin, R.M., 2006. Coal dust dispersal around a marine coal terminal (1977-1999), British Columbia: The fate of coal dust in the marine environment. Int. J. Coal Geol. 68, 57–69. https://doi.org/10.1016/j.coal.2005.10.003

Kelly, F.J., 2003. Oxidative stress: Its role in air pollution and adverse health effects. Occup. Environ. Med. 60, 612–616. https://doi.org/10.1136/oem.60.8.612

Kenny, L.C., Hurley, F., Warren, N.D., 2002. Estimation of the risk of contracting pneumoconiosis in the UK coal mining industry. Ann. Occup. Hyg. 46, 257–260. https://doi.org/10.1093/annhyg/46.suppl-1.257

Kerolli-Mustafa, M., Fajković, H., Rončević, S., Ćurković, L., 2015. Assessment of metal risks from different depths of jarosite tailing waste of Trepça Zinc Industry, Kosovo based on BCR procedure. J. Geochemical Explor. 148, 161–168. https://doi.org/10.1016/j.gexplo.2014.09.001

Kim, A.G., 2004. Locating fires in abandoned underground coal mines. Int. J. Coal Geol. 59, 49–62. https://doi.org/10.1016/j.coal.2003.11.003

Kizil, G. V., Donoghue, A.M., 2002. Coal dust exposures in the longwall mines of New South Wales, Australia: A respiratory risk assessment. Occup. Med. (Chic. Ill). 52, 137–149. https://doi.org/10.1093/occmed/52.3.137

Kolitsch, U., Pking, A., 2001. Crystal chemistry of the crandallite, beudantite and alunite groups: A reéiew and eéaluation of the suitability as storage materials for toxic metals. J. Mineral. Petrol. Sci. https://doi.org/10.2465/jmps.96.67

Kolker, A., 2012. Minor element distribution in iron disulfides in coal: A geochemical review. Int. J. Coal Geol. https://doi.org/10.1016/j.coal.2011.10.011

Koplitz, S.N., Jacob, D.J., Sulprizio, M.P., Myllyvirta, L., Reid, C., Paulson, J.A., 2017. Burden of Disease from Rising Coal-Fired Power Plant Emissions in Southeast Asia. https://doi.org/10.1021/acs.est.6b03731

Kossovich, E.L., Borodich, F.M., Epshtein, S.A., Galanov, B.A., 2020. Indentation of bituminous coals: Fracture, crushing and dust formation. Mech. Mater. 150, 103570. https://doi.org/10.1016/j.mechmat.2020.103570

Kuai, N., Huang, W., Yuan, J., Du, B., Li, Z., Wu, Y., 2012. Experimental investigations of coal dust-inertant mixture explosion behaviors. Procedia Eng. 26, 1337–1345. https://doi.org/10.1016/j.proeng.2011.11.2309

Küçük, A., Kadioğlu, Y., Gülaboğlu, M.Ş., 2003. A study of spontaneous combustion characteristics of a Turkish lignite: Particle size, moisture of coal, humidity of air. Combust. Flame 133, 255–261. https://doi.org/10.1016/S0010-2180(02)00553-9

Kurniawan, R., Managi, S., 2018. Coal consumption, urbanization, and trade openness linkage in

Indonesia. Energy Policy 121, 576–583. https://doi.org/10.1016/j.enpol.2018.07.023

Kurth, L.M., McCawley, M., Hendryx, M., Lusk, S., 2014. Atmospheric particulate matter size distribution and concentration in West Virginia coal mining and non-mining areas. Mod. Pathol. 27, 405–411. https://doi.org/10.1038/jes.2014.2

Landen, D.D., Wassell, J.T., McWilliams, L., Patel, A., 2011. Coal dust exposure and mortality from ischemic heart disease among a cohort of U.S. coal miners. Am. J. Ind. Med. 54, 727–733. https://doi.org/10.1002/ajim.20986

Laney, A.S., Attfield, M.D., 2010. Coal workers' pneumoconiosis and progressive massive fibrosis are increasingly more prevalent among workers in small underground coal mines in the United States. Occup. Environ. Med. 67, 428–431. https://doi.org/10.1136/oem.2009.050757

Laney, A.S., Weissman, D.N., 2014. Respiratory diseases caused by coal mine dust, in: Journal of Occupational and Environmental Medicine. Lippincott Williams and Wilkins, pp. S18–S22. https://doi.org/10.1097/JOM.0000000000000260

Lapp, N.L., Castranova, V., 1993. How silicosis and coal workers' pneumoconiosis develop--a cellular assessment. Occup. Med. 8, 35–56.

Lashgari, A., Kecojevic, V., 2016. Comparative analysis of dust emission of digging and loading equipment in surface coal mining. Int. J. Mining, Reclam. Environ. 30, 181–196. https://doi.org/10.1080/17480930.2015.1028516

Latvala, S., Hedberg, J., Di Bucchianico, S., Möller, L., Odnevall Wallinder, I., Elihn, K., Karlsson, H.L., 2016. Nickel Release, ROS Generation and Toxicity of Ni and NiO Micro- and Nanoparticles. PLoS One 11, e0159684. https://doi.org/10.1371/journal.pone.0159684

Lee, S., 1990. Oil Shale Technology. CRC Press, 280.

Lei, M., Rao, Z., Wang, H., Chen, Y., Zou, L., Yu, H., 2021. Maceral groups analysis of coal based on semantic segmentation of photomicrographs via the improved U-net. Fuel 294, 120475. https://doi.org/10.1016/j.fuel.2021.120475

León-Mejía, G., Espitia-Pérez, L., Hoyos-Giraldo, L.S., Da Silva, J., Hartmann, A., Henriques, J.A.P., Quintana, M., 2011. Assessment of DNA damage in coal open-cast mining workers using the cytokinesis-blocked micronucleus test and the comet assay. Sci. Total Environ. 409, 686–691. https://doi.org/10.1016/j.scitotenv.2010.10.049

León-Mejía, G., Espitia-Pérez, L., Linares, J.C., Hartmann, A., Quintana, M., 2007. Genotoxic effects in wild rodents (Rattus rattus and Mus musculus) in an open coal mining area. Mutat. Res. Toxicol. Environ. Mutagen. 630, 42–49. https://doi.org/10.1016/j.mrgentox.2007.02.007

Leonard, R., Zulfikar, R., Stansbury, R., 2020. Coal mining and lung disease in the 21st century. Curr. Opin. Pulm. Med. 26, 135–141. https://doi.org/10.1097/MCP.0000000000000653

Li, B., Liu, G., Bi, M.S., Li, Z.B., Han, B., Shu, C.M., 2021. Self-ignition risk classification for coal dust layers of three coal types on a hot surface. Energy 216, 119197.

https://doi.org/10.1016/j.energy.2020.119197

Li, B., Zhuang, X., Li, J., Querol, X., Font, O., Moreno, N., 2017. Enrichment and distribution of elements in the Late Permian coals from the Zhina Coalfield, Guizhou Province, Southwest China. Int. J. Coal Geol. 171, 111–129. https://doi.org/10.1016/j.coal.2017.01.003

Li, B., Zhuang, X., Querol, X., Moreno, N., Córdoba, P., Shangguan, Y., Yang, L., Li, J., Zhang, F., 2020. Geological controls on the distribution of REY-Zr (Hf)-Nb (Ta) enrichment horizons in late Permian coals from the Qiandongbei Coalfield, Guizhou Province, SW China. Int. J. Coal Geol. 231, 103604. https://doi.org/10.1016/j.coal.2020.103604

Li, J., Hu, S., 2017. History and future of the coal and coal chemical industry in China. Resour. Conserv. Recycl. 124, 13–24. https://doi.org/10.1016/j.resconrec.2017.03.006

Li, Q., Lin, B., Zhao, S., Dai, H., 2013. Surface physical properties and its effects on the wetting behaviors of respirable coal mine dust. Powder Technol. 233, 137–145. https://doi.org/10.1016/j.powtec.2012.08.023

Li, S., Lu, Y., Yan, J., Chen, B., Xie, X., 1999. Late Permian sequence stratigraphic framework and controlling factors in southern Yangtze platform and its margin. J. China Univ. Geosci. 10, 153–160.

Li, S., Xia, W., Cheng, S., Xie, X., 1990. The Late Permian tectonopalaeogeography and distribution of coal-rich zones in southwest China, in: Tectonopalaeogeography and Palaeobiogeography of China and Adjacent Regions. China Univ. Geosciences Wuhan, pp. 127–142.

Liang, Y., Wong, O., Yang, L., Li, T., Su, Z., 2006. The development and regulation of occupational exposure limits in China. Regul. Toxicol. Pharmacol. 46, 107–113. https://doi.org/10.1016/j.yrtph.2006.02.007

Liao, Q., Feng, G., Fan, Y., Hu, S., Shao, H., Huang, Y., 2018. Experimental investigations and field applications of chemical suppressants for dust control in coal mines. Adv. Mater. Sci. Eng. 2018. https://doi.org/10.1155/2018/6487459

Liao, Y., Wang, J., Wu, J., Driskell, L., Wang, W., Zhang, T., Xue, G., Zheng, X., 2010. Spatial analysis of neural tube defects in a rural coal mining area. Int. J. Environ. Health Res. 20, 439–450. https://doi.org/10.1080/09603123.2010.491854

Lighty, J.A.S., Veranth, J.M., Sarofim, A.F., 2000. Combustion aerosols: Factors governing their size and composition and implications to human health. J. Air Waste Manag. Assoc. 50, 1565–1618. https://doi.org/10.1080/10473289.2000.10464197

Lin, B., Raza, M.Y., 2020. Coal and economic development in Pakistan: A necessity of energy source. Energy 207, 118244. https://doi.org/10.1016/j.energy.2020.118244

Liu, G., Vassilev, S. V., Gao, L., Zheng, L., Peng, Z., 2005. Mineral and chemical composition and some trace element contents in coals and coal ashes from Huaibei coal field, China. Energy Convers. Manag. 46, 2001–2009. https://doi.org/10.1016/j.enconman.2004.11.002

Liu, Q., Bai, C., Li, X., Jiang, L., Dai, W., 2010. Coal dust/air explosions in a large-scale tube. Fuel.

https://doi.org/10.1016/j.fuel.2009.07.010

Liu, R., Zhou, G., Wang, C., Jiang, W., Wei, X., 2020. Preparation and performance characteristics of an environmentally-friendly agglomerant to improve the dry dust removal effect for filter material. J. Hazard. Mater. 397, 122734. https://doi.org/10.1016/j.jhazmat.2020.122734

Liu, T., Liu, S., 2020. The impacts of coal dust on miners' health: A review. Environ. Res. https://doi.org/10.1016/j.envres.2020.109849

Liu, X., Liu, H., Han, D., 2016. Analysis of the current situation of occupational safety and health in the world. Mod. Occup Saf. 3, 91–93.

Lloyd, D.R., Phillips, D.H., 1999. Oxidative DNA damage mediated by copper(II), iron(II) and nickel(II) Fenton reactions: Evidence for site-specific mechanisms in the formation of double-strand breaks, 8-hydroxydeoxyguanosine and putative intrastrand cross-links. Mutat. Res. - Fundam. Mol. Mech. Mutagen. 424, 23–36. https://doi.org/10.1016/S0027-5107(99)00005-6

Lou, Z., Li, P., Han, K., 2015. Redox-responsive fluorescent probes with different design strategies. Acc. Chem. Res. 48, 1358–1368. https://doi.org/10.1021/acs.accounts.5b00009

Lu, C., Song, G., Lin, J.M., 2006. Reactive oxygen species and their chemiluminescence-detection methods. TrAC - Trends Anal. Chem. 25, 985–995. https://doi.org/10.1016/j.trac.2006.07.007

Lungs at Work, 2015. Courier Journal Archives, n.d. About Black Lung Disease. URL https://lungsatworkpa.org/?page_id=53

Ma, D., Qin, B., Gao, Y., Jiang, J., Feng, B., 2020. Study on the explosion characteristics of methane–air with coal dust originating from low-temperature oxidation of coal. Fuel 260, 116304. https://doi.org/10.1016/j.fuel.2019.116304

Ma, Q., Nie, W., Yang, S., Xu, C., Peng, H., Liu, Z., Guo, C., Cai, X., 2020. Effect of spraying on coal dust diffusion in a coal mine based on a numerical simulation. Environ. Pollut. 114717. https://doi.org/10.1016/j.envpol.2020.114717

Ma, Y., Zhou, G., Ding, J., Li, S., Wang, G., 2018. Preparation and characterization of an agglomeration-cementing agent for dust suppression in open pit coal mining. Cellulose 25, 4011–4029. https://doi.org/10.1007/s10570-018-1826-z

Maclaren, W.M., Hurley, J.F., Collins, P.R., Cowie, A.J., 1989. Factors associated with the development of progressive massive fibrosis in British coalminers: a case-control study. Br. J. ofIndustrial Med. 46, 597–607. https://doi.org/10.1136/oem.46.9.597

MacNee, W., 2001. Oxidative stress and lung inflammation in airways disease. Eur. J. Pharmacol. https://doi.org/10.1016/S0014-2999(01)01320-6

MacNee, W., Rahman, I., 2001. Is oxidative stress central to the pathogenesis of chronic obstructive pulmonary disease? Trends Mol. Med. 7, 55–62. https://doi.org/10.1016/S1471-4914(01)01912-8

Madzivire, G., Maleka, R.M., Tekere, M., Petrik, L.F., 2019. Cradle to cradle solution to problematic waste materials from mine and coal power station: Acid mine drainage, coal fly ash and carbon dioxide. J. Water Process Eng. 30, 100474. https://doi.org/10.1016/j.jwpe.2017.08.012

Marmur, A., n.d. Soft contact: measurement and interpretation of contact angles. https://doi.org/10.1039/b514811c

Marsalek, R., Sassikova, M., 2016. Characterization of the size distribution of subbituminous coal by laser diffraction. Instrum. Sci. Technol. 44, 233–240. https://doi.org/10.1080/10739149.2015.1113429

Marts, J.A., Gilmore, R.C., Brune, J.F., Saki, S.A., Bogin, G.E., Grubb, J.W., 2015. Optimizing nitrogen injection for progessively sealed panels. 2015 SME Annu. Conf. Expo C. 117th Natl. West. Min. Conf. - Min. Navig. Glob. Waters 447–450.

Masto, R.E., George, J., Rout, T.K., Ram, L.C., 2017. Multi element exposure risk from soil and dust in a coal industrial area. J. Geochemical Explor. 176, 100–107. https://doi.org/10.1016/j.gexplo.2015.12.009

McCallum, R.I., 2005. Occupational exposure to antimony compounds, in: Journal of Environmental Monitoring. Royal Society of Chemistry, pp. 1245–1250. https://doi.org/10.1039/b509118g

McCunney, R.J., Morfeld, P., Payne, S., 2009. What Component of Coal Causes Coal Workers' Pneumoconiosis? J. Occup. Environ. Med. 51, 462–471. https://doi.org/10.1097/JOM.0b013e3181a01ada

McPherson, M.J., 1993. Subsurface ventilation systems, in: Subsurface Ventilation and Environmental Engineering. Springer Netherlands, pp. 91–133. https://doi.org/10.1007/978-94-011-1550-6_4

Mira, M.M., Huang, S., Hill, R.D., Stasolla, C., 2021. Tolerance to excess moisture in soybean is enhanced by over-expression of the Glycine max Phytoglobin (GmPgb1). Plant Physiol. Biochem. 159, 322–334. https://doi.org/10.1016/j.plaphy.2020.12.033

Mohanty, A.K., Lingaswamy, M., Rao, V.G., Sankaran, S., 2018. Impact of acid mine drainage and hydrogeochemical studies in a part of Rajrappa coal mining area of Ramgarh District, Jharkhand State of India. Groundw. Sustain. Dev. 7, 164–175. https://doi.org/10.1016/j.gsd.2018.05.005

Moore, P.D., 1987. Ecological and hydrological aspects of peat formation. Geol. Soc. Spec. Publ. 32, 7–15. https://doi.org/10.1144/GSL.SP.1987.032.01.02

Morawska, L., Ristovski, Z., Jayaratne, E.R., Keogh, D.U., Ling, X., 2008. Ambient nano and ultrafine particles from motor vehicle emissions: Characteristics, ambient processing and implications on human exposure. Atmos. Environ. https://doi.org/10.1016/j.atmosenv.2008.07.050

Moreno, T., Higueras, P., Jones, T., McDonald, I., Gibbons, W., 2005. Size fractionation in mercury-bearing airborne particles (HgPM 10) at Almadén, Spain: Implications for

inhalation hazards around old mines. Atmos. Environ. 39, 6409–6419. https://doi.org/10.1016/j.atmosenv.2005.07.024

Moreno, T., Kelly, F.J., Dunster, C., Oliete, A., Martins, V., Reche, C., Minguillón, M.C., Amato, F., Capdevila, M., de Miguel, E., Querol, X., 2017. Oxidative potential of subway PM2.5. Atmos. Environ. 148, 230–238. https://doi.org/10.1016/j.atmosenv.2016.10.045

Mraw, S.C., De Neufville, J.P., Freund, H., Baset, Z., Gorbaty, M.L., Wright, F.J., 1983. Science of Mineral Matter in Coal., Coal Sci. https://doi.org/10.1016/B978-0-12-150702-2.50007-4

Mudway, I.S., Stenfors, N., Duggan, S.T., Roxborough, H., Zielinski, H., Marklund, S.L., Blomberg, A., Frew, A.J., Sandström, T., Kelly, F.J., 2004. An in vitro and in vivo investigation of the effects of diesel exhaust on human airway lining fluid antioxidants. Arch. Biochem. Biophys. 423, 200–212. https://doi.org/10.1016/j.abb.2003.12.018

Murphy, P.J., Smith, A.M.L., Hudson-Edwards, K.A., Dubbin, W.E., Wright, K., 2009. Raman and ir spectroscopic studies of alunite-supergroup compounds containing Al, Cr3+, Fe3+ AND V3+ at the B site. Can. Mineral. 47, 663–681. https://doi.org/10.3749/canmin.47.3.663

Murphy, R., Strongin, D.R., 2009. Surface reactivity of pyrite and related sulfides. Surf. Sci. Rep. https://doi.org/10.1016/j.surfrep.2008.09.002

Myers, J.E., TeWaterNaude, J., Fourie, M., Zogoe, H.B.A., Naik, I., Theodorou, P., Tassel, H., Daya, A., Thompson, M. Lou, 2003. Nervous system effects of occupational manganese exposure on South African manganese mineworkers. Neurotoxicology 24, 649–656. https://doi.org/10.1016/S0161-813X(03)00035-4

National Health Commission of the People's Republic of China. http://en.nhc.gov.cn/2020-05/14/c_80150.htm

Nawrot, T., Geusens, P., Nulens, T.S., Nemery, B., 2010. Occupational cadmium exposure and calcium excretion, bone density, and osteoporosis in men. J. Bone Miner. Res. 25, 1441–1445. https://doi.org/10.1002/jbmr.22

NIOSH, 2010. Best Practices for Dust Control in Coal Mining. Pittsburgh, PA • Spokane, WA, US. https://www.cdc.gov/niosh/mining/userfiles/works/pdfs/2010-110.pdf

NIOSH, 2002. Health Effects of Occupational Exposure to Respirable Crystalline Silica, DEPARTMENT OF HEALTH AND HUMAN SERVICES, Centers for Disease Control and Prevention, National Institute for Occupational Safety and Health. https://doi.org/2002-129

NIOSH, 1995. Criteria for recomend standard: Occupational exposure to respirable coal mine dust, NIOSH Pub 95-106. https://www.cdc.gov/niosh/docs/95-106/default.html

NIOSH, (National Institute for Occupational Safety and Health), 2021. NIOSH Mining Program Information Circular IC 9532 Best Practices for Dust Control in Coal Mining. https://doi.org/10.26616/NIOSHPUB2021119

Nishita-Hara, C., Hirabayashi, M., Hara, K., Yamazaki, A., Hayashi, M., 2019. Dithiothreitol-Measured Oxidative Potential of Size-Segregated Particulate Matter in Fukuoka, Japan:

Effects of Asian Dust Events. GeoHealth 3, 160–173. https://doi.org/10.1029/2019GH000189

O'Keefe, J.M.K., Bechtel, A., Christanis, K., Dai, S., DiMichele, W.A., Eble, C.F., Esterle, J.S., Mastalerz, M., Raymond, A.L., Valentim, B. V., Wagner, N.J., Ward, C.R., Hower, J.C., 2013. On the fundamental difference between coal rank and coal type. Int. J. Coal Geol. 118, 58–87. https://doi.org/10.1016/j.coal.2013.08.007

O'Keefe, J.M.K., Henke, K.R., Hower, J.C., Engle, M.A., Stracher, G.B., Stucker, J.D., Drew, J.W., Staggs, W.D., Murray, T.M., Hammond, M.L., Adkins, K.D., Mullins, B.J., Lemley, E.W., 2010. CO2, CO, and Hg emissions from the Truman Shepherd and Ruth Mullins coal fires, eastern Kentucky, USA. Sci. Total Environ. 408, 1628–1633. https://doi.org/10.1016/j.scitotenv.2009.12.005

Oberdörster, G., Ferin, J., Lehnert, B.E., 1992. Correlation between particle size, in vivo particle persistence, and lung injury. Environ. Health Perspect. 102, 173–179. https://doi.org/10.1289/ehp.102-1567252

Oberdörster, G., Oberdörster, E., Oberdörster, J., 2005. Nanotoxicology: An emerging discipline evolving from studies of ultrafine particles. Environ. Health Perspect. https://doi.org/10.1289/ehp.7339

Onifade, M., Lawal, A.I., Abdulsalam, J., Genc, B., Bada, S., Said, K.O., Gbadamosi, A.R., 2021. Development of multiple soft computing models for estimating organic and inorganic constituents in coal. Int. J. Min. Sci. Technol. https://doi.org/10.1016/j.ijmst.2021.02.003

Orem, W.H., Finkelman, R.B., 2003. Coal Formation and Geochemistry, in: Treatise on Geochemistry. Elsevier Inc., pp. 191–222. https://doi.org/10.1016/B0-08-043751-6/07097-3

Oskarsson, P., Nielsen, K.B., Lahiri-Dutt, K., Roy, B., 2021. India's new coal geography: Coastal transformations, imported fuel and state-business collaboration in the transition to more fossil fuel energy. Energy Res. Soc. Sci. 73, 101903. https://doi.org/10.1016/j.erss.2020.101903

Ozbayoglu, G., 2018. Energy Production From Coal, in: Comprehensive Energy Systems. Elsevier Inc., pp. 788–821. https://doi.org/10.1016/B978-0-12-809597-3.00341-2

Pallarés, J., Herce, C., Bartolomé, C., Peña, B., 2017. Investigation on co-firing of coal mine waste residues in pulverized coal combustion systems. Energy 140, 58–68. https://doi.org/10.1016/j.energy.2017.07.174

Pandey, S., Fosso-kankeu, E., Redelinghuys, J., Kim, J., Kang, M., 2021. Science of the Total Environment Implication of bio fi lms in the sustainability of acid mine drainage and metal dispersion near coal tailings. Sci. Total Environ. 788, 147851. https://doi.org/10.1016/j.scitotenv.2021.147851

Pedroso-Fidelis, G. dos S., Farias, H.R., Mastella, G.A., Boufleur-Niekraszewicz, L.A., Dias, J.F., Alves, M.C., Silveira, P.C.L., Nesi, R.T., Carvalho, F., Zocche, J.J., Pinho, R.A., 2020. Pulmonary oxidative stress in wild bats exposed to coal dust: A model to evaluate the

impact of coal mining on health. Ecotoxicol. Environ. Saf. https://doi.org/10.1016/j.ecoenv.2020.110211

Peng, J., Yu, B.Y., Liao, H., Wei, Y.M., 2018. Marginal abatement costs of CO2 emissions in the thermal power sector: A regional empirical analysis from China. J. Clean. Prod. 171, 163–174. https://doi.org/10.1016/j.jclepro.2017.09.242

Perret, J.L., Plush, B., Lachapelle, P., Hinks, T.S.C., Walter, C., Clarke, P., Irving, L., Brady, P., Dharmage, S.C., Stewart, A., 2017. Coal mine dust lung disease in the modern era. Respirology 22, 662–670. https://doi.org/10.1111/resp.13034

Petsonk, E.L., Rose, C., Cohen, R., 2013. Coal mine dust lung disease: New lessons from an old exposure. Am. J. Respir. Crit. Care Med. 187, 1178–1185. https://doi.org/10.1164/rccm.201301-0042CI

Phaniendra, A., Jestadi, D.B., Periyasamy, L., 2015. Free Radicals: Properties, Sources, Targets, and Their Implication in Various Diseases. Indian J. Clin. Biochem. https://doi.org/10.1007/s12291-014-0446-0

Pinho, R.A., Bonatto, F., Andrades, M., Frota, M.L.C., Ritter, C., Klamt, F., Dal-Pizzol, F., Uldrich-Kulczynski, J.M., Moreira, J.C.F., 2004. Lung oxidative response after acute coal dust exposure. Environ. Res. 96, 290–297. https://doi.org/10.1016/j.envres.2003.10.006

Pizzino, G., Irrera, N., Cucinotta, M., Pallio, G., Mannino, F., Arcoraci, V., Squadrito, F., Altavilla, D., Bitto, A., 2017. Oxidative Stress: Harms and Benefits for Human Health. Oxid. Med. Cell. Longev. https://doi.org/10.1155/2017/8416763

Plumlee, G.S., Morman, S.A., 2011. Mine wastes and human health. Elements 7, 399–404. https://doi.org/10.2113/gselements.7.6.399

Potter, J., Stasiuk, L.D., Cameron, A.R., Petrology., C.S. for C.S. and O., (Calgary), G.S. of C., Technology., C.C. for M. and E., 1998. Petrographic atlas of Canadian coal macerals and dispersed organic matter. Geological Survey of Canada. https://www.osti.gov/etdeweb/biblio/20501570

Prasanta, K.M., Patrick, G.H., 1993. Composition of coal: Chapter 4, in: Hydrocarbons from Coal. pp. 79–118. https://doi.org/10.1038/154056a0

Qian, Q.Z., Cao, X.K., Qian, Q.Q., Shen, F.H., Wang, Q., Liu, H.Y., Tong, J.W., 2016. Relationship of cumulative dust exposure dose and cumulative abnormal rate of pulmonary function in coal mixture workers. Kaohsiung J. Med. Sci. 32, 44–49. https://doi.org/10.1016/j.kjms.2015.11.003

Qiao, H., Chen, S., Dong, X., Dong, K., 2019. Has China's coal consumption actually reached its peak? National and regional analysis considering cross-sectional dependence and heterogeneity. Energy Econ. 84, 104509. https://doi.org/10.1016/j.eneco.2019.104509

Querol, X., Izquierdo, M., Monfort, E., Alvarez, E., Font, O., Moreno, T., Alastuey, A., Zhuang, X., Lu, W., Wang, Y., 2008. Environmental characterization of burnt coal gangue banks at Yangquan, Shanxi Province, China. Int. J. Coal Geol. 75, 93–104. https://doi.org/10.1016/j.coal.2008.04.003

Querol, X., Zhuang, X., Font, O., Izquierdo, M., Alastuey, A., Castro, I., van Drooge, B.L., Moreno, T., Grimalt, J.O., Elvira, J., Cabañas, M., Bartroli, R., Hower, J.C., Ayora, C., Plana, F., López-Soler, A., 2011. Influence of soil cover on reducing the environmental impact of spontaneous coal combustion in coal waste gobs: A review and new experimental data. Int. J. Coal Geol. 85, 2–22. https://doi.org/10.1016/j.coal.2010.09.002

Reche, C., Querol, X., Alastuey, A., Viana, M., Pey, J., Moreno, T., Rodríguez, S., González, Y., Fernández-Camacho, R., de la Rosa, J., Dall'Osto, M., Prévôt, A.S.H., Hueglin, C., Harrison, R.M., Quincey, P., 2011. New considerations for PM, Black Carbon and particle number concentration for air quality monitoring across different European cities. Atmos. Chem. Phys. 11, 6207–6227. https://doi.org/10.5194/acp-11-6207-2011

Reichert, M., Bensadoun, E.S., 2009. PET imaging in patients with coal workers pneumoconiosis and suspected malignancy. J. Thorac. Oncol. 4, 649–651. https://doi.org/10.1097/JTO.0b013e31819d4778

Reichman, L.B., 1991. The U-shaped curve of concern. Am. Rev. Respir. Dis. https://doi.org/10.1164/ajrccm/144.4.741

Ren, Q., Zhang, Y., Arauzo, I., Shan, L., Xu, J., Wang, Y., Su, S., Hu, S., Xiang, J., 2021. Roles of moisture and cyclic loading in microstructures and their effects on mechanical properties for typical Chinese bituminous coals. Fuel 293, 120408. https://doi.org/10.1016/j.fuel.2021.120408

Ren, X.W., Wang, M.D., Kang, H.Z., Lu, X.X., 2012. Engineering Case Report. J. Occup. Environ. Hyg. 9, D77–D83. https://doi.org/10.1080/15459624.2012.667288

Rosita, W., Bendiyasa, I.M., Perdana, I., Anggara, F., 2020. Sequential particle-size and magnetic separation for enrichment of rare-earth elements and yttrium in Indonesia coal fly ash. J. Environ. Chem. Eng. 8, 103575. https://doi.org/10.1016/j.jece.2019.103575

Rutstein, D.D., Mullan, R.J., Frazier, T.M., Halperin, W.E., Melius, J.M., Sestito, J.P., 1984. Sentinel health events (occupational): A basis for physician recognition and public health surveillance. Arch. Environ. Health 39, 159–168. https://doi.org/10.1080/00039896.1984.9939518

Sánchez Jiménez, A., Van Tongeren, M., Cherrie, J.W., 2011. A review of monitoring methods for inhalable hardwood dust. Inst. Occup. Med. P937/1A. ttps://www.semanticscholar.org/paper/A-review-of-monitoring-methods-for-inhalable-dust-Jim%C3%A9nez-Tongeren/54bcd0b387fc922a983d24cbcc7771df7b40334c

Sapko, M.J., Cashdollar, K.L., Green, G.M., 2007. Coal dust particle size survey of US mines. J. Loss Prev. Process Ind. 20, 616–620. https://doi.org/10.1016/j.jlp.2007.04.014

Sarver, E., Keles, C., Rezaee, M., 2019. Beyond conventional metrics: Comprehensive characterization of respirable coal mine dust. Int. J. Coal Geol. 207, 84–95. https://doi.org/10.1016/j.coal.2019.03.015

Schins, R.P.F., Borm, P.J.A., 1999. Mechanisms and Mediators in Coal Dust Induced Toxicity: a Review. Ann. Occup. Hyg. 32, 7–33. https://doi.org/10.1093/annhyg/43.1.7

Scott, A.C., 2002. Coal petrology and the origin of coal macerals: A way ahead? Int. J. Coal Geol. 50, 119–134. https://doi.org/10.1016/S0166-5162(02)00116-7

Seaton, A., Dodgson, J., Dick, J.A., Jacobsen, M., 1981. Quartz and Pneumoconiosis in Coalminers. Lancet 318, 1272–1275. https://doi.org/10.1016/S0140-6736(81)91503-8

Sevim, Ö., Demir, İ., 2019. Optimization of fly ash particle size distribution for cementitious systems with high compactness. Constr. Build. Mater. 195, 104–114. https://doi.org/10.1016/j.conbuildmat.2018.11.080

Shao, L., Zhang, P., Ren, D., Lei, J., 1998. Late Permian coal-bearing carbonate successions in southern China: Coal accumulation on carbonate platforms. Int. J. Coal Geol. 37, 235–256. https://doi.org/10.1016/S0166-5162(98)00008-1

Sharma, Y.C., Aggarwal, P., Singh, T.N., 2009. Economic liabilities of environmental pollution by coal mining: Indian scenario. Environ. Dev. Sustain. 11, 589–599. https://doi.org/10.1007/s10668-007-9131-2

Shekarian, Y., Rahimi, E., Rezaee, M., Su, W.C., Roghanchi, P., 2021. Respirable coal mine dust: A review of respiratory deposition, regulations and characterization. Minerals 11, 1–25. https://doi.org/10.3390/min11070696

Shi, X., Dalal, N.S., 1992. The role of superoxide radical in chromium(VI)-generated hydroxyl radical: The Cr(VI) haber-weiss cycle. Arch. Biochem. Biophys. 292, 323–327. https://doi.org/10.1016/0003-9861(92)90085-B

Shi, X., Dalal, N.S., Kasprzak, K.S., 1992. Generation of free radicals from lipid hydroperoxides by Ni2+ in the presence of oligopeptides. Arch. Biochem. Biophys. 299, 154–162. https://doi.org/10.1016/0003-9861(92)90257-W

Shimura, K., Matsuo, A., 2019. Using an extended CFD-DEM for the two-dimensional simulation of shock-induced layered coal-dust combustion in a narrow channel. Proc. Combust. Inst. 37, 3677–3684. https://doi.org/10.1016/j.proci.2018.07.066

Sies, H., Berndt, C., Jones, D.P., 2017. Oxidative Stress. Annu. Rev. Biochem. 86, 715–748. https://doi.org/10.1146/annurev-biochem-061516-045037

Silva, L.F.O., Hower, J.C., Dotto, G.L., Oliveira, M.L.S., Pinto, D., 2021a. Titanium nanoparticles in sedimented dust aggregates from urban children's parks around coal ashes wastes. Fuel 285, 119162. https://doi.org/10.1016/j.fuel.2020.119162

Silva, L.F.O., Santosh, M., Schindler, M., Gasparotto, J., Dotto, G.L., Oliveira, M.L.S., Hochella, M.F., 2021b. Nanoparticles in fossil and mineral fuel sectors and their impact on environment and human health: A review and perspective. Gondwana Res. 92, 184–201. https://doi.org/10.1016/j.gr.2020.12.026

Simate, G.S., Ndlovu, S., 2014. Acid mine drainage: Challenges and opportunities. J. Environ. Chem. Eng. 2, 1785–1803. https://doi.org/10.1016/j.jece.2014.07.021

Singh, R., Singh, S., Parihar, P., Singh, V.P., Prasad, S.M., 2015. Arsenic contamination, consequences and remediation techniques: A review. Ecotoxicol. Environ. Saf.

https://doi.org/10.1016/j.ecoenv.2014.10.009

Skousen, J.G., Sexstone, A., Ziemkiewicz, P.F., 2015. Acid mine drainage control and treatment. Reclam. Drastically Disturb. Lands 131–168. https://doi.org/10.2134/agronmonogr41.c6

Smith, A. 6, Diamond, W.P., Mucho, T.P., Organiscak, A., 1994. Bleederless Ventilation Systems as a Spontaneous Combustion Control Measure in U.S. Coal Mines. United States Department of the Interlor. Bureau of Mines, Information Circular 9377.

Smith, A.M.L., Hudson-Edwards, K.A., Dubbin, W.E., Wright, K., 2006. Dissolution of jarosite [KFe3(SO4)2 (OH)6] at pH 2 and 8: Insights from batch experiments and computational modelling. Geochim. Cosmochim. Acta 70, 608–621. https://doi.org/10.1016/j.gca.2005.09.024

Smith, A.H. V., 1997. Provenance of Coals from Roman Sites in England and Wales. Britannia 28, 297. https://doi.org/10.2307/526770

Soltani, N., Keshavarzi, B., Sorooshian, A., Moore, F., Dunster, C., Dominguez, A.O., Kelly, F.J., Dhakal, P., Ahmadi, M.R., Asadi, S., 2018. Oxidative potential (OP) and mineralogy of iron ore particulate matter at the Gol-E-Gohar Mining and Industrial Facility (Iran). Environ. Geochem. Health 40, 1785–1802. https://doi.org/10.1007/s10653-017-9926-5

Spackman, W., 1958. Section of Geology and Mineralogy: the Maceral Concept and the Study of Modern Environments As a Means of Understanding the Nature of Coal*. Trans. N. Y. Acad. Sci. 20, 411–423. https://doi.org/10.1111/j.2164-0947.1958.tb00602.x

Sperazza, M., Moore, J.N., Hendrix, M.S., 2004. High-Resolution Particle Size Analysis of Naturally Occurring Very Fine-Grained Sediment Through Laser Diffractometry. J. Sediment. Res. 74, 736–743. https://doi.org/10.1306/031104740736

Stach, E., Mackowsky, M.-T., Teichmüller, M., Taylor, G.H., Chandra, D., Teichmüller, R., 1982. Stach's Textbook of Coal Petrology. Gebrüder Borntraeger. Berlin · Stuttgart.

Stayner, L., Smith, R., Thun, M., Schnorr, T., Lemen, R., 1992. A quantitative assessment of lung cancer risk and occupational cadmium exposure. IARC Sci. Publ. 447–455.

Stohs, S.J., Bagchi, D., 1995. Oxidative mechanisms in the toxicity of metal ions. Free Radic. Biol. Med. 18, 321–336. https://doi.org/10.1016/0891-5849(94)00159-H

Storz, G., Imlayt, J.A., 1999. Oxidative stress. Curr. Opin. Microbiol. 2, 188–194. https://doi.org/10.1016/S1369-5274(99)80033-2

Strlič, M., Kolar, J., Šelih, V.S., Kočar, D., Pihlar, B., 2003. A comparative study of several transition metals in fenton-like reaction systems at circum-neutral pH. Acta Chim. Slov. 50, 619–632. https://www.semanticscholar.org/paper/A-comparative-study-of-several-transition-metals-in-Strli%C4%8D-Kolar/44f3f49802b48667b1958892e187b0ed3dc26e44

Suárez-Ruiz, I., Crelling, J., 2008. Applied coal petrology, Applied Coal Petrology. Elsevier Ltd. https://doi.org/10.1016/B978-0-08-045051-3.X0001-2

Suarthana, E., Laney, A.S., Storey, E., Hale, J.M., Attfield, M.D., 2011. Coal workers' pneumoconiosis in the United States: Regional differences 40 years after implementation

of the 1969 Federal Coal Mine Health and Safety Act. Occup. Environ. Med. 68, 908–913. https://doi.org/10.1136/oem.2010.063594

Sundar, S., Chakravarty, J., 2010. Antimony toxicity. Int. J. Environ. Res. Public Health 7, 4267–4277. https://doi.org/10.3390/ijerph7124267

Sunkpal, M., Roghanchi, P., Kocsis, K.C., 2017. A Method to Protect Mine Workers in Hot and Humid Environments. Saf. Health Work 9, 149–158. https://doi.org/10.1016/j.shaw.2017.06.011

Swaine, D.J., 1990. Trace Elements in Coal. Elsevier. https://doi.org/10.1016/C2013-0-00949-8

Tang, Z., Chai, M., Cheng, J., Jin, J., Yang, Y., Nie, Z., Huang, Q., Li, Y., 2017. Contamination and health risks of heavy metals in street dust from a coal-mining city in eastern China. Ecotoxicol. Environ. Saf. 138, 83–91. https://doi.org/10.1016/j.ecoenv.2016.11.003

Teichmüller, M., 1989. The genesis of coal from the viewpoint of coal petrology. Int. J. Coal Geol. 12, 1–87. https://doi.org/10.1016/0166-5162(89)90047-5

Teng, J., Mastalerz, M., Hampton, L.B., 2017. Maceral controls on porosity characteristics of lithotypes of Pennsylvanian high volatile bituminous coal: Example from the Illinois Basin. Int. J. Coal Geol. 172, 80–94. https://doi.org/10.1016/j.coal.2017.02.001

Tirado-Ballestas, I., Caballero-Gallardo, K., Olivero-Verbel, J., 2020. Toxicological effects of bituminous coal dust on the earthworm Eisenia fetida (Oligochaeta: Lumbricidae). Ecotoxicology 29, 1422–1430. https://doi.org/10.1007/s10646-020-02263-8

Tomášková, H., Šplíchalová, A., Šlachtová, H., Urban, P., Hajduková, Z., Landecká, I., Gromnica, R., Brhel, P., Pelclová, D., Jirák, Z., 2017. Mortality in Miners with Coal-Workers' Pneumoconiosis in the Czech Republic in the Period 1992–2013. Int. J. Environ. Res. Public Health 14, 269. https://doi.org/10.3390/ijerph14030269

Tsitonaki, A., Petri, B., Crimi, M., Mosbk, H., Siegrist, R.L., Bjerg, P.L., 2010. In situ chemical oxidation of contaminated soil and groundwater using persulfate: A review. Crit. Rev. Environ. Sci. Technol. 40, 55–91. https://doi.org/10.1080/10643380802039303

Valko, M., Morris, H., Cronin, M.T.D., 2005. Metals, Toxicity and Oxidative Stress. Curr. Med. Chem. 12, 1161–1208. https://doi.org/10.2174/0929867053764635

Vassilev, S. V., Kitano, K., Vassileva, C.G., 1996. Some relationships between coal rank and chemical and mineral composition. Fuel 75, 1537–1542. https://doi.org/10.1016/0016-2361(96)00116-0

Wagner, N.J., Hlatshwayo, B., 2005. The occurrence of potentially hazardous trace elements in five Highveld coals, South Africa. Int. J. Coal Geol. 63, 228–246. https://doi.org/10.1016/j.coal.2005.02.014

Wang, D., Zhao, L., Guo, L.H., Zhang, H., 2014. Online Detection of reactive oxygen species in ultraviolet (UV)-irradiated nano-TiO2 suspensions by continuous flow chemiluminescence. Anal. Chem. 86, 10535–10539. https://doi.org/10.1021/ac503213m

Wang, H., Dlugogorski, B.Z., Kennedy, E.M., 2003. Coal oxidation at low temperatures: Oxygen

consumption, oxidation products, reaction mechanism and kinetic modelling. Prog. Energy Combust. Sci. https://doi.org/10.1016/S0360-1285(03)00042-X

Wang, H., Du, M.L., Zhang, G.T., 2014. Concentration and distribution of Cr, Pb and Zn in the Jurassic coals from northern Shaanxi and Ningxia, China. Adv. Mater. Res. 989–994, 1415–1418. https://doi.org/10.4028/www.scientific.net/AMR.989-994.1415

Wang, H., Zhang, L., Wang, D., He, X., 2017. Experimental investigation on the wettability of respirable coal dust based on infrared spectroscopy and contact angle analysis. Adv. Powder Technol. 28, 3130–3139. https://doi.org/10.1016/j.apt.2017.09.018

Wang, J., Zeng, X.C., Zhu, X., Chen, X., Zeng, X., Mu, Y., Yang, Y., Wang, Y., 2017. Sulfate enhances the dissimilatory arsenate-respiring prokaryotes-mediated mobilization, reduction and release of insoluble arsenic and iron from the arsenic-rich sediments into groundwater. J. Hazard. Mater. 339, 409–417. https://doi.org/10.1016/j.jhazmat.2017.06.052

Wang, P., Tan, X., Zhang, L., Li, Y., Liu, R., 2019. Influence of particle diameter on the wettability of coal dust and the dust suppression efficiency via spraying. Process Saf. Environ. Prot. 132, 189–199. https://doi.org/10.1016/j.psep.2019.09.031

Wang, Q., Ge, S., 2020. Uncovering the effects of external demand on China's coal consumption: A global input–output analysis. J. Clean. Prod. 245, 118877. https://doi.org/10.1016/j.jclepro.2019.118877

Wang, Q., Song, X., 2021. Why do China and India burn 60% of the world's coal? A decomposition analysis from a global perspective. Energy 227, 120389. https://doi.org/10.1016/j.energy.2021.120389

Wang, X., Yuan, S., Li, X., Jiang, B., 2019. Synergistic effect of surfactant compounding on improving dust suppression in a coal mine in Erdos, China. Powder Technol. 344, 561–569. https://doi.org/10.1016/j.powtec.2018.12.061

Wang, Y., Chen, H., Long, R., Yang, M., 2020. Health economic loss measurement and risk assessment of new cases of coal worker's pneumoconiosis in China. Saf. Sci. 122, 104529. https://doi.org/10.1016/j.ssci.2019.104529

Ward, C.R., 2016. Analysis, origin and significance of mineral matter in coal: An updated review. Int. J. Coal Geol. 165, 1–27. https://doi.org/10.1016/j.coal.2016.07.014

Ward, C.R., 2002. Analysis and significance of mineral matter in coal seams. Int. J. Coal Geol. 50, 135–168. https://doi.org/10.1016/S0166-5162(02)00117-9

Ward, C.R., 1984. Coal geology and coal technology. Blackwell Scientific Publications, Inc.,Palo Alto, CA, United States.

WCA, 2020. World Coal Association. https://www.worldcoal.org/coal-facts/coals-contribution/

Weber, R.J., Guo, H., Russell, A.G., Nenes, A., 2016. High aerosol acidity despite declining atmospheric sulfate concentrations over the past 15 years. Nat. Geosci. 9, 282–285. https://doi.org/10.1038/ngeo2665

Welch, S.A., Kirste, D., Christy, A.G., Beavis, F.R., Beavis, S.G., 2008. Jarosite dissolution II-

Reaction kinetics, stoichiometry and acid flux. Chem. Geol. 254, 73–86. https://doi.org/10.1016/j.chemgeo.2008.06.010

WHO, 2000. Air Quality Guidelines for Europe. Second edition. WHO Regional Publications, European Series, No. 91. World Health Organization, Regional Office for Europe, Copenhagen, Denmark. http://www.euro.who.int/en/health-topics/environment-and-health/air-quality/publications/pre2009/air-quality-guidelines-for-europe

WHO, 1986. Recommended health-based limits in occupational exposure to selected mineral dusts (silica, coal : report of a WHO study group [meeting held in Geneva from 6 to 12 March 1984]. World Health Organization technical report series ; no. 734. https://apps.who.int/iris/handle/10665/38001?locale-attribute=es&locale=en

WHO, 1999. Hazard prevention and control in the work environment: : airborne dust. Occupational and environmental health series. WHO/SDE/OEH/99.14, https://apps.who.int/iris/handle/10665/66147

Więckol-Ryk, A., Krzemień, A., Sánchez Lasheras, F., 2018. Assessing the breathing resistance of filtering-facepiece respirators in Polish coal mines: A survey and laboratory study. Int. J. Ind. Ergon. 68, 101–109. https://doi.org/10.1016/j.ergon.2018.07.001

Woskoboenko, F., 1988. Explosibility of Victorian brown coal dust. Fuel 67, 1062–1068. https://doi.org/10.1016/0016-2361(88)90371-7

Wu, Q., Han, L., Xu, M., Zhang, H., Ding, B., Zhu, B., 2019. Effects of occupational exposure to dust on chest radiograph, pulmonary function, blood pressure and electrocardiogram among coal miners in an eastern province, China. BMC Public Health 19, 1229. https://doi.org/10.1186/s12889-019-7568-5

Xi, Z., Jiang, M., Yang, J., Tu, X., 2014. Experimental study on advantages of foam–sol in coal dust control. Process Saf. Environ. Prot. 92, 637–644. https://doi.org/10.1016/j.psep.2013.11.004

Xiu, Z., Nie, W., Yan, J., Chen, D., Cai, P., Liu, Q., Du, T., Yang, B., 2020. Numerical simulation study on dust pollution characteristics and optimal dust control air flow rates during coal mine production. J. Clean. Prod. 248, 119197. https://doi.org/10.1016/j.jclepro.2019.119197

Xu, C., Wang, D., Wang, H., Xin, H., Ma, L., Zhu, X., Zhang, Y., Wang, Q., 2017. Effects of chemical properties of coal dust on its wettability. Powder Technol. 318, 33–39. https://doi.org/10.1016/j.powtec.2017.05.028

Yan, X., Dai, S., Graham, I.T., French, D., Hower, J.C., 2019. Mineralogy and geochemistry of the Palaeogene low-rank coal from the Baise Coalfield, Guangxi Province, China. Int. J. Coal Geol. 214, 103282. https://doi.org/10.1016/j.coal.2019.103282

Yang, L., Zhu, Z., Li, D., Yan, X., Zhang, H., 2019. Effects of particle size on the flotation behavior of coal fly ash. Waste Manag. 85, 490–497. https://doi.org/10.1016/j.wasman.2019.01.017

Yates, D.H., Gibson, P.G., Hoy, R., Zosky, G., Miles, S., Johnson, A.R., Silverstone, E., Brims, F.,

2016. Down under in the coal mines. Am. J. Respir. Crit. Care Med. https://doi.org/10.1164/rccm.201603-0615LE

Yu, H., Gao, Y., Zhou, R., 2020. Oxidative Stress From Exposure to the Underground Space Environment. Front. Public Heal. https://doi.org/10.3389/fpubh.2020.579634

Yu, H., Wei, J., Cheng, Y., Subedi, K., Verma, V., 2018. Synergistic and Antagonistic Interactions among the Particulate Matter Components in Generating Reactive Oxygen Species Based on the Dithiothreitol Assay. Environ. Sci. Technol. 52, 2261–2270. https://doi.org/10.1021/acs.est.7b04261

Yu, W., Zhao, L., 2021. Chemiluminescence detection of reactive oxygen species generation and potential environmental applications. TrAC - Trends Anal. Chem. https://doi.org/10.1016/j.trac.2021.116197

Yuan, J., Han, R., Esther, A., Wu, Q., Yang, J., Yan, W., Ji, X., Liu, Y., Li, Y., Yao, W., Ni, C., 2017. Polymorphisms in autophagy related genes and the coal workers' pneumoconiosis in a Chinese population. Gene 632, 36–42. https://doi.org/10.1016/j.gene.2017.08.017

Yuan, J., Wei, W., Huang, W., Du, B., Liu, L., Zhu, J., 2014. Experimental investigations on the roles of moisture in coal dust explosion. J. Taiwan Inst. Chem. Eng. 45, 2325–2333. https://doi.org/10.1016/j.jtice.2014.05.022

Yürüm, Y., 1988. New Trends in Coal Science, NATO ASI Series. Springer Netherlands, Dordrecht. https://doi.org/10.1007/978-94-009-3045-2

Zablotska, L.B., Lane, R.S.D., Frost, S.E., 2013. Mortality (1950-1999) and cancer incidence (1969-1999) of workers in the Port Hope cohort study exposed to a unique combination of radium, uranium and γ-ray doses. BMJ Open 3. https://doi.org/10.1136/bmjopen-2012-002159

Zazouli, M.A., Dehbandi, R., Mohammadyan, M., Aarabi, M., Dominguez, A.O., Kelly, F.J., Khodabakhshloo, N., Rahman, M.M., Naidu, R., 2021. Physico-chemical properties and reactive oxygen species generation by respirable coal dust: Implication for human health risk assessment. J. Hazard. Mater. 405, 124185. https://doi.org/10.1016/j.jhazmat.2020.124185

Zendehboudi, S., Bahadori, A., 2017. Production Methods in Shale Oil Reservoirs, Shale Oil and Gas Handbook. https://doi.org/10.1016/b978-0-12-802100-2.00008-3

Zeng, R., Zhuang, X., Koukouzas, N., Xu, W., 2005. Characterization of trace elements in sulphur-rich Late Permian coals in the Heshan coal field, Guangxi, South China. Int. J. Coal Geol. 61, 87–95. https://doi.org/10.1016/j.coal.2004.06.005

Zhang, L., Wang, C., Yan, Q., Zhang, T., Han, Z., Jiang, G., 2017. Diagnostic and clinical application value of magnetic resonance imaging (MRI) for progressive massive fibrosis of coal worker pneumoconiosis. Med. (United States) 96. https://doi.org/10.1097/MD.0000000000006890

Zhang, R., Liu, S., Zheng, S., 2021. Characterization of nano-to-micron sized respirable coal dust: Particle surface alteration and the health impact. J. Hazard. Mater. 413, 125447.

https://doi.org/10.1016/j.jhazmat.2021.125447

Zhang, Y., Dai, M., Yuan, Z., 2018. Methods for the detection of reactive oxygen species. Anal. Methods. https://doi.org/10.1039/c8ay01339j

Zhivin, S., Laurier, D., Guseva Canu, I., 2014. Health effects of occupational exposure to uranium: Do physicochemical properties matter? Int. J. Radiat. Biol. 90, 1104–1113. https://doi.org/10.3109/09553002.2014.943849

Zhou, Z., Yuan, X., Long, D., Liu, M., Li, K., Xie, Y., 2021. A pyridine-Si-rhodamine-based near-infrared fluorescent probe for visualizing reactive oxygen species in living cells. Spectrochim. Acta - Part A Mol. Biomol. Spectrosc. 246, 118927. https://doi.org/10.1016/j.saa.2020.118927

Zielonka, J., Kalyanaraman, B., 2018. Small-molecule luminescent probes for the detection of cellular oxidizing and nitrating species. Free Radic. Biol. Med. 128, 3–22. https://doi.org/10.1016/j.freeradbiomed.2018.03.032

Zosky, G.R., Hoy, R.F., Silverstone, E.J., Brims, F.J., Miles, S., Johnson, A.R., Gibson, P.G., Yates, D.H., 2016. Coal workers' pneumoconiosis: An Australian perspective. Med. J. Aust. 204, 414-418.e2. https://doi.org/10.5694/mja16.00357

Annex

ANNEX A. ADDITIONAL SCIENTIFIC CONTRIBUTIONS

Research publications contributions

i) *Behaviour and speciation of inorganic trace pollutants in a coal-fired power plant equipped with DENOX-SCR-ESP-NH3FGD controls.* Patricia Córdoba, Baoqing Li, Jing Li, Yunfei Shangguan, **Pedro Trechera**, Xinguo Zhuang, Xavier Querol. 2021. *Fuel*, 282, 119927. DOI: 10.1016/j.fuel.2020.119927

ii) *Mineralogical and geochemical variations from coal to deposited dust and toxicity of size-segregated respirable dust in a blasting mining underground coal mine in Hunan Province, South China.* Yunfei Shangguan, Xinguo Zhuang, Xavier Querol, Baoqing Li, Jing Li, natalia Moreno, **Pedro Trechera**, Patriciaa Córdoba, Gaëlle Uzu. 2021. *International Journal of Coal Geology,* 248, 103863.*DOI: 10.1016/j.coal.2021.103863*

Oral presentations

i) **Pedro Trechera**, Teresa Moreno, Xavier Querol. Reducing risks from Occupational exposure to Coal Dust (ROCD) 1st Progress Meeting.

ii) **Pedro Trechera**, Teresa Moreno, Xavier Querol. Reducing risks from Occupational exposure to Coal Dust (ROCD) 2nd Progress Meeting. 2018. 7th-8th November, Barcelona.

iii) **Pedro Trechera**, Teresa Moreno, Xavier Querol. Reducing risks from Occupational exposure to Coal Dust (ROCD) 3rd Progress Meeting. 2019. 15th-16th May, Exeter.

iv) **Pedro Trechera**, Teresa Moreno, Xavier Querol. Reducing risks from Occupational exposure to Coal Dust (ROCD) 4th Progress Meeting. 2019. 27th-28th November, Essen.

v) **Pedro Trechera**, Teresa Moreno, Patricia Córdoba, Natalia Moreno, Xinguo Zhuang, Baoqing Li, Jing Li, Yunfei Shangguan, Ana Oliete Dominguez, Frank Kelly, Xavier Querol. *Mineralogy, Geochemistry, and Toxicity of Size-segregated Respirable Deposited Dust in Chinese Coal Mines.* 2020. IDAEA Young Research Week, September 14th – 18th, Barcelona.

vi) **Pedro Trechera**, Teresa Moreno, Xavier Querol. Reducing risks from Occupational exposure to Coal Dust (ROCD) 5th Progress Meeting. 2020. 29th September.

Poster presentations

i) **Pedro Trechera**, Teresa Moreno, Xavier Querol, Robi Lah, Ben Williamson, Diane Johnson, Aleksander Wrana. *Separation and chemical analysis of underground coal mine PM_{10} and $PM_{2.5}$: a contribution to the new ROCD project*. 2018. 5th Working & Indoor Aerosols Conference, 18th-20th April, Cassino.

ii) **Pedro Trechera**, Teresa Moreno, Xavier Querol, Robi Lah, Ben Williamson, Diane Johnson, Aleksander Wrana. *Chemistry of inhalable coal dust in underground mines*. 2018. Reunión Ibérica de Ciencia y Tecnología de Aerosoles. 20th-22th, June, Bilbao.

iii) **Pedro Trechera**, Teresa Moreno, Xavier Querol, Robert Lah, Diane Johnson, Aleksander Wrana, Ben Williamson. *Size fractionation of metallic elements in inhalable coal mine dust*. 2019. European Aerosol Conference. 25th-30th August, Gothenburg.

ANNEX B. FOUNDING SOURCES

The financial support from this PhD thesis was carried out by the ROCD (Reducing risks from Occupational exposure to Coal Dust) project supported by the European Commission Research Fund for Coal and Steel; Grant Agreement Number 754205; by Generalitat de Catalunya (AGAUR 2017 SGR41), Spain; by the National Science Foundation of China (grant 41972180); by the Program of Introducing Talents of Discipline to Universities (grant B14031) and Overseas Top Scholars Program for the Recruitment of Global Experts, China; by the Spanish Ministry of Science and Innovation (Excelencia Severo Ochoa, Project CEX2018-000794-S). Specials thanks to the partners list of ROCD Project, http://emps.exeter.ac.uk/csm/rocd/